The University Of Sheffield.

The molecular basis of high-level methicillin resistance in *Staphylococcus aureus*

By

Viralkumar Vijaybhai Panchal, BSc. MSc.

(Oxford Brookes University)

A thesis submitted for the degree of Doctor of Philosophy

July 2018

Department of Molecular Biology and Biotechnology, University of Sheffield,

Firth Court, Western Bank, Sheffield, S10 2TN

Summary

Staphylococcus aureus continues to be a clinical burden globally due to its ability to rapidly adapt to antibiotic stress. The overwhelming majority of clinical MRSA (methicillin-resistant *Staphylococcus aureus*) isolates exhibit a low-level β-lactam resistance (oxacillin MIC 2-4 µg/ml). Yet, these are capable of developing high-level resistance to oxacillin (MIC ≥256 µg/ml) by an unknown mechanism(s). Therefore, an experimental system to explore underlying molecular basis of high-level resistance was developed here.

The aim of the project was to construct genetically amenable MRSA strains by introducing plasmid-borne and single copy chromosomal *mecA* into well-characterised, methicillin sensitive genetic background SH1000 which allowed to mimic the resistance phenotype identical to the naturally occurring MRSA clinical isolates. The progression of resistance and whole genome sequencing data revealed single nucleotide polymorphisms in c-di-AMP phosphodiesterase (*gdpP*) to be responsible for high-level resistance when plasmid-borne *mecA* was used. When, single copy *mecA* was introduced mutations in either *rpoB* (RNA polymerase β subunit) or *rpoC* (RNA polymerase β' subunit) were found associated with increased resistance properties.

The impact of the genetic mutations (*rpoB* and *rpoC*) responsible for high-level resistance were examined at the transcriptional level using RNA-seq. Introduction of *mecA* induces metabolic stress resulting in substantial gene expression compared to SH1000 but is reversed upon acquisition of *rpoB/rpoC* mutations. These findings suggested that expression of high-level resistance requires not only elevated amounts of cellular PBP2A but also normalised gene expression. Collectively, this study offers some important insights into physiological aspects of *S. aureus*.

Acknowledgments

I would like firstly thank Prof. Simon Foster and the international strategic alliance scholarship, University of Sheffield for giving me the opportunity to carry out my PhD. Thanks to Simon for his continued guidance and support throughout the course of the project.

Thanks to all past and present members of Foster lab for their scientific help. Particularly to Kasia and Mark for their valuable suggestions and many useful discussions. Thanks to Sid for his help with heatmaps.

I extend my special thanks and gratitude to my mammy, pappa, bhai, motimammy and dada for their endless support, patience and encouragement.

Finally, I would like to express special thanks to Priyal for being there and helping and supporting me in countless ways.

List of Abbreviations

%	Percentage
~	Approximately
º	Degree
ºC	Degree Celsius
2D	Two dimensional
3D	Three dimensional
µg	Microgram
µl	Microlitre
µM	Micromolar
Φ	Phage
Amp	Ampicillin
APS	Ammonium persulphate
ATP	Adenosine triphosphate
attB	Bacterial attachment site
attP	Phage attachment site
BHI	Brain heat infusion
bp	Base pair
BSA	Bovine serum albumin
Cm	Chloramphenicol
D-Ala	D-alanine
dH_2O	Distilled water
DEGs	Differentially expressed genes
DMSO	Dimethyl sulphoxide
DNA	Deoxyribonucleic acid
dNTP	Deoxyribonucleoside-5'-triphosphate
DTT	Dithiothreitol
EDTA	Ethylenediamine tetra-acetic acid
Ery	Erythromycin
eYFP	Enhanced yellow fluorescent protein
FITC	Fluorescein isothiocyanate
g	Grams
Glc*N*Ac	*N*-acetyl glucosamine
h	Hour
HMW	High molecular weight
HRP	Horseradish peroxidase
hVISA	Heterogeneous vancomycin intermediate *Staphylococcus aureus*
Kan	Kanamycin
kb	Kilobase pair
kDa	Kilodalton
kV	Kilovolt

l	Litre
LB	Lysogeny broth
Lin	Lincomycin
LMW	Low molecular weight
LTA	Lipoteichoic acid
M	Molar
mg	Milligram
MIC	Minimum inhibitory concentration
Min	Minute
ml	Millilitre
mM	Millimolar
MSSA	Methicillin Sensitive *Staphylococcus aureus*
MRSA	Methicillin Resistant *Staphylococcus aureus*
Mur*N*Ac	*N*-acetyl muramic acid
mW	Milliwatt
NAD	Oxidised nicotinamide adenine dinucleotide
NADH	Reduced nicotinamide adenine dinucleotide
ng	Nanogram
nm	Nanometres
nM	Nanomolar
nt	Nucleotide
OD_{600}	Optical density measure at 600 nm
pApA	5’-phosphadenylyl-adenosine
PBP	Penicillin binding protein
PBS	Phosphate buffered saline
PCA	Perchloric acid
PCR	Polymerase chain reaction
PDH	Pyruvate dehydrogenase complex
PG	Peptidoglycan
ppGpp	Guanosine tetraphosphate
RBS	Ribosomal binding site
rcf	Relative centrifugal force
RNA	Ribonucleic acid
RNA-Seq	RNA sequencing
rpm	Revolutions per minute
s	Second
sdH_2O	Sterile distilled water
SDS	Sodium dodecyl sulphate
SDS-PAGE	Sodium dodecyl sulphate polyacrylamide gel electrophoresis
TAE	Tris-acetate EDTA
Taq	Thermostable DNA polymerase derived from *Thermus aquaticus*

TBSI	Tris buffered saline containing a protease inhibitor cocktail
TBST	Tris buffered saline tween
TE	Tris-EDTA (buffer)
TEMED	N,N,N',N'-tetramethyl-ethylenediamine
Tet	Tetracycline
TES	Tris-EDTA NaCl
TGase	Transglycosylase
Tn	Transposon
TPase	Transpeptidase
Tris	Tris (hydroxymethyl) aminomethane
TSS	Toxic shock syndrome
U	Units (of enzyme activity)
UV	Ultra violet
v/v	Volume per volume
VISA	Vancomycin Intermediate *Staphylococcus aureus*
VRSA	Vancomycin Resistant *Staphylococcus aureus*
w/v	Weight per volume
WTA	Wall teichoic acid
x	Times

Table of contents

Table of Figures

List of Tables

Chapter 1

Introduction

1.1 *Staphylococcus aureus*

Staphylococcus aureus is a Gram-positive, facultative anaerobic coccal bacterium, approximately 0.5-1.5 µm in diameter, known for an array of diseases in both the community and the hospital settings. Staphylococcal cell division occurs in multiple planes (Tzagoloff and Novick, 1977) resulting in either a single cell following separation or if cells do not separate, form pairs, tetrads and 'bunch of grapes' like formation. This irregular grape-like structure, after which it was named, from the Greek, *staphyle* (bunch of grapes) and *kokkos* (granules), was first discovered from post-operative wound by Sir Alexander Ogoston in 1880. *S. aureus* is a commensal, non-spore forming, non-motile opportunistic pathogen able to colonise all mammalian species causing minor to life-threatening infections given the right circumstances. Preferably, it commonly colonises in the upper respiratory tract, particularly anterior nares (Stapleton and Taylor, 2007). Infections caused by *S. aureus* include, infections of skin (cellulitis and impetigo), bacteraemia, food poisoning, endocarditis, mastitis (mammary gland infection), pneumonia, toxic shock syndrome (TSS) and osteomyelitis (bone infection) (Boucher and Corey, 2008; Choi et al., 1989; Richards et al., 1999).

S. aureus produces circular, glistening, smooth and raised colonies on solid culture medium. The distinctive golden colour of *S. aureus* colonies is due to the carotenoid, staphyloxanthin, involved in oxidative stress resistance mechanism (Clauditz et al., 2006).

1.1.1 *Staphylococcus aureus* infections and epidemiology

A large number of staphylococci species is known to infect humans and other mammals and in some cases birds. *S. aureus* plays the most significant role in causing infections and diseases in humans compared to

other major pathogenic staphylococci include, *S. saprophyticus, S. hemolyticus* and *S. lugdunesis* (Couto et al., 2001). It is estimated that about 30% of the human population are transient carriers and 10% to 20% of are long-term carriers (Lowy, 1998). Most commonly, patients suffering from cancer, type l diabetes, circulatory system diseases, intravenous drug users and surgical patients are at high risk for staphylococcal infections (Archer, 1998; Lowy, 1998). Nine out of ten patients suffering from atopic dermatitis were found to be colonised with *S. aureus* (Abeck and Mempel, 1998). *S. aureus* is the most prevalent causative agent of joint infections (septic arthritis) by producing proteolytic enzymes leading to induction of pro-inflammatory cytokines (Sharff et al., 2013). *S. aureus*-induced pneumonia is highly life threatening with 50% mortality among infections in Europe (Kumar et al., 2009). Staphylococcal pneumonia is associated with cytotoxins such as PVL, enhancing bacterial virulence which contributes to neutrophil cell lysis (Löffler et al., 2010).

S. aureus infections have increasingly been reported throughout the world, mainly in United States, China, Canada, Europe and parts of the Western Pacific (Chuang and Huang, 2013; Diekema et al., 2001). Because of the complex medical issues of the infected patients, the treatment of these infections has become increasingly difficult, imposing a higher burden on healthcare resources (Chu et al., 2005), coupled with increasing morbidity and mortality. During 2016/2017, more than 12,500 cases of *S. aureus*-induced infections were reported in England, representing a 24.6% and 7.7 increase from 2011/2012 and 2015/2016, respectively (Public Health England Reports, 2017).

1.2 Staphylococcal metabolism: an overview

S. aureus is a highly adaptive commensal which possess a number of genes that allow the bacterium to grow and divide in the wide range of environments from aerobic to anaerobic during the course of an infection (Park et al., 1992). The ability to grow and divide in a variety of niches is provided by the metabolic capability of the bacterium which supplies

essential nutrients to ATP-producing pathways, both in the presence and absence of oxygen (Hall and Ji, 2013).

Under aerobic and anaerobic growth conditions, *S. aureus* grows well using oxygen and nitrate/nitrite, respectively as terminal electron acceptors (Fuchs et al., 2007; Somerville and Proctor, 2009). *S. aureus* utilises menaquinone for transfer of electrons regardless of oxygen availability (Lester and Crane, 1959). NADH dehydrogenase transfers electrons to menaquinone from NADH by hydrolysing NADH to NAD^+ under aerobic condition (Somerville and Proctor, 2009). The electrons are then transferred to oxygen through cascade of cytochrome oxidases from menaquinone which drives out protons across the membrane and generates water. Protons exterior to the membrane maintain electrochemical gradient and pH (Somerville and Proctor, 2009). In order to generate new ATP, protons return to the cytoplasm through the ATP synthase complex, however disruption of the electron transfer chain results in anaerobic or fermentative growth phenotype (Fuchs et al., 2007; Somerville and Proctor, 2009). Under anaerobic growth conditions, *S. aureus* ferment sugars and amino acids and enhances dissimilatory nitrate reduction in order to maintain redox poise of the cell (Fuchs et al., 2007; Hall and Ji, 2013).

1.3 *S. aureus* cell division

Cell division is a highly coordinated and controlled process which permits continual growth and division without affecting physiology of the cells (Errington et al., 2003). The main structural component of the cell wall which is peptidoglycan, must be continuously synthesised in a timely manner (Turner et al., 2014). Peptidoglycan makes up to 55% of the total cell wall mass (Heijenoort, 2001) which protects cells from osmotic shock as well as withstands internal turgor (Macheboeuf et al., 2006). *S. aureus* cell division machinery (divisome) comprises of two groups of proteins that coordinate division and peptidoglycan insertion (Figure 1.1). One of the most important divisome component is a mammalian protein tubulin homologue FtsZ which recruits other division proteins such as FtsA, in a sequential order to the division site (Bi and Lutkenhaus, 1991). EzrA, ZapA and SepF are also

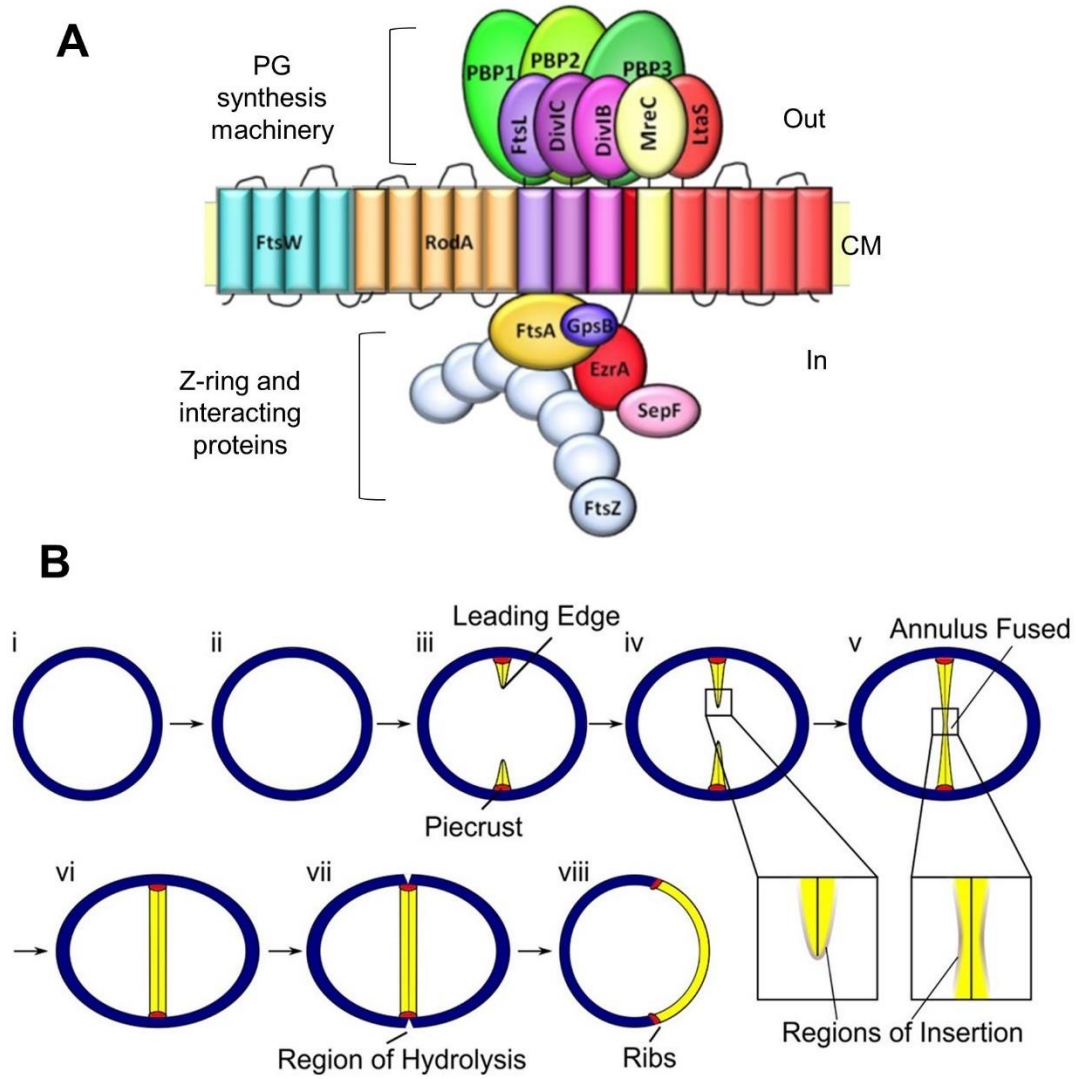

Figure 1.1 *S. aureus* divisome and cell cycle

A) Schematic illustrating cell division machinery from *S. aureus*. CM, cytoplasmic membrane. Taken from (Bottomley, 2011).
B) Model of *S. aureus* cell cycle and peptidoglycan insertion. Cell division begins with an increase in cell size followed by continuous insertion of peptidoglycan to the midcell to form a septum with uniform thickness. Following completion of the septum, the daughter cells separate from each other. Taken from (Lund et al., 2018)

recruited for Z-ring formation (Chaudhuri et al., 2009; Steele et al., 2011). The remaining cell division components are recruited to the midcell after Z-ring formation as late cell division proteins such as, FtsL, DivlC, DivlB, FtsW, GpsB, and PBPs, which are required for peptidoglycan remodelling and degradation (Chaudhuri et al., 2009; Pinho et al., 2000, 2001a).

Splitting of the cell into two hemispherical daughter cells is then enabled by the addition of cell wall hydrolases (e.g. autolysins). There are approximately 20 putative PG hydrolases but their roles are largely unknown (Wheeler et al., 2015).

1.3.1 Peptidoglycan synthesis in *Staphylococcus aureus*

Peptidoglycan is the major constituent of the bacterial cell wall which provides cell-shape as well as enabling resistance to intracellular turgor pressure (Sauvage et al., 2008). Insertion of the new peptidoglycan is mediated by penicillin binding proteins (PBPs) on the exterior of the cytoplasmic membrane following the cooperative activity of a number of other proteins involved in its building block synthesis in the cytoplasm (De Jonge et al., 1992).

Staphylococcal peptidoglycan consists glycan chains of alternating disaccharides, *N*-acetylmuramic acid (Mur*N*Ac) and *N*-acetylglucosamine (Glc*N*Ac) linked by short stem peptides attached to Mur*N*Ac (Figure 1.2) (Ghuysen, 1968; Vollmer et al., 2008a). Glc*N*Ac-Mur*N*Ac units are crosslinked by β-1, 4 glycosidic bonds through a PBP-mediated transglycosylation (TGase) reaction (Vollmer, 2008). *S. aureus* forms ~6 disaccharide long Glc*N*Ac-Mur*N*Ac polymers (Vollmer, 2008), crosslinked covalently by the pentapeptide stem consists of L-alanine, D-glutamine, L-lysine and a D-alanyl-D-alanyl moiety to the Mur*N*Ac residue through PBP-mediated transpeptidation (TPase) reaction (Pinho et al., 2013; Vollmer, 2008a; Vollmer et al., 2008). This flexible crosslinking of glycan units occurs between D-alanine at the 4th residue from one side chain and L-lysine at the position 3 on the other side chain through a pentaglycine bridge (Figure 1.2) (Pinho et al., 2013; Vollmer et al., 2008a). *S. aureus* peptidoglycan has a

high degree of crosslinking from 72% to over 93% of crosslinked peptidoglycan (Vollmer et al., 2008a).

Synthesis of peptidoglycan occurs in three different stages which takes place in three different locations in the cell (Figure 1.3). During the first stage in the cytoplasm, nucleotide sugar-linked precursors UDP-*N*-acetylglucosamine (UDP-Glc*N*Ac) and UDP-*N*-acetylmuramic acid (UDP-Mur*N*Ac) are synthesised from fructose-6-phosphate. Subsequently, amino acids are added by Mur ligases to UDP-Mur*N*Ac resulting in UDP-Mur*N*Ac pentapeptide. The second stage occurs to the cytoplasmic membrane, UDP-Mur*N*Ac pentapeptide precursor is linked to the transport lipid, bactoprenol forming lipid I. Subsequently, Glc*N*Ac is added from UDP-Glc*N*Ac to lipid I, forming lipid II. The subsequent addition of pentaglycine bridge to the 3rd position at L-lysine, resulting in Lipid II-Gly_5, is catalysed by FemABX-like proteins. Lipid II-Gly_5 is then flipped across the cell membrane by FtsW for peptidoglycan incorporation through PBPs. During the final stage, PBPs catalyse transglycosylation and transpeptidation reactions, resulting in respective polymerisation of Lipid II-Gly_5 and crosslinking of flexible pentapeptide stem into nascent peptidoglycan (Macheboeuf et al., 2006; Pinho et al., 2013; Typas et al., 2012).

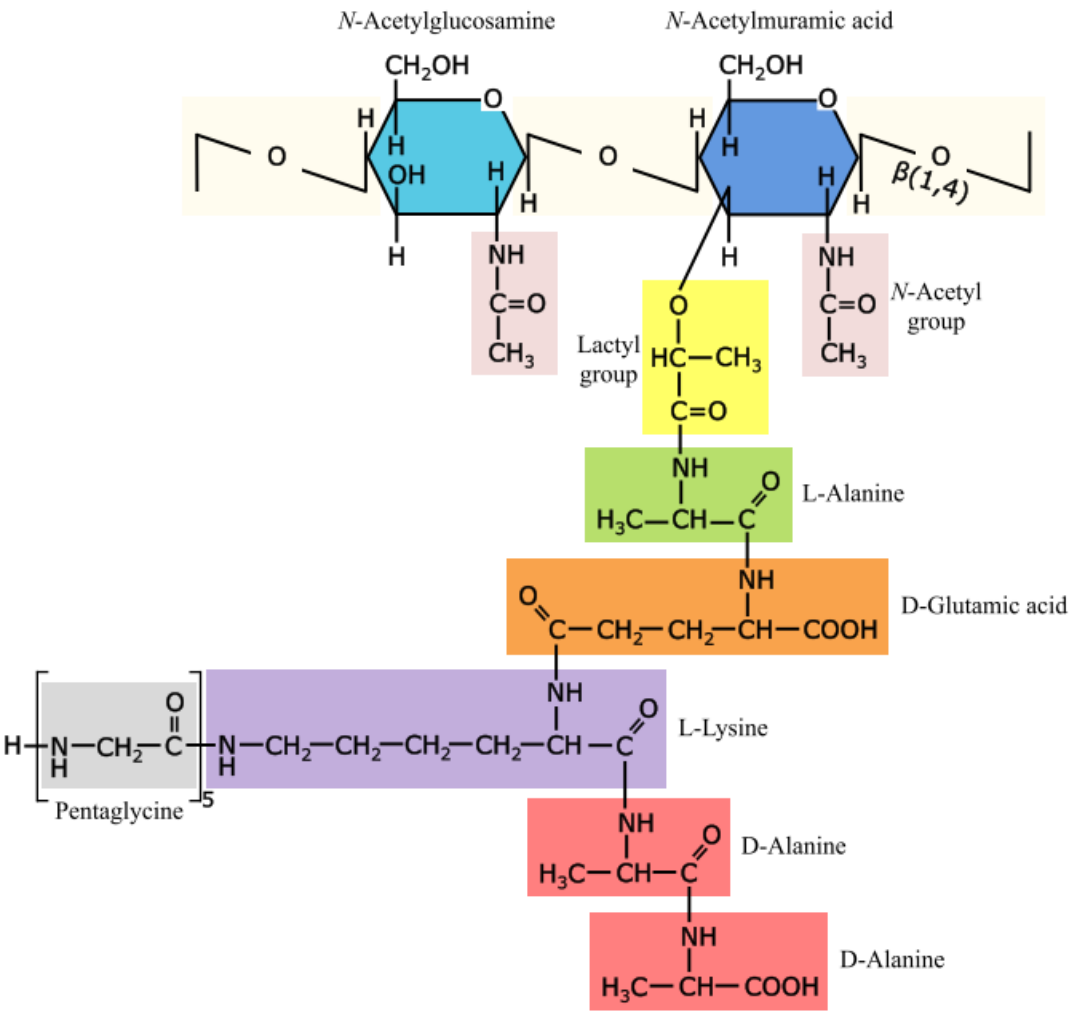

Figure 1.2 The chemical structure of *S. aureus* peptidoglycan

Chemical composition of single peptidoglycan disaccharide pentapeptide with a pentaglycine cross bridge unit is illustrated. The glycan polymer consists of *N*-acetylmuramic acid and *N*-acetylglucosamine are linked covalently to the peptide stem via lactyl group. A pentaglycine bridge linked to L-lysine at the 3rd position of the side chain is shown. Taken from (Fournier and Philpott, 2005; Macheboeuf et al., 2006).

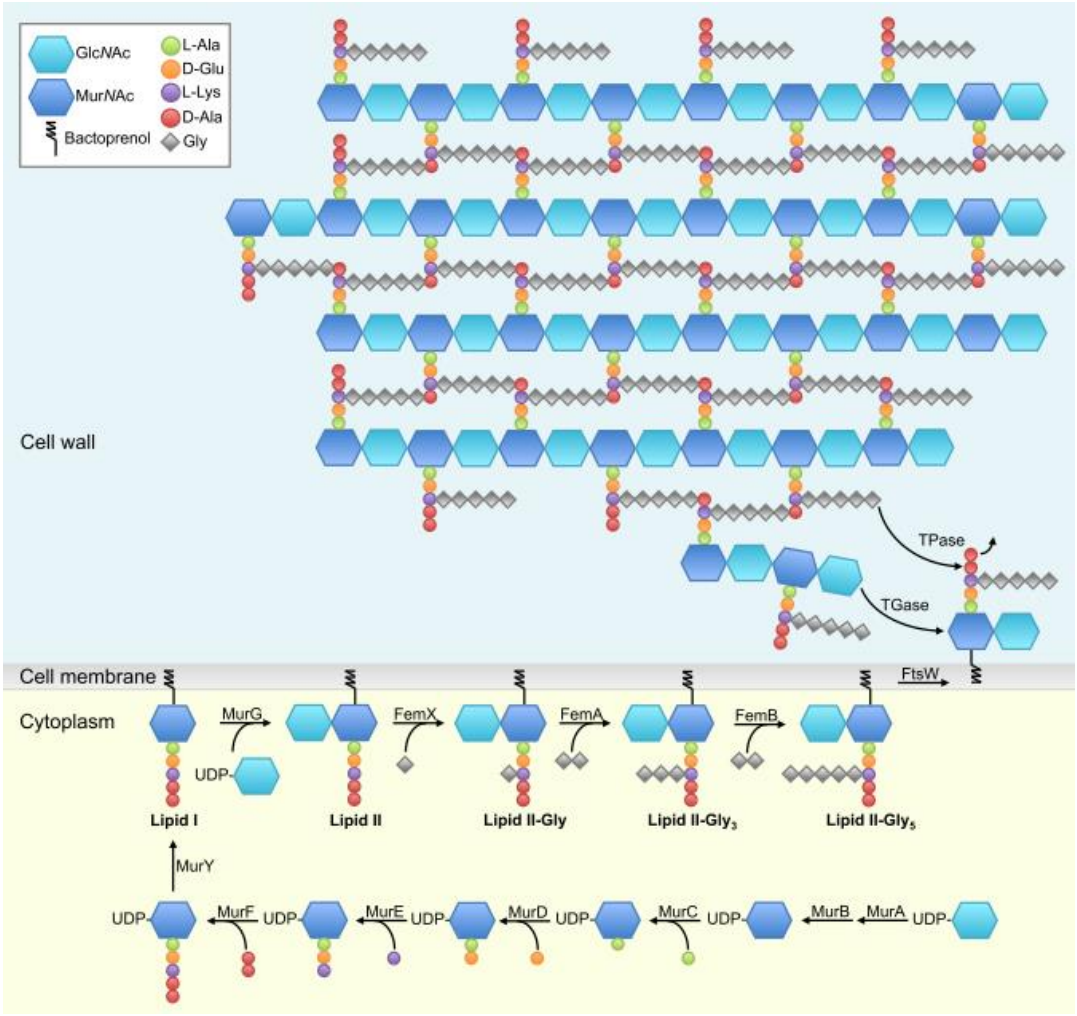

Figure 1.3 Peptidoglycan synthesis in *S. aureus*

Peptidoglycan precursors are synthesised and assembled in the cytoplasm through a series of steps. They are subsequently linked to transport lipid forming lipid I and lipid II. Lipid II is translocated across the cell membrane via FtsW activity. On the exterior of the cell membrane, PBPs catalyse transpeptidation and transglycosylation reactions to incorporate substrate (lipid II) into nascent peptidoglycan. Taken from (Pinho et al., 1998; Typas et al., 2012).

1.3.2 Penicillin binding proteins

Penicillin binding proteins (PBPs) are a group of enzymes with transpeptidation and/or transglycosylation activities, involved in the final stages of peptidoglycan metabolism (Goffin and Ghuysen, 1998; Sauvage et al., 2008). PBPs have particularly been the subject of interest since their discovery as β-lactam targets, as well as their role in the development of β-lactam resistance in some of the most important pathogens such as *Streptococcus pneumoniae, Staphylococcus aureus* and Enterococci (Zapun et al., 2008).

The PBPs are classified into two major groups based on their molecular weight: high molecular weight (HMW) and low molecular weight (LMW), and further according to the number of reactions a single enzyme is able to catalyse (Table 1.1). Depending on their catalytic activity and the structure, HMW PBPs are divided into two classes, class A of bifunctional PBPs and class B of monofunctional PBPs (Goffin and Ghuysen, 1998; Sauvage et al., 2008). Their topology comprises of a two functional domains joined by a β-rich linker on the exterior of cytoplasmic membrane, a transmembrane anchor and a cytoplasmic tail (Goffin and Ghuysen, 1998; Lovering et al., 2007; Macheboeuf et al., 2006). HMW class A PBPs can have N-terminal transglycosylase activity domain and a C-terminal transpeptidase activity domain (Goffin and Ghuysen, 1998; Sauvage et al., 2008). Whereas, HMW class B PBPs can contain an N-terminal domain with unknown function and a C-terminal transpeptidase activity domain (Goffin and Ghuysen, 1998; Sauvage et al., 2008). LMW PBPs possess either endopeptidase or carboxypeptidase activity to hydrolyse pentapeptide stems into tetrapeptides, preventing further peptidoglycan crosslinking (Goffin and Ghuysen, 2002; Macheboeuf et al., 2006). Thereby, the level of peptidoglycan crosslinking is controlled by LMW PBPs (Morlot et al., 2004).

The number of native PBPs possessed, varies amongst bacterial species. *B. subtilis* contains 16 PBPs, of which four are class A PBPs (Table 1.1). PBPs are involved in sporulation and vegetative peptidoglycan synthesis (Sauvage et al., 2008; Scheffers, 2005; Scheffers and Errington, 2004). Six of its 16

PBPs are class B (Table 1.1) of which, PBP2b containing transpeptidase activity is required for cell division (Daniel et al., 2000). *E. coli* possesses a total of 12 PBPs of which there are three class A (PBP1a, PBP1b and PBP1c) and two class B (PBP2 and PBP3) (Table 1.1). PBP1a and PBP1b are the main transpeptidases and transglycosylases whilst PBP2 and PBP3 are monofunctional transpeptidases (Den Blaauwen et al., 2008). PBP2 is specific to cell elongation while PBP3 is major constituent of the divisome (Den Blaauwen et al., 2008). The seven LMW PBPs are associated with peptidoglycan maturation or recycling and cell separation (Sauvage et al., 2008; Vollmer et al., 2004, 2008b). The different modes of growth and cell shape of bacteria might reflect the number of PBPs that they possess.

In *S. aureus*, the cell does not elongate therefore, peptidoglycan is mainly synthesised at the septum during cell division (Figure 1.1 B) (Lund et al., 2018; Pinho and Errington, 2003; Pinho et al., 2013), making *S. aureus* a minimalist model for studying cell division. It produces only four native PBPs (Table 1.1). *S. aureus* strains susceptible to β-lactam antibiotics contain two HMW class B PBPs, PBP1 and PBP3 of which PBP1 is essential for growth and survival (Pereira et al., 2009). Both enzymes are important of their transpeptidase activity. Depletion of PBP1 halts cell division and causes rapid loss in viability (Pereira et al., 2007). However, inactivation of the transpeptidase activity of PBP1 showed no alterations in peptidoglycan composition, signifying its function independent of its functional transpeptidase domain (Pereira et al., 2007, 2009). Its unique HMW class A PBP, PBP2 localises to the septum (Pinho and Errington, 2003), required for its transpeptidase and transglycosylase activities and deletion of this enzyme is lethal to the cell (Pinho et al., 2001a). Dispersed localisation of bifunctional PBP2 was observed when *S. aureus* cells were treated with oxacillin unlike in MRSA where transpeptidase activity of native PBP2 was taken over by PBP2A – a non-native HMW class A PBP, in the presence of oxacillin (Pinho and Errington, 2005; Tan et al., 2012a). Moreover, inhibition of substrate synthesis also delocalises PBP2, resembling the results found with oxacillin treatment, suggesting the importance of transpeptidation substrates for PBP2 recruitment to the septum (Pinho and Errington, 2005). Moreover, in

the presence of functional PBP2A, PBP2 localises to the septum explaining the essentiality of the transpeptidase activity of PBP2A for substrate recognition (Pinho and Errington, 2005; Pinho et al., 2001a). The methicillin resistance determinant, PBP2A is an acquired PBP encoded by the *mecA* gene in MRSA. This β-lactam insensitive transpeptidase undertakes the normal function of native PBPs in the presence of low-levels of all available β-lactam antibiotics (Pinho et al., 2001b). However, high-level resistance is only conferred by the presence of transglycosylase activity of native PBP2 (Pinho et al., 2001a). Inactivation of PBP3 showed no significant alteration in peptidoglycan composition or growth defects except significant decrease in autolytic rate (Pinho et al., 2000), suggesting the importance of PBP3 in cell division but not for cell survival as the transpeptidase activity of PBP3 may have thought to be taken over by PBP1 and/or PBP2 (Pinho et al., 2000). The exact role of PBP3 is yet to be identified. *S. aureus* encodes only one LMW PBP, PBP4 which unlike *E. coli* PBP5, has a transpeptidase activity necessary to achieve high degree of peptidoglycan crosslinking (Wyke et al., 1981). Loss of PBP4 is associated with reduction in the transcription of PBP2 in both MSSA and MRSA strains resulting in decreased peptidoglycan crosslinking (Memmi et al., 2008), suggesting a putative interaction between them. However, the expression of PBP2A remained unchanged upon the loss of PBP4 (Memmi et al., 2008). These observations suggest the cooperative function of PBP4, PBP2 and PBP2A and their structural and organisational relationships (Leski and Tomasz, 2005; Memmi et al., 2008). Moreover, inactivation of PBP4 in MRSA is associated with significant reduction in oxacillin resistance suggesting the role of PBP4 in in mediating high-level β-lactam resistance (Memmi et al., 2008).

Species	PBPs	Classification	Molecular function	References
Staphylococcus aureus	PBP2 (*pbp2*)	HMW Class A	Essential for cell division	(Pinho et al., 2001a)
	PBP2a (*mecA*)[a]	HMW Class B	Require for PG synthesis	(Pinho et al., 2001b)
	PBP1 (*pbpA*)		Essential for cell growth and survival	(Pereira et al., 2009)
	PBP3 (*pbpC*)		Involved in septum formation	(Pinho et al., 2000)
	PBP4 (*pbp4*)	LMW	Involved peptidoglycan crosslinking	(Memmi et al., 2008)
Bacillus subtilis	PBP1 (*ponA*)	HMW Class A	Important for the assembly of division septum	(Scheffers and Errington, 2004)
	PBP4 (*pbpD*)		Require for synthesis and remodelling of PG	(Sauvage et al., 2007)
	PBP2c (*pbpF*)		Require for cell growth	(Scheffers, 2005)
	PBP2d (*pbpG*)		Involved in cell growth	(Mcpherson and Popham, 2003)
	PBP3 (*pbpC*)	HMW Class B	Involved in cell division	(Murray et al., 1996)
	SpoVD (*spoVD*)		Required for spore morphogenesis	(Zhang et al., 1997)
	PBP2b (*pbpB*)		Involved in cell division	(Daniel et al., 2000)
	PBP2a (*pbpA*)		Involved in rod shape formation	(Wei et al., 2003)
	PbpH (*pbpH*)		Involved in PG synthesis	(Wei et al., 2003)
	PBP4b (*yrrR*)		Involved in spore PG synthesis	(Scheffers and Errington, 2004)
	PBP4a (*dacC*)	LMW	Cell separation and peptidoglycan maturation	(Sauvage et al., 2008)
	DacF (*dacF*)		Spore peptidoglycan crosslinking	(Popham et al., 1999)
	PBP5 (*dacA*)		Peptidoglycan maturation	(Scheffers, 2005)
	PBP5* (*dacB*)		Spore cortex synthesis	(Popham et al., 1999)
	PBP4* (*pbpE*)		Involved in sporulation	(Scheffers, 2005)
	PbpX (*pbpX*)		Involved in sporulation	(Scheffers, 2005)
Escherichia coli	PBP1a (*ponA*)	HMW Class A	Essential for cell growth and survival	(Denome et al., 1999)
	PBP1b (*ponB*)		Essential for cell growth and survival	(Denome et al., 1999)
	PBP1c (*pbpC*)		Involved in PG synthesis	(Schiffer and Höltje, 1999)
	PBP2 (*pbpA*)	HMW Class B	Required for cell shape	(Schiffer and Höltje, 1999)
	PBP3 (*ftsi*)		Essential for PG synthesis in the absence of PBP1b	(Denome et al., 1999)
	PBP4 (*dacB*)	LMW	Cell separation and peptidoglycan maturation	(Vollmer et al., 2004)
	PBP5 (*dacA*)		Peptidoglycan maturation	(Sauvage et al., 2008)

	PBP6 (*dacC*)		Peptidoglycan maturation	(Sauvage et al., 2008)
	PBP6b (*dacD*)		Peptidoglycan maturation	(Sauvage et al., 2008)
	PBP7 (*pbpG*)		Cell separation and peptidoglycan maturation	(Vollmer et al., 2004)
	PBP4b (*yefw*)		Not determined	(Vega and Ayala, 2006)
	AmpH (*ampH*)		Peptidoglycan recycling	(Henderson et al., 1997)

Table 1.1 Classification of PBPs

[a], only found in MRSA.

1.4 PBP-based antibiotic resistance

A multi-layered mesh of highly crosslinked peptidoglycan protects the cell from environmental stresses as well as contributing to resistance and virulence essential for survival and pathogenicity (McCallum et al., 2010). The Gram-positive bacterial cell wall also consists of wall teichoic acids covalently linked to the peptidoglycan, lipoteichoic acids attached to the cytoplasmic membrane and other membrane associated proteins including peptidoglycan-anchored surface proteins and extracellular proteins. All of these components make the cell envelope an attractive target for numerous antibiotics which either block or disrupt peptidoglycan synthesis (Figure 1.4) (McCallum et al., 2010). For continual cell growth and division, peptidoglycan precursor synthesis, polymerisation, cell wall degradation and turnover are essential processes.

As mentioned above, the last enzymatic reactions of peptidoglycan synthesis are carried out by PBPs. Any perturbation of cell wall metabolism caused by an inhibition of PBPs is lethal for growth and survival. The two major classes of cell wall antibiotics include β-lactams and glycopeptides. β-lactam antibiotics, such as penicillin, methicillin and oxacillin target native PBPs of *S. aureus* by inhibiting transpeptidase activity, hindering access to their substrate (Goffin and Ghuysen, 1998). Glycopeptides, such as vancomycin and teicoplanin target the D-ala-D-ala terminus of the lipid ll and uncrosslinked nascent peptidoglycan exterior to the cytoplasm, thereby blocking PBP reactions (Reynolds, 1989). However, various means of antibiotic resistance have been emerged and investigated, such as decrease affinity to the antibiotic by utilising non-native PBPs or degradation of the antibiotic by β-lactamases (Sabath, 1982)

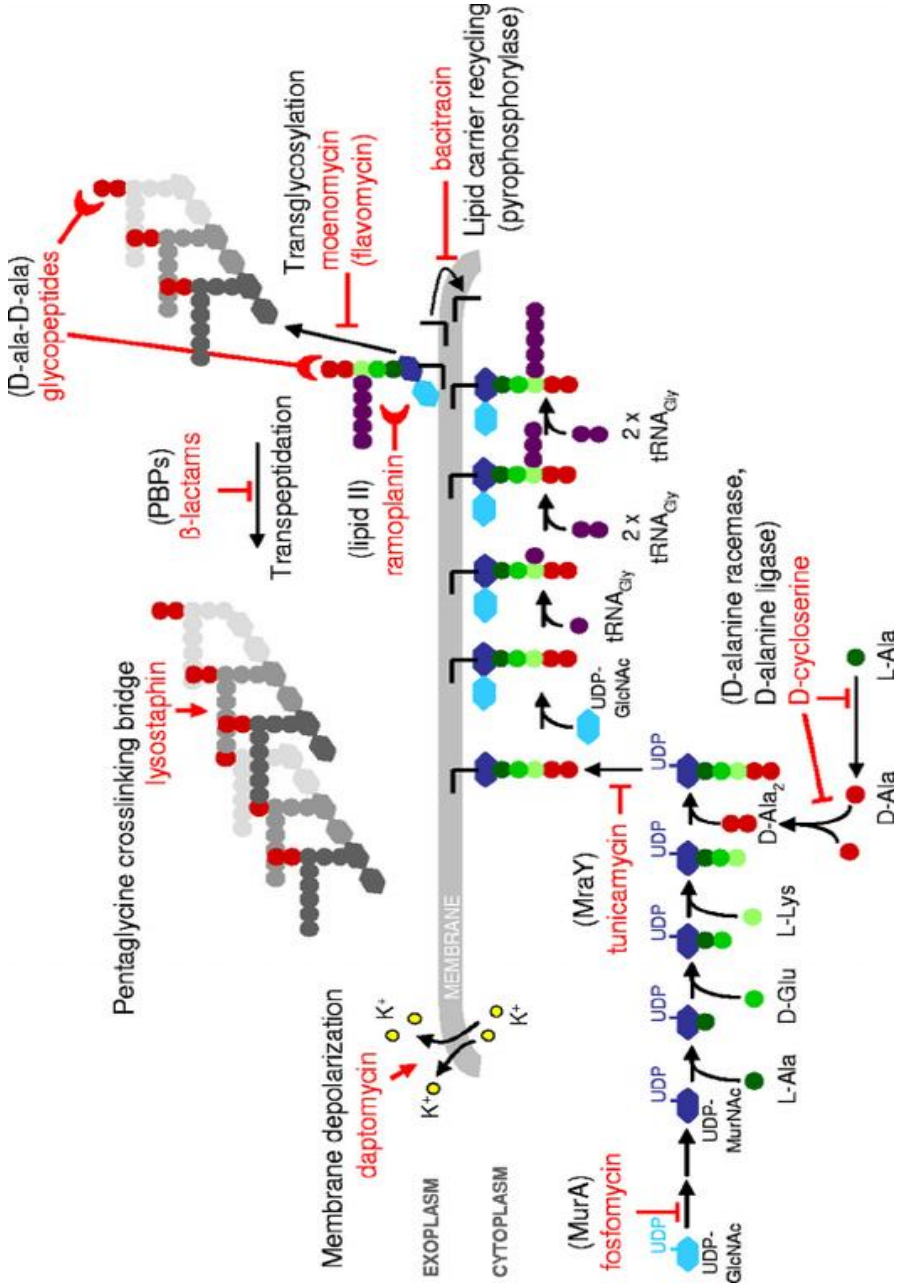

Figure 1.4 *S. aureus* peptidoglycan synthesis and cell wall active antibiotics targets

Red blocked arrows indicate inhibition of enzymatic reactions; red half-moon arrows indicate inhibition of cell wall synthesis; red arrows indicate pentaglycine bridge cleavage and membrane disruption. Taken from (McCallum et al., 2010, 2011).

1.4.1 β-lactam resistance in *Staphylococcus aureus*

There are two main mechanisms acquired by *S. aureus* to become resistant to the β-lactams. One is enzyme-mediated resistance conferred by penicillinase (β-lactamase) production which hydrolyses the β-lactam class of antibiotics, such as penicillin (Sabath, 1982). The second and broader mechanism is the expression of *mecA* encoding the additional PBP, PBP2A with decreased affinity for β-lactams, maintaining cell wall biosynthesis in the presence of β-lactams (Hartman and Tomasz, 1984; Lim and Strynadka, 2002; Reynolds and Brown, 1985) with the help of native bifunctional PBP, PBP2 for its transglycosylase activity (Pinho et al., 2001b).

A distinctive feature of methicillin-resistant *S. aureus* (MRSA) is their heterogeneous resistance expression, meaning that individual strains can produce a subpopulations with different levels of higher resistance (Tomasz et al., 1991). Resistance levels also varies between different MRSA lineages, ranging from an oxacillin MIC of <0.5 to >1000 µg/ml (McCallum et al., 2010).

1.5 The history of MRSA

In the early 1940s penicillin was first introduced to treat patients with *S. aureus* bacteraemia but penicillin resistant *S. aureus* (PRSA) were isolated as soon as 1942 (Rammelkamp and Maxon, 1942). The development of penicillin resistance was mediated by an enzyme, penicillinase/β-lactamase encoded by *blaZ* which cleaves the β-lactam ring and inhibits the action of antibiotic (Bondi and Dietz, 1945; Sabath, 1982).

In response to the spread and emergence of penicillin resistance, a semisynthetic β-lactam named methicillin, resistant to penicillinase was developed and introduced into the clinic in 1959 (Jevons, 1961; Lowy, 2003). One year later after the introduction of methicillin to treat *S. aureus* mediated infections, an MRSA isolate was recovered from a patient diagnosed with osteomyelitis and septic arthritis (Jevons et al., 1963). Later, a large proportion of cases were reported in hospital followed by community settings. The outcomes of MRSA mediated infections are worse than the outcomes from MSSA (Cosgrove et al., 2003). A rapid spread of MRSA was noted as

soon as its first appearance in a new setting, accounting for an increasing cases of nosocomial infections (Couto et al., 1995; Panlilio et al., 1992). The notorious ability of *S. aureus* to develop and acquire antibiotic resistance mechanisms makes it a major healthcare problem (Figure 1.5). Currently, MRSA mediated infections account for significantly high morbidity and mortality rates (Dantes et al., 2013; Klein et al., 2007). Even though methicillin is no longer produced commercially or used clinically, the term MRSA has continued to be used. In addition, methicillin resistance means resistance to nearly all available β-lactams (Stryjewski and Corey, 2014).

In order to identify the genetic determinants of methicillin resistance, the chromosomal localisation of *mec* gene complex encoding novel penicillin-binding protein (PBP2A) (Katayama et al., 2000) was determined by Sjöström et al (1975). Later, it was confirmed that *mec* was only found on a chromosomal region of MRSA and not MSSA (Stewart and Rosenblum, 1980). Using the penicillin-binding assay, several researchers also identified the novel low affinity PBP2A encoded by *mecA* in MRSA strains (Brown and Reynolds, 1980; Hartman and Tomasz, 1984; Utsui and Yokota, 1985). *mecA* is encoded on a mobile genetic element found in all MRSA called staphylococcal cassette chromosome (SCC*mec*) (Katayama et al., 2000). The types and classification of SCC*mec* are further described later in this chapter.

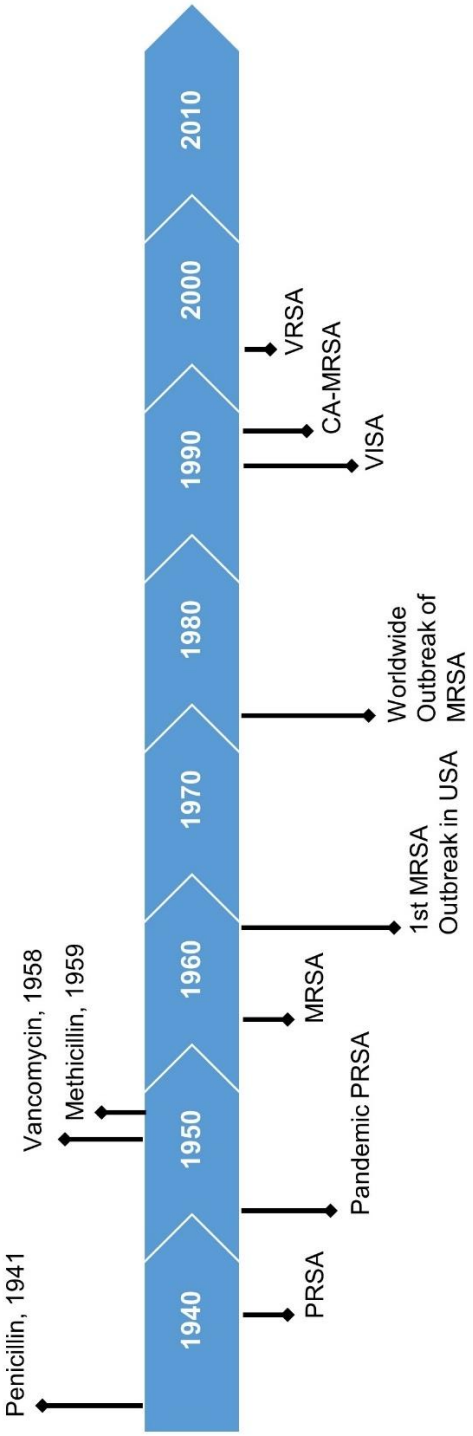

Figure 1.5 Timeline illustrating the introduction of antibiotics and subsequent emergence of antibiotic resistance in *S. aureus*

PRSA, Penicillin-resistant *S.* aureus; MRSA, Methicillin-resistant *S.* aureus; VISA, Vancomycin-intermediate *S. aureus*; VRSA, Vancomycin-resistant *S. aureus*; CA-MRSA, Community-acquired MRSA. Taken from (McGuinness et al., 2017).

1.5.1 Signalling and regulation of β-lactam resistance

The variable phenotypic expression of methicillin resistance is regulated by the *mecI* and *mecR1* regulatory elements (Archer and Bosilevac, 2001). The regulatory components, *mecI* and *mecR1* are encoded within the *mec* gene complex adjacent to the *mecA* on SCC*mec* element which integrates in the chromosome (Ito et al., 2001). The *mec* regulatory genes, *mecR1* and *mecI* are structurally and functionally similar to the *blaZ* regulatory components, *blaR1* and *blaI* (Figure 1.6) which in response to β-lactam antibiotics induces the expression of *mecA* or *blaZ*, respectively (Gregory et al., 1997; Lowy, 2003).

Exposure to β-lactams enables the activation of a signal-transduction protein, MecR1. Its extracellular penicillin-binding domain (PBD) senses the presence of antibiotic which then allows the activation of its cytoplasmic domain (Zhang et al., 2001). The cytoplasmic metalloproteinase domain (MPD) of MecR1 has a protease activity. Its activation results in direct or indirect cleavage of MecI repressor therefore, initiating the transcription of *mecA* (Figure 1.7) (Archer and Bosilevac, 2001; Zapun et al., 2008; Zhang et al., 2001). Recently, Arêde et al (2012) characterised an anti-repressor encoded by *mecR2* gene whose function is essential for complete induction of *mecA* enabling optimal β-lactam resistance. In addition to *mecR1-mecI*, the *mecR2* gene is localised in an unusual three-component arrangement and cotranscribed with *mecR1-mecI* (Figure 1.7) (Arêde et al., 2012). An inefficient *mecR1*-dependent *mecA* expression is compensated by *mecR2* which interacts with *mecI* directly enabling destabilisation of *mecI* binding to the *mecA* promoter (Arêde et al., 2012, 2013). Mutations or deletions of the operator region or the *mecI* results in constitutive expression of *mecA* (Niemeyer et al., 1996). It was demonstrated that either *blaI* or *mecI* must be functional in order to repress the expression of *mecA* suggesting the importance of preventing the overproduction of PBP2A (Rosato et al., 2003). Unexpectedly, methicillin resistance had no effect upon overexpression of *mecI* in *S. aureus* strains, suggesting the presence of an additional regulatory gene (Oliveira and de Lencastre, 2011).

Moreover, it is important to note that not all MRSA strains carry an intact *mec* regulatory system as some strains carries truncated genes or lack *mecI* (Hurlimann-Dalel et al., 1992; Suzuki et al., 1993). Those having a complete regulatory system tend to be slow in developing resistance upon exposure to methicillin (Ryffel et al., 1992). For example, the N315 strain carries both regulatory systems resulting in a tight repression of *mecA* by both *mecI* and *blaI* which can lead to inhibition of β-lactam resistance (Hiramatsu, 1995; Niemeyer et al., 1996). Yet, the strains with de-repressed *mecA* expression exhibit only low-level resistance in the absence of β-lactam selection. Also, the promoter region, *mecA*, and regulatory genes (*mecI* and *mecR1*) are highly conserved among MRSA strains (Chambers, 1997). This highlights the need for tightly controlled *mecA* expression.

The genetic background of the strains also plays an important role in the stability of *mecA* as the composition of *mec* regulatory system is greatly diverse between community-acquired MRSA (CA-MRSA) and hospital-acquired MRSA (HA-MRSA) strains (Katayama et al., 2005). In some MRSA, the penicillinase regulatory system is required as the induction of *mecA* by *mecI* is slower which could be lethal for the cell in the presence of β-lactam antibiotic (Cha et al., 2007; Ryffel et al., 1992). This explains the presence of non-functional regulatory elements in many clinical MRSA, resulting in constitutive PBP2A production which leads to increased resistance (Katayama et al., 2004; Niemeyer et al., 1996; Rosato et al., 2003).

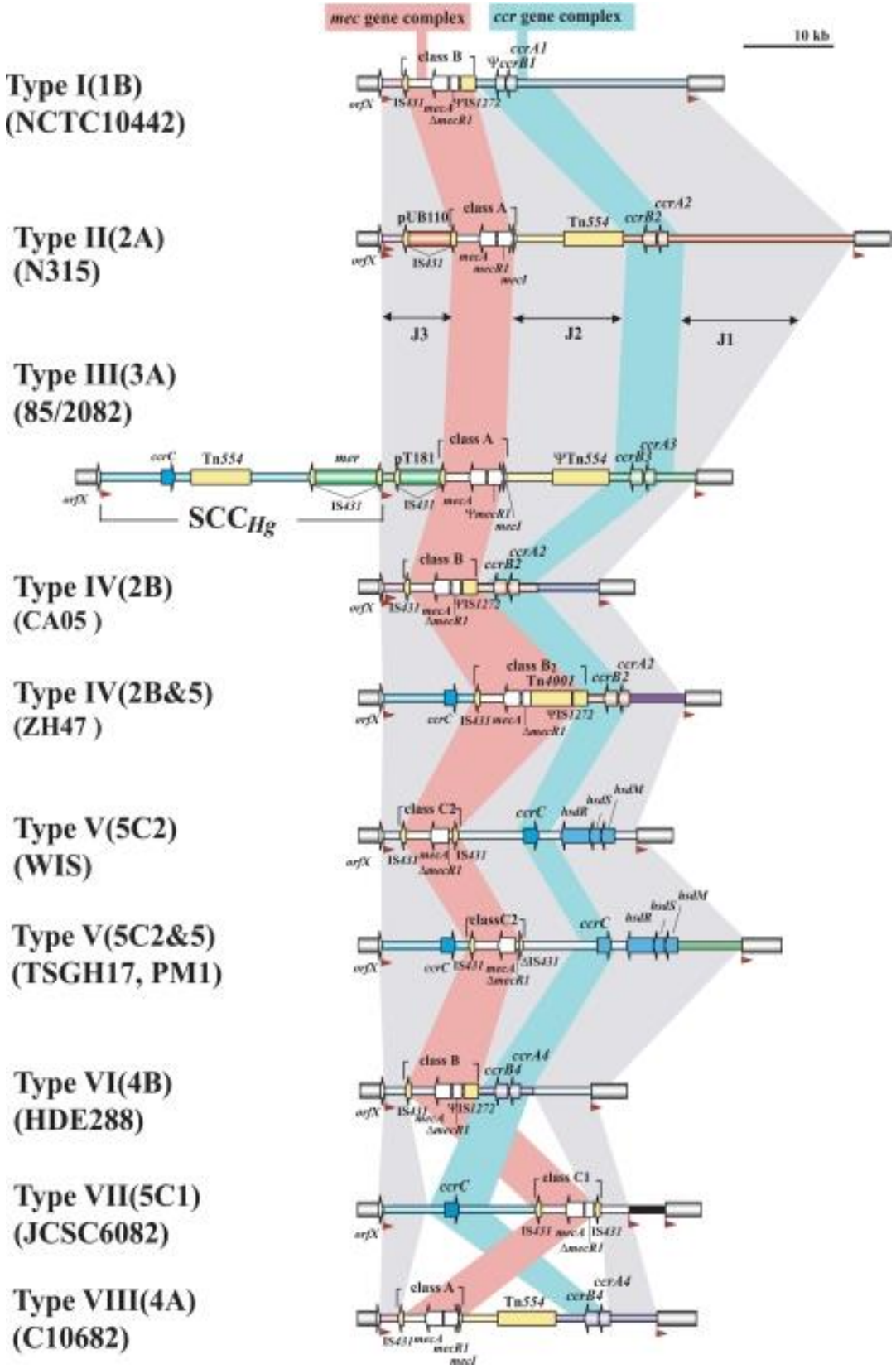

Figure 1.6 Structural organisation of SCC*mec* elements

The structures of SCC*mec* elements from representative strains are shown based on their nucleotide sequences available in databases. Taken from (Ito et al., 2009).

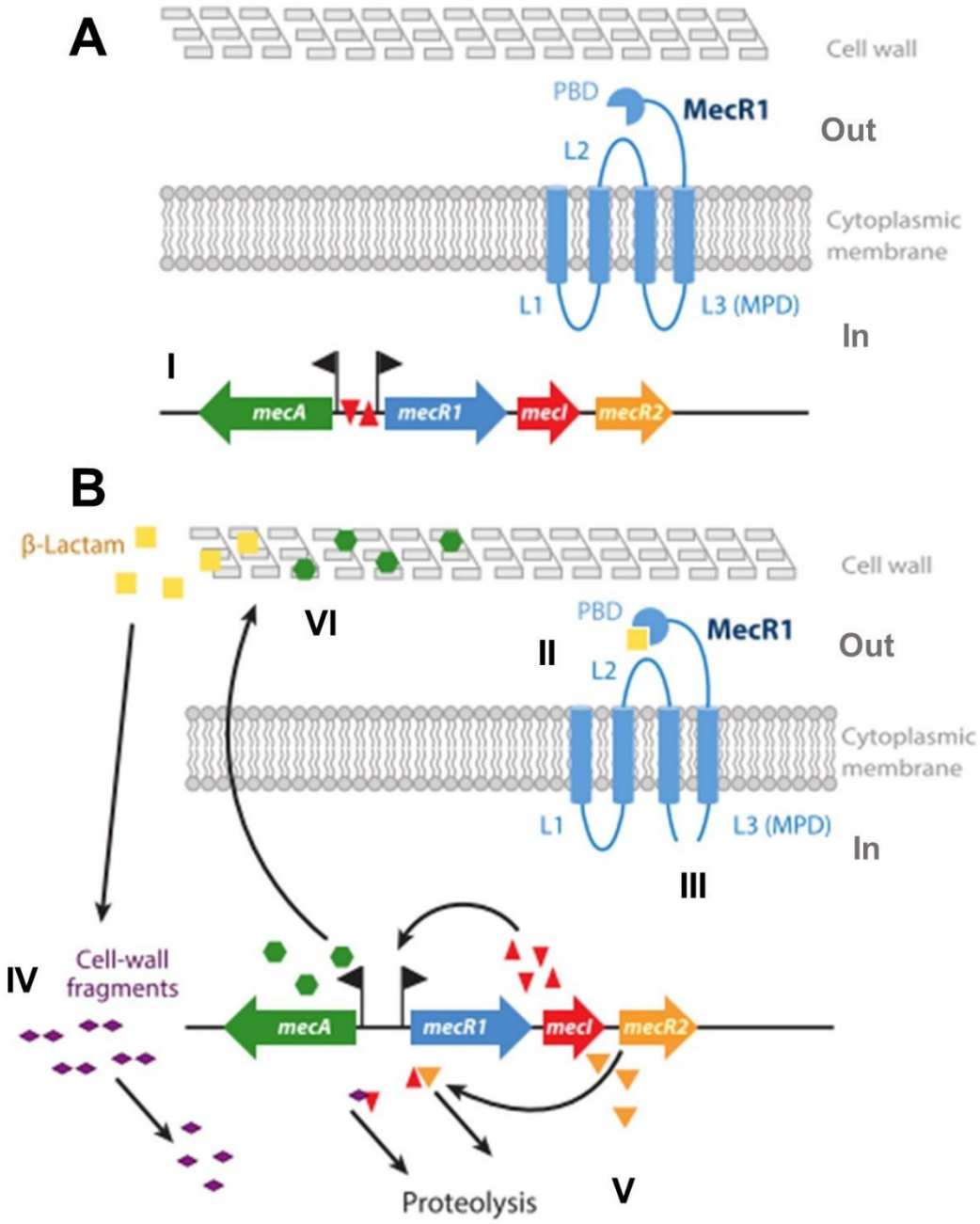

Figure 1.7 Regulation of methicillin resistance in *S. aureus*

A) In the absence of β-lactams, (I) *mecA* transcription is prevented by the binding of *mecI* (red triangle) to the *mec* operator/promoter region.
B) In the presence of β-lactams, (II) penicillin-binding domain (PBD) of MecR1 detects β-lactams which (III) triggers the activation of intracellular metalloproteinase domain (MPD) resulting in proteolysis of MecI. (IV) β-lactam disrupted cell-wall biosynthesis generates dipeptide cell-wall fragments which might be involved in the activation of MPD of MecR1. However, how the cell-wall fragments specifically, γ-D-Glu-L-Lys are generated in cytoplasm is not understood (Amoroso et al., 2012). (V) MecR2, a second anti-repressor is transcribed in the presence of antibiotic leading to MecI proteolysis. (VI) MecI degradation causes the transcription of *mecA* and subsequent production of PBP2A resulting in the expression of methicillin resistance.
Adapted from (Peacock and Paterson, 2015).

1.5.2 Characteristics of Staphylococcal cassette chromosome *mec* (SCC*mec*)

The evolution of MSSA to MRSA is due to the acquisition of a genetic element, staphylococcal cassette chromosome (SCC*mec*) which encodes for methicillin resistance along with the regulatory network which controls its expression in *Staphylococcus* genus. It was first identified and characterised in 1999 (Ito et al., 1999). Preliminary work suggested that the evolution of SCC*mec* occurred in multiple stages in the most primitive *Staphylococcus* species, the *Staphylococcus sciuri.* The study showed that *mecA1* encoding a penicillin-binding protein in *S. sciuri* had 80% nucleotide identity to *S. aureus mecA* (Couto et al., 1996; Wu et al., 1996a). Other homologues to *mecA* were also identified namely, *mecA* of *Staphylococcus fleurettii* (99% identity) and *mecA2* of *Staphylococcus vitulinus* (90% identity) (Schnellmann et al., 2006; Tsubakishita et al., 2010), however the structural organisation of *mecA* and its regulatory system was different to that of *S*. *sciuri* (Tsubakishita et al., 2010). Only recently investigators examined the origin and distribution of *S. aureus* SCC*mec* elements by using whole genome sequencing and SNP analysis approaches which demonstrated that the evolutionary stages comprised a possible contribution from several *Staphylococcus* species which included *S. sciuri, S. vitulinus* and *S. fleurettii* (Rolo et al., 2017). Moreover, iterative phylogenetic tree inferred the level of relatedness between SCC elements and SCC*mec* which suggested that SCC*mec* was assembled through series of recombination events involving at least three species even before the introduction of β-lactam antibiotics (Rolo et al., 2017).

SCC*mec* integrates into the *S. aureus* genome near the origin of replication at the 3' end of the *orfX* gene at the attachment site sequence *attB* in all cases (Figure 1.8) (Katayama et al., 2003a; Noto et al., 2008). The integration of SCC*mec* is mediated by *ccr*-based recombination at the *attB* site of the genome and the circularised SCC*mec* specific *att*S site (Ito et al., 1999; Katayama et al., 2000). This generates new pair of sites called *attL* and *attR*; which flanks the SCC*mec* elements. However, upon excision of

SCC*mec* results in regeneration of the original *attB* and *att*S sites (Figure 1.8) (Katayama et al., 2000; Misiura et al., 2013).

The complete sequence of *orfX* is maintained upon acquisition of the SCC*mec* without altering its expression during growth (Boundy et al., 2013). The molecular function of *orfX* was not clear until recently, the crystal structural analysis revealed its structural homology to ribosomal methyltransferase YbeA of *E. coli* 70 S ribosomal methyltransferase RlmH (Ero et al., 2008). OrfX-dependent 70 S ribosome methylation was demonstrated to have methyltransferase activity in *S. aureus* (Boundy et al., 2013).

SCC*mec* elements contain three basic genetic elements and share structurally similar backbone, that consists of (I) a *mec* gene complex carrying *mecA* and its regulators, surrounding ORFs and insertion sequences, (II) a cassette chromosome recombinase (*ccr*) gene complex containing *ccrAB* and or *ccrC* ensuring the mobility of SCC*mec* and surrounding ORFs and (III) the joining region (J region) (Ito et al., 2009; Liu et al., 2016a; Turlej et al., 2011). See *mec* organisation diagram for structural organisation of genetic components (Figure 1.6). Moreover, it may also carry housekeeping genes inside J regions as well as transposons and plasmids (Katayama et al., 2000). Currently, SCC*mec* elements are classified into I to XI types on the basis of the nature of *ccr* and *mec* gene complexes (Table 1.2) (Liu et al., 2016a). They are further classified into different subtypes based on the location and DNA segments of the J regions (Liu et al., 2016a).

1.5.2.1 The *ccr* gene complex

The *ccr* gene complex contains *ccr* gene(s) and surrounded ORFs. The *ccr* genes encoded DNA recombinases catalyse precise site and orientation-specific integration as well as excision of the SCC*mec* elements into and from staphylococcal chromosome (Katayama et al., 2000). Based on phylogenetic analysis, there are three distinct *ccr* genes; *ccrA*, *ccrB* and *ccrC* have been identified in *S. aureus* (Ito et al., 2009). These are further classified into 8 allotypes based on allelic variation in *ccr* (Ito et al., 2009; Liu

et al., 2016a). Type 1 comprises of *ccrA1* and *ccrB1* genes, type 2 comprises of *ccrA2* and *ccrB2* genes, type 3 carries *ccrA3* and *ccrB3* genes, type 4 comprises of *ccrA4* and *ccrB4* genes, type 5 contains the *ccrC1* gene, type 6 comprises of *ccrA5* and *ccrB3* genes, type 7 carries *ccrA1* and *ccrB6* genes, and type 8 comprises of *ccrA1* and *ccrB3* genes (Figure 1.6) (Table 1.2) (Liu et al., 2016a). The types of *ccr* genes were defined based on frequency of DNA sequence similarities in different *S. aureus* (Ito et al., 2009).

1.5.2.2 The *mec* gene complex

Apart from *mecA* and its regulatory genes, the *mec* gene complex is composed of insertion sequences (IS) and hypervariable region (HVR). Based on the differences in IS and the location and integrity of regulatory genes, the *mec* gene complex was classified into 5 classes (Table 1.2). The class A *mec* gene complex contains intact *mecR1* and *mecI* regulatory genes upstream of *mecA*, insertion sequence IS*431* downstream of *mecA* and HVR (Ito et al., 2009). The class B *mec* gene complex carries IS*1272* upstream of *mecA* resulting in truncated *mecR1* and IS*431* downstream of *mecA* and HVR (Ito et al., 2009). The class C *mec* gene complex is divided into two classes based on the orientation of IS*431*: class C1 and C2. Both classes contain truncated *mecR1* due to IS*431* upstream of *mecA* and HVR and IS*431* to the downstream of *mecA*. IS*431* of class C1 has the same orientation upstream and downstream of *mecA* while class C2 carries IS*431* flanking *mecA* and regulatory components is in the opposite orientation to class C1 (Ito et al., 2009). The class D *mec* gene complex comprises of a partly deleted *mecR1* with no IS*431* downstream of *mec* complex (Ito et al., 2009; Katayama et al., 2001). The class E *mec* gene complex has recently been identified from livestock MRSA isolate which contains *blaz*, *mecA, mecR1 and mecI* (Liu et al., 2016a; Turlej et al., 2011).

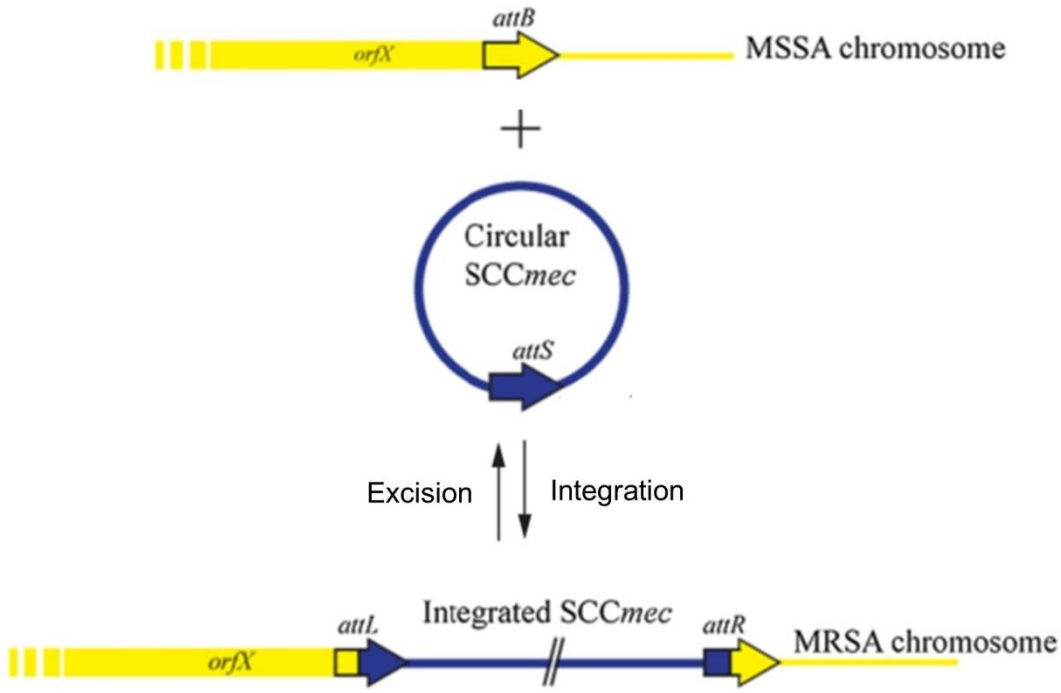

Figure 1.8 Schematic representation of SCC*mec* transposition

Circularised SCC*mec* (dark blue) integrates into the *S. aureus* genome (yellow), specifically to the *attB* site at the 3' end of the *orfX* gene. MRSA chromosome shows the integration of linearised SCC*mec* in the chromosome generating *attL* and *attR* sites. Upon excision of SCC*mec* from the chromosome creates circularised SCC*mec*. Integration and excision of SCC*mec* is modulated by *ccr* genes. Modified from (Stojanov et al., 2015).

SCC*mec* type	*Mec* gene complex	Structure of *mec* gene complex	*Ccr* gene complex	*Ccr* genes	Original strain	Reference
I	Class B	IS*1272*-△*mecR1*-*mecA*-IS*431*	Type 1	*ccrA1, ccrB1*	NCTC10442	(Ito et al., 2001)
II	Class A	*mecI*-*mecR1*-*mecA*-IS*431*	Type 2	*ccrA2, ccrB2*	N315	(Ito et al., 1999, 2001; Katayama et al., 2000)
III	Class A	*mecI*-*mecR1*-*mecA*-IS*431*	Type 3	*ccrA3, ccrB3*	85/2082	(Ito et al., 2001)
IV	Class B	IS*1272*-△*mecR1*-*mecA*-IS*431*	Type 2	*ccrA2, ccrB2*	JCSC1986, JCSC1978	(Ma et al., 2002)
V	Class C2	IS*431*- *mecA*-△*mecR1*-IS*431*	Type 5	*ccrC1*	JCSC3624	(Ito et al., 2004)
VI	Class B	IS*1272*-△*mecR1*-*mecA*-IS*431*	Type 4	*ccrA4, ccrB4*	HDE288	(Oliveira et al., 2001, 2006)
VII	Class C1	IS*431*- *mecA*-△*mecR1*-IS*431*	Type 5	*ccrC1*	JCSC6082	(Zhang et al., 2009)
VIII	Class A	*mecI*-*mecR1*-*mecA*-IS*431*	Type 4	*ccrA4, ccrB4*	C10682	(Zhang et al., 2009)
IX	Class C2	IS*431*- *mecA*-△*mecR1*-IS*431*	Type 1	*ccrA1, ccrB1*	JCSC6943	(Li et al., 2011)
X	Class C1	IS*431*- *mecA*-△*mecR1*-IS*431*	Type 7	*ccrA1, ccrB6*	JCSC6945	(Li et al., 2011)
XI	Class E	*blaZ*-*mecA*-*mecR1*-*mecI*	Type 8	*ccrA1, ccrB3*	LGA251, M10/0061	(García-Álvarez et al., 2011)

Table 1.2 Types of SCC*mec* and their composition

Modified from (Liu et al., 2016a)

1.5.2.3 The joining (J) regions

Besides, *mec* and *ccr* gene complexes, the J regions are essential for the biological functions of the SCC*mec*. The J regions are epidemiologically significant as they could be use as potential targets for transposons or plasmids. The J regions carry additional resistance determinants for a range of antibiotics and heavy metals resulting in a multidrug resistance phenotype (Turlej et al., 2011). Based on the location of J regions in SCC*mec*, they are classified in J1, located at the right side of the cassette; J2, between the *mec* and *ccr* gene complexes; and J3, located at the left side between the chromosomal junction adjoining *orfX* and the *mec* complex (Ito et al., 2009; Liu et al., 2016a; Turlej et al., 2011).

1.6 Structural basis of resistance

The transpeptidation step of peptidoglycan biosynthesis is inhibited by the β-lactams which act as substrate analogues of the peptidoglycan side chain D-Ala-D-Ala (Tipper and Strominger, 1965). PBPs require to access pentapeptide, specifically D-Ala-D-Ala dipeptides chain for catalysing the transpeptidation reaction in order to continue cell wall synthesis. β-lactam forms a covalent acyl-enzyme complex between the nucleophilic serine residue of the PBP and the antibiotic impeding the transpeptidation reaction which results in inhibition of cell wall synthesis (Lim and Strynadka, 2002; Peacock and Paterson, 2015). The interaction of PBPs with β-lactam antibiotics is shown in Figure 1.9 A. Moreover, the β-lactam occupies the deacylating acceptor moiety resulting in slower deacylation of the acyl-enzyme complex leading to blockage of regeneration of the PBP (Lim and Strynadka, 2002; Peacock and Paterson, 2015). This slower rate (k_3) of regeneration of the PBP renders the enzyme effectively irreversibly inactivated. Consequently, loss of peptidoglycan cross-linking results in a weaker cell wall formation causing cell death (Peacock and Paterson, 2015). However, mechanistic understanding leading to cell death is poorly understood. Giesbrecht et al (1998) demonstrated that the penicillin-induced cell death results from the high internal turgor pressure leading to cytoplasmic leakage due to a weak cell wall.

The enzyme kinetic parameters for resistance conferred by PBP2A showed that PBP2A has a reduced β-lactam mediated acylation rate compared to the native PBPs resulting inefficient formation of acyl-PBP complex as a result of poorer fit of β-lactam to the active site (Fuda et al., 2004; Graves-Woodward and Pratt, 1998). Therefore, reduced acylation rate (k_2) of PBP2A is important for developing high-level resistance. Secondly, PBP2A showed absence of high affinity (K_d) for β-lactams. The PBP2A crystal structure showed that the active-site serine of PBP2A is less accessible compared to the susceptible PBPs to β-lactams as the active site is located in a narrow cleft (Figure 1.9 B and C) (Lim and Strynadka, 2002). β-lactam sensitive PBPs undergo conformational changes to facilitate acylation reaction unlike PBP2A (Lim and Strynadka, 2002). However, structural analysis of PBP2A showed that the activity of PBP2A is under the control of allosteric site, located within the non-penicillin-binding domain (Figure 1.9 C) (Otero et al., 2013). Nascent peptidoglycan access to this allosteric site by recognition of the D-Ala-D-Ala dipeptide stimulates conformational changes allowing opening the active site for the transpeptidation reaction (Otero et al., 2013). Therefore, poor efficiency for acylation together with restricted access to the active site is an important aspect of PBP2A based resistance.

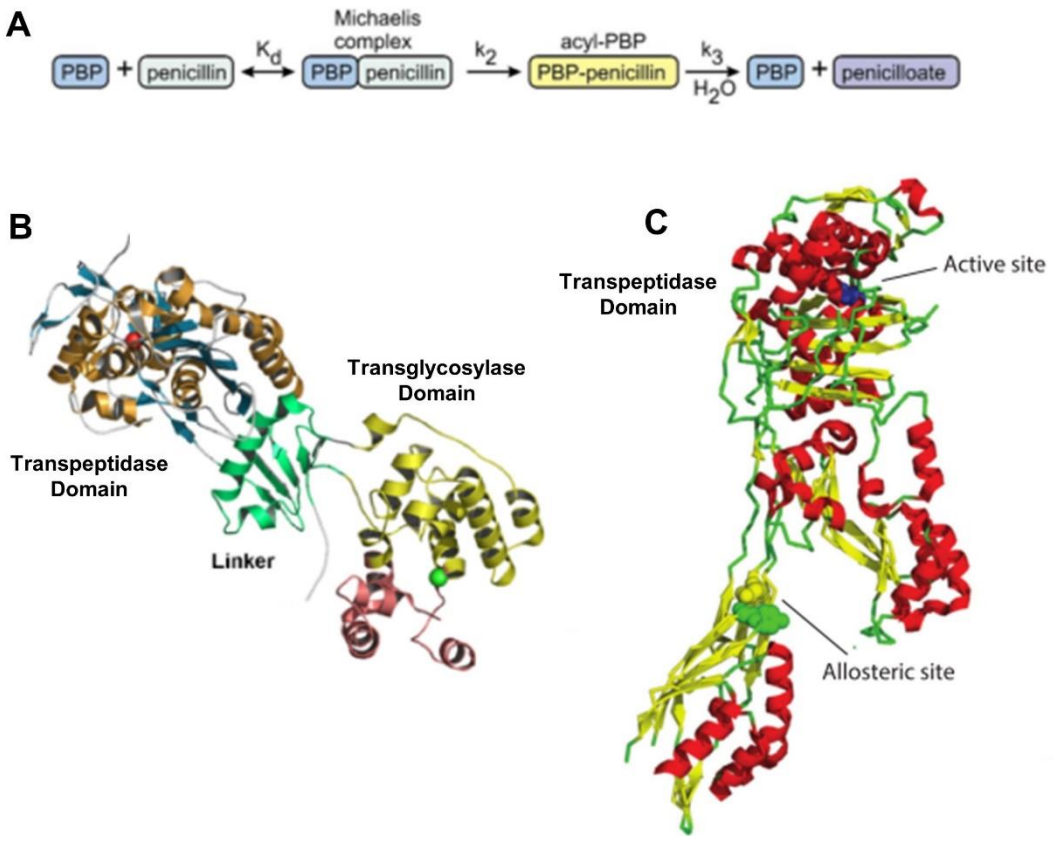

Figure 1.9 Interaction of *S. aureus* PBPs with β-lactam and their structures

A) Diagrammatic representation of the interaction of PBPs with β-lactams (represented by penicillin). A reversible, noncovalent pre-acylation Michaelis complex (represented by K_d as the dissociation constant) is formed upon interaction. The acyl-PBP intermediate is formed from the Michaelis complex measured by a rate constant k_2. Deacylation rate constant k_3 measures the regeneration of PBPs due to hydrolysis of acyl-PBP intermediate. Taken from (Lim and Strynadka, 2002).
B) Structural representation of PBP2 showing the catalytic serine residue (red sphere) of transpeptidase domain and the catalytic glutamic acid residue (green sphere) of the transglycosylase domain. Taken from (Sauvage et al., 2008).
C) Crystal structure of MRSA PBP2A showing allosteric site highlighted with yellow spheres and the active-site serine highlighted with blue sphere within the transpeptidase domain. Taken from (Peacock and Paterson, 2015).

1.7 The genetic basis of methicillin resistance

Unlike penicillin resistance in *S. aureus* which is mediated by plasmid-borne β-lactamase (Dyke et al., 1966), methicillin resistance is mediated by the acquisition of *mecA* encoding a fifth low affinity PBP named PBP2A in addition to the four native PBPs (Hartman and Tomasz, 1984; Utsui and Yokota, 1985). The expression of *mecA* is often induced by the presence of β-lactams maintaining peptidoglycan synthesis while the activity of the resident PBPs is inhibited (Fuda et al., 2005). PBP2A is the most abundant among all native PBPs of MRSA cell, approximately 800 molecules per cell (Pucci and Dougherty, 2002); nonetheless, the level of resistance does not fully correlate with the amount of PBP2A (Berger-Bächi and Rohrer, 2002; Niemeyer et al., 1996; Ryffel et al., 1994). It has also been demonstrated that the amount of native PBPs; approximately 150 to 450 molecules per cell, do not alter due to the abundance of PBP2A (Pucci and Dougherty, 2002). The acquisition of *mecA* is a prerequisite for the development of resistance (Kim et al., 2013; Mwangi et al., 2013).

1.7.1 Heterogeneous low-level expression of methicillin resistance

The level of methicillin resistance of MRSA isolate is diverse according to the β-lactam and the culture conditions used. A distinctive feature displayed by all MRSA is a heterogeneous expression of methicillin resistance which means that the majority of bacterial population is sensitive to low concentrations of antibiotic (<5 μg/ml methicillin); however, contains a small proportion of cells exhibiting high-level resistance (>50 μg/ml) (Hartman and Tomasz, 1986; Tomasz et al., 1991). The frequency at which highly resistance subpopulation arises is about 10^{-4}, which is reproducible and strain-specific (Tomasz et al., 1991). Earlier studies by Tomasz et al (1991) classified MRSA into four classes based on methicillin MICs. Class I, II and II contained heterogeneously resistant strains with methicillin MIC 1.5-3, 6-12 and 50-200 μg/ml, respectively; class IV strains exhibited homogeneous high-level resistance to methicillin (MIC ≥800 μg/ml) (Tomasz et al., 1991). Most MRSA strains expresses heterogeneous resistance under normal growth conditions, however growth in hypertonic media containing sucrose or

NaCl or incubation at 30°C appeared to develop homogeneous high-level resistance (Sabath and Wallace, 1971). While incubation at 37 to 43°C or addition of EDTA (pH 5.2) only favours heterogeneous resistance. Incubation of heterogeneously resistant strain in the presence of β-lactam antibiotic altered the resistance and selected highly resistant clones (Sabath and Wallace, 1971).

Methicillin resistant variants from pre-MRSA strain N315 were isolated upon exposure to 3 µg/ml of methicillin, carried mutations or deletions in their *mecI* gene or at the operator of the *mecA* gene exhibited class III heterotypic resistance pattern (Suzuki et al., 1993). However, deletion of *mecI* by gene-replacement with *tetL* strain showed concomitant constitutive expression of *mecA* accompanied by class III heterogeneous resistance (Kuwahara-Arai et al., 1996). This observation demonstrates that the constitutive expression of *mecA* through its derepression and concomitant production of PBP2A can make the strain resistant to methicillin but only to the heterogeneous level. Consistent with this, 38 epidemic MRSA strains isolated from 20 countries had either deletion of the *mecI* gene or mutations in *mecI* or mutations in the operator region of *mecA* further supporting the importance of the inactivated *mecI* gene for developing methicillin resistance (Hiramatsu, 1995).

In an effort to understand the underlying mechanism of heterogeneous resistance, earlier evidence suggested that the presence of *mec* gene regulators could not alone be responsible for class I heterogeneity in N315 as inactivation of *mecI* leaves N315 strain heterogeneously resistant as well as PBP2A remains inducible; therefore, it is likely that other factor(s) are involved in the heterogeneous expression of resistance (Hiramatsu, 1995).

1.7.2 Factors influencing methicillin resistance levels

To investigate the genes responsible for the heterogeneity, transposon mutagenesis was carried out using homogeneously resistant MRSA strains. This approach identified several genes involved in peptidoglycan synthesis which led to change from homogeneously resistant to either susceptible or heterogeneously resistant (Berger-Bächi et al., 1992; Berger Bachi, 1983;

Kornblum et al., 1986). Subsequently, De Lencastre and Tomasz (1994) identified 14 independent loci, auxiliary (*aux*) factors or *fem* (factors essential for methicillin resistance) responsible for the decrease in methicillin resistance of MRSA strains, evidently, unlinked to SCC*mec* and *mecA* but influencing methicillin resistance (Berger-Bächi et al., 1992; De Lencastre and Tomasz, 1994; De Lencastre et al., 1999).

The characterised *fem* or *aux* factors have shown to be housekeeping genes and present in the genomes of all wild-type *S. aureus* strains. Their activity influence the expression of resistance (Berger-Bächi and Rohrer, 2002). Many of these chromosomal genes are directly or indirectly involved in peptidoglycan biosynthesis and turnover or have regulatory functions (Table 1.3). However, none of them has been shown to alter *mecA* expression (Berger-Bächi and Rohrer, 2002; Roemer et al., 2013). Tightly controlled cell wall synthesising processes, such as stem peptide synthesis (*femD/glmM*), addition of lysine to the stem peptide (*murE/femF*), glutamine reduction of precursor stem peptide (*femC/glnR*) are all required for the expression of methicillin resistance (Berger-Bächi and Rohrer, 2002). It is also shown that the inhibition of the pentaglycine side chain synthesis through mutated *femA, femB* and *femhB*, leads to hypersusceptibility as PBP2A strictly requires pentaglycine side chain to mediate resistance (Berger-Bächi and Rohrer, 2002; Rohrer et al., 1999).

Moreover, teichoic acids have also been implicated in methicillin resistance as they are linked to peptidoglycan while lipoteichoic acids are anchored to membrane glycolipids. Teichoic acids regulate autolytic activities (Wecke et al., 1997) through modulating their charge by addition of phosphate groups carrying negative charge and alanine carrying positive charge. Alteration in transfer of alanine into teichoic acids through the *dlt* operon leads to increased negative charge influencing cell wall metabolism through altered autolytic activities, therefore increases methicillin resistance (Nakao et al., 2000). Increase in negative charge of the membrane surface have also been shown to influence the binding of antimicrobial peptides to the surface (Peschel et al., 2001). Other cellular processes involving protein secretion

(*spsB*) and cell division (*ftsA* and *ftsZ*) as well as signal transduction systems (*pknB*/SAV1220) were also identified in contributing to methicillin resistance when a specific gene transcript of COL and USA300 isolates were targeted using a plasmid library containing an inducible antisense interference fragment (Lee et al., 2011; Roemer et al., 2013). This observation demonstrated that methicillin resistance is multifactorial where the coordinated activity of a network of processes contributes in providing resistance in addition to the expression of *mecA*.

The cell wall two-component system (TCS) *vraSR* of *S. aureus* senses cell surface damage through cell wall active antibiotics and subsequently induces a cell wall stress stimulon (CWSS) comprising a number of genes including, *murZ, fmtA, tarA* and *pbp2* (Jordan et al., 2008; Kuroda et al., 2003). Mutations in *vraSR* have been shown to severely affect the cell wall stress response resulting in hypersusceptibility not only to *vraSR* inducing agents but also β-lactam antibiotics (Gardete et al., 2006; Kuroda et al., 2003). Consistent with this, oxacillin efficacy was restored in an animal infection model against USA300 lacking *vraSR* (Jo et al., 2011).

Besides the genetic background of MRSA, the levels of methicillin resistance also strongly influenced by the environmental factors such as osmolarity, temperature, pH, visible light, the composition of growth media and the availability of divalent cations (Matthews and Stewart, 1984).

Gene (alternative names)	Function	References
fmhB (femX)	Addition of the first glycine to the peptide stem, inactivation lethal	(Rohrer et al., 1999)
femA	Addition of the 2nd and 3rd glycine to the peptide stem, inactivation disrupts methicillin resistance	(Strandén et al., 1997)
femB	Addition of the 4th and 5th glycine to the peptide stem, inactivation reduces methicillin resistance	(Henze et al., 1993)
femC (glnR)	Glutamine synthetase repressor, inactivation reduces methicillin resistance	(Gustafson et al., 1994)
femD (glmM)	Phosphoglucosamine mutase, inactivation reduces methicillin resistance	(Jolly et al., 1997)
femE	Function unknown; inactivation reduces methicillin resistance	(de Lencastre et al., 1994)
femF (murE)	Catalyses incorporation of lysine into the peptide stem; inactivation reduces methicillin resistance	(Ornelas-Soares et al., 1994)
fmtA	Membrane protein; inactivation reduces methicillin resistance	(Komatsuzawa et al., 2001)
fmtB (mrp)	Cell surface protein, inactivation reduces methicillin resistance	(Wu and de Lencastre, 1999)
fmtC (mprF)	Membrane-associated protein; inactivation reduces methicillin resistance	(Komatsuzawa et al., 2001)
lytH	Lytic enzyme, inactivation increases methicillin resistance	(Fujimura and Murakami, 1997)
pbp2	Penicillin-binding protein 2, functional transglycosylase domain of PBP2 is needed for methicillin resistance	(Pinho et al., 2001b)
sigB	Transcription factor, inactivation reduces methicillin resistance	(Wu et al., 1996b)
hmrA	Putative aminohydrolase; overexpression increases methicillin resistance	(Kondo et al., 2001)
hmrB	Homologue of acyl carrier protein; overexpression increases methicillin resistance	(Kondo et al., 2001)
dlt operon	Transfer of D-alanine into teichoic acids; inactivation increases methicillin resistance	(Nakao et al., 2000)
glmS	Glucosamine-6-phosphate synthase, required for methicillin resistance	(Lee et al., 2011)
murA	Transferase; converts UDP-GlcNAc to UDP-GlcNAc-enoylpyruvate, required for methicillin resistance	(Lee et al., 2011)
murB	Reductase; converts UDP-GlcNAc-enoylpyruvate to UDP-MurNAc, required for methicillin resistance	(Lee et al., 2011)
glyS	Glycine tRNA synthetase, required for methicillin resistance	(Lee et al., 2011)
gatD	Glutamine amidotransferase, required for methicillin resistance	(Figueiredo et al., 2012)
murT	Mur ligase homolog, required for methicillin resistance	(Figueiredo et al., 2012)
SAV1754 (mviN, murJ)	Proposed lipid II translocase, required for methicillin resistance	(Huber et al., 2009)

ftsW	Proposed lipid II translocase, required for methicillin resistance	(Lee et al., 2011)
pbp1 (pbpA)	PBP with transpeptidation activity	(Lee et al., 2011)
pbp4	PBP with transpeptidation activity, required for methicillin resistance	(Memmi et al., 2008)
ftsA	Divisome component, required for methicillin resistance	(Lee et al., 2011)
ftsZ	Bacterial ortholog of tubulin, Divisome component, required for methicillin resistance	(Lee et al., 2011)
tarO	Forms first precursor in WTA synthesis, required for methicillin resistance	(Maki et al., 1994)
tarA	Forms second intermediate in WTA synthesis, required for methicillin resistance	(Wang et al., 2013)
tarB	Forms third intermediate in WTA synthesis, required for methicillin resistance	(Wang et al., 2013)
tarD	WTA synthesis, required for methicillin resistance	(Wang et al., 2013)
tarL	Required for poly ribitol-phosphate extension of WTA	(Lee et al., 2011)
tarI	WTA synthesis, required for methicillin resistance	(Wang et al., 2013)
tarS	Glycosyltransferase, required for methicillin resistance	(Brown et al., 2012)
ltaS	Lipoteichoic acid synthase, required for methicillin resistance	(De Lencastre et al., 1999)
pknB (stk1, aux2)	Eukaryotic-like serine/threonine kinase, required for methicillin resistance	(De Lencastre et al., 1999)
spsB	Signal peptidase I, required for methicillin resistance	(Lee et al., 2011)
vraSR	Two component signal transduction sensor of cell wall stress, inactivation reduces resistance	(Kuroda et al., 2003)
prsA	Required for post-translational maturation of PBP2A, Inactivation increases susceptibility to ceftaroline	(Jousselin et al., 2016)

Table 1.3 Chromosomal genes influencing methicillin resistance levels

1.7.3 Homogeneous high-level expression of methicillin resistance

The mechanism of heterogeneity is particularly intriguing because homogeneous high-level resistance arises from *S. aureus* isolates exhibiting heterotypic resistance upon exposure to a β-lactam antibiotic (Hartman and Tomasz, 1986). The majority of CA-MRSA exhibit heterogeneous resistance such as USA300 while HA-MRSA exhibit homogeneously high-level resistance such as COL. Such isolates expressing high-level resistance exhibited uniformly stable expression of resistance with little variation in colony size to heterogeneous population (Tomasz et al., 1991). Early research to examine the transition from heterogeneous to homogeneous resistance suggested that the development of stable high-level resistance required the acquisition of genetic mutations at non-*mec* and non-*fem* loci (Ryffel et al., 1994). Selection of homogeneous resistance did not revert to heterogeneous resistance following growth in drug-free medium indicating the selection of mutations driving the stability and not the induction of resistance pathway (Finan et al., 2002; Ryffel et al., 1994).

Consistent with this hypothesis, introduction of *mecA* into a strain carrying a chromosomal mutation or naturally occurring homogeneously resistant strain with inactivated *mecA* reproduced homogeneously high-level resistance (Chambers, 1997; Ryffel et al., 1994). This demonstrates that the chromosomally encoded determinant does not function in the absence of *mecA* to express homogeneous high-level resistance. Mwangi et al (2013) demonstrated that introduction of plasmid-borne *mecA* into an MSSA background display relatively low resistance, however, is capable of developing homogenously high-level resistance upon exposure to a β-lactam antibiotic. Genome sequencing of such a highly resistant population identified a nonsense mutation in *relA* resulting in induction of the stringent response (Gandara et al., 2018) through constitutive (p)ppGpp production (Mwangi et al., 2013). Moreover, introduction of SCC*mec* into an MSSA strain led to the subsequent development of the mutation in *relA* with concomitant (p)ppGpp accumulation (Kim et al., 2013). Using a similar methodological approach, Pozzi et al (2012) identified that the

homogeneously high-level resistance phenotype was associated with a nonsense mutation in *gdpP*, encoding a recently identified c-di-AMP phosphodiesterase (Corrigan et al., 2011). Also, disruption of *gdpP* was implicated in β-lactam and glycopeptide-mediated high-level resistance and tolerance (Griffiths and O'Neill, 2012).

Conversion of heterogeneous to homogeneous resistance in N315 strain is promoted by the acquisition of mutations in the *rpoB* gene, encoding the RNA polymerase β-subunit (Aiba et al., 2013). The effect of *rpoB* mutation was reversed upon replacing amino acid substitutions to wildtype suggesting the *rpoB* mutations being the major cause for heterogeneous to homogeneous conversion (Aiba et al., 2013). Mutations of *rpoB* are also implicated in the conversion from hVISA to VISA phenotype (Matsuo et al., 2011; Watanabe et al., 2011). In addition, selection of high-level resistance in historic early MRSA isolates identified mutations in 27 genes and 3 intergenic sequences representing a range of functional diversity (Dordel et al., 2014). These mutations were identified in agreement with previous research including, *rpoB* (Aiba et al., 2013), *relA* (Mwangi et al., 2013) and 17 different genes sufficient to confer homogeneous high-level resistance (Dordel et al., 2014). Transcriptional profiling comparing both heterogeneous and subsequent homogeneously resistant population demonstrated that the β-lactam mediated SOS response is associated with development of homogeneous expression of resistance by the selection of chromosomal mutations (Cuirolo et al., 2009). It is important to note that each of the aforementioned mutations associated with elevated resistance, accompanied an increase in the cellular levels of PBP2A. Also, when repressed, reduction of *mecA* transcription prevents the conversion from heterogeneous to homogeneous resistance signifying the requirement for increased *mecA* transcription and concomitant increase in the quantity of PBP2A for conversion (Finan et al., 2002).

In the absence of antibiotics, the chemical structures of peptidoglycan from heterogeneously resistant, USA300 (Müller et al., 2015) and susceptible strains are indistinguishable from highly resistant strains COL (De Jonge et

al., 1992) while in the presence of methicillin poorly cross-linked peptidoglycan was produced (de Jonge and Tomasz, 1993) possibly by functional PBP2A which is required in increased amounts for high-level resistance.

1.8 Current treatments for MRSA infections

One of the major problems in the fight against resistant pathogens is the difficulty in identifying novel suitable antimicrobial agents. The evolutionary perfection of bacterial resistance mechanisms has threatened the effectiveness of every antibiotic ever introduced disregarding the molecular target of the drug or its chemical class (Payne et al., 2007). The introduction of penicillin gave rise to many other new β-lactam related class of antibiotics for the treatment of infections.

1.8.1 New β-lactam antibiotics targeting PBP2A

Development of novel β-lactam antibiotics with high affinity for PBP2A targeting its transpeptidase activity should help for the treatments of MRSA-associated infections. This includes a newer class of cephalosporin β-lactams such as ceftobiprole and ceftaroline; for their broad spectrum activity against both gram-positive and gram-negative bacteria, including MRSA (Barbour et al., 2009; Saravolatz et al., 2011). Compared to other β-lactams, ceftaroline and ceftobiprole have lower MIC values against MRSA due to their significantly high affinity for PBP2A (Davies et al., 2007; Kosowska-Shick et al., 2010). Structural studies of ceftaroline-PBP2A complex have shown that it binds to an allosteric site and activates the binding of a second ceftaroline molecule to the active site of PBP2A resulting in acyl-enzyme complex (Villegas-estrada et al., 2008). It is not clear whether ceftobiprole acts in a similar way. Resistance to ceftaroline has already been reported among MRSA isolates (Otero et al., 2013). Nonsense mutations have been identified in transpeptidase domain as well as the allosteric domain of PBP2A, presumably lowering the affinity of ceftaroline binding (Fishovitz et al., 2014; Otero et al., 2013). These mutations have been characterised to

disrupt the salt bridges required for the allosteric activation of PBP2A activity (Fishovitz et al., 2014).

1.8.2 Vancomycin

The vancomycin group of antibiotics are a class of glycopeptide antibiotics. Vancomycin targets the cell wall biosynthesis specifically, the D-Ala-D-ala terminus of the pentapeptide stem of the peptidoglycan precursors (Barna and Williams, 1984). Vancomycin has become the drug of choice for due to its broad-spectrum activity against MRSA. However, *S. aureus* isolates with decreased susceptibility to vancomycin were reported in Japan (Chambers, 1997) rendering it sufficient for vancomycin treatment failures in some cases. Complete resistance to vancomycin was first discovered in enterococci (Murray, 2000) due to the acquisition of the transposon Tn*1546* encoding the *vanA* operon (Arthur et al., 1993). The first appearance of *S. aureus* isolate with complete vancomycin resistance (MIC ≥16 µg/ml) also carried the *vanA* operon, originally detected in a vancomycin resistant enterococci (VRE) (Chang et al., 2003).

Vancomycin disrupts the late-stages of peptidoglycan biosynthesis by blocking the penultimate D-Ala-D-Ala dipeptide residues through formation of non-covalent hydrogen bonds, therefore inhibiting cell wall synthesis (Barna and Williams, 1984). Mutations in two-component systems, such as *walKR* and *graSR* have also implicated in reduced susceptibility to vancomycin (Meehl et al., 2007). Also, mutations in RNA polymerase subunit β (*rpoB*) and β' (*rpoC*) are also commonly associated with reduced susceptibility to vancomycin, leading to increased cell wall thickness and prolonged doubling time (Matsuo et al., 2011, 2015).

1.8.3 Teicoplanin

Similar to vancomycin, teicoplanin is a glycopeptide antibiotic active against both MSSA and MRSA as well as other gram-positive cocci. Unlike vancomycin, teicoplanin has a longer half-life and can be administered intramuscularly (Chambers, 1997), however it is less effective than vancomycin. Moreover, treatment with teicoplanin has 25% less clinical

success rate compared to vancomycin (Chambers, 1997). Emergence of teicoplanin resistance has been reported during therapy and it is also possible to select teicoplanin resistant mutants *in vitro* (Kaatz et al., 1990). Mutations in *sigB* operon was shown to be preferred mutation site contributing to the development of teicoplanin resistance in the *rsbU* mutant (Bischoff and Berger-Bachi, 2001). Also, mutations in other genetic loci such as *yvqF/vraSR*, *trfAB*, *tcaA* were implicated in reduced susceptibility to teicoplanin (Kato et al., 2010).

1.8.4 Fluoroquinolones

Fluoroquinolones, such as ciprofloxacin, pefloxacin and ofloxacin have shown potent activity against staphylococcal infections. Fluoroquinolones primarily targets topoisomerase IV in staphylococci, unlike DNA gyrase in *E. coli* (Ng et al., 1996). Clinically significant levels of resistance have been documented due to the acquisition of mutation in the *grlA* gene encoding the A subunit of topoisomerase IV (Ferrero et al., 1995). Additionally, mutations in DNA gyrase subunit A are also implicated in fluoroquinolone resistance suggesting it as a secondary target of fluoroquinolone (Ferrero et al., 1995). As a result of the ability of *S. aureus* to develop resistance to monotherapy of fluoroquinolone, combination of rifampicin and fluoroquinolone has been used as the development of resistance is less likely (Kaatz et al., 1989).

1.8.5 Rifampicin

Rifampicin is a highly potent antistaphylococcal agent with an MIC of ≤0.05 µ/ml. Rifampicin inhibits protein synthesis by directly blocking RNA polymerase which disrupts transcription elongation of RNA (Campbell et al., 2001). Mutations in the target of rifampicin, *rpoB* (RNA polymerase subunit β) alone confers high-level resistance if rifampicin is used as monotherapy, therefore is subject to use in combination with another antibiotic active against *S. aureus* to which it also is susceptible (Chambers, 1997). Such rifampicin combination regimens include nafcillin or vancomycin for the treatment of serious infections caused by MRSA (Chambers, 1997).

1.8.6 Mupirocin

Mupirocin, also known as pseudomonic acid A is an antibacterial agent produced by *Pseudomonas fluorescens* which is effective against staphylococci and streptococci (Morton et al., 1995). Mupirocin acts by inhibiting bacterial isoleucyl-tRNA synthetase, thereby disrupting protein synthesis (Hughes and Mellows, 1978). Mupirocin is a topical antibacterial agent with higher success rate in eradicating colonised staphylococci (Morton et al., 1995). Two types of mupirocin resistance have been discovered. First and very common is low to intermediate level resistance caused by mutations in target enzyme with MICs from 8 to 256 µg/ml (Morton et al., 1995). Second, high-level resistance (MIC = >500 µg/ml) is mediated by the acquisition of a non-native plasmid encoding isoleucyl-tRNA synthetase which renders mupirocin ineffective (Morton et al., 1995).

1.8.7 Alternative to antibiotics

Finally, the developments of new antimicrobial agents have been variably successful therefore, *S. aureus* vaccine candidates are also currently being investigated. *S. aureus* capsular polysaccharide protein conjugate was clinically trailed with haemodialysis patients which showed encouraging results, however inconclusive (Shinefield et al., 2002). Other vaccine candidates such as enterotoxins or surface adhesins directed to *S. aureus* virulence were also proposed to be developed (Lowy, 2003).

An active immunisation strategy using a staphylococcal surface protein, IsdB was tested which resulted in a failure during the phase II/III trial (Bagnoli et al., 2012; Kuklin et al., 2006). Even though IsdB is conserved and expressed in different *S. aureus* strains as an important virulence factor, it was reported that as an antigen, IsdB vaccine was unable to generate complete protection in mouse models with lethal infection (Kuklin et al., 2006; Stranger-Jones et al., 2006). In order to improve the efficacy of the vaccine, a combination of four surface proteins including IsdA, IsdB, SdrD and SdrE showed high levels of protective immunity compared to single component against infections with diverse human *S. aureus* isolates (Stranger-Jones et al.,

2006). These four proteins bind to haemoglobin on the staphylococcal surface which is required for iron uptake from heme compounds of hosts (Mazmanian and al., 2003).

1.9 Aims of the study

Several research have been carried out in an attempt to understand the molecular basis of methicillin resistance which revealed a number of essential genes for developing resistance, however how *mecA* interacts with division machinery and confer resistance is not well understood. Therefore, the aim of the study was to investigate the underlying mechanism of high-level methicillin resistance and studying the localisation of PBP2A. This study employed a combination of next generation sequencing techniques at genomic and transcriptional level coupled with protein labelling. This approach allowed to the tracking of the evolutionary progression of resistance from low-level to high-level resistance.

Chapter 2

Materials and methods

2.1 Growth media

All bacterial growth media were prepared in distilled water (dH2O) and sterilised by autoclaving at 121ºC for 20 min, 103 kilopascals, unless otherwise stated.

2.1.1 Brain heart infusion (BHI)

Brain heart infusion (Sigma)	37 g /l

2.1.2 BHI agar

Brain heart infusion agar (Sigma)	52 g/l

2.1.3 Lysogeny broth (LB)

Tryptone (Oxoid)	5 g/l
Yeast extract (Oxoid)	10 g/l
NaCl	5 g/l

2.1.4 LB agar

Tryptone (Oxoid)	5 g/l
Yeast extract (Oxoid)	10 g/l
NaCl	5 g/l

1.5% (w/v) Sigma Bacteriological agar was added to make LB agar.

2.1.5 LK broth

Tryptone (Oxoid)	5 g/l
Yeast extract (Oxoid)	10 g/l
KCl	5 g/l

2.1.6 LK agar

Tryptone (Oxoid)	5 g/l
Yeast extract (Oxoid)	10 g/l
KCl	5 g/l

1.5% (w/v) Sigma Bacteriological agar was added to make LB agar.

2.2 Antibiotics

Antibiotics used in this study are listed in Table 2.1. Stock solutions were filter sterilised using 0.2 μm pore size filter and stored at -20ºC until needed. Antibiotics stock solutions were added to agar plates after media was cooled to 55ºC. Antibiotic stock solutions were thawed and added to liquid media prior to use.

Antibiotic	**Stock concentration (mg/ml)**	***S. aureus* working concentration (μg/ml)**	***E. coli* working concentration (μg/ml)**	**Solvent**
Ampicillin (Amp)	100	-	100	dH_2O
Chloramphenicol (Cm)	10	10	-	95% (v/v) ethanol
Erythromycin (Ery)	5	5	-	95% (v/v) ethanol
Kanamycin (Kan)	50	50	-	dH_2O
Lincomycin (Lin)	25	25	-	95% (v/v) ethanol
Methicillin (Met)	10	5	-	dH_2O
Oxacillin (Ox)	10	5	-	dH_2O
Tetracycline (Tet)	5	5	-	50% (v/v) ethanol

Table 2.1 List of antibiotics used in this study

2.3 Bacterial strains and plasmids

2.3.1 *Staphylococcus aureus* strains

All strains of *Staphylococcus aureus* listed in Table 2.2 were stored at -80ºC in Microbank (Pro-lab Diagnostics) bead vials. Strains were grown on BHI agar plate containing appropriate antibiotic where required to maintain selection of resistance markers. Agar plates were stored at 4ºC for two weeks and for long-term storage single colony was stocked in bead stocks and stored at -80ºC.

Liquid cultures were grown in a sterile universal tube inoculated with a single colony and incubated overnight at 37ºC on a shaker at 250 rpm.

Strain	Characteristic(s)	Reference
SH1000	Functional *rsbU*+ derivative of 8325-4	(Horsburgh et al., 2002)
RN4220	Restriction deficient transformation recipient	(Kreiswirth et al., 1983)
SJF4978	8325-4 p*mecA* HeR; 8325-4 carrying p*mecA* expression heterogeneous resistance to oxacillin; Cm^R	(Pozzi et al., 2012)
SJF4979	8325-4 p*mecA* HoR; 8325-4 carrying p*mecA* expression homogenous resistance to oxacillin; Cm^R	(Pozzi et al., 2012)
SJF4981	SH1000 p*mecA*; SH1000 carrying pRB474 p*mecA* expressing low-level resistance to oxacillin (Untrained); Cm^R	This study
SJF4984	SH1000 p*mecA* -TI1*; SH1000 carrying pRB474 p*mecA* expressing low-level resistance to oxacillin (Trained-Intermediate); Cm^R	This study
SJF4989	SH1000 p*mecA* -TI2*; SH1000 carrying pRB474 p*mecA* expressing low-level resistance to oxacillin (Trained-Intermediate); Cm^R	This study
SJF4992	SH1000 p*mecA* -TI3*; SH1000 carrying pRB474 p*mecA* expressing low-level resistance to oxacillin (Trained-Intermediate); Cm^R	This study
SJF4985	SH1000 p*mecA* -TR1†; SH1000 carrying pRB474 p*mecA* expressing high-level resistance to oxacillin (Trained-Resistant); Cm^R	This study
SJF4990	SH1000 p*mecA* -TR2†; SH1000 carrying pRB474 p*mecA* expressing high-level resistance to oxacillin (Trained-Resistant); Cm^R	This study
SJF4991	SH1000 p*mecA* -TR3†; SH1000 carrying pRB474 p*mecA* expressing high-level resistance to oxacillin (Trained-Resistant); Cm^R	This study
SJF4986	SH1000 p*mecA* -TIR1‡; SH1000 carrying pRB474 p*mecA* expressing high-level resistance to oxacillin (Trained-Intermediate to Resistant); Cm^R	This study
SJF4987	SH1000 p*mecA* -TIR2‡; SH1000 carrying pRB474 p*mecA* expressing high-level resistance to oxacillin (Trained-Intermediate to Resistant); Cm^R	This study
SJF4988	SH1000 p*mecA* - TIR3‡; SH1000 carrying pRB474 p*mecA* expressing high-level resistance to oxacillin (Trained-Intermediate to Resistant); Cm^R	This study
SJF4993	SH1000 pRB474 p*mecA* cured; SJF4991 from which pRB474 p*mecA* removed	This study
SJF4995	SH1000 pRB474 p*mecA*+; SJF4993 with pRB474 p*mecA* reintroduced; Cm^R	This study
SJF5015	ANG1959; SEJ1 Δ*gdpP*::*Kan*^{R}; marked *gdpP* deletion	(Corrigan et al., 2011)
SJF5025	SJF5015; SH1000 Δ*gdpP*::*Kan*^{R}; marked *gdpP* deletion	This study
SJF5026	SJF5025; SH1000 p*mecA* Δ*gdpP*::*Kan*^{R}; marked *gdpP* deletion	This study

SJF4994	RN4220 *lysA*::p*mecA*; Ery^R, Lin^R. Single copy expression of *mecA* under its own promoter from *lysA* locus	This study
SJF4996	SH1000 *lysA*::p*mecA*; Ery^R, Lin^R. Single copy expression of *mecA* under its own promoter from *lysA* locus	This study
SJF4998	SH1000 *lysA*::p*mecA* -TI1* (Trained-Intermediate); Ery^R, Lin^R. Expressing low-level resistance to oxacillin	This study
SJF4999	SH1000 *lysA*::p*mecA* -TI2* (Trained-Intermediate); Ery^R, Lin^R. Expressing low-level resistance to oxacillin	This study
SJF5001	SH1000 *lysA*::p*mecA* -TI4* (Trained-Intermediate); Ery^R, Lin^R. Expressing low-level resistance to oxacillin	This study
SJF5002	SH1000 *lysA*::p*mecA* -TI4* (Trained-Intermediate); Ery^R, Lin^R. Expressing low-level resistance to oxacillin	This study
SJF5000	SH1000 *lysA*::p*mecA* -TR1* (Trained-Resistant); Ery^R, Lin^R. Expressing high-level resistance to oxacillin	This study
SJF5003	SH1000 *lysA*::p*mecA* -TR2* (Trained-Resistant); Ery^R, Lin^R. Expressing high-level resistance to oxacillin	This study
SJF5004	SH1000 *lysA*::p*mecA* -TR3* (Trained-Resistant); Ery^R, Lin^R. Expressing high-level resistance to oxacillin	This study
SJF5005	SH1000 *lysA*::p*mecA* -TR4* (Trained-Resistant); Ery^R, Lin^R. Expressing high-level resistance to oxacillin	This study
SJF5006	SH1000 *lysA*::p*mecA* -TIR1* (Trained-Intermediate to Resistant); Ery^R, Lin^R. Expressing high-level resistance to oxacillin	This study
SJF5007	SH1000 *lysA*::p*mecA* -TIR2* (Trained-Intermediate to Resistant); Ery^R, Lin^R. Expressing high-level resistance to oxacillin	This study
SJF5008	SH1000 *lysA*::p*mecA* -TIR3* (Trained-Intermediate to Resistant); Ery^R, Lin^R. Expressing high-level resistance to oxacillin	This study
SJF5009	RN4220 *lysA::kan*; empty vector at *lysA*	This study
SJF5010	SJF5003; SH1000 *lysA::kan* empty vector at *lysA*	This study
SJF5011	SJF5010; SH1000 *lysA*::p*mecA*+; Ery^R, Lin^R. p*mecA* reintroduced at *lysA* locus replaced with empty vector	This study
SJF4997	SJF4993; SH1000 pRB474-p*mecA*-cured *lysA*::p*mecA*. Ery^R, Lin^R.	This study
SJF5024	SJF5010; SH1000 *lysA*::*kan* pRB474-p*mecA*. Cm^R.	This study
8325-4	Restriction deficient derivative of 8325	(Kreiswirth et al., 1983)
SJF5035	8325-4 *lysA*::p*mecA*; Ery^R, Lin^R. Single copy expression of *mecA* under its own promoter from *lysA* locus	This study
SJF5031	SH1000 *lysA*::p*mecA* -TR5* (Trained-Resistant); Ery^R, Lin^R. Expressing high-level resistance to oxacillin	This study
SJF5032	SH1000 *lysA*::p*mecA* -TR6* (Trained-Resistant); Ery^R, Lin^R. Expressing high-level resistance to oxacillin	This study
SJF5033	SH1000 *lysA*::p*mecA* -TR7* (Trained-Resistant); Ery^R, Lin^R. Expressing high-level resistance to oxacillin	This study
SJF5034	SH1000 *lysA*::p*mecA* -TR8* (Trained-Resistant); Ery^R, Lin^R. Expressing high-level resistance to oxacillin	This study

SJF315	COL; HA-MRSA (type I SCC*mec*).	(Shafer and Iandolo, 1979)
SJF4821	MRSA252; HA-MRSA (type II SCC*mec*)	(Enright et al., 2000)
SJF5041	Mu50; HA-MRSA (VISA clinical isolate)	(Hiramatsu et al., 1997a)
SJF5042	Mu3; HA-MRSA (hVISA clinical isolate)	(Hiramatsu et al., 1997b)
SJF4703	USA300_FPR3757; CA-MRSA (type IV SCC*mec*).	(Fey et al., 2013)
SJF5043	MW2; CA-MRSA (type IV SCC*mec*)	(Baba et al., 2002)
SJF5036	AJ1008 – AR1089, with *kanA* near *rpoBC*, Kan^R. Complementation strain for *rpoB* and *rpoC* allele.	(Villanueva et al., 2016)
SJF5037	MV42 – AR1089, *ermB* near *rpoB*+, Ery^R. Erythromycin cassette inserted near *rpoB* genomic region.	(Villanueva et al., 2016)
SJF5044	SJF5003, *rpoB*+, Kan^R. Complemented to carry WT *rpoB* allele.	This study
SJF5045	SJF5034, *rpoC*+, Kan^R. Complemented to carry WT *rpoC* allele.	This study
SJF5049	SJF315 (COL), *rpoB*+, Kan^R. Complemented to carry WT *rpoB* allele.	This study
SJF5046	SJF5003, SH1000 *lysA*::p*mecA rpoB*-H929Q Kan^R, Ery^R, Lin^R. Oxacillin and kanamycin resistant *rpoB*-H929Q marked mutation.	This study
Newman	Clinical isolate (ATCC25904), *rsbU*$^+$. High-level clumping factor	(Duthie and Lorenz, 1952)
SJF5048	Newman *rpoB*-H929Q, Kan^R.	This study
SJF5050	Newman *lysA*::p*mecA rpoB*-H929Q, Kan^R, Ery^R, Lin^R. Expressing high-level resistance to oxacillin.	This study
SJF5021	RN4220 *lysA*::eYFP-PBP2A, Ery^R, Lin^R. eYFP-PBP2A fusion at *lysA* locus.	This study
SJF5022	SH1000 *lysA*::eYFP-PBP2A, Ery^R, Lin^R. eYFP-PBP2A fusion at *lysA* locus.	This study
SJF5023	SJF4993, SH1000 pRB474-p*mecA*-cured *lysA*::eYFP-PBP2A, Ery^R, Lin^R. eYFP-PBP2A fusion at *lysA* locus of multicopy *mecA* cured background.	This study
SJF5066	SJF5010, *mecA*-cured-*rpoB* (H929Q) *lysA*::eYFP-PBP2A, Ery^R, Lin^R. eYFP-PBP2A fusion at *lysA* locus of single copy *mecA*-cured-*rpoB* (H929Q) background.	This study
SJF5018	RN4220 *lysA*::PBP2A-SNAP Ery^R, Lin^R. PBP2A-SNAP fusion at *lysA* locus.	This study
SJF5020	SH1000 *lysA*::PBP2A-SNAP Ery^R, Lin^R. PBP2A-SNAP fusion at *lysA* locus.	This study
SJF5027	SJF4993, pRB474-p*mecA*-cured lysA::PBP2A-SNAP, Ery^R, Lin^R. PBP2A-SNAP fusion at *lysA* locus of multi copy *mecA* cured background.	This study
SJF5028	SJF5010, *mecA*-cured-*rpoB* (H929Q) *lysA*::PBP2A-SNAP, Ery^R, Lin^R. PBP2A-SNAP fusion at *lysA* locus of single copy *mecA* cured background.	This study

SJF5030	SJF5025, Δ*gdpP*::KanR lysA::PBP2A-SNAP, Ery^R, Lin^R. PBP2A-SNAP fusion at *lysA* locus of *gdpP* mutant.	This study
SJF5051	JMB4556; SH1000 *srrAB*::*tet*. Tetracycline marked *srrAB* deletion strain.	(Mashruwala and Boyd, 2017)
SJF5054	SH1000 *srrAB*::*tet*. Tetracycline marked *srrAB* deletion strain.	This study

Table 2.2 *S. aureus* strains used in this study

Cm^R, chloramphenicol resistant; Ery^R, erythromycin resistant; Kan^R, kanamycin resistant; Lin^R, lincomycin resistant; Tet ^{R}, tetracycline resistant.

2.3.2 *Escherichia coli* strains

E. coli strains listed in Table 2.3 were grown and stored similar to *S. aureus* strains using LB broth and agar instead of BHI growth media.

Strain	Characteristic(s)	Reference
DH5α	*E. coli, fhuA2Δ(argF-lacZ)U169 phoA glnV44 Φ80Δ (lacZ)M15 gyrA96 recA1 relA1 endA1 thi-1 hsdR17*	New England Biolabs
SJF4983	DH5α *E. coli* pVP01-p*mecA*; Amp^R.	This study
SJF5065	DH5α *E. coli* pVP02-*orfX*; Amp^R.	This study
SJF5017	DH5α *E. coli* pMK-RQ_eYFP-PBP2A, Kan^R.	This study
SJF5019	DH5α *E. coli* pVP03_eYFP-PBP2A, Amp^R.	This study
SJF5012	DH5α *E. coli* pVP04_PBP2A-SNAP, Amp^R.	This study
SJF5013	DH5α *E. coli* pMA-T_CLIP-tag, Amp^R.	This study
SJF5014	DH5α *E. coli* pVP05_PBP2A-CLIP, Amp^R.	This study
SJF5029	DH5α *E. coli* pVP06_PBP2A-CLIP, Amp^R.	This study

Table 2.3 *E. coli* strains used in this study

Amp^R, ampicillin resistant marker; Kan^R, kanamycin resistant marker.

2.3.3 Plasmids

Plasmids listed in Table 2.4 were purified using GeneJET Plasmid Miniprep kit (Thermo Fischer Scientific). See section 2.9.2 for details.

Plasmid	Characteristic(s)	Reference
pRB474	Low copy *E. coli-Staphylococcus* shuttle vector. Amp^R (*E. coli*), Cm^R (*S. aureus*)	(Brückner, 1997)
p*mecA*	2,867 bp EcoRI fragment containing *mecA* from pSA*mecA*5 subcloned into the EcoRI site of pRB474	(Pozzi et al., 2012; Rudkin et al., 2012)

pMUTIN4	Derivative of pMUTIN which contains promoterless transcriptional *lacZ* fusion, non-replicating in gram positive bacteria; Amp^R (*E. coli*), Ery^R, Lin^R (*S. aureus*)	(Vagner et al., 1998)
pGM068	pMUTIN4 derived insertion vector including *lysA* 3' fragment	(McVicker et al., 2014)
pVP01-p*mecA*	pGM068, insertion vector carrying *mecA* under its native promoter; Amp^R (*E. coli*), Ery^R, Lin^R (*S. aureus*)	This study
pVP02-*orfX*	pGM068 including 3' *orfX* fragment, insertion vector carrying *mecA* under its native promoter; Amp^R (*E. coli*), Ery^R, Lin^R (*S. aureus*)	This study
pMK-RQ_eYFP-PBP2A	High copy *E. coli* shuttle vector for eYFP-PBP2A fragment supplied by Invitrogen, Kan^R.	This study
pVP03_eYFP-PBP2A	pGM068, insertion vector carrying eYFP upstream of *mecA* under its native promoter; Amp^R (*E. coli*), Ery^R, Lin^R (*S. aureus*)	This study
pVP04_PBP2A-SNAP	pGM068, insertion vector carrying *mecA* under its native promoter and C-terminal SNAP-tag; Amp^R (*E. coli*), Ery^R, Lin^R (*S. aureus*)	This study
pMA-T_CLIP-tag	High copy *E. coli* shuttle vector for CLIP-tag fragment supplied by Invitrogen, Amp^R.	This study
pVP05_PBP2A-CLIP	pGM068, insertion vector carrying *mecA* under its native promoter and C-terminal CLIP-tag; Amp^R (*E. coli*), Ery^R, Lin^R (*S. aureus*)	This study
pVP06_PBP2A-CLIP	pGM068, insertion vector carrying *mecA* under its native promoter and C-terminal CLIP-tag; Amp^R (*E. coli*), Tet^R (*S. aureus*)	This study
pCQ11-FtsZ-SNAP	*E. coli-S. aureus* shuttle vector containing *ftsZ-snap* and *lacI* gene under Pspac; Amp^R (*E. coli*), Ery^R, Lin^R (*S. aureus*)	Fabien Grein

Table 2.4 Plasmids used in this study

Amp^R, ampicillin resistant; Cm^R, chloramphenicol resistant; Ery^R, erythromycin resistant; Lin^R, lincomycin resistant.

2.4 Buffers and solutions

All buffers and solutions were prepared using dH_2O and stored at room temperature. Solutions were sterilised by autoclaving when required.

2.4.1 Phage buffer

$MgSO_4$	1 mM
$CaCl_2$	4 mM
Tris-HCl pH 7.8	50 mM
NaCl	0.6% (w/v)
Gelatin	0.1% (w/v)

2.4.2 Phosphate buffered saline (PBS)

NaCl	8 g/l
Na_2HPO_4	1.4 g/l
KCl	0.2 g/l
KH_2PO_4	0.2 g/l

The pH was adjusted to 7.4 with NaOH.

2.4.3 TAE (50X)

Tris base	242 g/l
Glacial acetic acid	5.7% (v/v)
Na_2EDTA pH 8.0	0.05 M

1x TAE working solution was made by diluting 50x stock solution with dH_2O.

2.4.4 TBSI

Tris-HCl pH 7.5	50 mM
NaCl	0.1 M

EDTA-free protease cocktail inhibitor (Roche) was dissolved in buffer prior to use.

2.4.5 Fixative preparation

2.4.5.1 Preparation of 16% (w/v) paraformaldehyde

2.4.5.1.1 100 mM sodium phosphate buffer (pH 7.0)

1 M $NaH2PO_4$	42.3 ml
1 M $Na2HPO_4$	57.7 ml

The final volume was adjusted to 1:1.

2.4.5.1.2 16% (w/v) paraformaldehyde

Paraformaldehyde	8 g
100 mM sodium phosphate buffer (pH 7.0)	50 ml

In 40 ml 100 mM sodium phosphate buffer (pH 7.0), 8 g of paraformaldehyde was added and the solution was heated to 60°C with vigorous mixing. While heating and mixing the solution, ≥5 M NaOH solution was added dropwise until the solution cleared. The solution was stored at 4°C for up to 3 months.

2.4.5.2 Fixative

PBS	2 ml
16% (w/v) paraformaldehyde	0.5 ml

2.4.6 SDS-PAGE solutions

2.4.6.1 SDS-PAGE reservoir buffer (10X)

Tris	30.3 g/l
Glycine	144 g/l
SDS	10 g/l

1x SDS-PAGE working solution was made using dH_2O.

2.4.6.2 SDS-PAGE loading buffer (5x)

Glycerol	50% (v/v)
Tris-HCl pH 6.8	250 mM
SDS	10% (w/v)
DTT	0.5 M
Bromophenol blue	0.5% (w/v)

2.4.6.3 Coomassie Blue stain

Coomassie Blue	0.1% (w/v)
Glacial acetic acid	10% (v/v)
Methanol	5% (v/v)

2.4.6.4 Coomassie destain

Glacial acetic acid	10% (v/v)
Methanol	5% (v/v)

2.4.7 Western blotting solutions

2.4.7.1 Blotting buffer

Glycine	11.26 g/l
Tris	2.4 g/l
Ethanol	20% (v/v)

Blotting buffer was stored in 4ºC room.

2.4.7.2 TBST (20x)

Tris	48.4 g/l

Tween-20	2% (v/v)
NaCl	20 g/l

The pH was adjusted to 7.6. 1x TBST working buffer was made using 1:20 dilution with dH_2O.

2.4.7.3 Blocking buffer

5% (w/v) dried semi-skimmed milk powder was added to 1x TBST buffer prior to use.

2.5 Chemicals and enzymes

All chemicals and enzymes were of analytical grade quality and were purchased from Fischer Scientific, MP Biomedicals or Roche unless otherwise stated. All restriction enzymes, ligases, DNA polymerases, Gibson master mix and appropriate buffers were purchased from Fermentas, New England Biolabs or Bioline. Concentrations of stock solutions and storage conditions are shown in Table 2.5.

Stock solution	Concentration	Solvent	Storage
Ammonium persulfate (APS)	10% (w/v)	dH_2O	-20ºC
Lysostaphin (Sigma)	5 mg/ml	20 mM Sodium acetate pH 5.2	-20ºC
Pronase (Sigma)	10 mg/ml	TES pH 8.0	-20ºC

Table 2.5 List of chemical stock solutions used in this study

2.6 Centrifugation

The following list of centrifuges were used to harvest samples:

- Eppendorf microcentrifuge 5424, capacity to 24 x 1.5-2 ml microfuges, maximum speed of 21,130 x g (14,800 rpm).
- Sigma centrifuge 4K15C, capacity up to 16 x 50 ml falcon tubes, and maximum speed of 5,525 rcf (5,100 rpm).
- Avanti High Speed J25I centrifuge, Beckman Coulter:
- JA-10.5, capacity up to 6 x 400 ml; maximum speed of 18, 500 rcf (10,000 rpm)
- JA-25.50, capacity up to 6 x 50 ml, maximum speed of 75,000 rcf (25,000 rpm)

Centrifugation was carried out at room temperature unless otherwise stated.

2.7 Determination of bacterial cell density

2.7.1 Optical density measurements

Spectrophotometric measurements were taken at 600 nm (OD_{600}) to determine the bacterial yield of a culture using a Biochrom WPA Biowave DNA spectrophotometer. 1:10 dilution was made using sterile culture media whenever necessary.

2.8 Determination of antibiotic minimum inhibitory concentration (MIC)

2.8.1 Determination of MIC by Etest

An overnight culture was diluted to an OD_{600} of ~2 using fresh culture media. The diluted bacterial culture was inoculated on BHI agar plated using cotton swab. An antibiotic Etest strip was then placed onto the pre-inoculated BHI agar plate using tweezers. Etest strips were stored at 4ºC fridge. Plates were incubated overnight at 37ºC developing zone of inhibition around the strip following incubation. The antibiotic Etests used in this study were oxacillin (Oxoid), Penicillin G (Oxoid), Cefoxitin (Liofilchem) and Rifampicin (Liofilchem). For anaerobic MICs, plates were supplied with 2 mM $NaNO_3$ and incubated in anaerobic jar at 37ºC until visible growth was observed.

2.8.2 Determination of MIC by Microdilution method

An overnight culture was diluted to an OD_{600} of ~2 using fresh culture media. The desired test antibiotic was diluted to 2X the top concentration desired. 100 µl of BHI broth was dispensed into all wells of the 96 well microtitre plate. Subsequently, 100 µl of test antibiotic solution was pipetted into the wells of column 1. The antibiotics was mixed thoroughly by pipetting up and down without introducing bubbles. 100 µl of antibiotic-media mixture was withdrew from column 1 and added to column 2 followed by thorough mixing with pipette. Similarly, the mixture was transferred to column 3 and the procedure was repeated to column 10. Pipette tips were changed with every

transfer to prevent cross-contamination. Next, 100 µl of mixture was discarded from column 10. Then, 5 µl of bacteria was inoculated into wells in columns 1 to 11. Column 12 was not inoculated as it was sterility control and blank for reading plates. The plates were incubated at 37ºC for 12-18 hours. For anaerobic MICs, BHI broth was supplied with 2 mM $NaNO_3$ and incubated in anaerobic jar at 37ºC until visible growth was observed in column 11 (positive control). The readings were measured with a Perkin VICTOR x3 2030 plate reader.

2.9 DNA purification techniques

2.9.1 Genomic DNA extraction

Extraction and purification of *S. aureus* genomic DNA was carried out using a Qiagen DNeasy Blood and Tissue kit. 1 ml of an overnight culture was spun at 14,000 rpm for 5 min. The cell pellet was resuspended in 190 µl of dH_2O and 10 µl of Lysostaphin (5 mg/ml) was added, followed by 1-hour incubation at 37ºC. Genomic DNA was isolated in accordance with the manufacturer's instructions.

2.9.2 Plasmid purification

Plasmid purification from *E. coli* was carried out using a GeneJET Plasmid Miniprep kit. Manufacturer's instructions were followed.

2.9.3 Gel extraction of DNA

DNA was separated using TAE agarose gel (1% w/v) stained with ethidium bromide (0.5 µg/ml). UV transilluminator was used to visualise DNA bands. The required band was excised from the gel using a clean scalpel. GeneJET Gel Extraction kit was used to purify DNA from agarose gel slice. Manufacturer's instructions were followed.

2.9.4 Purification of PCR products

To purify DNA fragments from PCR reactions, GeneJET PCR Purification kit was used in accordance with manufacture guidelines.

2.9.5 Ethanol precipitation

Following purification of DNA, 0.1 volume of 3 M sodium acetate pH 6.2 and 2.5x volume of 95% (v/v) ethanol were added to the sample. The purified DNA sample was spun at 14,000 rpm for 30 min at room temperature. The supernatant was discarded and the pellet was washed in 1 ml 70% (v/v) ethanol and centrifuged at 14,000 rpm for 15 min. the supernatant was discarded and the pellet was dried under laminar flow to remove ethanol. The pellet was then resuspended in an appropriate volume of sterile dH_2O (sdH_2O).

2.10 *In vitro* DNA manipulation techniques

2.10.1 Primer design

For PCR amplification, primers were synthesised by Eurofins MWG Operon, usually 20-35 nucleotides. Primers were designed based on the DNA sequences of *S. aureus* 8325 or plasmids or fluorescent proteins. For Gibson assembly, primers were designed to be ~50 nucleotides long. For cloning, a suitable restriction sites were introduced at the 5' end of primers followed by additional bases for efficient restriction digestions at these sites. Primers were resuspended in sdH_2O. For stock and working solutions, primers were diluted to 100 and 10 µM and stored at -20ºC, respectively. Primers used in this study are listed in Table 2.6.

2.10.2 PCR amplification

2.10.2.1 Phusion polymerase

Phusion High Fidelity Master Mix (Thermo Scientific) was used for PCR amplification where 3'-5' proofreading activity is required. A final reaction volume contained:

Phusion High Fidelity Master Mix (2x)	25 µl
Forward primer (10 µM)	2.5 µl
Reverse primer (10 µM)	2.5 µL
Template DNA	50-100 ng
sdH_2O	up to 50 µl

PCR amplification was carried out in Veriti Thermal Cycler (Applied Biosystems). Pre-heated lid (105ºC) was used under the following reaction conditions:

1x	Initial denaturation	98ºC	30 s
30x	Denaturation	98ºC	10 s
	Annealing	55-62ºC	10 s
	Extension	72ºC	15-30 s/kb
1x	Final extension	72ºC	3-5 min

2.10.2.2 Taq polymerase

PCR amplification was performed using DreamTaq Green Master Mix (Thermo Scientific). This was used when accurate amplification was not needed. Reaction volume was prepared as follows:

DreamTaq Green Master Mix (2x)	25 µl
Forward primer (10 µM)	2.5 µl
Reverse primer (10 µM)	2.5 µL
Template DNA	50-100 ng
sdH_2O	up to 50 µl

PCR amplification was carried out in Veriti Thermal Cycler (Applied Biosystems). Pre-heated lid (105ºC) was used under the following reaction conditions:

1x	Initial denaturation	95ºC	1 min
30x	Denaturation	95ºC	30 s
	Annealing	50-60ºC	30 s
	Extension	72ºC	1 min/kb
1x	Final extension	72ºC	5-7 min

2.10.2.3 High-Fidelity DNA polymerase

For difficult and long amplification, Q5 High-Fidelity DNA Polymerase 2x Master Mix (NEB) was used for PCR reactions. Reaction volume was prepared as follows:

Q5 High-Fidelity Master Mix (2x)	25 µl
Forward primer (10 µM)	2.5 µl
Reverse primer (10 µM)	2.5 µL
Template DNA	50-100 ng

sdH_2O up to 50 µl

PCR amplification was carried out in Veriti Thermal Cycler (Applied Biosystems). Pre-heated lid (105ºC) was used under the following reaction conditions:

1x	Initial denaturation	98ºC	30 s
30x	Denaturation	98ºC	5-10 s
	Annealing	50-72ºC	10-30 s
	Extension	72ºC	20-30 s/kb
1x	Final extension	72ºC	2 min

PCR products were analysed by agarose gel electrophoresis (section 2.10.6).

Primer	Sequence (5'-3')	Application	Source
p*mecA*_F1	TGACGATTCCAATGACGAAC	Amplification of *mecA*. Forward primer	This study
p*mecA*_R1	TCATCTATATCGTATTTTTTATTACCGTTC	Amplification of *mecA*. Reverse primer	This study
p*mecA*2_seqF1	CATCAGTCAAACGTGGAGACTATC	Amplifies *mecA* and its own promoter. Sequencing forward primer	This study
p*mecA*2_seqR1	GTTATTTAACCCAATCATTGCTG	Amplifies *mecA* and its own promoter. Sequencing reverse primer	This study
p*mecA*2_seqF2	GAAAGACCAAAGCATACATATTG	Amplifies *mecA* and its own promoter. Sequencing forward primer	This study
p*mecA*2_seqR2	GCGGTCGCGTTCGGTTGCAC	Amplifies *mecA* and its own promoter. Sequencing reverse primer	This study
*mecA*_F	AGTTGTAGTTGTCGGGTTTGG	Amplifies *mecA*. Forward primer	(Pozzi et al., 2012)
*mecA*_R	GCATTGTAGCTAGCCATTCCTT	Amplifies *mecA*. Reverse primer	(Pozzi et al., 2012)
KanR_FW_For	GTTCCAAAGGTCCTGCACTTTG	Amplifies kanamycin cassette. Forward primer	This study
KanR_FW_Rev	CTTACTTTGCCATCTTTCACAAAGATG	Amplifies kanamycin cassette. Reverse primer	This study

pMUTIN4_OL_FP1	GGGGAATTTTTATGCATTATAGATGACTGTAGAAAACATGGTAGGATCCTGACGATTCCAATGACG	Amplification of *mecA* along with its own promoter. Gibson forward primer.	This study
pMUTIN4_OL_RP1	AGCGGCTTACCATCCAGCGCCACCATCCAGTGCAGGAGCTCAGGAGCTCTTATTCATCTATATCGTATTTTTTATTACCG	Amplification of *mecA* along with its own promoter. Gibson reverse primer.	This study
lysA_5'_For	ATGGCGAATTAACAATGGATG	Amplification of *lysA*. Forward primer.	This study
VP62_SeqF3	CTATTGGTTATCGGTACAATACTGAC	Amplifies upstream of *gdpP.* Forward primer.	This study
VP63_SeqR3	GTTGCTTCTACAGCATAATTCTTTTTC	Amplifies downstream of *gdpP.* Reverse primer.	This study
VP58_SeqF1	ATGAATCGGCAGTCCACTAAG	*gdpP* sequencing primer. Forward primer.	This study
VP59_SeqR1	TCATGCATCTTCACTCCTACTTAATTG	*gdpP* sequencing primer. Reverse primer.	This study
VP60_SeqF2	GTCATTAGTCGATGGGCAACTG	*gdpP* sequencing primer. Forward primer.	This study
VP61_SeqR2	CACCACGTCTATGATGATCGATAAC	*gdpP* sequencing primer. Reverse primer.	This study
RNAP_F1	GAATCTGTTTGGCAGGTCAAGTTG	*rpoBC* sequencing forward primer.	This study
RNAP_F2	GATTAATACGCAATTTACAAAAC	*rpoBC* sequencing forward primer.	This study
RNAP_F3	GTTGAAGAAGGTACAGTGCTTG	*rpoBC* sequencing forward primer.	This study
RNAP_F4	CTTGTGAAAGATGACGTGTATAC	*rpoBC* sequencing forward primer.	This study
RNAP_F5	CTATTTAAACCATTCGTAATGAAAG	*rpoBC* sequencing forward primer.	This study
RNAP_F6	CAGCATTTACTTGTAACGCACGAC	*rpoBC* sequencing forward primer.	This study
RNAP_R1	TCCTCCAAAGTTCTGCTTGCATC	*rpoBC* sequencing reverse primer.	This study
RNAP_R2	GAAATTATTTACATCAATCAAGGA	*rpoBC* sequencing reverse primer.	This study
RNAP_R3	CTTTCACGTACAACTCTTTCCATTC	*rpoBC* sequencing reverse primer.	This study
RNAP_R4	CTTCACGATTGAATACTTTTAC	*rpoBC* sequencing reverse primer.	This study
RNAP_R5	CATCAACATTCTTGCTTCAGCTTG	*rpoBC* sequencing reverse primer.	This study
RNAP_R6	CATTAGCACCTTTAACAACAATTTC	*rpoBC* sequencing reverse primer.	This study

Kpn_rpoC_nearby5	ATGCGGTACCCTTGTAACGCACGACATGGTG	*rpoBC* marker insertion nearby. Forward primer.	(Villanueva et al., 2016)
Pst1_rpoC_nearby	GCATCTGCAGGCATCACGACCACTGCGTTGTTC	*rpoBC* marker insertion nearby. Reverse primer.	(Villanueva et al., 2016)
orfx_GF2	GTGGCATAATGTGTGGAATTGTGAGCGCTCACAATTAAGCTTAATATATTGAAAATAATAC	Gibson forward primer for *orfX* amplification	This study
orfx_GR2	GTTATTAAAAGTTCGTCATTGGAATCGTCAGGATCCTGCTCTGTACACTTGTTCAATTAAC	Gibson reverse primer for *orfX* amplification	This study
5orfx	AATATATTGAAAATAATACTAC	*OrfX* sequencing forward primer	This study
3orfx	TGCTCTGTACACTTGTTCAATTAAC	*orfX* sequencing reverse primer	This study
3*mecA*_F1	GTTCAGGTGGTGGTTCATTACACATATCGTGAGCAATGAACTGATTATAC	eYFP-PBP2A amplification from pMK-RQ; forward primer.	This study
3*mecA*_R1	AGCGCCACCATCCAGTGCAGGAGCTCTTATTCATCTATATCGTATTTTTTATTACCGTTCTCATATAGCTC	eYFP-PBP2A amplification from pMK-RQ; reverse primer.	This study
VP49_F	GATGACTGTAGAAAACATGGATCCTGACGATTCCAATGACGAACTTTTAATAAC	p*mecA* insert amplification; forward primer.	This study
VP50_R	GTCCATTGAACCACCACCTGAACCTTCATCTATATCGTATTTTTTATTACCG	p*mecA* insert amplification; reverse primer.	This study
VP51_F	GAAGGTTCAGGTGGTGGTTCAATGGACAAAGATTGCGAAATGAAACG	PBP2A-SNAP insert amplification; forward primer.	This study
VP52_R	GCGCCACCATCCAGTGCAGGAGCTCTCATCCCAGACCCGGTTTACCCAG	PBP2A-SNAP insert amplification; reverse primer.	This study
VP53_R	GAACCACCACCTGAACCTTCATCTATATCGTATTTTTTATTACCGTTCTC	PBP2A-CLIP insert amplification; reverse primer	This study
VP54_F	CGATATAGATGAAGGTTCAGGTGGTGGTTCAATGGACAAAG	CLIP-tag amplification; forward primer.	This study
VP55_R	CCAGCGCCACCATCCAGTGCAGGAGCTCTTAACCTAAACCTGGCTTTCCCAATC	CLIP-tag amplification; reverse primer.	This study
3*mecA*_F	AAGGGTTCAGGTGGTGGTTCATTACACATATCGTGAGCAATGAAC	eYFP-PBP2A amplification; forward primer	This study
3*mecA*_R	AGCGCCACCATCCAGTGCAGGAGCTCTTATTCATCTATATCGTATTTTTTATTACCGTTC	eYFP-PBP2A amplification; reverse primer.	This study

VP56_F	GGTTCAGGTGGTGGTTCAATGG	Amplifies CLIP-tag. Forward primer.	This study
VP57_R	TTAACCTAAACCTGGCTTTCCCAATC	Amplifies CLIP-tag. Reverse primer.	This study
srrAB_5'_up	CTTCTACACCATCATCTTTACCTAC	Amplifies upstream of *srrAB*. Forward primer.	This study
srrAB_3'_down	GTCAGAAGAATGTTCGAACATTTTGGTC	Amplifies downstream of *srrAB*. Reverse primer.	This study

Table 2.6 Primers used in this study

2.10.2.4 Colony PCR screening of *E. coli*

The PCR reaction mixture was prepared as described above, without the addition of template DNA. Using a sterile pipette tip, a single colony from an agar plate was introduced into the PCR reaction mixture. The PCR reaction was performed according to the protocol described above.

2.10.3 Restriction endonuclease digestion

Restriction digestion of DNA was performed using restriction enzymes (NEB) according to the manufacturer's instructions, using the buffers provided. The reaction mixture was incubated at 37ºC for between 2 to 16 h. Digested DNA was separated using agarose gel electrophoresis and purified for downstream experiments.

2.10.4 DNA ligation

Plasmid DNA and insert were prepared for ligation reaction by restriction digestion or PCR amplification and purified as described above. The ligation reaction was prepared in a total of 10 µl volume as follows:

Linearised plasmid DNA	50 ng
Insert DNA	3-fold excess of plasmid DNA
T4 DNA ligase	0.5 µl (200 U)
T4 DNA ligase buffer (10x)	1 µl
sdH_2O	up to 10 µl

The reaction mixture was incubated overnight at 16ºC. The ligated products were transformed to competent *E. coli* cells.

2.10.5 Gibson assembly

Plasmid DNA was prepared by restriction endonuclease digestion (section 2.10.3). Inserts were prepared by PCR amplification using Gibson assembly primers (section 2.10.2). Purified DNA fragments were added to reaction mixture. The assembly was performed in a final volume of 10 µl:

Plasmid DNA	50 ng
Insert	3-fold excess of plasmid DNA
Gibson assembly Master Mix (2x)	5 µl
sdH_2O	up to 10 µl

The reaction was performed at 50ºC for 1 h. Ligated DNA fragments were diluted to 1:3 using sdH_2O. Assembled plasmid was used to transform competent *E. coli* cells.

2.10.6 Agarose gel electrophoresis

1% (w/v) agarose gel was used to separate DNA fragments stained with 0.5 µg/ml ethidium bromide, in 1x TAE buffer. DNA samples were mixed with 6x DNA loading dye (Thermo Scientific) before loading into the wells of the gel. To resolve DNA probes, 120 V for 30 min was applied at room temperature. DNA bands were visualised using an UV transilluminator and photograph was taken using UVi Tec Digital camera and UVi Doc Gel documentation system. The size of DNA bands was compared with the fragments of DNA ladder (Table 2.7).

2.10.7 DNA sequencing

Purified PCR products were sequenced by GATC Biotech. Sequencing results were analysed using SnapGene software.

2.10.8 Determining DNA concentration

DNA concentration in a sample was measured using NanoDrop 3300 spectrophotometer and operating software v.2.9.1. The blank measurement

was taken for 1 µl buffer used for DNA elution. 1 µl of the sample was loaded onto the lever to measure DNA concentration at 260 nm.

Marker	DNA fragment size (kb)
GeneRuler 1 kb DNA ladder (Thermo Scientific)	10.0
	8.0
	6.0
	5.0
	4.0
	3.5
	3.0
	2.5
	2.0
	1.5
	1.0
	0.75
	0.50
	0.25

Table 2.7 DNA fragments used as size markers for agarose gel electrophoresis

2.11 RNA purification techniques

2.11.1 Total RNA extraction

Extraction and purification of *S. aureus* total RNA was carried out using a Qiagen RNeasy Plus Mini kit. Using fresh bacterial culture with the OD_{600} ~0.05, culture was grown in fresh media until it reaches OD_{600} ~0.5. 8 ml of Qiagen RNAprotect Bacteria Reagent was added to 8 ml of culture in a 50 ml tube and incubated for 5 mins at room temperature. Cells were recovered by centrifugation at 4000 rpm for 10 min at 4°C. Pellets can be stored at -70°C for future. 200 µl of TE buffer (30 mM Tris-HCl, 1 mM EDTA, pH 8.0) and 200 µl proteinase K solution was added to the RNAprotect Bacteria Reagent treated pellet and vortexed. Tubes were incubated for 1 hour at 37°C in a waterbath. The cell suspension was mixed by vortexing every 10 min for at least 10 s. Following centrifugation as above, pellet was resuspended in 700 µl of RLT buffer containing β-mercaptoethanol. Cells were then disrupted using MP Biomedicals FastPrep 24 Homogeniser (3x, speed 6.5, 30 s). Cells

were incubated on ice for 5 min between each cycle. The samples were centrifuged for 30 s at 13,000 rpm to separate lysing matrix. Supernatant was harvested in a gDNA eliminator column and spun for 30 s at 10,000 rpm. An equal volume of 100% ethanol was added to flow-through and the spin column was discarded. 700 µl of mixture was transferred to RNeasy Mini Spin Column and centrifuged for 30 s at 10,000 rpm. Flow-through was discarded. This step was repeated until all mixture was passed through the column. 700 µl of RW1 buffer was added to the column and spun for 30 s at 13,000 rpm. Flow-through was discarded. 500 µl of RPE buffer was added to the column and spun as before. This step was repeated two more times. Column was placed in a new collection tube and centrifuged for 90 s at 13,000 rpm to remove any remaining buffer. To elute RNA from the membrane, spin column was placed in a clean microfuge tube and 40 µl of nuclease-free water was added onto the membrane and the tube was incubated at room temperature for 1 min before spinning at 13,000 rpm for 1 min. To improve the yield, flow-through was transferred to the membrane and spun as before. RNA concentration was measured using NanoDrop. RNA samples were stored at -4°C for a month or -70°C for longer period.

2.12 Protein analysis

2.12.1 Preparation of whole cell lysate

S. aureus cells were grown to an OD_{600} ~1 in 100 ml BHI. Cells were collected by centrifugation for 10 min at 5,000 rcf in a pre-chilled centrifuge. The cell pellet was resuspended in PBS and spun as before. This step was performed two more times. The pellet was resuspended on 500 µl PBS and added to pre-chilled lysing matrix tubes containing 0.1 mm acid-washed glass beads (Sigma). Cells were broken using an MP Biomedicals FastPrep 24 Homogeniser (12x, speed 6.5, 30 s). Samples were incubated on ice between each cycle. FastPrep beads were separated by a brief spin for 30 s at 13,000 rpm. The supernatant was stored at -20°C until needed.

2.12.2 Preparation of membrane fraction

S. aureus cultures were grown to an OD_{600} ~1 in 1 l BHI. Cells were collected by centrifugation at 5,000 rcf for 10 min at 4°C. Cells were resuspended using PBS and centrifuged at 5,000 rpm for 10 min at 4°C. This step was repeated 2 more times. TBSI resuspended pellet was then added to chilled lysing matrix tubes containing 0.1 mm acid washed glass beads (Sigma) and disrupted using an MP Biomedicals FastPrep 24 Homogeniser (12x, speed 6.5, 30 s). Samples were incubated on ice for 5 min between each cycle. The supernatant was recovered by centrifugation for 10 min at 3,500 rpm at 4°C. To remove any remaining glass beads or unbroken cells, supernatant was transferred to 15 ml Falcon tube and spun at 5,000 rcf for 10 min at 4°C. The supernatant was then centrifuged twice for 10 min at 15,000 rcf at 4°C to sediment cell wall material. The supernatant was transferred to new centrifuge tube and membrane fractions were sedimented by centrifugation at 70,000 rcf for 60 min at 4°C. The pellet was resuspended in PBS and stored at -20°C.

2.12.3 Bradford protein assay

In order to determine concentration of unknown protein, first different known concentration (0, 1.6, 4, 8 and 12 µg) of bovine serum albumin (BSA) were prepared using 800 µl of PBS and standard curve was plotted (Figure 2.1). BSA and PBS solution was transferred into a spectrophotometer cuvette (Fisherbrand). 200 µl of BioRad Protein Assay Dye was added to each sample and mixed by pipetting. The absorbance at 595 nm was measured after 5 min incubation at room temperature. The sample containing 0 µg of BSA was used as a blank to calibrate spectrophotometer to zero. Protein concentration was calculated based on the dilution factor used and the standard curve.

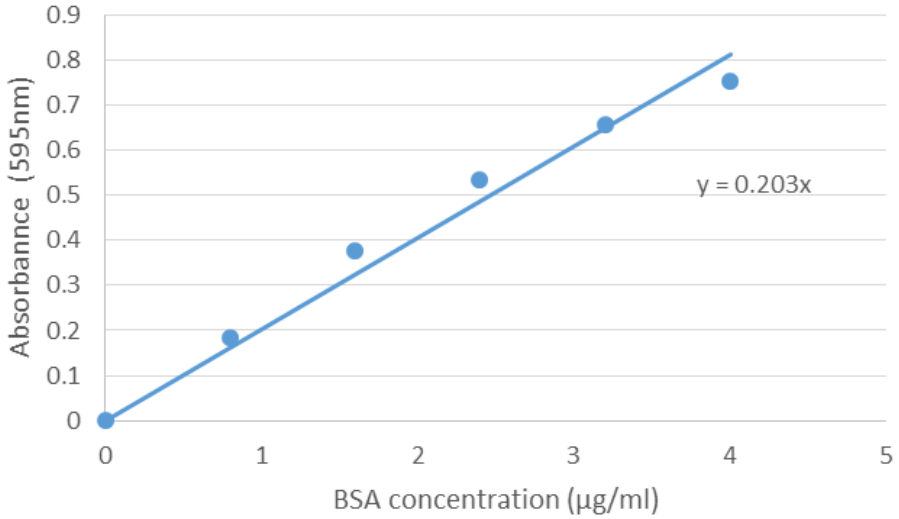

Figure 2.1 Standard curve for Bradford Protein Assay

The linear regression method was used for estimation of the concentration of protein samples. The trend line equation is also shown.

2.12.4 SDS-PAGE

Laemmli SDS-PAGE was used to analyse membrane fractions and cell lysates. Composition of resolving gel is as follows:

SDS-PAGE 10% (w/v) resolving gel

dH_20	4 ml
1.5 M Tris-HCl pH 8.8	2.5 ml
10% (w/v) SDS	100 µl
30% (w/v) acrylamide/bis (37.5:1)	3.5 ml
10% (w/v) APS	100 µl
TEMED	20 µl

N,N,N'N'-tetramethyl-ethylenediamine (TEMED) and ammonium persulfate (APS) were added to the gel solution immediately before use. The components were mixed gently using a pipette without introducing air bubbles. The mixture was loaded between the glass plates of a gel casting apparatus (BioRad). To isolate gel from air, 100% (v/v) isopropanol was added on top of the gel. Isopropanol was drained using filter paper once gel was solidified. Composition of stacking gel is as follows:

SDS-PAGE 4% (w/v) stacking gel

dH_20	3.6 ml
0.5 M Tris-HCl pH 6.8	750 µl
10% (w/v) SDS	50 µl
30% (w/v) acrylamide/bis (37.5:1)	650 µl
10% (w/v) APS	50 µl
TEMED	20 µl

Mixed stacking gel components were loaded on top of solidified resolving gel. To create sample loading wells, a plastic comb was inserted in to the stacking gel. The gel was transferred to BioRad tank containing 1x SDS-PAGE reservoir buffer after it had solidified. To prepare samples, 5x SDS-PAGE loading buffer was mixed with samples and incubated for 5 min at 100ºC and appropriate amount of sample was loaded in the wells. 6 µl of Color Prestained Protein Standard, Broad Range (NEB) was also loaded as a protein size marker (Table 2.8). Proteins were separated by electrophoresis at 120 V until the loading dye reached the base of the glass plate.

Protein size marker	Molecular mass (kDa)
Color Prestained Protein Standard, Broad Range (NEB)	245
	190
	135
	100
	80
	54
	46
	32
	25
	22
	17
	11

Table 2.8 Protein size markers

2.12.5 Coomassie straining

SDS-PAGE gel was submerged in Coomassie Blue stain following electrophoresis for between 30 min to 1 hour in order to visualise protein

bands. Subsequently, gel was then destained in Coomassie destain solution overnight on shaker until the background was clear. The protein standards of known molecular mass were used for comparison of molecular sizes of proteins.

2.12.6 Western blotting

Following separation of protein samples by SDS-PAGE (section 2.12.4), the gel was soaked in blotting buffer for 10 min. Nitrocellulose membrane (GE Healthcare) was cut to the same size as gel and soaked in blotting buffer for 10 min. Using the Mini-Protean Tetra cell system (BioRad), proteins were transferred to the membrane from the gel by wet transfer in ice-cold blotting buffer. The power was set to 100 V for 90 min. Subsequently, the membrane was rinsed with 1x TBST and then the blot was blocked in blocking buffer for 1 h at room temperature with gentle shaking. The membrane was then rinsed and washed three times in TBST for 10 min at room temperature. The membrane was incubated with blocking buffer containing appropriate dilution of primary antibodies overnight at 4°C with gentle shaking. To remove the primary antibody solution, the membrane was rinsed and washed three times with TBST for three times for 10 min as before. The membrane was then incubated with blocking buffer containing 1:10,000 horseradish peroxidase (HRP) conjugated anti-rabbit IgG secondary antibodies (Sigma) for 1 h at room temperature with gentle shaking. To remove unbound antibodies, the membrane was rinsed and washed with TBST for three times as before. In order to detect proteins bound to the membrane, the blot was covered with Clarity Western ECL blotting substrates (BioRad) and incubated for 3 min in dark room at room temperature. The excess substrate was then removed and the blot was scanned using ChemiDoc MP Systems (BioRad) for chemiluminescent detection.

2.12.7 Gel-based analysis of penicillin binding proteins

For the detection of penicillin binding proteins, membrane fraction was isolated (section 2.12.2). Approximately 25 µg of total protein was incubated with 30 µM Bocillin FL (ThermoFisher) at 37°C for 30 min. Subsequently, 5x

SDS-PAGE loading buffer was added and incubated for 5 min at 100°C. The proteins were separated by SDS-PAGE gel electrophoresis and visualised with ChemiDoc MP Systems (BioRad).

2.13 Transformation techniques

2.13.1 Transformation of *E. coli*

2.13.1.1 Transformation of electrocompetent *E. coli*

A 50 µl of *E. coli* NEB5α electrocompetent cells (NEB) was defrosted on ice. 1 ng of Gibson assembly mix or plasmid DNA was added to the cells. The mixture was pipetted into a pre-chilled 1 mm electroporation cuvette (BioRad). Electroporation was carried out at 25 µF, 1.75 kV and 200 Ω using a GenePulser Xcell Electroporation system (BioRad). To recover cells, 1 ml of LB was immediately added to the cuvette. *E. coli* cells were incubated for 1 h at 37°C with shaking at 250 rpm. 100-150 µl of cells were spread on LB agar plates containing appropriate antibiotics. The plates were incubated for 24-48 hours at 37°C until colonies appeared.

2.13.2 Transformation of *S. aureus*

2.13.2.1 Preparation of electrocompetent *S. aureus* cells

A single colony of RN4220 *S. aureus* was inoculated to 400 ml of BHI and incubated for 10-12 h at 37°C with shaking at 250 rpm. Using overnight culture, fresh 400 ml of BHI was inoculated with a starting OD_{600} of 0.1. Cells were incubated at 37°C with shaking at 250 rpm until the OD_{600} reaches 0.4-0.6. Cells were harvested by centrifugation at 5,000 rcf for 10 min at room temperature. Pellets were resuspended in 25 ml sdH_2O and spun as before. This step was repeated three times. Subsequently, pellets were resuspended in 20 ml 10% (v/v) glycerol and centrifuged as before for 10 min. This step was repeated twice. Then, 10 ml of 10% (v/v) glycerol was used to resuspend the pellet and tubes were incubated at room temperature for 30 min. The cells were centrifuged as before for 10 min. The pellet was

resuspended in 200 µl 10% (v/v) glycerol. From this, 50 µl of aliquots were prepared and stored at -80°C.

2.13.2.2 Transformation of electrocompetent *S. aureus*

An aliquot of 50 µl electrocompetent RN4220 *S. aureus* cells was thawed at room temperature and ~1 µg plasmid DNA was added to the cells. The mixture was pipetted to a pre-chilled 1 mm electroporation cuvette (BioRad). Electroporation was carried out at 25 µF, 2.3 kV and 100 Ω using a GenePulser Xcell Electroporation system (BioRad). To recover cells, 1 ml of BHI was immediately added to the cuvette. Cells were incubated for 3 h at 37°C with shaking at 250 rpm. 100-150 µl of cells were spread on BHI agar plates containing appropriate antibiotics. The plates were incubated for 24-48 hours at 37°C until colonies appeared.

2.14 Phage techniques

2.14.1 Bacteriophage

In order to perform phage transduction of *S. aureus,* bacteriophage Φ11 was used (Mani et al., 1993).

2.14.2 Preparation of phage lysate

The donor strain of *S. aureus* was grown overnight. 200 µl of the overnight culture was mixed with 5 ml phage buffer, 5 ml BHI and 100 µl of a phage lysate stock (Φ11). The mixture was incubated overnight at 25°C, until it was clear. Subsequently, the lysate was filter-sterilised using 0.2 µm pore filter (Merck) and stored at 4°C.

2.14.3 Phage transduction

Recipient *S. aureus* strain was inoculated in 50 ml LK and incubated at 37°C overnight, 250 rpm. The overnight culture was centrifuged at 5,000 rcf at room temperature for 10 min. The pellet was resuspended in fresh 3 ml LK. 500 µl of recipient strain was mixed with 1 ml LK, 10 µl 1 M $CaCl_2$ and 500 µl phage lysate. The tubes were incubated without shaking at 37°C for 25 min

and then with shaking for 15 min. 1 ml ice cold 0.02 M sodium citrate was added to the mixture and incubated the tube for 5 min on ice. The cells were centrifuged for 10 min at 5,000 rpm and 4°C. The supernatant was discarded and the pellet was resuspended with 1 ml ice cold 0.02 M sodium citrate and incubated on ice for 50-100 min. 100-150 µl of cells were spread on LK agar plate containing 0.05% (w/v) sodium citrate and appropriate antibiotics for selection. Plates were incubated for 24-72 hour at 37°C. Single colonies were picked and streaked onto BHI agar plate containing antibiotic for further confirmation.

2.15 Microscopy imaging

2.15.1 Fixing of cells for imaging

Cell pellets were resuspended with 0.5 ml PBS. 0.5 ml of freshly prepared fixative (section 2.4.5) was added to the cells incubated at room temperature for 30 min. After fixation, cells were washed twice with sdH_2O by centrifugation (14,000 rcf, 1 min, room temperature) and resuspension.

2.15.2 Labelling of SNAP fusion proteins

For conventional microscopy, strains producing SNAP fusions were grown to an OD_{600} ~0.05 (early exponential phase). 1 ml of cell culture was incubated with 0.5 to 1 µM SNAP substrate, SNAP-Cell TMR-Star for 10 min at 37°C. After labelling, the cells were washed with PBS by centrifugation for 1 min at 10,000 rpm at room temperature and resuspended. The cells were then fixed for imaging.

2.15.3 Conventional fluorescence microscopy

DeltaVision deconvolution microscope (Applied, precision, GE Healthcare) was used to acquire fluorescence images. All the images obtained were deconvolved using SoftWoRx v.3.5.1 software. Appropriate wavelengths and filters used for imaging of fluorophores are listed in Table 2.9. Brightness and contrast adjustment was done using Fiji (ImageJ 1.52c).

Filter	DeltaVision		Fluorophore(s)
	Excitation filter/bandpass (nm)	Emission filter/band pass (nm)	
FITC	492/20	528/38	eYFP
RD-TR-PE/TxRED	555/28	617/73	TMR-Star

Table 2.9 DeltaVision filter sets used for imaging

2.16 Rate of respiration

2.16.1 Clark-type oxygen electrode

Clark-type oxygen electrode (Rank Bros Ltd) was used to measure rate of respiration. The apparatus contains an electrode operating at a polarising voltage of 0.6 V separated by a chamber with an oxygen-permeable Teflon membrane. The reduction in the oxygen concentration was measured at the cathode which creates a potential difference. The potential difference is measured by LabTrax-4 and LabScribe2 software (World Precision Instruments). The temperature of the chamber was maintained at 37°C and stirred at a constant rate. Prior to experiment, the chamber was calibrated to a 100% to 0% oxygen determined by the addition of sodium dithionate.

2.16.2 Sample preparation

50 ml of BHI was inoculated with a single colony and incubated overnight at 37°C with 250 rpm shaking. Next morning, overnight culture was diluted to 1:50 in 50 ml fresh BHI and incubated to produce log phase culture for 3 hours at 37°C with 250 rpm shaking. The cultures were centrifuged at 3,380 rcf for 10 min at 4°C and supernatant discarded. The pellet was washed twice by resuspension in ice-cold 0.02 M PBS followed by centrifugation as described above. The washed cell pellet was resuspended in 1 ml ice-cold 0.02 M PBS and kept on ice until needed.

2.16.3 Experimental procedure

Following electrode calibration, 1950 µl of 0.02 M PBS was added to the electrode chamber and the system was left idle for 15 min to stabilise oxygen concentration inside the chamber. 50 µl of sample (2.16.2) was added to the chamber and allowed to stabilise for 5 min. The chamber was then sealed with the lid. After 5 min, 50 µl of 1 M glucose was injected into the chamber through the lid to begin respiration. The oxygen consumption was recorded and respiration rates were calculated as nmolO_2/min.

2.17 Quantification of extracellular lactate

2.17.1 Sample preparation

10 ml of BHI was inoculated with a single colony and incubated overnight at 37°C with 250 rpm shaking. Overnight culture was used to inoculate fresh 10 ml BHI and incubated until OD600 reaches ~1. Cells were centrifuged for 10 min at 5,000 rcf at 4°C.

2.17.1.1 Deproteinisation procedure

For deproteinisation, 75 µl of supernatant sample (section 2.17.1) was added to a clean microfuge tube. In order to precipitate protein, 30 µl of 4 M ice-cold perchloric acid (PCA) was mixed well with sample by vortex. Samples were incubated on ice for 5 min and centrifuged at 13,000 rpm for 2 min. The supernatant was transferred to the new microfuge tube for the sample neutralisation step. Samples were neutralised by adding ice-cold 2 M KOH that equals 34 % of the supernatant (e.g. 34 µl of 2 M KOH to 100 µl sample) and mixed by vortex briefly. This step neutralised the sample and precipitated excess PCA. The tubes were left open to release any CO_2 formation. The pH was adjusted between 6.5 to 8.0. To adjust pH, 0.1 M KOH or PCA was used when necessary. Samples were centrifuged at 13,000 rpm for 15 min and supernatant was collected. L-Lactate Assay Kit (Colorimetric/Fluorometric) (Abcam) was used to detect lactate in samples and manufacturer's instructions were followed.

2.18 Whole genome sequencing

Whole genome sequencing was provided by MicrobesNG, University of Birmingham. Strains were sent as a bead stock.

2.18.1 Sample preparation

For genomic DNA extraction, three beads were washed with extraction buffer containing Lysostaphin and RNase A followed by incubation at 37°C for 25 min. Proteinase K and RNase A was added and further incubated at 65°C for 5 min. In order to purify genomic DNA, equal volume of SPRI (Solid Phase Reversible Immobilisation) beads resuspended in EB buffer was used. DNA was quantified in triplicates using Quantit dsDNA HS assay in a plate reader (Eppendorf).

Genomic DNA libraries were prepared using Nextera XT Library Prep Kit (Illumina) in accordance with manufacturer's instructions. Library preparation and DNA quantification was carried out on a liquid handling system (Hamilton Microlab STAR). Pooled libraries were quantified using Kapa Biosystems Library Quantification Kit for illumine on a Roche light cycler 96 qPCR machine. Libraries were sequenced on the Illumina HiSeq using a 250 bp paired end protocol.

Above optimised method is taken from MicrobesNG.

2.18.2 Data analysis

Reads were trimmed using Trimmomatic 0.30 with a sliding window cutoff of Q15 (Bolger et al., 2014). De novo assembly was performed on samples using SPAdes version 3.7 (Bankevich et al., 2012). For contigs annotation, Prokka 1.11 was used (Seemann, 2014). NCTC8325 whole genome sequence was used as a reference for comparison.

This pipeline for data analysis was optimised and performed by MicrobesNG.

2.19 RNA-Sequencing

RNA-Seq for transcriptome analysis was performed by Glasgow Polyomics, University of Glasgow. Total RNA was extracted from representative strains and sent for sequencing. See section 2.11.1 for RNA extraction method.

2.19.1 Data analysis

Total RNA samples of three biological replicates for each strain were subject to QC prior to library preparation followed by ribosomal depletion using TruSeq stranded total RNA kits (Illumina). The generated raw data was compared to NCTC8325 reference sequence for expression quantification and transcript annotation. Preliminary bioinformatics support for data analysis was provided by Glasgow Polyomics which included expression quantification, statistics and differential expression analysis.

Chapter 3

Expression of high-level methicillin resistance using multi copy plasmid-borne *mecA*

3.1 Introduction

Methicillin resistance in staphylococci is a major health problem and is due to an acquisition of a non-native penicillin binding protein (PBP2A). PBP2A is encoded by *mecA,* involved in the final assembly of crosslinked peptidoglycan in the cell wall (Matthews and Stewart, 1984). This additional PBP, confers an intrinsic resistance to all available β-lactams due to its low binding affinity (Hartman and Tomasz, 1986). Consequently, production of PBP2A allows cells to continue growth and division and enables cell wall biosynthesis even in the presence of high concentrations of the antibiotics (Aedo and Tomasz, 2016). The central genetic determinant, *mecA*; is carried by a mobile genetic element the staphylococcal chromosomal cassette (SCC*mec*), which incorporates into the chromosome at a unique site (Ito et al., 2009). The promoter and gene sequences of *mecA* among most MRSA strains are well conserved (Ryffel et al., 1990), except some of the recently identified strains carrying a new *mec* gene homologue (García-Álvarez et al., 2011; Kim et al., 2012). However, the carrier SCC has been shown to have considerable structural diversity (Ito et al., 2009).

A distinctive characteristic of most MRSA is the heterotypic expression of methicillin resistance under normal growth conditions (Chambers et al., 1989; Pozzi et al., 2012). Heterogeneous expression is characterised by the majority of cells being susceptible to low concentrations of drug in the presence of a β-lactam antibiotic, however, a subpopulation is able to develop high-level homogenous resistance (Berger-Bächi and Rohrer, 2002; Finan et al., 2002; Kim et al., 2013; Pozzi et al., 2012; Sabath and Wallace, 1971). This phenomenon of exhibiting heterogeneous or low-level resistance of MRSA depends on the genetic background of the strain that acquired *mecA* (Berger-Bächi and Rohrer, 2002). Importantly, one of the most

significant observations made is that the high-level homogenous resistance will arise from low-level resistance following exposure of a staphylococcal population to a β-lactam antibiotic (Finan et al., 2002; Hartman and Tomasz, 1986). Factors found to be influencing high-level resistance have been described in several studies in the past (Berger-Bächi and Rohrer, 2002; Matthews and Stewart, 1984). The factors with the most profound effect to obtain stable resistance are pH, osmolarity, temperature, visible light and growth in the presence of β-lactam antibiotic (Berger-Bächi and Rohrer, 2002; Matthews and Stewart, 1984; Pozzi et al., 2012). While most MRSA isolates exhibit varied resistance, the activity of regulatory genes (*mecI/mecR*) which controls *mecA* transcription cannot be simply involved (Mwangi et al., 2013). However, the molecular basis of transition from low-level to high-level has not yet been examined systematically.

In an effort to understand the cause of heterogeneous resistance, chromosomal genes affecting methicillin resistance were characterised (Berger-Bächi and Rohrer, 2002). Many of them play an important role in cell wall biosynthesis (Berger-Bächi and Rohrer, 2002; De Lencastre et al., 1999) which has given valuable insight into the physiology of this pathway but none of them have shown to affect the production of PBP2A so far (Rohrer et al., 2003). In addition, oxacillin was found to be associated with mediating the accessory gene regulator (Agr) dependent SOS response linked with increased expression of *mecA* during conversion from heterogeneous (HeR) to homogeneous resistance (HoR) (Cuirolo et al., 2009). Transcriptional profiles of MRSA strains, selected for HeR-HoR phenotype, revealed increased expression of the *agr* global regulatory system together with increased *mecA* expression (Plata et al., 2011). However, HeR cells overexpressing of ectopic *agr* were unable to undergo HeR-HoR transition in the presence of oxacillin, indicating the importance of increased *mecA* expression (Cuirolo et al., 2009). However, this observation alone is insufficient to explain transition from HeR to HoR resistance as highly resistant isolates are not deficient in accessory factors (Pozzi et al., 2012).

In an attempt to better understand the underlying mechanism of heterogeneous β-lactam resistance, Mwangi et al (2013) developed a model system. It was shown that introduction of *mecA* carried on a multicopy plasmid into a methicillin sensitive strain produced a heterogeneous population from which a highly resistant homogeneous subpopulation was selected upon exposure to β-lactam antibiotic. This subpopulation exhibited high-level β-lactam resistance indistinguishable from that of the phenotypes of most MRSA isolates (Antignac and Tomasz, 2009). This observation indicated that some determinants of methicillin resistance may reside in the chromosomal genetic background (Mwangi et al., 2013). Whole genome sequencing identified point mutations in the *relA* gene which encodes for synthesis of an alarmone (p)ppGpp during the stringent stress response suggesting its role in defining high-level β-lactam resistance (Mwangi et al., 2013). Similar results were obtained when *mecA* was transferred via an entire SCC*mec* element into an MSSA strain (Kim et al., 2013). However, intracellular levels of (p)ppGpp could be modulated by not only genetic changes but also by environmental factors.

Subsequently, Dordel et al (2014) identified 44 different chromosomal mutations associated with high-level resistance using whole genome sequencing of laboratory isolated early MRSA lineages expressing heterogeneous resistance (De Lencastre et al., 2000). Taken together, the influence of these genetic factors on the level of methicillin resistance in MRSA should be systematically investigated, as the link between genetic determinant and high-level expression of resistance is inconclusive.

It is plausible that the heterogeneous methicillin resistance is an effect of a complex regulatory mechanism capable of producing highly resistant subclones, only comparison of transcriptional patterns together with proteome analysis of the genomes from low-level resistant parents with highly resistant strains may shed some light on the identity of pleiotropic regulatory networks. It is therefore essential to elucidate the origin of heterogeneous low-level methicillin resistance.

3.1.1 Aims of the chapter

The overall aim of this chapter at the outset was to construct a high-level methicillin resistant strain in the genetically amenable background an SH1000. Then to use super resolution microscopy approaches to study the subcellular localisation and dynamics of PBP2A. The specific aims of this chapter were to:

i. Construct genetically amenable MRSA strain using the SH1000 background
ii. Experimental evolution of MRSA strains to isolate highly resistant MRSA derivatives
iii. Determine the mechanism of high-level resistance using a WGS approach

3.2 Results

3.2.1 Construction of a genetically amenable MRSA strain

Previous studies by Pozzi et al., (2012) and Kim et al., (2013) demonstrated that plasmid-borne copies of the *mecA* could be introduced into an MSSA strain to generate low-level methicillin resistance. In order to understand the molecular basis of methicillin resistance in *Staphylococcus aureus,* the multicopy shuttle plasmid pRB474 p*mecA,* carrying *mecA* was transduced into the lab strain SH1000 (Pozzi et al., 2012; Rudkin et al., 2012). SH1000 was chosen because it is amenable to genetic manipulation. The expression of *mecA* was controlled by its native promoter. A phage lysate was made using SJF4978 (8325-4 *pmecA* HeR) and transduced into SH1000. The resulting strain SJF4981 (SH1000 p*mecA*) was selected using BHI chloramphenicol (10 µg/ml) plates.

SJF4981 (SH1000 p*mecA*) was verified by using an oxacillin Etest (Oxoid M.I.C.E) for detection of MIC and by PCR using primers for *mecA* amplification following isolation of pRB474 p*mecA* (Figure 3.1 B below).

8325-4 derived strains are susceptible to oxacillin with MICs ranging from 0.12 to 0.25 µg/ml (Bæk et al., 2014). To verify susceptibility of SH1000, the oxacillin MIC using Etest method was carried out which revealed the SH1000 MIC to be 0.12 µg/ml (Figure 3.1 A below). Acquisition of plasmid-borne *mecA* by SH1000 produces a low-level resistance with an oxacillin MIC value of 0.25 µg/ml (Figure 3.1 A below). This observation verified the functionality of *mecA* expression. In addition, SJF4981 (SH1000 p*mecA*) grows on BHI agar plates containing 10 µg/ml chloramphenicol. Furthermore, the plasmid-borne *mecA* was confirmed by PCR, following isolation of pRB474 *pmecA* plasmid from SJF4981 (SH1000 p*mecA*), using primers p*mecA*_F1 and p*mecA*_R1 (Figure 3.1 B). PCR and oxacillin MIC results confirmed SJF4981 (SH1000 p*mecA*) to have the expected phenotype. This observation is similar to previous work (Kim et al., 2013; Peacock and Paterson, 2015; Pozzi et al., 2012).

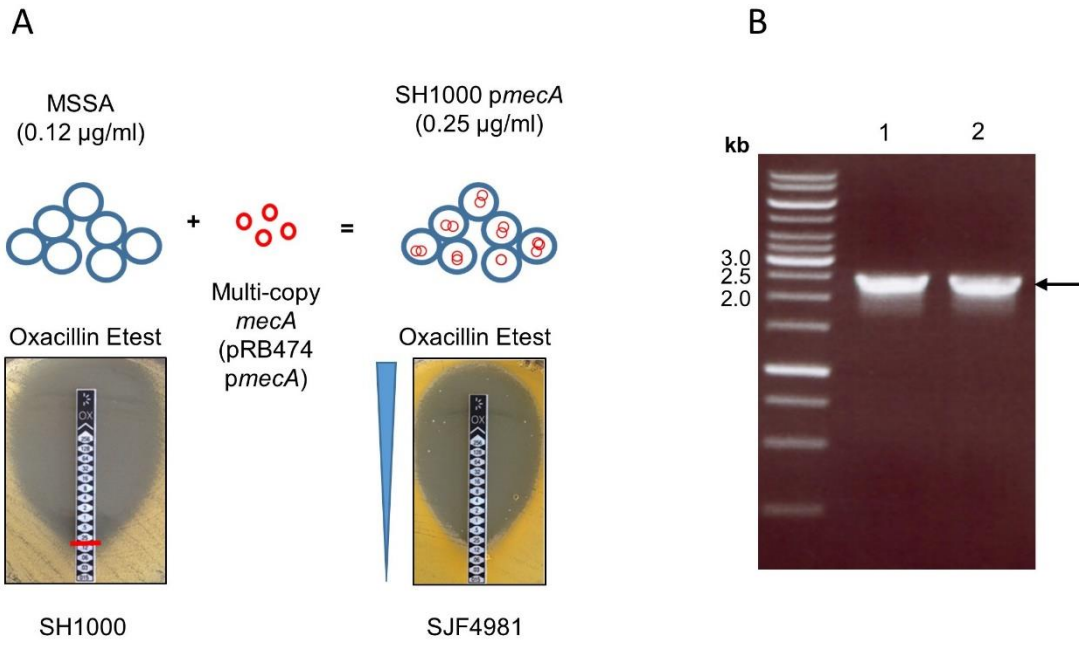

Figure 3.1 Construction of an SH1000 p*mecA* MRSA derivative from an MSSA strain

A) SJF4981 (SH1000 p*mecA*) construct was produced by transduction using an 8325-4 HeR (SJF4978) phage lysate containing pRB474 p*mecA* plasmid carrying *mecA* under its own promoter. Oxacillin MIC was measured using Etest strip for antibiotic susceptibility testing. MICs are listed in brackets.
B) 1% (w/v) TAE agarose gel showing products of PCR amplification of *mecA* (lane 1) and positive control (COL genomic DNA) (lane 2) using p*mecA*_F1 (forward) and p*mecA*_R1 (reverse) primer. The expected DNA fragment of 2.5 kb is indicated with a black arrow for both lanes. Sizes of a DNA ladder are shown in kb. DNA fragments were used as size markers for agarose gel electrophoresis.

3.2.1.1 Isolation of highly oxacillin resistant derivatives of SH1000 p*mecA*

Transformation of plasmid-borne *mecA* to SH1000 is accompanied by low-level oxacillin resistance (Section 3.2.1). To investigate the transition to high-level resistance to oxacillin, a modified gradient plate technique (Szybalski and Bryson, 1952) was used (Figure 3.2 A). Two layers of agar were poured into an OmniTray (Thermo Scientific). The bottom layer (slanted) consists of plain BHI agar covering the entire OmniTray bottom. The top flat layer contains 5 µg/ml methicillin (Figure 3.2 A). A heavy suspension of SJF4981 (SH1000 p*mecA*) was spread over the surface of the agar covering the whole area of the agar in the OmniTray containing the 0-5 µg/ml methicillin gradient (Figure 3.2 A below). Only resistant cells are able to grow in the regions of highest methicillin concentration whereas, confluent growth is obtained in the regions with less methicillin (Figure 3.2 C and D). This method allowed the selection of subsequent mutants exhibiting variable resistance levels toward oxacillin, with MICs ranging from <2 µg/ml (comparable to those of susceptible isolates) to ≥256 µg/ml in highly resistant strains. This approach also showed the progression of resistance in experimentally evolved oxacillin resistant strains. This screening was repeated twice to select enough spontaneous mutants with variable oxacillin MIC. Originally, a total of 42 isolates were selected from two separate gradient plates containing 0-5 µg/ml methicillin (See Appendix 1 Table 1). Of these 42 strains, a total of ten representative strains were selected for further study. An evolutionary lineage from SH1000 is shown in Figure 3.3 and associated oxacillin MICs are listed in Table 3.1.

To determine oxacillin MICs for spontaneous mutants isolated from the gradient plate, Etest was performed by spreading, using a cotton swab, a small aliquot of overnight cultures diluted to an OD_{600} of 0.1. Oxacillin Etest strips were placed on spread plates for overnight incubation. Most isolates produced a low-level of resistance to oxacillin MIC value ranging from 2-4 µg/ml. However, some isolates exhibited higher oxacillin MIC (≥256 µg/ml). Isolates producing low-level resistance (2-4 µg/ml) were further spread on a

methicillin gradient plate supplied with up to 20 µg/ml methicillin to select for increased resistance. This approach allowed the sequential acquisition of resistance to be determined at the molecular level. SJF4986 (SH1000 p*mecA* TIR1) was considered to be highly resistant to oxacillin (MIC = ≥256 µg/ml), as Etest results show partial growth around the Etest strip. All representative isolates derived from SJF4981 (SH1000 p*mecA*) are shown in Figure 3.3 along with oxacillin MIC Table 3.1. The presence of pRB474 p*mecA* was confirmed by growing isolates on agar plates supplied with 10 µg/ml chloramphenicol. Moreover, an increase in oxacillin MIC was evidence of a functional p*mecA* plasmid.

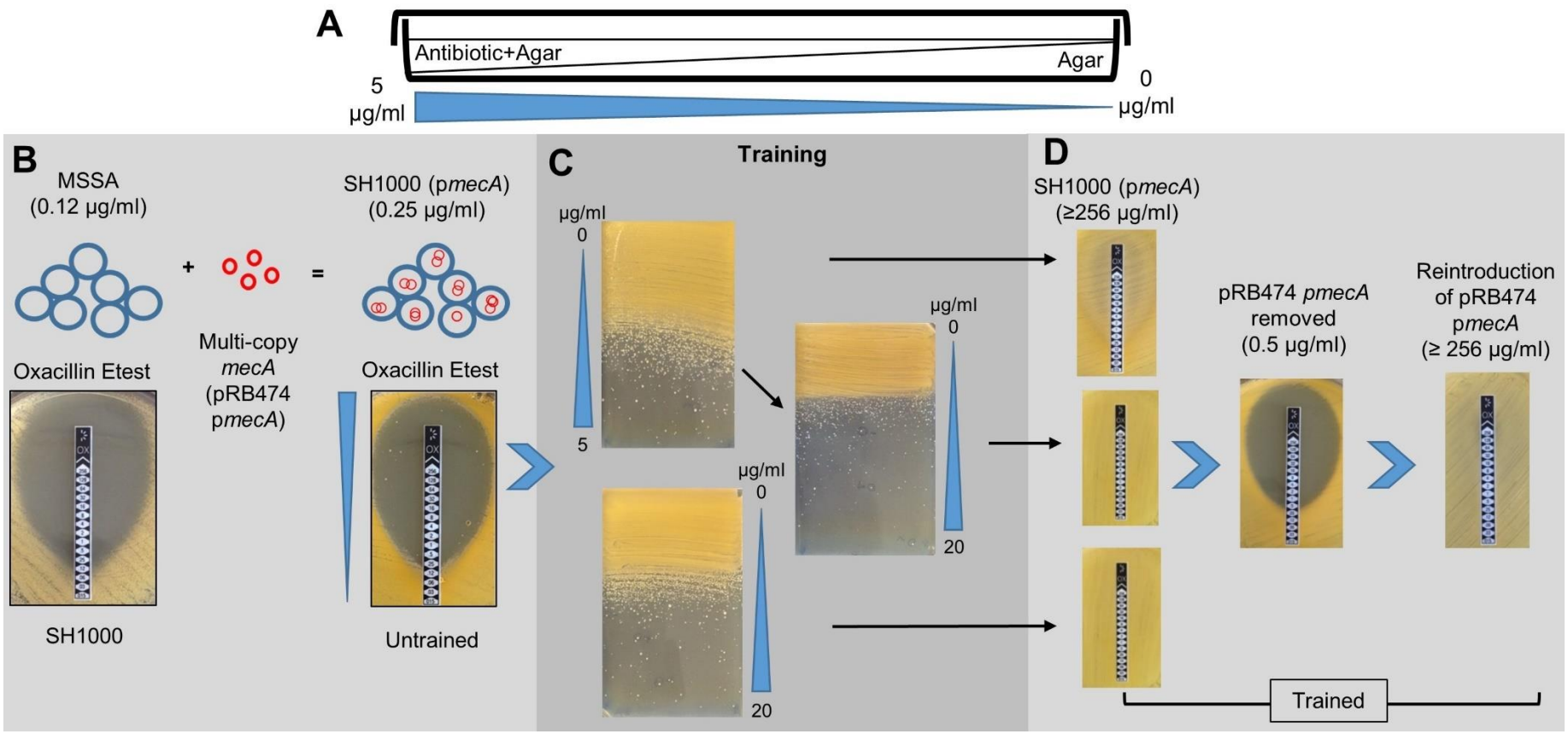

Figure 3.2 Scheme of high-level MRSA selection using plasmid-borne *mecA* expression and subsequent strain evolution

A) Schematic representation of antibiotic gradient plate of two layers. Bottom layer consists of plain BHI agar, top layer containing 5/20 µg/ml methicillin.
B) Resistance properties of SJF4981 (SH1000 p*mecA*) and its parental MSSA, SH1000 strain.
C) Use of a gradient plate to select for high-level methicillin resistance.
D) The Etest strips revealed high-level oxacillin resistance which required presence of the p*mecA*.

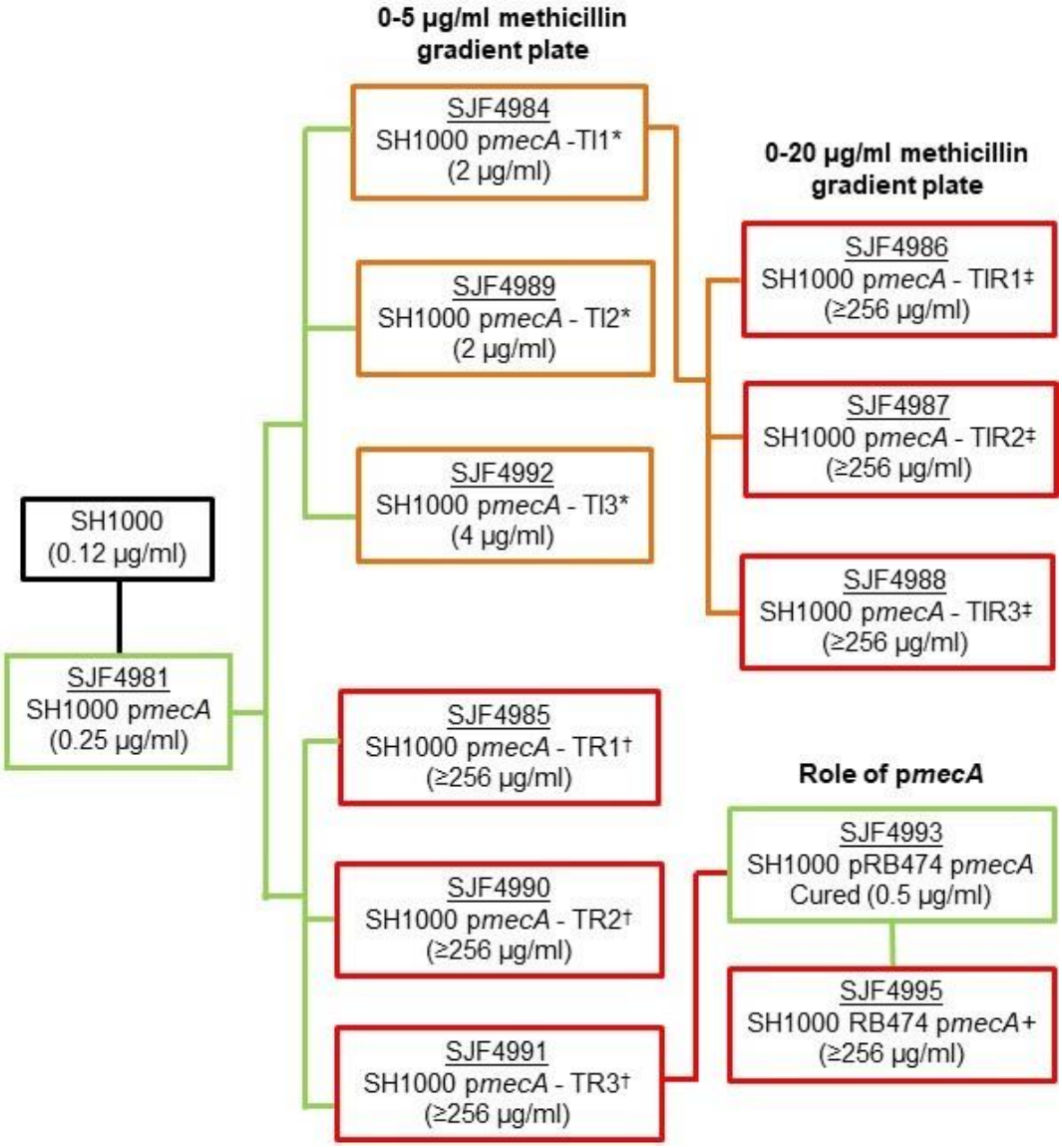

Figure 3.3 Lineage of SH1000 showing progression of methicillin resistance

Oxacillin MICs are listed in brackets for all strains. Ten representative strains were selected for further study. *, denotes isolates expressing intermediate oxacillin resistance (TI – trained-intermediate), listed in orange boxes; †, denotes isolates expressing high-level oxacillin resistance (TR – trained-resistant), listed in red boxes; ‡, denotes isolates expressing high-level oxacillin resistance following selection on 0-20 µg/ml methicillin gradient plate using TI1 strain (TIR – trained-intermediate to resistant), also listed in red boxes.

Strain	Gradient plate	Oxacillin MIC
SH1000		0.12 µg/ml
Parental strain SH1000		
SH1000 p*mecA* (SJF4981)		0.25 µg/ml
Parental strain SH1000 p*mecA* (SJF4981)		
SH1000 p*mecA* -TI1* (SJF4984)	0-5 µg/ml methicillin	2 µg/ml
SH1000 p*mecA* -TI2* (SJF4989)	0-5 µg/ml methicillin	2 µg/ml
SH1000 p*mecA* -TI3* (SJF4992)	0-5 µg/ml methicillin	4 µg/ml
Parental strain SH1000 p*mecA* -TI1* (SJF4984)		
SH1000 p*mecA* -TIR1‡ (SJF4986)	0-20 µg/ml methicillin	≥256 µg/ml
SH1000 p*mecA* -TIR2‡ (SJF4987)	0-20 µg/ml methicillin	≥256 µg/ml
SH1000 p*mecA* -TIR3‡ (SJF4988)	0-20 µg/ml methicillin	≥256 µg/ml
Parental strain SH1000 p*mecA* (SJF4981)		
SH1000 p*mecA* -TR1† (SJF4985)	0-5 µg/ml methicillin	≥256 µg/ml
SH1000 p*mecA* -TR2† (SJF4990)	0-5 µg/ml methicillin	≥256 µg/ml
SH1000 p*mecA* -TR3† (SJF4991)	0-5 µg/ml methicillin	≥256 µg/ml
Parental strain SH1000 p*mecA* -TR3† (SJF4991)		
SH1000 pRB474 p*mecA* cured (SJF4993)		0.5 µg/ml
Parental strain SH1000 pRB474 p*mecA* cured (SJF4993)		
SH1000 pRB474 p*mecA*+ (SJF4995)		≥256 µg/ml

Table 3.1 List of representative strains

*, denotes isolates expressing intermediate oxacillin resistance (TI – trained-intermediate); †, denotes isolates expressing high-level oxacillin resistance (TR – trained-resistant); ‡, denotes isolates expressing high-level oxacillin resistance (TIR – trained-intermediate to resistant.

3.2.1.2 Removal of plasmid-borne *mecA*

From the original screening, a total of 18 isolates were picked expressing variable oxacillin resistance with MIC ranging from 1 to ≥256 µg/ml. Subsequently, 24 more isolates were selected from second screening expressing variable oxacillin resistance (Appendix 1 Table 1).

The results from section 3.2.1.1 showed a vastly variable oxacillin resistance developed from a single clone (SJF4981; SH1000 p*mecA* TI1) upon exposure to an antibiotic gradient. This observation is similar to the MRSA isolates found in clinical settings exhibiting large variations in the resistance level – this may not be simply due to the level of expression of *mecA* (Hartman and Tomasz, 1986; Sieradzki et al., 2008). Therefore, it was important to see whether removal of plasmid-borne *mecA* leads to susceptibility to oxacillin with MIC values identical to that of the parental strain SH1000 (oxacillin MIC = 0.12 µg/ml).

To address this question, a highly resistant strain (SJF4991 - SH1000 p*mecA* -TR3) with an oxacillin MIC of ≥256 µg/ml was selected. Initially, chloramphenicol selection was used to retain plasmid. Growth of highly resistant SJF4991 (SH1000 p*mecA* -TR3) in the absence of chloramphenicol generated a plasmid free derivative of SJF4991 (SH1000 p*mecA* -TR3). The strain was subcultured thirty times without chloramphenicol for the removal of pRB474-p*mecA*. In order to eliminate the possibility of inducing non-specific spontaneous mutations in the genome, SJF4991 (SH1000 p*mecA* -TR3) was not grown using curing agents or other procedures such as elevated growth temperature (Trevors, 1986) unlike in previous studies (Kim et al., 2013; Mwangi et al., 2013).

The plasmid-free SJF4993 (SH1000 pRB474 p*mecA* cured) derivative was isolated from BHI agar plate and tested for oxacillin sensitivity. SJF4993 (SH1000 pRB474 p*mecA* cured) regained susceptibility to oxacillin with an MIC value (0.5 µg/ml) similar to that of the parental strain SH1000 Figure 3.2 D and Figure 3.4 A). The successful removal of *mecA* was also confirmed by

PCR to amplify *mecA* using primers p*mecA*_F1 and p*mecA*_R1, as expected this PCR did not yield a product (Figure 3.4 A).

These observations suggest that *mecA* is a prerequisite for producing high-level β-lactam resistance (Finan et al., 2002; Hiramatsu et al., 2002; Lim and Strynadka, 2002; Peacock and Paterson, 2015; Walsh, 2000). Reintroduction of pRB474 p*mecA* by phage transduction into SJF4993 (SH1000 pRB474 p*mecA* cured) produced a strain SJF4995 (SH1000 pRB474 p*mecA*+) with high-level resistance to oxacillin (MIC = ≥256 μg/ml) indistinguishable from that of the original SJF4991 (SH1000 p*mecA* -TR3) (Figure 3.2 D and Figure 3.4 B). The presence of plasmid-borne *mecA* was confirmed by PCR to amplify *mecA* using primers p*mecA*2_SeqF2 and p*mecA*2_SeqR1 – yielding a product of 838 bp (Figure 3.4 B).

The findings showed that restoration of high-level oxacillin resistance did not require re-training on a methicillin gradient plate. This suggests that once an apparent chromosomal mutation(s) has been selected, *mecA* could be removed (SJF4993 - SH1000 pRB474 p*mecA* cured) and replaced (SJF4995 - SH1000 pRB474 p*mecA*+) to give high-level resistance. The evolutionary lineages for resultant strains SJF4993 (SH1000 pRB474 p*mecA* cured) and SJF4995 (SH1000 pRB474 p*mecA*+) are shown in Figure 3.3 and Table 3.1.

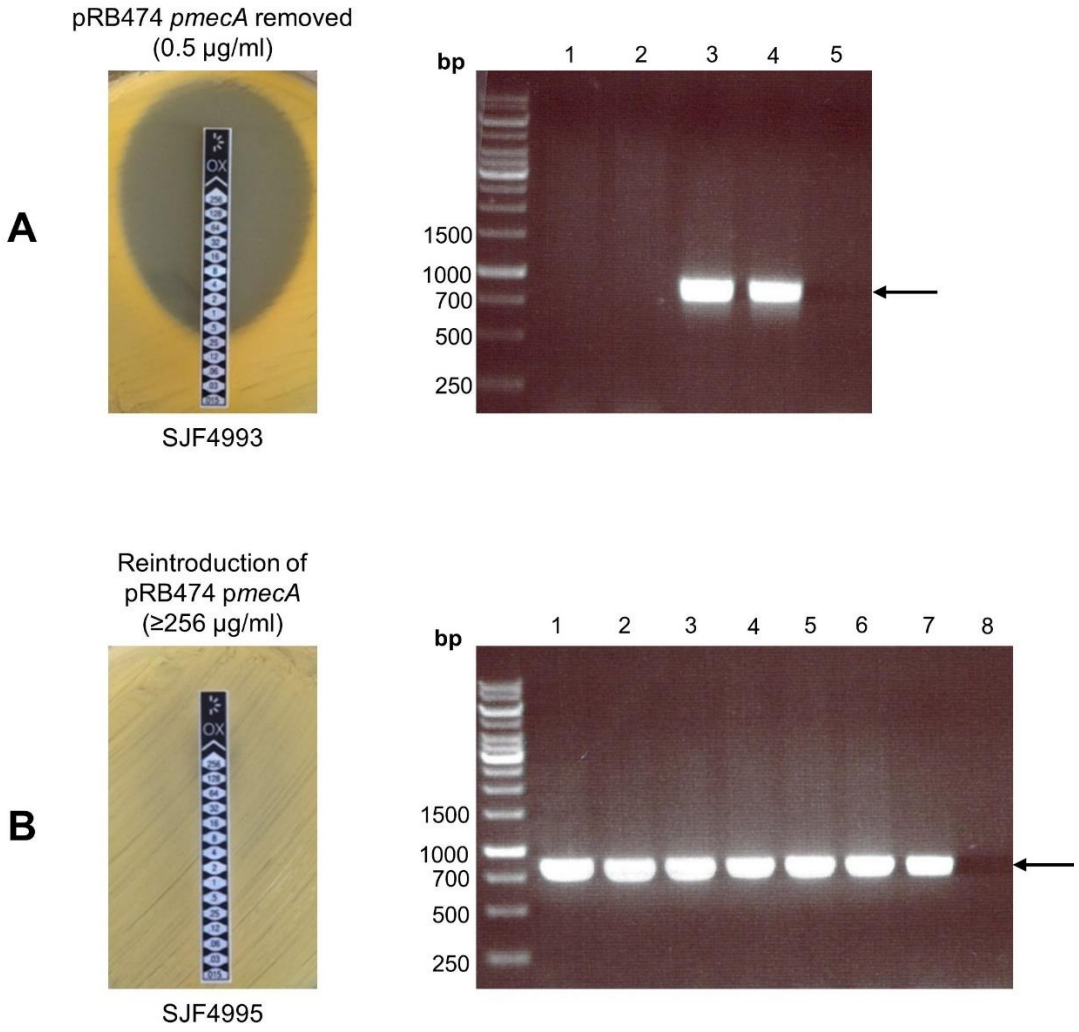

Figure 3.4 Removal and reintroduction of pRB474 p*mecA*

A) SH1000 p*mecA* -TR3 (SJF4991) was cured of pRB474 p*mecA* resulting in SH1000 pRB474 p*mecA* cured (SJF4993) regained susceptibility to oxacillin. 1% (w/v) TAE agarose gel showing no products (lane 1 and 2) for *mecA* fragment, positive control using COL genomic DNA (lanes 3 and 4) for *mecA* and non-template control (lane 5) using p*mecA*2_SeqF2 (forward) and p*mecA*2_SeqR1 (reverse) primers. The expected DNA fragment of 838 bp is indicated with black arrow for both lanes. DNA fragments were used as size markers for agarose gel electrophoresis.
B) Subsequently, reintroduction of pRB474 p*mecA* restored resistance to oxacillin resulting in SH1000 pRB474 p*mecA*+ (SJF4995). Introduction of *mecA* was confirmed by amplification of *mecA* fragment (lanes 1 to 6), positive control using COL genomic DNA (lane 7) and non-template control (lane 8). DNA fragments were used as size markers for agarose gel electrophoresis.

3.2.2 Identification of genetic determinants required for high-level resistance

Several studies have shown a connection between development of resistance and a compensatory mutation(s) in the genome that support the phenotypic expression of resistance (Bæk et al., 2015; Baquero, 2001; Kim et al., 2013; Martinez and Baquero, 2000; McCallum et al., 2010; Pozzi et al., 2012). The results obtained above (section 3.2.1.2) indicate involvement of genetic determinant(s) that define the level of oxacillin resistance in highly resistant trained derivatives (Table 2.2) of SJF4981.

3.2.2.1 Disruption of *gdpP* leads to high-level resistance

To better understand the selection of high-level resistance and to test the hypothesis of the involvement of chromosomal mutations, the genomes of untrained-SH1000 p*mecA* (SJF4981) and its derivatives, trained – expressing intermediate (low-level) resistance and trained – highly resistant strains (Table 3.1 and Figure 3.3) were sequenced using Illumina MiSeq and HiSeq 2500 platforms (MicrobesNG, University of Birmingham). Reads from strains were mapped to the fully sequenced reference genome of NCTC8325 (accession no. NC_007795.1). Variant calling was done using VarScan (MicrobesNG, University of Birmingham). A total of 93 mutations were identified. These included 5 frameshifts, 33 non-synonymous, 14 synonymous and 2 nonsense mutations. All identified mutations are listed in Appendix 1 Table 2 together with locus tag or gene name and mutation strength. From these, 77 of the identified mutations were not considered as they were present in all strains including control strain SH1000 p*mecA* (SJF4891).

When SH1000 p*mecA* (SJF4981) was compared to its highly resistant derivatives, whole genome sequencing identified that all trained - highly resistant strains have acquired range of mutations in a gene encoding a protein named GdpP (GGDEF domain protein containing phosphodiesterase) (Figure 3.5 B and Table 3.2), a recently identified c-di-AMP phosphodiesterase (Corrigan et al., 2011). Previous studies have

reported similar findings associated with different phenotypic observations (Banerjee et al., 2010; Corrigan et al., 2011; Greninger et al., 2016; Griffiths and O'Neill, 2012; Pozzi et al., 2012).

In *S. aureus*, *gdpP* is part of an operon that contains an upstream gene with unknown function and the two downstream genes, *rplI*, the gene encoding 50s ribosomal protein L9 and *dnaC*, the gene encoding DnaC protein that is important for DNA replication (Corrigan and Gründling, 2013) (Figure 3.5 A). In *B. subtilis*, the regulation of *gdpP* expression is controlled by a transcription factor σ^D which is involved in motility, chemotaxis and autolysis genes (Luo and Helmann, 2012a). GdpP (655 amino acids) contains two transmembrane domains; a degenerate Per-Arnt-Sim (PAS) sensory domain, involved in small molecule ligands binding and redox responses; a highly modified GGDEF motif that produces neither c-di-GMP nor c-di-AMP (Rao et al., 2010); a Desert hedgehog (DHH) domain, a characteristic of phosphodiesterases (Pde); and a DHH-associated DHHA1 domain (Figure 3.5 B) (Corrigan and Gründling, 2013). Two amino acid substitutions were identified in GGDEF motif of SJF4987 (SH1000 p*mecA* TIR2) and SJF4990 (SH1000 p*mecA* TR2). There were no mutations identified in either PAS motif, DHH or DHHA1 domains (Figure 3.5 B). The GGDEF motif, when present in a protein containing phosphodiesterase activity have shown to be involved in regulation of phosphodiesterase activity of the protein and not the synthesis of c-di-GMP or c-di-AMP (Rao et al., 2010). This observation suggests that the GGDEF domain has a regulatory function. The other three amino acid substitutions in SJF4991 (SH1000 p*mecA* TR3), SJF4985 (SH1000 p*mecA* TR1) and SJF4998 (SH1000 p*mecA* TIR3) could be linked with preventing the ability of the protein to restore susceptibility to oxacillin due to loss of catalytic activity of the protein.

In addition to altered *gdpP,* other genetic changes were also identified (Table 3.2) in strains exhibiting low-level and high-level resistance to oxacillin. However, mutations in *gdpP* were only found in highly resistant strains of SH1000 pRB474 p*mecA.* Other seven genes encoding proteins including SAOUHSC_00006, DNA gyrase subunit A *gyrA*; SAOUHSC_00162, Type I

site-specific deoxyribonuclease *hsdR*; SAOUHSC_00370, Hypothetical protein; SAOUHSC_01137, Hypothetical protein; SAOUHSC_01812, Hypothetical protein; SAOUHSC_02685, putative uncharacterised protein (*nirR*) and SAOUHSC_02932, Oxygen-dependent choline dehydrogenase (*betA*). These seven mutations were discarded because it is likely that these genetic changes were introduced during further training of SH1000 p*mecA* TI1 (SJF4984) using a 0-20 µg/ml methicillin gradient to obtain high-level resistance (Table 3.2 and Figure 3.3). It is also possible that one or more mutations listed in Table 3.2 may have emerged during passage and not be linked to a change in resistance (See Appendix 1 Table 2 for derivation of strains).

The strains listed in Table 3.1 used for whole genome sequencing were also used for isolation of pRB474 p*mecA*. DNA Sequencing (GATC Biotech, Germany) of the isolated plasmid (pRB474 p*mecA*) region containing p*mecA* revealed no mutations in plasmid-borne *mecA* - strongly suggesting the role of mutated *gdpP* in developing high-level resistance.

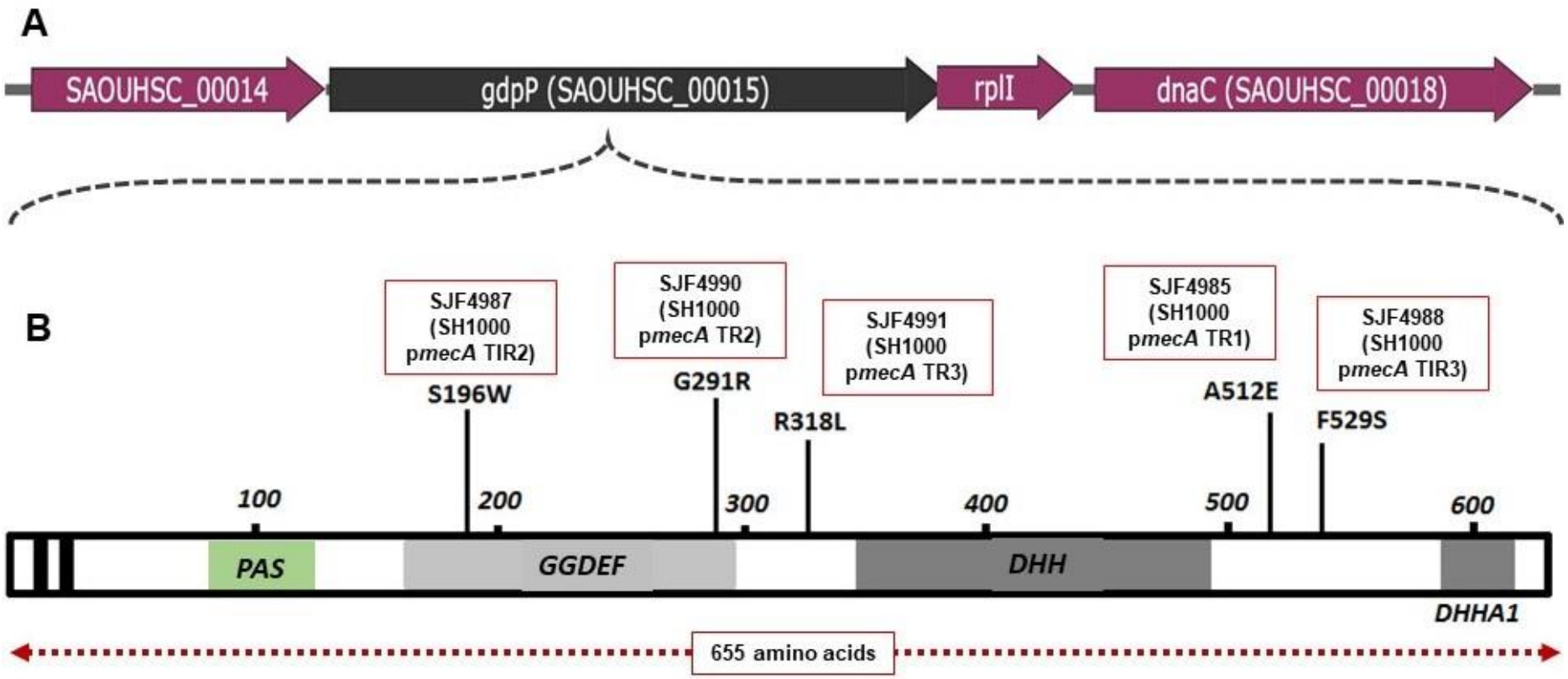

Figure 3.5 Schematic representation of the GdpP operon and SNP locations

A) Schematic representation of the genomic region containing the *gdpP* operon, and the *rplI* and *dnaC* genes.
B) The N-terminus of the GdpP protein contains two transmembrane helices (black boxes), a PAS domain, GGDEF, DHH and DHHA1 domains. Amino acid substitutions identified in highly resistant derivatives of SJF4981 (SH1000 pRB474 p*mecA*) are indicated and strain details are in red boxes.

Genome position	Oxacillin MIC (µg/ml)	Nucleotide change	Amino acid Change	Locus tag (Gene)	Protein
Parental strain SH1000 (SJF682)					
SH1000 p*mecA* (SJF4981)	0.25				
Parental strain SH1000 p*mecA* (SJF4981)					
TI1 (SJF4984) 9045	2	C-T	R681C	SAOUHSC_00006 (*gyrA*)	DNA gyrase subunit A
176626		G-A	D784N	SAOUHSC_00162 (*hsdR*)	Type I site-specific deoxyribonuclease
2698103		C-T	S511L	SAOUHSC_02932 (*betA*)	Oxygen-dependent choline dehydrogenase
TI2 (SJF4989) 9045	2	C-T	R681C	SAOUHSC_00006 (*gyrA*)	DNA gyrase subunit A
176626		G-A	D784N	SAOUHSC_00162 (*hsdR*)	Type I site-specific deoxyribonuclease
TI3 (SJF4992) 9045	4	C-T	R681C	SAOUHSC_00006 (*gyrA*)	DNA gyrase subunit A
176626		G-A	D784N	SAOUHSC_00162 (*hsdR*)	Type I site-specific deoxyribonuclease
2471861		C-T	H173Y	SAOUHSC_02685 (*nirR*)	Hypothetical protein
Parental strain SH1000 p*mecA* -TI1 (SJF4984)					
TIR1 (SJF4986) 9045	≥256	C-T	R681C	SAOUHSC_00006 (*gyrA*)	DNA gyrase subunit A
176626		G-A	D784N	SAOUHSC_00162 (*hsdR*)	Type I site-specific deoxyribonuclease
1718656		G-A	G54D	SAOUHSC_01812	Hypothetical protein
TIR2 (SJF4987) 9045	≥256	C-T	R681C	SAOUHSC_00006 (*gyrA*)	DNA gyrase subunit A
18904		C-G	S196W	SAOUHSC_00015 (*gdpP*)	c-di-AMP phosphodiesterase
176626		G-A	D784N	SAOUHSC_00162 (*hsdR*)	Type I site-specific deoxyribonuclease
TIR3 (SJF4988) 9045	≥256	C-T	R681C	SAOUHSC_00006 (*gyrA*)	DNA gyrase subunit A
19903		T-C	F529S	SAOUHSC_00015 (*gdpP*)	c-di-AMP phosphodiesterase
176626		G-A	D784N	SAOUHSC_00162 (*hsdR*)	Type I site-specific deoxyribonuclease
Parental strain SH1000 p*mecA* (SJF4981)					
TR1 (SJF4985) 19852	≥256	C-A	A512E	SAOUHSC_00015 (*gdpP*)	c-di-AMP phosphodiesterase
TR2 (SJF4990) 19188	≥256	G-C	G291R	SAOUHSC_00015 (*gdpP*)	c-di-AMP phosphodiesterase
TR3 (SJF4991) 19270	≥256	G-T	R318L	SAOUHSC_00015 (*gdpP*)	c-di-AMP phosphodiesterase
376633		G-T	E212*	SAOUHSC_00370	Hypothetical protein
1089537		C-G	P216A	SAOUHSC_01137	Hypothetical protein

Table 3.2 Mutations identified by whole genome sequencing in SH1000 pRB474 p*mecA* derivatives relative to NCTC8325

3.2.2.2 Inactivation of GdpP results in increased resistance to oxacillin

The genetic mechanism involving GdpP high-level resistance was further investigated to examine whether mutations in *gdpP*, directly affect oxacillin resistance. A strain SEJ1 Δ*gdpP*::*kan* (SJF5015) containing a kanamycin resistance cassette marked *gdpP* deletion (Corrigan et al., 2011) was lysed using bacteriophage Φ 11. Phage transduction introducing the *gdpP* deletion into SH1000 background resulting in strain SJF5025 (SH1000 Δ*gdpP*::*kan*) upon selection on agar plate supplied with 50 µg/ml kanamycin. The insertion of the *gdpP* deletion was confirmed by PCR amplification (Figure 3.6 A) and verified by genomic DNA sequencing (GATC Biotech, Germany).

Next, SJF5025 (SH1000 Δ*gdpP*::*kan*) was transduced with pRB474 p*mecA* to investigate resistance properties in the presence of *gdpP*. The resultant strain, SJF5026 (SH1000 p*mecA* Δ*gdpP*::*kan*) was isolated using an agar plate supplemented with 10 µg/ml chloramphenicol. PCR amplification of *mecA* by using *mecA*_F and *mecA*_R primers verified the presence of pRB474 p*mecA* Figure 3.6 B).

Following this, oxacillin MIC was determined for *gdpP* deleted strains, SJF5025 (SH1000 Δ*gdpP*::*an*) and SJF5026 (SH1000 p*mecA* Δ*gdpP*::*kan*) using an Etest strip (Figure 3.6 A and B). Oxacillin MICs for SJF5025 (MIC = 0.25 µg/ml) and SJF5026 (MIC = ≥256 µg/ml) revealed that inactivation of *gdpP* leads to high-level resistance. This is supported by the observations of Corrigan et al., 2011 and Griffiths and O'Neill, 2012 who noted increased resistance in USA300 LAC and Newman strains, respectively.

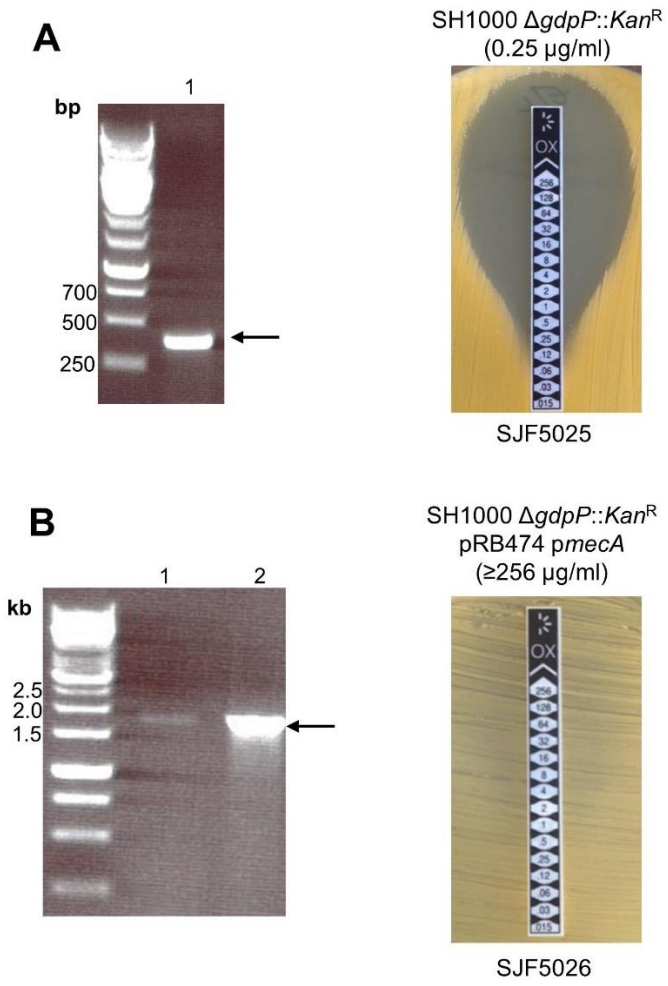

Figure 3.6 Increased oxacillin resistance is caused by inactivation of *gdpP*

A) A phage lysate of SEJ1 Δ*gdpP*::*kan* (SJF5015) was transduced into SH1000 resulting into SH1000 Δ*gdpP*::*kan* (SJF5025). The deletion of *gdpP* in SH1000 Δ*gdpP*::*kan* (SJF5025) was confirmed by a kanamycin cassette PCR resulting in a product marked with a black arrow of 395 bp (Lane 1). The MIC for oxacillin determined by Etest is listed in brackets. DNA fragments were used as size markers for agarose gel electrophoresis. **B)** Subsequently, pRB474 p*mecA* was introduced into SJF5025 (SH1000 Δ*gdpP*::*kan*) resulting in SJF5026 (SH1000 p*mecA* Δ*gdpP*::*kan*) (lane 2). This was confirmed by *mecA* PCR using primers *mecA*_F (forward) and *mecA*_R (reverse). The expected fragment of 1902 bp is shown with a black arrow. The MIC for oxacillin determined by Etest is listed in brackets. DNA fragments were used as size markers for agarose gel electrophoresis.

3.3 Discussion

A notable feature of heterogeneous (low-level) expression of methicillin resistance in *Staphylococcus aureus* is that it is mediated by an optimal level of production of PBP2A (Kim et al., 2013). However, the level of resistance depends on the background of the strains and varies from borderline (oxacillin MIC 2-4 µg/ml) resistance to high-level resistance (Tomasz et al., 1991). Prior studies have noted the importance of selection of chromosomal mutations or genetic rearrangements in developing highly resistant populations from populations exhibiting low-level resistance (Chan et al., 2016; Griffiths and O'Neill, 2012; Kim et al., 2013; Mwangi et al., 2013; Pozzi et al., 2012). This is further supported by the genetically amenable experimental design demonstrated in this study.

SH1000, a lab strain expressing *mecA* under its native promoter on plasmid pRB474 produced low-level oxacillin resistance as predicted. Oxacillin sensitivity for SH1000 p*mecA* (MIC 0.25 µg/ml) transductants revealed similar observations to previously described studies (Pozzi et al., 2012; Ryffel et al., 1994), this expression of low-level resistance is similar to parental SH1000 (MSSA) strains as well as most MRSA strains. This observation suggests variations in basal resistance due to the background of the strains. Resistance to a high-level of oxacillin was obtained upon exposure to an antibiotic gradient plate containing 5 µg/ml methicillin suggesting a small increment in methicillin exposure is sufficient for the selection of high-level oxacillin resistance up to ≥256 µg/ml similar to that of clinical MRSA isolates containing SCC*mec* determinant in the chromosome (Finan et al., 2002). The selection of high-level resistance developed in the presence of *mecA* alone, without the additional *mec*-associated SCC element. Therefore, we can rule out any role of SCC*mec* in leading to high-level resistance. In addition, highly resistant mutants retained a high-level resistance phenotype under drug-free growth conditions once selected. Removal of pRB474 p*mecA* from one of the highly resistant mutant restored susceptibility to oxacillin similar to parental SH1000 confirming *mecA* as a prerequisite for conferring high-level resistance. When pRB474 p*mecA* was

reintroduced into cured methicillin sensitive (formerly highly resistant) strains, this restored high-level resistance phenotype without further training on antibiotic concentration gradient. Therefore, *mecA* alone cannot promote high-level resistance. These observations indicate that a genetic determinant(s) reside in the chromosomal genetic background of bacteria which define the level of oxacillin resistance.

It is interesting that the development of high-level methicillin resistance is a consequence of genetic rearrangement(s) in the chromosome. Once a chromosomal mutation is selected in a strain expressing high-level resistance, *mecA* could be removed and reintroduced resulting in immediate high-level resistance to oxacillin. Therefore, the genetic modification of the chromosome was confirmed to be responsible for the high-level resistance as if the *mecA* was removed from a highly resistant strain, it became low-level resistant and reintroduction of the *mecA* led to concomitant high-level resistance without the need for training.

Whole genome sequencing identified a number of amino acid substitutions in the recently identified SAOUHSC_00015, *gdpP* (GGDEF domain protein containing phosphodiesterase) gene in five out of six highly resistant strains (Table 3.2 and Figure 3.5). This observation is consistent with the previously described studies in which disruption of the *gdpP* gene supports expression of high-level β-lactam resistance (Griffiths and O'Neill, 2012). However, its role in producing high methicillin resistance is yet to be studied. *S. aureus* GdpP, a membrane located signalling protein was recently characterised by Corrigan et al., 2011 and shown to have an *in vitro* cyclic dinucleotide, c-di-AMP phosphodiesterase activity. GdpP contains two N-terminal transmembrane domains, a PAS sensory domain, a GGDEF domain, a DHH domain and a DHH-associated DHHA1 domain (Figure 3.5). The GGDEF domain is capable of synthesising c-di-GMP nucleotide messenger however *S. aureus* GdpP lacks critical residues for catalysing cyclic diguanylate (Griffiths and O'Neill, 2012). The closest homologue of *S. aureus* GdpP protein is the *Bacillus subtilis* YybT protein, recently shown to have a strong phosphodiesterase activity mediated by DHH/DHHA1 domains (Rao et al.,

2010). The C-terminal DHH/DHHA1 domains of *S. aureus* GdpP possess phosphodiesterase activity therefore mediates hydrolysis of c-di-AMP (Griffiths and O'Neill, 2012; Rao et al., 2010).

c-di-AMP is a novel secondary messenger molecule synthesised by DacA and broken down to phosphadenylyl-adenosine (pApA) by GdpP in *S. aureus* as shown in Figure 3.7 (Corrigan and Gründling, 2013). *B. subtilis* possess three diadenylate cyclase (DAC) domain containing proteins (Witte et al., 2008), compared to only one in *S. aureus* (Dengler et al., 2013). The *dacA* is often found in an operon containing YbbR sensory domain protein (Figure 3.8) which physically interacts with DacA and stimulates cyclase activity (Corrigan and Gründling, 2013; Dengler et al., 2013). However, deletion of *ybbR* do not affect oxacillin resistance or c-di-AMP levels in *S. aureus* (Bowman et al., 2016). The *dacA* operon also contain the phosphoglucosamine mutase encoding gene (*glmM*), GlmM is involved in peptidoglycan biosynthesis, which suggests a link between the expression of the three-gene (*dacA-ybbR-glmM*) operon and levels of c-di-AMP resulting in concomitant cell wall structures and homeostasis (Corrigan and Gründling, 2013).

c-di-AMP has already been characterised in *Listeria monocytogenes* and shown to be involved in a range of cellular processes such as immunogenicity and sensing DNA damage (Corrigan and Gründling, 2013; Woodward et al., 2010). Corrigan et al., 2011 showed that disruption of *gdpP* leads to increased levels of intracellular c-di-AMP that is capable of changing cell wall properties resulting into increased resistance to cell wall targeting antibiotics such as oxacillin in a lipoteichoic acid (LTA) negative strain. Taking this into consideration, it seems possible that increased resistance is due to elevated levels of intracellular c-di-AMP due to GdpP being inactivated. However, levels of c-di-AMP have not been measured in highly resistant mutants studied in this work. Previous study by Dengler et al., (2013) showed that an MRSA carrying a naturally acquired mutation in *dacA* gene resulted in a small decrease in the levels of intracellular c-di-AMP, which, however had a pronounced effect on oxacillin resistance as the *dacA*

mutant became heterogeneously resistant from being homogeneously resistant and the MIC decreased from >256 µg/ml to 64 µg/ml. The cellular levels of c-di-AMP have been shown to have a direct influence on cell envelope characteristics. In the *gdpP* mutant strain with increased intracellular c-di-AMP, a highly cross-linked peptidoglycan structure was observed (Corrigan et al., 2011). This could be potentially linked with increased resistance to oxacillin by strengthening the cell wall. However, this remains to be confirmed.

So far, four c-di-AMP target proteins have been identified in *S. aureus* (Figure 3.8 A); KtrA (SAOUHSC_01034), the potassium transporter-gating component; CpaA (SAOUHSC_00946), a predicted proton/cation antiporter; PstA (SAOUHSC_00456), a P-ll like signal transduction protein; and KdpD (SAOUHSC_2314), a phosphate regulon sensor kinase (Corrigan and Gründling, 2013; Corrigan et al., 2013). Three of these proteins (KdpD, KtrA and CpaA) are implicated in potassium transport system which provides a link between c-di-AMP and ion transport (Corrigan et al., 2013). Very recently, OpuCA (SAOUHSC_02744), an ATPase component of the carnitine ABC transporter, was identified as c-di-AMP receptor protein (Schuster et al., 2016). However, individually, none of these genes have shown to be essential (Campeotto et al., 2015; Corrigan et al., 2013; Fey et al., 2013; Moscoso et al., 2016; Schuster et al., 2016). The varying cellular levels of c-di-AMP is implicated in an altered ability for potassium ion transport (Corrigan et al., 2013) which plays major role in maintaining cell physiology by regulating membrane potential and osmotic tolerance (Gries et al., 2013).

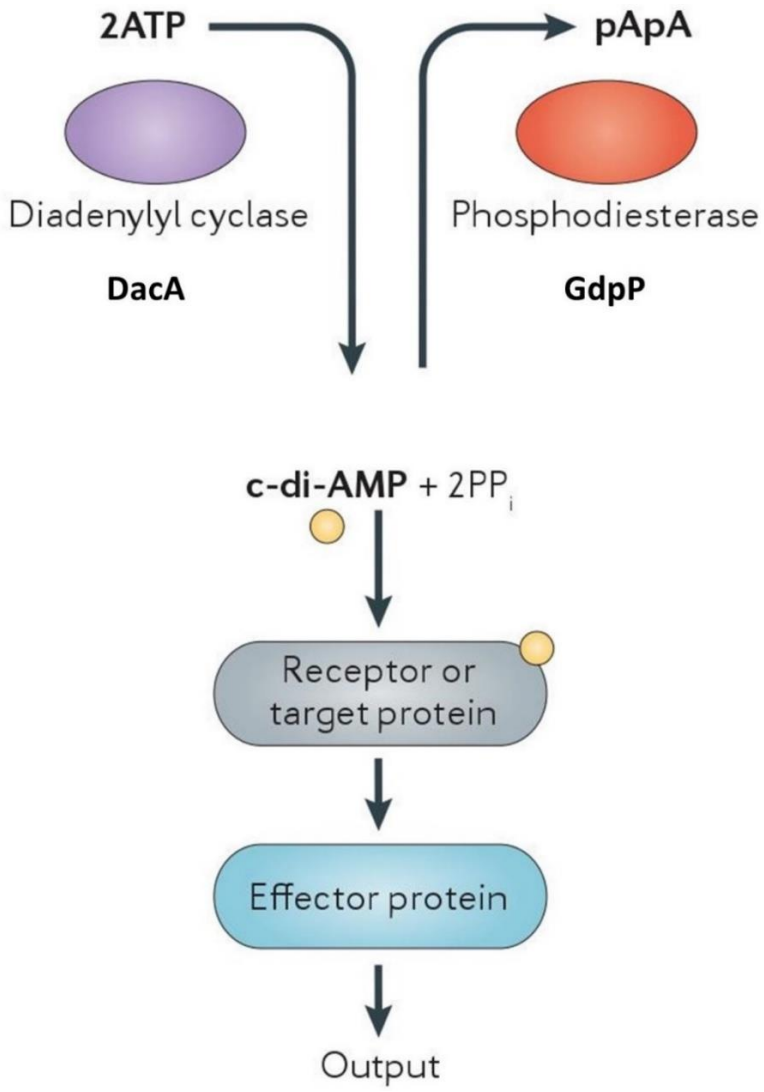

Figure 3.7 Synthesis and hydrolysis of c-di-AMP in *S. aureus*.

c-di-AMP is synthesised by diadenylyl cyclase (Dac) enzymes using two ATP molecules. Phosphodiesterases (PDEs) breaks down c-di-AMP into pApA. GdpP is the only characterised PDE containing GGDEF domain. It has been speculated that c-di-AMP bind to the specific receptor proteins which affect the activity of effector proteins, resulting into a regulation of specific cellular pathways. PP_i, inorganic pyrophosphate. Adapted from (Corrigan and Gründling, 2013).

Gries et al., (2013) demonstrated that cells lacking a functional Ktr potassium uptake system showed increased membrane potential resulting in increased susceptibility to aminoglycosides and cationic antibiotics, thereby altered cellular c-di-AMP levels exhibited an important role in regulating potassium uptake and concomitant membrane potential (Zeden et al., 2018). The *gdpP* mutant (Corrigan et al., 2011) with increased intracellular c-di-AMP showed increase membrane potential whereas, the *dacA* mutant (Bowman et al., 2016) with reduced intracellular c-di-AMP showed a reduced membrane potential (Zeden et al., 2018). Besides, the *dacA* mutant (Zeden et al., 2018) strain completely lacking cellular c-di-AMP found to have reduced oxacillin MIC, indicating the importance of an adequate membrane potential to produce high-level antibiotic resistance.

In an effort to understand β-lactam tolerance in *S. aureus*, Griffiths and O'Neill, (2012) studied the impact of inactivated *gdpP* by truncation of the DHH domain. This resulted in a completely abolished catalytic activity of the phosphodiesterase activity of DHH motif. In addition, disruption of the GGDEF motif alone was also enough to confer high-level oxacillin resistance. Therefore, strains missing both catalytic activity of GGDEF and DHH motif are highly oxacillin resistant. However, in the current study, the identified substitutions of GdpP are distributed covering most regions of the protein including an inter-domain sequence. Therefore, it appears that the disruption of GdpP supports high-level β-lactam resistance possibly as a result of misfolding or destabilisation of the protein. Consequently, loss of activity of GdpP protects *S. aureus* from β-lactams.

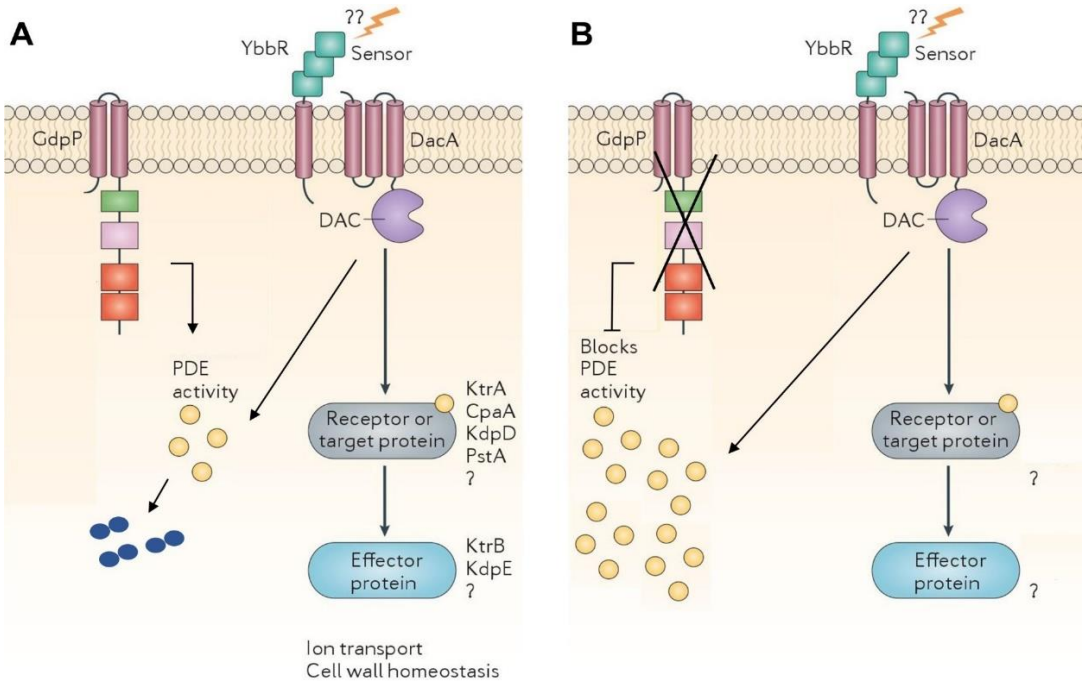

Figure 3.8 The c-di-AMP signalling network in *S. aureus*

A) In *S. aureus*, environmental changes (yellow lightning bolt) are sensed by YbbR or yet-unidentified mechanisms. YbbR interacts with the DacA protein, influencing the cyclase activity to synthesise c-di-AMP (yellow circles) from ATP. c-di-AMP binds to recently identified receptor proteins (KtrA, CpaA, KdpD, PtsA, OpuCA) potassium uptake system (Corrigan et al., 2013; Schuster et al., 2016). This affects the activity of effector proteins directly or indirectly. Phosphodiesterase (PDE) activity of GdpP protein hydrolyses c-di-AMP into 5' -pApA, resulting in maintenance of cellular c-di-AMP levels (Corrigan and Gründling, 2013; Corrigan et al., 2011). Modified from (Corrigan and Gründling, 2013; Corrigan et al., 2011). Blue solid circles denotes 5' pApA.
B) It is speculated that the highly resistant SH1000 p*mecA* (SJF4981) derivatives containing mutated *gdpP* are unable to hydrolyse c-di-AMP, resulting into accumulation of intracellular c-di-AMP levels affecting the activity of yet unknown receptor protein directly or indirectly to produce high-level oxacillin resistance. Modified from (Corrigan and Gründling, 2013; Corrigan et al., 2011).

To better understand the role of lack of GdpP activity supporting high-level resistance, a marked *gdpP* mutation was transduced into SH1000 p*mecA*. The resultant *gdpP* deletion strain exhibited high-level oxacillin resistance.

However, interestingly no *gdpP* SNP was identified in one (SH1000 p*mecA* TIR1/SJF4986) of the six highly resistant derivatives selected. The mutation was amino acid substitution at residue 54 of SAOUHSC_01812. Bioinformatics analysis of SAOUHSC_01812, a hypothetical protein revealed to possess a putative DHH/DHHA1 motif, characteristic of phosphodiesterases (Pde) and its activity is essential for maintaining intracellular c-di-AMP levels. Recently, the function of SAUSA300_1650 (Pde2), DHH/DHHA1 domain protein; an orthologue of SAOUHSC_01812 has recently been assessed by using a strain lacking the *pde2* gene (Bowman et al., 2016). Bowman et al., (2016) demonstrated that Pde2 can hydrolyses c-di-AMP and pApA to AMP but preferentially hydrolyses pApA to AMP over c-di-AMP. Therefore, similar to the *gdpP* mutant, the *pde2* mutant leads to accumulation of pApA and increased cellular c-di-AMP levels which has shown to be associated with increased oxacillin resistance (Bowman et al., 2016). This observation suggests that the SAOUHSC_01812 contributes to c-di-AMP metabolism and oxacillin resistance.

Moreover, there were six other mutations identified in SH1000 p*mecA* derived strains (Table 3.2) accompanying low-level and high-level resistance to oxacillin. These mutations were discarded as it is likely that these mutations arose due to passaging to construct highly resistant derivative.

Several recent studies described a connection between cellular c-di-AMP levels and the composition of bacterial cell wall. For instance, Corrigan et al., 2011 showed 15-fold increase in cellular c-di-AMP caused by inactivation of *gdpP* allowed a *S. aureus* mutant lacking the essential cell wall polymer, LTA to grow normally. This phenotype was accompanied by a reduced cell size with increased c-di-AMP level. Mutated *gdpP* in *S. aureus*, *B. subtilis* and *L. monocytogenes* leads to increased β-lactam resistance (Banerjee et al., 2010; Corrigan et al., 2011; Griffiths and O'Neill, 2012; Luo and Helmann, 2012; Pozzi et al., 2012; Witte et al., 2013). This evidence further supports

the hypothesis of significant physiological changes occur due to accumulation of intracellular c-di-AMP. Overproduction of GdpP decreases c-di-AMP levels in *B. subtilis* and *L. monocytogenes* and restores sensitivity to cell-wall targeting antibiotics (Luo and Helmann, 2012; Witte et al., 2013).

Together, these data suggest that the transition from low-level to high-level methicillin resistance is associated with c-di-AMP levels by regulating cell wall synthesis and allowing cells to cope with membrane and cell-wall damage upon exposure to β-lactam antibiotics. Overall, these results underscore the potential role of *gdpP* in β-lactam resistance in *S. aureus*. Further work is required to investigate the role of c-di-AMP and target genes contributing to cell wall homeostasis.

Chapter 4

Expression of high-level methicillin resistance using single copy chromosomal *mecA*

4.1 Introduction

Since the discovery of first clinical MRSA isolate in 1960 in England (Jevons, 1961), MRSA has become resistant to nearly all available β-lactam (methicillin, nafcillin, dicloxacillin oxacillin, etc.) and cephalosporin antibiotics (Katayama et al., 2000). Soon after the occurrence of resistance, various hospital-acquired MRSA (HA-MRSA) and community-acquired MRSA (CA-MRSA) were found disseminated worldwide (Rice, 2006). In addition, MRSA has a remarkable ability to acquire resistance to other classes of antibiotics such as, vancomycin – an antibiotic of last resort, tetracyclines, macrolides, quinolones and aminoglycosides (Hiramatsu et al., 1997a; Tenover et al., 1998). The appearance of vancomycin-intermediate (VISA) strains is thought to be due to an increased cell wall thickness, resulting into restricted access of vancomycin to its target (Howden et al., 2010). Whereas, the molecular basis of methicillin resistance in *S. aureus* is yet to be studied. Currently, key areas of methicillin resistance research include; the evolution of resistance and the effects of genetic factors to the physiology of MRSA.

The first step for the development of methicillin resistance is the acquisition of *mecA* via a mobile genetic element – staphylococcal cassette chromosome *mec* (SCC*mec*), integrated into the chromosome of an MSSA strain (Hiramatsu, 1995). The composition of SCC*mec* is highly diverse in MRSA (Berglund et al., 2008; Liu et al., 2016a) and its integration into the chromosome is driven by site-specific recombinases, *ccrA* and *ccrB* (Katayama et al., 2000). SCC*mec* possess three basic genetic elements: the *mec* gene complex, the *ccr* gene complex, insertion sequences (IS) and the junk regions (J region) (Berglund et al., 2008; Liu et al., 2016a). Other than *mecA*, the *mec* gene complex carries *mecA* regulatory genes, *mecR1* – encoding the signal transducer protein MecR1 and *mecI* – encoding the

repressor protein MecI (Archer and Bosilevac, 2001). Based on high diversity in the structural organisation and the integrity of genetic content of SCC*mec* elements, they are currently classified into type I to XI and further classified into different subtypes (Ito et al., 2009; Liu et al., 2016a).

The *mecA* gene encodes for a non-native penicillin binding protein (PBP2A), a transpeptidase involved in cell wall biosynthesis (Brown and Reynolds, 1980; Hartman and Tomasz, 1986). Native PBPs (PBP1, PBP2, PBP3 and PBP4) of *S. aureus* are involved in final assembly of peptidoglycan synthesis but have higher affinity for β-lactam antibiotics (Tipper and Strominger, 1965). Unlike, native PBPs of *S. aureus*, PBP2A has low affinity for β-lactam antibiotics and therefore in the presence of antibiotics, it takes over the transpeptidase activities of conventional PBPs and cell can continue to grow (Lim and Strynadka, 2002). Even though PBP2A takes over transpeptidase activities of native PBPs, previous experiments indicated that transglycosylase activity of PBP2 is required for the expression of methicillin resistance (Pinho et al., 2001b), suggesting that cell wall synthesis is coordinated via convoluted interactions between PBPs.

Most MRSA strains carry intact regulatory genes, *mecI* and *mecR1*, resulting into strong repression of *mecA* (Kuwahara-Arai et al., 1996), however truncated *mecI* and *mecR1* results into constitutive expression of *mecA* (Katayama et al., 2001). While *mecA* is essential for methicillin resistance, the majority of MRSA strains only exhibit low-level resistance (MIC = 2-4 µg/ml) (Ryffel et al., 1994) however these cells are capable of developing uniform high-level resistance upon exposure to antibiotics (Finan et al., 2002; Sabath and Wallace, 1971; Tomasz et al., 1991). This indicates that acquisition of *mecA* alone cannot impart high-level resistance. It is not necessary for the production of PBP2A to increase substantially for the expression of high-level resistance, even when it is constitutively expressed (Hartman and Tomasz, 1986). Therefore, the quantity of PBP2A does not correlate with the variable levels of resistance, indicating other genetic determinants other than PBP2A must be responsible for conferring high-level resistance (Hartman and Tomasz, 1986).

Early research of transposon mutant libraries identified a range of *fem* (factors essential for methicillin resistance) genes and *aux* (auxiliary factors) that are unlinked to *mecA* but are linked to influence methicillin resistance (Berger-Bächi and Rohrer, 2002; Berger-Bächi et al., 1992; De Lencastre and Tomasz, 1994). Many of *fem* genes are directly or indirectly involved in peptidoglycan biosynthesis or regulatory processes (Berger-Bächi and Rohrer, 2002). However, the mechanistic insights of high-level resistance remain to be studied.

4.1.1 Aims of the chapter

The overall aim of this chapter was to construct a high-level methicillin resistant strain in the genetically amenable background, SH1000 with chromosomal expression of *mecA* under its native promoter. Using super resolution microscopy approaches to study the subcellular localisation and dynamics of PBP2A. The specific aims of this chapter were to:

i. Construction of genetically amenable MRSA strain using well defined lab strain SH1000
ii. Experimental evolution of MRSA derivatives and isolation of highly resistant MRSA mutants
iii. Determine the molecular basis of high-level oxacillin resistance

4.2 Results

4.2.1 Construction of a genetically amenable MRSA train

Previous studies have demonstrated the importance of compensatory mutations acquired by the genetic background in leading to high-level resistance. These studies were conducted using plasmid-borne *mecA* expression.

In order to investigate the effect of a single copy *mecA* within SH1000 chromosome on antibiotic resistance, *mecA* and its native promoter was amplified using genomic DNA of COL strain as a template. For chromosomal integration of *mecA*, the suicide vector pMUTIN4 (Vagner et al., 1998) based pGM068 lysine insertion plasmid (McVicker et al., 2014) was used to integrate *mecA* under its own promoter (p*mecA*) downstream of the *lysA* gene. pGM068 contains a truncated 3' region of a *lysA* gene encoding the terminal enzyme of lysine biosynthesis pathway in *S. aureus*. This provides a region of homology with a chromosomal *lysA* gene which upon transformation in *S. aureus* results in recombination between 3' *lysA* of the plasmid and the chromosomal region. This created an insertional duplication providing erythromycin resistance without undesired disruption of *lysA* causing lysine auxotrophs. The gel purified p*mecA* was cloned into the BamHl /Sacl site of pGM068 using Gibson assembly resulting in pVP01-p*mecA* plasmid (Figure 4.1 A and C) and transformed into *E. coli* DH5α (NEB). Recombinant plasmids were isolated and tested by restriction enzyme digest with BamHl/Sacl site producing two bands 7669 bp and 2550 bp for linear pVP01 backbone and p*mecA*, respectively (Figure 4.1 C and D) and validated by DNA sequencing. The resulting plasmid pVP01-p*mecA* was electroporated into RN4220 resulting into RN4220 *lysA*::p*mecA* (SJF4994) and transduced into SH1000 creating SH1000 *lysA*::p*mecA* (SJF4996). The insert p*mecA* was amplified to confirm integration of the pVP01-p*mecA* into the chromosome (Figure 4.1 C). The correct insertion of plasmid at *lysA* locus was also confirmed by PCR using a forward primer residing in the chromosome and a reverse in p*mecA* insert generating a product of ~4000 bp, larger than p*mecA* (2550 bp) as predicted (Figure 4.1 E).

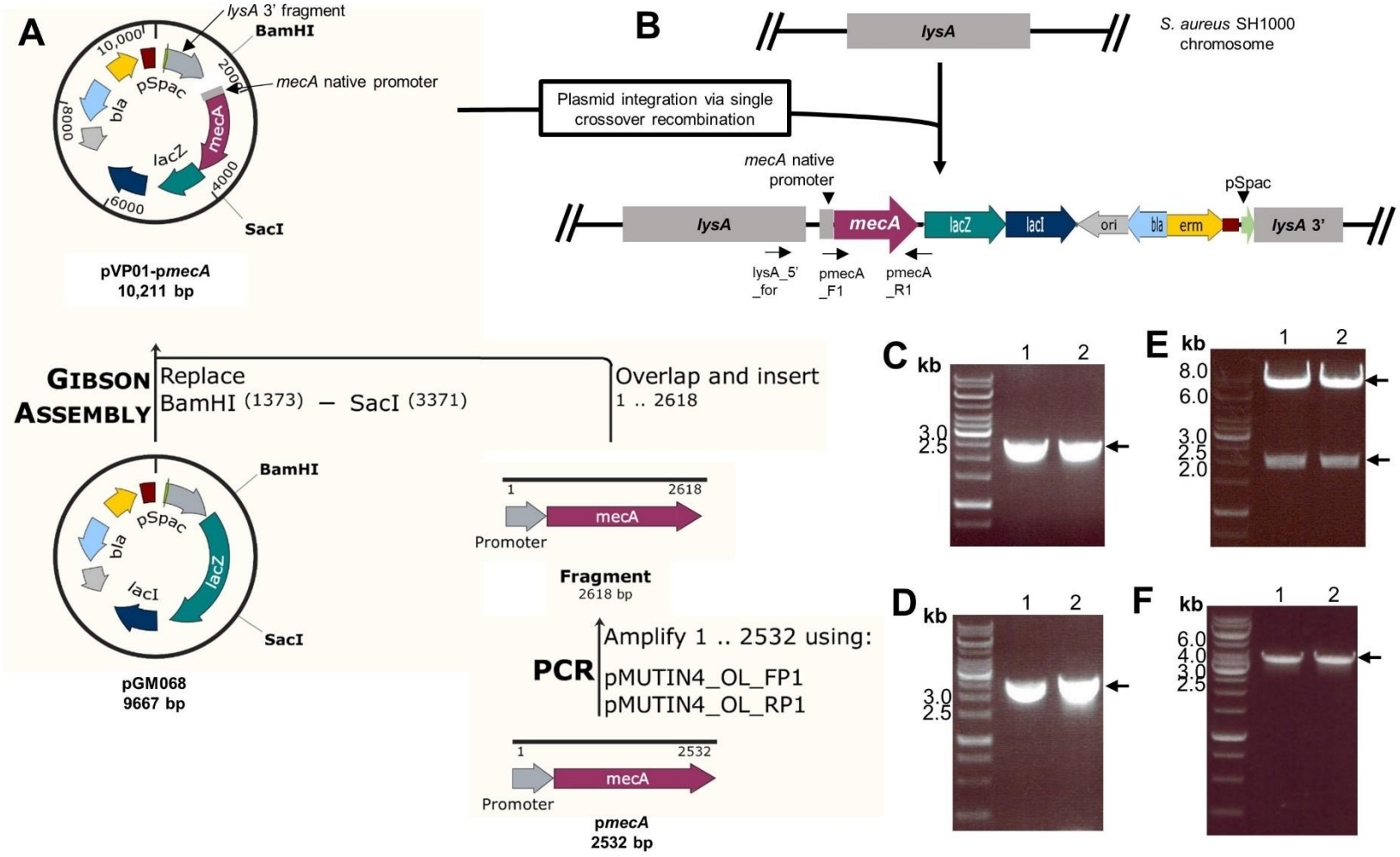

Figure 4.1 Construction of a chromosomal p*mecA* fusion in *S. aureus* SH1000

A) Diagrammatic illustration of pVP01-p*mecA* construction. A 2532 bp fragment including the *mecA* gene and its native promoter (p*mecA*) was PCR amplified from COL genomic DNA using pMUTIN4_OL_FP1 and pMUTIN4_OL_RP1. These primers were designed to regenerate restriction site BamHI/SacI. The pGM068 plasmid was linearised using BamHI/SacI restriction enzymes. The linearised plasmid backbone and PCR amplified p*mecA* fragments were joined by Gibson assembly, resulting into pVP01-p*mecA*.
B) Schematic overview of genomic region of *lysA* in SH1000 and post integration of pVP01-p*mecA* resulting into *lysA*::p*mecA* (SJF4996). Primer binding sites are shown with black arrows.
C) p*mecA* insert was amplified using overlapping primers pMUTIN4_OL_FP1 and pMUTIN4_OL_FR1 creating overhanging strands at both ends of the product. The expected band size of 2618 bp for p*mecA* insert is marked by black arrows (lane 1, 2). DNA fragments were used as size markers for agarose gel electrophoresis.
D) The insertion of p*mecA* fragment into pGM068 was verified by PCR using p*mecA*_F1 and p*mecA*_R1 primers resulting in 2550 bp product marked by a black arrow (lane 1, 2). DNA fragments were used as size markers for agarose gel electrophoresis.
E) pGM068 was digested with BamHI and SacI enzymes resulting in 7669 bp linear vector backbone and an addition fragment of 1998 bp marked with black arrows (lane 1, 2). DNA fragments were used as size markers for agarose gel electrophoresis.
F) The chromosomal integration of pVP01-p*mecA* was verified by using forward primer lysA_5'_for and p*mecA*_R1 resulting in a product of ~4000 bp marked by a black arrow (lane 1, 2). DNA fragments were used as size markers for agarose gel electrophoresis.

4.2.1.1 Detection of oxacillin susceptibility of SH1000 *lysA*::p*mecA*

The oxacillin MIC by Etest method was compared for SH1000 and its derived SH1000 *lysA*::p*mecA* (SJF4996). As shown in section 3.2.1, SH1000 is susceptible to oxacillin (MIC 0.12 µg/ml) whereas SH1000 *lysA*::p*mecA* (SJF4996) expresses low-level resistance to oxacillin with an MIC of 2 µg/ml (Figure 4.2), similar to most clinical isolates of MRSA with borderline or heterogeneous resistance (Gerberding et al., 1991; Varaldo et al., 1993). This confirms the introduction of functional single copy expression of chromosomal integrated *mecA* at *lysA* locus of SH1000 *lysA*::p*mecA* (SJF4996). The insertion of *mecA* further verified by PCR (Figure 4.1 F).

4.2.1.2 Isolation of highly oxacillin resistant derivatives of SH1000 *mecA*

The SH1000 *lysA*::p*mecA* (SJF4996) strain was trained to produce high-level resistance to oxacillin using antibiotic gradient plate technique as described in section 3.2.1.1 and Figure 3.2 A. A heavy suspension of SH1000 *lysA*::p*mecA* (SJF4996) was streaked over the surface of the agar containing 0-5 µg/ml methicillin gradient (Figure 4.3 B). Only resistant cells were able to grow towards the region with highest concentration of methicillin.

From this initial screening, a total of eight spontaneous mutants were selected (Figure 4.3 B). Subsequent (trained) mutants exhibited variable levels of resistance to oxacillin, with MICs ranging from 2 to ≥256 µg/ml (Figure 4.4). Oxacillin susceptibility testing was carried out by using the Etest method. Similar to the results obtained in section 3.2.1.1, progression of resistance was achieved in experimentally evolved strains. Four isolates (SH1000 *lysA*::p*mecA* -TI1, SJF4998; SH1000 *lysA*::p*mecA* -TI2, SJF4999; SH1000 *lysA*::p*mecA* -TI3, SJF5001; SH1000 *lysA*::p*mecA* -TI4, SJF5002) exhibiting low-level (2-4 µg/ml) or intermediate level (<16 µg/ml) resistance were picked (Figure 4.4 and Table 4.1). Four isolates (SH1000 *lysA*::p*mecA* -TR1, SJF5000; SH1000 *lysA*::p*mecA* -TR2, SJF5003; SH1000 *lysA*::p*mecA* -TR3, SJF5004; SH1000 *lysA*::p*mecA* -TR4, SJF5005) exhibiting high-level

(≥256 µg/ml) resistance were also found from the first screen (Figure 4.4 and Table 4.1). SH1000 *lysA*::p*mecA* -TI1 (SJF4998) was further trained on a methicillin gradient plate supplied with 20 µg/ml methicillin to select for isolates with increased resistance with an MIC of ≥256 µg/ml (oxacillin). The resultant trained-intermediate-to-resistant strains were SH1000 *lysA*::p*mecA* -TIR1 (SJF5006), SH1000 *lysA*::p*mecA* -TIR2 (SJF5007) and SH1000 *lysA*::p*mecA* -TIR3 (SJF5007) with oxacillin MIC of ≥256 µg/ml (Table 4.1). This methodology allowed the detection of the progression of resistance for each strain.

The evolutionary lineage of SH1000 to SH1000 *lysA*::p*mecA* for all derived representative strains is shown in Figure 4.4 along with oxacillin MIC (Table 4.1).

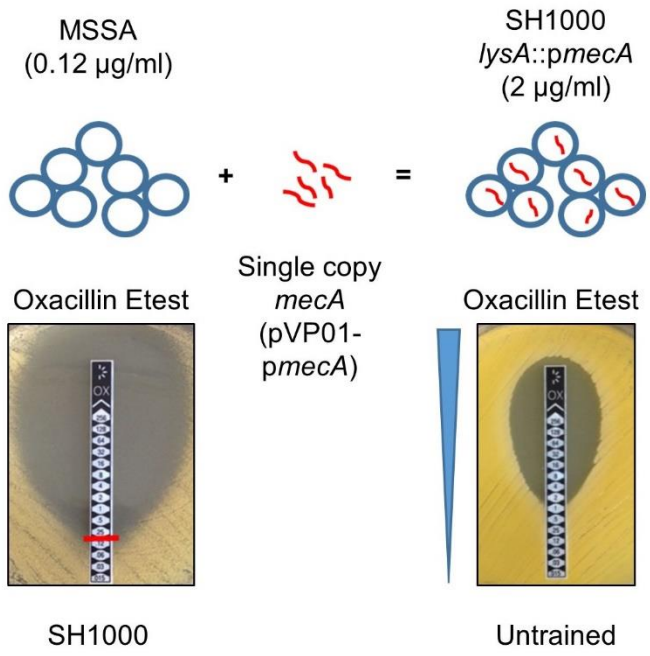

Figure 4.2 Construction and oxacillin MIC of SH1000 and SJF4996

Oxacillin MICs for both strains are listed in brackets.

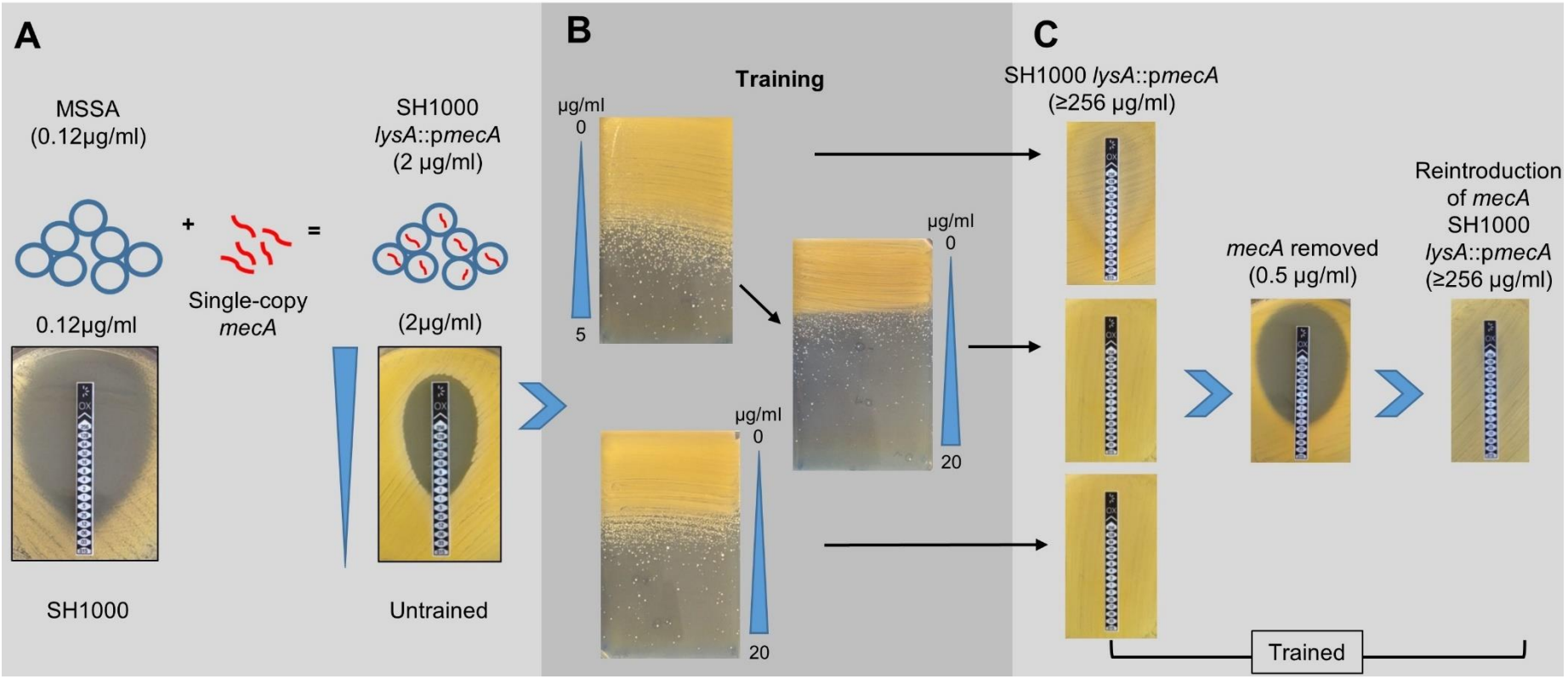

Figure 4.3 Scheme of high-level MRSA construction using single copy chromosomal insertion of *mecA* and subsequent strain evolution

A) SH1000 *lysA*::p*mecA* (SJF4996) construct was produced by transduction from RN4220 *lysA*::p*mecA* (SJF4994). This led to single copy *mecA* at the *lysA* locus with *mecA* expressed under its native promoter. Oxacillin MICs shown in brackets were measured using the Etest strip.
B) Subsequently, spontaneous mutants exhibiting oxacillin resistance were selected using a gradient plate containing either 0-5 or 0-20 µg/ml of methicillin. Strains with low-level resistance were further trained using an antibiotic gradient plate containing 0-20 µg/ml methicillin to select high-level resistance.
C) The Etest strips revealed high-level oxacillin resistance which could be cured by removal of *mecA* and restored via subsequent reintroduction of *mecA* at *lysA* locus.

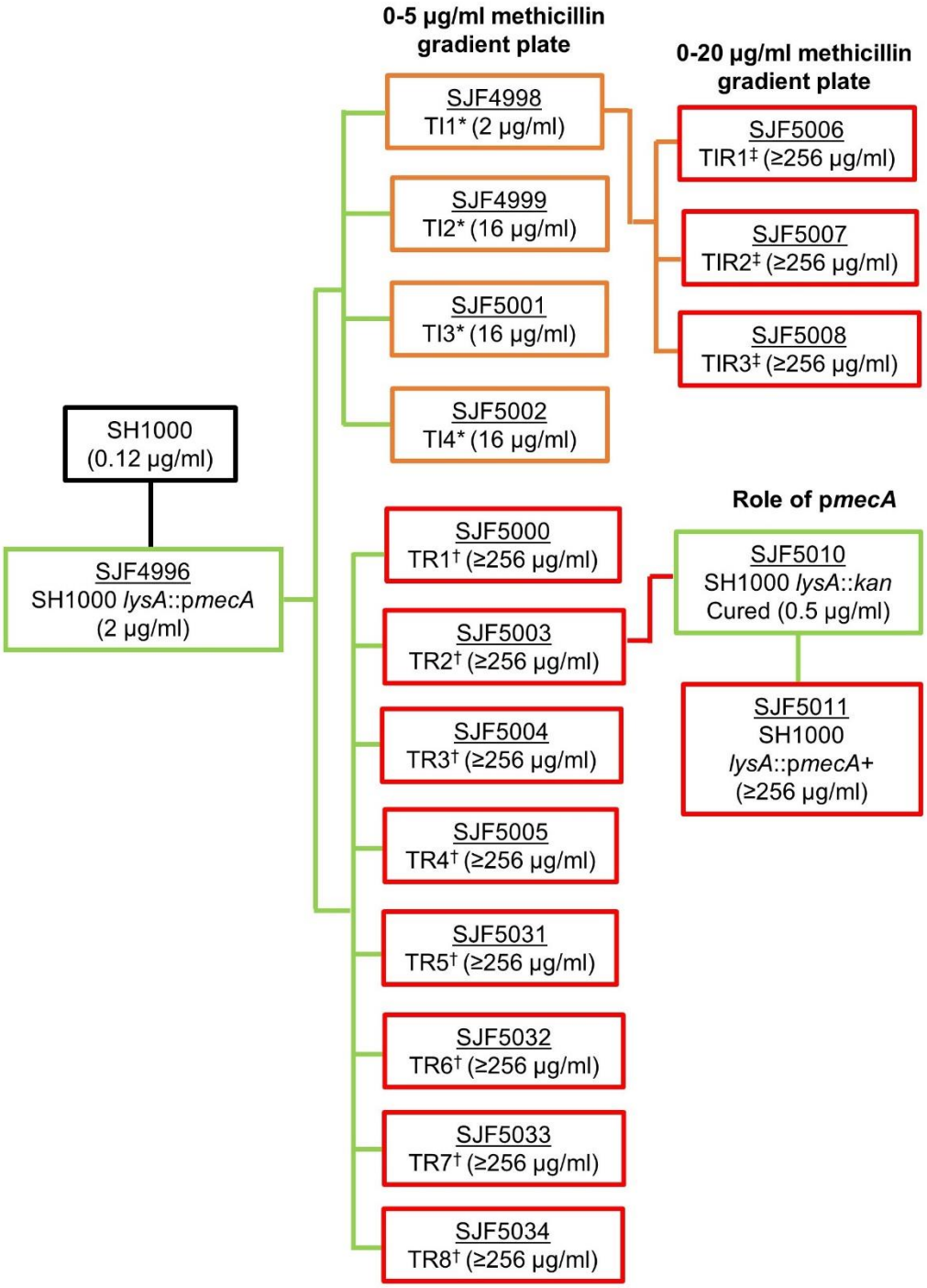

Figure 4.4 Lineage of SH1000 showing progression of methicillin resistance

Oxacillin MICs are listed in brackets for all strains. *, denotes isolates expressing intermediate oxacillin resistance (TI – trained-intermediate) listed in orange boxes; †, denotes isolates expressing high-level oxacillin resistance (TR – trained-resistant) listed in red boxes; ‡, denotes isolates expressing high-level oxacillin resistance following selection on 0-20 µg/ml methicillin gradient plate using TI1 strain (TIR – trained-intermediate to resistant) also listed in red boxes. Further description of the strains is in Table 4.1.

Strain	Gradient plate	Oxacillin MIC
SH1000		0.12 µg/ml
Parental strain SH1000		
SH1000 *lysA*::p*mecA* (SJF4996)		2 µg/ml
Parental strain SH1000 *lysA*::p*mecA* (SJF4996)		
SH1000 *lysA*::p*mecA* -TI1* (SJF4998)	0.5 µg/ml methicillin	2 µg/ml
SH1000 *lysA*::p*mecA* -TI2* (SJF4999)	0.5 µg/ml methicillin	16 µg/ml
SH1000 *lysA*::p*mecA* -TI3* (SJF5001)	0.5 µg/ml methicillin	16 µg/ml
SH1000 *lysA*::p*mecA* -TI4* (SJF5002)	0-20 µg/ml methicillin	16 µg/ml
Parental strain SH1000 *lysA*::p*mecA* -TI1 (SJF4998)		
SH1000 *lysA*::p*mecA* -TIR1‡ (SJF5006)	0-20 µg/ml methicillin	≥256 µg/ml
SH1000 *lysA*::p*mecA* -TIR2‡ (SJF5007)	0-20 µg/ml methicillin	≥256 µg/ml
SH1000 *lysA*::p*mecA* -TIR3‡ (SJF5008)	0-20 µg/ml methicillin	≥256 µg/ml
Parental strain SH1000 *lysA*::p*mecA* (SJF4996)		
SH1000 *lysA*::p*mecA* -TR1† (SJF5000)	0.5 µg/ml methicillin	≥256 µg/ml
SH1000 *lysA*::p*mecA* -TR2† (SJF5003)	0-20 µg/ml methicillin	≥256 µg/ml
SH1000 *lysA*::p*mecA* -TR3† (SJF5004)	0-20 µg/ml methicillin	≥256 µg/ml
SH1000 *lysA*::p*mecA* -TR4† (SJF5005)	0-20 µg/ml methicillin	≥256 µg/ml
Parental strain SH1000 *lysA*::p*mecA* (SJF4996)		
SH1000 *lysA*::p*mecA* -TR5† (SJF5031)	0.5 µg/ml methicillin	≥256 µg/ml
SH1000 *lysA*::p*mecA* -TR6† (SJF5032)	0.5 µg/ml methicillin	≥256 µg/ml
SH1000 *lysA*::p*mecA* -TR7† (SJF5033)	0.5 µg/ml methicillin	≥256 µg/ml
SH1000 *lysA*::p*mecA* -TR4† (SJF5034)	0.5 µg/ml methicillin	≥256 µg/ml
Parental strain SH1000 *lysA*::p*mecA* -TR2† (SJF5003)		
SH1000 *lysA::kan* cured (SJF5010)		0.5 µg/ml
Parental strain SH1000 *lysA::kan* cured (SJF5010)		
SH1000 *lysA*::p*mecA*+ (SJF5011)		≥256 µg/ml

Table 4.1 List of representative strains

*, denotes isolates expressing intermediate oxacillin resistance (TI – trained-intermediate); †, denotes isolates expressing high-level oxacillin resistance (TR – trained-resistant); ‡, denotes isolates expressing high-level oxacillin resistance (TIR – trained-intermediate to resistant.

4.2.1.3 Removal of a single copy chromosomal *mecA*

The vast differences in the level of oxacillin resistance obtained in SH1000 *lysA*::p*mecA* (SJF4996) trained derivatives (Figure 4.4 and Table 4.1) is similar to clinical MRSA isolates; this could not be simply due to the level of expression of *mecA* (Hartman and Tomasz, 1986; Sieradzki et al., 2008). Therefore, it was hypothesised that excision of chromosomal *mecA* from one of the highly resistant strains would lead to restored oxacillin susceptibility identical to that of the parental strain SH1000 (oxacillin MIC = 0.12 µg/ml).

To address this, SH1000 *lysA*::p*mecA* -TR2 (SJF5003) with oxacillin MIC ≥256 µg/ml was selected for removal of chromosomally integrated p*mecA*. An empty pGM068 suicide vector with kanamycin marker was transduced into RN4220 strain resulting in RN4220 *lysA::kan* (SJF5009). SH1000 *lysA*::p*mecA* -TR2 (SJF5003) was transduced with Φ11 lysate from RN4220 *lysA::kan* (SJF5009) and transductants selected on BHI agar plate containing kanamycin (50 µg/ml). The resulting strain lost *mecA* to give SH1000 *lysA::kan* (SJF5010). The removal of *mecA* was confirmed by PCR to amplify *mecA* (Figure 4.5 A). The insertion of empty vector was further verified by PCR amplifying the kanamycin cassette (Figure 4.5 A). SH1000 *lysA::kan* (SJF5010) regained susceptibility to oxacillin (MIC 0.5 µg/ml) similar to that of the parental strain SH1000 (Figure 4.3 A, Figure 4.4 and Figure 4.5 A). These observations further strongly suggest that *mecA* is a prerequisite for developing high-level β-lactam resistance.

Reintroduction of pVP01-p*mecA* into *mecA* cured strain - SH1000 *lysA::kan* (SJF5010) by phage transduction using Φ11 lysate from SJF4994 (RN4220 *lysA*::p*mecA*) produced SH1000 *lysA*::p*mecA*+ (SJF5011). This strain produced high-level resistance to oxacillin indistinguishable from that of the original SH1000 *lysA*::p*mecA* -TR2 (SJF5003) (Figure 4.5 B). The chromosomal integration of *mecA* was confirmed by PCR to amplify *mecA* and oxacillin MIC was verified using an Etest for SH1000 *lysA*::p*mecA*+ (SJF5011) (Figure 4.5 B).

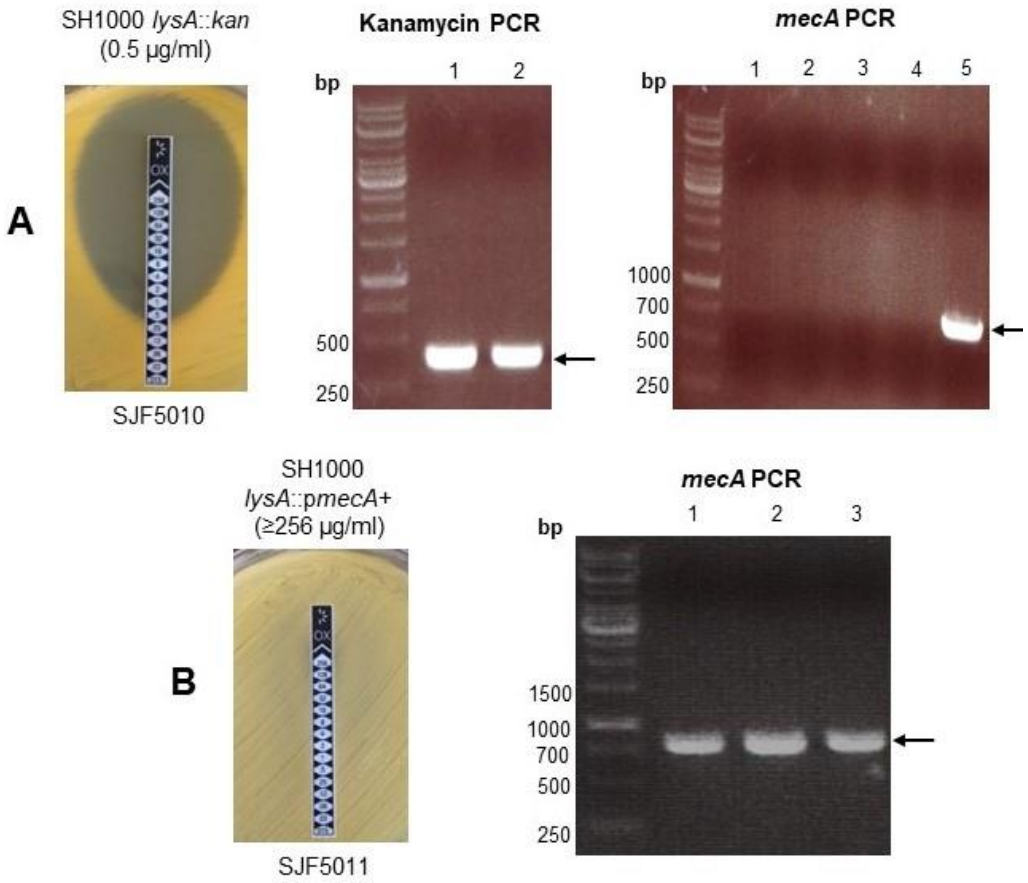

Figure 4.5 Removal and reintegration of *lysA*::p*mecA*

A) SH1000 *lysA*::p*mecA* -TR2 (SJF5003) was transduced with *lysA*::*kan* to replace *lysA*::p*mecA.* This resulted in oxacillin susceptible SH1000 *lysA*::*kan* (SJF5010). 1% (w/v) TAE agarose gel shows *kan* (lane 1, 2) with product size of 395 bp (marked by an arrow) using KanR_FW_For (Forward) and KanR_FW_Rev (Reverse) primers. SJF5010 showed no band for *mecA* (lane 1 to 4) using p*mecA*2_SeqF2 (forward) and p*mecA*2_SeqR1 (reverse) primers. *mecA* positive control using COL genomic DNA showed a product of 838 bp (lane 5). DNA fragments were used as size markers for agarose gel electrophoresis.
B) Subsequently, reintroduction of *lysA*::p*mecA* into SH1000 *lysA*::*kan* (SJF5010) resulted into SH1000 *lysA*::p*mecA*+ (SJF5011). This was confirmed by an oxacillin Etest and PCR to amplify *mecA* using p*mecA*2_SeqF2 (forward) and p*mecA*2_SeqR1 (reverse) primers. Oxacillin MICs are listed in brackets for both strains. DNA fragments were used as size markers for agarose gel electrophoresis.

4.2.1.4 Does *MecA* copy number affect oxacillin resistance level?

It is interesting to note that removal of *mecA* in both SJF4993 (SH1000 pRB474 p*mecA* cured) as described in section 3.2.1.2 (Figure 3.4 A); as well as SJF5010 (SH1000 *lysA*::*kan*), resulting in abolition of oxacillin resistance. Subsequently, reintroduction of multi copy pRB474-p*mecA* plasmid into SH1000 pRB474 p*mecA* cured (SJF4993) (Figure 3.4 B); and single copy chromosomal *mecA* reintroduction into SH1000 *lysA*::*kan* (SJF5010) background exhibited high-level oxacillin resistance upon acquisition of *mecA*. This led to a question as to whether reintroduction of plasmid borne *mecA* into the single copy cured strain (SJF5010) would result in high-level resistance to oxacillin, and vice versa?

SH1000 pRB474 p*mecA* cured (SJF4993 - multi copy *mecA* cured) background was transduced with a single copy *mecA* (pVP01-p*mecA*) resulting in SJF4997 (SH1000 pRB474-p*mecA*-cured *lysA*::p*mecA*), also SH1000 *lysA*::*kan* (SJF5010 - single copy *mecA* cured) was transduced with multi copy *mecA* (pRB474-p*mecA*) resulting in SJF5024 (SH1000 *lysA*::*kan* pRB474-p*mecA*) (Figure 4.6). Interestingly, SJF4997 (SH1000 pRB474-p*mecA*-cured *lysA*::p*mecA* developed only low-level resistance to oxacillin (MIC = 8 µg/ml; Figure 4.6 A) whereas, SJF5024 (SH1000 *lysA*::*kan* pRB474-p*mecA*) retained susceptibility to oxacillin (MIC = 0.5 µg/ml) similar to the parental strain SH1000 *lysA*::*kan* (SJF5010) (Figure 4.6 B).

Taken together, these results suggest that the development of high-level resistance is specific to the strain background. As a result, *mecA* cured backgrounds do not mutually support high-level resistance suggesting involvement of two independent mechanisms for conferring high-level resistance.

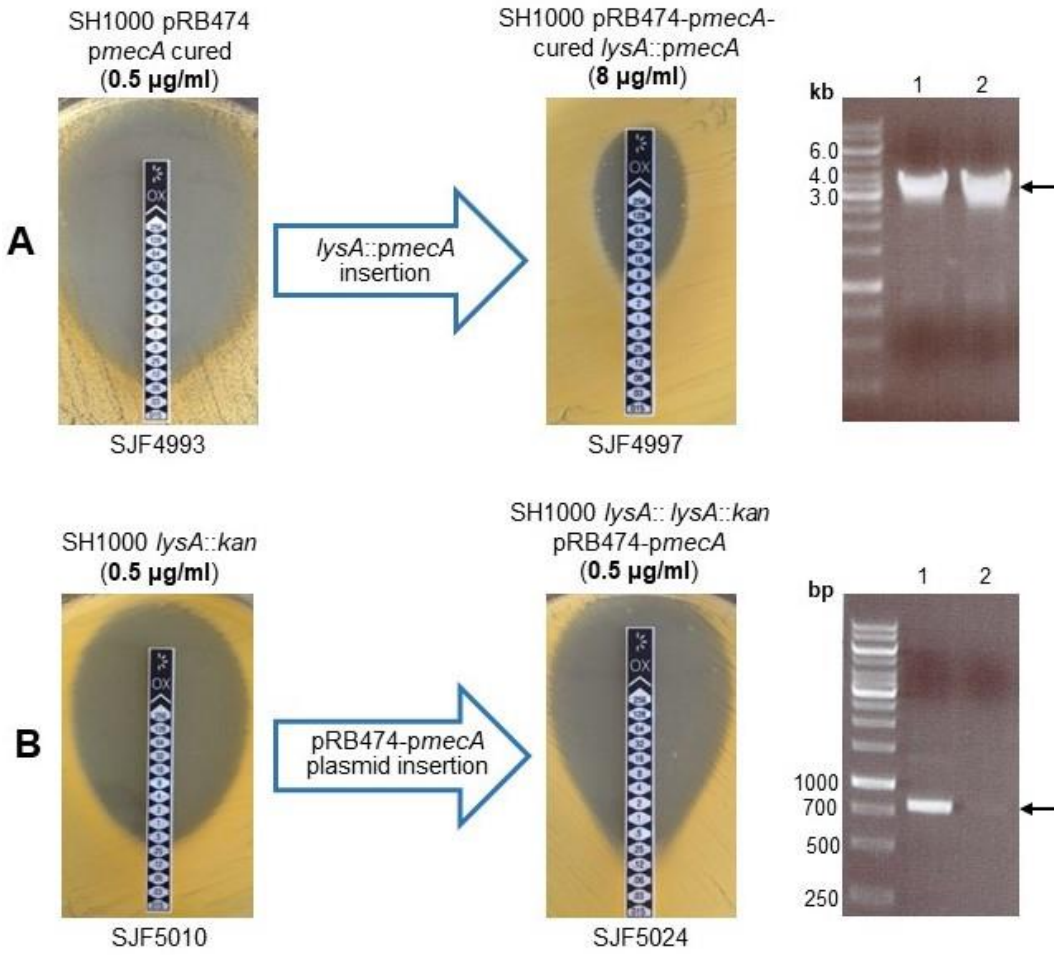

Figure 4.6 Reintroduction of *mecA* into p*mecA* cured backgrounds

A) SH1000 pRB474 p*mecA* cured (SJF4993) was transduced with RN4220 *lysA*::p*mecA* (SJF4994) phage lysate for chromosomal integration of *mecA* into the multicopy *mecA* cured background. 1% (w/v) TAE agarose gel shows *mecA* insertion at the *lysA* locus (lane 1, 2) with product size of ~4000 bp using lysA_5'_For (Forward) and p*mecA*_R1 (Reverse) primers. DNA fragments were used as size markers for agarose gel electrophoresis.
B) SH1000 *lysA::kan* (SJF5010) was transduced with multi copy pRB474-p*mecA* into the single copy *mecA* cured background (SJF5010). PCR amplification of *mecA* using p*mecA*2_SeqF2 (forward) and p*mecA*2_SeqR1 (reverse) primers verified *mecA* at 838 bp indicated with a black arrow. Oxacillin MICs are listed in brackets for all strains. DNA fragments were used as size markers for agarose gel electrophoresis.

4.2.1.5 Are *gdpP* mutations responsible for elevated antibiotic resistance in single copy *mecA* trained strains?

In order to investigate whether mutation of *gdpP* is involved in producing high-level resistance in SH1000 *lysA*::p*mecA* derivatives (Table 4.1), genomic DNA was isolated from these strains. The *gdpP* gene was amplified using primers VP62_F3 and VP63_R3 (see Figure 4.7 A for primer binding sites). The PCR products were purified using a GeneJET PCR purification kit (Thermo Fischer Scientific). Interestingly, DNA sequencing (GATC Biotech, Germany) revealed no alterations in *gdpP*.

The insertion of p*mecA* at *lysA* was also verified by gene sequencing (GATC Biotech, Germany). Genomic DNA was isolated from all SH1000 *lysA*::p*mecA* derivatives (Table 4.1) using primers p*mecA*2_seqF1 and p*mecA*2_seqR2 (see Figure 4.7 B for construct map). p*mecA* sequencing confirmed no alteration of *mecA* gene or its native promoter at the *lysA* locus.

4.2.2 Identification of chromosomal mutations in highly resistant strains

In order to identify compensatory mutation(s) in highly resistant SH1000 *lysA*::p*mecA* derivatives, full genomes of representative strains (listed in Figure 4.4 and Table 4.1) were sequenced using Illumina MiSeq and HiSeq 2500 platforms (MicrobesNG, University of Birmingham). Reads from strains were mapped to the fully sequenced reference genome of NCTC8325 (accession no. NC_007795.1). Variant calling was done using VarScan (MicrobesNG, University of Birmingham). A total of 93 mutations were identified. These included 5 frameshifts, 32 non-synonymous, 15 synonymous and 1 nonsense mutations. All identified mutations are listed in Appendix 1 Table 3 together with locus tag or gene name and mutation strength. From these, 73 identified mutations were not considered as they were present in all strains including control strain SH1000 *lysA*::p*mecA* (SJF4996) as well SH1000 p*mecA* (SJF4891) derivatives (Appendix 1 Table 2).

The sequencing data for SH1000 *lysA*::p*mecA* (SJF4996) was compared with its trained isolates (Figure 4.4). Whole genome sequencing identified a number of genetic polymorphisms in trained strains with oxacillin MIC from 2 to ≥256 µg/ml (Table 4.2). However, the single most striking observation to emerge from sequencing data was that resistant strains have acquired mutations that caused an amino acid substitution in either SAOUHSC_00524, *rpoB* (DNA-directed RNA polymerase subunit β) or SAOUHSC_00525, *rpoC* (DNA-directed RNA polymerase subunit β') (Figure 4.8 B and Table 4.2). RpoB and RpoC enzymes are components of RNA polymerase (RNAP) holoenzyme. The *rpoB* and *rpoC* genes in *S. aureus* share an operon (Figure 4.8 A) with other downstream genes, 50S ribosomal protein encoded by *rplGB* (SAOUHSC_00526), two 30S ribosomal proteins encoded by *rpsL* (SAOUHSC_00527) and *rpsG* (SAOUHSC_00528) and two elongation factors encoded by *fusA* (SAOUHSC_00529) and *tuf* (SAOUHSC_00530).

It has been shown that mutations in *rpoB* are commonly associated with rifampicin resistance (Gao et al., 2013). In addition, some studies have also noted that alterations in *rpoB* to be involved in developing resistance to methicillin, vancomycin and daptomycin (Matsuo et al., 2011). Moreover, mutation in *rpoC* converts heterogeneously vancomycin-intermediate *S. aureus* (hVISA) into slow VISA which results in increased oxacillin resistance (Matsuo et al., 2015; Saito et al., 2014). Nevertheless, how *rpo* mutations lead to high-level resistance is not well studied.

The positions of the nonsynonymous mutations that were identified in *rpoB* and *rpoC* are depicted on physical maps with corresponding gene regions (Figure 4.8 B). Originally, whole genome sequencing of SH1000 *lysA*::p*mecA* -TIR3 (SJF5008), a highly oxacillin resistant isolate trained to produce high-level resistance from expressing low-level resistance did not reveal any alterations in either *rpoB* or *rpoC* genes. Therefore, the genomic DNA was isolated from SH1000 *lysA*::p*mecA* -TIR3 (SJF5008) for DNA sequencing of *rpoB* and *rpoC* genes using sequencing primers (Figure 4.10 C). Reads for *rpoB* and *rpoC* were mapped to NCTC8325 genomic region corresponding to

rpoB and *rpoC* genes. The sequence alignment identified two amino acid substitutions in *rpoB* at residue 639 and 949 (Figure 4.8 B and Table 4.2). This observation further confirms the role of *rpo* alterations in concomitant development of high-level resistance.

Besides *rpo* mutations, some resistant strains had also acquired other mutations. Two of these mutations in SH1000 *lysA*::p*mecA* -TI4 (SJF5002) and SH1000 *lysA*::p*mecA* -TIR1 (SJF5006) included amino acid substitutions in SAOUHSC_00270, a hypothetical protein and SAOUHSC_00269, hypothetical protein, respectively (Table 4.2). Four out of seven highly resistant strains acquired a point deletion, resulting in disruption of the reading frame leading to a frameshift in the gene encoding SAOUHSC_00591, a hypothetical protein (Table 4.2). However, it is likely that these genetic changes were introduced during passaging and not a direct consequence of increased oxacillin resistance as they are not present in all highly resistant mutants. Therefore, these mutations were discarded for being linked to increased oxacillin resistance.

For two of the highly resistant strains, SH1000 *lysA*::p*mecA* -TIR1 (SJF5006) and SH1000 *lysA*::p*mecA* -TR2 (SJF5003); whole genome sequencing identified 12-bp insertion at genome position 2134372 when compared to the genome of NCTC8325 strain. This genomic region maps to SAOUHSC_02031 (*rsbU*), the sigma B regulatory protein. NCTC8325 strain carries a deletion in *rsbU* which is repaired in SH1000 by 11-bp insertion to repair defective *rsbU* of NCTC8325 derived SH1000 (Horsburgh et al., 2002). Therefore, this means that the SH1000 *lysA*::p*mecA* derivatives with increased resistance have regained a defective *rsbU* allele similar to the parental NCTC8325 strain.

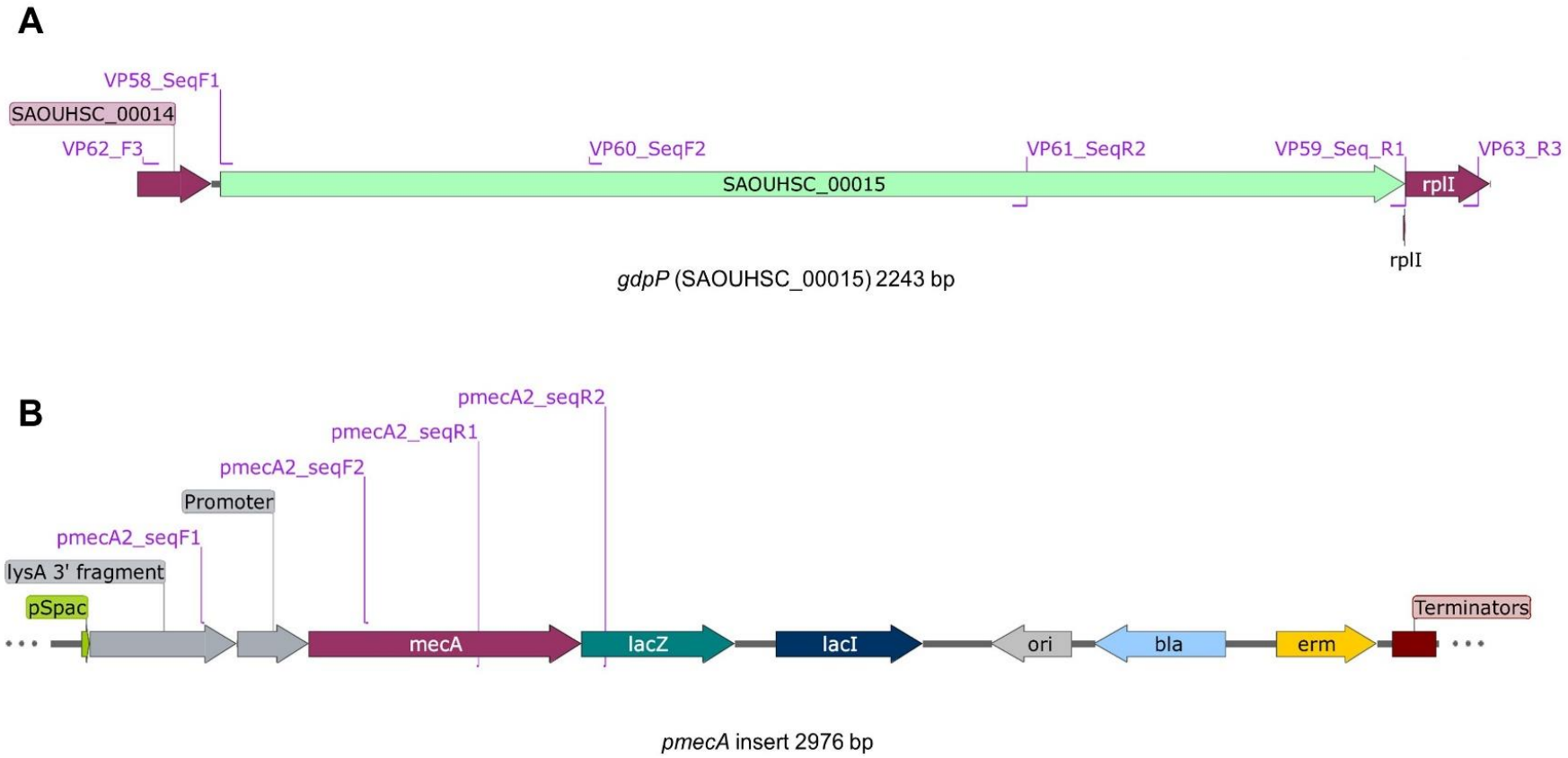

Figure 4.7 Location of sequencing primers for *gdpP* and the p*mecA* insert

A) Genomic region of *gdpP* and sequencing primer binding sites.
B) Sequencing primer binding sites mapped to pVP01-p*mecA* plasmid. Promoter region is covered by sequencing primers.

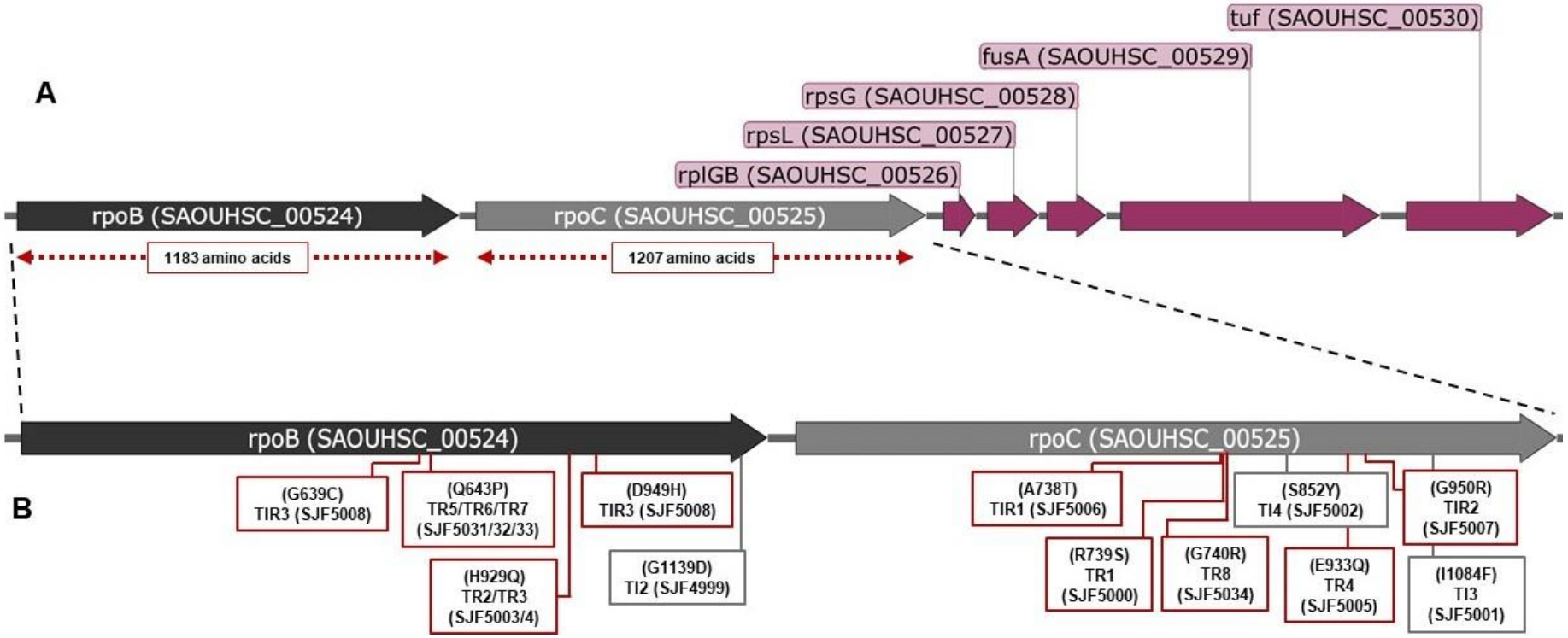

Figure 4.8 Physical map depicting SNPs identified in highly resistant SH1000 *lysA*::p*mecA* derivatives

A) Schematic representation of the genomic region of *rpoB, rpoC* operon, and downstream genes.
B) Amino acid substitutions identified in resistant derivatives of SJF4996 (SH1000 *lysA*::p*mecA*) are indicated with a red box representing highly resistant mutants with oxacillin MIC of ≥256 µg/ml and a grey box representing intermediate resistant mutants with oxacillin MIC of up to 16 µg/ml.

Genome position		Oxacillin MIC	Nucleotide change	Amino acid Change	Locus tag (Gene)	Protein
Parental strain SH1000						
SH1000 *lysA*::p*mecA* (SJF4996)		2				
Parental strain SH1000 *lysA*::p*mecA* (SJF4996)						
TI1 (SJF4998)		2				
TI2 (SJF4999)	525575	16	G-A	G1139D	SAOUHSC_00524 (*rpoB*)	DNA-directed RNA polymerase subunit β
TI3 (SJF5001)	529097	16	A-T	I1084F	SAOUHSC_00525 (*rpoC*)	DNA-directed RNA polymerase subunit β'
TI4 (SJF5002)	290628	16	T-G	S169A	SAOUHSC_00270	Hypothetical protein
	528402		C-A	S852Y	SAOUHSC_00525 (*rpoC*)	DNA-directed RNA polymerase subunit β'
TR1 (SJF5000)	528062	≥256	C-A	R739S	SAOUHSC_00525 (*rpoC*)	DNA-directed RNA polymerase subunit β'
	590401†		CG-C	R189	SAOUHSC_00591	Hypothetical protein
TR2 (SJF5003)	524946	≥256	T-A	H929Q	SAOUHSC_00524 (*rpoB*)	DNA-directed RNA polymerase subunit β
	590401†		CG-C	R189	SAOUHSC_00591	Hypothetical protein
	2134372‡		A-AAGCCTTTAACG		SAOUHSC_02301 (*rsbU*)	Sigma B regulatory protein
TR3 (SJF5004)	524946	≥256	T-A	H929Q	SAOUHSC_00524 (*rpoB*)	DNA-directed RNA polymerase subunit β
	590401†		CG-C	R189	SAOUHSC_00591	Hypothetical protein
TR4 (SJF5005)	528644	≥256	G-C	E933Q	SAOUHSC_00525 (*rpoC*)	DNA-directed RNA polymerase subunit β'
TR5 (SJF5031)*	524087	≥256	A-C	Q643P	SAOUHSC_00524 (*rpoB*)	DNA-directed RNA polymerase subunit β
TR6 (SJF5032)*	524087	≥256	A-C	Q643P	SAOUHSC_00524 (*rpoB*)	DNA-directed RNA polymerase subunit β
TR7 (SJF5033)*	524087	≥256	A-C	Q643P	SAOUHSC_00524 (*rpoB*)	DNA-directed RNA polymerase subunit β
TR8 (SJF5034)*	528065	≥256	G-C	G740R	SAOUHSC_00525 (*rpoC*)	DNA-directed RNA polymerase subunit β'
Parental strain SH1000 *lysA*::p*mecA* -TI1 (SJF4998)						
TIR1 (SJF5006)	289906	≥256	T-A	L161Q	SAOUHSC_00269	Hypothetical protein
	528059		G-A	A738T	SAOUHSC_00525 (*rpoC*)	DNA-directed RNA polymerase subunit β'
	2134372‡		A-AAGCCTTTAACG		SAOUHSC_02301 (*rsbU*)	Sigma B regulatory protein
TIR2 (SJF5007)	528695	≥256	G-C	G950R	SAOUHSC_00525 (*rpoC*)	DNA-directed RNA polymerase subunit β'
TIR3 (SJF5008)	524074	≥256	G-T	G639C	SAOUHSC_00524 (*rpoB*)	DNA-directed RNA polymerase subunit β
	525004		G-C	D949H	SAOUHSC_00524 (*rpoB*)	DNA-directed RNA polymerase subunit β

Table 4.2 Mutations identified by whole genome sequencing in SH1000 pRB474 p*mecA* derivatives relative to NCTC8325

*, DNA sequencing was performed only for the *rpoB* and *rpoC* genes; †, frameshift mutation; ‡, 11-bp insertion. Oxacillin MIC listed in µg/ml.

In order to investigate the effects of this small deletion on high-level resistance, a phage lysate from RN4220 *lysA*::p*mecA* (SJF4994) was transduced into NCTC8325-4 strain, a derivative of 8325 strain with three prophages removed (O'Neill, 2010). The transductants were selected on BHI agar plate supplied with erythromycin 5 µg/ml and lincomycin 25 µg/ml. The resultant strain 8325-4 *lysA*::p*mecA* (SJF5035) was further confirmed by *mecA* PCR verification (Figure 4.9). It was hypothesised that if defective *rsbU* is linked with the development of high-level oxacillin resistance then 8325-4 *lysA*::p*mecA* (SJF5035) would exhibit high-level resistance to oxacillin upon acquisition of *mecA* without needing training on methicillin gradient plate. However, 8325-4 *lysA*::p*mecA* (SJF5035) retained susceptibility to oxacillin (MIC = 0.5 µg/ml) comparable to that of its parental strain 8325-4 (MIC = 0.12 µg/ml) as shown in Figure 4.9. Therefore, the involvement of defective *rsbU* in developing high-level resistance was ruled out.

In order to assess if the selection of *rpo* mutations is linked with high-level resistance and not a consequence of one-off spontaneous event, SH1000 *lysA*::p*mecA* (SJF4996) was further streaked on methicillin gradient plate similar to the method described in section 4.2.1.2 and shown in Figure 4.3. Subsequently, four trained strains; SH1000 *lysA*::p*mecA* TR5 to TR8 (SJF5031, SJF5032, SJF5033 and SJF5034) were isolated with increased oxacillin resistance (MIC = ≥256 µg/ml) (Table 4.1 and Figure 4.10 A). PCR amplification verified the correct insertion of *mecA* at *lysA* locus (Figure 4.10 B). The gene sequencing of *mecA* revealed no alteration in the sequence. It was predicted that these strains may have acquired mutations in either *rpoB* or *rpoC*. Therefore, genomic DNA was isolated from four strains, SH1000 *lysA*::p*mecA* TR5 to TR8 (SJF5031, SJF5032, SJF5033 and SJF5034) for *rpoB* and *rpoC* gene sequencing. The genomic region of *rpoBC* was amplified using primers RNAP_F1 and RNAP_R1 producing 7449 bp product. Purified PCR products were used for DNA sequencing (GATC Biotech, Germany) using primers shown in Figure 4.10 C. Gene sequencing reads for *rpoBC* were mapped to NCTC8325 genome using SnapGene

software. The sequencing alignment identified amino acid substitutions in either *rpoB* or *rpoC* genes of all four strains. These results strongly suggest the role of *rpoBC* in developing high-level oxacillin resistance. Three of the strains SH1000 *lysA*::p*mecA* TR5 to TR7 (SJF5031, SJF5032 and SJF5033) carried same amino acid substitution in the *rpoB* gene. Whereas, SH1000 *lysA*::p*mecA* TR8 (SJF5034) carried a SNP in the *rpoC* gene (Table 4.2).

Interestingly, all strains with SNPs in *rpoBC* exhibited high-level oxacillin resistance and these SNPs are located towards the C-terminal of the protein. It has previously been reported that depending on the locations of the SNPs in *rpoB* gene decides the resistance to specific antibiotics. One of the most frequent mutations in *rpoB* is H481Y, associated with producing high-level resistance to rifampicin and vancomycin intermediate resistance in *S. aureus* (Matsuo et al., 2011). Two of the mutations in *rpoB* (N967I and R644H) are associated with increased methicillin resistance but do not affect susceptibility to rifampicin (Aiba et al., 2013).

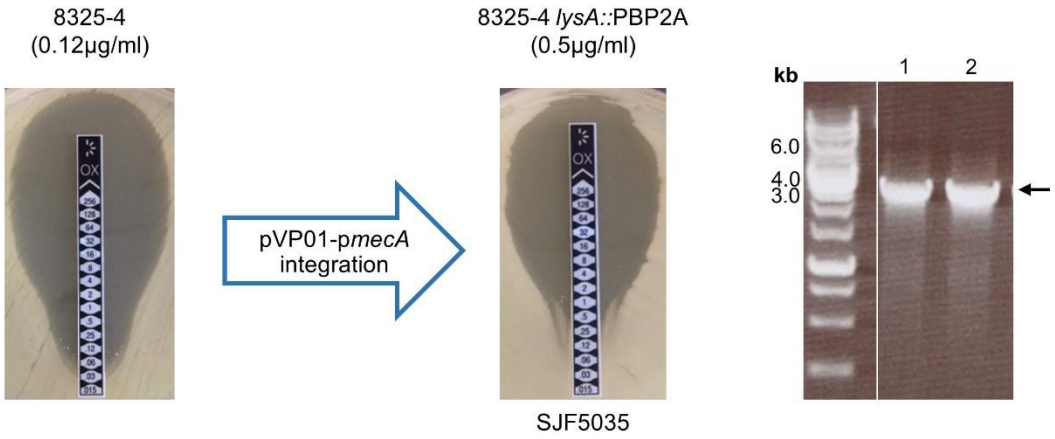

Figure 4.9 Construction and oxacillin MIC of 8325-4 *lysA*::p*mecA*

8325-4 was transduced with RN4220 *lysA*::p*mecA* (SJF4994) lysate for chromosomal integration of *mecA* at the *lysA* locus. 1% (w/v) TAE agarose gel shows *mecA* insertion at *lysA* locus (lane 1) with product size of ~4000 bp using lysA_5'_For (Forward) and p*mecA*_R1 (Reverse) primers. SH1000 *lysA*::p*mecA* (SJF4996) genomic DNA was used as a template for positive control (lane 2). DNA fragments were used as size markers for agarose gel electrophoresis.

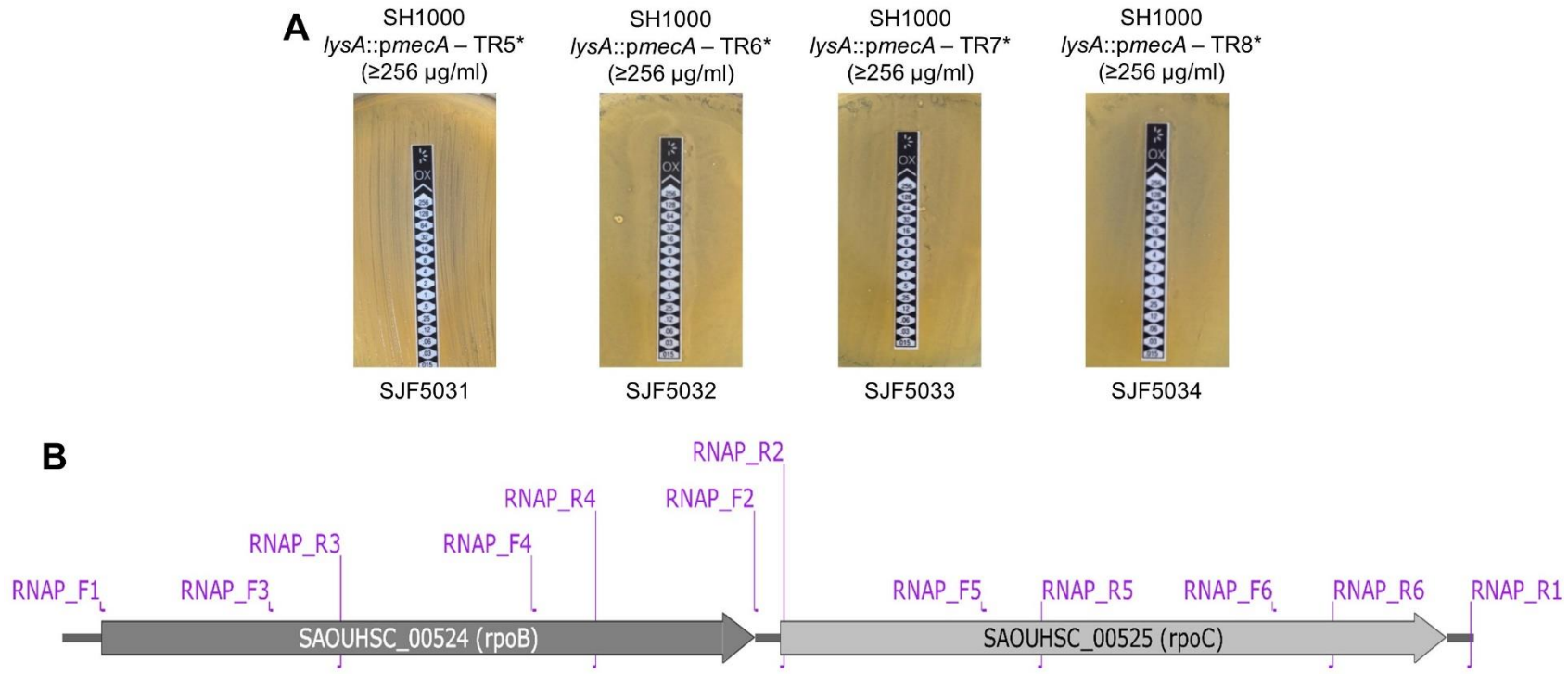

Figure 4.10 Evolution of SJF4996 derived highly oxacillin resistant *rpo* mutants and their verification

A) SJF4996 (Untrained-SH1000 *lysA*::p*mecA*) was trained to develop high-level resistance. Subsequently, selection of three isolates (SJF5031, SJF5032, SJF5033) acquired *rpoB* and one (SJF5034) acquired *rpoC* SNPs. Oxacillin MICs are listed in bracket for each strain.
B) Schematic overview of the native genomic region of *rpoB*, *C* and sequencing primer binding sites.

4.2.2.1 Influence of *rpo* mutations on other β-lactam and rifampicin susceptibilities

In order to investigate whether *rpoBC* mutations affect susceptibility to other antibiotics including rifampicin, β-lactams including cefoxitin and penicillin G, Etest was performed to determine the MIC for each strain carrying *rpo* mutations (Table 4.1). Rifampicin was chosen for antibiotic susceptibility testing because it has specific inhibitory effects on RNA polymerase which inactivates the enzyme at very low concentrations, resulting into inhibition of RNA synthesis which stops bacterial growth (Wehrli, 1983). All highly resistant strains harbouring *rpo* mutations were sensitive to rifampicin (Table 4.3). This observation suggests that the acquired *rpoB* mutations do not support rifampicin resistance.

Besides oxacillin MIC, cefoxitin and penicillin G MICs were tested using Etest method. For cefoxitin, MIC value of ≤4 µg/ml was considered to be sensitive and an MIC value of ≥8 µg/ml was considered to be resistant (Wu et al., 2016). All strains were found to be resistant to cefoxitin apart from SH1000 (Table 4.3). However, only strains exhibiting high-level oxacillin resistance with MIC value of ≥256 µg/ml showed high-level cefoxitin resistance with MIC value of ≥256 µg/ml. For penicillin G, MIC value of ≤2 µg/ml was considered to be sensitive and an MIC value of ≥2 µg/ml was considered to be resistant based on the quality control ranges supplied by Oxoid. All strains exhibiting high-level resistance to oxacillin with an MIC value of ≥256 µg/ml showed increased resistance to penicillin G with MIC value of ≥4 µg/ml (Table 4.3). MIC values for antibiotics used were compared against SH1000 and SH1000 *lysA*::p*mecA* (SJF4996).

Taken together, these observations suggest that the *rpo* mutations acquired by highly oxacillin resistant SH1000 *lysA*::p*mecA* (SJF4996) derivatives specifically confer resistance to β-lactam antibiotics.

Strain	Gene	Amino acid Change	MIC (µg/ml)			
			Oxacillin	Cefoxitin	Penicillin G	Rifampicin
SH1000			0.12	2	0.064	S
SH1000 *lysA*::p*mecA* (SJF4996)			2	24	0.75	S
SH1000 *lysA*::p*mecA* - TI2 (SJF4999)	*rpoB*	G1139D	16	24	2	S
SH1000 *lysA*::p*mecA* - TI3 (SJF5001)	*rpoC*	I1084F	16	24	1.5	S
SH1000 *lysA*::p*mecA* - TI4 (SJF5002)	*rpoC*	S852Y	16	16	1	S
SH1000 *lysA*::p*mecA* - TIR1 (SJF5006)	*rpoC*	A738T	≥256	≥256	8	S
SH1000 *lysA*::p*mecA* - TIR2 (SJF5007)	*rpoC*	G950R	≥256	≥256	12	S
SH1000 *lysA*::p*mecA* - TIR3 (SJF5008)	*rpoB*	G639C D949H	≥256	≥256	16	S
SH1000 *lysA*::p*mecA* - TR1 (SJF5000)	*rpoC*	R739S	≥256	≥256	8	S
SH1000 *lysA*::p*mecA* - TR2 (SJF5003)	*rpoB*	H929Q	≥256	≥256	12	S
SH1000 *lysA*::p*mecA* - TR3 (SJF5004)	*rpoB*	H929Q	≥256	≥256	6	S
SH1000 *lysA*::p*mecA* - TR4 (SJF5005)	*rpoC*	E933Q	≥256	≥256	16	S
SH1000 *lysA*::p*mecA* - TR5 (SJF5031)	*rpoB*	Q643P	≥256	≥256	12	S
SH1000 *lysA*::p*mecA* - TR6 (SJF5032)	*rpoB*	Q643P	≥256	≥256	12	S
SH1000 *lysA*::p*mecA* - TR7 (SJF5033)	*rpoB*	Q643P	≥256	≥256	8	S
SH1000 *lysA*::p*mecA* - TR8 (SJF5034)	*rpoC*	G740R	≥256	≥256	12	S

S, Sensitive.

Table 4.3 Antibiogram of SH1000 derived oxacillin resistant strains

4.2.2.2 Mapping *rpoB* and *rpoC* mutations to the core RNAP structure

It is important to examine the impact of *rpo* mutations (Table 4.3) on the physical properties of the RNAP core enzyme and its activity. A single point mutation can have pleiotropic effects on the stability and structure of the protein. In order to map mutations, the cryoEM structure of *E. coli* RNA polymerase elongation complex (Kang et al., 2017) was used to provide a structural framework as the *S. aureus* crystal structure of RNAP is not resolved yet. All mutations identified in *rpoB* are in conserved residues in *E. coli*, whereas except one of the *rpoC* residues (S852), the rest are conserved in *E. coli* (Appendix 3). These point mutations are mapped on the *E. coli* RNAP as shown in Figure 4.11 A. All mutations occurred either on the surface or towards the surface far from the catalytic center (Nudler, 2009). Additionally, none of the mutations were shown to be interacting with the nearby RNAP subunit interaction site (Figure 4.11 A). All *rpoB* mutations were mapped on *E. coli rpoB* to determine if any of the residue resides in the rifampicin binding pocket regions (Figure 4.11 B). None of the mutations detected in this study are located in the rifampicin binding regions I and II (Campbell et al., 2001; Villanueva et al., 2016). Therefore, all *rpoB* and *rpoC* mutants are susceptible to rifampicin (Table 4.3).

Interestingly, each mutation detected in *rpoB* and *rpoC* brought a change to the physicochemical properties of the amino acids (Pommié et al., 2004). The *rpoB* and *rpoC* mutations result in amino acid substitutions G1139D and G740R which cause the introduction of positive and negative charge, respectively as well as substantial change in hydropathy from neutral to hydrophilic. Whereas, G639C of *rpoB* amino acid substitution results into hydrophobicity without altering its polarity. D949H and R739S mutations brought in charged basic amino acids from acidic and uncharged amino acids from a charged basic amino acid, respectively, resulting in neutral hydropathy from hydrophilic. The H929Q substitution resulted in loss of electrical charge by replacing a neutral basic amino acid with a hydrophilic uncharged amino acid. The I1084F substitution did not change polarity but replaced an aliphatic amino acid with an aromatic amino acid. The A738T

substitution brought in a neutral polar amino acid in place of a hydrophobic nonpolar amino acid. The S852Y substitution did not alter polarity but substituted an aromatic amino acid with very large molar volume (Pommié et al., 2004). Moreover, the Q643P substitution brought in substantial change in polarity accompanying a sharp structural variation introducing abrupt changes to the direction of the chain (Pommié et al., 2004). All these amino acid changes suggest severe effects on the activity and/or interaction of RNAP resulting into a common phenotype of high-level β-lactam resistance.

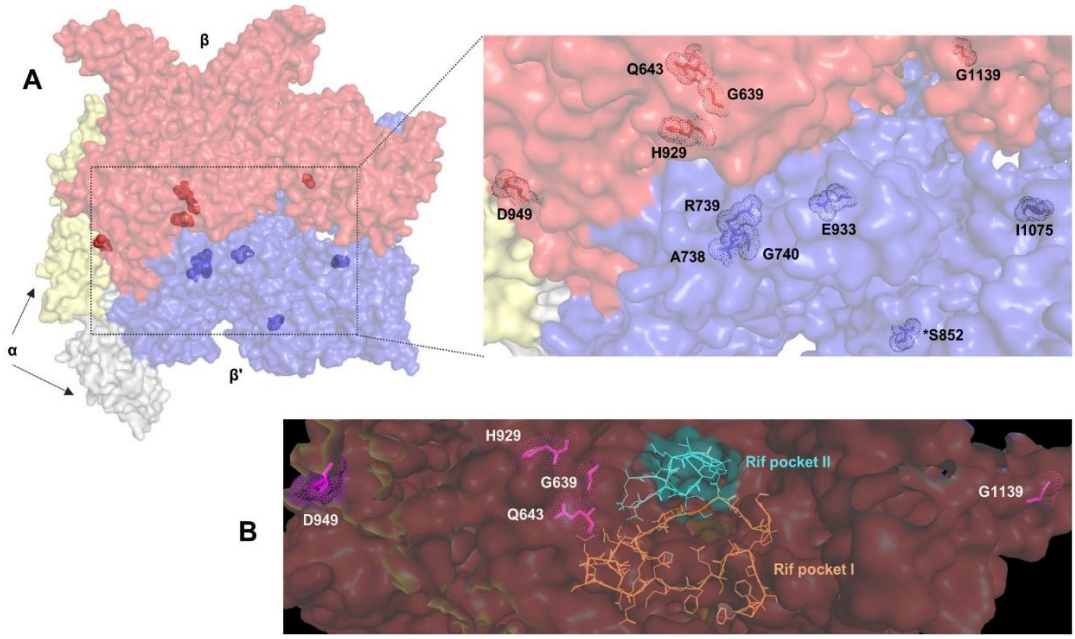

Figure 4.11 Location of *rpo* mutations on *E. coli* RNAP core enzyme complex

A) The three-dimensional structure of *E. coli* RNAP elongation complex (Kang et al., 2017) was used to map the *rpoB* and *rpoC* mutations identified in this study. The core RNAP complex consists of two α subunits (grey and pale yellow), β subunit (red) and β' subunit (blue) marked with colour coded molecular surface with reduced transparency. The mapped *rpoB* and *rpoC* (*S. aureus*) mutated residues are shown as sticks and highlighted with dots (Zoom in section). *S. aureus* residue numbering was used to label structural locations of mutated alleles. *, residue not conserved in *E. coli* (Appendix 3). Figures were generated from Protein Data Bank code 6ALH using PyMOL protein modelling software.
B) All identified *rpoB* mutations were mapped to the *E. coli* RpoB structure and are marked on the red molecular surface with reduced transparency. Other molecular structures of two α and a β' subunits were hidden. Rifampicin binding pocket regions I and II (Campbell et al., 2001) are marked as orange and cyan lines, respectively and mapped mutations are shown as sticks highlighted with dots (magenta). *S. aureus* residue numbering was used to label structural locations of mutated alleles. The figure was generated from Protein Data Bank code 6ALH using PyMOL protein modelling software.

4.2.2.3 Prevalence of *rpo* mutations in clinical MRSA isolates

Previous studies have identified mutations in *rpo* genes which confer antibiotic resistance in laboratory-derived highly resistant isolates (Aiba et al., 2013; Matsuo et al., 2015; Saito et al., 2014; Villanueva et al., 2016; Zhou et al., 2012). In order to investigate the existence of *rpo* alterations in MRSA isolates found in clinical settings and their effect on developing high-level resistance to β-lactam antibiotics, a total of seven MRSA isolates were selected for protein sequence alignment of RpoB and RpoC using the Clustal Omega tool. Multiple sequence alignments of RpoB and RpoC identified non-synonymous amino acid substitutions in JH9, COL, USA300, MRSA252 and Mu50 relative to NCTC8325 (Table 4.4 and Appendix 2).

In order to verify these results and determine oxacillin susceptibility, the genomic DNA from HA-MRSA (COL, MRSA252, Mu50 and Mu3) and CA-MRSA (USA300 and MW2) strains were isolated and the *rpoBC* genomic region was PCR amplified using RNAP_F1 and RNAP_R1 (Figure 4.10 C). The purified products of 7461 bp were used for DNA sequencing (GATC biotech, Germany). The sequencing data was aligned with NCTC8325 which identified mutations in *rpoBC* of four strains similar to the results obtained from Clustal Omega alignment (Appendix 2). Antibiotic susceptibility tests and amino acid substitutions are listed in Table 4.4

There were no nonsynonymous mutations identified in *rpoBC* of Mu3 and MW2 irrespective of exhibiting high-level and low-level β-lactam resistance, respectively. This suggests involvement of an unknown mechanism independent of *rpo* alterations in the development of high-level resistance. In addition, USA300 has been reported to be resistant to oxacillin with an MIC ranging from 32-48 µg/ml (Bæk et al., 2014) and also carries an amino acid substitution in *rpoC* at residue 857. Mwangi et al., 2007 reported that the JH9 strain to have four SNPs in *rpoB* (D471Y, A473S, A477S, A478D) and one in *rpoC* (E854K) but it is susceptible to oxacillin (MIC = 0.75 µg/ml) and resistant to vancomycin (MIC = 8 µg/ml) and rifampicin (MIC = 16 µg/ml). JH9 was isolated *in vivo* following multidrug therapy resulting in vancomycin intermediate resistance (Mwangi et al., 2007).

The direct homologues of *S. aureus rpoB* and *rpoC* in *B. subtilis, E. coli* and *T. aquaticus* are highly conserved. Alignment of *S. aureus* RpoB with *B. subtilis, E. coli* and *T. aquaticus* RpoB revealed that three out of five substitutions found in RpoB of strains listed in Table 4.3 are conserved residues, while two residues are in conservative regions but either with strong or weak similar properties (highlighted in green Appendix 3). Alignment of *S. aureus* RpoC with *B. subtilis, E. coli* and *T. aquaticus* RpoC revealed that four out of seven substitutions found in strains listed in Table 4.3 are conserved residues, while one resides in conservative region with strong similar properties whereas one is found to be in not conserved region (highlighted in green Appendix 3). Similarly, alignment of RpoB and RpoC of clinical isolates listed in Table 4.4 revealed that not all identified SNPs are located in conserved regions of the genes (highlighted in yellow Appendix 3).

Taken together, these observations suggest that the location of the mutations could not simply determine if the level of antibiotic resistance and a disruption of either RpoB or RpoC are sufficient to confer high-level antibiotic resistance.

Strains	Mutation	MIC (µg/ml)			
		Oxacillin	Cefoxitin	Penicillin G	Rifampicin
COL	*rpoB* (A798V, S875L)	≥256	≥256	32	S
MRSA252	*rpoB* (Y737F), *rpoC* (I864V)	≥256	≥256	≥256	S
Mu50	*rpoB* (H481Y)	≥256	≥256	24	≥256
Mu3		≥256	≥256	48	S
USA300	*rpoC* (R857H)	1	16	0.25	S
MW2		8	32	32	S
JH9*	*rpoB* (D471Y, A473S, A477S, E478D) *rpoC* (E854K)	0.75	ND	ND	16

S, Sensitive; ND, not done; *, not tested for antibiotic susceptibility testing as the strain was not available, data taken from (Mwangi et al., 2007)

Table 4.4 Antibiogram and detection of *rpo* SNPs in clinical MRSA isolates

4.2.3 Effect of *rpo* mutations on growth characteristics of representative strains

The frequent occurrence of *rpoB* and *rpoC* mutations have previously been shown to be involved in not only the conversion of heterogeneous vancomycin resistance to vancomycin intermediate resistance but also heterogeneous to homogenous conversion of methicillin resistance (Aiba et al., 2013; Matsuo et al., 2011, 2015; Watanabe et al., 2011). This conversion is accompanied by a slower growth rate (Aiba et al., 2013; Matsuo et al., 2011).

In order to test if *rpo* mutations have an impact on growth rate of SH1000 *lysA*::p*mecA* (SJF4996) and derived mutants, their growth characteristics in liquid medium was examined and compared to the SH1000 in the absence of antibiotic. From the strains listed in Table 4.1, Table 4.3 and Table 4.4, WT control, SH1000; MRSA control, COL; untrained, SH1000 *lysA*::p*mecA* (SJF4996); trained *rpoB* (H929Q), SH1000 *lysA*::p*mecA* (SJF5003); trained-*mecA*-cured-*rpoB* (H929Q), SH1000 *lysA::kan* cured (SJF5010); and trained *rpoC* (G740R), SH1000 *lysA*::p*mecA* (SJF5034) strains were selected as representatives for growth rate assays. Optical density measurements showed the parental strain SJF4996 (*mecA* only) exhibited a growth rate similar to that of SH1000 (Figure 4.12 A). However, both the *rpo* mutants (SJF5003 and SJF5034) including *mecA*-cured-*rpoB* mutant (SJF5010) had a similar but slower growth rate than the parental strain SJF4996 and SH1000. Optical density measurements were used to calculate doubling time. SH1000 and untrained, SH1000 *lysA*::p*mecA* (SJF4996) doubling time was approximately 35 min and 34 min, respectively. Whereas, COL, trained-*rpoB* (SJF5003) and trained-*mecA*-cured-*rpoB* (SJF5010) required more time (~48 min) to double than parent strain. While, trained-*rpoC* (SJF5034) showed the slowest growth rate with doubling time of 55 min.

The growth rates of the *rpo* mutants did not show a defect compared to COL (Figure 4.12 A). As aforementioned, the COL strain also harbours two SNPs in *rpoB* (A798V, S875L) gene. This observation suggests that the growth

defect in *rpo* mutants is due to the acquisition of mutations in either *rpoB* (SJF5003 and SJF5010) or *rpoC* (SJF5034).

Furthermore, the growth characteristics of the representative strains (SH1000, COL, SJF4996, SJF5003 and SJF5034) were also tested in the presence of oxacillin (Figure 4.12 B). Following inoculation of fresh culture into 50 ml pre-warmed BHI, the cultures were grown for one hour and oxacillin was added (Figure 4.12 B). 0.5 µg/ml of oxacillin was added to SH1000 and SJF4996 cultures and 20 µg/ml of oxacillin was added to COL, SJF5003 and SJF5034 cultures after one hour of incubation. Optical density measurements showed that SH1000 was unable to grow in the presence of oxacillin. Whereas, SJF4996 grew for two hours before cessation but showed same doubling time of 35 min as compared to in the absence of oxacillin (Figure 4.12 B). The growth rate of *rpo* mutants (SJF5003 and SJF5034) and COL was unaffected in the presence of oxacillin (Figure 4.12 B). SJF5003 retained same doubling time of 47 min in the presence of 20 µg/ml oxacillin, whereas SJF5034 and COL needed less time (51 min and 44 min, respectively) to double in the presence of 20 µg/ml oxacillin compared to in the absence of oxacillin.

These observations suggest that the growth of highly resistant *rpo* mutants remains stable in the presence of oxacillin, similar to the clinical isolate COL. Therefore, the acquisition of compensatory mutations in *rpoB* and *rpoC* allow cells to grow in the presence of oxacillin to cope with antibiotic pressure, resulting into homogenous high-level resistance.

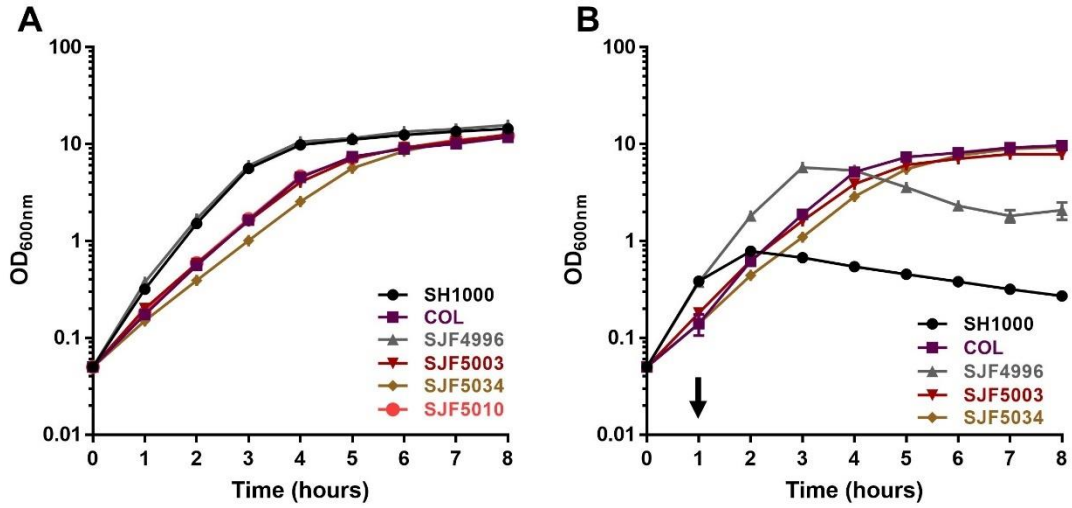

Figure 4.12 Growth characteristics of *rpo* mutants relative to SH1000

A) Growth of representative *rpo* mutants, SH1000 *lysA*::p*mecA rpoB* (H929Q) (SJF5003), SH1000 *lysA::kan mecA* cured *rpoB* (H929Q) (SJF5010), SH1000 *lysA*::p*mecA rpoC* (G740R) (SJF5034) was compared to SH1000, COL and a parental strain SH1000 *lysA*::p*mecA* (SJF4996). Bacterial cultures were prepared in triplicate and the error bars represent standard deviation of the mean.
B) Growth of representative *rpo* mutants, SH1000 *lysA*::p*mecA rpoB* (H929Q) (SJF5003) and SH1000 *lysA*::p*mecA rpoC* (G740R) (SJF5034) was compared to SH1000, COL and parent strain SH1000 *lysA*::p*mecA* (SJF4996). Bacterial cultures were prepared in triplicate and the error bars represent standard deviation of the mean. 0.5 µg/ml of oxacillin was added to SH1000 and SJF4996 cultures following one hour of incubation. 20 µg/ml of oxacillin was added to COL, SJF5003 and SJF5034 cultures following one hour of incubation, indicated with a black arrow.

4.2.4 Effect of *rpo* mutations on the level of PBP2A and other PBPs

In order to test the amount of PBP2A being produced in SH1000; COL; SH1000 *lysA*::p*mecA* (SJF4996); trained *rpoB* (H929Q), SH1000 *lysA*::p*mecA* (SJF5003); trained-*mecA*-cured-*rpoB* (H929Q), SH1000 *lysA::kan* cured (SJF5010); and trained *rpoC* (G740R), SH1000 *lysA*::p*mecA* (SJF5034) strains, Western blot using anti-PBP2A antibodies was performed. To avoid cross reactivity of antibodies against other cellular proteins, crude antiserum containing anti-PBP2A antibodies was incubated at room temperature with *E. coli* whole cell lysate followed by incubation with *S. aureus* SH1000 whole cell lysate for four hours prior to use. To test the specificity, blots were probed with polyclonal anti-PBP2A antibodies using a range of serum dilutions of 1:5,000; 1:10,000 and 1:15,000 prepared in blocking buffer. An intense band was observed at ~76 kDa for PBP2A. Similarly, a range of membrane fraction concentrations were tested and ~10 µg of membrane protein was then used as standard. As an endogenous control for membrane proteins, anti-DivlB antibodies were purified to avoid cross reactivity using an *E. coli* whole cell lysate. DivlB was selected as it is located in the membrane (Bottomley et al., 2014). To test the specificity, blots were probed with anti-DivlB antiserum using a range of serum dilutions of 1:5,000; 1:10,000 and 1:15,000 with 10 µg of membrane protein. An intense band of reactivity with anti-DivlB was observed at ~50 kDa for DivlB.

Western blot analysis using anti-PBP2A antibodies identified the expected band of ~76 kDa identified in COL, SJF4996, SJF5003, SJF5034 in the absence and presence of 20 µg/ml oxacillin (SJF5003 and SJF5034) as shown in Figure 4.13 A. In addition, Western blot analysis using anti-DivlB identified a band of ~50 kDa with similar intensity for each sample (Figure 4.13 A, bottom panel), confirming equal amount of membrane fraction used for the detection of membrane proteins (~10 µg). As predicted, SH1000 and SJF5010 (*mecA*-cured-*rpoB*-H929Q) did not show a band for PBP2A. whereas, trained-*rpo* mutants (SJF5003 and SJF5034) produced increased amounts of PBP2A compared to SJF4996 (untrained) which produced low-levels of PBP2A, however similar to the relative amount of PBP2A being

produced by COL (Figure 4.13 B). The relative levels of PBP2A was calculated for all samples using ImageLab™ (BioRad) software by selecting untrained-*mecA*-only (SJF4996) as a point of reference (=1). Interestingly, in the presence of 20 µg/ml oxacillin in SJF5003 (trained-*rpoB*-H929Q) and SJF5034 (trained-*rpoC*-G740R) showed no difference in the relative levels of PBP2A production when compared in the absence of oxacillin (Figure 4.13 A and B). Both *rpo* mutations resulted into up to 2-fold increase in PBP2A compared to untrained (SJF4996) parental strain (Figure 4.13 A and B) suggesting that each mutation resulted in elevated levels of PBP2A in the cell membranes. This observation was in agreement with the results reported by other research groups (Dordel et al., 2014).

The production of PBP2A was also compared in strains carrying multicopy *mecA* (pRB474-p*mecA* based) untrained-SH1000-p*mecA* (SJF4981) and trained-*gdpP* (R318L) (SJF4991) alongside single copy *mecA* strains, untrained (SJF4996), trained-*rpoB* (SJF5003) and trained-*rpoC* (SJF5034) (Figure 4.13 D). For Western blot analysis, whole cell lysate (~10 µg) was used instead of membrane fractions. SJF4991 (trained-*gdpP*) showed increased levels of PBP2A compared to parental strain (SJF4981). These observations were similar to the single copy *mecA* expressing, untrained (SJF4996) and trained (SJF5003 and SJF5034) strains (Figure 4.13 D). This result indicate that increased in the production of PBP2A is required to confer high-level oxacillin resistance regardless of how *mecA* is being expressed.

The profiles of PBPs in SH1000; COL; untrained, SH1000 *lysA*::p*mecA* (SJF4996); trained *rpoB* (H929Q), SH1000 *lysA*::p*mecA* (SJF5003); trained-*mecA*-cured-*rpoB* (H929Q), SH1000 *lysA::kan* cured (SJF5010); and trained *rpoC* (G740R), SH1000 *lysA*::p*mecA* (SJF5034) were studied by an SDS-PAGE gel-based Bocillin-FL labelling. Membrane fractions were isolated from each strain grown to an OD_{600} of ~1. The membrane proteins (~50 µg) were incubated with 25 µM Bocillin-FL for 25 min at 37ºC and separated in a 10% (w/v) SDS-PAGE gel. As expected, four bands were detected representing PBP1 (~82.7 kDa), PBP2 (~80 kDa), PBP3 (~77.3 kDa) and PBP4 (~48.2 kDa). Due to similar size of PBP1, PBP2 and PBP3, some

samples showed brighter bands (Figure 4.13 C). However, there was no obvious difference observed in the production of PBPs in the aforementioned representative strains. Moreover, both *rpo* mutants (SJF5003, *rpoB*-H929Q and SJF5034, *rpoC*-G740R) were grown in the presence of 20 µg/ml of oxacillin prior to membrane fraction isolation. However, the presence of oxacillin did not alter the production of native PBPs, suggesting *rpo* mutations do not impact the production of PBPs.

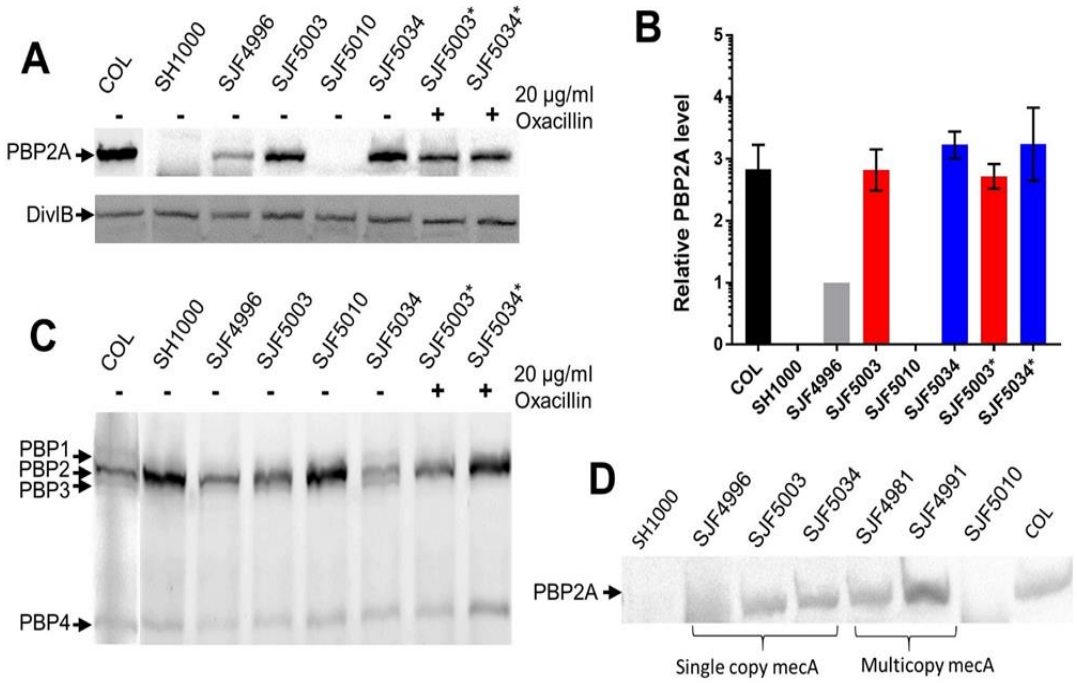

Figure 4.13 Cellular levels of PBP2A and other PBPs of SJF4996 and its derivatives

A) Membranes fractions (~10 µg of protein) of COL, SH1000, SJF4996 (untrained-*mecA*-only), SJF5003 (trained-*rpoB*-H929Q), SJF5010 (trained-*mecA*-cured-*rpoB*-H929Q) and SJF5034 (trained-*rpoC*-G740R) were probed with anti-PBP2A antibodies at a 1:5000 dilution (first row). Anti-DivIB antibodies were used as an endogenous control for membrane proteins (second row) at a 1:10000 dilution simultaneously. Bands of ~76 kDa and 50 kDa, corresponding to PBP2A and DivIB, respectively, are indicated with black arrows.
B) Relative levels of PBP2A for representative strains (COL, SH1000, SJF5003, SJF5010, SJF5034) were calculated using ImageLab™ (BioRad) quantitation tool, selecting SJF4996 (untrained-*mecA*-only) as a point of reference (=1). The results of relative concentrations of PBP2A are the average of three independent repeats where error bars represent standard deviation of the mean (±SEM).
C) Analysis of penicillin binding protein (PBPs) profiles in representative strains (COL, SH1000, SJF4996, SJF5003, SJF5010, SJF5034) by Bocillin-FL labelling. The membrane fractions (~50 µg protein) were labelled with 25 µM Bocillin-FL at 37°C for 20 mins. The identified bands for PBP1 (~82.7 kDa), PBP2 (~80 kDa), PBP3 (~77.3 kDa) and PBP4 (~48.2 kDa) are indicated with black arrows.
D) Whole cell lysate (~10 µg protein) of SH1000, SJF4996 (untrained-*mecA*-only), SJF5003 (trained-*rpoB*-H929Q), SJF5034 (trained-*rpoC*-G740R), SJF4981 (untrained-multicopy *mecA*), SJF4991 (trained-*gdpP* mutant), SJF5010 (trained-*mecA*-cured-*rpoB*-H929Q) and COL were probed with anti-PBP2A antibodies at a 1:5000 dilution. Bands of ~76 kDa are indicated with a black arrow.

*, cells were grown in the presence of 20 µg/ml of oxacillin prior to membrane fractionations.

4.2.5 Complementation of *S. aureus rpoB* and *rpoC*

To determine if the *rpo* mutations were the reason for the development of high-level β-lactam resistance, mutated *rpoBC* were complemented with the respective a wild type allele. A phage lysate from AJ1008 with a *kan* insertion next to *rpoBC* was used (Villanueva et al., 2016) (SJF5036). The kanamycin resistance gene is in the intergenic region between *rpoC* and SAOUHSC_00526. Phage transduction of both *rpo* mutants (SJF5003, *rpoB*-H929Q and SJF5034, *rpoC*-G740R) were carried out with selection on agar containing kanamycin (50 µg/ml). Kanamycin resistant transductants were verified by PCR-based assays for the insertion of the *kan* next to the *rpoBC* genomic region (Figure 4.14 A). The genomic DNA was isolated from the resultant strains SJF5044 (SJF5003, *rpoB*+), SJF5045 (SJF5034, *rpoC*+) for DNA sequencing to verify replacement of mutated *rpoB*-H929Q and *rpoC*-G740R to wildtype *rpoB* and *rpoC*, respectively. This would occur via co-transduction of *kan* and the WT *rpoBC* allele as they are genetically linked. Both genetically complemented strains (SJF5044 and SJF5045) regained susceptibility to oxacillin with an MIC value of 1 µg/ml (Figure 4.14 B and C). Furthermore, the amount of PBP2A production was also determined using Western blot showed reduction in the levels of PBP2A similar to that of untrained, SH1000 *lysA*::p*mecA* (SJF4996) strain (Figure 4.13 A and Figure 4.14 E). Moreover, COL was transduced using phage lysate from SJF5036 (AJ1008 with *kan* near *rpoBC* (Villanueva et al., 2016)). The resultant transductant SJF5049 (COL *rpoB*+) was verified by PCR based assays (Figure 4.14 A) and DNA sequencing confirmed replacement of native *rpoB* (A798V, S875L) to WT *rpoB*. Surprisingly, the genetically complemented SJF5049 (COL *rpoB*+) became highly sensitive to oxacillin with an MIC of 0.5 µg/ml (Figure 4.14 D). However, some colonies were seen to grow in the zone of inhibition (Figure 4.14 D). Western blot analysis showed reduction in the production of PBP2A of SJF5049 (COL *rpoB*+) compared to its parent (Figure 4.14 E). Collectively, these observations further confirm the role of *rpo* mutations in leading to high-level oxacillin resistance.

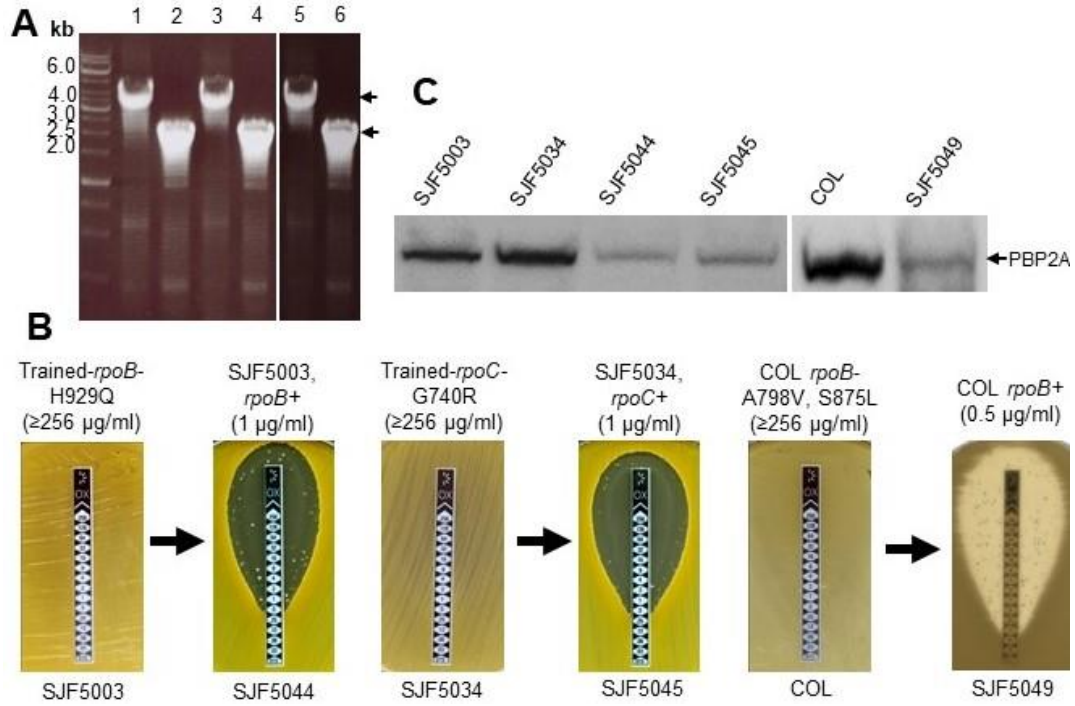

Figure 4.14 Correlation between oxacillin resistance and the production of PBP2A

A) A phage lysate from SJF5036 (AJ1008, AR1089 with *kanA* near *rpoBC* (Villanueva et al., 2016)) was used to replace mutated *rpoB*-H929Q (SJF5003), *rpoC*-G740R (SJF5034) and COL to WT *rpoB* and *C* regions. The resultant SJF5044 (SJF5003, *rpoB*+), SJF5045 (SJF5034, *rpoC*+) and SJF5049 (COL *rpoB*+) kanamycin resistant transductants for complemented strains were verified by PCR using Kpn_rpoC_nearby5 and Pst1_rpoC_nearby (Villanueva et al., 2016) producing a band of 3.5 kb marked by black arrows (SJF5044-lane 1, SJF5045-lane 3 and SJF5049-lane 5). SJF5003 (lane 2), SJF5034 (lane 4) and COL genomic DNA was used as a positive control, producing a product of 2 kb marked by a black arrow. DNA fragments were used as size markers for agarose gel electrophoresis.
B) Oxacillin susceptibility for parental and genetically complemented strains, SJF5003 and SJF5044, SJF5034 and SJF5045, COL and SJF5049 (COL *rpoB*+) were compared using the Etest method. Oxacillin MIC are listed in brackets for all strains.
C) Membranes fractions (~10 µg of protein) of SJF5003 (trained-*rpoB*-H929Q), SJF5034 (trained-*rpoC*-G740R), SJF5044 (SJF5003, *rpoB*+), SJF5045 (SJF5034, *rpoC*+), COL and SJF5049 (COL *rpoB*+) were probed with anti-PBP2A antibodies at a 1:5000 dilution. A band of ~76 kDa corresponding to PBP2A is indicated with a black arrow.

4.2.6 Reconstitution of the high-level resistance in a naïve MSSA background

In order to examine whether the phenotypic expression of high-level oxacillin resistance is not SH1000 strain background specific phenomenon, a clinical MSSA isolate Newman was chosen for complete reconstitution of the high-level resistance phenotype. Newman, a clinical strain isolated in 1952 is commonly used for genetic manipulation (Duthie and Lorenz, 1952). In order to introduce mutation in the *rpoB* gene of Newman, phage lysate from SJF5036 (AJ1008 with *kanA* near *rpoBC* (Villanueva et al., 2016)) was transduced into SJF5003 (trained-*rpoB*-H929Q) as described in section 2.14.3 and resultant transductants were screened for kanamycin as well as high-level oxacillin resistance. This would show kanamycin resistance but without co-transduction of the WT *rpoB* allele. Genomic DNA was isolated and the insertion of *kan* nearby *rpoBC* was confirmed by PCR resulting into kanamycin resistance marked *rpoB* (H929Q) mutant, SH1000 *lysA*::p*mecA* *rpoB*-H929Q (SJF5046). A phage lysate from SJF5046 was used to transduce the *rpoB*-H929Q mutation across to Newman. The transductant was selected on agar plate containing kanamycin (50 µg/ml). The resultant Newman *rpoB*-H929Q (SJF5048) strain was verified for the insertion of *rpoB*-H929Q mutation by DNA sequencing. The PCR based assay confirmed insertion of *kan* next to *rpoBC* (Figure 4.15 A).

Subsequently, in order to introduce *mecA*, SJF5048 (Newman *rpoB*-H929Q) was transduced using a phage lysate from SJF4994 (RN4220 *lysA*::p*mecA*). Transductants were selected on agar containing erythromycin (5 µg/ml) and lincomycin (25 µg/ml). Genomic DNA was isolated from the resultant transductant Newman *lysA*::p*mecA* *rpoB*-H929Q (SJF5050) and verified by PCR to amplify *mecA* at the *lysA* locus (Figure 4.15 B). Oxacillin susceptibility of SJF5050 (Newman *lysA*::p*mecA* *rpoB*-H929Q) showed increased oxacillin MIC value of ≥256 µg/ml unlike its parental strain (oxacillin MIC 0.12 µg/ml) (Figure 4.15 C). Therefore, the successful reconstitution of an MRSA phenotype in Newman ensured that development

of resistance is not strain specific phenomenon, further emphasising on the correlation between *rpo* mutations and *mecA*.

4.2.6.1 Insertion of *mecA* nearby *orfX* locus

The *mec* gene complex is located within a mobile genetic element, SCC*mec* (Staphylococcal Chromosome Cassette *mec*), which carries *mecA* and its regulatory genes (Beck et al., 1986). All MRSA isolates possess a *mec* gene complex, specifically located within the 3' end of *orfX* (SAOUHSC_00027), known as the SCC*mec* attachment site (*attB*) (Noto et al., 2008).

In order to determine whether expression of *mecA* from the native *orfX* locus could regenerate high-level β-lactam resistance, pMUTIN4 derived (Vagner et al., 1998) plasmid was used to introduce *mecA* and its own promoter downstream of the *orfX* gene. For chromosomal insertion of *mecA* at *orfX* site, the pVP01-p*mecA* plasmid was restriction digested using HindIII/BamHI enzymes to cut out 3' *lysA* fragment of 1084 bp resulting in a linear plasmid backbone. Genomic DNA was isolated from SH1000 to amplify the *orfX* gene including downstream sequence (Figure 4.16 A) and subsequently cloned into the linear plasmid using Gibson assembly master mix, resulting into pVP02-*orfX* (Figure 4.16 A). Transformation of plasmid, pVP02-*orfX* into electrocompetent *E. coli* DH5α (NEB) (SJF5065) was used for amplification of plasmid prior to verification. The insertion of *orfX* fragment and presence of intact p*mecA* was verified by DNA sequencing and PCR-based assays (Figure 4.16 B and C). However, transformation of pVP02-o*rfX* into RN4220 did not produce transformants. Several unsuccessful attempts were made by changing parameters for RN4220 transformation.

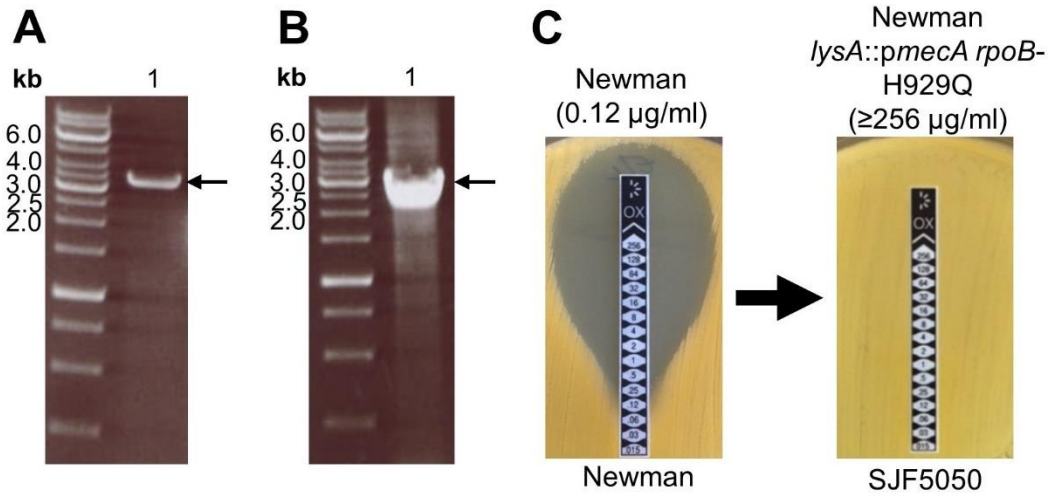

Figure 4.15 Reconstitution of high-level oxacillin resistance in Newman

A) A phage lysate from SH1000 *lysA*::p*mecA rpoB*-H929Q (SJF5046) was used to move kanamycin marked *rpoB*-H929Q (SJF5003) into Newman. The resultant Newman *rpoB*-H929Q (SJF5048) kanamycin resistant strain was verified by PCR using Kpn_rpoC_nearby5 and Pst1_rpoC_nearby (Villanueva et al., 2016) producing a band of 3.5 kb marked by a black arrow (lane 1). DNA fragments were used as size markers for agarose gel electrophoresis.
B) Subsequently, a phage lysate from SJF4994 (RN4220 *lysA*::p*mecA*) was used to transduce SJF5048 (Newman *rpoB*-H929Q) with *mecA* insertion at the *lysA* locus. The resultant strain, Newman *lysA*::p*mecA rpoB*-H929Q (SJF5050) was verified by PCR using lysA_5'_For (Forward) and p*mecA*_R1 (Reverse) primers producing a band of ~4000 bp marked by a black arrow (lane 1). DNA fragments were used as size markers for agarose gel electrophoresis.
C) The introduction of *rpoB*-H929Q and *mecA* into Newman resulted in the development of high-level resistance. Oxacillin susceptibility of SJF5050 (Newman *lysA*::p*mecA rpoB*-H929Q) and its parental strain Newman were compared using Etest method. Oxacillin MICs are listed in brackets for both strains.

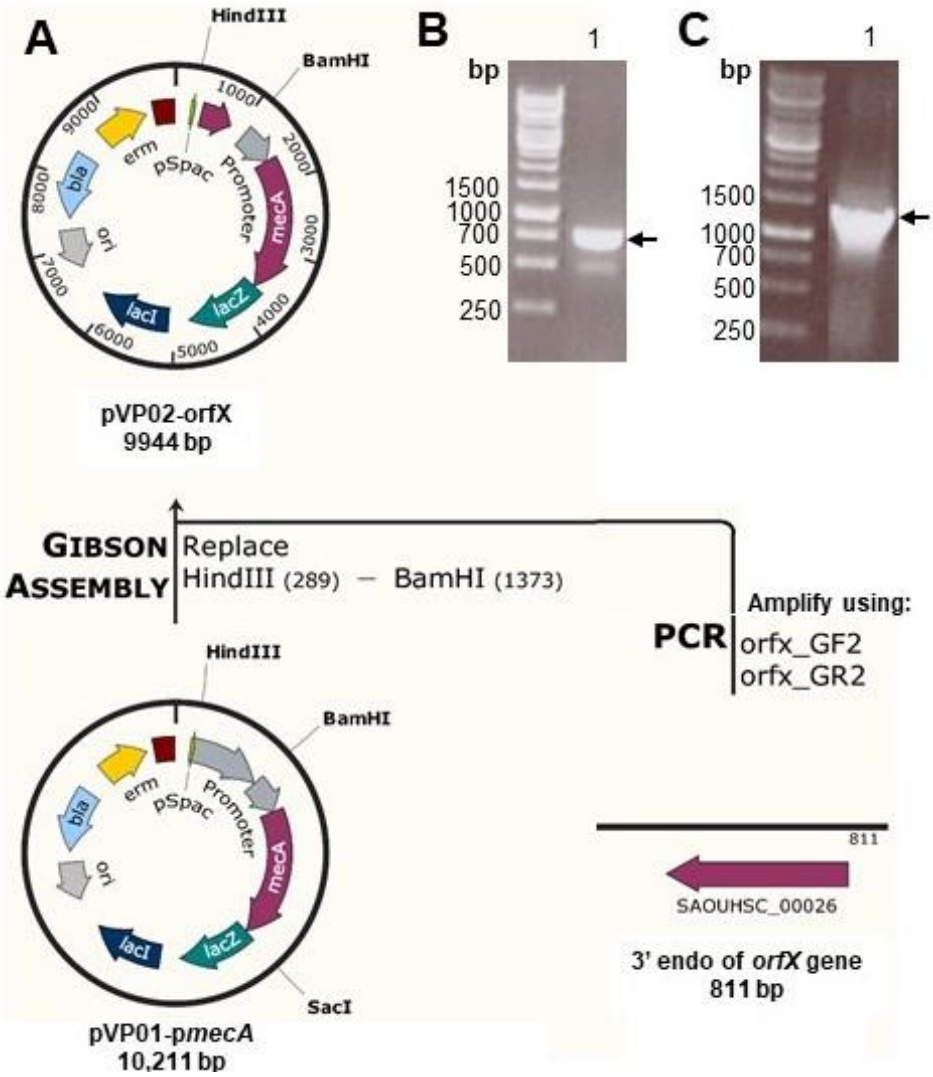

Figure 4.16 Construction of a suicide vector for p*mecA* expression from the *orfX* site in *S. aureus*

A) Diagrammatic illustration of pVP02-*orfX* construction. An 811 bp fragment covering downstream region of the *orfX* gene and the intergenic region was PCR amplified from *S. aureus* genomic DNA using orfX_GF2 and orfX_GR2. These primers were designed to regenerate the restriction site HindIII/BamHI. The pVP01-p*mecA* plasmid was linearised using HindIII/BamHI restriction enzymes. The linearised plasmid backbone and *orfX* fragments were joined by Gibson assembly, resulting into pVP02-orfX.
B) 1% w/v TAE agarose gel showing product of ~811 bp representing *orfX* 3' fragment using sequencing primers 5orfX and 3orfX. The expected band is marked by an arrow. DNA fragments were used as size markers for agarose gel electrophoresis.
C) The p*mecA* insert was amplified using overlapping primers *mecA*_F and *mecA*_R producing a band of ~1902 bp marked by a black arrow. DNA fragments were used as size markers for agarose gel electrophoresis.

4.2.7 Screen for functional PBP2A fluorescent fusions

In MRSA, an acquired PBP2A, encoded by the *mecA* gene is a membrane associated protein penicillin binding protein with transpeptidation activity (Macheboeuf et al., 2006; Pinho et al., 2001b). It is required for the final assembly of peptidoglycan in the presence of β-lactam antibiotics (Sauvage et al., 2008), when the activity of native PBPs is inhibited, however the presence of PBP2 is still required (Pinho et al., 2001b, 2001a). Previous studies have shown that PBP2 mainly localised to the septum throughout the cell division (Pinho and Errington, 2005) even when the cells are treated with oxacillin (Tan et al., 2012a). However, the subcellular localisation of PBP2A is not yet studied. In an effort to understand the localisation of PBP2A in a well-defined genetically amenable MRSA background, PBP2A fluorescent fusions were constructed with eYFP, CLIP and SNAP.

4.2.7.1 Construction of *S. aureus* eYFP-PBP2A strains

In an attempt to study the localisation of PBP2A, an *S. aureus* strain producing PBP2A fused with eYFP was constructed. N-terminal fusion of eYFP joined to PBP2A by a 6-amino acid flexible linker (GSGGGS) was constructed using pGM068 (McVicker et al., 2014) integration plasmid. The expression of eYFP-PBP2A was under the native promoter of *mecA*.

The full-length fragment containing the *mecA* promoter, *eyfp* and *mecA* sequences was gene synthesised by GeneArt Gene Synthesis service (Invitrogen). The synthetic eYFP-PBP2A encoding fragment was inserted into pMK-RQ (KanR), an *E. coli* shuttle vector. pMK-RQ_eYFP-PBP2A was transformed into electrocompetent *E. coli* DH5α (SJF5017). The eYFP-PBP2A fragment was PCR amplified using 3*mecA*_F1 and 3*mecA*_R1 primers and PCR purified insert was cloned into BamHl/Sacl cut linearised pGM068 *lysA* plasmid, resulting in pVP03_eYFP-PBP2A (Figure 4.17 A). Subsequently, pVP03_eYFP-PBP2A was transformed into electrocompetent DH5α *E. coli* resulting into SJF5019. Next, pVP03_eYFP-PBP2A was isolated from SJF5019 using a Plasmid Midiprep Kit (Sigma) followed by transformation into RN4220 to create RN4220 *lysA*::eYFP-PBP2A

(SJF5021). Integration of plasmid was confirmed by selection of transformants on agar containing erythromycin (5 µg/ml) and lincomycin (25 µg/ml). The chromosomal *lysA* region containing eYFP-PBP2A (Figure 4.17 B) was then moved to SH1000, multicopy copy *mecA* cured background SJF4993 (SH1000 pRB474 p*mecA* cured) and single copy *mecA* cured background SJF5010 (SH1000 *lysA::kan* cured) by phage transduction creating SJF5022 (SH1000 *lysA*::eYFP-PBP2A), SJF5023 (pRB474-p*mecA*-cured *lysA*::eYFP-PBP2A) and SJF5066 (*mecA*-cured-*rpoB* (H929Q) *lysA*::eYFP-PBP2A), respectively. The insertion of eYFP-PBP2A was verified by PCR amplification of p*mecA* and *lysA*-*mecA* fragment (Figure 4.17 C and D).

Based on the observations reported in previous sections 3.2.1.2 and 4.2.1.3, removal and subsequent reintroduction of *mecA* resulted into concomitant high-level oxacillin resistance. Therefore, it was predicted that insertion of eYFP-PBP2A into multicopy copy *mecA* cured background SJF4993 (SH1000 pRB474 p*mecA* cured) and single copy *mecA* cured background SJF5010 (SH1000 *lysA::kan* cured) would promote high-level resistance. In order to determine oxacillin susceptibility of SJF5022 (SH1000 *lysA*::eYFP-PBP2A), SJF5023 (SJF4993, pRB474-p*mecA*-cured *lysA*::eYFP-PBP2A) and SJF5066 (SJF5010, *mecA*-cured-*rpoB* (H929Q) *lysA*::eYFP-PBP2A) Etest was performed which showed that all three strains were sensitive to oxacillin with MIC value of 0.25 (SJF5022 and SJF5023) and 0.12 (SJF5066) µg/ml (Figure 4.17 E). Furthermore, SJF5022, SJF5023 and SJF5066 were grown in BHI broth containing methicillin (2, 4 and 6 µg/ml), showed no growth after overnight incubation at 37ºC.

Taken together, sensitivity to oxacillin would suggest that the eYFP-PBP2A fusion is not functional due to misfolding of PBP2A.

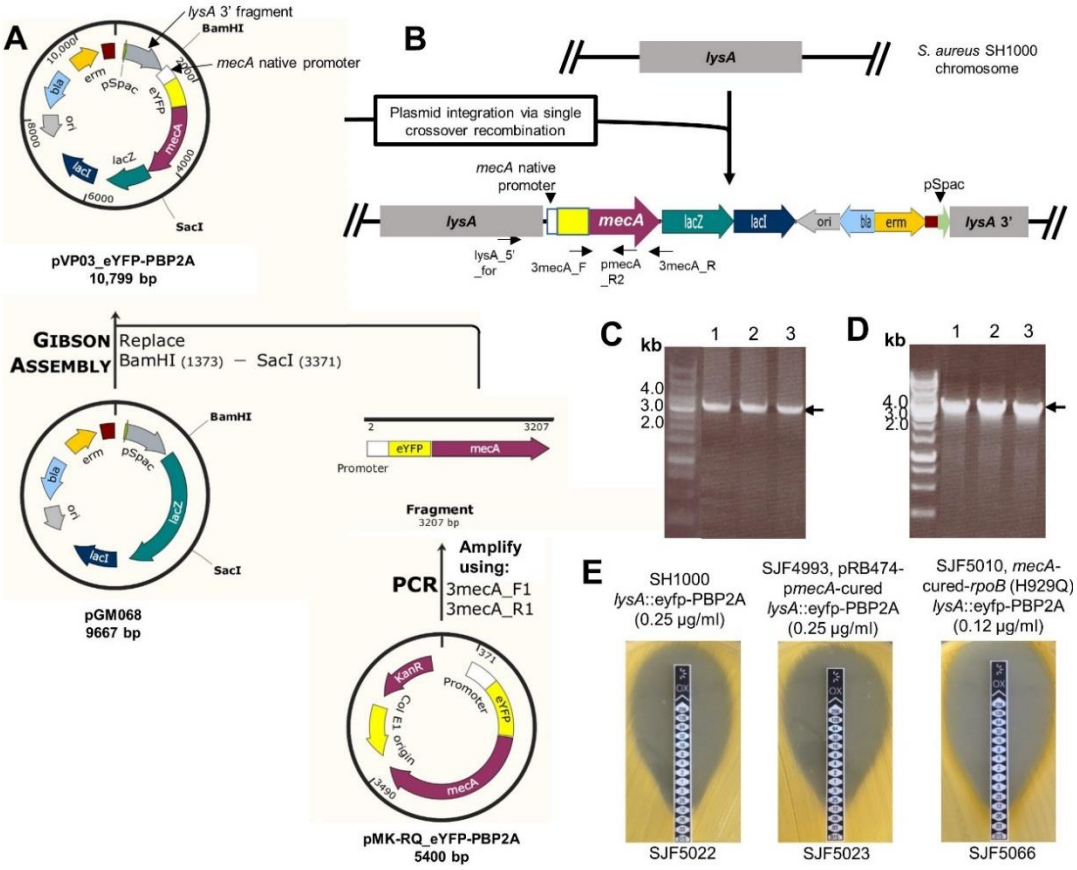

Figure 4.17 Construction SH1000 *lysA*::eYFP-PBP2A using p*mecA* cured backgrounds

A) Diagrammatic illustration of pVP03_eYFP-PBP2A construction. The full length insert comprising native *mecA* promoter, eYFP joined by a 6-amino acid linker and *mecA* was synthesised by GeneArt (Invitrogen) services cloned into an *E. coli* shuttle vector pMK-RQ_eYFP-PBP2A (SJF5017). The plasmid was isolated and an insert was amplified using overlapping primers 3*mecA*_F1 and 3*mecA*_R1. The PCR product was cloned into BamHI and SacI cut integration plasmid, pGM068 by Gibson assembly, resulting in pVP03_eYFP-PBP2A (*E. coli* pVP03_eYFP-PBP2A, SJF5019).
B) Physical map showing insertion of pVP03-eYFP-PBP2A plasmid at the *lysA* locus. Primer binding sites are also shown with arrows.
C) Genomic DNA was isolated from SJF5022 (lane 1), SJF5023 (lane 2) and SJF5066 (lane 3) for PCR verification. 1% w/v TAE agarose gel showing a product of 3207 bp representing the insertion of eYFP-PBP2A fragment using sequencing primers 3*mecA*_F and 3*mecA*_R. The expected band is marked by an arrow. DNA fragments were used as size markers for agarose gel electrophoresis.
D) Genomic DNA was isolated from SJF5022 (lane 1), SJF5023 (lane 2) and SJF5066 (lane 3) for PCR verification. 1% w/v TAE agarose gel showing a product of ~4000 bp representing the insertion of eYFP-PBP2A fragment at *lysA* locus using sequencing primers lysA_5'_For (Forward) and p*mecA*2_seqR2 (Reverse). The expected band is marked by an arrow. DNA fragments were used as size markers for agarose gel electrophoresis.
E) The oxacillin susceptibility of eYFP-PBP2A constructs SJF5022 (SH1000 *lysA*::eYFP-PBP2A), SJF5023 (SJF4993, pRB474-p*mecA*-cured *lysA*::eYFP-PBP2A) and SJF5066 (SJF5010, *mecA*-cured-*rpoB* (H929Q) *lysA*::eYFP-PBP2A) was determined using the Etest method. Oxacillin MICs are listed in brackets for all strains.

4.2.7.2 Construction of *S. aureus* PBP2A-CLIP strains

The CLIP-tag (NEB) is a small protein tag (20 kDa) based on a human DNA repair enzyme, O^6-alkylguanine-DNA-alkyltransferase (AGT) that covalently binds with CLIP-tag substrates derived from benzylcytosine (BC) (Keppler et al., 2003). The CLIP-tag can be fused to any protein of interest and labelled with range of synthetic CLIP-tag substrates conjuncted with a fluorophore.

The full-length CLIP-tag fragment encoding a flexible linker of 6-amino acids (GSGGGS) upstream of CLIP-tag was gene synthesised by GeneArt Gene Synthesis service (Invitrogen). The CLIP-tag DNA sequence was codon optimised for *S. aureus* prior to synthesis. The synthetic CLIP-tag fragment was supplied in an *E. coli* shuttle vector, pMA-T_CLIP-tag (AmpR) (Invitrogen). pMA-T_CLIP-tag was transformed into electrocompetent *E. coli* DH5α upon arrival (SJF5013). The CLIP-tag fragment together with a linker was amplified by PCR using pMA-T_CLIP-tag as a template and overlapping VP54_F and VP55_R primers, resulting in a 613 bp product. Simultaneously, p*mecA* fragment was amplified by PCR using overlapping VP49_F and VP53_R primers, resulting in a 2579 bp product. Both PCR purified fragments were cloned into BamHI/SacI cut version of pGM068 (TetR) plasmid backbones, with tetracycline resistant cassette. This resulted in pVP06_PBP2A-CLIP (Figure 4.18 A) creating SJF5029 (pVP06_PBP2A-CLIP) following transformation into electrocompetent *E. coli* DH5α. The insertion of CLIP-tag was verified by PCR amplification using VP56_F and VP57_R primers resulting in a 567 bp product (Figure 4.18 B). The insertion of p*mecA* was verified by PCR amplification using p*mecA*2_seqF1 and p*mecA*2_seqR2 primers resulting in a 3500 bp product (Figure 4.18 C). Subsequently, pVP06_PBP2A-CLIP was isolated from SJF5029 for RN4220 transformation. However, there was no positive RN4220 transformants recovered from agar plate containing tetracycline (5 µg/ml). Several unsuccessful attempts were made to obtain RN4220 *lysA*::PBP2A-CLIP fusion.

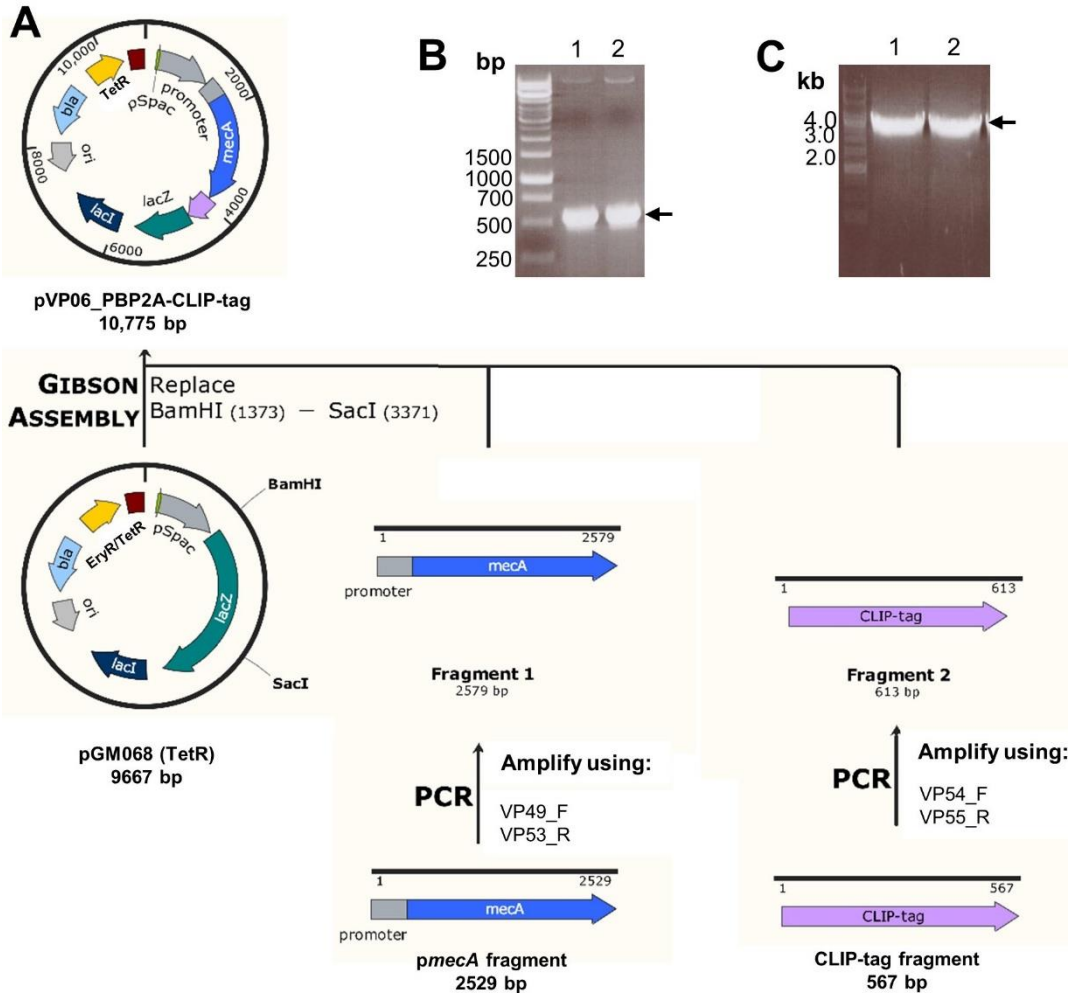

Figure 4.18 Construction of pVP06_PBP2A-CLIP

A) Diagrammatic illustration of pVP06_PBP2A-CLIP construction. Codon optimised, full-length CLIP-tag sequence along with 6-amino acid flexible linker upstream was synthesised by GeneArt (Invitrogen) services and cloned into an *E. coli* shuttle vector pMA-T_CLIP-tag (SJF5013). CLIP-tag fragment was amplified from using pMA-T_CLIP-tag (SJF5013) as a template with VP54_F and VP55_R primers. The p*mecA* fragment was amplified using VP49_F and VP53_R primers. Both fragments were PCR purified and cloned into BamHI and SacI cut integration plasmid, pGM068 (TetR) by Gibson assembly, resulting in pVP06_PBP2A-CLIP.
B) The insertion of CLIP-tag into pVP06_PBP2A-CLIP of SJF5029 was verified by PCR using VP56_F and VP57_R primers producing a band of 567 bp marked by a black arrow. DNA fragments were used as size markers for agarose gel electrophoresis.
C) The insertion of p*mecA* into pVP06_PBP2A-CLIP of SJF5029 was verified by PCR using p*mecA*2_seqF1 and p*mecA*2_seqR2 primers producing a band of 3500 bp marked by a black arrow. DNA fragments were used as size markers for agarose gel electrophoresis.

4.2.7.3 Construction of *S. aureus* PBP2A-SNAP strains

Similar to CLIP-tag (NEB), the SNAP-tag (NEB) is a highly engineered, small protein (20 kDa) tag based on a human DNA repair enzyme, O^6-alkylguanine-DNA-alkyltransferase (AGT). However, SNAP-tag covalently binds to benzylguanine (BG) substrates (Keppler et al., 2003). The SNAP-tag can be fused to any protein of interest and labelled with range of synthetic SNAP-tag substrates conjuncted with a fluorophore without affecting the reaction with SNAP-tag.

The full-length SNAP-tag fragment was PCR amplified from pCQ11-FtsZ-SNAP (Fabien Grein) as a template using VP51_F and VP52_R. the overlapping primers were designed to insert a flexible linker of 6-amino acids (GSGGGS) upstream of SNAP-tag. Simultaneously, p*mecA* fragment was amplified by PCR using overlapping VP49_F and VP50_R primers, resulting in a 2588 bp product. Both fragments were PCR purified and cloned into BamHI/SacI cut version of pGM068 plasmid backbones, with erythromycin/lincomycin for *S. aureus*; resulting in pVP04_PBP2A-SNAP (Figure 4.19 A). The plasmid was transformed into *E. coli* DH5α electrocompetent strain (NEB), creating SJF5012. The insertion of SNAP-tag was verified by PCR amplification using VP51_F and VP52_R primers resulting in a 558 bp product (Figure 4.19 B). The insertion of p*mecA* was verified by PCR amplification using p*mecA*2_seqF1 and p*mecA*2_seqR2 primers resulting in a 3500 bp product (Figure 4.19 C). pVP04_PBP2A-SNAP was isolated from SJF5012 and transformed into electrocompetent RN4220. The transformants were selected on agar plate containing erythromycin (5 µg/ml) and lincomycin (25 µg/ml). Genomic DNA was isolated from positive transformants to verify the integration of pVP04_PBP2A-SNAP at the *lysA* locus. PCR amplification using lysA_5'_For and p*mecA*2_SeqR2 primers produced a ~4000 bp product. A phage lysate from RN4220 *lysA*::PBP2A-SNAP (SJF5018) was used to move *lysA* region containing PBP2A-SNAP (Figure 4.19 D) into SH1000; multicopy copy *mecA* cured background, SJF4993 (SH1000 pRB474 p*mecA* cured); single copy *mecA* cured background, SJF5010 (SH1000 *lysA::kan* cured) and a *gdpP*

mutant, (SJF5025) by phage transduction creating SJF5020 (SH1000 *lysA*::PBP2A-SNAP), SJF5027 (pRB474-p*mecA*-cured *lysA*::PBP2A-SNAP), SJF5028 (*mecA*-cured-*rpoB* (H929Q) *lysA*::PBP2A-SNAP) and SJF5030, (Δ*gdpP*::*kan lysA*::PBP2A-SNAP), respectively.

In order to determine the oxacillin susceptibility of PBP2A-SNAP strains, the oxacillin Etest method was performed. SJF5020 (SH1000 *lysA*::PBP2A-SNAP) remained sensitive to oxacillin (0.5 µg/ml) whereas, reintroduction of *mecA* via PBP2A-SNAP fusion into *mecA* cured backgrounds, SJF5027 (pRB474-p*mecA*-cured *lysA*::PBP2A-SNAP), SJF5028 (*mecA*-cured-*rpoB* (H929Q) *lysA*::PBP2A-SNAP) only showed sensitivity (oxacillin MIC = 1 µg/ml) or intermediate resistance to oxacillin (MIC = 8 µg/ml), respectively (Figure 4.19 F). Similar to SJF5027, PBP2A-SNAP in the *gdpP* mutant background (SJF5030) remained sensitive to oxacillin (MIC = 1 µg/ml) (Figure 4.19 F). The detection of intermediate level resistance (SJF5028) to oxacillin suggests that the C-terminal SNAP fused to PBP2A is likely to be affecting its function.

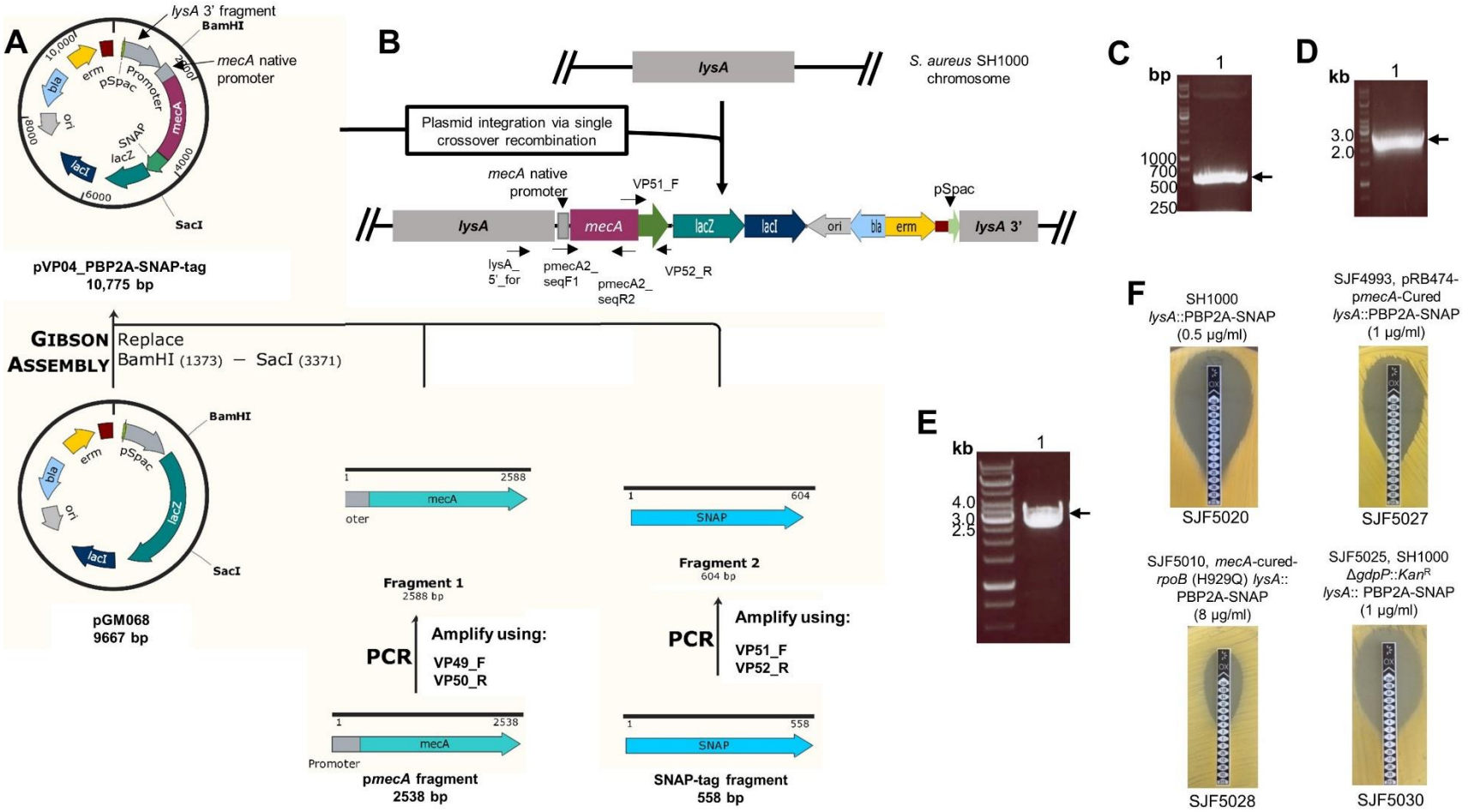

Figure 4.19 Construction of SH1000 *lysA*::PBP2A-SNAP fusion

A) Diagrammatic illustration of pVP04_PBP2A-SNAP construction. SNAP-tag was amplified with pCQ11-FtsZ-SNAP (Fabien Grein) as a template using overlapping primers VP51_F and VP52_R primers producing 604 bp fragment. Primers were designed to insert a flexible linker (6-amino acids) upstream of SNAP. The p*mecA* fragment was PCR amplified using VP49_F and VP50_R producing 2588 bp fragment. The purified PCR products were cloned into BamHI/SacI cut pGM068 by Gibson assembly, resulting in pVP04_PBP2A-SNAP (*E. coli* pVP04_PBP2A-SNAP, SJF5012).
B) Physical map showing insertion of pVP04_PBP2A-SNAP plasmid at the *lysA* locus. Primer binding sites are also shown with arrows.
C) The insertion of the SNAP-tag in pVP04_PBP2A-SNAP (lane 1) was verified by PCR using VP51_F and VP52_R primers producing a band of 558 bp marked by a black arrow. DNA fragments were used as size markers for agarose gel electrophoresis.
D) The insertion of p*mecA* in pVP04_PBP2A-SNAP (lane 1) was verified by PCR using p*mecA*2_seqF1 and p*mecA*2_seqR2 primers producing a band of 3500 bp marked by a black arrow. DNA fragments were used as size markers for agarose gel electrophoresis.
E) Genomic DNA was isolated from RN4220 PBP2A-SNAP (SJF5018) (lane 1) for PCR verification. 1% w/v TAE agarose gel showing a product of ~4000 bp representing the insertion of PBP2A-SNAP at the *lysA* locus using sequencing primers lysA_5'_For (Forward) and p*mecA*2_SeqR2 (Reverse). The expected band is marked by an arrow. DNA fragments were used as size markers for agarose gel electrophoresis.
F) Oxacillin susceptibility of SH1000 *lysA*::PBP2A-SNAP (SJF5020); SJF4993, pRB474-p*mecA*-cured *lysA*::PBP2A-SNAP (SJF5027); SJF5010, *mecA*-cured-*rpoB* (H929Q) *lysA*::PBP2A-SNAP (SJF5028) and SJF5025, Δ*gdpP*::*kan lysA*::PBP2A-SNAP (SJF5030) was determined using the Etest method. Oxacillin MICs are listed in brackets for all strains.

4.2.7.3.1 Localisation of PBP2A-SNAP in *S. aureus* in the absence of oxacillin

The subcellular localisation of *S. aureus* PBP2A was visualised using fluorescence microscopy of SJF5020 (SH1000 *lysA*::PBP2A-SNAP) and SJF5028 (*mecA*-cured-*rpoB* (H929Q) *lysA*::PBP2A-SNAP). The cells were grown to an OD_{600} 0.5 in the absence of oxacillin. To optimise the labelling conditions, different concentrations (0.25 and 0.5 µM) of SNAP-Cell TMR-Star (NEB) substrate was tested but did not produce a fluorescence signal. Therefore, the collected cells were incubated with 1 µM SNAP-Cell TMR-Star at 37ºC for 30 min for labelling. SNAP-Cell TMR-Star is a cell permeable substrate based on 6-carboxytetramethylrhodamine. It is a red fluorescent dye which covalently binds to SNAP-tag fusion proteins.

Previous studies have shown that PBP2 localises at the septum (Pinho and Errington, 2003) and that PBP2A takes over its transpeptidase activity in the presence of oxacillin (Pinho and Errington, 2005; Pinho et al., 2001b). This suggests that PBP2A is recruited at the septum. SH1000 was labelled as a control which showed no signal with the same contrast for SJF5020 and SJF5028 (Figure 4.20 A). Preliminary data from the raw images of SJF5020 showed cytoplasmic signal whereas, deconvolution revealed a collection of patches distributed around the cell surface (Figure 4.20 B). In SJF5028, in the presence of *rpoB* (H929Q) mutation, a bright signal at the septum was observed, this was further highlighted by deconvolution which reduced the cytoplasmic signals (Figure 4.20 C). However, not all cells in the field showed septal localisation of PBP2A-SNAP. Based on preliminary data, this observation suggests that PBP2A is able to localise at the midcell in the absence of oxacillin when the cells have acquired an *rpoB* mutation. However, this experiment was a trial to optimise for a brighter fluorescence substrate and requires further tests to verify the findings.

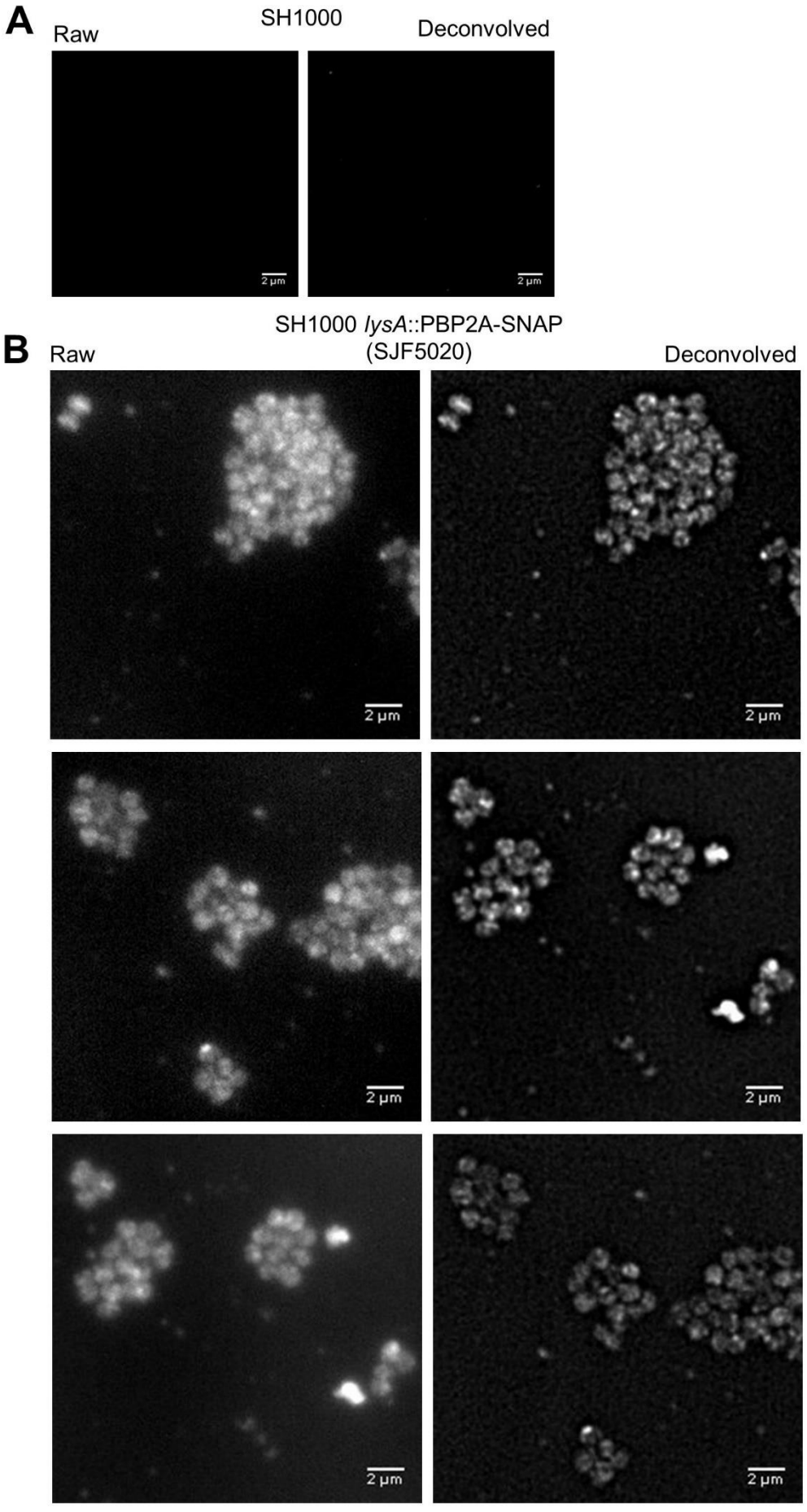
A
SH1000
Raw
Deconvolved
2 µm
2 µm
B
SH1000 lysA::PBP2A-SNAP
(SJF5020)
Raw
Deconvolved
2 µm
2 µm
2 µm
2 µm
2 µm
2 µm

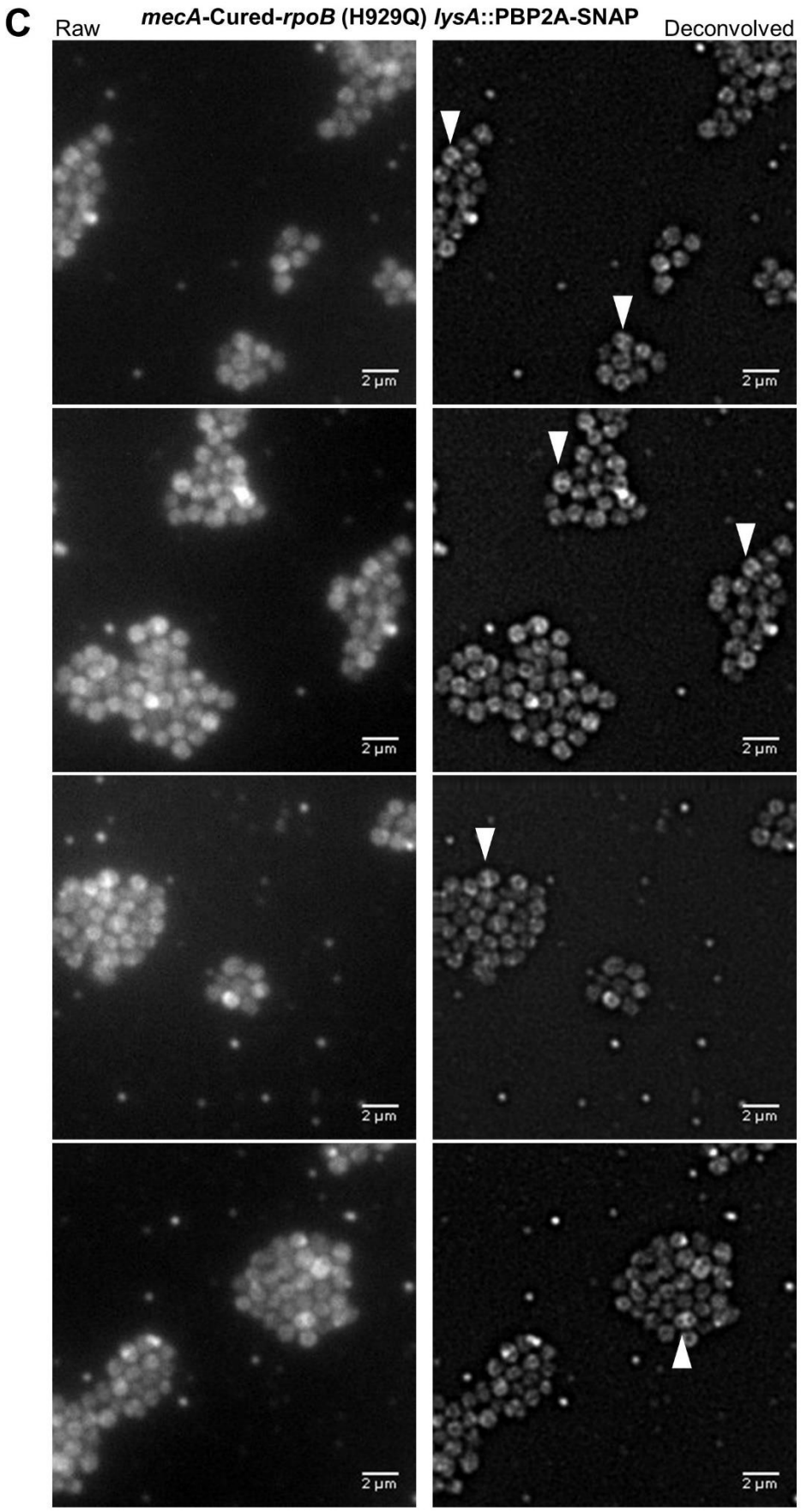

Figure 4.20 Localisation of PBP2A-SNAP TMR-Star in the absence of oxacillin

A) SH1000 labelled with 1 µM SNAP-Star showed no signal. The images are average intensity projections of z-stacks images acquired at 250 nm z-intervals. The same contrast was adjusted for all images
B) PBP2A-SNAP in SJF5020 (SH1000 *lysA*::PBP2A-SNAP) was labelled with 1 µM SNAP-Cell TMR-Star for 30 mins. The images are z-stack images with average intensity projections are acquired at 250 nm z-intervals. Same contrast was adjusted for all raw and deconvolved images separately.
C) For SJF5028 (*mecA*-cured-*rpoB* (H929Q) *lysA*::PBP2A-SNAP), PBP2A-SNAP was labelled with 1 µM SNAP-Cell TMR-Star for 30 mins. Some cells showed a brighter signal at the septum marked by a white arrowhead. The z-stack images with average intensity projections are acquired at 250 nm z-intervals. Same contrast was adjusted for all raw and deconvolved images separately.

4.2.7.3.2 Localisation of PBP2A-SNAP in *S. aureus* in the presence of oxacillin

The localisation of the PBP2A-SNAP fusion was visualised using fluorescence microscopy with SJF5020 (SH1000 *lysA*::PBP2A-SNAP) and SJF5028 (*mecA*-cured-*rpoB* (H929Q) *lysA*::PBP2A-SNAP. The cells were grown in BHI to an OD_{600} 0.5 (early-exponential phase). and then SJF5020 (SH1000 *lysA*::PBP2A-SNAP; oxacillin MIC = 0.5 µg/ml) was sub-cultured into fresh BHI broth containing 0.2 µg/ml of oxacillin. SJF5028 (*mecA*-cured-*rpoB* (H929Q) *lysA*::PBP2A-SNAP; oxacillin MIC = 8 µg/ml) was sub-cultured into fresh BHI containing 2 µg/ml of oxacillin. During the experiment, it was noted that in the presence of 0.2 µg/ml of oxacillin, SJF5020 grew slower than in the absence of oxacillin, suggesting a severe growth defect due to PBP2A-SNAP fusion (results not shown). SJF5028 also grew slower in the presence of 2 µg/ml oxacillin (results not shown).

Following incubation with oxacillin, the cells were then collected and labelled with 1 µM SNAP-Cell TMR-Star for 30 mins and incubated at 37ºC. The labelled cells were washed and then fixed with paraformaldehyde. The cells were then washed and resuspended in dH_2O. The samples were examined using deconvolution fluorescence microscopy. A control (SH1000) did not show fluorescence (Figure 4.21 A). Preliminary data from the raw images of SJF5020 showed cytoplasmic localisation in the presence of oxacillin whereas, deconvolution revealed that some cells appeared to have increased signal distributed around cell surface (Figure 4.21 B). Moreover, SJF5020 appeared to have increased cell size compared to cells grown without oxacillin (Figure 4.20 B).

In SJF5028, in the presence of the *rpoB* (H929Q) mutation, a bright signal at the septum was observed, this was further highlighted by deconvolution which reduced the cytoplasmic signals (Figure 4.21 C). A number of cells showed brighter PBP2A-SNAP signal at the septum compared to the cells grown in the absence of oxacillin (Figure 4.20 C). Based on preliminary data, this observation suggests that PBP2A is able to localise at the midcell more effectively in the presence of oxacillin when the cells have acquired a *rpoB*

mutation. However, this experiment was a trial to optimise for a brighter fluorescence substrate and requires further tests to verify the findings. Further localisation study is needed to determine differences in cell size with and without oxacillin treatment.

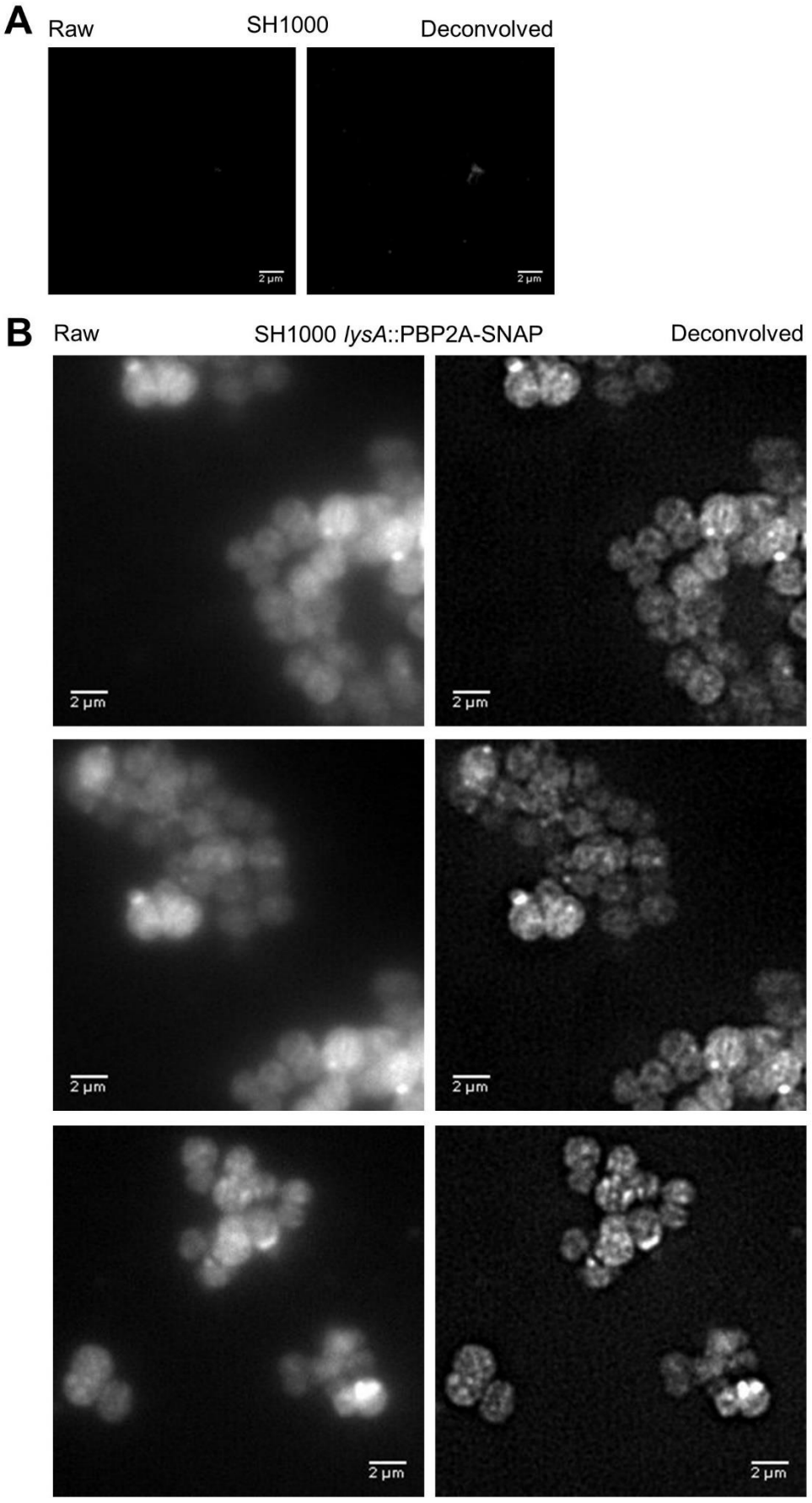
A
Raw
SH1000
Deconvolved
2 µm
2 µm
B
Raw
SH1000 lysA::PBP2A-SNAP
Deconvolved
2 µm
2 µm
2 µm
2 µm
2 µm
2 µm

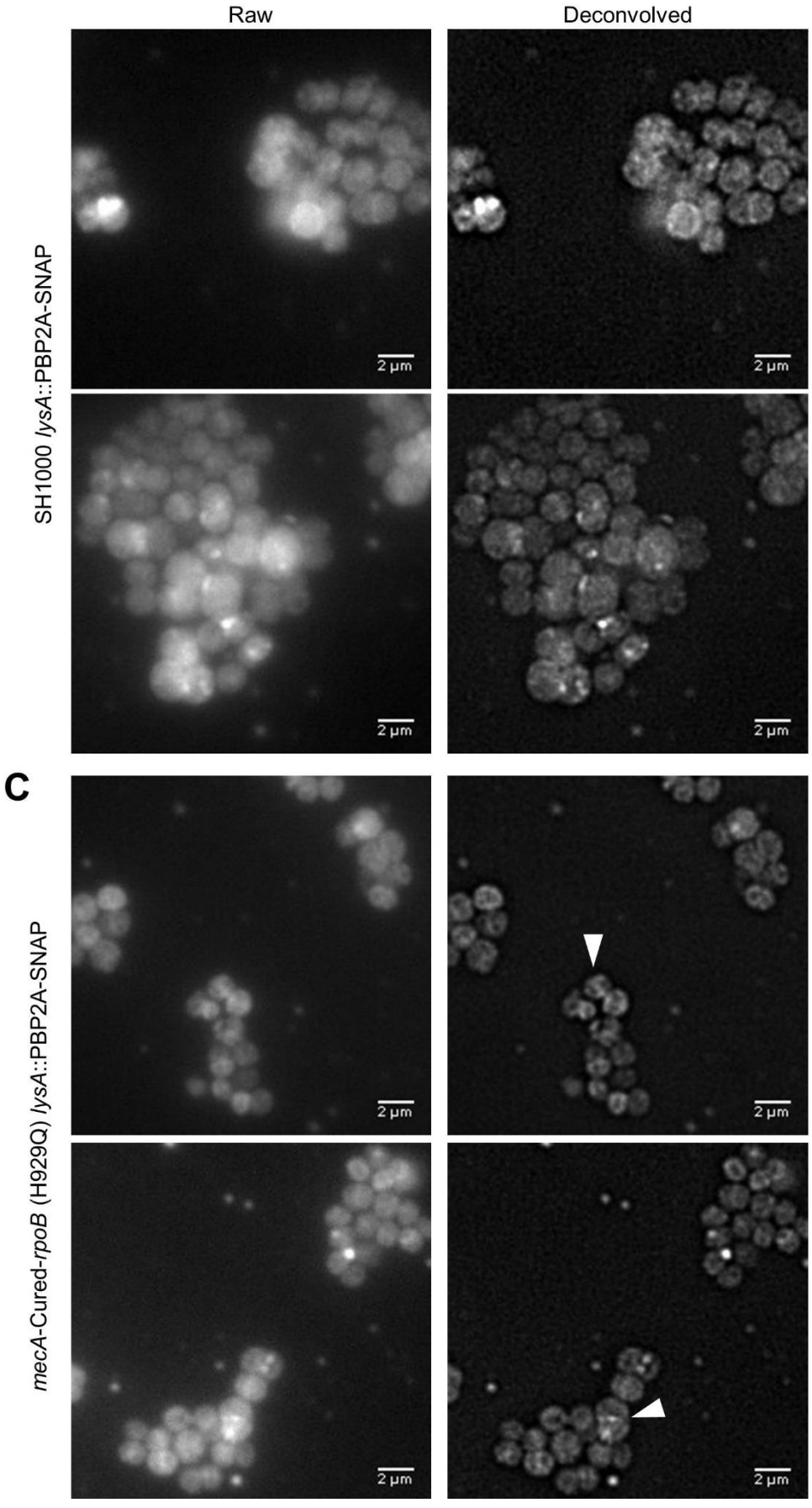
Raw
Deconvolved
SH1000 lysA::PBP2A-SNAP
2 µm
C
mecA-Cured-rpoB (H929Q) lysA::PBP2A-SNAP

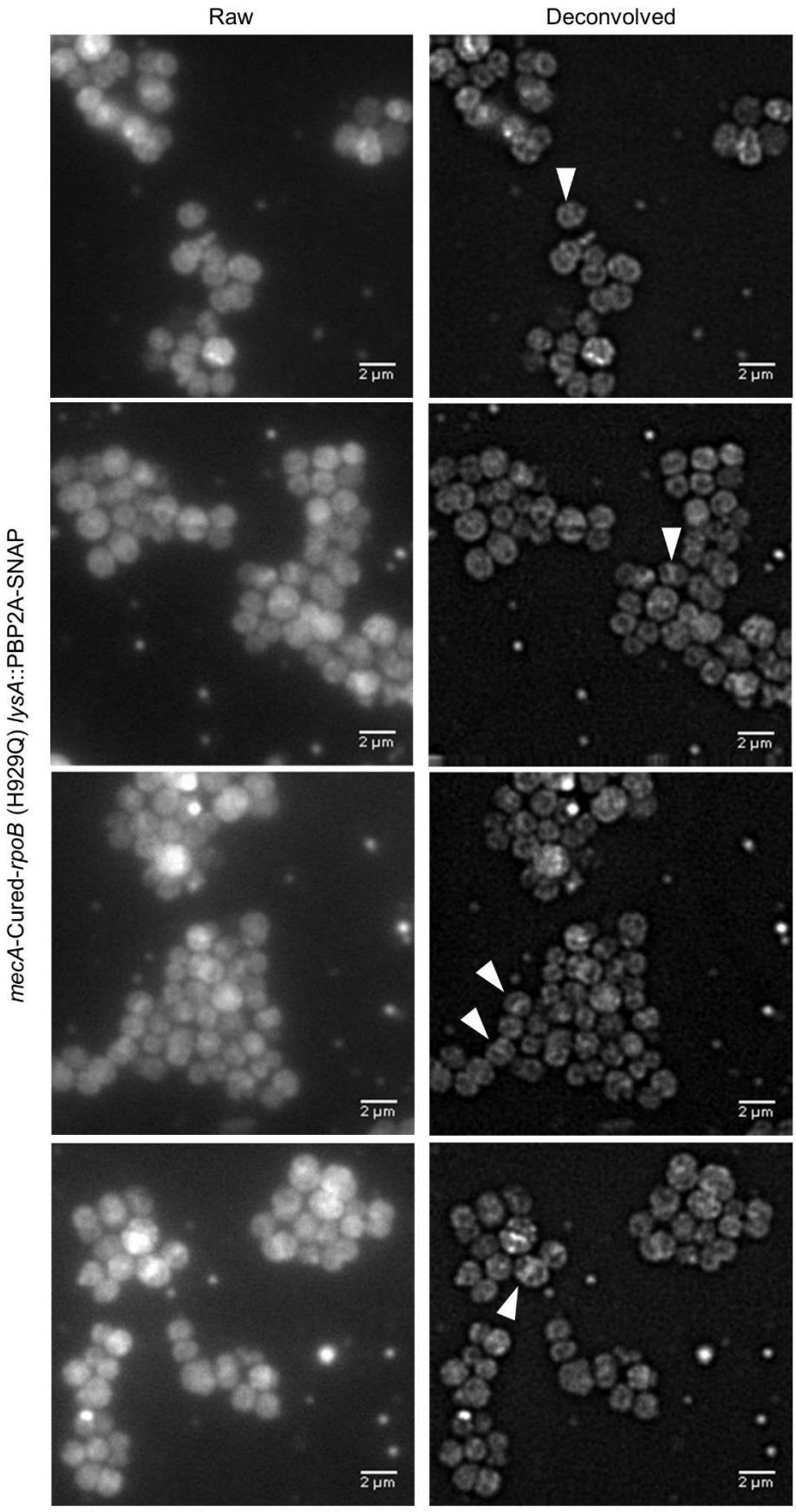

Figure 4.21 Localisation of PBP2A-SNAP TMR-Star in the presence of oxacillin

A) SH1000 labelled with 1 µM SNAP-Star showed no signal. The images are average intensity projections of z-stacks images acquired at 250 nm z-intervals. The same contrast was adjusted for all images
B) SJF5020 (SH1000 *lysA*::PBP2A-SNAP) was grown in the presence of 0.2 µg/ml of oxacillin (MIC = 0.5 µg/ml). PBP2A-SNAP was labelled with 1 µM SNAP-Cell TMR-Star for 30 mins. The images are z-stack images with average intensity projections are acquired at 250 nm z-intervals. Same contrast was adjusted for all raw and deconvolved images separately.
C) SJF5028 (*mecA*-cured-*rpoB* (H929Q) *lysA*::PBP2A-SNAP) grown in the presence of 2 µg/ml of oxacillin (MIC = 8 µg/ml) was labelled with 1 µM SNAP-Cell TMR-Star for 30 mins. Some cells showed a brighter signal at the septum marked by a white arrowhead. The z-stack images with average intensity projections are acquired at 250 nm z-intervals. Same contrast was adjusted for all raw and deconvolved images separately.

4.3 Discussion

An expression of heterogeneous methicillin resistance in *S. aureus* is a characteristic feature capable of developing a stable high-level homogeneous resistance upon exposure to β-lactam antibiotics (Matthews and Stewart, 1984). The introduction of plasmid-borne *mecA* into clinical MSSA leads to low-level resistance (Kim et al., 2013; Murakami et al., 1987; Pozzi et al., 2012) which was able to develop homogeneous high-level resistance upon selection with antibiotic exposure. However, it is difficult to study the underlying mechanism of developing high-level resistance using clinical MSSA and MRSA strains as it limits the experimental genetic manipulation. Therefore, similar to the naturally occurring MRSA carrying chromosomally located *mecA* gene on SCC*mec* element; in this study, an MSSA strain with constitutive expression of single copy *mecA* under its native promoter was constructed using a genetically amenable lab strain, SH1000 (SJF4996), exhibiting low-level of resistance to oxacillin (MIC = 2 µg/ml). Highly oxacillin resistant spontaneous mutants were selected upon exposure to ≥5 µg/ml of methicillin, similar to the results obtained in section 3.2.1.1 (see section 4.2.1.2). However, when single copy chromosomal *mecA* was removed (SJF5010) and replaced with plasmid-borne *mecA* (SJF5024) did not result into high-level resistance (Figure 4.6). This observation suggested the importance of the chromosomal background contributing to the development of high-level resistance.

Prior studies have noted considerable increase in the production of PBP2A (Aedo and Tomasz, 2016; Dordel et al., 2014; Pozzi et al., 2012) was associated with the expression of high-level resistance yet Murakami et al., (1987) demonstrated that strains exhibiting low-level resistance produced large amount of PBP2A similar to those produced by highly resistant strains. This data suggested an apparent noncorrelation between the amount of PBP2A being produced and the MIC, implicating an existence of different genetic determinants responsible for varied resistance pattern. To further examine the correlation between the amount of PBP2A and resistance, Katayama et al., (2003) introduced plasmid-borne *mecA* into naïve (i.e.,

MSSA strains that have not carried *mecA* previously) and experienced (i.e., MRSA strains that have SCC*mec* removed) hosts, showing diminished amounts of PBP2A in naïve compared to experienced strains. Also, upon re-acquisition of *mecA* into experienced the strains exhibited high-level resistance accompanied by increased production of PBP2A (Antignac and Tomasz, 2009), highlighting the importance of the genetic background in regulating β-lactam resistance. Similar results were obtained in this study with highly resistant derivatives (SJF5003 and SJF5034) of SJF4996 (SH1000 *lysA*::p*mecA*) produced up to 3-fold more PBP2A even in the presence of oxacillin, comparable to clinical isolate COL (Figure 4.13 A and B).

It has been proposed that additional compensatory mutations in the genome played a prominent role in supporting high-level resistance (Hartman and Tomasz, 1986; Murakami et al., 1987). To better understand the role of genetic determinants in causing high-level resistance from low-level resistance, four clones of MRSA (De Lencastre et al., 2000) carrying type l SCC*mec* element containing inactive form of regulatory genes, *mecI* and *mecR1* (Hiramatsu et al., 1992) were grown in the presence of oxacillin to obtain homogeneously and highly resistant populations (Dordel et al., 2014). Genome comparisons with their parental strains revealed a number of functionally diverse genetic determinants influencing high-level resistance. Functional categorisation of these genes included guanine metabolism (*guaA*, *prsA*, *hpt* and *relA2*), transcription (*rpoB* and *rpoC*), ribosome structure or translation (*metS*, *lysS*, *cysS*, *valS*, *gcp*, *rpsM* and *sua-5*) (Dordel et al., 2014). Most of these genes have been shown to be involved in inducing the stringent stress response resulting in the development of high-level resistance (Kim et al., 2013; Mwangi et al., 2013). Kim et al (2013) proposed that mutations in genes involved in nutrient uptake, maintaining bacterial metabolism or in transcription systems (RNA polymerase) lead to constitutive expression of *relA* which would be predicted to activate production of (p)ppGpp, invoking the stringent response and concomitant high-level resistance (Figure 4.22). However, the correlation between specific mutations carried by MRSA isolates resulting in a common

consequence remains to be determined. This is because not all highly resistant clones of MRSA carry an altered *relA* system.

In this study, it has been shown that *mecA* is essential for resistance, yet chromosomal genes influence the level of expression of resistance. This is because when chromosomal *mecA* of highly oxacillin resistant mutant (SJF5003, MIC = ≥256 µg/ml) was replaced with kanamycin resistance gene *kan*, it regained susceptibility (SJF5010, MIC = 0.5 µg/ml) however, subsequent reintroduction of *mecA* produced high-level resistance (SJF5011, MIC = ≥256 µg/ml) without further training indicating the contribution of genetic determinant which defines the level of resistance.

The comparison of full genome sequences of highly resistant strains (Table 4.1) Table 4.2 versus low-level resistant parental strain (SJF4996) identified mutations in either *rpoB* or *rpoC* genes (Table 4.2). Acquisition of either *rpo* mutations not only conferred resistance to oxacillin but also to other β-lactams such as cefoxitin and penicillin G (Table 4.3). However, all strains carrying highly resistant strains remained sensitive to rifampicin. Rifampicin resistance is most commonly associated with mutations in *rpoB*, one of the most frequent mutations in *rpoB* (H481Y) promotes rifampicin as well as vancomycin resistance (Matsuo et al., 2011). The identification of *rpo* mutations in this study is not coincidental as *rpo* mutations are also identified in clinical MRSA isolates associated with resistance to specific antibiotics (Table 4.4). Alignment of the RpoB and RpoC sequences from clinical MRSA isolates, COL, Mu50, Mu3, MW2, USA300, JH9, MRSA252; with the Clustal Omega program revealed number of alterations highlighted in green (Appendix 2). The mutations identified in both *rpoB* and *rpoC* of JH9 were previously reported by Mwangi et al (2007). The *rpoB* mutations of COL were previously reported by Dordel et al (2014) and Hiramatsu et al (2013), and further verified using DNA sequencing along with other clinical MRSA isolate used in this study.

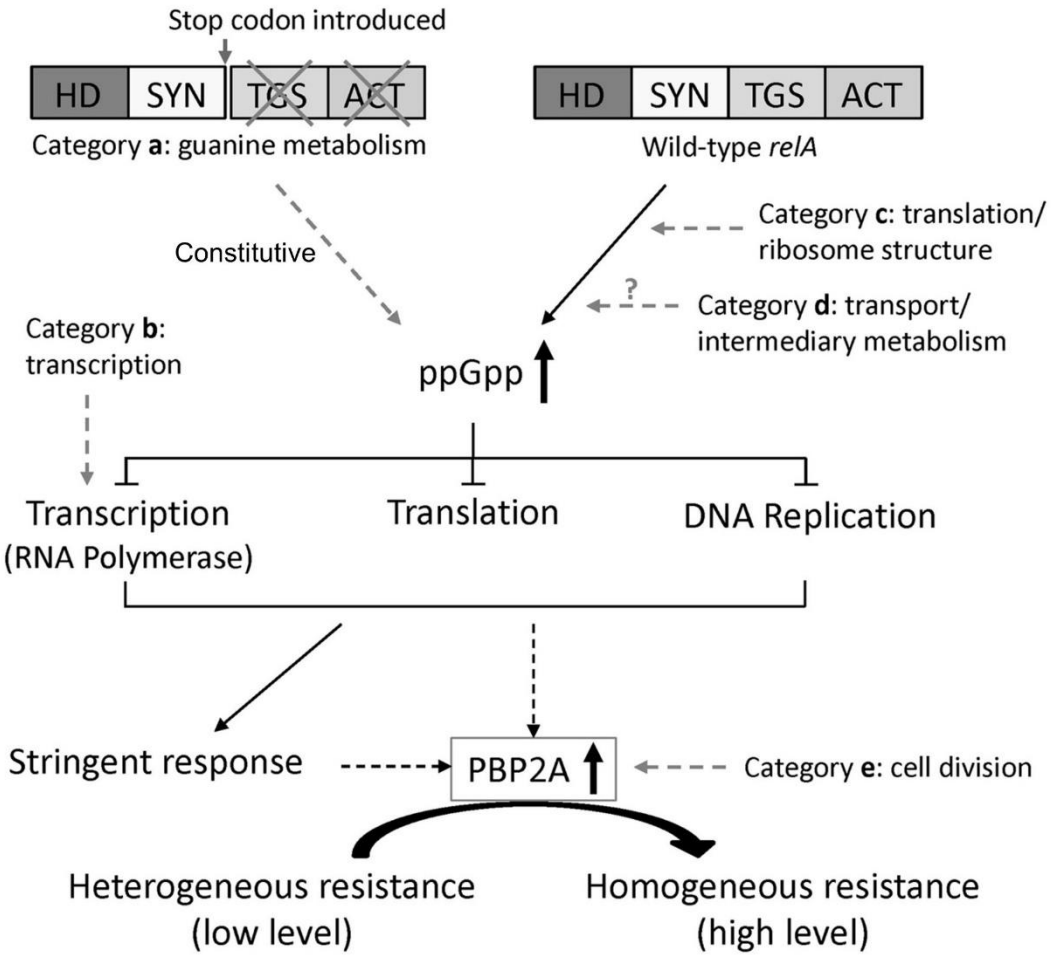

Figure 4.22 Schematic model for stringent response mediated high-level resistance in *S. aureus*

Mutations identified (Dordel et al., 2014; Kim et al., 2013) involved in diverse cellular functions could trigger stringent stress response by increasing cellular ppGpp which controls biosynthetic activities through direct interaction with ribosomal protein and its regulation, resulting into increased production of PBP2A and antibiotic resistance. Taken from (Dordel et al., 2014).
HD, hydrolase; SYN, synthetase; TGS, a domain containing three enzyme activities, threonyl-tRNA synthetase (ThrRS), GTPase and guanosine 3', 5' -bis(diphosphate) 3' -pyrophosphohydrolase (SpoT); ACT, domain containing three enzyme activities, aspartate kinase, chorismite mutase and prephenate dehydrogenase (TyrA).

Genetic complementation of *rpoB* and *rpoC* in representative strains SJF5003 (trained, SH1000 *lysA*::p*mecA rpoB*-H929Q) and SJF5034 (trained, SH1000 *lysA*::p*mecA rpoC*-G740R) not only restored oxacillin susceptibility (MIC = 1 µg/ml) in SJF5044 (SJF5003, *rpoB*+) and SJF5045 (SJF5034, *rpoC*+), respectively but also diminished the production of PBP2A (Figure 4.14 E) similar to the parental strain SJF4996 (Figure 4.13 A). These results were not specific to the strains constructed in this study as replacing COL *rpoB* (A798V and S875L) to WT *rpoB* (NCTC8325) resulted into not only restoration of oxacillin susceptibility comparable to the parental strain SJF4996 (oxacillin MIC = 2 µg/ml) but also reduction in the amount of cellular PBP2A being produced (Figure 4.14 and F). Another possible explanation is that COL carries type l SCC*mec* which contains truncated *mecA* regulatory genes *mecI* and *mecRI* (Deurenberg et al., 2007), resulting in derepression of the *mecA* gene, therefore constitutive production of PBP2A (Figure 4.14 F) however, this can be reversed by replacing *rpoB* to WT (NCTC8325), resulting into decreased production of PBP2A (Figure 4.14 F). Therefore, the *rpo* mutations can be considered 'regulatory mutations'. Moreover, introduction of *mecA* and *rpoB* (H929Q) mutation into Newman strain produced highly oxacillin resistant clones (SJF5050). Collectively, these observations confirm the importance of mutations in either RNA polymerase subunits for the conversion of low-level to high-level homogeneous methicillin resistance.

Recent studies by Aiba et al (2013) demonstrated that two point mutations in *rpoB* (N967I and R644H) were able to cause heterogeneous to homogeneous resistance in N315 upon selection with imipenem. N315 is a hospital-acquired MRSA which carries type ll SCC*mec* element containing a functional *mecI* (*mecA* repressor gene), resulting in strongly repressed *mecA* expression (Hiramatsu et al., 1992). Both *rpoB* mutants had prolonged doubling time and thickened cell wall accompanied by increased amount of cellular PBP2A. Similar features were noted for *rpoB* (H481Y) mutation which raises rifampicin and vancomycin resistance (Katayama et al., 2009; Matsuo et al., 2011). Transcriptional analysis of *rpoB* (N967I) mutant relative to the parental strain showed decrease in expression of *cidABC* and increase

in the expression of *lrgAB* (Aiba et al., 2013). Disruption of *lrgAB* operon is associated with decreased antibiotic tolerance (Groicher et al., 2000) and inactivation of *cid* operon causes increased tolerance to antibiotics (Rice et al., 2003). This suggests the expression of *cid* and *lrg* is modulated by *rpoB* mutations.

rpoB mutations have also been identified in the progression of vancomycin resistance from hetero-VISA→slow-VISA→VISA accompanied by rifampicin resistance (Matsuo et al., 2011; Watanabe et al., 2011). Slow-VISA is a novel phenotype associated with prolonged doubling time (Saito et al., 2014). Not only *rpoB* mutations have shown to be a frequent underlying cause for antibiotic resistance but also mutations in *rpoC* (P440L) showed increase vancomycin resistance (Matsuo et al., 2015). The revertants of *rpoC* (P440L) mutant showed increased susceptibility to vancomycin accompanied by decreased doubling time with reduced cell wall thickness (Matsuo et al., 2015). Surprisingly, a number of revertants had acquired different *rpoC* mutations that were considered to be compensatory, suggesting its influence on the overall gene expression profile (Matsuo et al., 2015). Taken together, it is plausible that *rpo* mutations lead to changes in the way RNA polymerase subunits interact with each other which influences diverse transcriptional regulation, supporting elevated resistance. Therefore, the next chapter moves on to discuss the impact of *rpoB* (H929Q) and *rpoC* (G740R) mutations on global transcription in *S. aureus.*

Chapter 5

The role of *rpoB* and *rpoC* mutations in *S. aureus* high-level methicillin resistance

5.1 Introduction

Early research by Hartman and Tomasz (1986) and Sabath and Wallace (1971) in the study of the molecular basis of expression of methicillin resistance strongly suggested the involvement of genetic determinants in the conversion of low-level to high-level resistance. With the technological advancements in recent years, several studies using whole genome sequencing have revealed a number of genetic factors required for high-level β-lactam resistance.

Mwangi et al (2013) identified a nonsense mutation in *relA* by introducing plasmid-borne *mecA* into an MSSA strain to reproduce high-level β-lactam resistance. Inactivation of *relA* is predicted to result in constitutive production of (p)ppGpp, leading to the stringent stress response (Mwangi et al., 2013). Similar observations were noted when an entire SCC*mec* element was introduced into an MSSA strain (Kim et al., 2013). Furthermore, Griffiths and O'Neill (2012) and Pozzi et al (2012) identified mutations in *gdpP* required for conversion of heterogeneous to homogeneous methicillin resistance. Disruption in *gdpP* is associated with reduced phosphodiesterase activity, resulting into increased intracellular c-di-AMP (Corrigan et al., 2011). Mutations in *gdpP* were also found to be associated with resistance to other broad-spectrum β-lactams such as, ceftobiprole and ceftaroline (Chan et al., 2016). Aiba et al (2013) reported a mutation in the *rpoB* gene implicated in the conversion from low-level to high-level homogeneous resistance by altering the expression of autolysis genes, resulting in reduced autolytic activity associated with a prolonged doubling time. Similarly, nonsense mutations in *relA* and *rpoB* were identified along with other mutations in 25 genes found to be associated with the development of high-level resistance (Dordel et al., 2014).

Moreover, systematic tracking of evolution in the JH lineage *in vivo*, identified 35 point mutations between JH1 (first) and JH9 (last) isolates associated with multidrug resistance (Mwangi et al., 2007). Characterisation of compensatory mutations have led us to one step towards understanding the genomic changes leading to high-level resistance. However, it is important to examine the role of chromosomal mutations on not only of the genomic level but also their effect on bacterial physiology via alterations in the transcriptional and translational capacity. To better understand the transcriptional changes caused by mutations for the conversion of JH1 to multidrug resistant JH9, transcriptional profiling revealed 224 differentially expressed genes; where 48 genes were found to be controlled by *vraR* (Kuroda et al., 2003), and other 32 genes were controlled by *yycF* (Dubrac and Msadek, 2004) and 244 genes positively regulated by the *agr* (Liang et al., 2005) locus. These three transcriptional regulators *agr*, *vraR* and *yycF* also appear to be involved in increased tolerance to vancomycin (Mwangi et al., 2007). Additionally, the expression of many genes are affected by nonsynonymous mutations in *rpoB* that causes pleiotropic effects that are responsible for rifampicin resistance in *B. subtilis* (Maughan et al., 2004). The impacts of *rpoB* H481Y and *relA* F128Y mutations on global gene expression revealed significant upregulation in genes associated with *agr* activity as well as genes involved in capsule biosynthesis (Gao et al., 2013).

Investigating proteins induced by oxacillin in MSSA, Singh et al., (2001) revealed nine proteins were produced in elevated amounts, these include, MsrA (methionine sulfoxide reductase), signal transduction proteins encoded by the *agr* locus, GreA (transcription elongation factor) and GroES (heat shock protein). Comparison of proteomic profiles of MSSA and MRSA in the absence of methicillin showed only the FemA protein with an elevated amount (Cordwell et al., 2002; Lee et al., 2015). FemA is characterised as a factor essential for the expression of methicillin resistance in *S. aureus.* (Berger-Bächi et al., 1989). Another report exploring proteome profiles in MSSA and MRSA identified a total of ten proteins with an elevated amount in MRSA compared to MSSA (Enany et al., 2014). These were Asp23 (alkaline shock protein 23), AhpC (alkyl hydroperoxide reductase subunit C), a

general stress protein, LdhD (D-lactate dehydrogenase), LdhA (L-lactate dehydrogenase), PdhB (pyruvate dehydrogenase E1 component β subunit), SodA (superoxide dismutase), LipA (triacylglycerol lipase precursor), TpiA (triosephosphate isomerase) and a universal stress protein family protein (Enany et al., 2014). Whereas, proteomic response prior to oxacillin treatment in MRSA showed 72 differentially expressed proteins involved in diverse functional categories, such as oxidation-reduction homeostasis and cell wall biosynthesis, indicating a diverse response of the bacteria to oxacillin (Liu et al., 2016c).

Despite several studies, there is no mechanistic understanding of the processes underpinning the ability of *S. aureus* to attain high-level β-lactam resistance. My work has identified mutations in *rpoB* or *rpoC* as being solely responsible for resistance in the presence of *mecA*. It is now important to explain how this effect is mediated.

5.1.1 Aims

The overall aim of this chapter was to establish an RNA-seq approach to understand the molecular basis of methicillin resistance in a well-defined strain background. The specific aims of this chapter were to:

i. Examine transcriptomic responses of experimentally evolved strains expressing low-level and high-level resistance
ii. Systematic identification and comparative analysis of differentially expressed genes associated with high-level resistance
iii. Determine putative regulatory mechanism(s) responsible for increased resistance to β-lactam antibiotics

5.2 Results

5.2.1 Transcriptomics project workflow and data analysis

The popularity of deep sequencing of cDNA molecules (RNA-Seq) has become the tool of choice for global gene expression studies, replacing microarrays to measure simultaneous expression of genes (Wang et al., 2008). Transcriptome profiling using RNA-Seq is a high-throughput sequencing method to map and quantify the complete set of transcripts in order to understand the importance of functional elements of the genome involved in cellular physiology under various conditions (Wang et al., 2009).

My previous work (Chapter 4) determined that development of high-level resistance is conferred by the acquisition of nonsynonymous mutations in either *rpoB* or *rpoC*. In order to better understand the impact of these mutations on global gene expression, RNA-Seq and preliminary analysis was performed by the Glasgow Polyomics facility at the University of Glasgow (Figure 5.1) for comparative transcriptome profiling of five representative strains listed in Table 4.1. Total RNA was isolated from WT control (SH1000), untrained (SJF4996; SH1000 *lysA*::p*mecA*), trained-*rpoB* (SJF5003; SH1000 *lysA*::p*mecA rpoB*-H929Q), trained-*mecA*-cured-*rpoB* (SJF5010; SH1000 *lysA*::*kanA rpoB*-H929Q) and trained-*rpoC* (SJF5034; SH1000 *lysA*::p*mecA rpoC*-G740R) strains. These five representative strains used for transcriptome analysis will be referred to as WT, untrained, trained-*rpoB*, trained-*mecA*-cured-*rpoB* and trained-*rpoC*. The integrity of total RNA was measured prior to the preparation of cDNA library followed by rRNA (ribosomal RNA) depletion. All samples were supplied with three biological replicates to control sample variation. cDNA libraries were sequenced with a 75-basepair single-end read using an Illumina NextSeq™ 500 platform.

For differential gene expression analysis, reads were aligned to the NCTC8325 genome and expression values were determined as normalised counts using DESeq2 package (Love et al., 2014) for each gene. The *mecA* DNA sequence was added to the reference genome prior to alignment.

Differential expression of each gene was tested for variance and estimated differential expression was corrected for multiple comparisons (Padj).

5.2.1.1 Principal Component analysis

DESeq2 is a method which enables a quantitative analysis of comparative transcriptomics data by using a number of computational packages (Love et al., 2014). In order to detect a possible variation in large data sets principal component analysis (PCA) was used, a statistical method which uses gene expression values to define unrelated variables and assign as a principal component(s), allowing the identification of outliers (Stacklies et al., 2007).

PCA analysis of 15 samples (5 representative strains, each with three biological replicates) identified two outliers clustered with a group of different strains. The samples with swapped groups were one of the replicates of WT control (SH1000) and one of the replicates of trained-*mecA*-cured-*rpoB* (SJF5010; SH1000 *lysA*::*kanA rpoB*-H929Q) (Figure 5.2). For comparative data analysis, both replicates were excluded.

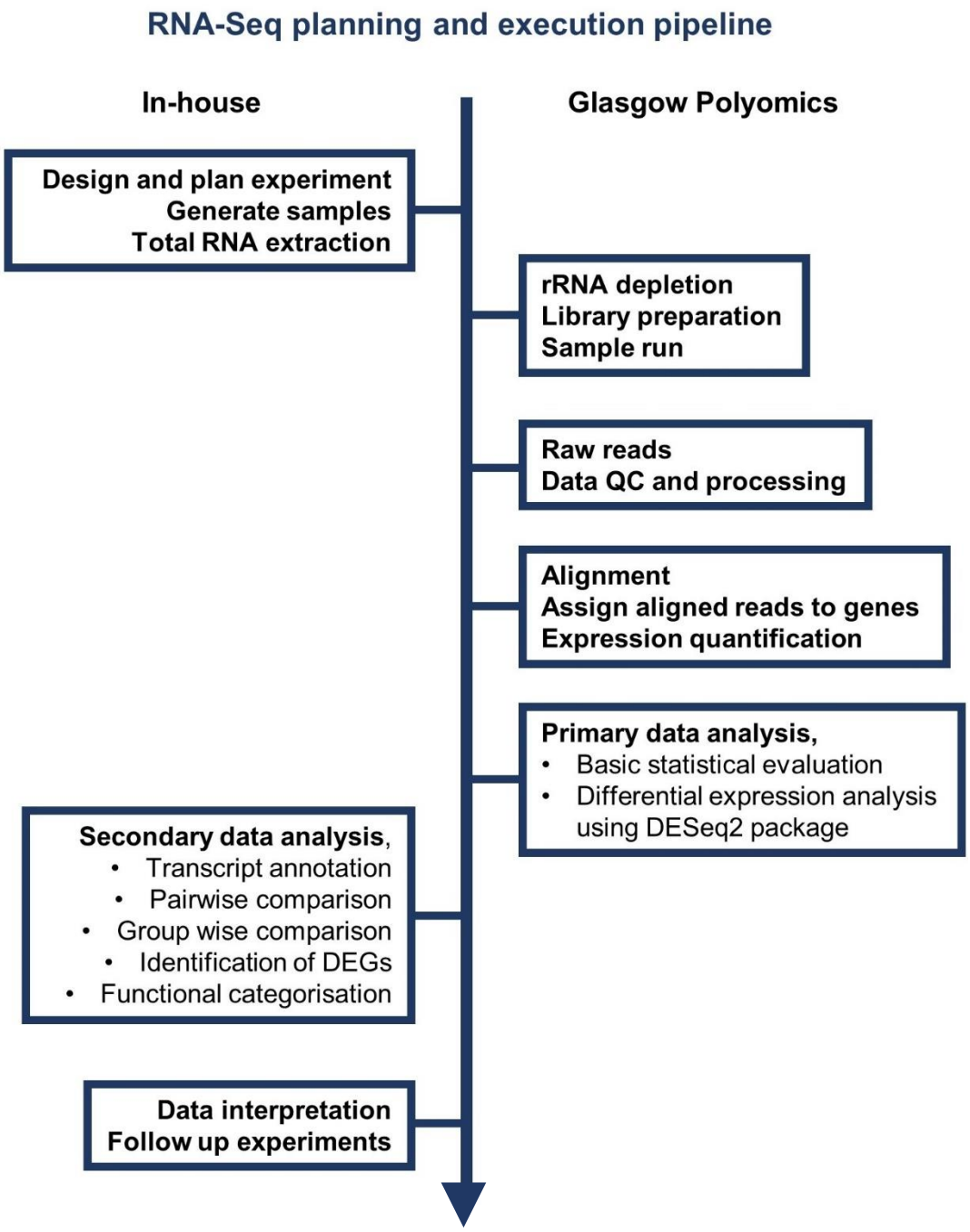

Figure 5.1 RNA-Seq pipeline for transcriptome profiling

Stepwise process illustrating RNA-Seq workflow of five representative strains, WT, untrained, trained-rpoB, trained-*mecA*-cured-rpoB and trained-rpoC. Steps listed on the left side were performed in-house. Steps listed on the right side were carried out by Glasgow Polyomics.

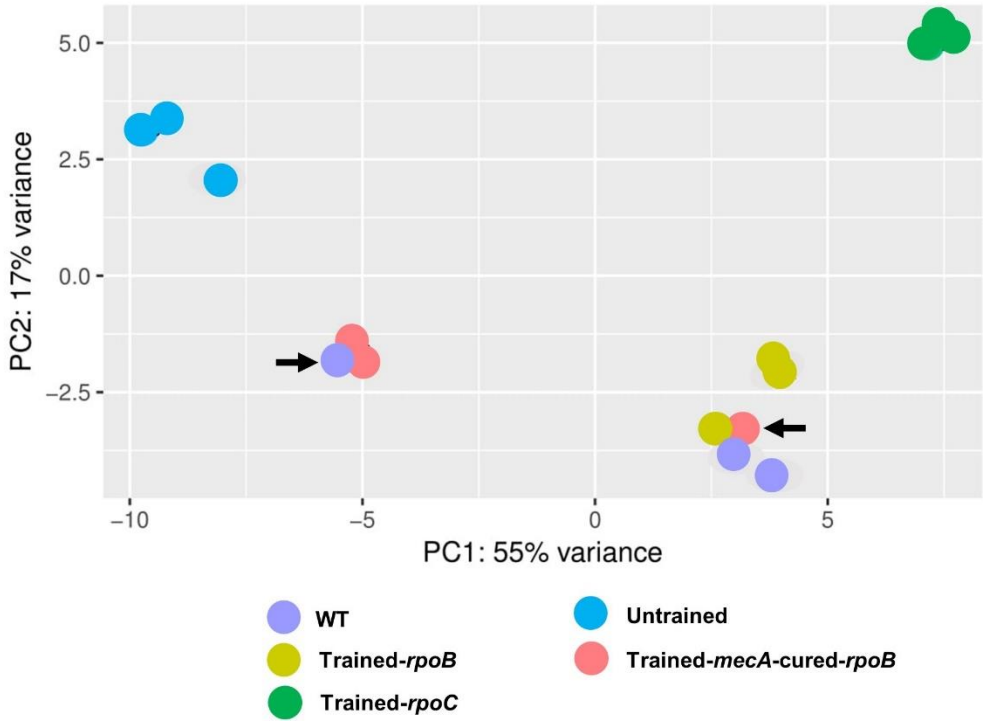

Figure 5.2 Principal component analysis to identify sample variation

2D PCA score plot displaying three biological replicates of each strain clustered together. The samples are WT, untrained, trained-*rpoB*, trained-*mecA*-cured-*rpoB* and trained-*rpoC*. The replicates which are not clustered within the corresponding group are marked with black arrows.

5.2.2 Comparative pairwise analysis of expressed genes

The goal of transcriptomics analysis was to identify differentially expressed genes among five strains in an accurate and unbiased manner. Primary data analysis using the DESeq2 platform generated raw files for each sample containing expression values (normalised counts), p value, padj (adjusted p value) and log2foldchange (log2fc) for each gene. The data was then compared in a pairwise manner between the five samples, resulting in a total of ten pairwise comparisons. In order to carry out secondary analysis to identify statistically significant differentially expressed genes (DEGs), all genes from each pairwise comparisons were annotated using the NCTC8325 genome which produced raw gene names. Next, raw gene names were used to retrieve UniProt protein accession, gene ids (locus tags) and their description using the UniProtKB database. Subsequently, from each pairwise comparison, genes with an adjusted P value <0.05 and log2fc ≥±1 were identified as being statistically significant DEGs. Therefore, the non-significant gene sets were removed retaining only important gene sets for each pairwise comparison. Important gene sets were used to retrieve common genes with differential expression between pairwise and group wise comparisons.

5.2.2.1 Identification of DEGs in untrained compared to SH1000

In order to determine the impact of the acquisition of chromosomal *mecA* and concomitant transcriptional changes in MRSA, global gene expression profiles from untrained exhibiting low-level oxacillin resistance (MIC = 2 µg/ml) and WT were compared. Pairwise comparison of RNA-Seq data identified 193 DEGs with a significant threshold of padj <0.05 and log2fc ≥±1 (2-fold change) (Figure 5.3 A). The variability in all samples of WT and untrained (columns) for 193 DEGs is shown in a heatmap created based on log2 transformed normalised counts which identified changes in expression profiles of both strains (Figure 5.3 A). The full list of 193 DEGs with differential expression is shown in Appendix 4 Table 1. This data suggests that acquisition of *mecA* on its own influenced profound transcriptional changes whilst exhibiting low-level resistance.

5.2.2.2 Identification of DEGs in trained-*rpoB* (H929Q) mutant compared to SH1000

In order to assess the transcriptional response due to the acquisition of a nonsynonymous mutation in *rpoB* (H929Q) of trained-*rpoB* mutant compared to WT, differentially expressed genes from both strains were identified. Based on a pairwise comparison using both strains, there were 9 DEGs identified with significant differential expression (Figure 5.4 A). Three and two biological replicates of trained-*rpoB* mutant and WT were used for transcriptome comparison, respectively. The full list of 9 DEGs with expression values are listed in Appendix 4 Table 2. The expression of *mecA* between strains was demonstrated by boxplot (Figure 5.4 B). Surprisingly, this observation revealed that even though the trained-*rpoB* mutant exhibits high-level oxacillin resistance (MIC ≥256 µg/ml), it requires minimal transcriptional alterations to be able to produce such a high-level resistance. This observation is further supported by PCA analysis as both these strains cluster close to each other (Figure 5.2).

5.2.2.3 Identification of DEGs in trained-*mecA*-cured-*rpoB* (H929Q) compared to SH1000

In order to analyse the impact of *rpoB* mutation on gene expression, trained-*mecA*-cured-*rpoB* was used for comparative analysis against WT. Trained-*mecA*-cured-*rpoB* was derived from trained-*rpoB* by removal of *mecA* (section 4.2.1.3), resulting into restored susceptibility to oxacillin. Therefore, this background allowed to investigate transcriptional changes implemented by *rpoB* mutation alone. Pairwise comparison of RNA-Seq data identified 122 DEGs in trained-*mecA*-cured-*rpoB* (Figure 5.5). Two biological replicates from both strains were used for data analysis. The full list of 122 DEGs with differential expression are shown in Appendix 4 Table 3. This observation indicates that mutation in *rpoB* induces a substantial transcriptional change which can be restored back to WT level in the presence of *mecA* (section 5.2.2.2).

5.2.2.4 Identification of DEGs in trained-*rpoC* (G740R) compared to SH1000

In order to examine the transcriptional changes acquired by trained-*rpoC* strain compared to WT, RNA-Seq data was compared from all biological replicates of both strains. There were 120 DEGs identified between two strains (Figure 5.6 A). The details of DEGs are listed in Appendix 4 Table 4. The expression of *mecA* was significantly higher compared to WT due to lack of *mecA* gene (Figure 5.6 B). Unlike transcriptional responses observed due acquisition of *rpoB* mutation (in the presence of a chromosomal copy of *mecA*), *rpoC* mutant shown to have considerable transcriptional changes compared to WT. However, there were 73 genes found to be reverted back to WT level compared to the original 193 DEGs identified in untrained strain (section 5.2.2.1). Taken together, this data suggests that *rpoC* mutations caused significant changes in transcriptional profile while exhibiting high-level oxacillin resistance (MIC ≥256 µg/ml) similar to that of *rpoB* mutant (SJF5003).

5.2.2.5 Identification of DEGs in trained-*rpoB* (H929Q) compared to untrained

In the presence of *mecA*, the acquisition of the *rpoB* mutation caused a dramatic increase in the resistance phenotype compared to its parental strain, untrained. This observation indicates obvious transcriptional changes have occurred for concomitant increased resistance. In order to examine the transcriptional response in trained-*rpoB*. This was compared to untrained. Pairwise comparative analysis of transcriptional profiles from untrained and trained conditions identified 172 DEGs with significant differential expression (Figure 5.7 A), potentially associated with high-level oxacillin resistance. Furthermore, the acquisition of the *rpoB* mutation led to increased *mecA* expression (Figure 5.7 B), suggesting some increase in the expression of *mecA* is required but not sufficient for developing high-level resistance. Three biological replicates of both conditions were used for comparison. The full list of 172 DEGs with expression values are listed in Appendix 4 Table 5.

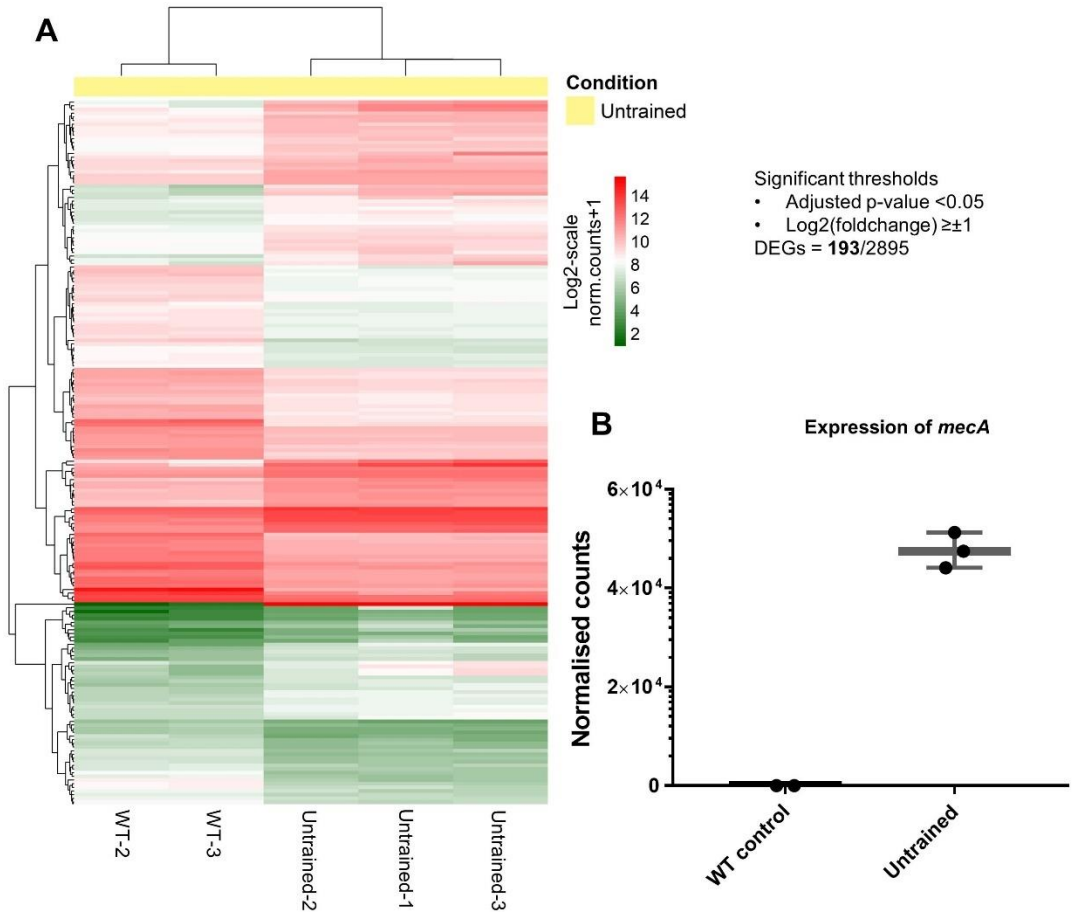

Figure 5.3 The diversity of expression profiles in untrained compared to WT

A) Heatmap representation of 193 (out of 2895) statistically significant DEGs (*padj <0.05, log2fc ≥±1*) in untrained relative to WT across all biological replicates. The rows (genes) and columns (replicates) of the heatmap were linked using hierarchical clustering. Heatmap was generated using R software (R Development core team, 2012), *pheatmap* package.
B) Boxplot comparing the *mecA* gene expression data using normalised counts from five samples (WT-2, 3 and Untrained-1, 2, 3). Boxplots were created using GraphPad Prism software.

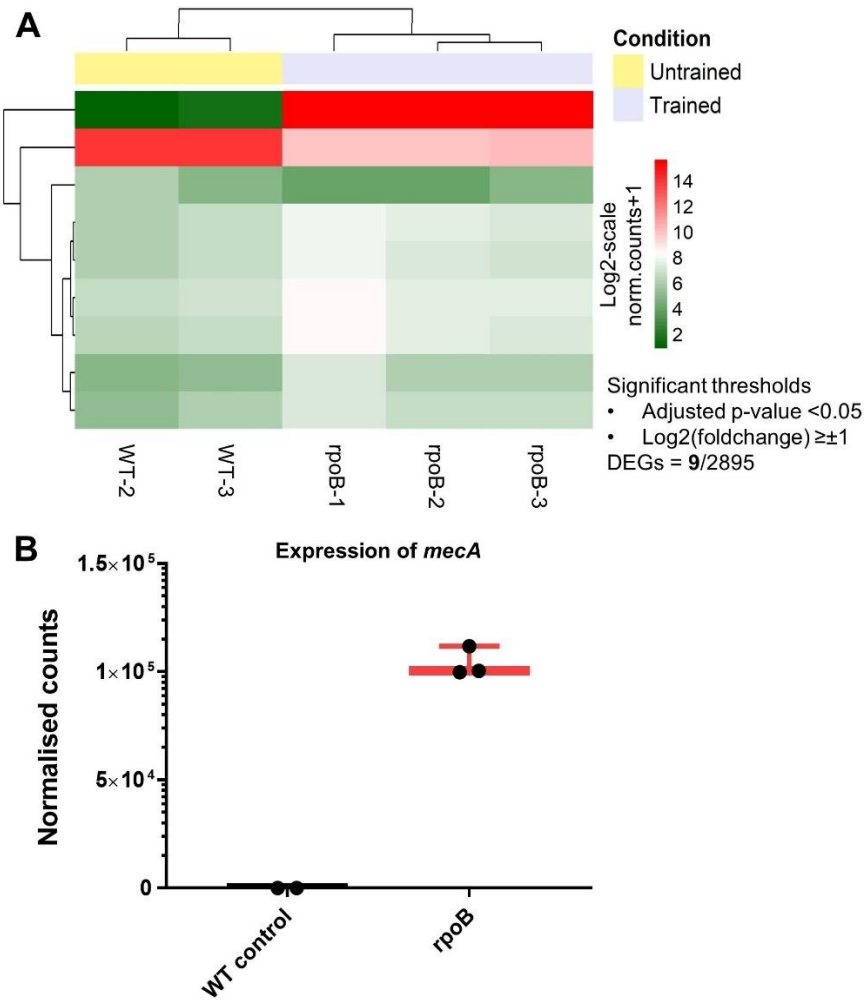

Figure 5.4 The diversity of expression profiles in trained-*rpoB* mutant compared to SH1000

A) Heatmap representation of 9 (out of 2895) statistically significant DEGs (*padj <0.05, log2fc ≥±1*) in trained-*rpoB* relative to WT across all biological replicates. The rows (genes) and columns (replicates) of the heatmap were linked using hierarchical clustering. Heatmap was generated using R software (R Development core team, 2012), *pheatmap* package.
B) Boxplot comparing the *mecA* gene expression data using normalised counts from five samples (WT-2, 3 and trained-*rpoB*-1, 2, 3). Boxplots were created using GraphPad Prism software.

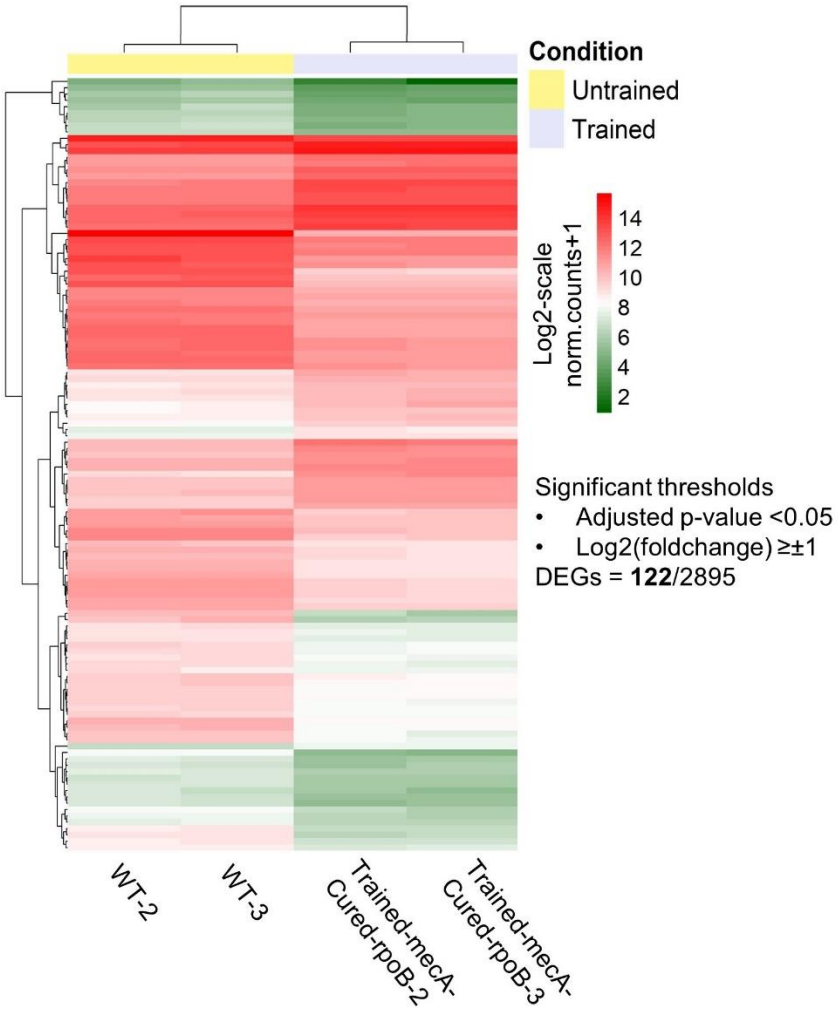

Figure 5.5 The diversity in expression profiles of *mecA*-cured *rpoB* mutant compared to SH1000

Heatmap representation of 122 (out of 2895) statistically significant DEGs (*padj <0.05, log2fc ≥±1*) in trained-*mecA*-cured-*rpoB* relative to WT across all biological replicates. The rows (genes) and columns (replicates) of the heatmap were linked using hierarchical clustering. Heatmap was generated using R software (R Development core team, 2012), *pheatmap* package.

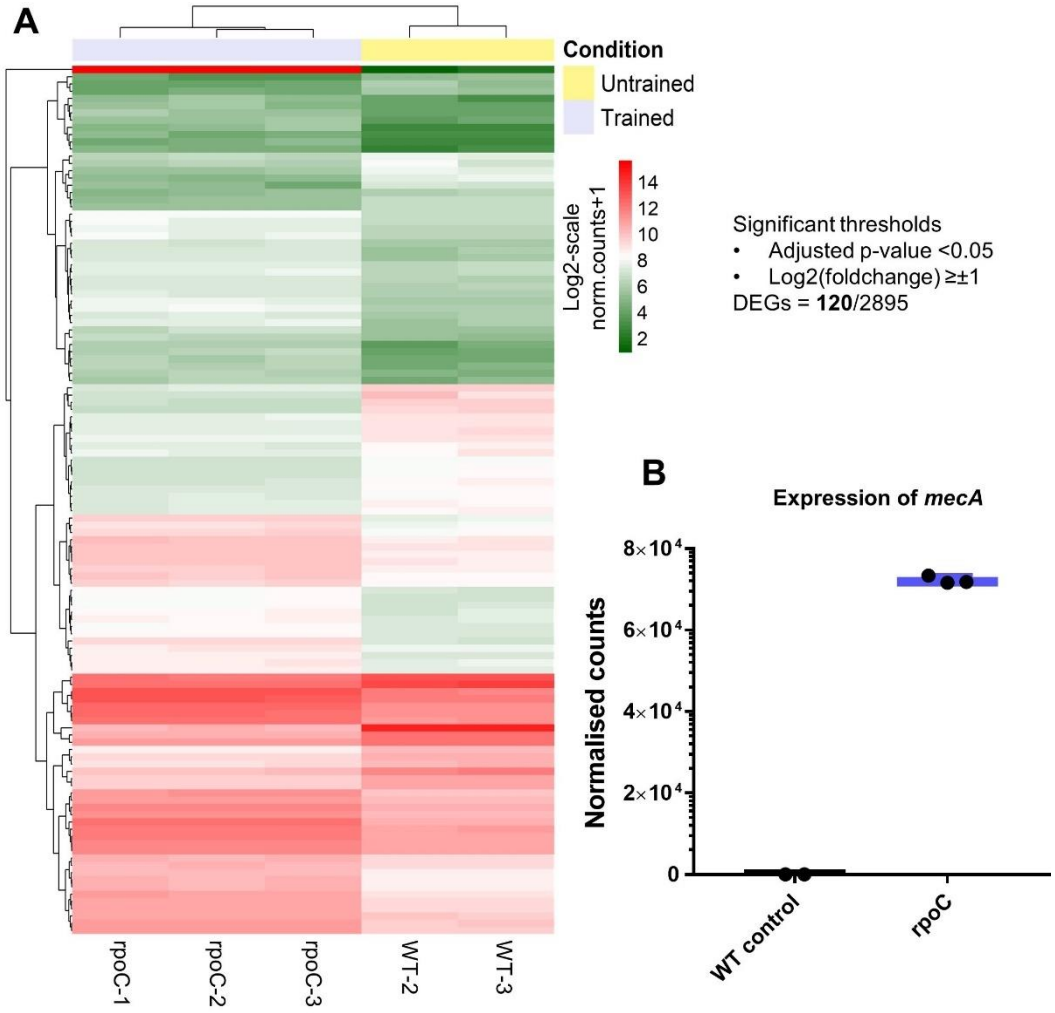

Figure 5.6 The diversity of expression profiles in *rpoC* mutant compared to SH1000

A) Heatmap representation of 120 (out of 2895) statistically significant DEGs (*padj <0.05, log2fc ≥±1*) in trained-*rpoC* relative to WT across all biological replicates. The rows (genes) and columns (replicates) of the heatmap were linked using hierarchical clustering. Heatmap was generated using R software (R Development core team, 2012), *pheatmap* package.
B) Boxplot comparing the *mecA* gene expression data using normalised counts from five samples (WT-2, 3 and trained-*rpoC*-1, 2, 3). Boxplots were created using GraphPad Prism software.

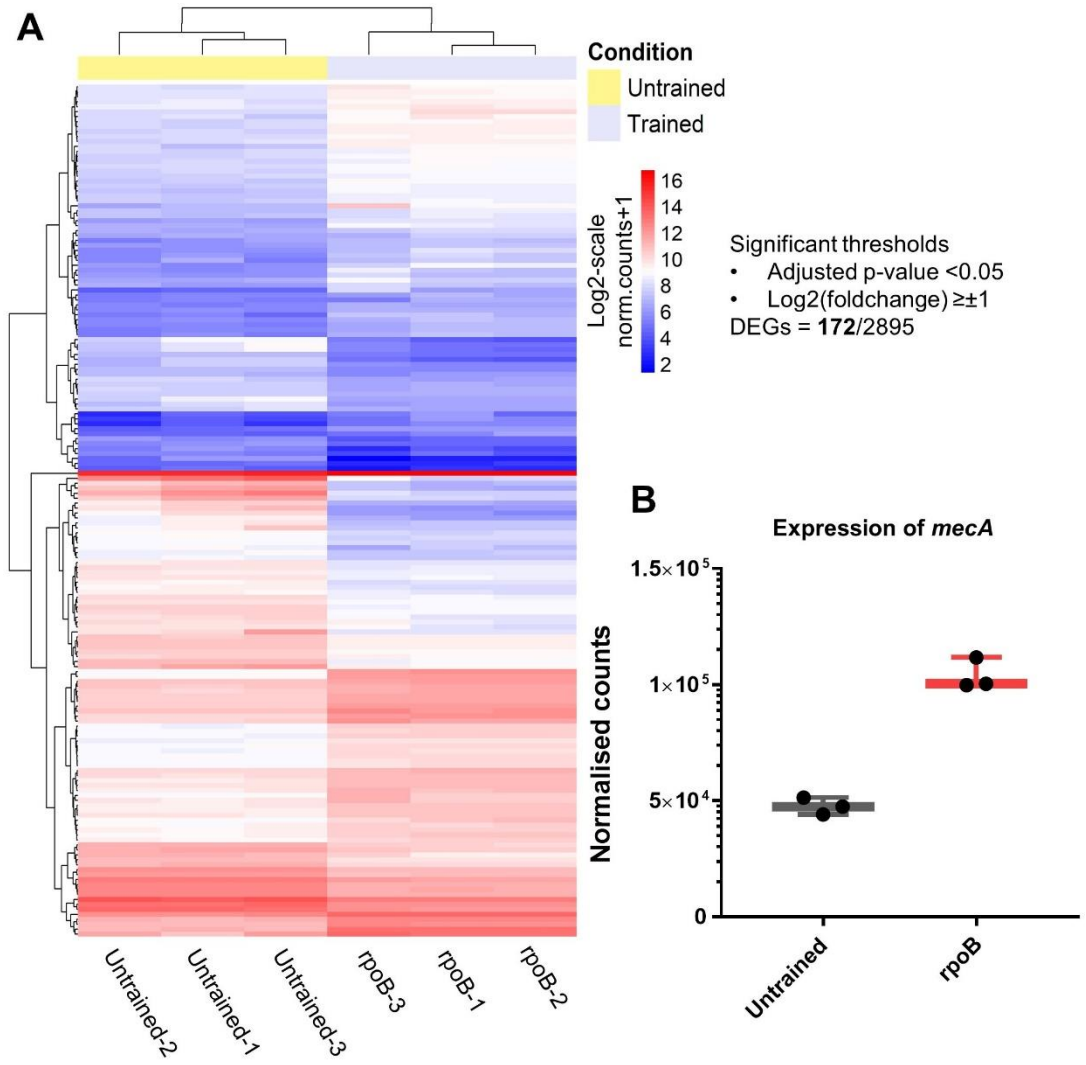

Figure 5.7 The diversity of expression profiles in trained-*rpoB* mutant compared to untrained

A) Heatmap representation of 172 (out of 2895) statistically significant DEGs (*padj <0.05, log2fc* ≥±*1*) in trained-*rpoB* relative to untrained across all biological replicates. The rows (genes) and columns (replicates) of the heatmap were linked using hierarchical clustering. Heatmap was generated using R software (R Development core team, 2012), *pheatmap* package.
B) Boxplot comparing the *mecA* gene expression data using normalised counts from six samples (Untrained-1, 2, 3 and trained-*rpoB*-1, 2, 3). Boxplots were created using GraphPad Prism software.

5.2.2.6 Identification of DEGs in trained-*mecA*-cured-*rpoB* (H929Q) compared to untrained

In order to determine the transcriptional response in the presence of *rpoB* mutation alone, transcriptional profiles of trained-*mecA*-cured-*rpoB* and untrained was compared. Pairwise comparison identified 57 DEGs with differential expression (Figure 5.8 A). Three biological replicates of both strains were used for the data analysis. The full list of 57 DEGs with differential expression are listed in Appendix 4 Table 6. This observation identified the transcriptional changes caused by the *rpoB* mutation independent of *mecA*. There was an obvious significant increase in *mecA* expression in untrained compared to *mecA*-cured-*rpoB* strain (Figure 5.8 B).

5.2.2.7 Identification of DEGs in trained-*rpoC* (G740R) compared to untrained

In order to determine the transcriptional changes acquired due to the *rpoC* mutation, RNA-Seq data was compared between untrained and trained-*rpoC* strains. There were 291 DEGs identified with differential expression (Figure 5.9 A). The details of DEGs are listed in Appendix 4 Table 7. A significant increase in the expression of *mecA* was also noted in trained-*rpoC* compared to the untrained strain (Figure 5.9 B). This data further supports the hypothesis that some increase in *mecA* expression is associated with the development of high-level resistance but is not sufficient as the *rpoC* mutation influenced substantial transcriptional changes. It is also important to note that acquisition of *rpoC* mutation induces increased transcriptional changes compared to the *rpoB* mutation (Figure 5.7 A).

5.2.2.8 Identification of DEGs in trained-*rpoB* (H929Q) compared to trained-*mecA*-cured-*rpoB* (H929Q)

In order to determine the transcriptional changes that occurred between trained-*rpoB* and trained-*mecA*-cured-*rpoB*, pairwise comparison was carried out. Subsequently, the data analysis identified 170 DEGs with differential expression between two strains (Figure 5.10 A). The full list of DEGs are listed in Appendix 4 Table 8. This observation suggested that removal of

mecA led to considerable transcriptional changes and was unable to revert back to WT level in the absence of *mecA*. There was an obvious significantly increased *mecA* expression in trained-*rpoB* compared to *mecA*-cured-*rpoB* strain (Figure 5.10 B).

5.2.2.9 Identification of DEGs in trained-*rpoB* (H929Q) compared to trained-*rpoC* (G740R)

To assess the transcriptional changes between trained-*rpoB* and trained-*rpoC* and subsequently investigate *mecA* dependent common DEGs (described in detail later in this chapter), pairwise comparison was carried out. There were 111 DEGs identified between trained-*rpoB* and trained-*rpoC* strains (Figure 5.11 A). Three biological replicates of each strain were included prior to data analysis. The detailed list of 111 DEGs are shown in Appendix 4 Table 9. The expression of *mecA* was noted to have less than 0.5-fold decrease for trained-*rpoC* compared to trained-*rpoB* but both strains have significant increase over untrained, resulting in high-level oxacillin resistance in both cases (Figure 5.11 B).

5.2.2.10 Identification of DEGs in trained-*rpoC* (G740R) compared to trained-*mecA*-cured-*rpoB* (H929Q)

Transcriptional profiles of trained-*rpoC* and trained-*mecA*-cured-*rpoB* were compared for pairwise data analysis. There were 251 DEGs identified with significant differential expression (Figure 5.12 A). The full list of DEGs are listed in Appendix 4 Table 10. Significantly higher expression of *mecA* was reported for trained-*rpoC* compared to trained-*mecA*-cured-*rpoB* as expected (Figure 5.12 B).

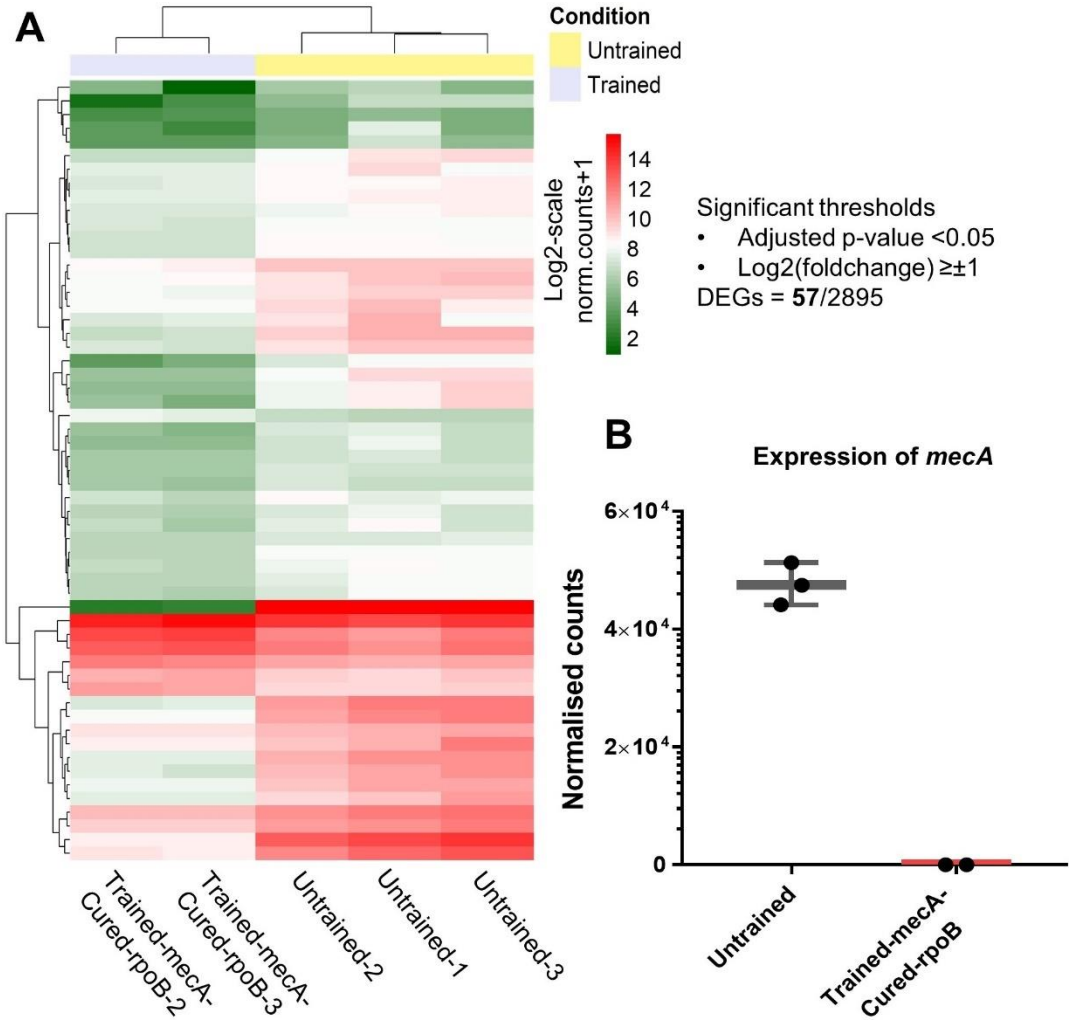

Figure 5.8 The diversity of expression profiles in *mecA*-cured-*rpoB* mutant compared to untrained

A) Heatmap representation of 57 (out of 2895) statistically significant DEGs (*padj <0.05, log2fc ≥±1*) in trained-*mecA*-cured-*rpoB* relative to untrained across all biological replicates. The rows (genes) and columns (replicates) of the heatmap were linked using hierarchical clustering. Heatmap was generated using R software (R Development core team, 2012), *pheatmap* package.
B) Boxplot comparing the *mecA* gene expression data using normalised counts from six samples (Untrained-1, 2, 3 and trained-*mecA*-cured-*rpoB*-2, 3). Boxplots were created using GraphPad Prism software.

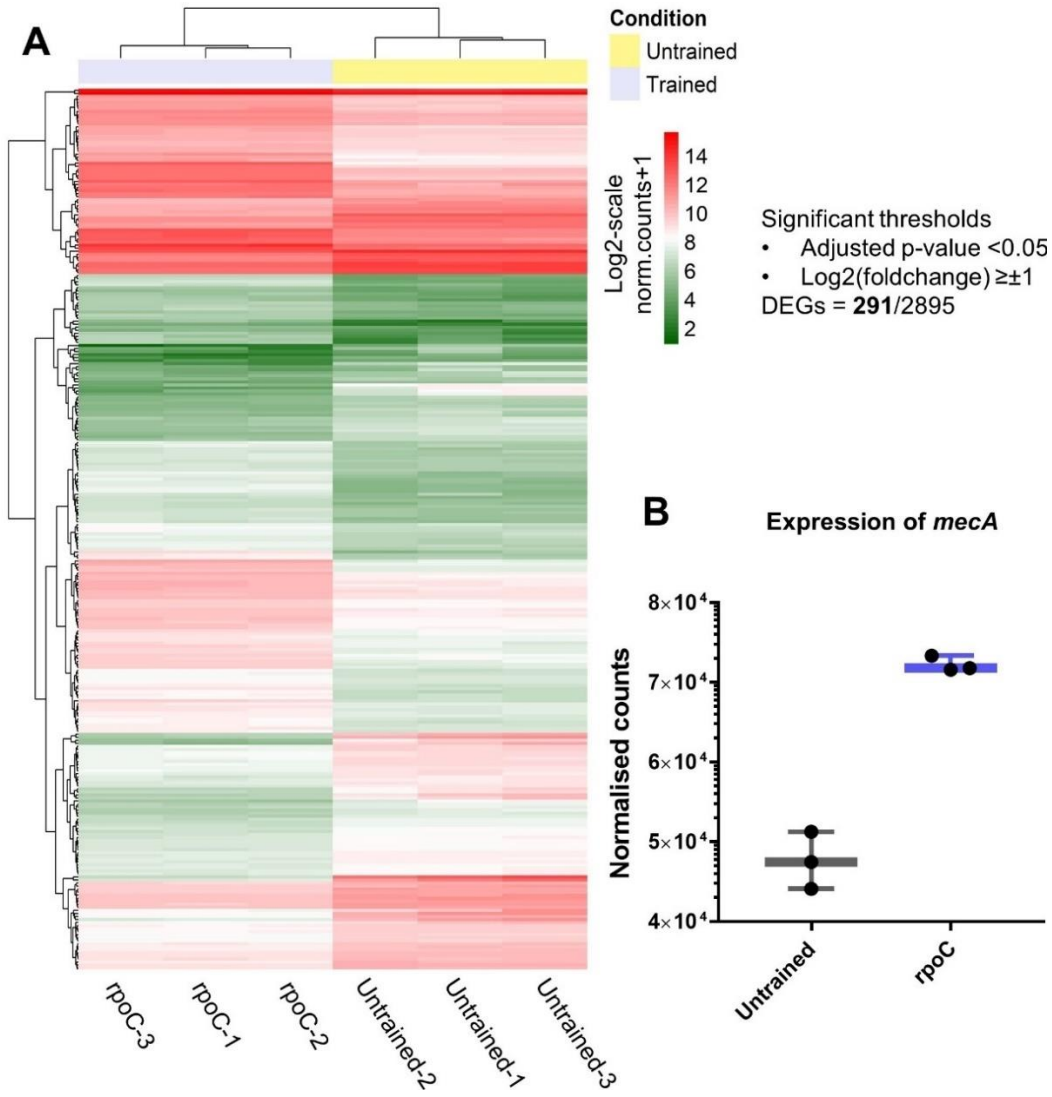

Figure 5.9 The diversity of expression profiles in trained-*rpoC* mutant compared to untrained

A) Heatmap representation of 291 (out of 2895) statistically significant DEGs (*padj <0.05, log2fc ≥±1*) in trained-*rpoC* relative to untrained across all biological replicates. The rows (genes) and columns (replicates) of the heatmap were linked using hierarchical clustering. Heatmap was generated using R software (R Development core team, 2012), *pheatmap* package.
B) Boxplot comparing the *mecA* gene expression data using normalised counts from six samples (Untrained-1, 2, 3 and trained-*rpoC*-1, 2, 3). Boxplots were created using GraphPad Prism software.

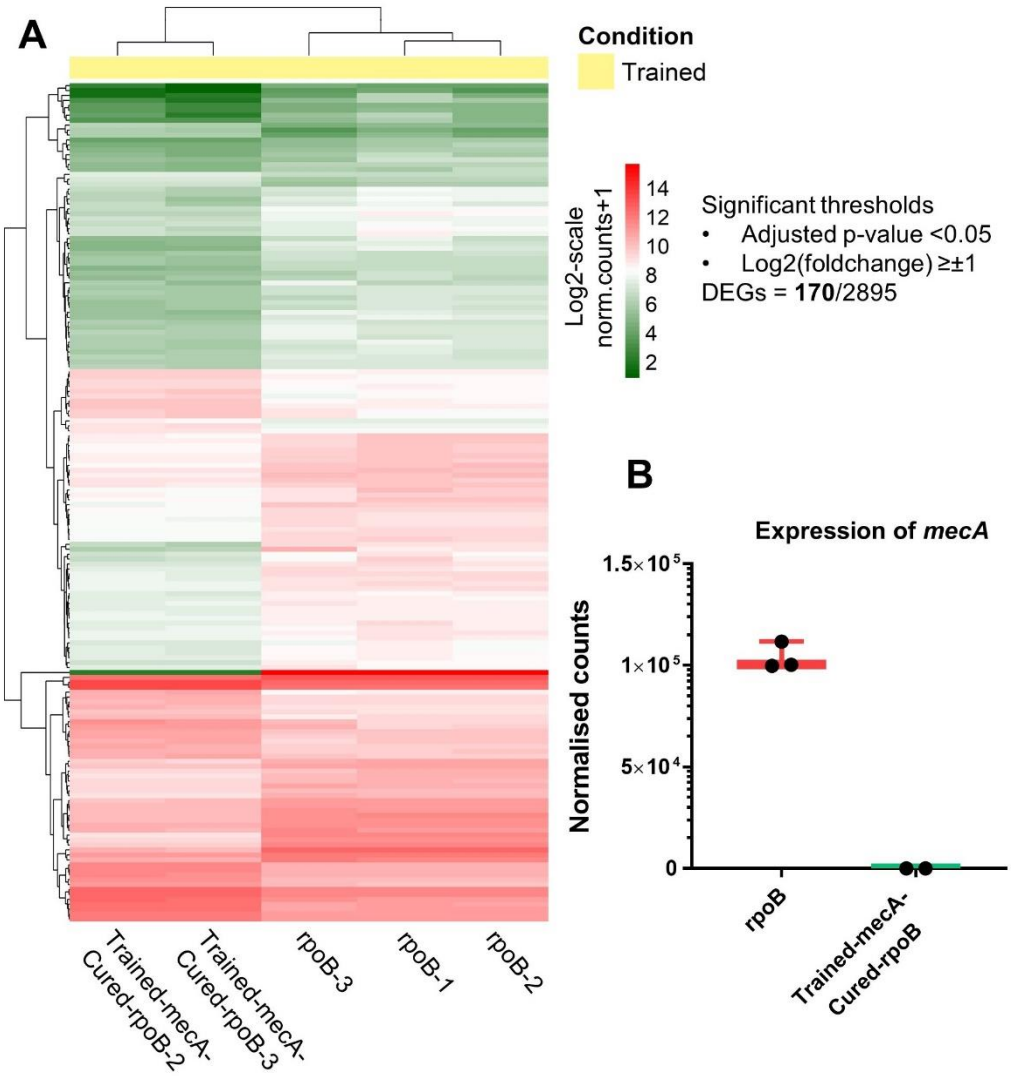

Figure 5.10 The diversity of expression profiles in trained-*rpoB* mutant compared to *mecA*-cured-*rpoB* mutant

A) Heatmap representation of 170 (out of 2895) statistically significant DEGs (*padj <0.05, log2fc* ≥±*1*) in trained-*mecA*-cured-*rpoB* relative to trained-*rpoB* across all biological replicates. The rows (genes) and columns (replicates) of the heatmap were linked using hierarchical clustering. Heatmap was generated using R software (R Development core team, 2012), *pheatmap* package.
B) Boxplot comparing the *mecA* gene expression data using normalised counts from five samples (trained-*rpoB*-1, 2, 3 and trained-*mecA*-cured-*rpoB*-2, 3). Boxplots were created using GraphPad Prism software.

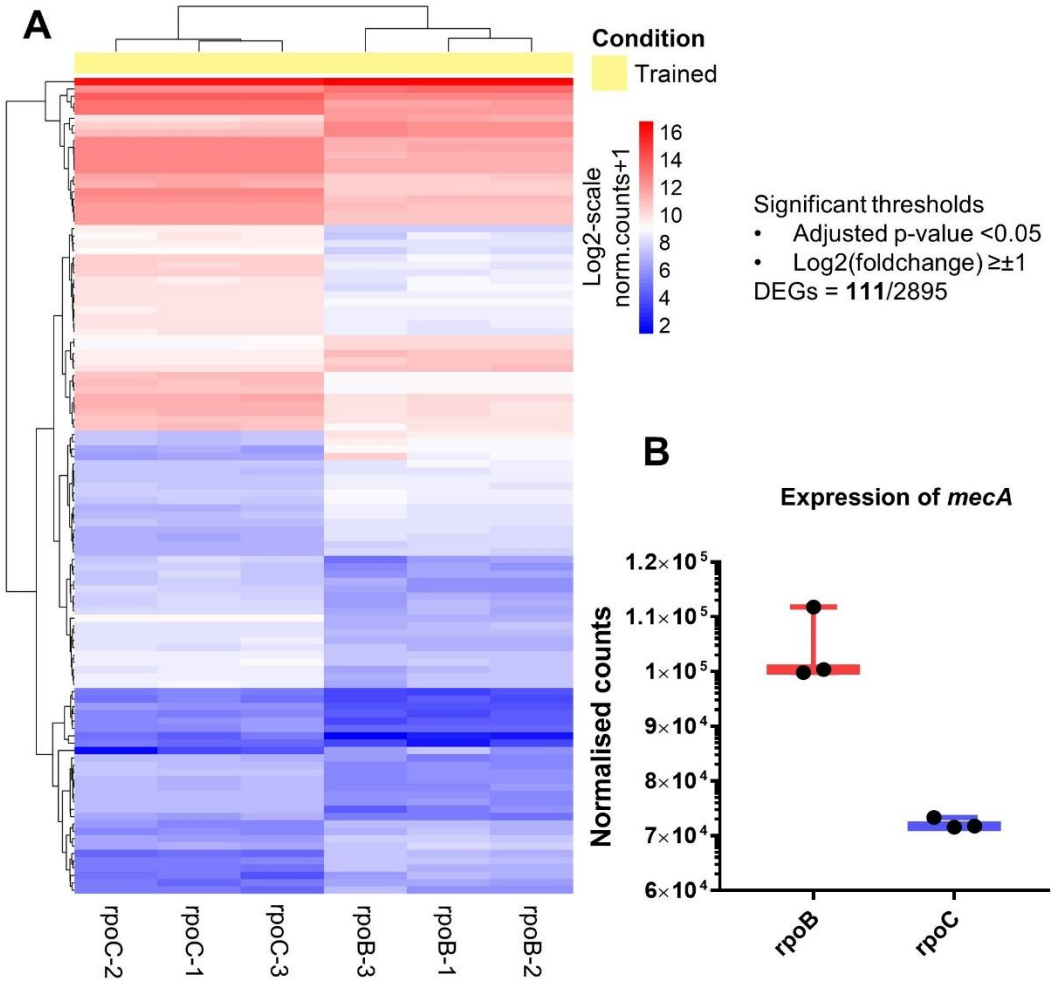

Figure 5.11 The diversity of expression profiles in trained-*rpoC* mutant compared to trained-*rpoB* mutant

A) Heatmap representation of 111 (out of 2895) statistically significant DEGs (*padj <0.05, log2fc ≥±1*) in trained-*rpoC* relative to trained-*rpoB* across all biological replicates. The rows (genes) and columns (replicates) of the heatmap were linked using hierarchical clustering. Heatmap was generated using R software (R Development core team, 2012), *pheatmap* package.
B) Boxplot comparing the *mecA* gene expression data using normalised counts from six samples (trained-*rpoB*-1, 2, 3 and trained-*rpoC*-1, 2, 3). Boxplots were created using GraphPad Prism software.

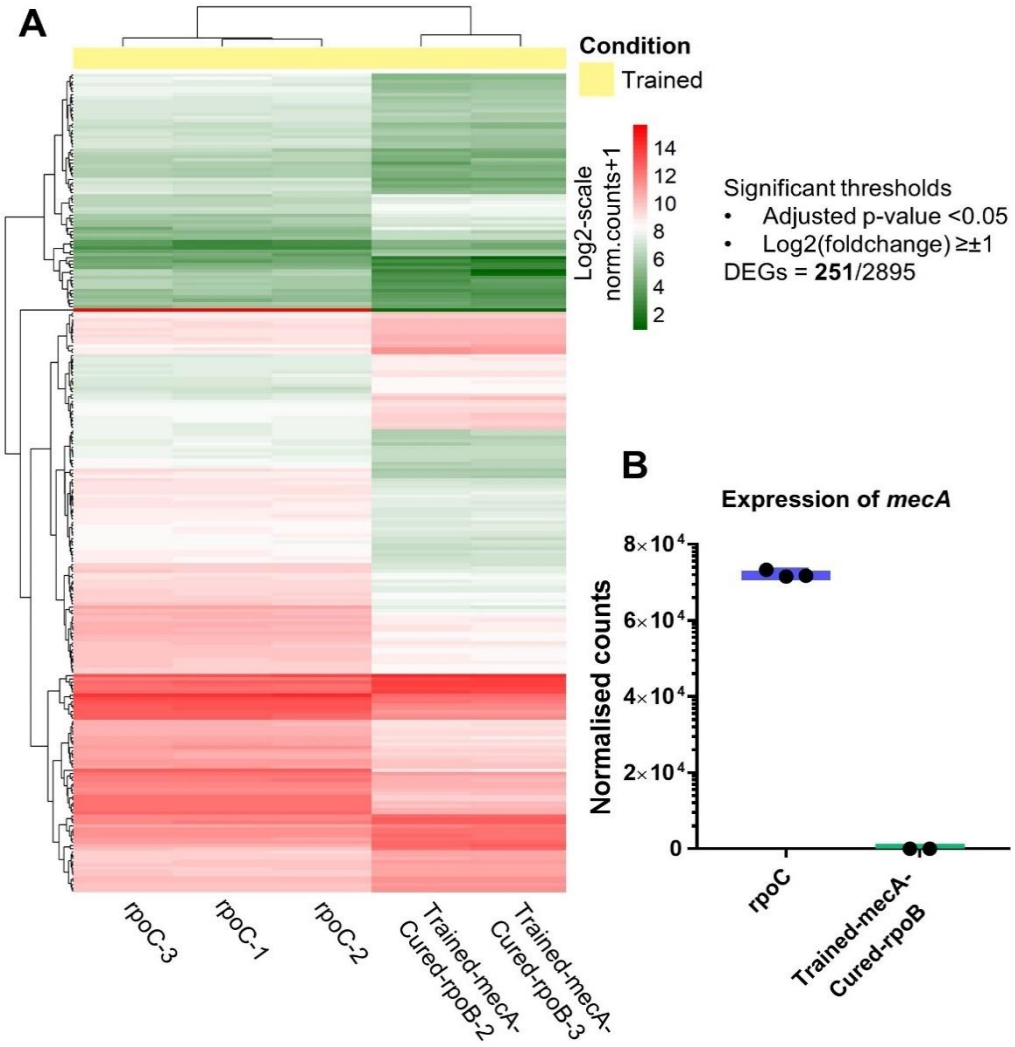

Figure 5.12 The diversity of expression profiles in trained-*rpoC* mutant compared to *mecA*-cured-*rpoB* mutant

A) Heatmap representation of 251 (out of 2895) statistically significant DEGs (*padj <0.05, log2fc ≥±1*) in trained-*rpoC* relative to trained-*mecA*-cured-*rpoB* across all biological replicates. The rows (genes) and columns (replicates) of the heatmap were linked using hierarchical clustering. Heatmap was generated using R software (R Development core team, 2012), *pheatmap* package.
B) Boxplot comparing the *mecA* gene expression data using normalised counts from five samples (trained-*rpoC*-1, 2, 3 and trained-*mecA*-cured-*rpoB*-2, 3). Boxplots were created using GraphPad Prism software.

5.2.3 Identification of unique and shared DEGs among untrained and trained strains relative to WT

To identify the expression level distribution of shared gene content among untrained and trained strains compared to WT, DEGs obtained from pairwise comparisons were analysed for common gene pools between strains. This approach was used to distinguish between unique and overlapping gene pools by comparing two pairwise comparisons relative to WT. There were only 3 common DEGs identified between untrained and trained-*rpoB* compared to WT (Figure 5.13 A) even though, the pairwise comparison of untrained against WT identified a substantial transcriptional change. Whereas, untrained and trained-*rpoC* shared 29 common DEGs when compared to WT (Figure 5.13 C). It is important to note that trained-*rpoB* showed a similar transcriptional profile as WT while trained-*rpoC* retained higher differential gene expression. In addition, trained-*rpoB* and trained-*rpoC* demonstrated 3 overlapping DEGs compared to WT (Figure 5.13 B). Moreover, 90 common DEGs were identified between untrained and trained-*mecA*-cured-*rpoB* compared to WT (Figure 5.13 D). This observation suggests that acquisition of the *rpoB* mutation led to minimal transcriptional change by shifting gene expression to the WT level in the presence of *mecA* but removal of *mecA* induced a considerable transcriptional change. The unique DEGs identified by the pairwise comparisons were not considered for further analysis.

In order to further investigate the shared gene content expressed by both groups, untrained and trained (*rpoB* and *rpoC*) strains compared to WT, the data from three pairwise comparisons were merged and visualised using a three-set proportional Venn diagram (Figure 5.13 E). This approach detected 3 common genes with differential gene expression among both groups of strains. These genes included *lysA* encoding the terminal enzyme of the lysine biosynthesis pathway, *mecA* encoding PBP2A and *nirR* (SAOUHSC_02685) encoding nitrite reductase transcriptional regulator. The *mecA* gene was introduced at the 3’ of the *lysA* gene via pGM072 vector (McVicker et al., 2014). Therefore, *lysA* was found to be downregulated in

untrained and trained-*rpoB* and *rpoC* strains compared to WT (Figure 5.13 E). It is obvious to have found *mecA* as one of the common DEGs because of its elevated expression and production of PBP2A in trained-*rpoB* and *rpoC* strains compared to untrained as well as WT. In addition, upregulation of *nirR* was observed in untrained whereas, trained-*rpoB* and *rpoC* showed downregulation of *nirR*, suggesting that the presence of *mecA* alone induces the expression of *nirR* which is repressed by the acquisition of either *rpo* mutations (Figure 5.13 D, bar plot). Nitrite reductase regulator (*nirR*) is positively and negatively regulated by *nreC* (response regulator) and *rex* (redox-sensing transcriptional repressor), respectively during nitrogen and anaerobic metabolism (Schlag et al., 2008; Somerville and Proctor, 2009).

In an effort to determine the common DEGs amongst untrained, trained-*rpoB*-*rpoC* and trained-*mecA*-cured-*rpoB* strains compared to WT, a four-set Venn diagram was created by introducing the data obtained from pairwise comparisons of trained-*mecA*-cured-*rpoB* relative to WT (Figure 5.14). Only one gene, *lysA* was found to be common between all four strains compared to WT exhibiting reduced expression.

An interesting observation provided by the comparative analysis for the identification of DEGs is that the presence of *mecA* alone induces a significant amount of stress to the cell which is compensated by the acquisition of *rpoB* and partially compensated by *rpoC* mutations to lead to WT level of gene expression, accompanied by concomitant high-level oxacillin resistance.

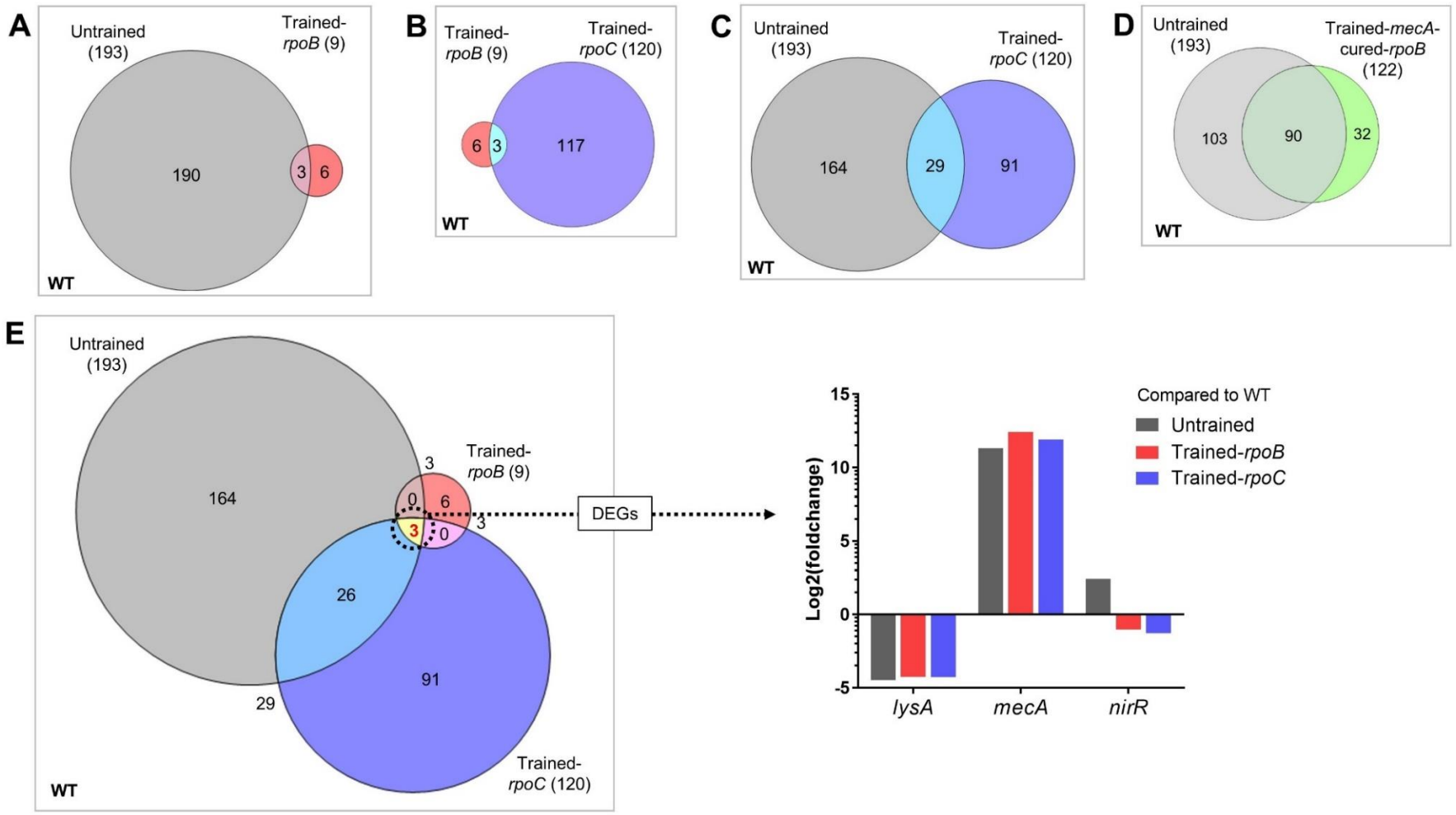

Figure 5.13 Detection of shared and unique DEGs among strains

A) Two-set proportional Venn diagram illustrating the total number of DEGs (listed in brackets) altered in untrained and trained-*rpoB* compared to WT. The identified DEGs using a significance threshold (*padj <0.05, log2fc ≥±1*) from pairwise comparisons of untrained (grey) and trained-*rpoB* (red) against WT (white background) determined 190 and 6 unique DEGs for untrained and trained-*rpoB*, respectively and 3 overlapping DEGs between them.
B) Two-set proportional Venn diagram illustrating the total number of DEGs (listed in brackets) altered in trained-*rpoB* and trained-*rpoC* compared to WT. The identified DEGs using a significance threshold (*padj <0.05, log2fc ≥±1*) from pairwise comparisons of trained-*rpoB* (red) and trained-*rpoC* (blue) against WT (white background) determined 6 and 117 unique DEGs for trained-*rpoB* and trained-*rpoC*, respectively and 3 overlapping DEGs between them.
C) Two-set proportional Venn diagram illustrating the total number of DEGs (listed in brackets) altered in untrained and trained-*rpoC* compared to WT. The identified DEGs using a significance threshold (*padj <0.05, log2fc ≥±1*) from pairwise comparisons of untrained (grey) and trained-*rpoC* (blue) against WT (white background) determined 164 and 91 unique DEGs for untrained and trained-*rpoC*, respectively and 29 overlapping DEGs between them.
D) Two-set proportional Venn diagram illustrating the total number of DEGs (listed in brackets) altered in untrained and trained-*mecA*-cured-*rpoB* compared to WT. The identified DEGs using a significance threshold (*padj <0.05, log2fc ≥±1*) from pairwise comparisons of untrained (grey) and trained-*mecA*-cured-*rpoB* (green) against WT (white background) determined 103 and 32 unique DEGs for untrained and trained-*mecA*-cured-*rpoB*, respectively and 90 overlapping DEGs between them.
E) Three-set proportional Venn diagram facilitate visualising the shared DEGs among untrained (grey), trained-*rpoB* (red) and trained-*rpoC* (blue) compared to WT (white background). Two-set Venn diagrams (A, B, C) were merged together to identify overlapping DEGs among the strains. 3 common DEGs are marked by a dotted circle. Bar plot indicates log2FoldChange of expression levels of three common DEGs (*lysA*, *mecA*, *nirR*) compared to WT.

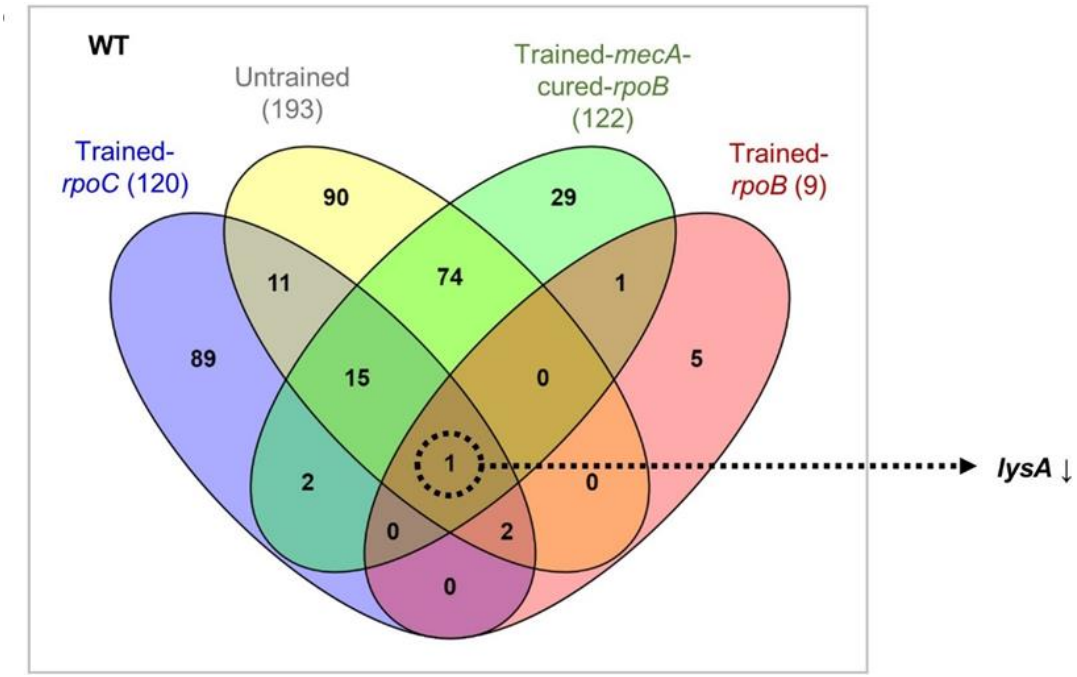

Figure 5.14 Four-set Venn diagram illustrating unique and common DEGs between untrained and trained strains

The *lysA* gene (marked by a dotted circle) was shared among four strains based on pairwise comparison of untrained (yellow), trained-*rpoB* (red), trained-*mecA*-cured-*rpoB* (green) and trained-*rpoC* (blue) compared to control (WT; white background). *lysA* was downregulated in all four strains compared WT, marked by a downward arrow.

5.2.4 Identification of DEGs associated with high-level resistance

To determine the transcriptional response promoted by *mecA* alone and following acquisition of *rpoB* or *rpoC* mutations, comparative analysis of untrained versus trained transcriptomes was performed by combining the data obtained from pairwise analysis. This approach enabled the identification and characterisation of DEGs associated with high-level resistance developed by trained-*rpoB* or *rpoC* strains. The data obtained from two pairwise comparisons of trained- *rpoB* or *rpoC* identified 121 common DEGs between these two strains compared to untrained (Figure 5.15 A), suggesting that the common gene pool may contain a gene or number of genes associated with high-level oxacillin resistance (Table 5.1). The transcriptomic profile of trained-*rpoC* showed an extensive transcriptional change compared to untrained. However, there were only 35 common DEGs identified between trained-*rpoC* and trained-*mecA*-cured-*rpoB* relative to untrained (Figure 5.15 B). Additionally, two pairwise comparisons of trained-*rpoB* and trained-*mecA*-cured-*rpoB* against untrained were combined to determine the transcriptional change introduced by *rpoB* (H929Q) mutation. There were 28 common DEGs identified, suggesting that the permanent differential expression of these genes is due to the presence of *rpoB* mutation alone regardless of *mecA* presence (Figure 5.15 C). The identified unique gene sets from combined pairwise comparisons were not considered for further analysis.

By combining the data obtained from all trained strains and comparing against untrained enabled the identification of overlapping DEGs between untrained and trained strains. Three-set proportional Venn diagram showed 26 DEGs shared by all three trained strains compared to untrained (Figure 5.16 A). These 26 DEGs were part of 121 DEGs originally identified following acquisition of *rpoB* or *rpoC* mutations in the presence of *mecA* (Figure 5.15 A). Notably, out of 26 overlapping DEGs within all three trained strains, 22 genes were upregulated in untrained whereas, the same 22 genes were downregulated in all three trained strains (Figure 5.16 A). This observation suggests that acquisition of the *mecA* induced severe alterations in the gene

expression whereas, *rpo* mutations restored expression levels for most of these genes to WT levels. The rest of the 95 (Figure 5.17) genes showed a similar distribution of differential expression for 56 genes (out of 83 genes) accompanying reduced expression in untrained while trained- *rpoB* or *rpoC* showed increased expression in 66 genes out of 95 (Figure 5.16 A).

The database of Clusters of Orthologous Groups (COGs) was used for functional categorisation of 121 genes (Figure 5.16 B and C and Table 5.1) (Tatusov et al., 2000). These set of common genes were shared between trained-*rpoB* and *rpoC* which also contains 26 DEGs shared by all three trained strains (*rpoB, rpoC* and *mecA*-cured-*rpoB*) (Figure 5.16). All DEGs were classified into broad functional categories and then COG categories were retrieved manually for each gene by searching UniProt accession NCBI database (Table 5.1). Functional categorisation detected that 52 genes affected were involved in metabolism, 19 genes associated with cellular processes and signalling and 12 genes related to information storage and processes. The term 'multi class' was applied to 14 genes as they matched to more than one COG categories of same or different broad functional groups (Figure 5.18 A). 24 genes were assigned to poorly characterised category as their function was either based on prediction (R) or unknown to categories (S).

From 95 key genes (Figure 5.16 A and Figure 5.17), specifically associated with high-level resistance in response to the acquisition of *rpoB* and *rpoC*, 16 genes assigned to the category "Cellular processes and signalling" were upregulated compared to untrained. 11 genes assigned to "Information storage and processing" were also upregulated compared to untrained. Moreover, 21 genes related to the category "Metabolism", were considerably upregulated in trained- *rpoB* and *rpoC* strains compared to untrained (Table 5.1). The differential expression of identified genes was found to be controlled by different transcriptional regulators without affecting their own expression (Figure 5.18 C). Six genes (*yusE*, *yusF*, *proP*, Saouhsc_00356, *yfcH* and *yhbs*) were found to be controlled by *sigB,* a general stress response alternative sigma factor (Bischoff et al., 2004). Ferric uptake

repressor (*fur*) controlled genes (*sirB*, *sirA*, *ocd2*, *sbnA* and *sbnC*) were also identified with higher expression in trained-*rpoB* and *rpoC* compared to untrained (Horsburgh et al., 2001; Mäder et al., 2016). These observations indicate that the presence of *mecA* may induce oxidative stress resulting into substantial transcriptional changes. In addition, four genes (*aur*, *hisZ*, *yrbD* and *sodM*) were identified to be negatively regulated by CodY, which regulates the expression of metabolic and virulence genes associated with nucleotide transport, energy production and defence mechanisms (Pohl et al., 2009). Three genes (*fib*, *lukG* and *saeP*) were found to be controlled by the SaeRS two-component system (TCS). SaeRS regulates the production of virulence factors including surface proteins, leukocidins and hemolysins (Liu et al., 2016b). Moreover, NreBC TCS which regulates nitrate/nitrite reduction in response to oxygen (Schlag et al., 2008) showed reduced expression in trained-*rpoB* and *rpoC* strains compared to untrained (Figure 5.19 A). NreBC is dually regulated by NreC and Rex - a redox sensing transcriptional repressor (Pagels et al., 2010). This suggests that *mecA* alone induces partial anaerobiosis even in the presence of oxygen. This phenomenon is then reversed back to aerobic respiration upon acquisition of *rpoB* or *rpoC* mutations.

Interestingly, comparison of all three trained strains including *mecA*-cured-*rpoB* against untrained identified an overlapping pool of 26 genes associated with anaerobic fermentative metabolism (22 genes), involved in nitrite and nitrate reduction, found to be down regulated (Figure 5.19 B). It is known that the expression of these genes is regulated dually by Rex and NreC (Pagels et al., 2010; Schlag et al., 2008). Based on these observations, it appears that the untrained strain initiated anaerobic growth to adapt to the presence of non-native gene, *mecA*; as reflected by elevated expression of fermentation enzymes such as, lactate dehydrogenase (*ldh1*), alcohol dehydrogenases (*adhE* and *adh*) and alanine dehydrogenase (*ald1*) (Figure 5.19 B). The remaining four DEGs exhibited reduced expression in the untrained strain compared to WT. These genes are *spa* encoding IgG binding protein A, *sbi* encoding IgG binding protein Sbi, *ecb* encoding fibrinogen-binding protein and *icaB* encoding polysaccharide intercellular

adhesin (PIA) biosynthesis deacetylase (Figure 5.19 B). Of these four genes *sbi, spa* and *ecb* exhibited increased expression in the trained strains compared to the untrained strain. *icaB* was only found to be upregulated in trained-*rpoB* (Figure 5.19). Overexpression of *icaB* has been shown to lead to synthesis of increased levels of PIA, producing a heavy biofilm (Cerca et al., 2007). The increased expression of *spa* and SaeRS-dependent genes (*sbi* and *ecb*) in the trained strains compared to the untrained strain reflects the importance of host evasion immune response in *S. aureus* (Mäder et al., 2016; Serruto et al., 2010).

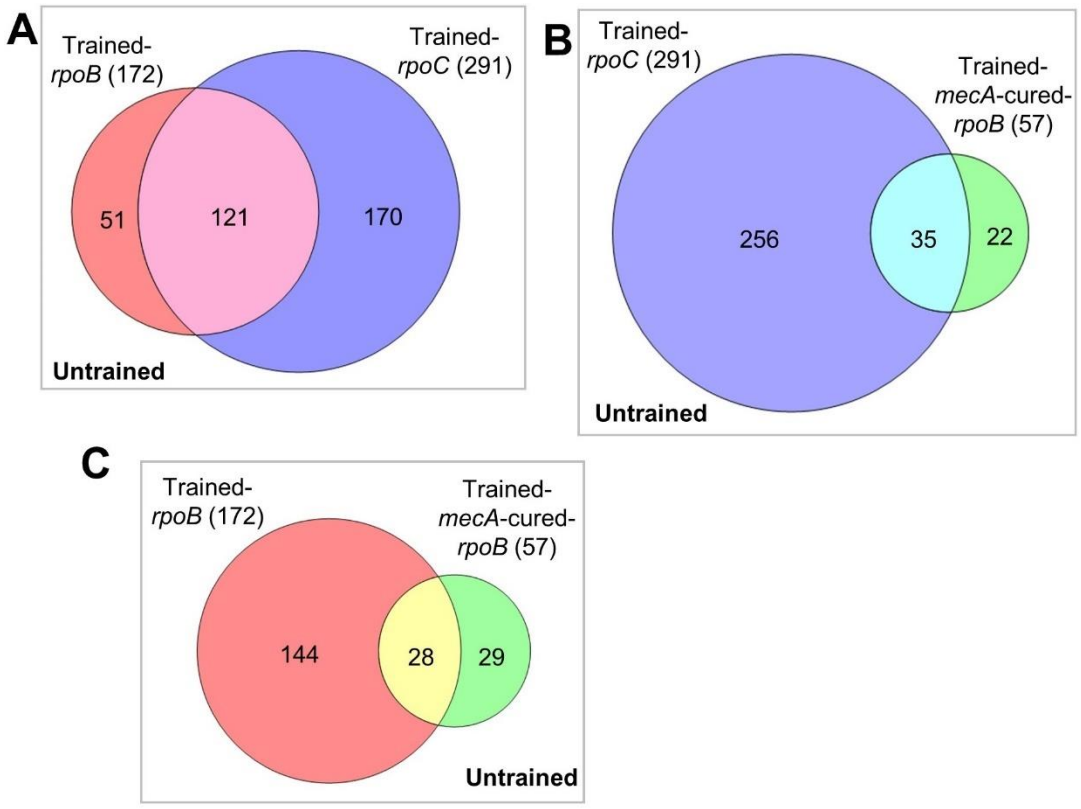

Figure 5.15 Identification of overlapping genes in the trained strains compared to untrained

A) Two-set proportional Venn diagram displaying the total number of DEGs (listed in brackets) altered in trained-*rpoB* and trained-*rpoC* compared to untrained. The identified DEGs using significant threshold (*padj <0.05, log2fc ≥±1*) from pairwise comparisons of trained-*rpoB* (red) and trained-*rpoC* (blue) against untrained (white background) determined 51 and 170 unique DEGs for trained-*rpoB* and trained-*rpoC*, respectively and 121 shared genes between them.
B) Two-set proportional Venn diagram displaying the total number of DEGs (listed in brackets) altered in trained-*rpoC* and trained-*mecA*-cured-*rpoB* compared to untrained. The identified DEGs using significant threshold (*padj <0.05, log2fc ≥±1*) from pairwise comparisons of trained-*rpoC* (blue) and trained-*mecA*-cured-*rpoB* (green) against untrained (white background) determined 256 and 22 unique DEGs for trained-*rpoC* and trained-*mecA*-cured-*rpoB*, respectively and 35 shared genes between them.
C) Two-set proportional Venn diagram displaying the total number of DEGs (listed in brackets) altered in trained-*rpoB* and trained-*mecA*-cured-*rpoB* compared to untrained. The identified DEGs using significant threshold (*padj <0.05, log2fc ≥±1*) from pairwise comparisons of trained-*rpoB* (red) and trained-*mecA*-cured-*rpoB* (green) against untrained (white background) determined 114 and 29 unique DEGs for trained-*rpoB* and trained-*mecA*-cured-*rpoB*, respectively and 28 shared genes between them.

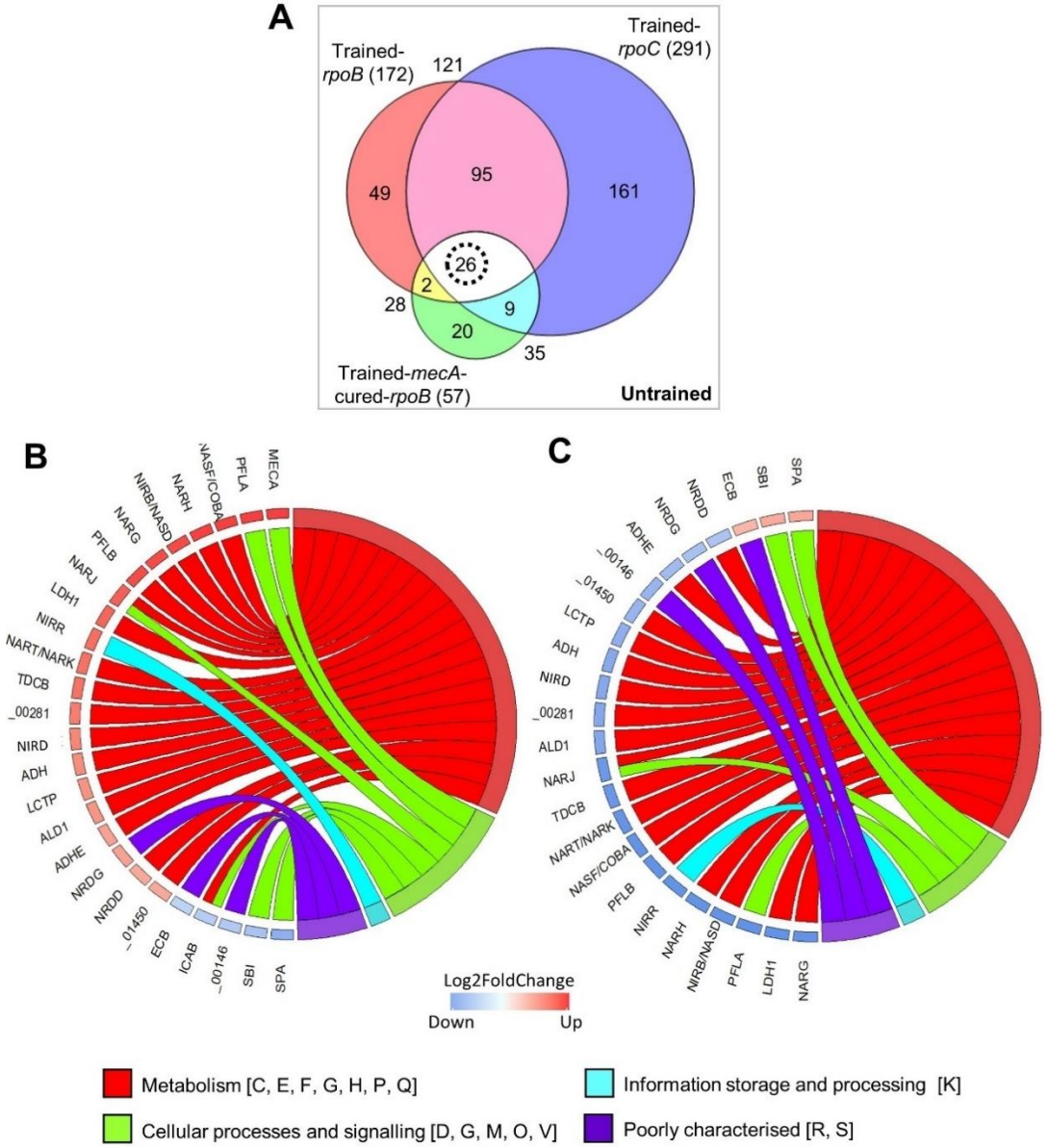

Figure 5.16 Identification of shared gene pool in the trained strains compared to untrained

A) Three-set proportional Venn diagram constructed by merging Figure 5.15 A, B and C facilitated visualising the shared DEGs among all three trained strains (*rpoB*, *rpoC* and *mecA*-cured-*rpoB*) compared to untrained (white background). 26 common DEGs are marked by a dotted circle.
B) Chord plot illustrating 26 common genes (intersecting genes from Figure 5.16 A) that were differentially expressed in untrained (SJF4996) compared to WT. The log2FoldChange of individual genes is shown on the left and their corresponding functional categories on the right side of chord diagram. Chord connects gene names (left) with COG classification based functional categories (right, key below).
C) Chord plot displaying 24 common genes (intersecting genes from Figure 5.16 A) out of 26 genes that were differentially expressed in the three trained strains compared to the untrained (SJF4996). *mecA* was not included as SJF5010 (*mecA* cured) showed an obvious reduced *mecA* expression. *icaB* was not included because it was upregulated only in trained-*rpoB* (SJF5003). Each segment on the left represents the average log2FoldChange of individual genes from the three trained strains which connects to their functional categories on the right. Chord diagrams were generated using GOplot R package (Walter et al., 2015).

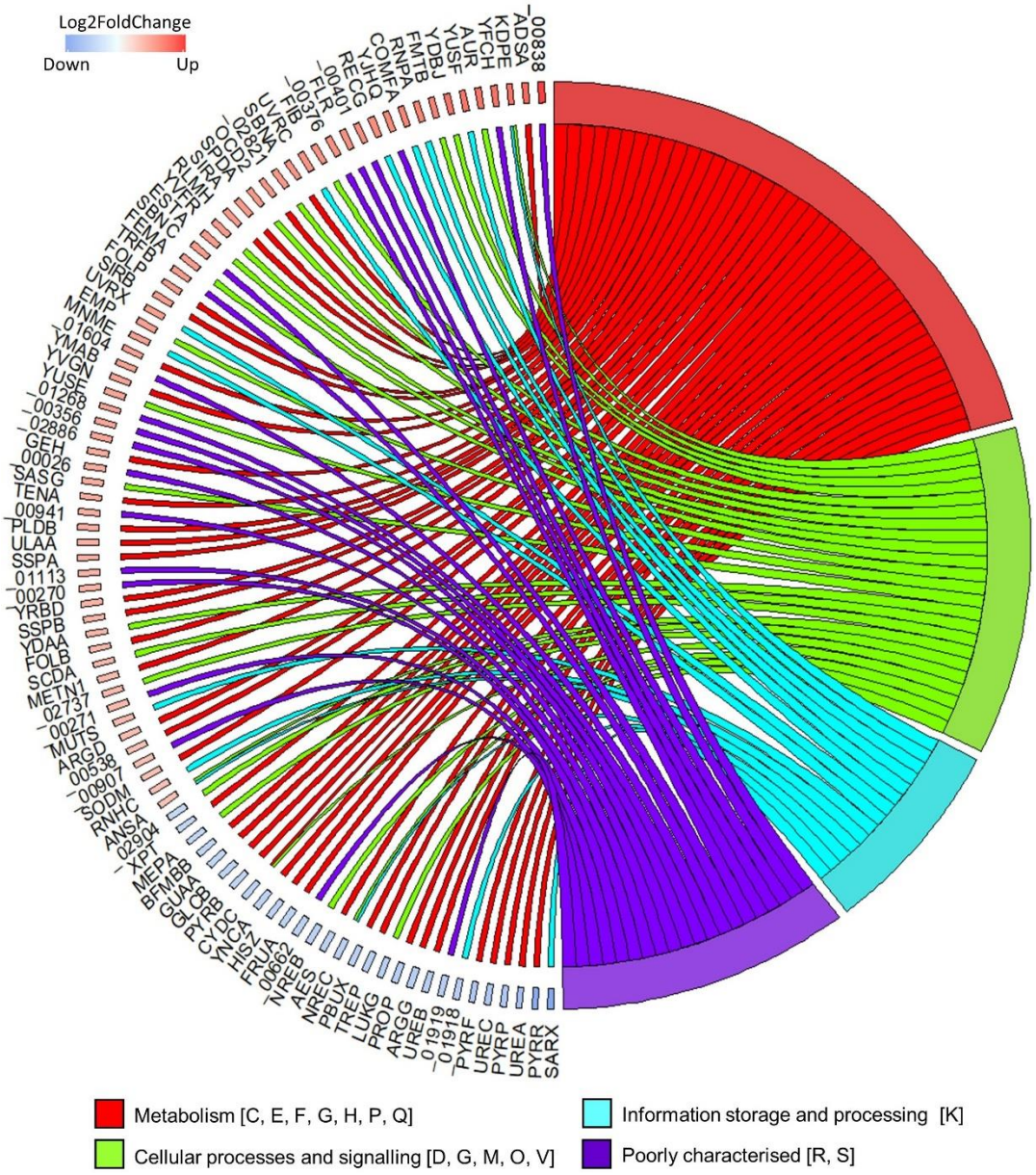

Figure 5.17 Identification of shared genes between trained-*rpoB* and *rpoC* compared to the untrained

Chord diagram displaying 95 common genes between trained-*rpoB* and trained-*rpoC* (intersecting genes from Figure 5.16 A) out of 121 common genes (differentially expressed in the three trained strains) compared to the untrained strain (SJF4996). Each segment on the left represents the average log2FoldChange of individual genes from the three trained strains which connects to their functional categories on the right. Numbers on the left refer to NCTC8325 locus tag. Chord diagram was generated using GOplot R package (Walter et al., 2015).

COG Functional categories	UniProt accession	Gene name	Locus tag	Protein product	Log2FC				Predicated Regulators
					Untrained*	Trained-*rpoB*†	Trained-*mecA*-cured-*rpoB*†	Trained-*rpoC*†	
Cellular processes and signalling									
VW	Q2G012	*emp*	SAOUHSC_00816	Extracellular matrix protein-binding protein emp	-1.77	1.88	-	1.41	-
V	Q2G140	*mepA*	SAOUHSC_00315	Multidrug export protein MepA (Staphylococcal virulence regulator protein A)	1.14	-1.06	-	-1.10	MepR
T	Q2FVM6	*nreB*	SAOUHSC_02676	Oxygen sensor histidine kinase NreB (Nitrogen regulation protein B)	1.12	-1.14	-	-1.29	Rex, NreC
O	Q2FZZ3	*yusE*	SAOUHSC_00841	Uncharacterized protein	-	1.33	-	1.82	SigB
VW	Q2FZB8	*fib*	SAOUHSC_01114	Fibrinogen-binding protein	-1.60	1.85	-	1.89	SaeR
V	Q2FYW3	*yvfR*	SAOUHSC_01311	ABC transporter, ATP-binding protein, putative	-	1.25	-	2.22	-
T	Q2FXL6	*ydaA/uspA1*	SAOUHSC_01819	Putative universal stress protein	-1.50	1.33	-	1.23	-
O	Q2FXE9	*spdA*	SAOUHSC_01900	Uncharacterized protein membrane spanning protein	-1.25	1.41	-	2.12	-
V	Q2FWP0	*lukG*	SAOUHSC_02241	Uncharacterized leukocidin-like protein 1	1.20	-1.17	-	-1.36	SaeR
M	Q2FW95	*fmtB*	SAOUHSC_02404	Extracellular matrix-binding protein	-1.28	1.19	-	3.04	-
M	Q2FVL5	*fmhA/femA*	SAOUHSC_02696	methicillin resistance determinant protein	-1.15	1.19	-	2.19	-
M	Q2FVH5		SAOUHSC_02737	Epimerase/dehydratase, putative	-1.35	1.22	-	1.20	-
V	Q2FVB4	*ydbJ*	SAOUHSC_02820	ABC-type multidrug transport system	-2.65	2.48	-	2.18	-
M	Q2FVB3		SAOUHSC_02821	Membrane spanning protein, putative	-2.09	1.97	-	1.60	-
O	Q2FV35		SAOUHSC_02904	Uncharacterized protein monooxygenase/thioredoxin reductase	-	-1.00	-	-1.05	Zur
V	Q2FUY3	*estA/xynC*	SAOUHSC_02962	Tributyrin esterase, putative	-1.69	1.22	-	2.23	-
O	Q2FUX4	*aur*	SAOUHSC_02971	Aureolysin, putative	-1.75	1.52	-	3.18	CodY
VM	Q2G2B2	*sasG*	SAOUHSC_02798	Surface protein G	-1.54	1.34	-	1.58	-
O	P72360	*scdA*	SAOUHSC_00229	Iron-sulfur cluster repair protein ScdA (Cell wall-related protein ScdA)	-1.50	1.33	-	1.17	-
DM	A0A0H2WXF8	*mecA*	SACOL0033	Penicillin-binding protein 2A	11.31	1.12	-11.19	0.60	-
O	Q2G1D7	*pflA*	SAOUHSC_00188	Pyruvate formate-lyase-activating enzyme	3.16	-3.72	-3.15	-4.10	CcpA, Rex
V	Q2FVK5	*sbi*	SAOUHSC_02706	Immunoglobulin-binding protein sbi	-1.63	1.66	1.40	1.38	SaeR
V	P02976	*spa*	SAOUHSC_00069	Immunoglobulin G-binding protein A (IgG-binding protein A)	-2.21	1.67	1.90	1.01	CcpA
Cellular processes and signalling, information storage and processing									
TK	Q2FVM7	*nreC*	SAOUHSC_02675	Oxygen regulatory protein NreC (Nitrogen regulation protein C)	1.31	-1.27	-	-1.20	Rex, NreC

Information storage and processing									
J	Q2FUQ2	*mnmE/trmE*	SAOUHSC_03053	tRNA modification GTPase MnmE	-1.68	1.33	-	1.96	-
L	O50581	*recG*	SAOUHSC_01194	ATP-dependent DNA helicase RecG	-1.58	1.59	-	2.30	-
L	Q2FZD7	*rnhC*	SAOUHSC_01095	Ribonuclease HIII (RNase HIII)	-1.12	1.00	-	1.18	-
K	Q2FUQ1	*rnpA*	SAOUHSC_03054	Ribonuclease P protein component (RNase P protein)	-2.10	1.67	-	2.53	-
L	Q2G057	*comFA*	SAOUHSC_00765	Uncharacterized protein comF operon protein 1	-1.68	1.49	-	2.65	-
J	Q2FZZ4	*yusF*	SAOUHSC_00840	5S rRNA maturation endonuclease (Ribonuclease M5)	-2.17	1.92	-	2.75	SigB
L	Q2FYS2	*uvrX*	SAOUHSC_01363	Nucleotidyltransferase	-1.21	1.26	-	2.08	LexA
L	Q2G2Y4		SAOUHSC_01918	Uncharacterized protein excalibur calcium-binding domain protein	1.04	-1.08	-	-1.58	-
L	Q2FWL3	*mutS*	SAOUHSC_02276	MutS domain V protein	-	1.12	-	1.27	-
K	Q2G0D1	*sarX*	SAOUHSC_00674	HTH-type transcriptional regulator SarX (Staphylococcal accessory regulator X)	1.54	-1.63	-	-3.24	-
L	Q2FZD0	*uvrC*	SAOUHSC_01102	UvrABC system protein C (Protein UvrC) (Excinuclease ABC subunit C)	-1.47	1.29	-	2.40	-
K	Q2G1V2	*nirR*	SAOUHSC_02685	Transcriptional regulator, Nitrite reductase	2.41	-3.45	-3.26	-3.70	Rex, NreC
Information storage and processing or cellular processes and signalling									
JU	Q2FYF4	*ansA*	SAOUHSC_01497	L-asparaginase, putative	-1.17	1.15	-	1.00	-
TK	Q2FWH6	*kdpE*	SAOUHSC_02315	DNA-binding response regulator, putative	-1.25	1.21	-	3.55	-
Metabolism									
E	Q2FZU1	*argG*	SAOUHSC_00899	Argininosuccinate synthase	1.11	-1.28	-	-1.36	ArgR, CodY
G	Q2FV87	*glcB*	SAOUHSC_02848	Phosphotransferase system IIC components, glucose/maltose/N-acetylglucosamine-specific	-	-1.11	-	-1.19	-
F	Q2G0Y6	*guaA*	SAOUHSC_00375	GMP synthase, PP-ATPase domain/subunit	1.13	-1.08	-	-1.18	-
E	Q2FUT6	*hisZ*	SAOUHSC_03015	ATP phosphoribosyltransferase regulatory subunit	1.00	-1.27	-	-1.06	CodY, HisR
I	Q2G155	*geh/lip2*	SAOUHSC_00300	Lipase 2 (Glycerol ester hydrolase 2)	-1.71	1.61	-	1.34	-
E	Q2G0V2	*metN1*	SAOUHSC_00423	Methionine import ATP-binding protein MetN 1	-1.21	1.06	-	1.39	CymR
F	Q2FZ75	*pyrB*	SAOUHSC_01166	Aspartate carbamoyltransferase	1.03	-1.13	-	-1.18	-
F	Q2FZ71	*pyrF*	SAOUHSC_01171	Orotidine 5'-phosphate decarboxylase (OMP decarboxylase)	1.18	-1.34	-	-1.57	-
F	Q2FZ77	*pyrR*	SAOUHSC_01164	Pyrimidine operon attenuation protein/uracil phosphoribosyltransferase	2.03	-2.12	-	-2.50	-
G	Q2G252	*rlmH*	SAOUHSC_00027	Ribosomal RNA large subunit methyltransferase H	-1.69	1.55	-	1.92	-
E	Q2G1H3	*rocD/argD*	SAOUHSC_00150	Acetylornithine/succinyldiaminopimelate/putrescine aminotransferase	-1.32	1.05	-	1.22	ArgR
F	Q2G253	*adsA*	SAOUHSC_00025	Uncharacterized protein	-2.94	2.60	-	2.41	-
P	Q2G1N5	*sirB*	SAOUHSC_00072	Lipoprotein, SirB, putative	-1.38	1.17	-	2.18	Fur

P	Q2G1N4	*sirA*	SAOUHSC_00074	Periplasmic binding protein, putative SirA	-1.59	1.50	-	1.99	Fur
E	Q2G1N2	*ocd2*	SAOUHSC_00076	Ornithine cyclodeaminase, putative	-1.16	1.03	-	2.53	Fur
G	Q2G145	*ulaA*	SAOUHSC_00310	PTS system ascorbate-specific transporter subunit IIC	-1.31	1.24	-	1.55	-
F	Q2G0Y8	*pbuX*	SAOUHSC_00373	Xanthine permease, putative	1.31	-1.26	-	-1.20	-
G	Q2G0U0	*treP*	SAOUHSC_00437	Uncharacterized protein	1.43	-1.35	-	-1.15	CcpA
H	Q2G0Q7	*folP*	SAOUHSC_00489	Dihydropteroate synthase (DHPS)	-1.55	1.55	-	1.81	-
H	Q2G0Q6	*folB*	SAOUHSC_00490	7,8-dihydroneopterin aldolase	-1.04	1.11	-	1.41	-
C	Q2G0M2		SAOUHSC_00538	Haloacid dehalogenase-like hydrolase, putative	-1.08	1.10	-	1.13	-
GEPR	Q2G0K4	*proP*	SAOUHSC_00556	Proline/betaine transporter, putative	1.63	-1.37	-	-1.22	SigB
I	Q2G0E5	*aes*	SAOUHSC_00661	Acetyl esterase/lipase	1.34	-1.36	-	-1.08	-
G	Q2G239	*fruA*	SAOUHSC_00708	Fructose specific permease, putative	1.23	-1.12	-	-1.22	FruR, CcpA
E	Q2FZQ1	*yrbD*	SAOUHSC_00949	Uncharacterized protein	-1.27	1.07	-	1.61	CodY
F	Q2FZ76	*pyrP*	SAOUHSC_01165	Uracil permease, putative	1.52	-1.44	-	-1.57	-
I	Q2FYZ3	*pldB*	SAOUHSC_01279	Hydrolase, alpha/beta fold family domain protein	-1.07	1.26	-	1.60	-
Q	Q2FY61		SAOUHSC_01604	Uncharacterized protein glyoxalase/bleomycin resistance protein/dioxygenase	-1.65	1.57	-	1.69	-
C	Q2FY54	*bfmBB*	SAOUHSC_01611	Dihydrolipoamide acetyltransferase component of pyruvate dehydrogenase complex	1.09	-1.03	-	-1.23	-
Q	Q2FXE2	*yvgN*	SAOUHSC_01907	Aldo/keto reductase, related to diketogulonate reductase	-1.64	1.35	-	1.81	-
E	Q2FV98	*yncA*	SAOUHSC_02836	L-amino acid N-acyltransferase	1.02	-1.18	-	-1.16	-
E	Q2G1N3	*sbnA*	SAOUHSC_00075	Probable siderophore biosynthesis protein SbnA	-1.18	1.04	-	2.62	Fur
P	Q2G261	*sodM*	SAOUHSC_00093	Superoxide dismutase [Mn/Fe]	-1.28	1.09	-	1.10	CodY
E	Q2FZL2	*sspA*	SAOUHSC_00988	V8-like Glu-specific endopeptidase	-1.36	1.07	-	1.68	-
E	Q2FZL3	*sspB*	SAOUHSC_00987	Staphylococcal cysteine proteinase B	-1.19	1.03	-	1.53	-
H	Q2FWG0	*tenA*	SAOUHSC_02331	Aminopyrimidine aminohydrolase (Thiaminase II)	-	1.16	-	1.73	-
E	Q2FVW5	*ureA*	SAOUHSC_02558	Urease subunit gamma	1.96	-1.88	-	-1.54	-
E	Q2G2K6	*ureB*	SAOUHSC_02559	Urease subunit beta	1.62	-1.38	-	-1.27	-
E	Q2G2K5	*ureC*	SAOUHSC_02561	Urease subunit alpha	1.72	-1.63	-	-1.32	-
F	Q2G0Y9	*xpt*	SAOUHSC_00372	Xanthine phosphoribosyltransferase (XPRTase)	1.09	-1.13	-	-1.00	-
H	Q2FVM0	*nasF/cobA*	SAOUHSC_02682	Uroporphyrin-III C-methyltransferase, putative	3.13	-3.33	-2.74	-3.49	Rex, NreC
C	Q2FVQ4	*lctP*	SAOUHSC_02648	L-lactate permease	1.85	-2.25	-1.72	-2.64	Rex
CP	Q2FVM2	*narH*	SAOUHSC_02680	Nitrate reductase, beta subunit	3.08	-3.49	-3.27	-3.74	Rex, NreC
C	Q2FVL8	*nirB/nasD*	SAOUHSC_02684	Assimilatory nitrite reductase [NAD(P)H], large subunit, putative	2.88	-3.40	-3.40	-3.78	Rex, NreC
CP	Q2FVM1	*narG*	SAOUHSC_02681	Nitrate reductase, alpha subunit	2.87	-3.73	-3.67	-4.06	Rex, NreC
C	Q2G218	*ldh1*	SAOUHSC_00206	L-lactate dehydrogenase 1 (L-LDH 1)	2.39	-3.45	-3.40	-4.13	Rex

C	Q2G1D8	*pflB*	SAOUHSC_00187	Formate acetyltransferase (Pyruvate formate-lyase)	2.87	-3.41	-3.05	-3.57	Rex, CcpA
P	Q2FVN1	*narT/narK*	SAOUHSC_02671	Probable nitrate transporter NarT	2.39	-2.94	-3.06	-2.96	Rex, NreC
P	Q2G172		SAOUHSC_00281	Uncharacterized protein, formate-nitrite transporter	2.21	-2.66	-2.40	-2.23	Rex
F	Q2FV02	*nrdD*	SAOUHSC_02942	Anaerobic ribonucleoside-triphosphate reductase, putative	1.51	-1.58	-1.46	-1.67	NrdR
E	Q2FYJ3	*tdcB*	SAOUHSC_01451	L-threonine dehydratase (Threonine deaminase)	2.37	-2.72	-3.11	-2.92	CodY
CPO	Q2FVM3	*narJ*	SAOUHSC_02679	Respiratory nitrate reductase, delta subunit, putative	2.63	-2.53	-3.03	-2.97	Rex, NreC
E	Q2FYJ4		SAOUHSC_01450	Uncharacterized protein amino acid permease	1.50	-1.76	-2.06	-2.17	CodY
G	Q2G0G1	*adh*	SAOUHSC_00608	Alcohol dehydrogenase	1.97	-2.15	-2.34	-2.57	Rex
C	Q2FYJ2	*ald1*	SAOUHSC_01452	Alanine dehydrogenase 1	1.84	-2.31	-2.50	-2.52	Rex
PQ	Q2FVL9	*nirD/nasE*	SAOUHSC_02683	Assimilatory nitrite reductase [NAD(P)H], small subunit, putative	2.07	-2.38	-2.40	-2.41	Rex, NreC
C	Q2G1K9	*adhE*	SAOUHSC_00113	Aldehyde-alcohol dehydrogenase	1.63	-1.85	-1.78	-1.80	Rex
				Metabolism and cellular processes and signalling					
CO	Q2G0B2	*cydC*	SAOUHSC_00693	ATP-binding/permease protein	1.12	-1.10	-	-1.23	-
GM	Q9RQP7	*icaB*	SAOUHSC_03004	Peptidoglycan/xylan/chitin deacetylase, PgdA/CDA1 family	-1.33	1.06	-1.08	-1.04	CodY, IcaR
				Poorly characterised					
R	Q2FZC0	*flr*	SAOUHSC_01112	FPRL1 inhibitory protein	-1.35	1.86	-	1.93	-
S	Q2G249		SAOUHSC_00026	Uncharacterized protein	-1.53	1.37	-	1.56	-
S	Q2G1N1	*sbnC*	SAOUHSC_00077	Uncharacterized protein	-1.02	1.00	-	2.41	Fur
S	Q2G177		SAOUHSC_00270	Uncharacterized protein putative lipoprotein	-	1.32	-	1.37	-
S	Q2G176		SAOUHSC_00271	Uncharacterized protein	-	1.14	-	1.27	-
S	Q2G105		SAOUHSC_00356	Uncharacterized protein	-1.65	1.88	-	1.22	SigB
S	Q2G0Y5		SAOUHSC_00376	Uncharacterized protein	-1.07	1.53	-	2.23	-
S	Q2G0X2		SAOUHSC_00401	Uncharacterized protein	-1.74	1.94	-	1.90	-
S	Q2G0E3		SAOUHSC_00662	Uncharacterized protein	1.26	-1.13	-	-1.25	-
S	Q2G2G0	*SaeP*	SAOUHSC_00717	Uncharacterized protein putative lipoprotein	-1.16	1.41	-	1.46	SaeR
R	Q2G035	*yfcH*	SAOUHSC_00792	Epimerase family protein	-2.45	2.12	-	2.62	SigB
R	Q2G016	*yjhQ/Yhbs*	SAOUHSC_00811	Predicted N-acetyltransferase	-1.96	1.80	-	2.22	SigB
S	Q2FZZ6		SAOUHSC_00838	Uncharacterized protein	-3.62	3.18	-	4.14	-
S	Q2FZT3		SAOUHSC_00907	UPF0344 membrane protein	-	1.00	-	1.22	-
R	Q2G1U4	*trfB*	SAOUHSC_00936	Uncharacterized protein, transcription factor	-	1.01	-	2.36	-
S	Q2G200		SAOUHSC_00941	UPF0738 protein	-1.54	1.51	-	1.37	-
S	Q2FZB9		SAOUHSC_01113	Uncharacterized protein membrane protein	-	1.35	-	1.34	-
S	Q2FZ03		SAOUHSC_01268	Uncharacterized protein	-1.08	1.32	-	1.80	-

S	Q2FXQ3	*ymaB*	SAOUHSC_01782	Uncharacterized protein	-1.38	1.10	-	2.10	-
S	Q2G2Y3		SAOUHSC_01919	Uncharacterized protein membrane protein	1.13	-1.13	-	-1.53	-
R	Q2FV53		SAOUHSC_02886	Uncharacterized protein	-	1.13	-	1.97	-
S	Q2G1H7		SAOUHSC_00146	Uncharacterized protein integral membrane protein	-1.42	-2.01	-1.42	-2.53	-
R	Q2FV03	*nrdG*	SAOUHSC_02941	Anaerobic ribonucleoside-triphosphate reductase-activating protein	1.62	-1.61	-1.60	-1.75	NrdR
R	Q2FZC2	*ecb*	SAOUHSC_01110	Fibrinogen-binding protein-related	-1.16	1.33	1.17	1.29	SaeR

Table 5.1 Functional classification and differential gene expression of shared gene content of untrained, trained-*rpoB* and *rpoC*

*, compared against WT; †, compared against untrained; 26 DEGs shared by all three trained strains are highlighted in blue, related to Figure 5.16 A.
Clusters of orthologues groups of proteins (COGs) were retrieved from NCBI for 121 common DEGs associated with high-level resistance as follows:
CELLULAR PROCESSES AND SIGNALING
[M] Cell wall/membrane/envelope biogenesis; [O] Post-translational modification, protein turnover, and chaperones; [T] Signal transduction mechanisms; [V] Defence mechanisms
INFORMATION STORAGE AND PROCESSING
[J] Translation, ribosomal structure and biogenesis; [K] Transcription; [L] Replication, recombination and repair
METABOLISM
[C] Energy production and conversion; [E] Amino acid transport and metabolism; [F] Nucleotide transport and metabolism; [G] Carbohydrate transport and metabolism; [H] Coenzyme transport and metabolism; [I] Lipid transport and metabolism; [P] Inorganic ion transport and metabolism; [Q] Secondary metabolites biosynthesis, transport, and catabolism
POORLY CHARACTERIZED
[R] General function prediction only; [S] Function unknown

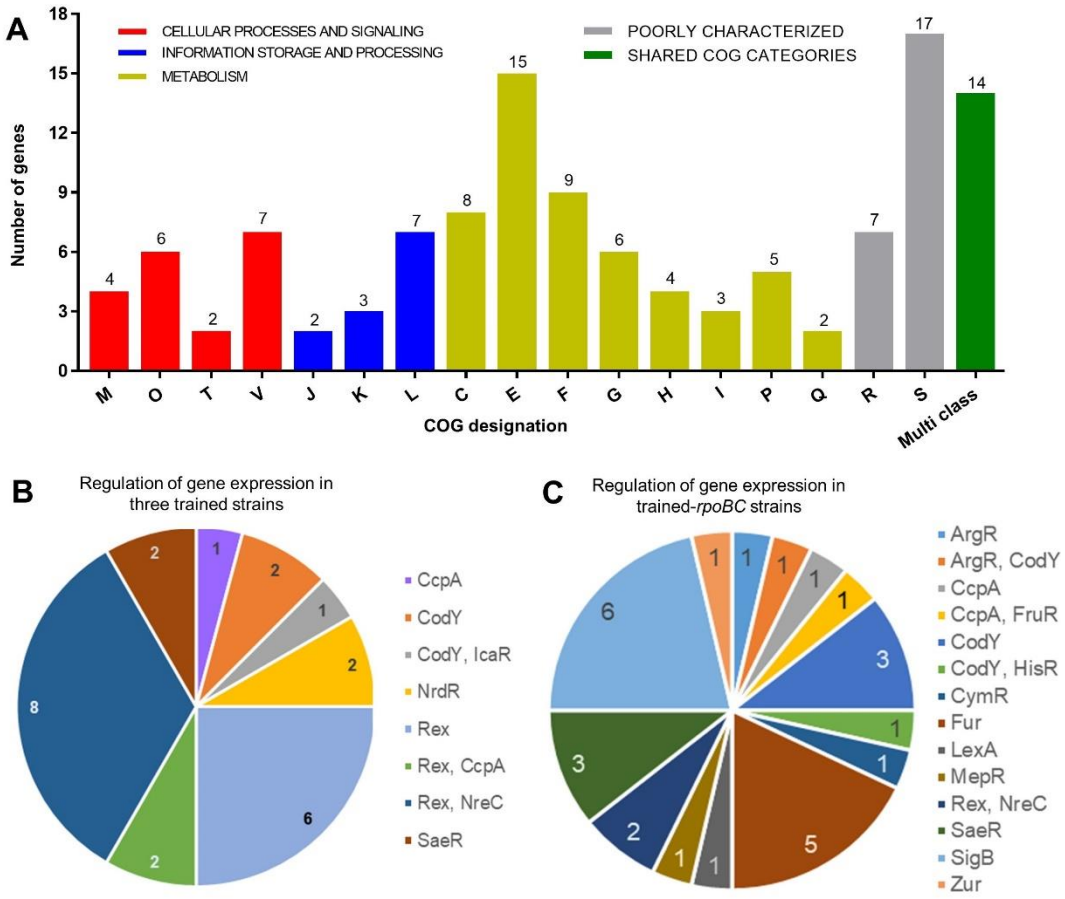

Figure 5.18 Functional classification and regulation of the differentially expressed genes

A) The 121 overlapping DEGs from Table 5.1 were classified into broad functional categories using Clusters of Orthologous Groups (COGs) classification. Different colours illustrate different COG functions. This demonstrates transcriptional changes due to significant metabolic stress. C, Energy production and conversion; E, amino acid transport and metabolism; F, nucleotide transport and metabolism; G, carbohydrate transport and metabolism; H, coenzyme transport and metabolism; I, lipid transport and metabolism; P, inorganic ion transport and metabolism; Q, secondary metabolites biosynthesis, transport, and catabolism; M, cell wall/membrane/envelope biogenesis; O, post-translational modification, protein turnover, and chaperones; T, signal transduction mechanisms; V, defence mechanisms; J, translation, ribosomal structure and biogenesis; K, transcription; L, replication, recombination and repair; R and S are function prediction only or function unknown categories. Total number of genes associated with each category are listed outside the bar.
B) The transcriptional regulators were predicted for 24 genes out of 26 common DEGs identified in three trained strains (*rpoB, rpoC* and *mecA*-cured-*rpoB*) compared to untrained, related to Figure 5.16. A total of 16 out of 24 genes were directly or indirectly controlled by Rex.
C) Subsequently, transcriptional regulators were predicted for 95 (Figure 5.17) DEGs associated with high-level resistance in trained-*rpoB* and *rpoC*.

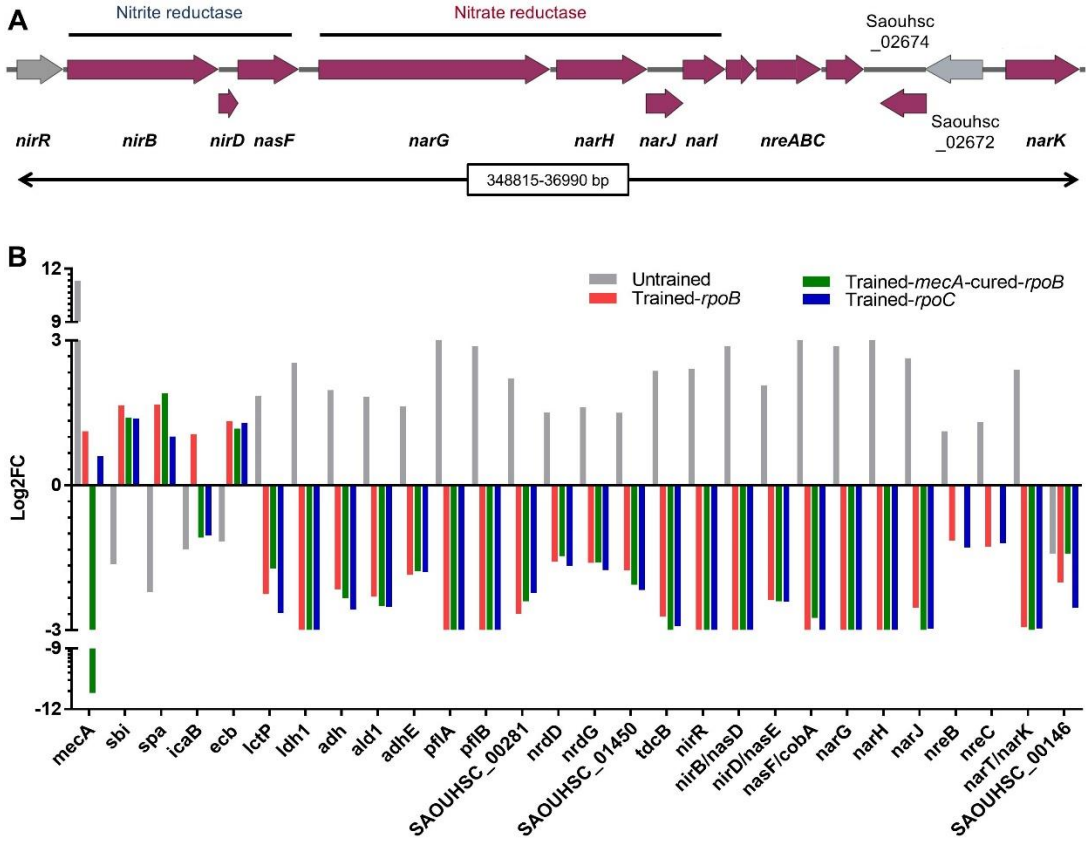

Figure 5.19 Gene expression profiles of nitrite and nitrate reductase genes

A) Chromosomal region of the genes involved in nitrite and nitrate reduction in *S. aureus*. A membrane bound nitrate reductase system (*narGHJI*) reduces nitrate to nitrite. Subsequently, nitrite is reduced to ammonia by NADH-dependent nitrite reductase system (*nirBD*) (Schlag et al., 2008). NreABC has been identified as an oxygen sensing system which regulates the expression of nitrate and nitrite reductase system as well as *narK* (Fedtke et al., 2002).
B) Transcriptional profiles of the common gene pool involved in nitrate and nitrite reduction showed upregulation in untrained compared to three trained strains. The expression of *nreBC* genes were not found to be significant in trained-*mecA*-cured-*rpoB* strain compared to the untrained strain.

5.2.5 Influence of the absence of staphylococcal respiratory regulatory (SrrAB) system on antibiotic resistance

Higher expression of genes related to anaerobic metabolism was observed in the untrained strain compared to WT. A number of transcripts encoding pyruvate metabolism enzymes (Ldh1, PflB, LctP, Adh, AdhE) associated with anaerobic respiration were highly expressed in the untrained strain which exhibits low-level oxacillin resistance (MIC = 2 µg/ml). On the contrary, trained-*rpoB* and *rpoC* strains showed reduced expression of genes related to anaerobic respiration while accompanying high-level oxacillin resistance (MIC = ≥256 µg/ml). Therefore, it was predicted that inactivation of anaerobic metabolism may lead to increased resistance in the untrained strain aerobically and anaerobically because acquisition of the *rpoB* and *rpoC* mutations reduces the expression of alternative respiratory system.

In order to test this hypothesis, the oxygen-dependent regulator SrrAB was disrupted, leading to impaired anaerobic respiration. SrrAB is a two-component regulatory system (TCS), mediating the aerobic-anaerobic switch in *S. aureus* which shares a considerable homology with the ResDE two-component regulatory system of *B. subtilis* required for anaerobic respiration (Somerville and Proctor, 2009; Throup et al., 2001). ResDE positively regulates anaerobic metabolism by controlling the anaerobic regulator Fnr, flavohemoglobin gene *hmp* and the nitrate reductase system *nasDEF* (Throup et al., 2001). Similar to a *B. subtilis resDE* mutant, an inactivation of *srrAB* in *S. aureus* have shown to have severe growth defect anaerobically (Throup et al., 2001).

To construct an *srrAB* lacking strain, a phage lysate from of JMB4556, SH1000 *srrAB*::*tet* (Mashruwala and Boyd, 2017) was transduced into a clean SH1000 (SJF682) background and selected using tetracycline (5 µg/ml) resulting into SH1000 *srrAB*::*tet* (SJF5054). The replacement of *srrAB* by *tet* was confirmed by DNA sequencing and PCR using primers resulting in a band of 2.5 kb compared to 3.2 kb in WT (Figure 5.20 A). The growth of SH1000 *srrAB*::*tet* (SJF5054) was examined anaerobically using BHI agar plate supplied with 2 mM sodium nitrate as an alternative terminal electron

acceptor. For anaerobic growth, plates were incubated at 37ºC in an anaerobic jar (Oxoid) containing a GasPak EZ (BD) to produce an anaerobic environment.

In the absence of nitrate, strain lacking *srrAB* (SJF5054) produced small colonies compared to WT (Figure 5.20 B), suggesting a marked reduction in growth. However, in the presence of nitrate both (WT and SJG5054) strains produced identical colonies anaerobically (Figure 5.20 B).

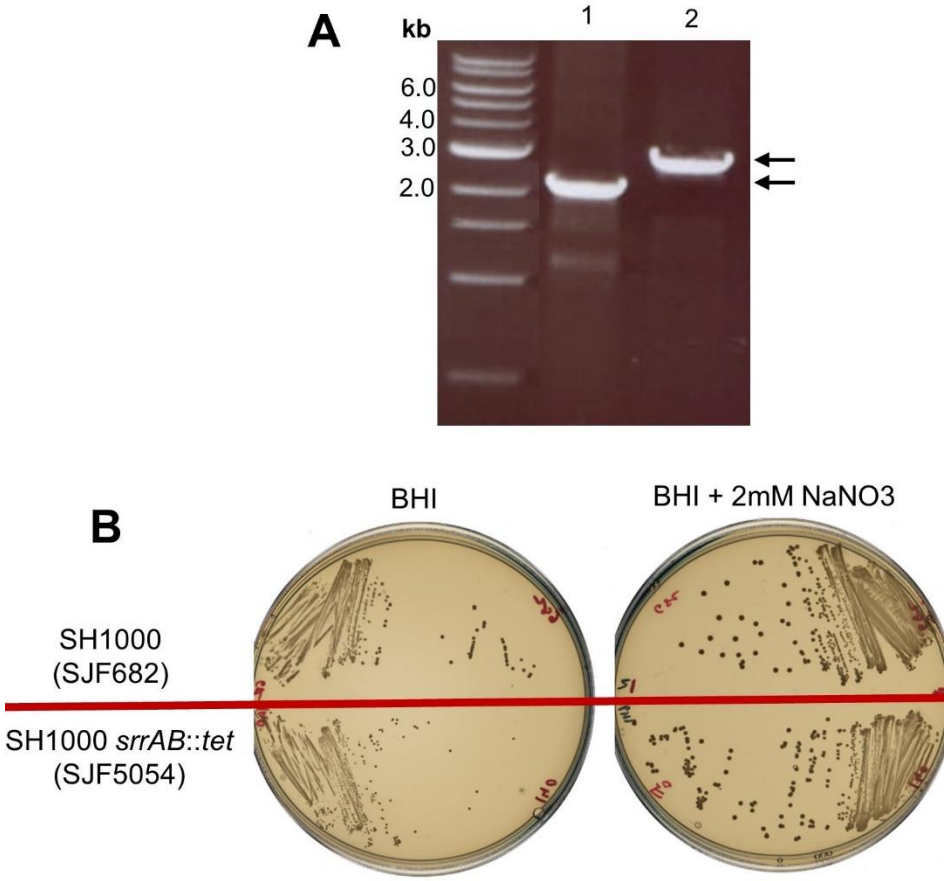

Figure 5.20 Construction and growth of SH1000 *srrAB*::*tet*

A) Phage lysate of JMB4556, SH1000 *srrAB*::*tet* (Mashruwala and Boyd, 2017) (SJF5051) was transduced into SH1000 (SJF682) resulting in SH1000 *srrAB*::*tet* named SJF5054. The transductant (lane 1) was verified by using primers srrAB_5'_up (forward) and srrAB_3'_down (reverse) binding upstream and downstream of *srrAB*, respectively, resulting in a band of ~2.5 kb (transductant, lane 1) and 3.2 kb for the positive control using SH1000 genomic DNA (lane 2). SH1000 genomic DNA was used as a template for the positive control. DNA fragments were used as size markers for agarose gel electrophoresis.
B) Subsequently, SH1000 (top half) and SH1000 *srrAB*::*tet* (SJF5054) (bottom half) were grown anaerobically on a BHI plate in the absence (left) and presence (right) of sodium nitrate.

5.2.5.1 Effect of aerobic and anaerobic growth conditions on antibiotic resistance

In order to examine oxacillin resistance, untrained, trained-*rpoB* and *rpoC* strains were transduced with a phage lysate from SJF5054 (SH1000 *srrAB*::*tet*). The resultant strains were named as untrained *lysA*::*pmecA srrAB*::*tet* (SJF5055); trained-*rpoB lysA*::*pmecA rpoB* (H929Q) *srrAB*::*tet* (SJF5056) and trained-*rpoC lysA*::*pmecA rpoB* (G740R) *srrAB*::*tet* (SJF5057). In addition to strains lacking *SrrAB* in SH1000, clinical MRSA COL and genetically complemented *rpoB*+ (SJF5044) and *rpoC*+ (SJF5045) were also tested for oxacillin resistance. A total of twelve strains were tested including five representative strains used for transcriptome analysis (Figure 5.21).

To test oxacillin sensitivity aerobically using Etest strips, strains were incubated for 24 hours at 37ºC on a BHI agar plate. For anaerobic growth conditions, agar plates were supplied with 2 mM $NaNO_3$ and incubated for 24 hours at 37ºC in an anaerobic jar as described above (section 5.2.5). In the absence of nitrate, poor or no growth was observed for all strains after 48 hours incubation at 37ºC anaerobically. Reduced oxacillin MICs were noted for trained-*rpoC* (Figure 5.21 E) from ≥256 aerobically to 32 µg/ml anaerobically and untrained *srrAB*::*tet* (Figure 5.21 J) from 4 aerobically to 0.5 µg/ml anaerobically. Similarly, untrained (Figure 5.21 B) showed reduced oxacillin MIC from being 1 aerobically to 0.25 µg/ml anaerobically. All other strains showed no alterations to oxacillin resistance under aerobic or anaerobic conditions.

To evaluate the performance of the agar plate method for antibiotic susceptibility testing, MICs were tested using broth microdilution method on 96-well plate as a reference method using oxacillin concentrations starting from 256 to 0.03 µg/ml. To determine the MIC under anaerobic growth conditions, BHI broth was supplied with 2 mM $NaNO_3$ and plates were incubated for 24 hours at 37ºC. Growth was assessed using plate reader. MICs obtained by broth microdilution and agar plate method under aerobic and anaerobic conditions were plotted using a bar plot for all test strains

(Figure 5.22). Oxacillin MICs obtained by broth microdilution method under both conditions showed overall reduction in MIC values of all highly resistant strains (Figure 5.22 A). Trained-*rpoC* showed no alteration in oxacillin MIC (128 µg/ml) under anaerobic growth compared to the agar plate method (Figure 5.22 A). Consistent with MICs determined by using the agar plate method, broth dilution method for untrained *srrAB*::*tet* showed reduced resistance from 4 aerobically to 1 µg/ml anaerobically.

To reproduce similar resistance profiles as oxacillin for all strains using another β-lactam antibiotic, methicillin susceptibility was determined using broth dilution method as methicillin Etest strips are not available commercially. Trained strains (Figure 5.22 B; trained-*rpoB, rpoC*, and trained-*rpoB srrAB*::*tet*) expressing high-level oxacillin resistance (MIC = >32 µg/ml) showed reduced methicillin resistance under anaerobic conditions. Interestingly, methicillin MIC for untrained strain displayed similar resistance characteristics to that of oxacillin resistance profile with methicillin MIC from 8 under aerobic to 4 µg/ml under anaerobic conditions (Figure 5.22 B). Overall, based on these observations, it is possible to speculate that the functionality of *mecA* may depend on aerobic over anaerobic growth conditions. However, this rationale required to be tested.

To assess if the development of oxacillin resistance affected antibiotic susceptibility to other class of antibiotics. Tetracycline and chloramphenicol MICs were determined using agar plate and broth dilution methods under aerobic and anaerobic conditions. MICs were determined for untrained, trained-*rpoB* and *rpoC*, COL, trained-*rpoB*+ and trained-*rpoC*+ strains and compared against SH1000 (Figure 5.23). These strains except COL, were found to be sensitive to tetracycline with MIC values ≤1 µg/ml under all conditions (Figure 5.23 A). With the agar plate approach, chloramphenicol MICs showed similar values under aerobic and anaerobic conditions. However, all strains except COL displayed 0.06 µg/ml MIC aerobically and ≥1 µg/ml anaerobically.

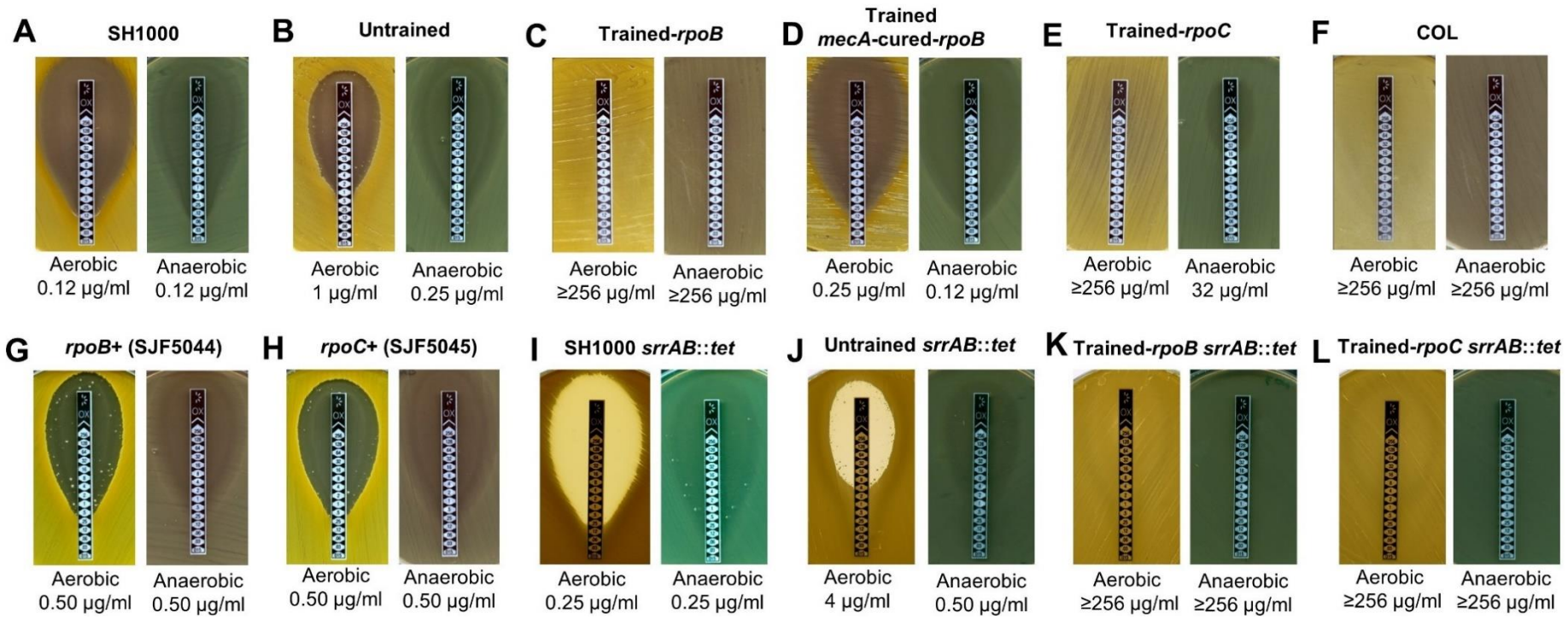

Figure 5.21 Oxacillin MIC of strains under aerobic and anaerobic growth conditions

Oxacillin sensitivity for strains in the absence and presence of SrrAB was determined using the Etest method under aerobic and anaerobic growth conditions. A BHI agar plate containing 2 mM sodium nitrate was used for anaerobic incubation at 37ºC for 24 hours. Strains used are **A)** SH1000 (WT); **B)** untrained (SJF4996, SH1000 *lysA*::*pmecA*); **C)** trained-*rpoB* (SJF5003, SH1000 *lysA*::p*mecA rpoB*-H929Q); **D)** trained-*mecA*-cured-*rpoB* (SJF5010; SH1000 *lysA*::*Kan rpoB*-H929Q); **E)** trained-*rpoC* (SJF5034; SH1000 *lysA*::p*mecA rpoC*-G740R); **F)** COL (SJF315, clinical MRSA isolate); **G)** *rpoB* (H929Q) complemented strain, *rpoB*+ (SJF5044); **H)** *rpoC* (G740R) complemented strain, *rpoC*+ (SJF5045); **I)** SH1000 *srrAB*::*tet* (SJF5054); **J)** untrained *lysA*::*pmecA srrAB*::*tet* (SJF5055); **K)** trained-*rpoB lysA*::*pmecA rpoB* (H929Q) *srrAB*::*tet* (SJF5056); **L)** trained-*rpoC lysA*::*pmecA rpoB* (G740R) *srrAB*::*tet* (SJF5057).

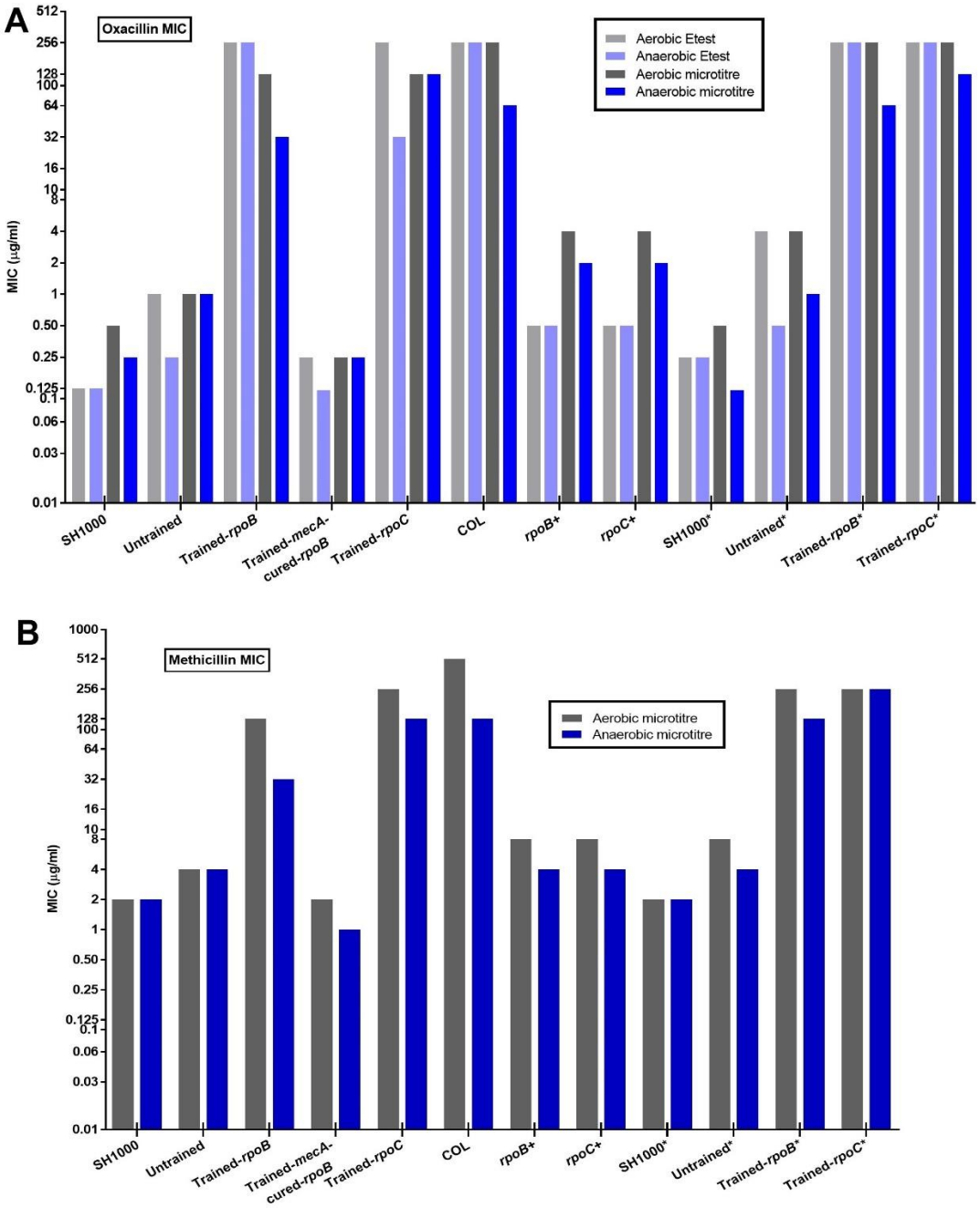

Figure 5.22 β-lactam resistance under aerobic and anaerobic growth

A) Oxacillin MIC was determined using the Etest and microdilution method under aerobic and anaerobic growth conditions for strains with or without the deletion of *srrAB*. 2 mM sodium nitrate was supplied to growth media prior to anaerobic incubation. The highest concentration of oxacillin (2048 µg/ml) was serially diluted to 0.03 µg/ml using 96-well plate.
B) Methicillin sensitivity was determined using the microdilution method under aerobic and anaerobic growth conditions for all representative strains including *srrAB* mutants. 2 mM sodium nitrate was added to growth media prior to anaerobic incubation. The highest concentration of methicillin (2048 µg/ml) was serially diluted to 0.03 µg/ml using a 96-well plate. *, strains lacking *srrAB*.

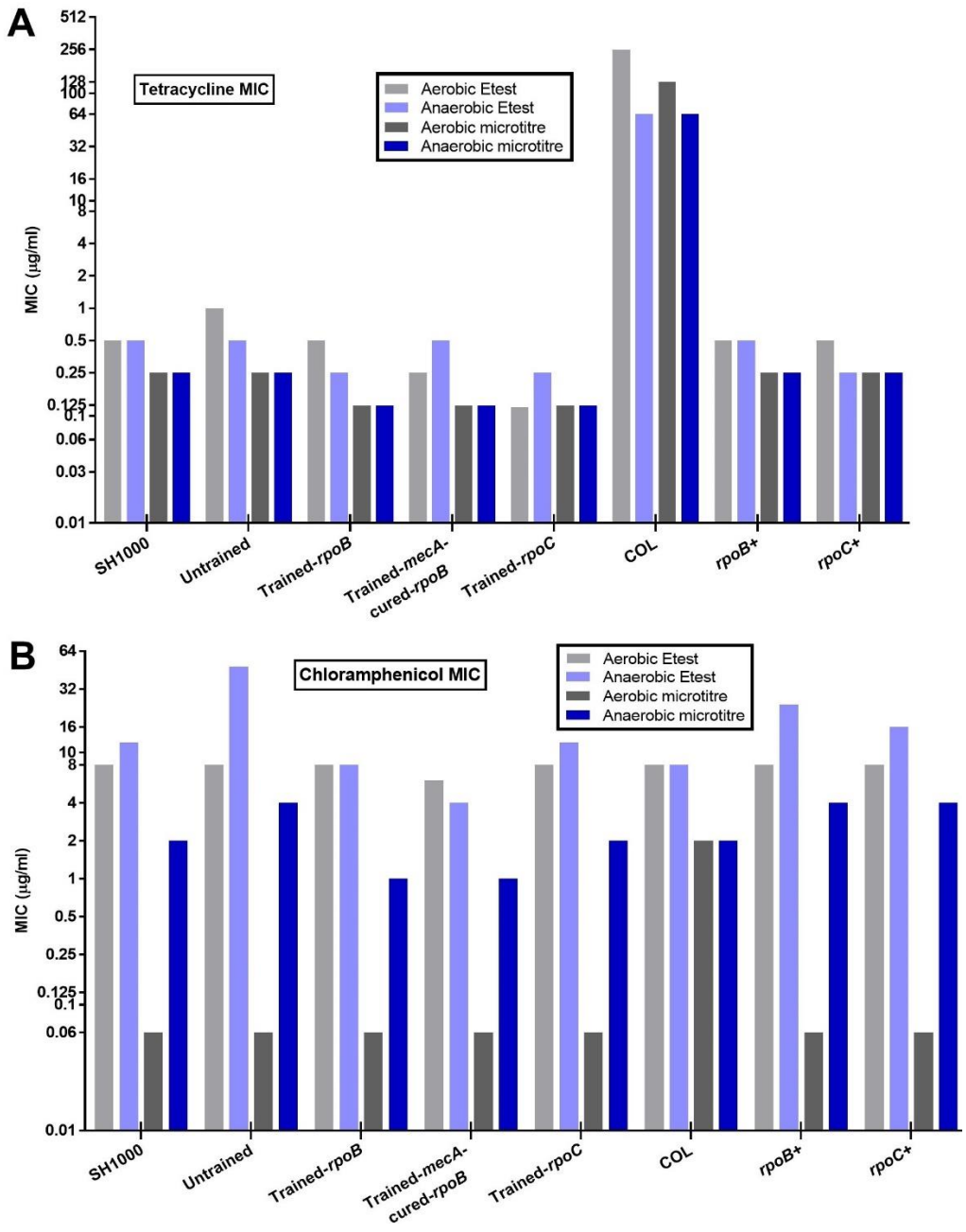

Figure 5.23 Tetracycline and chloramphenicol sensitivity test under aerobic and anaerobic growth conditions

A) Tetracycline sensitivity was determined using the Etest and microdilution method under aerobic and anaerobic growth conditions. 2 mM sodium nitrate was supplied to growth media prior to anaerobic incubation. The highest concentration of tetracycline (2048 µg/ml) was serially diluted to 0.03 µg/ml using a 96-well plate.
B) Chloramphenicol MIC was determined using the Etest and microdilution method under aerobic and anaerobic growth conditions. 2 mM sodium nitrate was added to growth media prior to anaerobic incubation. The highest concentration of methicillin (64 µg/ml) was serially diluted to 0.03 µg/ml using a 96-well plate.

5.2.6 Resistance to oxidative stress following a *mecA* induced transcriptional response

S. aureus is capable of resisting a wide range of stresses such as, oxidative, acid tolerance, osmotic with its ability to respond using an intrinsic repertoire of the regulatory mechanisms (Clements and Foster, 1999; Gaupp et al., 2012). A set of genes (*metN1*, *sirA*, *sirB*, *ocd2*, *sbnA*, *sbnC*, *sodM* and SAOUHSC_02904) regulated by stress regulators such as Fur, Zur, CodY and CymR were found to be upregulated in trained-*rpoB* and *rpoC* strains compared to the untrained strain (Table 5.1). In order to test whether the acquired differential expression alters the sensitivity of these strains to various oxidative stress stimuli, disk diffusion assays were performed for representative strains using three oxidative stress inducing compounds, 1 M diamide, 2 M paraquat (methyl viologen) and 200 mM potassium tellurite (K_2TeO_3).

Diamide is a specific thiol oxidant which causes disulphide stress resulting in damage to proteins (Pöther et al., 2009). *S. aureus* is resistant to tellurite (TeO_3^{2-}) toxicity because of its reductive detoxification by in part cysteine synthetase and cysteine containing molecules which reduces tellurite to black crystals of tellurium (Chasteen et al., 2009; Lithgow et al., 2004). Paraquat (methyl viologen) induces oxidative stress by reducing oxygen to superoxide anions causing superoxide stress conditions which causes DNA damage (Lin and Everse, 1987). Both untrained and trained strains showed no effect on sensitivity to diamide similar to SH1000 (Figure 5.24). All representative strains showed no detectable growth inhibition around the disk with either paraquat/tellurite indicating the level of paraquat/tellurite was not sufficient. Interestingly, there is the potential of some susceptibility to paraquat in the untrained compared to WT. These observations suggest that the resistance to oxidative stress was maintained in all strains, independent of transcriptional changes in stress associated genes. Moreover, it is important to note that differential expression of stress related genes involved were not found to be significant in trained-*mecA*-cured-*rpoB* strain, meaning that *rpoB* and *rpoC* mutations compensate for the stress induced by *mecA*.

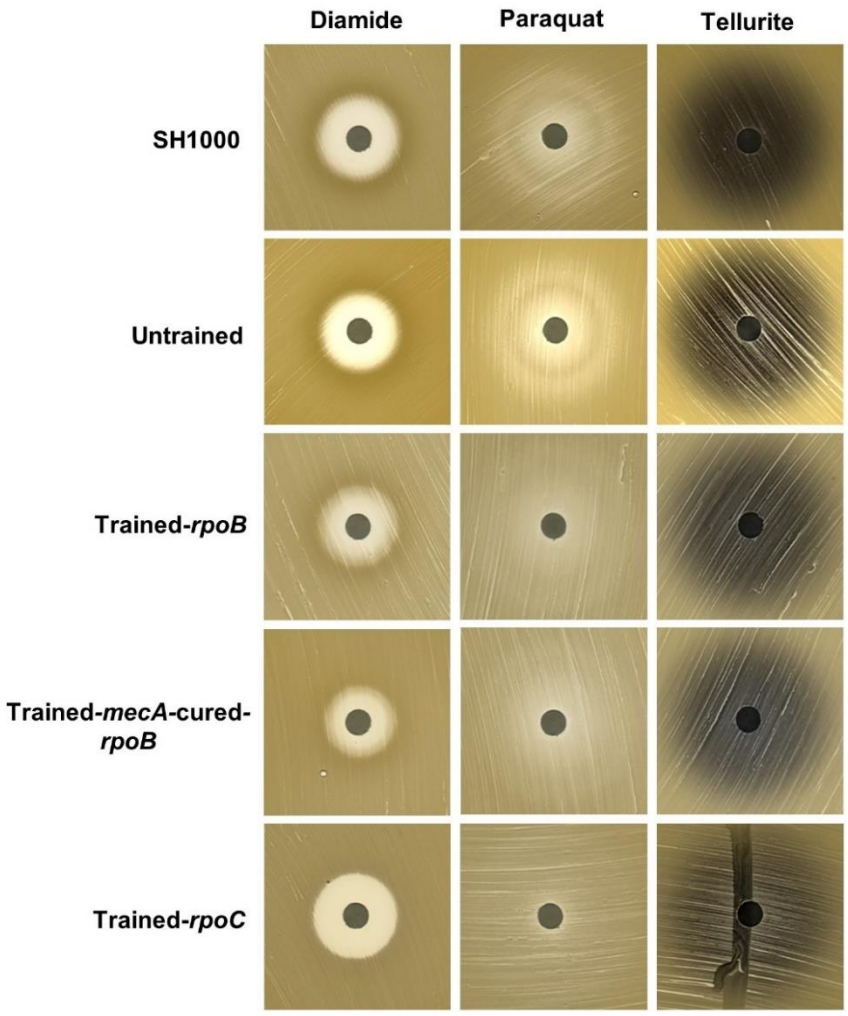

Figure 5.24 Stress resistance phenotypes of untrained and trained strains

Disk diffusion assays were performed with 1 M diamide, 2 M paraquat (methyl viologen) and 200 mM potassium tellurite (K_2TeO_3) for WT, untrained and the three trained strains. The results of stress sensitivity were compared against WT (SH1000).

5.2.7 Enzymatic determination of lactate from *S. aureus* culture supernatants

S. aureus is a facultative anaerobe with an ability to catabolise carbohydrates using tricarboxylic acid cycle (TCA) under aerobic conditions, however this depends on the oxygen and nutrient availability (Strasters and Winkler, 1963). Depending on the availability of oxygen, one of the most key growth-limiting factor varies from site to site in the host (Coleman et al., 1983). The physiological response of *S. aureus* to oxygen deprivation resulted in a switch from energy favourable respiratory state (aerobic) to anaerobic fermentative conditions (Fuchs et al., 2007), leading to the upregulation of fermentation genes encoding proteins such as, LDH, ADH accompanied by downregulation of TCA enzymes (Throup et al., 2001).

As mentioned above in section 5.2.5, genes associated with anaerobic fermentative growth showed increased transcripts in untrained compared to trained-*rpoB, rpoC* and *mecA*-cured strains. However, comparative analysis of the trained strains against WT showed no change in these set of genes. Considering these metabolic transcriptional changes induced by the acquisition of *mecA*, extracellular amount of lactate, a major end-product of fermentation was quantified using a colorimetric based lactate assay (Abcam). To examine the extracellular lactate, strains were grown under aerobic conditions until OD_{600} reached 1. Supernatant was collected and samples were processed in accordance with manufacturer's instructions.

The levels of secreted lactate showed significant reduction in the untrained strain compared to WT. Whereas, the three trained strains showed moderate reduction in the levels of lactate compared to WT (Figure 5.25). The concentration of extracellular lactate was measured using a standard curve of known lactate standards. These observations are in line with the recent study (Ferreira et al., 2013) demonstrated that *S. aureus* uses lactate as a carbon source to sustain growth during glucose limiting conditions aerobically. Therefore, in the presence of *mecA*, untrained strain likely uses lactate to regenerate NADH subsequently generating energy.

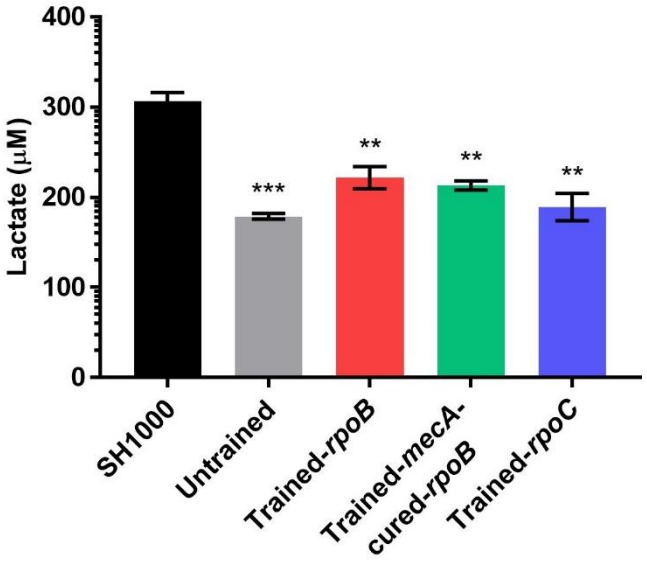

Figure 5.25 Quantification of extracellular lactate from *S. aureus* supernatant

Lactate measured in SH1000, untrained, trained-*rpoB*, trained-*mecA*-cured-*rpoB* and trained-*rpoC* supernatants showing quantity in µmol per ml of tested supernatant. Samples were deproteinised prior to processing. Results are the average of three independent repeats ±SEM. Unpaired t-test; *, p <0.05; **, p <0.01; ***, p <0.001.

5.2.8 Quantification of rate of cellular respiration

If the acquisition of *mecA* (untrained strain) disrupts the respiratory chain by inducing the expression of anaerobic fermentative genes, presumably it would lower the rate of oxygen consumption in untrained and it may be restored back to WT level of respiration rate in the trained strains following acquisition of *rpoB* or *rpoC* mutations. In order to investigate this hypothesis, a Clark-type oxygen electrode was used to measure rate of respiration at which oxygen is consumed. Oxygen electrode was calibrated using PBS prior to testing samples. Oxygen respiration rates (OCR) were measured at 37ºC and respiration was initiated by supplying glucose.

OCR measurements for untrained showed deceleration of cellular respiration, however not significant compared to WT. Whereas, trained-*rpoB* and *rpoC* strains showed significant acceleration of cellular respiration compared to untrained but similar to WT (Figure 5.26). These observations showed that the respiration rate affected by *mecA*-associated metabolic changes normalises to WT levels in trained-*rpoB* and *rpoC* strains. However, trained-*mecA*-cured-*rpoB* showed similar OCR to the untrained strain, suggesting *mecA* dependent cellular respiration in the presence of *rpoB* mutation alone.

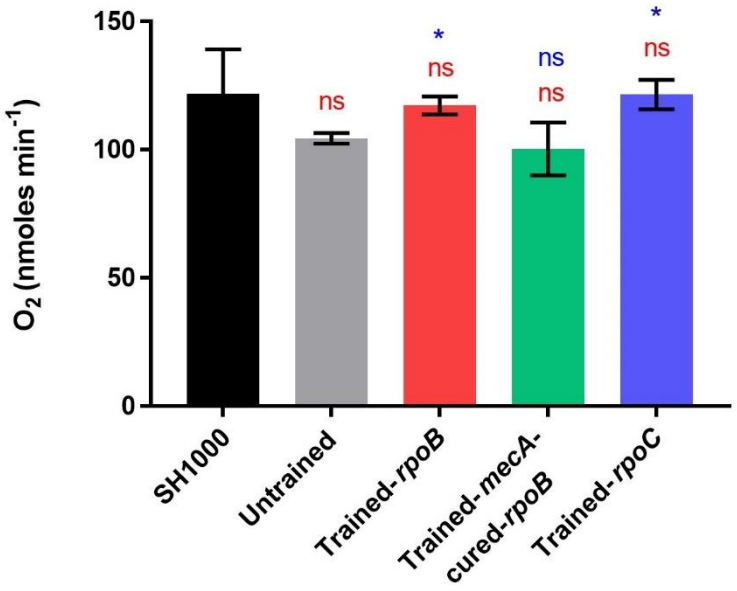

Figure 5.26 Determination rate of oxygen consumption in *S. aureus*

Cellular respiration was measured for SH1000, untrained, trained-*rpoB*, trained-*mecA*-cured-*rpoB* and trained-*rpoC* strains using Clark-type oxygen electrode. Data shown here reflect mean ±SEM of the three biological replicates. The results were compared against WT and untrained are shown in red and blue asterisks (above bar plot), respectively. Statistical analysis was performed using unpaired t-test. *, p <0.05; ns, not significant (p ≥0.05).

5.3 Discussion

The mechanisms of β-lactam resistance in *S. aureus* are poorly understood. Due to the pathogenic importance of this organism it is important to study gene expression and regulation and their contribution to the development of the high-level resistance. Previous studies have used the microarray analysis approach to investigate differential gene expression and identify virulence factors (Dunman et al., 2001; Korem et al., 2005). Here, transcriptional responses of *S. aureus* due to acquisition of *mecA* was successfully investigated using RNA-Seq, providing the distribution of differential gene expression required to confer oxacillin resistance. This data identified two important transcriptional responses induced by *mecA* and mutations in *rpoB* and *rpoC*.

First, the primary comparative transcriptome analysis of the strains (untrained and trained-*rpoC*, *mecA*-cured-*rpoB*) determined significant differences in the expression patterns due to the presence of *mecA* and subsequent acquisition of *rpoC* mutation compared to WT, whilst, the acquisition of *rpoB* mutation showed restored gene expression to WT levels, suggesting that at the transcription level, *S. aureus* has a complex regulatory network specific to the acquired mutations. In addition, over one hundred genes were differentially expressed in untrained, trained-*rpoC* and *mecA*-cured-*rpoB* strains, whereas only nine genes were shown to have differential expression in trained-*rpoB* (Figure 5.13). Surprisingly, only *lysA, mecA* and *nirR* were detected to be shared among untrained and trained-*rpoB* and *rpo*C strains. In the untrained strain, the reduced expression of *mecA* was accompanied by increased *nirR* transcripts and low-level oxacillin resistance (MIC = 2 µg/ml). Moreover, a substantial reduction in *nirR* transcription was observed upon acquisition of *rpoB* or *rpoC* mutations together with increased *mecA* expression and high-level oxacillin resistance (MIC = ≥256 µg/ml). This indicates that WT level *nirR* expression may be necessary together with increased *mecA* expression in order for the strain to develop high-level resistance which can be achieved by alterations in *rpo*.

Surprisingly, *nirR* was also identified to be the only transcriptional regulator found to be common among trained strains compared to the untrained strain along with other set of 121 DEGs. However, this group included a subset of 26 common genes with differential expression by comparative analysis of the trained strains against the untrained strain (Figure 5.15 and Figure 5.16). The remaining 95 genes were exclusively shared by *rpoB* and *rpoC* mutants only (Figure 5.16 A and Figure 5.17), suggesting their connection with increased resistance. Systematic analysis of 121 genes to determine functional categories based on COG designations revealed that the majority of genes were related to metabolism, suggesting a *mecA*-derived transcriptional perturbation of *S. aureus.* Upregulation of anaerobic nitrate/nitrite respiration related genes (*nirR, nirB, nirD, nasF, narG, narH, narJ, narT*) and fermentation-related genes (*adhE, adh, ldh1, ald1, lctP*) were identified in the untrained strain under aerobic growth conditions. However, these genes showed WT level expression in trained strains. Nitrate/nitrite respiration related genes are regulated dually by the NreBC TCS and Rex (repressor of anaerobic genes) (Pagels et al., 2010; Schlag et al., 2008). It is unclear whether NreBC specifically detects the presence of nitrate, where under oxygen deprived conditions it upregulates the nitrate and nitrite reductase systems (Kamps et al., 2004; Schlag et al., 2008). The redox sensing transcriptional regulator Rex plays an important role in the maintenance of the NADH/NAD+ ratio independent of oxygen availability (Pagels et al., 2010). Considering this, it is plausible to speculate that the untrained strain may favour mixed metabolism of anaerobic-nitrate fermentative respiration to generate energy to sustain growth rate similar to the WT while producing low-level resistance.

Second, the expression of oxidative stress response regulators, Fur, Zur, SigB and CymR regulated genes (*yusE*; SAOUHSC_02904, encoding putative thioredoxin reductase; *yusF; metN1; sirB; sirA; ocd2; prop; sbnA; sbnC;* SAOUHSC_00356, uncharacterised protein; *yfcH; yhbS*) were induced in trained strains. This induction was unable to alter the oxidative stress response in *S. aureus* upon exposure to exogenous oxidants (Figure 5.24). Additionally, oxacillin resistance remained largely unchanged under aerobic

and anaerobic growth conditions for trained strains. Whereas, the untrained strain lacking *srrAB* showed a reduction in oxacillin and methicillin MIC under anaerobic conditions, suggests that the expression of *mecA* may be dependent on the presence of oxygen. However, this could be tested by real-time qPCR. Meanwhile, the levels of extracellular lactate showed a reduction in untrained strain compared to trained strains (Figure 5.25).

It was shown previously that *S. aureus* may switch to mixed-acid (acetate, formate, and lactate) and butanediol fermentation under fermentative growth conditions, enabling pyruvate reduction to lactate or acetoin (Fuchs et al., 2007). Furthermore, under aerobic conditions pyruvate is metabolised to acetyl-CoA by PDH (pyruvate dehydrogenase complex), producing NADH. Similar to *E. coli* (Hansen and Henning, 1966), reduced expression of PDH complex was reported in *S. aureus* with simultaneous increase in the expression of pyruvate formate lyase (PflB) under anaerobic conditions (Fuchs et al., 2007). Therefore, increased expression of PflA and PflB along with SAOUHSC_00281 (encoding nitrate/formate transporter) in the untrained strain may have resulted in increased extracellular formate levels. Furthermore, formate oxidation and nitrate reduction reactions occur simultaneously under anaerobic condition in *E. coli* (Figure 5.27) (Sawers, 2005).

Transcriptomics data combined with oxygen consumption rate results (Figure 5.26), suggests that *mecA* might be interacting with respiratory genes resulting into disruption of respiration, therefore leading to a partial inhibition of oxygen consumption in the untrained strain. Subsequently, *rpoB* and *rpoC* mutations restore metabolic balance perturbed by having *mecA* alone.

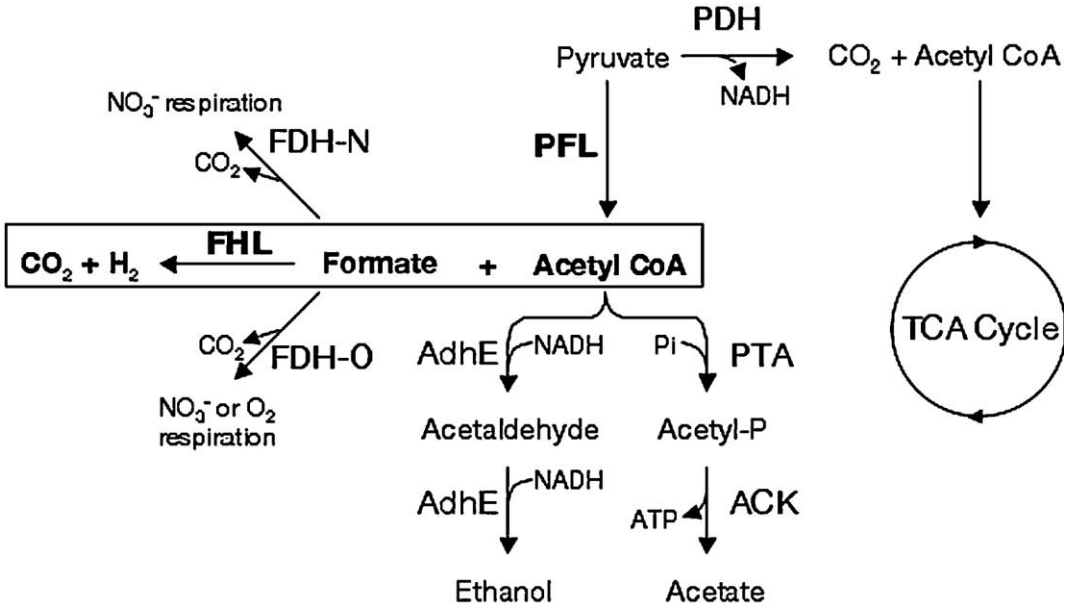

Figure 5.27 Scheme of pyruvate metabolism in *E. coli*

Key pathways of pyruvate and formate metabolism. Formate metabolism reactions are shown in bold and boxed. Taken from (Sawers, 2005).

Chapter 6

General Discussion

Antimicrobial resistance (AMR) is a global threat to the control of an increasing range of difficult-to-treat infections caused by bacteria, fungi, viruses and parasites. AMR emerges when the pathogens causing infection such as bacteria, survive upon exposure to antibiotics that would normally inhibit their growth or kill them. Therefore, the reduced efficacy of medicines renders the treatment of patients costly, difficult or even impossible. The magnitude of the impact of AMR on not only human health but also the economy has been assessed and the findings are particularly shocking (O'Neill, 2016). Currently, 700,000 people die due to infections that are resistant to antibiotics every year (O'Neill, 2016). The review on AMR by Jim O'Neill (2016) estimated that AMR could claim 10 million lives a year (1 person every 3 seconds) by 2050 costing up to 100 trillion USD to the economy if proactive solutions are not found to tackle AMR. The deaths attributable to AMR would be higher than that predicted for cancer.

The development of resistance to antibiotics is a natural process and has been noted since the introduction of the first antibiotic. This has resulted in the emergence of 'superbugs'. One such 'superbug' is methicillin-resistant *Staphylococcus aureus* (MRSA). Infections caused by MRSA are difficult or even impossible to treat, in some cases, due to its resistance to virtually all β-lactam antibiotics. The development of methicillin resistance in *S. aureus* is predominantly due to the acquisition of the *mecA* gene encoding a penicillin insensitive PBP (Hartman and Tomasz, 1984). The majority of MRSA isolates display a low-level resistance, barely above that exhibited by susceptible strains. However, these MRSA isolates are capable of developing high-level resistance upon exposure (during treatment) to β-lactam antibiotics. This characteristic of conversion of resistance level have shown to be induced by chromosomal mutations in the presence of antibiotic (Finan et al., 2002; Ryffel et al., 1994). This means that the acquisition and

expression of *mecA* is a prerequisite, but not sufficient, to develop high-level resistance. This conversion has formed the basis for my project.

To better understand the basis for the transition from low-level to high-level resistance, several studies by other researchers (Kim et al., 2013; Mwangi et al., 2013; Pozzi et al., 2012) and myself have employed a model system to introduce multicopy plasmid-borne *mecA* into an MSSA strain which produced derivatives with low-level resistance, capable of developing high-level homogeneous resistance upon exposure to elevated levels of antibiotics. Similar to previous studies by others (Banerjee et al., 2010; Griffiths and O'Neill, 2012; Pozzi et al., 2012), genome sequencing of highly resistant isolates identified mutations in the *gdpP* gene (Table 3.2) implicated in the development of high-level resistance. GdpP (c-di-AMP phosphodiesterase) regulates intracellular levels of c-di-AMP, assisting biofilm formation, cell wall architecture and more importantly resistance/tolerance to β-lactams (Corrigan et al., 2011; Griffiths and O'Neill, 2012). Elevated resistance due to deletion or disruption of *gdpP* indicates that misfolding or destabilisation of GdpP might lead to increased resistance and concomitant increased intracellular c-di-AMP levels which can contribute to the co-regulation of antibiotic resistance through its interaction with yet unknown c-di-AMP target proteins (Corrigan et al., 2013).

However, naturally occurring MRSA isolates carry a single copy of *mecA*, making it more interesting and relevant system to study compared to the multicopy plasmid-borne *mecA* approach. Therefore, the molecular basis of MecA activity was investigated by introducing a single copy *mecA* integrated into the chromosome of an MSSA strain. Derivatives exhibited low-level resistance but were capable of developing high-level resistance following antibiotic treatment. This approach allowed the systematic tracking of the evolutionary progression of resistance, setting this system apart from others studies. Interestingly, genome sequencing revealed amino acid substitutions in either *rpoB* or *rpoC* (Table 4.2) that were responsible for conferring high-level resistance. Such mutations have been identified before in highly resistant clinical isolates (Aiba et al., 2013; Dordel et al., 2014; Hiramatsu et

al., 2013; Mwangi et al., 2007) but have not really been highlighted as important genetic determinant(s) for developing high-level β-lactam resistance.

The selection of spontaneous *rpoB* and *rpoC* mutants allowed the examination of the role of the mutations promoting low-level to high-level conversion of β-lactam resistance. Specifically, the impact of *rpoB* (H929Q) (SJF5003) and *rpoC* (G740R) (SJF5034) mutations were further studied in the context of high-level resistance. The RNAP core enzyme consists of two α, a β and a β' subunits, whose activity is sufficient to carry out transcription (Delumeau et al., 2011). The effects of *rpoB* and *rpoC* mutations on the activity of RNAP and its interaction with other proteins were examined by employing an *in vitro* transcription assay in collaboration with Prof Nikolay Zenkin and Caitlin Griffiths (Newcastle University). Purified RNAPs from both trained-*rpoB* (H929Q) and trained-*rpoC* (G740R) showed prolonged pausing of RNAP elongation complexes at different sites of the template compared to the WT. RNAP pausing is a sequence-dependent process which is associated with coupling of transcription with translation (Landick et al., 1985), nascent RNA transcript folding (Pan et al., 1999), recruitment of regulatory factors to the complex (Artsimovitch and Landick, 2000) and a prerequisite for transcription termination (Farnham and Platt, 1981). However, differences in pausing due to the acquisition of *rpoB* and *rpoC* mutations might affect the global pattern of transcription in the cell through changes in transcriptional activity. Furthermore, the presence of oxacillin showed no effect on the transcription of the *rpoB* and *rpoC* mutants as well as WT suggesting oxacillin independent RNAP activity.

In *S. aureus*, the proteins that interact with RNAP resulting in regulation of its activity, have not been fully described. The RNAP interacting protein YsxC specifically binds to the β' subunit, and has been previously reported to have a role in ribosomal stability and growth (Cooper et al., 2009). Extensive studies in *B. subtilis* revealed that a unique thiol/oxidative stress global transcriptional regulator, Spx is an RNAP-binding protein which positively regulates transcription in response to oxidative stress (Nakano et al., 2003a;

Zuber, 2004). Spx contains an N-terminal Cys-X-X-Cys (CXXC) motif which regulates its activity during thiol-oxidising conditions (Nakano et al., 2005; Pamp et al., 2006). Spx positively regulates the transcription of *trxA*, encoding thioredoxin and *trxB*, thioredoxin reductase (Pamp et al., 2006; Villanueva et al., 2016). The activation of *trxA* and *trxB* results from a direct interaction of Spx with α subunit of RNAP under oxidised conditions (Nakano et al., 2005; Pamp et al., 2006). Spx specifically interacts with the α-CTD (C-terminal domain) of RNAP subunit α with no evidence of a direct Spx-DNA interaction (Nakano et al., 2003b). Even though oxidised Spx is thought to be the active form of Spx, recent studies on the identification of Spx regulated genes demonstrates new promoters activated by reduced Spx (Rochat et al., 2012; Rojas-Tapias and Helmann., 2018). Also, disruption of *S. aureus spx* led to pleiotropic effects (Jousselin et al., 2013; Pamp et al., 2006) which suggests its role in cellular physiology as a global regulator. Moreover, Spx also serves as a negative regulator which represses the energy consuming functions of the cells in order to recover from stress (Nakano et al., 2003a). Furthermore, Spx controls the *trfA* gene, encoding an adaptor protein implicated in genetic competence and proteolysis (Jousselin et al., 2013). Disruption of *trfA* led to loss of resistance to glycopeptides and oxacillin in MSSA and MRSA strains providing a link between cell wall antibiotic stress and response mediated by Spx (Jousselin et al., 2013).

Together, it might be possible that the gene(s) identified in my study (Figure 5.17 and Table 5.1) are potentially under the direct or indirect control of Spx. Figure 6.1 depicts a model summarising the transcriptional response due to the expression of *mecA* could be linked to Spx. Potentially, Spx controls the activity of RNAP and/or its specificity for a specific promoter selection during *mecA* induced stress (untrained SJF4996 strain) which can be reversed upon the acquisition of *rpoB* and *rpoC* mutations (trained strains, SJF5003 and SJF5034) without detectable alteration in the expression of Spx. Of particular significance in the work demonstrated herein was the identification of the set of overlapping genes from the three trained strains, implicated in anaerobic respiration that were upregulated in the presence of *mecA* alone and adjusted back to WT level in trained strains (Figure 5.16 and Table 5.1

highlighted in blue). The majority of these genes are regulated by Rex, a redox dependent transcriptional repressor implicated in monitoring metabolism and sensing O_2 by responding to the NADH/NAD^+ ratio (Somerville and Proctor, 2009). Upregulation of anaerobic-associated genes suggests that Rex activity has been compromised in response to *mecA*-induced metabolic stress in the untrained strain and that the *rpoB* and *rpoC* mutations has restored the production of Rex repressing anaerobic genes to WT levels. However, *rex* is not controlled at the transcriptional level. This suggests that PBP2A might be interacting with component(s) of the respiratory chain resulting in perturbation of respiration causing a deceleration of the respiration rate (Figure 5.26) and concomitant redox imbalance accompanied by low-level resistance. Subsequently, mutations in *rpoB* and *rpoC* potentially reduces the redox-related stress, suggesting that high-level resistance would only occur when there is optimal redox balance as well as less transcriptional burden to the cell.

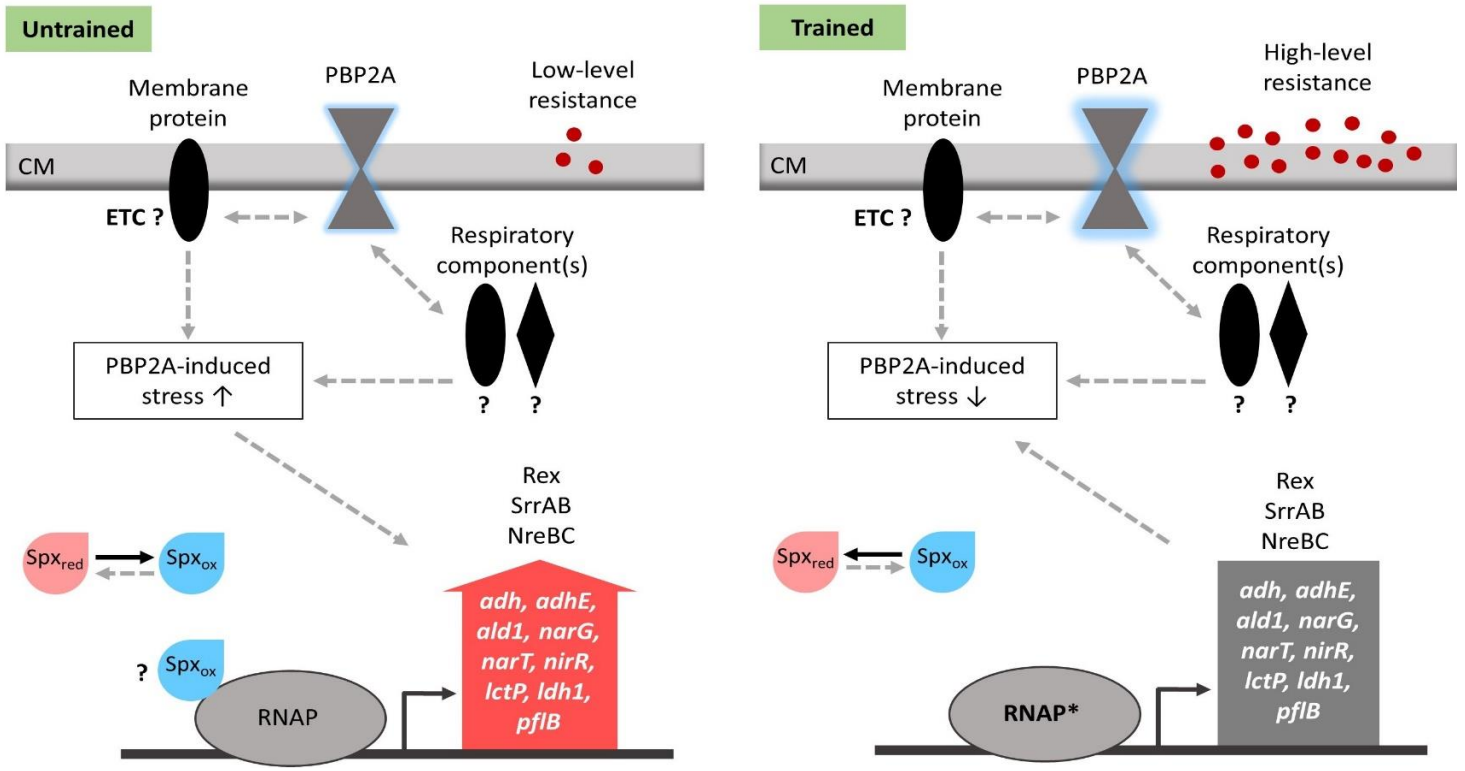

Figure 6.1 Model of proposed Spx-dependent transcriptional regulation

This model summarises the *mecA*-dependent cell wall stress and concomitant impact on global transcription might have induced Spx regulated mechanisms to recover from the stress in the untrained strain. This is probably due to a possible interaction of PBP2A with respiratory system. The mutation in *rpoB* and *rpoC* of the trained strains stabilises transcription to the WT level accompanied by increased PBP2A production leading to finely adjusted adaptation for the development of high-level β-lactam resistance. The dashed arrows indicate the proposed pathways and protein-protein interactions (left-right arrows).

6.1 Future perspectives

This work provides important information on the *mecA*-induced transcriptional response, specifically, upregulation of anaerobic metabolism which could be crucial for growth. Future work could be carried out to identify a possible direct or indirect interaction of *mecA* with anaerobic fermentative-related proteins. This could be done using the bacterial two-hybrid method. Understanding this will identify whether the wider PG synthesis machinery is actually interacting with the respiratory chain. Coupled with this, it would be particularly interesting to examine if the untrained strain has two populations or the whole population is carrying out mixed metabolism as the untrained strain showed upregulation of genes associated with anaerobic respiration. This could be performed by the localisation studies using fluorescent-labelled anaerobic gene, such as *ldh.*

The molecular localisation and role of PBP2A in cell division has not been studied yet. Prior studies have demonstrated that the cooperative function of PBP2 and PBP2A is required for continual cell wall biosynthesis in the presence of β-lactams (Pinho et al., 2001a). In the presence of oxacillin PBP2 is still required for its transglycosylation activity, suggesting its interaction with PBP2A (Pinho and Errington, 2005). However, the stoichiometry is unknown. From PBP2A localisation studies, preliminary data showed a strong PBP2A-SNAP signal to the septum in the presence of *rpoB* mutation and in the presence of oxacillin. However, septal localisation was also observed in the absence of oxacillin suggesting the importance of *rpoB* mutation for the recruitment of PBP2A to the septum. For co-localisation studies, utilisation of SNAP and CLIP labelled proteins combined with single molecule imaging using super-resolution microscopy approaches would shed more light on the mechanistic insight of *S. aureus* cell division.

To identify the link between the *rpoBC* mutations and high-level resistance, it would be interesting to study the activity of RNAP and its ability to interact with other proteins. This could include *in vitro* transcription assays using purified RNAP from the representative strains. Another hypothesis generated from this work would suggest that if the anaerobic respiration is inhibited

permanently by overexpressing Rex in the untrained strain would lead to increased oxacillin resistance without having *rpoBC* mutations, indicating the importance of aerobic respiration for the development of high-level resistance.

Another avenue for future work would include investigation of RNAP binding proteins in *S. aureus* and RNAP activity in the presence and absence of *rpoBC* mutations. Spx was characterised as a novel transcriptional regulator impacting thiol/oxidative stress tolerance (Pamp et al., 2006; Zuber, 2004). Identification of an *rpoB* mutation in *spx* mutant strain was found to be sufficient to compensate for the loss of an otherwise essential gene (Villanueva et al., 2016). It would be particularly interesting to examine whether the *rpoB* and *rpoC* mutations identified in this study would be sufficient to bypass the requirement for *spx* without altering resistance. This could be done by transducing the *spx* mutation into the *rpoBC* mutants. It would be important to determine the activity of Spx in the presence and absence of oxacillin. Finally, *in vitro* transcription assays using purified RNAP and Spx on specific promoters such as, *rex* or *nreBC,* would reveal whether such promoters are controlled by Spx.

Based on the comments from James O'Gara (external examiner) and Mike Brockhurst (internal examiner), it would be interesting to examine the amounts of PBP2A in other strains exhibiting low or intermediate level resistance to see if there is a correlation between the amounts of PBP2A being produced and concomitant resistance. It is also plausible to speculate that the expression of *mecA* requires certain codon(s) to be present in the cell for which the cell might have limited numbers of the rare corresponding tRNA(s) leading to codon bias. Therefore, it is tempting to speculate that this could then be solved by the acquisition of compensatory *rpoB* and *rpoC* mutations allowing efficient codon usage for *mecA*, resulting in concomitant increase in the production of PBP2A and oxacillin resistance.

Overall my work has revealed a novel effect of acquisition of *mecA* on cellular physiology by way of altering metabolism. This alludes to an interaction between cell wall synthesis and respiration. This observation

paves the way to begin to elucidate how such an important pathogen *S. aureus* is able to develop high-level drug resistance and give possible avenues for new therapeutic approaches.

References

Abeck, D., and Mempel, M. (1998). *Staphylococcus aureus* colonization in atopic dermatitis and its therapeutic implications. Br. J. Dermatol. *139*, 13–16.

Adams, D.W., and Errington, J. (2009). Bacterial cell division : assembly, maintenance and disassembly of the Z ring. Nat. Rev. Microbiol. *7*, 642–653.

Aedo, S., and Tomasz, A. (2016). Role of the Stringent Stress Response in the Antibiotic Resistance Phenotype of Methicillin-Resistant *Staphylococcus aureus*. Antimicrob. Agents Chemother. *60*, AAC.02697-15.

Aiba, Y., Katayama, Y., Hishinuma, T., Murakami-Kuroda, H., Cui, L., and Hiramatsu, K. (2013). Mutation of RNA polymerase β-subunit gene promotes heterogeneous-to-homogeneous conversion of β-lactam resistance in methicillin-resistant *Staphylococcus aureus*. Antimicrob. Agents Chemother. *57*, 4861–4871.

Amoroso, A., Boudet, J., Berzigotti, S., Duval, V., Teller, N., Mengin-Lecreulx, D., Luxen, A., Simorre, J.P., and Joris, B. (2012). A peptidoglycan fragment triggers β-lactam resistance in *Bacillus licheniformis*. PLoS Pathog. *8*.

Antignac, A., and Tomasz, A. (2009). Reconstruction of the phenotypes of methicillin-resistant *Staphylococcus aureus* by replacement of the staphylococcal cassette chromosome mec with a plasmid-borne copy of *Staphylococcus sciuri pbpD* gene. Antimicrob. Agents Chemother. *53*, 435–441.

Archer, G.L. (1998). *Staphylococcus aureus* : A Well–Armed Pathogen. Clin. Infect. Dis. *26*, 1179–1181.

Archer, G.L., and Bosilevac, J.M. (2001). Signaling in Resistance. Science (80). *291*, 1915–1916.

Arêde, P., Milheiriço, C., de Lencastre, H., and Oliveira, D.C. (2012). The anti-repressor MecR2 promotes the proteolysis of the *mecA* repressor and enables optimal expression of β-lactam resistance in MRSA. PLoS Pathog. *8*, 1–13.

Arêde, P., Botelho, T., Guevara, T., Usón, I., Oliveira, D.C., and Gomis-Rüth, F.X. (2013). Structure-function studies of the staphylococcal methicillin resistance antirepressor MecR2. J. Biol. Chem. *288*, 21267–21278.

Arthur, M., Molinast, C., and Depardieu, F. (1993). Characterization of Tn1546, a Tn3-Related Transposon Conferring Glycopeptide Resistance by Synthesis of Depsipeptide Peptidoglycan Precursors in *Enterococcus faecium* BM4147. J. Bacteriol. *175*, 117–127.

Artsimovitch, I., and Landick, R. (2000). Pausing by bacterial RNA polymerase is mediated by mechanistically distinct classes of signals. Proc. Natl. Acad. Sci. *97*, 7090–7095.

Baba, T., Takeuchi, F., Kuroda, M., Yuzawa, H., Aoki, K.I., Oguchi, A., Nagai, Y., Iwama, N., Asano, K., Naimi, T., et al. (2002). Genome and virulence determinants of high virulence community-acquired MRSA. Lancet *359*, 1819–1827.

Bæk, K.T., Gründling, A., Mogensen, R.G., Thøgersen, L., Petersen, A., Paulander, W., and Frees, D. (2014). β-lactam resistance in methicillin-resistant *Staphylococcus aureus* USA300 is increased by inactivation of the ClpXP protease. Antimicrob. Agents Chemother. *58*, 4593–4603.

Bæk, K.T., Thøgersen, L., Mogensen, R.G., Mellergaard, M., Thomsen, L.E., Petersen, A., and Skov, S. (2015). Stepwise Decrease in Daptomycin Susceptibility in Clinical

Staphylococcus aureus Isolates Associated with an Initial Mutation in *rpoB* and a Compensatory Inactivation of the *clpX* Gene. Antimicrob. Agents Chemother. *59*, 6983–6991.

Bagnoli, F., Bertholet, S., and Grandi, G. (2012). Inferring Reasons for the Failure of *Staphylococcus aureus* Vaccines in Clinical Trials. Front. Cell. Infect. Microbiol. *2*, 2–5.

Banerjee, R., Gretes, M., Harlem, C., Basuino, L., and Chambers, H.F. (2010). A *mecA*-negative strain of methicillin-resistant *Staphylococcus aureus* with high-level β-lactam resistance contains mutations in three genes. Antimicrob. Agents Chemother. *54*, 4900–4902.

Bankevich, A., Nurk, S., Antipov, D., Gurevich, A.A., Dvorkin, M., Kulikov, A.S., Lesin, V.M., Nikolenko, S.I., Pham, S., Prjibelski, A.D., et al. (2012). SPAdes: A New Genome Assembly Algorithm and Its Applications to Single-Cell Sequencing. J. Comput. Biol. *19*, 455–477.

Baquero, F. (2001). Low-level antibacterial resistance: a gateway to clinical resistance. Drug Resist. Updat. *4*, 93–105.

Barbour, A., Schmidt, S., Rand, K.H., and Derendorf, H. (2009). Ceftobiprole: a novel cephalosporin with activity against Gram-positive and Gram-negative pathogens, including methicillin-resistant *Staphylococcus aureus* (MRSA). Int. J. Antimicrob. Agents *34*, 1–7.

Barna, C., and Williams, D.H. (1984). The structure and mode of action of glycopeptide antibiotics of the vancomycin group. Annu. Rev. Microbiol. *38*, 339–357.

Beck, W.D., Berger-Bachi, B., and Kayser, F.H. (1986). Additional DNA in methicillin-resistant *Staphylococcus aureus* and molecular cloning of mec-specific DNA. J. Bacteriol. *165*, 373–378.

Berger-Bächi, B., and Rohrer, S. (2002). Factors influencing methicillin resistance in staphylococci. Arch. Microbiol. *178*, 165–171.

Berger-Bächi, B., Barberis-Maino, L., Strässle, a, and Kayser, F.H. (1989). FemA, a host-mediated factor essential for methicillin resistance in *Staphylococcus aureus*: molecular cloning and characterization. Mol. Gen. Genet. *219*, 263–269.

Berger-Bächi, B., Strässle, a, Gustafson, J.E., and Kayser, F.H. (1992). Mapping and characterization of multiple chromosomal factors involved in methicillin resistance in *Staphylococcus aureus*. Antimicrob. Agents Chemother. *36*, 1367–1373.

Berger Bachi, B. (1983). Insertional inactivation of staphylococcal methicillin resistance by Tn551. J. Bacteriol. *154*, 479–487.

Berglund, C., Ito, T., Ikeda, M., Xiao, X.M., Söderquist, B., and Hiramatsu, K. (2008). Novel type of staphylococcal cassette chromosome mec in a methicillin-resistant *Staphylococcus aureus* strain isolated in Sweden. Antimicrob. Agents Chemother. *52*, 3512–3516.

Bi, E., and Lutkenhaus, J. (1991). FtsZ ring structure associated with division in *Escherichia coli*. Nature *354*, 161–164.

Bischoff, M., and Berger-Bachi, B. (2001). Teicoplanin stress-selected mutations increasing sigma(B) activity in *Staphylococcus aureus*. Antimicrob. Agents Chemother. *45*, 1714–1720.

Bischoff, M., Dunman, P., Kormanec, J., Macapagal, D., Murphy, E., Mounts, W., Berger-ba, B., and Projan, S. (2004). Microarray-Based Analysis of the *Staphylococcus aureus* SigB Regulon. J. Bacteriol. *186*, 4085–4099.

Den Blaauwen, T., De Pedro, M.A., Nguyen-Distèche, M., and Ayala, J.A. (2008).

Morphogenesis of rod-shaped sacculi. FEMS Microbiol. Rev. *32*, 321–344.

Bolger, A.M., Lohse, M., and Usadel, B. (2014). Trimmomatic: A flexible trimmer for Illumina sequence data. Bioinformatics *30*, 2114–2120.

Bondi, A., and Dietz, C. (1945). Penicillin Resistant Staphylococci. Am. J. Clin. Pathol. *61*, 55–58.

Bottomley, A.L. (2011). Identification and characterisation of the cell division machinery in *Staphylococcus aureus*.

Bottomley, A.L., Kabli, A.F., Hurd, A.F., Turner, R.D., Garcia-Lara, J., and Foster, S.J. (2014). *Staphylococcus aureus* DivIB is a peptidoglycan-binding protein that is required for a morphological checkpoint in cell division. Mol. Microbiol. *94*, 1041–1064.

Boucher, H.W., and Corey, G.R. (2008). Epidemiology of Methicillin-Resistant *Staphylococcus aureus*. Clin. Infect. Dis. *46*, S344–S349.

Boundy, S., Safo, M.K., Wang, L., Musayev, F.N., O'Farrell, H.C., Rife, J.P., and Archer, G.L. (2013). Characterization of the *Staphylococcus aureus* rRNA methyltransferase encoded by *orfx*, the gene containing the staphylococcal chromosome cassette mec (SCCmec) insertion site. J. Biol. Chem. *288*, 132–140.

Bowman, L., Zeden, M.S., Schuster, C.F., Kaever, V., and Gründling, A. (2016). New insights into the cyclic di-adenosine monophosphate (c-di-AMP) degradation pathway and the requirement of the cyclic dinucleotide for acid stress resistance in *Staphylococcus aureus*. J. Biol. Chem. *291*, 26970–26986.

Brekasis, D., and Paget, M.S.B. (2003). A novel sensor of NADH / NAD + redox poise in *Streptomyces coelicolor* A3(2). EMBO J. *22*, 4856–4865.

Brown, D.F., and Reynolds, P.E. (1980). Intrinsic resistance to beta-lactam antibiotics in *Staphylococcus aureus*. FEBS Lett. *122*, 275–278.

Brown, S., Xia, G., Luhachack, L.G., Campbell, J., Meredith, T.C., Chen, C., Winstel, V., Gekeler, C., Irazoqui, J.E., Peschel, A., et al. (2012). Methicillin resistance in *Staphylococcus aureus* requires glycosylated wall teichoic acids. Proc. Natl. Acad. Sci. *109*, 18909–18914.

Brückner, R. (1997). Gene replacement in *Staphylococcus carnosus* and *Staphylococcus xylosus*. FEMS Microbiol. Lett. *151*, 1–8.

Campbell, E.A., Korzheva, N., Mustaev, A., Murakami, K., Nair, S., Goldfarb, A., and Darst, S.A. (2001). Structural mechanism for rifampicin inhibition of bacterial RNA polymerase. Cell *104*, 901–912.

Campeotto, I., Zhang, Y., Mladenov, M.G., Freemont, P.S., and Gründling, A. (2015). Complex structure and biochemical characterization of the *Staphylococcus aureus* cyclic diadenylate monophosphate (c-di-AMP)-binding protein PstA, the founding member of a new signal transduction protein family. J. Biol. Chem. *290*, 2888–2901.

Cerca, N., Jefferson, K.K., Maira-Litrán, T., Pier, D.B., Kelly-Quintos, C., Goldmann, D.A., Azeredo, J., and Pier, G.B. (2007). Molecular basis for preferential protective efficacy of antibodies directed to the poorly acetylated form of staphylococcal poly-N-acetyl-β-(1-6)-glucosamine. Infect. Immun. *75*, 3406–3413.

Cha, J., Vakulenko, S.B., and Mobashery, S. (2007). Characterization of the β-lactam antibiotic sensor domain of the MecR1 signal sensor/transducer protein from methicillin-resistant *Staphylococcus aureus*. Biochemistry *46*, 7822–7831.

Chambers, H.F. (1997). Methicillin resistance in staphylococci: molecular and biochemical basis and clinical implications. Clin. Microbiol. Rev. *10*, 781–791.

Chambers, H.F., Archer, G., and Matsuhashi, M. (1989). Low-Level Methicillin Resistance in Strains of *Staphylococcus aureus*. Antimicrob. Agents Chemother. *33*, 424–428.

Chan, L.C., Gilbert, A., Basuino, L., Costa, M., Hamilton, S.M., Santos, R., Chambers, H.F., and Chatterjee, S. (2016). PBP4 Mediates High-Level Resistance to New-Generation Cephalosporins in *Staphylococcus aureus*. Antimicrob. Agents Chemother. *60*, 3934–3941.

Chang, S., Sievert, D., Hageman, J., Boulton, M., and Al, E. (2003). Infection with Vancomycin-Resistant *Staphylococcus aureus* Containing the *vanA* Resistance Gene. N. Engl. J. Med. *384*, 1342–1347.

Chasteen, T.G., Fuentes, D.E., Tantaleán, J.C., and Vásquez, C.C. (2009). Tellurite: History, oxidative stress, and molecular mechanisms of resistance: Review article. FEMS Microbiol. Rev. *33*, 820–832.

Chaudhuri, R.R., Allen, A.G., Owen, P.J., Shalom, G., Stone, K., Harrison, M., Burgis, T. a, Lockyer, M., Garcia-Lara, J., Foster, S.J., et al. (2009). Comprehensive identification of essential *Staphylococcus aureus* genes using Transposon-Mediated Differential Hybridisation (TMDH). BMC Genomics *10*, 291.

Choe, D., Szubin, R., Dahesh, S., Cho, S., Nizet, V., Palsson, B., and Cho, B.K. (2018). Genome-scale analysis of Methicillin-resistant *Staphylococcus aureus* USA300 reveals a tradeoff between pathogenesis and drug resistance. Sci. Rep. *8*, 1–13.

Choi, Y.W., Kotzin, B., Herron, L., Callahan, J., Marrack, P.C., and Kappler, J.W. (1989). Interaction of *Staphylococcus aureus* toxin “superantigens” with human T cells. Proc. Natl. Acad. Sci. U. S. A. *86*, 8941–8945.

Chu, V.H., Crosslin, D.R., Friedman, J.Y., Reed, S.D., Cabell, C.H., Griffiths, R.I., Masselink, L.E., Kaye, K.S., Corey, G.R., Reller, L.B., et al. (2005). *Staphylococcus aureus* bacteremia in patients with prosthetic devices: Costs and outcomes. Am. J. Med. *118*.

Chuang, Y.Y., and Huang, Y.C. (2013). Molecular epidemiology of community-associated meticillin-resistant *Staphylococcus aureus* in Asia. Lancet Infect. Dis. *13*, 698–708.

Clauditz, A., Resch, A., Wieland, K.P., Peschel, A., and Götz, F. (2006). Staphyloxanthin plays a role in the fitness of *Staphylococcus aureus* and its ability to cope with oxidative stress. Infect. Immun. *74*, 4950–4953.

Clements, M.O., and Foster, S.J. (1999). Stress resistance in *Staphylococcus aureus*. Trends Microbiol. *7*, 458–462.

Coleman, G., Garbutt, I.T., and Demnitz, U. (1983). Ability of a *Staphylococcus aureus* Isolate from a Chronic Osteomyelitic Lesion to Survive in the Absence of Air. Eur. J. Clin. Microbiol *2*, 595–597.

Commichau, F.M., Gibhardt, J., Halbedel, S., Gundlach, J., and Stülke, J. (2018). A Delicate Connection: C-di-AMP Affects Cell Integrity by Controlling Osmolyte Transport. Trends Microbiol. *26*, 175–185.

Cooper, E.L., García-Lara, J., and Foster, S.J. (2009). YsxC, an essential protein in *Staphylococcus aureus* crucial for ribosome assembly/stability. BMC Microbiol. *9*, 266.

Cordwell, S.J., Larsen, M.R., Cole, R.T., and Walsh, B.J. (2002). Comparative proteomics of *Staphylococcus aureus* and the response of methicillin- resistant and methicillin-sensitive strains to Triton X-100. Microbiology *148*, 2765–2781.

Corrigan, R.M., and Gründling, A. (2013). Cyclic di-AMP: another second messenger enters the fray. Nat. Rev. Microbiol. *11*, 513–524.

Corrigan, R.M., Abbott, J.C., Burhenne, H., Kaever, V., and Gründling, A. (2011). C-di-amp is a new second messenger in *Staphylococcus aureus* with a role in controlling cell size and envelope stress. PLoS Pathog. *7*.

Corrigan, R.M., Campeotto, I., Jeganathan, T., Roelofs, K.G., Lee, V.T., and Gründling, A. (2013). Systematic identification of conserved bacterial c-di-AMP receptor proteins. Proc Natl Acad Sci U S A *110*, 9084–9089.

Cosgrove, S., Sakoulas, G., Perencevich, E., Schwaber, M., Karchmer, A., and Carmeli, Y. (2003). Comparison of Mortality Associated with Methicillin Resistant and Methicillin Susceptible *Staphylococcus aureus* Bacteremia: A Meta-analysis. Clin. Infect. Dis. *36*, 53–59.

Couto, I., Melo-Cristino, J., Fernandes, M.L., Garcia, T., Serrano, N., Salgado, M.J., Torres-Pereira, A., Sanches, I.S., and De Lencastre, H. (1995). Unusually large number of methicillin-resistant *Staphylococcus aureus* clones in a Portuguese hospital. J. Clin. Microbiol. *33*, 2032–2035.

Couto, I., de LENCASTRE, H., SEVERINA, E., KLOOS, W., WEBSTER, J.A., HUBNER, R.J., SANCHES, I.S., and TOMASZ, A. (1996). Ubiquitous Presence of a *mecA* Homologue in Natural Isolates of Staphylococcus sciuri. Microb. Drug Resist. *2*, 377–391.

Couto, I., Pereira, S., Miragaia, M., Santos, I., Couto, I., Pereira, S., Miragaia, M., and Sanches, I.S. (2001). Identification of Clinical Staphylococcal Isolates from Humans by Internal Transcribed Spacer PCR Identification of Clinical Staphylococcal Isolates from Humans by Internal Transcribed Spacer PCR. J. Clin. Microbiol. *39*, 3099–3103.

Cuirolo, A., Plata, K., and Rosato, A.E. (2009). Development of homogeneous expression of resistance in methicillin-resistant *Staphylococcus aureus* clinical strains is functionally associated with a β-lactam-mediated SOS response. J. Antimicrob. Chemother. *64*, 37–45.

Daniel, R. a., Harry, E.J., and Errington, J. (2000). Role of penicillin-binding protein PBP2B in assembly and functioning of the division machinery of *Bacillus subtilis*. Mol. Microbiol. *35*, 299–311.

Dantes, R., Mu, Y., Belflower, R., Aragon, D., Dumyati, G., Harrison, L.H., Lessa, F.C., Lynfield, R., Nadle, J., Petit, S., et al. (2013). National burden of invasive methicillin-resistant *Staphylococcus aureus* infections, United States, 2011. JAMA Intern. Med. *173*, 1970–1979.

Davies, T.A., Page, M.G.P., Shang, W., Andrew, T., Kania, M., and Bush, K. (2007). Binding of Ceftobiprole and Comparators to the Penicillin-Binding Proteins of *Escherichia coli*, *Pseudomonas aeruginosa*, *Staphylococcus aureus*, and *Streptococcus pneumoniae*. Antimicrob. Agents Chemother. *51*, 2621–2624.

Delumeau, O., Lecointe, F., Muntel, J., Guillot, A., Guédon, E., Monnet, V., Hecker, M., Becher, D., Polard, P., and Noirot, P. (2011). The dynamic protein partnership of RNA polymerase in *Bacillus subtilis*. Proteomics *11*, 2992–3001.

Dengler, V., McCallum, N., Kiefer, P., Christen, P., Patrignani, A., Vorholt, J. a., Berger-Bächi, B., and Senn, M.M. (2013). Mutation in the C-di-AMP Cyclase *dacA* Affects Fitness and Resistance of Methicillin Resistant *Staphylococcus aureus*. PLoS One *8*, e73512.

Denome, Elf, P., Henderson, T., Nelson, D., and Young, K. (1999). Escherichia coli mutants lacking all possible combinations of eight penicillin binding proteins: …. J. Bacteriol. *181*, 3981–3993.

Deurenberg, R.H., Vink, C., Kalenic, S., Friedrich, A.W., Bruggeman, C.A., and Stobberingh,

E.E. (2007). The molecular evolution of methicillin-resistant *Staphylococcus aureus*. Clin. Microbiol. Infect. *13*, 222–235.

Diekema, D., Pfaller, M., Schmitz, F., and Al., E. (2001). Survey of Infections Due To Staphylococcus Species: Frequency of Occurrence and Antimicrobial Susceptibility of Isolates Collected in the United States, Canada, Latin America, Europe and the Western Pacific Region for the Sentry Antimicrobial Surveillance. Clin. Infect. Dis. *32*, 114–132.

Dordel, J., Kim, C., Chung, M., de la Gándara, M.P., Holden, M.T.J., Parkhill, J., de Lencastre, H., Bentley, S.D., and Tomasz, A. (2014). Novel determinants of antibiotic resistance: Identification of mutated Loci in Highly methicillin-resistant subpopulations of methicillin-resistant *Staphylococcus aureus*. MBio *5*, 1–9.

Dubrac, S., and Msadek, T. (2004). Identification of genes controlled by the essential YycG / YycF two-component system of *Staphylococcus aureus*. J. Bacteriol. *186*, 1175–1181.

Dunman, P., Murphy, E., and Haney, S. (2001). Transcription Profiling-Based Identification of *Staphylococcus aureus* Genes Regulated by the agr and/or sarA Loci. J. Bacteriol. *183*, 7341–7353.

Duthie, E.S., and Lorenz, L.L. (1952). Staphylococcal Coagulase: Mode of Action and Antigenicity. Microbiology *6*, 95–107.

Dyke, K.G.H., Jevons, M.P., and Parker, M.T. (1966). Penicillinase production and intrinsic resistance to penicillins in *Staphylococcus aureus*. Lancet 835–838.

Enany, S., Yoshida, Y., and Yamamoto, T. (2014). Exploring extra-cellular proteins in methicillin susceptible and methicillin resistant *Staphylococcus aureus* by liquid chromatography-tandem mass spectrometry. World J. Microbiol. Biotechnol. *30*, 1269–1283.

Enright, M.C., Day, N.P.J., Davies, C.E., Peacock, S.J., and Spratt, B.G. (2000). Multilocus Sequence Typing for Characterization of Methicillin-Resistant and Methicillin-Susceptible Clones of *Staphylococcus aureus* Multilocus Sequence Typing for Characterization of Methicillin- Resistant and Methicillin-Susceptible Clones of Staphyloco. J. Clin. Microbiol. *38*, 1008–1015.

Ero, R., Peil, L., Liiv, A., and Remme, J. (2008). Identification of pseudouridine methyltransferase in Escherichia coli. RNA *14*, 2223–2233.

Errington, J., Daniel, R. a, and Scheffers, D.-J. (2003). Cytokinesis in bacteria. Microbiol. Mol. Biol. Rev. *67*, 52–65, table of contents.

Farnham, P.J., and Platt, T. (1981). Rho-independent termination: Dyad symmetry in DNA causes RNA polymerase to pause during transcription in vitro. Nucleic Acids Res. *9*, 563–577.

Fedtke, I., Kamps, A., Krismer, B., and Götz, F. (2002). The nitrate reductase and nitrite reductase operons and the narT gene of *Staphylococcus carnosus* are positively controlled by the novel two-component system NreBC. J. Bacteriol. *184*, 6624–6634.

Ferreira, M.T., Manso, A.S., Gaspar, P., Pinho, M.G., and Neves, A.R. (2013). Effect of Oxygen on Glucose Metabolism: Utilization of Lactate in *Staphylococcus aureus* as Revealed by In Vivo NMR Studies. PLoS One *8*.

Ferrero, L., Cameron, B., and Crouzet, J. (1995). Analysis of gyrA and grlA Mutations in Stepwise-Selected Ciprofloxacin-Resistant Mutants of *Staphylococcus aureus*. Antimicrob. Agents Chemother. *39*, 1554–1558.

Fey, P.D., Endres, J.L., Yajjala, K., Widhelm, T.J., Boissy, R.J., Bose, J.L., and Bayles, W. (2013). A Genetic Resource for Rapid and Comprehensive Phenotype Screening of

Nonessential *Staphylococcus aureus* Genes. MBio *4*, e00537-12-e00537-12.

Figueiredo, T.A., Sobral, R.G., Ludovice, A.M., de Almeida, J.M.F., Bui, N.K., Vollmer, W., de Lencastre, H., and Tomasz, A. (2012). Identification of genetic determinants and enzymes involved with the amidation of glutamic acid residues in the peptidoglycan of *Staphylococcus aureus*. PLoS Pathog. *8*.

Finan, J.E., Rosato, A.E., Dickinson, T.M., Ko, D., and Archer, G.L. (2002). Conversion of oxacillin-resistant staphylococci from heterotypic to homotypic resistance expression. Antimicrob. Agents Chemother. *46*, 24–30.

Fishovitz, J., Rojas-altuve, A., Otero, L.H., Dawley, M., Carrasco-lo, C., Chang, M., Hermoso, J.A., and Mobashery, S. (2014). Disruption of Allosteric Response as an Unprecedented Mechanism of Resistance to Antibiotics. JACS 1–4.

Fournier, B., and Philpott, D. (2005). Recognition of *Staphylococcus aureus* by the Innate Immune System. Clin. Microbiol. Rev. *18*, 521–540.

Fuchs, S., Pané-Farré, J., Kohler, C., Hecker, M., and Engelmann, S. (2007). Anaerobic gene expression in *Staphylococcus aureus*. J. Bacteriol. *189*, 4275–4289.

Fuda, C., Suvorov, M., Vakulenko, S.B., and Mobashery, S. (2004). The basis for resistance to beta-lactam antibiotics by penicillin-binding protein 2a of methicillin-resistant *Staphylococcus aureus*. J. Biol. Chem. *279*, 40802–40806.

Fuda, C.C.S., Fisher, J.F., and Mobashery, S. (2005). ??-Lactam resistance in *Staphylococcus aureus*: The adaptive resistance of a plastic genome. Cell. Mol. Life Sci. *62*, 2617–2633.

Fujimura, T., and Murakami, K. (1997). Increase of methicillin resistance in *Staphylococcus aureus* caused by deletion of a gene whose product is homologous to lytic enzymes . Increase of Methicillin Resistance in *Staphylococcus aureus* Caused by Deletion of a Gene Whose Product Is Homologous to. J. Bacterology *179*, 6294–6301.

Gandara, M., Borges, V., Chung, M., Milheirico, C., Gomes, J., de Lencastre, H., and Tomasz, A. (2018). Genetic Determinants of High-Level Oxacillin Resistance in Methicillin-Resistant *Staphylococcus aureus*. Antimicrob. Agents Chemother. *62*, 1–7.

Gao, W., Cameron, D.R., Davies, J.K., Kostoulias, X., Stepnell, J., Tuck, K.L., Yeaman, M.R., Peleg, A.Y., Stinear, T.P., and Howden, B.P. (2013). The RpoB H148Y rifampicin resistance mutation and an active stringent response reduce virulence and increase resistance to innate immune responses in *Staphylococcus aureus*. J. Infect. Dis. *207*, 929–939.

García-Álvarez, L., Holden, M.T.G., Lindsay, H., Webb, C.R., Brown, D.F.J., Curran, M.D., Walpole, E., Brooks, K., Pickard, D.J., Teale, C., et al. (2011). Meticillin-resistant *Staphylococcus aureus* with a novel *mecA* homologue in human and bovine populations in the UK and Denmark: A descriptive study. Lancet Infect. Dis. *11*, 595–603.

García, A.B., Viñuela Prieto, J.M., Lopez González, L., and Candel, F.J. (2017). Correlation between resistance mechanisms in *Staphylococcus aureus* and cell wall and septum thickening. Infect. Drug Resist. *Volume 10*, 353–356.

Gardete, S., Wu, S.W., Gill, S., and Tomasz, A. (2006). Role of VraSR in antibiotic resistance and antibiotic-induced stress response in *Staphylococcus aureus*. Antimicrob. Agents Chemother. *50*, 3424–3434.

Gaupp, R., Ledala, N., and Somerville, G.A. (2012). Staphylococcal response to oxidative stress. Front. Cell. Infect. Microbiol. *2*, 1–19.

Gerberding, J.L., Miick, C., Liu, H.H., and Chambers, H.F. (1991). Comparison of conventional susceptibility tests with direct detection of penicillin-binding protein 2a in borderline oxacillin-resistant strains of *Staphylococcus aureus*. Antimicrob. Agents Chemother. *35*, 2574–2579.

Ghuysen, J.-M. (1968). Use of Bacteriolytic Enzymes in Determination of Wall Structure and Their Role in Cell Metabolism. Bacteriol. Rev. *32*, 425–464.

Giesbrecht, P., Kersten, T., Maidhof, H., and Wecke, J. (1998). Staphylococcal cell wall: morphogenesis and fatal variations in the presence of penicillin. Microbiol. Mol. Biol. Rev. *62*, 1371–1414.

Goffin, C., and Ghuysen, J.-M. (1998). Multimodular Penicillin-Binding Proteins: An Enigmatic Family of Orthologs and Paralogs. Microbiol. Mol. Biol. Rev. *62*, 1079–1093.

Goffin, C., and Ghuysen, J.-M. (2002). Biochemistry and comparative genomics of SxxK superfamily acyltransferases offer a clue to the mycobacterial paradox: presence of penicillin-susceptible target proteins versus lack of efficiency of penicillin as therapeutic agent. Microbiol. Mol. Biol. Rev. *66*, 702–38, table of contents.

Graves-Woodward, K., and Pratt, R.F. (1998). Reaction of soluble penicillin-binding protein 2a of methicillin-resistant *Staphylococcus aureus* with β-lactams and acyclic substrates : kinetics in homogeneous solution. Biochem. J *332*, 755–761.

Gregory, P.D., Lewis, R. a, Curnock, S.P., and Dyke, K.G. (1997). Studies of the repressor (BlaI) of beta-lactamase synthesis in *Staphylococcus aureus*. Mol. Microbiol. *24*, 1025–1037.

Greninger, A.L., Chatterjee, S.S., Chan, L.C., Hamilton, S.M., Chambers, H.F., and Chiu, C.Y. (2016). Whole-Genome Sequencing of Methicillin-Resistant *Staphylococcus aureus* Resistant to Fifth-Generation Cephalosporins Reveals Potential Non-*mecA* Mechanisms of Resistance. PLoS One *11*, e0149541.

Gries, C.M., Bose, J.L., Nuxoll, A.S., Fey, P.D., and Bayles, K.W. (2013). The Ktr potassium transport system in *Staphylococcus aureus* and its role in cell physiology, antimicrobial resistance and pathogenesis. Mol. Microbiol. *89*, 760–773.

Griffiths, J.M., and O'Neill, a. J. (2012). Loss of function of the GdpP protein leads to joint β-lactam/ glycopeptide tolerance in *Staphylococcus aureus*. Antimicrob. Agents Chemother. *56*, 579–581.

Groicher, K.H., Firek, B.A., Fujimoto, D.F., and Bayles, K.W. (2000). The *Staphylococcus aureus* lrgAB operon modulates murein hydrolase activity and penicillin tolerance. J. Bacteriol. *182*, 1794–1801.

Gundlach, J., Herzberg, C., Kaever, V., Gunka, K., Hoffmann, T., Weiß, M., Gibhardt, J., Thürmer, A., Hertel, D., Daniel, R., et al. (2017). Control of potassium homeostasis is an essential function of the second messenger cyclic di-AMP in *Bacillus subtilis*. Sci. Signal. *10*, 1–10.

Gustafson, J., Strassle, A., Hachler, H., Kayser, F.H., and Berger-Bachi, B. (1994). The *femC* locus of *Staphylococcus aureus* required for methicillin resistance includes the glutamine synthetase operon. J. Bacteriol. *176*, 1460–1467.

Gyan, S., Shiohira, Y., Sato, I., Takeuchi, M., and Sato, T. (2006). Regulatory loop between redox sensing of the NADH/NAD+ratio by Rex (YdiH) and oxidation of NADH by NADH dehydrogenase Ndh in *Bacillus subtilis*. J. Bacteriol. *188*, 7062–7071.

Hall, J., and Ji, Y. (2013). Advances in Microbiology Chapter one.

Hansen, H.G., and Henning, U. (1966). Regulation of pyruvate dehydrogenase activity in

Escherichia coli K12. Biochim. Biophys. Acta *122*, 355–358.

Hartman, B.J., and Tomasz, A. (1984). Low-Affinity Penicillin-Binding Protein Associated with beta-Lactam Resistance in *Staphylococcus aureus*. J. Bacteriol. *158*, 513–516.

Hartman, B.J., and Tomasz, A. (1986). Expression of methicillin resistance in heterogeneous strains of *Staphylococcus aureus*. Antimicrob. Agents Chemother. *29*, 85–92.

Haydon, D.J., Stokes, N.R., Ure, R., Galbraith, G., Bennett, J.M., Brown, D.R., Baker, P.J., Barynin, V. V, Rice, D.W., Sedelnikova, S.E., et al. (2008). An Inhibitor of FtsZ with Potent and Selective Anti-Staphylococcal Activity. Science (80). *321*, 1673–1676.

Heijenoort, J. van (2001). Formation of the glycan chains in the synthesis of bacterial peptidoglycan. Glycobiology *11*, 25R–36R.

Henderson, T.A., Young, K.D., Denome, S.A., and Elf, P.K. (1997). AmpC and AmpH, proteins related to the class C β-lactamases, bind penicillin and contribute to the normal morphology of *Escherichia coli*. J. Bacteriol. *179*, 6112–6121.

Henze, U., Sidow, T., Wecke, J., Labischinski, H., and Berger-Bachi, B. (1993). Influence of *femB* on methicillin resistance and peptidoglycan metabolism in *Staphylococcus aureus*. J. Bacteriol. *175*, 1612–1620.

Hiramatsu, K. (1995). Molecular Evolution of MRSA. Microbiol. Immunol. *39*, 531–543.

Hiramatsu, K., Asada, K., Suzuki, E., K. Okonogi, and Yokota., T. (1992). Molecular cloning and nucleotide sequence determination of the regulator region of *mecA* gene in methicillin-resistant *Staphylococcus aureus* (MRSA). FEBS Lett *298*, 133–6.

Hiramatsu, K., Hanaki, H., Ino, T., Yabuta, K., Oguri, T., and Tenover, F.C. (1997a). Methicillin-resistant *Staphylococcus aureus* clinical strain with reduced vancomycin susceptibility. J. Antimicrob. Chemother. *40*, 135–136.

Hiramatsu, K., Aritaka, N., Hanaki, H., Kawasaki, S., Hosoda, Y., Hori, S., Fukuchi, Y., and Kobayashi, I. (1997b). Dissemination in Japanese hospitals of strains of *Staphylococcus aureus* heterogeneously resistant to vancomycin. Lancet *350*, 1670–1673.

Hiramatsu, K., Katayama, Y., Yuzawa, H., and Ito, T. (2002). Molecular genetics of methicillin-resistant *Staphylococcus aureus*. Int. J. Med. Microbiol. *292*, 67–74.

Hiramatsu, K., Ito, T., Tsubakishita, S., Sasaki, T., Takeuchi, F., Morimoto, Y., Katayama, Y., Matsuo, M., Kuwahara-Arai, K., Hishinuma, T., et al. (2013). Genomic Basis for Methicillin Resistance in *Staphylococcus aureus*. Infect. Chemother. *45*, 117–136.

Horsburgh, M.J., Ingham, E., and Foster, S.J. (2001). In *Staphylococcus aureus*, Fur is an interactive regulator with PerR, contributes to virulence, and is necessary for oxidative stress resistance through positive regulation of catalase and iron homeostasis. J. Bacteriol. *183*, 468–475.

Horsburgh, M.J., Aish, J.L., White, I.J., Shaw, L., Lithgow, J.K., and Foster, S.J. (2002). σ^B Modulates Virulence Determinant Expression and Stress Resistance: Characterization of a Functional *rsbU* Strain Derived from *Staphylococcus aureus* 8325-4. J. Bacteriol. *184*, 5457–5467.

Howden, B.P., Davies, J.K., Johnson, P.D.R., Stinear, T.P., and Grayson, M.L. (2010). Reduced vancomycin susceptibility in *Staphylococcus aureus*, including vancomycin-intermediate and heterogeneous vancomycin-intermediate strains: Resistance mechanisms, laboratory detection, and clinical implications. Clin. Microbiol. Rev. *23*, 99–139.

Huber, J., Donald, R.G.K., Lee, S.H., Jarantow, L.W., Salvatore, M.J., Meng, X., Painter, R., Onishi, R.H., Occi, J., Dorso, K., et al. (2009). Chemical Genetic Identification of Peptidoglycan Inhibitors Potentiating Carbapenem Activity against Methicillin-Resistant *Staphylococcus aureus*. Chem. Biol. *16*, 837–848.

Hughes, B.J., and Mellows, G. (1978). Inhibition of Isoleucyl-Transfer Ribonucleic Acid Synthetase in *Escherichia coli* by Pseudomonic Acid. Biochem. J *176*, 305–318.

Hurlimann-Dalel, R., Ryffel, C., Kayser, F., and Berger-Bächi, B. (1992). Survey of the Methicillin Resistance-Associated Genes *mecA*, *mecRI-mecI*, and *femA-femB* in Clinical Isolates of Methicillin-Resistant *Staphylococcus aureus*. Antimicrob. Agents Chemother. *36*, 2617–2621.

Ito, T., Katayama, Y., and Hiramatsu, K. (1999). Cloning and Nucleotide Sequence Determination of the Entire mec DNA of Pre-Methicillin-Resistant *Staphylococcus aureus* N315. Antimicrob. Agents Chemother. *43*, 1449–1458.

Ito, T., Katayama, Y., Asada, K., Mori, N., Tsutsumimoto, K., Tiensasitorn, C., and Hiramatsu, K. (2001). Structural Comparison of Three Types of Staphylococcal Cassette Chromosome mec Integrated in the Chromosome in Methicillin-Resistant *Staphylococcus aureus* Structural. Antimicrob. Agents Chemother. *45*, 1323–1336.

Ito, T., Takeuchi, F., Okuma, K., Yuzawa, H., and Hiramatsu, K. (2004). Novel Type V Staphylococcal Cassette Chromosome *mec* Driven by a Novel Cassette Chromosome Recombinase, *ccrC*. Antimicrob. Agents Chemother. *48*, 2637–2651.

Ito, T., Hiramatsu, K., Oliveira, D.C., De Lencastre, H., Zhang, K., Westh, H., O'Brien, F., Giffard, P.M., Coleman, D., Tenover, F.C., et al. (2009). Classification of staphylococcal cassette chromosome mec (SCC*mec*): Guidelines for reporting novel SCC*mec* elements. Antimicrob. Agents Chemother. *53*, 4961–4967.

Jevons, M.P. (1961). "Celbenin" -resistant Staphylococci. Br. Med. J. *1*, 124–125.

Jevons, P., Coe, A., and Parker, M. (1963). Methicillin resistance in staphylococci. Lancet *1*, 904–907.

Jo, D.S., Montgomery, C.P., Yin, S., Boyle-Vavra, S., and Daum, R.S. (2011). Improved oxacillin treatment outcomes in experimental skin and lung infection by a methicillin-resistant *Staphylococcus aureus* isolate with a *vraSR* operon deletion. Antimicrob. Agents Chemother. *55*, 2818–2823.

Jolly, L., Wu, S., Heijenoort, J. Van, De Lencastre, H., Mengin-Lecreulx, D., and Tomasz, A. (1997). The *femR315* gene from *Staphylococcus aureus*, the interruption of which results in reduced methicillin resistance, encodes a phosphoglucosamine mutase. J. Bacteriol. *179*, 5321–5325.

de Jonge, B.L.M., and Tomasz, A. (1993). Abnormal Peptidoglycan Produced in a Methicillin-Resistant Strain of *Staphylococcus aureus* Grown in the Presence of Methicillin: Functional Role for Penicillin-Binding Protein 2A in Cell Wall Synthesis. Antimicrob. Agents Chemother. *37*, 342–346.

De Jonge, B.L.M., Chang, Y.S., Gage, D., and Tomasz, A. (1992). Peptidoglycan composition of a highly methicillin-resistant *Staphylococcus aureus* strain: The role of penicillin binding protein 2A. J. Biol. Chem. *267*, 11248–11254.

Jordan, S., Hutchings, M.I., and Mascher, T. (2008). Cell envelope stress response in Gram-positive bacteria. FEMS Microbiol. Rev. *32*, 107–146.

Jousselin, A., Kelley, W.L., Barras, C., Lew, D.P., and Renzoni, A. (2013). The *Staphylococcus aureus* Thiol/Oxidative stress global regulator Spx controls *trfA*, a gene

implicated in cell wall antibiotic resistance. Antimicrob. Agents Chemother. *57*, 3283–3292.

Jousselin, A., Manzano, C., Biette, A., Reed, P., Pinho, M.G., Rosato, A.E., Kelley, W.L., and Renzoni, A. (2016). The *Staphylococcus aureus* chaperone PrsA is a new auxiliary factor of oxacillin resistance affecting penicillin-binding protein 2A. Antimicrob. Agents Chemother. *60*, 1656–1666.

Kaatz, G.W., Seo, S.M., Barriere, S.L., Albrecht, L.M., and Rybak, M.J. (1989). Ciprofloxacin and Rifampin , Alone and in Combination , for Therapy of Experimental *Staphylococcus aureus* Endocarditis. Antimicrob. Agents Chemother. *33*, 1184–1187.

Kaatz, G.W., Seo, S.M., Dorman, N.J., and Lerner, S.A. (1990). Emergence of Teicoplanin Resistance during Therapy of *Staphylococcus aureus* Endocarditis. J. Infect. Dis. *162*, 103–108.

Kamps, A., Achebach, S., Fedtke, I., Unden, G., and Götz, F. (2004). Staphylococcal NreB: An O2-sensing histidine protein kinase with an O2-labile iron-sulphur cluster of the FNR type. Mol. Microbiol. *52*, 713–723.

Kang, J.Y., Olinares, P.D.B., Chen, J., Campbell, E.A., Mustaev, A., Chait, B.T., Gottesman, M.E., and Darst, S.A. (2017). Structural basis of transcription arrest by coliphage HK022 nun in an *Escherichia coli* rna polymerase elongation complex. Elife *6*, 1–20.

Katayama, Y., Ito, T., and Hiramatsu, K. (2000). A new class of genetic element, staphylococcus cassette chromosome *mec*, encodes methicillin resistance in *Staphylococcus aureus*. Antimicrob Agents Chemother *44*, 1549–1555.

Katayama, Y., Ito, T., and Hiramatsu, K. (2001). Genetic Organization of the Chromosome Region Surrounding *mecA* in Clinical Staphylococcal Strains: Role of IS431- Mediated *mecI* Deletion in Expression of Resistance in *mecA*-Carrying, Low-Level Methicillin- Resistant *Staphylococcus haemolyticus*. Antimicrob. Agents Chemother. *45*, 1955–1963.

Katayama, Y., Takeuchi, F., Ito, T., Ui-mizutani, Y., Kobayashi, I., and Hiramatsu, K. (2003a). Identification in Methicillin-Susceptible Staphylococcus hominis of an Active Primordial Mobile Genetic Element for the Staphylococcal Cassette Chromosome *mec* of Methicillin-Resistant *Staphylococcus aureus*. J. Bacterology *185*, 2711–2722.

Katayama, Y., Zhang, H.Z., Hong, D., and Chambers, H.F. (2003b). Jumping the barrier to beta-lactam resistance in *Staphylococcus aureus*. J Bacteriol *185*, 5465–5472.

Katayama, Y., Zhang, H.Z., and Chambers, H.F. (2004). PBP 2a Mutations Producing Very-High-Level Resistance to Beta-Lactams. Antimicrob. Agents Chemother. *48*, 453–459.

Katayama, Y., Katayama, Y., Robinson, D.A., Robinson, D.A., Enright, M.C., Enright, M.C., Chambers, H.F., and Chambers, H.F. (2005). Genetic Background Affects Stability of *mecA* in *Staphylococcus aureus*. Microbiology *43*, 2380–2383.

Katayama, Y., Murakami-Kuroda, H., Cui, L., and Hiramatsu, K. (2009). Selection of heterogeneous vancomycin-intermediate *Staphylococcus aureus* by imipenem. Antimicrob. Agents Chemother. *53*, 3190–3196.

Kato, Y., Suzuki, T., Ida, T., and Maebashi, K. (2010). Genetic changes associated with glycopeptide resistance in *Staphylococcus aureus*: predominance of amino acid substitutions in YvqF/VraSR. J. Antimicrob. Chemother. *65*, 37–45.

Keppler, A., Gendreizig, S., Gronemeyer, T., Pick, H., Vogel, H., and Johnsson, K. (2003). A general method for the covalent labeling of fusion proteins with small molecules in vivo. Nat. Biotechnol. *21*, 86–89.

Kim, C., Milheiriço, C., Gardete, S., Holmes, M.A., Holden, M.T.G., De Lencastre, H., and

Tomasz, A. (2012). Properties of a novel PBP2A protein homolog from *Staphylococcus aureus* strain LGA251 and its contribution to the β-lactam-resistant phenotype. J. Biol. Chem. *287*, 36854–36863.

Kim, C., Mwangi, M., Chung, M., Milheirco, C., De Lencastre, H., and Tomasz, A. (2013). The mechanism of heterogeneous beta-lactam resistance in MRSA: Key role of the stringent stress response. PLoS One *8*, 1–10.

Kinkel, T.L., Ramos-Montañez, S., Pando, J.M., Tadeo, D. V., Strom, E.N., Libby, S.J., and Fang, F.C. (2016). An essential role for bacterial nitric oxide synthase in *Staphylococcus aureus* electron transfer and colonization. Nat. Microbiol. *2*, 1–7.

Klein, E., Smith, D.L., and Laxminarayan, R. (2007). Hospitalizations and deaths caused by methicillin-resistant *Staphylococcus aureus*, United States, 1999-2005. Emerg. Infect. Dis. *13*, 1840–1846.

Komatsuzawa, H., Ohta, K., Fujiwara, T., Choi, G.H., Labischinski, H., and Sugai, M. (2001). Cloning and sequencing of the gene, *fmtC* , which affects oxacillin resistance in methicillin-resistant *Staphylococcus aureus*. FEMS Microbiol. Lett. *203*, 49–54.

Kondo, N., Kuwahara-arai, K., Kuroda-murakami, H., Tateda-suzuki, E., and Hiramatsu, K. (2001). Eagle-Type Methicillin Resistance: New Phenotype of High Methicillin Resistance under. Antimicrob Agents Chemother *45*, 815–824.

Korem, M., Gov, Y., Kiran, M.D., and Balaban, N. (2005). Transcriptional profiling of target of RNAIII-activating protein, a master regulator of staphylococcal virulence. Infect. Immun. *73*, 6220–6228.

Kornblum, J., Hartman, B.J., Novick, R.P., and Tomasz, A. (1986). Conversion of a homogeneously methicillin-resistant strain of *Staphylococcus aureus* to heterogeneous resistance by Tn551-mediated insertional inactivation. Eur. J. Clin. Microbiol. *5*, 714–718.

Kosowska-Shick, K., Mcghee, P.L., and Appelbaum, P.C. (2010). Affinity of Ceftaroline and Other β-Lactams for Penicillin-Binding Proteins from *Staphylococcus aureus* and *Streptococcus pneumoniae*. Antimicrob. Agents Chemother. *54*, 1670–1677.

Kreiswirth, B.N., Löfdahl, S., Betley, M.J., O'reilly, M., Schlievert, P.M., Bergdoll, M.S., and Novick, R.P. (1983). The toxic shock syndrome exotoxin structural gene is not detectably transmitted by a prophage. Nature *305*, 709–712.

Kuklin, N. a, Clark, D.J., Secore, S., Cook, J., Cope, L.D., Mcneely, T., Noble, L., Brown, M.J., Zorman, J.K., Wang, X.M., et al. (2006). A Novel *Staphylococcus aureus* Vaccine: Iron Surface Determinant B Induces Rapid Antibody Responses in Rhesus Macaques and Specific Increased Survival in a Murine *S. aureus* Sepsis Model. Infect. Immun. *74*, 2215–2223.

Kumar, A., Zarychanski, R., Pinto, R., and Al., E. (2009). Critically Ill Patients With 2009 Influenza A(H1N1) Infection in Canada. Jama *302*, 1872.

Kuroda, M., Kuroda, H., Oshima, T., Takeuchi, F., Mori, H., and Hiramatsu, K. (2003). Two-component system VraSR positively modulates the regulation of cell-wall biosynthesis pathway in *Staphylococcus aureus*. Mol. Microbiol. *49*, 807–821.

Kuwahara-Arai, K., Kondo, N., Hori, S., Tateda-Suzuki, E., and Hiramatsu, K. (1996). Suppression of methicillin resistance in a *mecA*-containing pre-methicillin-resistant *Staphylococcus aureus* strain is caused by the mecI-mediated repression of PBP 2' production. Antimicrob. Agents Chemother. *40*, 2680–2685.

Landick, R., Carey, J., and Yanofsky, C. (1985). Translation activates the paused transcription complex and restores transcription of the trp operon leader region. Proc Natl

Acad Sci U S A *82*, 4663–4667.

Larsson, J.T., Rogstam, A., and von Wachenfeldt, C. (2005). Coordinated patterns of cytochrome bd and lactate dehydrogenase expression in *Bacillus subtilis*. Microbiology *151*, 3323–3335.

Lee, C.R., Lee, J.H., Park, K.S., Jeong, B.C., and Lee, S.H. (2015). Quantitative proteomic view associated with resistance to clinically important antibiotics in Gram-positive bacteria: A systematic review. Front. Microbiol. *6*, 1–29.

Lee, S.H., Jarantow, L.W., Wang, H., Sillaots, S., Cheng, H., Meredith, T.C., Thompson, J., and Roemer, T. (2011). Antagonism of chemical genetic interaction networks resensitize MRSA to β-lactam antibiotics. Chem. Biol. *18*, 1379–1389.

de Lencastre, H., de Jonge, B.L., Matthews, P.R., and Tomasz, a (1994). Molecular aspects of methicillin resistance in *Staphylococcus aureus*. J Antimicrob Chemother *33*, 7–24.

De Lencastre, H., and Tomasz, A. (1994). Reassessment of the number of auxiliary genes essential for expression of high-level methicillin resistance in *Staphylococcus aureus*. Antimicrob. Agents Chemother. *38*, 2590–2598.

De Lencastre, H., Wu, S.W., Pinho, M.G., Ludovice, a M., Filipe, S., Gardete, S., Sobral, R., Gill, S., Chung, M., and Tomasz, A. (1999). Antibiotic resistance as a stress response: complete sequencing of a large number of chromosomal loci in *Staphylococcus aureus* strain COL that impact on the expression of resistance to methicillin. Microb. Drug Resist. *5*, 163–175.

De Lencastre, H., Chung, M., and Westh, H. (2000). Archaic strains of methicillin-resistant *Staphylococcus aureus*: Molecular and microbiological properties of isolates from the 1960s in Denmark. Microb. Drug Resist. Mech. Epidemiol. Dis. *6*, 1–10.

Leski, T. a, and Tomasz, A. (2005). Role of Penicillin-Binding Protein 2 (PBP2) in the Antibiotic Susceptibility and Cell Wall Cross-Linking of *Staphylococcus aureus*. J. Bacteriol. *2*, 1815–1824.

Lester, R., and Crane, F. (1959). The Natural Occurrence of Coenzyme Q and Related Compounds The Natural and Occurrence of Coenzyme Related Compounds *. J. Biol. Chem. *234*, 2169–2175.

Li, S., Skov, R.L., Han, X., Larsen, A.R., Larsen, J., Sørum, M., Wulf, M., Voss, A., Hiramatsu, K., and Ito, T. (2011). Novel types of staphylococcal cassette chromosome *mec* elements identified in clonal complex 398 methicillin-resistant *Staphylococcus aureus* strains. Antimicrob. Agents Chemother. *55*, 3046–3050.

Liang, X., Zheng, L., Landwehr, C., Lunsford, D., and Holmes, D. (2005). Global Regulation of Gene Expression by ArlRS , a Two-Component Signal Transduction Regulatory System of *Staphylococcus aureus*. J. Bacteriol. *187*, 5486–5492.

Lim, D., and Strynadka, N.C.J. (2002). Structural basis for the beta lactam resistance of PBP2a from methicillin-resistant *Staphylococcus aureus*. Nat. Struct. Biol. *9*, 870–876.

Lin, H., and Everse, J. (1987). The cytotoxic activity of hematoheme: evidence for two different mechanisms. Anal. Biochem. *161*, 323–331.

Lithgow, J.K., Hayhurst, E.J., Cohen, G., Foster, S.J., and Aharonowitz, Y. (2004). Role of a Cysteine Synthase in *Staphylococcus aureus* Role of a Cysteine Synthase in *Staphylococcus aureus*. Society *186*, 1579–1590.

Liu, J., Chen, D., Peters, B.M., Li, L., Li, B., Xu, Z., and Shirliff, M.E. (2016a). Staphylococcal chromosomal cassettes mec (SCCmec): A mobile genetic element in methicillin-resistant

Staphylococcus aureus. Microb. Pathog. *101*, 56–67.

Liu, Q., Yeo, W.S., and Bae, T. (2016b). The SaeRS two-component system of *Staphylococcus aureus*. Genes (Basel). *7*.

Liu, X., Pai, P.J., Zhang, W., Hu, Y., Dong, X., Qian, P.Y., Chen, D., and Lam, H. (2016c). Proteomic response of methicillin-resistant S. aureus to a synergistic antibacterial drug combination: A novel erythromycin derivative and oxacillin. Sci. Rep. *6*, 1–12.

Löffler, B., Hussain, M., Grundmeier, M., Brück, M., Holzinger, D., Varga, G., Roth, J., Kahl, B.C., Proctor, R.A., and Peters, G. (2010). *Staphylococcus aureus* panton-valentine leukocidin is a very potent cytotoxic factor for human neutrophils. PLoS Pathog. *6*.

Love, M.I., Huber, W., and Anders, S. (2014). Moderated estimation of fold change and dispersion for RNA-seq data with DESeq2. Genome Biol. *15*, 1–21.

Lovering, A.L., De Castro, L.H., Lim, D., and Strynadka, N.C.J. (2007). Structural insight into the transglycosylation step of bacterial cell-wall biosynthesis. Science (80-.). *315*, 1402–1405.

Lowy, F. (1998). *Staphylococcus aureus* infections. N. Engl. J. Med. *339*, 520–532.

Lowy, F. (2003). Antimicrobial resistance: the example of *Staphylococcus aureus*. J. Clin. Invest. *111*, 1265–1273.

Lund, V.A., Wacnik, K., Turner, R.D., Cotterell, B.E., Walther, C.G., Fenn, S.J., Grein, F., Wollman, A.J.M., Leake, M.C., Olivier, N., et al. (2018). Molecular coordination of *Staphylococcus aureus* cell division. Elife 1–31.

Luo, Y., and Helmann, J.D. (2012a). A σ^D-dependent antisense transcript modulates expression of the cyclic-di-AMP hydrolase GdpP in *Bacillus subtilis*. Microbiol. (United Kingdom) *158*, 2732–2741.

Luo, Y., and Helmann, J.D. (2012b). Analysis of the role of *Bacillus subtilis* σ^M in β-lactam resistance reveals an essential role for c-di-AMP in peptidoglycan homeostasis. Mol. Microbiol. *83*, 623–639.

Ma, X.X., Ito, T., Tiensasitorn, C., Chongtrakool, P., Boyle-vavra, S., Daum, R.S., Hiramatsu, K., and Jamklang, M. (2002). Novel Type of Staphylococcal Cassette Chromosome mec Identified in *Staphylococcus aureus* Strains Novel Type of Staphylococcal Cassette Chromosome mec Identified in Community-Acquired Methicillin-Resistant *Staphylococcus aureus* Strains. Antimicrob. Agents Chemother. *46*, 1147–1152.

Macheboeuf, P., Contreras-Martel, C., Job, V., Dideberg, O., and Dessen, A. (2006). Penicillin binding proteins: Key players in bacterial cell cycle and drug resistance processes. FEMS Microbiol. Rev. *30*, 673–691.

Mäder, U., Nicolas, P., Depke, M., Pané-Farré, J., Debarbouille, M., van der Kooi-Pol, M.M., Guérin, C., Dérozier, S., Hiron, A., Jarmer, H., et al. (2016). *Staphylococcus aureus* Transcriptome Architecture: From Laboratory to Infection-Mimicking Conditions. PLoS Genet. *12*, 1–32.

Maki, H., Yamaguchi, T., and Murakami, K. (1994). Cloning and characterization of a gene affecting the methicillin resistance level and the autolysis rate in *Staphylococcus aureus*. J. Bacteriol. *176*, 4993–5000.

Mani, N., Tobin, P., and Jayaswal, R.K. (1993). Isolation and characterization of autolysis-defective mutants of *Staphylococcus aureus* created by Tn917-*lacZ* mutagenesis. J. Bacteriol. *175*, 1493–1499.

Martinez, J.L., and Baquero, F. (2000). Mutation Frequencies and Antibiotic Resistance. Antimicrob. Agents Chemother. *44*, 1771–1777.

Mashruwala, A.A., and Boyd, J.M. (2017). The *Staphylococcus aureus* SrrAB regulatory system modulates hydrogen peroxide resistance factors, which imparts protection to aconitase during Aerobic growth. PLoS One *12*, 1–30.

Matsuo, M., Hishinuma, T., Katayama, Y., Cui, L., Kapi, M., and Hiramatsu, K. (2011). Mutation of RNA polymerase β subunit (rpoB) promotes hVISA-to-VISA phenotypic conversion of strain Mu3. Antimicrob. Agents Chemother. *55*, 4188–4195.

Matsuo, M., Cui, L., Kim, J., and Hiramatsu, K. (2013). Comprehensive identification of mutations responsible for heterogeneous vancomycin-intermediate *Staphylococcus aureus* (hVISA)-to-VISA conversion in laboratory-generated VISA strains derived from hVISA clinical strain Mu3. Antimicrob. Agents Chemother. *57*, 5843–5853.

Matsuo, M., Hishinuma, T., Katayama, Y., and Hiramatsu, K. (2015). A mutation of RNA polymerase β' subunit (RpoC) converts heterogeneously vancomycin-intermediate *Staphylococcus aureus* (hVISA) into “slow VISA.” Antimicrob. Agents Chemother. *59*, 4215–4225.

Matthews, P.R., and Stewart, P.R. (1984). Resistance heterogeneity in methicillin-resistant *Staphylococcus aureus*. FEMS Microbiol. Lett. *22*, 161–166.

Maughan, H., Galeano, B., and Nicholson, W.L. (2004). Mutations Conferring Rifampin Resistance on *Bacillus subtilis*: Global Effects on Growth, Competence, Sporulation, and Germination. J. Bacteriol. *186*, 2481–2486.

Mazmanian, S.K., and al., et (2003). Passage of ehme-iron across the envelope of *Staphylococcus aureus*. Science (80). *299*, 906–909.

McCallum, N., Berger-Bächi, B., and Senn, M.M. (2010). Regulation of antibiotic resistance in *Staphylococcus aureus*. Int. J. Med. Microbiol. *300*, 118–129.

McCallum, N., Stutzmann Meier, P., Heusser, R., and Berger-Bächi, B. (2011). Mutational analyses of open reading frames within the *vraSR* operon and their roles in the cell wall stress response of *Staphylococcus aureus*. Antimicrob. Agents Chemother. *55*, 1391–1402.

McGuinness, W.A., Malachowa, N., and DeLeo, F.R. (2017). Vancomycin resistance in *Staphylococcus aureus*. Yale J. Biol. Med. *90*, 269–281.

Mcpherson, D.C., and Popham, D.L. (2003). Peptidoglycan Synthesis in the Absence of Class A Penicillin-Binding Proteins in *Bacillus subtilis*. J. Bacteriol. *185*, 1423–1431.

McVicker, G., Prajsnar, T.K., Williams, A., Wagner, N.L., Boots, M., Renshaw, S. a., and Foster, S.J. (2014). Clonal Expansion during *Staphylococcus aureus* Infection Dynamics Reveals the Effect of Antibiotic Intervention. PLoS Pathog. *10*.

Meehl, M., Herbert, S., Go, F., and Cheung, A. (2007). Interaction of the GraRS Two-Component System with the VraFG ABC Transporter To Support Vancomycin-Intermediate Resistance in *Staphylococcus aureus*. Antimicrob. Agents Chemother. *51*, 2679–2689.

Memmi, G., Filipe, S.R., Pinho, M.G., Fu, Z., and Cheung, A. (2008). *Staphylococcus aureus* PBP4 is essential for β-lactam resistance in community-acquired methicillin-resistant strains. Antimicrob. Agents Chemother. *52*, 3955–3966.

Michalik, S., Bernhardt, J., Otto, A., Moche, M., Becher, D., Meyer, H., Lalk, M., Schurmann, C., Schlüter, R., Kock, H., et al. (2012). Life and Death of Proteins: A Case Study of Glucose-starved *Staphylococcus aureus*. Mol. Cell. Proteomics *11*, 558–570.

Misiura, A., Pigli, Y.Z., Boyle-Vavra, S., Daum, R.S., Boocock, M.R., and Rice, P.A. (2013). Roles of two large serine recombinases in mobilizing the methicillin-resistance cassette SCC*mec*. Mol. Microbiol. *88*, 1218–1229.

Morlot, C., Noirclerc-Savoye, M., Zapun, A., Dideberg, O., and Vernet, T. (2004). The D,D-carboxypeptidase PBP3 organizes the division process of *Streptococcus pneumoniae*. Mol. Microbiol. *51*, 1641–1648.

Morton, T.M., Johnston, J.L., Patterson, J.A.N., and Archer, G.L. (1995). Characterization of a Conjugative Staphylococcal Mupirocin Resistance Plasmid. Antimicrob. Agents Chemother. *39*, 1272–1280.

Moscoso, J.A., Schramke, H., Zhang, Y., Tosi, T., Dehbi, A., Jung, K., and Gründling, A. (2016). Binding of cyclic di-AMP to the *Staphylococcus aureus* sensor kinase KdpD occurs via the universal stress protein domain and downregulates the expression of the Kdp potassium transporter. J. Bacteriol. *198*, 98–110.

Müller, S., Wolf, A.J., Iliev, I.D., Berg, B.L., Underhill, D.M., and Liu, G.Y. (2015). Poorly cross-linked peptidoglycan in MRSA due to *mecA* induction activates the inflammasome and exacerbates immunopathology. Cell Host Microbe *18*, 604–612.

Murakami, K., Nomura, K., Doi, M., and Yoshida, T. (1987). Production of Low-Affinity Penicillin-Binding Protein by Low- and High-Resistance Groups of Methicillin-Resistant Staphylococcus. Antimicrob. Agents Chemother. *31*, 1307–1311.

Murray, B. (2000). Vancomycin-Resistant Enterococcal infections. N. Engl. J. Med.

Murray, T., Popham, D.L., and Setlow, P. (1996). Identification and characterization of *pbpC*, the gene encoding *Bacillus subtilis* penicillin-binding protein 3. J. Bacteriol. *178*, 6001–6005.

Mwangi, M.M., Wu, S.W., Zhou, Y., Sieradzki, K., de Lencastre, H., Richardson, P., Bruce, D., Rubin, E., Myers, E., Siggia, E.D., et al. (2007). Tracking the in vivo evolution of multidrug resistance in *Staphylococcus aureus* by whole-genome sequencing. Proc. Natl. Acad. Sci. *104*, 9451–9456.

Mwangi, M.M., Kim, C., Chung, M., Tsai, J., Vijayadamodar, G., Benitez, M., Jarvie, T.P., Du, L., and Tomasz, A. (2013). Whole-genome sequencing reveals a link between β-lactam resistance and synthetases of the alarmone (p)ppGpp in *Staphylococcus aureus*. Microb. Drug Resist. *19*, 153–159.

Nakano, S., Küster-Schöck, E., Grossman, A.D., and Zuber, P. (2003a). Spx-dependent global transcriptional control is induced by thiol-specific oxidative stress in *Bacillus subtilis*. Proc. Natl. Acad. Sci. U. S. A. *100*, 13603–13608.

Nakano, S., Nakano, M.M., Zhang, Y., Leelakriangsak, M., and Zuber, P. (2003b). A regulatory protein that interferes with activator-stimulated transcription in bacteria. Proc. Natl. Acad. Sci. U. S. A. *100*, 4233–4238.

Nakano, S., Erwin, K.N., Ralle, M., and Zuber, P. (2005). Redox-sensitive transcriptional control by a thiol/disulphide switch in the global regulator, Spx. Mol. Microbiol. *55*, 498–510.

Nakao, A., Imai, S. ichiro, and Takano, T. (2000). Transposon-mediated insertional mutagenesis of the D-alanyl-lipoteichoic acid (dlt) operon raises methicillin resistance in *Staphylococcus aureus*. Res. Microbiol. *151*, 823–829.

Ng, E., Trucksis, M., and Hooper, D. (1996). Quinolone Resistance Mutations in Topoisomerase IV : Relationship to the flqA Locus and Genetic Evidence that Topoisomerase IV Is the Primary Target and DNA Gyrase Is the Secondary Target of Fluoroquinolones in *Staphylococcus aureus*. Antimicrob. Agents Chemother. *40*, 1881–1888.

Niemeyer, D.M., Pucci, M.J., Thanassi, J. a., Sharma, V.K., and Archer, G.L. (1996). Role of *mecA* transcriptional regulation in the phenotypic expression of methicillin resistance in *Staphylococcus aureus*. J. Bacteriol. *178*, 5464–5471.

Noto, M.J., Kreiswirth, B.N., Monk, A.B., and Archer, G.L. (2008). Gene acquisition at the insertion site for SCC*mec*, the genomic island conferring methicillin resistance in *Staphylococcus aureus*. J. Bacteriol. *190*, 1276–1283.

Nudler, E. (2009). RNA Polymerase Active Center: The Molecular Engine of Transcription. Annu. Rev. Biochem. *78*, 335–361.

Núñez, M.F., Aguilar, J., Baldoma, L., Kwon, O., Wilson, T.H., and Lin, E.C.C. (2002). Transport of L-lactate, D-lactate, and glycolate by the LldP and GlcA membrane carriers of Escherichia coli. Biochem. Biophys. Res. Commun. *290*, 824–829.

O'Neill, A.J. (2010). *Staphylococcus aureus* SH1000 and 8325-4: comparative genome sequences of key laboratory strains in staphylococcal research. Lett. Appl. Microbiol. *51*, 358–361.

O'Neill, J. (2016). Tackling Drug-Resistant Infections Globally: Final Report and Recommendations the Review on Antimicrobial Resistance.

O'Neill, A.J., Huovinen, T., Fishwick, C.W.G., and Chopra, I. (2006). Molecular Genetic and Structural Modeling Studies of *Staphylococcus aureus* RNA Polymerase and the Fitness of Rifampin Resistance Genotypes in Relation to Clinical Prevalence. Antimicrob. Agents Chemother. *50*, 298–309.

Oliveira, D.C., and de Lencastre, H. (2011). Methicillin-resistance in *Staphylococcus aureus* is not affected by the overexpression in trans of the *mecA* gene repressor: A surprising observation. PLoS One *6*.

Oliveira, D.C., Tomasz, A., and de Lencastre, H. (2001). The Evolution of Pandemic Clones of Methicillin-Resistant *Staphylococcus aureus* : Identification of Two Ancestral Genetic Backgrounds and the Associated *mec* Elements. Microb. Drug Resist. *7*, 349–361.

Oliveira, D.C., Milheiriço, C., and De Lencastre, H. (2006). Redefining a structural variant of staphylococcal cassette Chromosome mec, SCC*mec* type VI. Antimicrob. Agents Chemother. *50*, 3457–3459.

Ornelas-Soares, A., De Lencastre, H., De Jonge, B.L.M., and Tomasz, A. (1994). Reduced methicillin resistance in a new *Staphylococcus aureus* transposon mutant that incorporates muramyl dipeptides into the cell wall peptidoglycan. J. Biol. Chem. *269*, 27246–27250.

Otero, L.H., Rojas-Altuve, A., Llarrull, L.I., Carrasco-Lopez, C., Kumarasiri, M., Lastochkin, E., Fishovitz, J., Dawley, M., Hesek, D., Lee, M., et al. (2013). How allosteric control of *Staphylococcus aureus* penicillin binding protein 2a enables methicillin resistance and physiological function. Proc. Natl. Acad. Sci. *110*, 16808–16813.

Pagels, M., Fuchs, S., Pané-Farré, J., Kohler, C., Menschner, L., Hecker, M., McNamarra, P.J., Bauer, M.C., Von Wachenfeldt, C., Liebeke, M., et al. (2010). Redox sensing by a Rex-family repressor is involved in the regulation of anaerobic gene expression in *Staphylococcus aureus*. Mol. Microbiol. *76*, 1142–1161.

Pamp, S.J., Frees, D., Engelmann, S., Hecker, M., and Ingmer, H. (2006). Spx is a global effector impacting stress tolerance and biofilm formation in *Staphylococcus aureus*. J. Bacteriol. *188*, 4861–4870.

Pan, T., Artsimovitch, I., Fang, X.W., Landick, R., and Sosnick, T.R. (1999). Folding of a large ribozyme during transcription and the effect of the elongation factor NusA. Proc. Natl. Acad. Sci. U. S. A. *96*, 9545–9550.

Panlilio, A.L., Culver, D.H., Gaynes, R.P., Banerjee, S., Henderson, T.S., Tolson, J.S., and Martone, W.J. (1992). Methicillin-resistant *Staphylococcus aureus* in U.S. hospitals, 1975-1991. Infect. Control Hosp. Epidemiol. *13*, 582–586.

Park, M.K., Myers, R.A., and Marzella, L. (1992). Oxygen tensions and infections: modulation of microbial growth, activity of antimicrobial agents, and immunologic responses. Clin. Infect. Dis. *14*, 720–740.

Payne, D.J., Gwynn, M.N., Holmes, D.J., and Pompliano, D.L. (2007). Drugs for bad bugs: confronting the challenges of antibacterial discovery. Nat. Rev. Drug Discov. *6*, 29–40.

Peacock, S.J., and Paterson, G.K. (2015). Mechanisms of Methicillin Resistance in *Staphylococcus aureus*. Annu. Rev. Biochem. *84*, 577–601.

Pereira, S.F.F., Henriques, a. O., Pinho, M.G., De Lencastre, H., and Tomasz, a. (2007). Role of PBP1 in cell division of *Staphylococcus aureus*. J. Bacteriol. *189*, 3525–3531.

Pereira, S.F.F., Henriques, A.O., Pinho, M.G., De Lencastre, H., and Tomasz, A. (2009). Evidence for a dual role of PBP1 in the cell division and cell separation of *Staphylococcus aureus*. Mol. Microbiol. *72*, 895–904.

Peschel, A., Jack, R.W., Otto, M., Collins, L.V., Staubitz, P., Nicholson, G., Kalbacher, H., Nieuwenhuizen, W.F., Jung, G., Tarkowski, A., et al. (2001). *Staphylococcus aureus* Resistance to Human Defensins and Evasion of Neutrophil Killing via the Novel Virulence Factor Mprf Is Based on Modification of Membrane Lipids with l-Lysine. J. Exp. Med. *193*, 1067–1076.

Pinho, M.G., and Errington, J. (2003). Dispersed mode of *Staphylococcus aureus* cell wall synthesis in the absence of the division machinery. Mol. Microbiol. *50*, 871–881.

Pinho, M.G., and Errington, J. (2005). Recruitment of penicillin-binding protein PBP2 to the division site of *Staphylococcus aureus* is dependent on its transpeptidation substrates. Mol. Microbiol. *55*, 799–807.

Pinho, M.G., de Lencastre, H., and Tomasz, a (1998). Transcriptional analysis of the *Staphylococcus aureus* penicillin binding protein 2 gene. J. Bacteriol. *180*, 6077–6081.

Pinho, M.G., De Lencastre, H., and Tomasz, A. (2000). Cloning, characterization, and inactivation of the gene *pbpC*, encoding penicillin-binding protein 3 of *Staphylococcus aureus*. J. Bacteriol. *182*, 1074–1079.

Pinho, M.G., Filipe, S.R., De Lencastre, H., and Tomasz, a. (2001a). Complementation of the essential peptidoglycan transpeptidase function of penicillin-binding protein 2 (PBP2) by the drug resistance protein PBP2A in *Staphylococcus aureus*. J. Bacteriol. *183*, 6525–6531.

Pinho, M.G., de Lencastre, H., and Tomasz, a (2001b). An acquired and a native penicillin-binding protein cooperate in building the cell wall of drug-resistant staphylococci. Proc. Natl. Acad. Sci. U. S. A. *98*, 10886–10891.

Pinho, M.G., Kjos, M., and Veening, J.-W. (2013). How to get (a)round: mechanisms controlling growth and division of coccoid bacteria. Nat. Rev. Microbiol. *11*, 601–614.

Plata, K.B., Rosato, R.R., and Rosato, A.E. (2011). Fate of mutation rate depends on agr locus expression during oxacillin-mediated heterogeneous-homogeneous selection in methicillin-resistant *Staphylococcus aureus* clinical strains. Antimicrob. Agents Chemother. *55*, 3176–3186.

Pohl, K., Francois, P., Stenz, L., Schlink, F., Geiger, T., Herbert, S., Goerke, C., Schrenzel, J., and Wolz, C. (2009). CodY in *Staphylococcus aureus*: A regulatory link between metabolism and virulence gene expression. J. Bacteriol. *191*, 2953–2963.

Pommié, C., Levadoux, S., Sabatier, R., Lefranc, G., and Lefranc, M.P. (2004). IMGT standardized criteria for statistical analysis of immunoglobulin V-Region amino acid properties. J. Mol. Recognit. *17*, 17–32.

Popham, D.L., Gilmore, M.E., Setlow, P., and Documentacion, S.D.E. (1999). Roles of Low-Molecular-Weight Penicillin-Binding Proteins in *Bacillus subtilis* Spore Peptidoglycan Synthesis and Spore Properties. J. Bacteriol. *181*, 126–132.

Pöther, D.C., Liebeke, M., Hochgräfe, F., Antelmann, H., Becher, D., Lalk, M., Lindequist, U., Borovok, I., Cohen, G., Aharonowitz, Y., et al. (2009). Diamide triggers mainly S thiolations in the cytoplasmic proteomes of *Bacillus subtilis* and *Staphylococcus aureus*. J. Bacteriol. *191*, 7520–7530.

Poupel, O., Proux, C., Jagla, B., Msadek, T., and Dubrac, S. (2018). SpdC, a novel virulence factor, controls histidine kinase activity in *Staphylococcus aureus*. PLoS Pathog. *14*, 1–32.

Pozzi, C., Waters, E.M., Rudkin, J.K., Schaeffer, C.R., Lohan, A.J., Tong, P., Loftus, B.J., Pier, G.B., Fey, P.D., Massey, R.C., et al. (2012). Methicillin resistance alters the biofilm phenotype and attenuates virulence in *Staphylococcus aureus* device-associated infections. PLoS Pathog. *8*.

Pucci, M.J., and Dougherty, T.J. (2002). Direct quantitation of the numbers of individual penicillin-binding proteins per cell in *Staphylococcus aureus*. J. Bacteriol. *184*, 588–591.

Qin, N., Tan, X., Jiao, Y., Liu, L., Zhao, W., Yang, S., and Jia, A. (2015). RNA-Seq-based transcriptome analysis of methicillin-resistant *Staphylococcus aureus* biofilm inhibition by ursolic acid and resveratrol. Sci. Rep. *4*, 5467.

Rammelkamp, C.H., and Maxon, T. (1942). Resistance of *Staphylococcus aureus* to the Action of Penicillin. Exp. Biol. Med. *51*, 386–389.

Rao, F., See, R.Y., Zhang, D., Toh, D.C., Ji, Q., and Liang, Z.X. (2010). YybT is a signaling protein that contains a cyclic dinucleotide phosphodiesterase domain and a GGDEF domain with ATPase activity. J. Biol. Chem. *285*, 473–482.

Reynolds, P.E. (1989). Structure, biochemistry and mechanism of action of glycopeptide antibiotics. Eur. J. Clin. Microbiol. Infect. Dis. *8*, 943–950.

Reynolds, P.E., and Brown, D.F. (1985). Penicillin-binding proteins of beta-lactam-resistant strains of *Staphylococcus aureus*. Effect of growth conditions. FEBS Lett. *192*, 28–32.

Rice, L.B. (2006). Antimicrobial resistance in gram-positive bacteria. Am. J. Infect. Control *34*, 11–19.

Rice, K.C., and Bayles, K.W. (2008). Molecular Control of Bacterial Death and Lysis. Microbiol. Mol. Biol. Rev. *72*, 85–109.

Rice, K.C., Firek, B. a, Nelson, J.B., Patton, T.G., Bayles, K.W., and Yang, S. (2003). The *Staphylococcus aureus cidAB* Operon : Evaluation of Its Role in Regulation of Murein Hydrolase Activity and Penicillin Tolerance. *185*, 2635–2643.

Richards, M.J., Edwards, J.R., and Culver, D.H. (1999). Nosocomial Infections in Pediatric Intensive Care Units in the United States. Pediatrics *103*.

Rochat, T., Nicolas, P., Delumeau, O., Rabatinová, A., Korelusová, J., Leduc, A., Bessières, P., Dervyn, E., Krásný, L., and Noirot, P. (2012). Genome-wide identification of genes directly regulated by the pleiotropic transcription factor Spx in *Bacillus subtilis*. Nucleic Acids Res. *40*, 9571–9583.

Roemer, T., Schneider, T., and Pinho, M.G. (2013). Auxiliary factors: A chink in the armor of MRSA resistance to β-lactam antibiotics. Curr. Opin. Microbiol. *16*, 538–548.

Rohrer, S., Ehlert, K., Tschierske, M., Labischinski, H., and Berger-Bächi, B. (1999). The essential *Staphylococcus aureus* gene fmhB is involved in the first step of peptidoglycan pentaglycine interpeptide formation. Proc. Natl. Acad. Sci. *96*, 9351–9356.

Rohrer, S., Maki, H., and Berger-Bächi, B. (2003). What makes resistance to methicillin heterogeneous? J. Med. Microbiol. *52*, 605–607.

Rojas-Tapias, D., and Helmann, J. (2018). Induction of the Spx regulon by cell wall stress reveals novel regulatory mechanisms in *Bacillus subtilis*. Mol. Micro. 107(5), 659-674.

Rolo, J., Worning, P., Nielsen, J., Bowden, R., Bouchami, O., Damborg, P., Guardabassi, L., Perreten, V., Tomasz, A., Westh, H., et al. (2017). Evolutionary Origin of the Staphylococcal Cassette Chromosome mec (SCCmec). Antimicrob. Agents Chemother. *61*, 1–16.

Rosato, A.E., Kreiswirth, B.N., Craig, W. a, Eisner, W., Climo, M.W., and Archer, G.L. (2003). *mecA* - blaZ Corepressors in Clinical *Staphylococcus aureus* Isolates. Antimicrob. Agents Chemother. *47*, 1460–1463.

Rudkin, J.K., Edwards, A.M., Bowden, M.G., Brown, E.L., Pozzi, C., Waters, E.M., Chan, W.C., Williams, P., O'Gara, J.P., and Massey, R.C. (2012). Methicillin resistance reduces the virulence of healthcare-associated methicillin-resistant *Staphylococcus aureus* by interfering with the agr quorum sensing system. J. Infect. Dis. *205*, 798–806.

Ryffel, C., T, W., Reynolds, P.E., Barberis-maino, L., Kayser, F.H., Berger-bgehi, B., February, T. a B., and Hara, O. (1990). Sequence comparison of *mecA* genes isolated from methicillin-resistant Staphylococcus ureus and Staphylococcus epidermidis *. Gene *94*, 137–138.

Ryffel, C., Kayser, F.H., and Berger-Bachi, B. (1992). Correlation between regulation of *mecA* transcription and expression of methicillin resistance in staphylococci. Antimicrob. Agents Chemother. *36*, 25–31.

Ryffel, C., Strassle, a., Kayser, F.H., and Berger-Bachi, B. (1994). Mechanisms of heteroresistance in methicillin-resistant *Staphylococcus aureus*. Antimicrob. Agents Chemother. *38*, 724–728.

Sabath, L.D. (1982). Mechanisms of resistance to beta-lactam antibiotics in strains of *Staphylococcus aureus*. Ann.Intern.Med. *97*, 339–344.

Sabath, L., and Wallace, S. (1971). Factors influencing methicillin resistance in staphylococci. Ann. N. Y. Acad. Sci. *182*, 258–266.

Saito, M., Katayama, Y., Hishinuma, T., Iwamoto, A., Aiba, Y., Kuwahara-Arai, K., Cui, L., Matsuo, M., Aritaka, N., and Hiramatsua, K. (2014). "Slow VISA," a novel phenotype of vancomycin resistance, found in vitro in heterogeneous vancomycin-intermediate *Staphylococcus aureus* strain Mu3. Antimicrob. Agents Chemother. *58*, 5024–5035.

Saravolatz, L.D., Stein, G.E., and Johnson, L.B. (2011). Ceftaroline : A Novel Cephalosporin with Activity against Methicillin-resistant *Staphylococcus aureus*. Rev. Anti-Infective Agents *52*.

Sauvage, E., Duez, C., Herman, R., Kerff, F., Petrella, S., Anderson, J.W., Adediran, S. a., Pratt, R.F., Frère, J.M., and Charlier, P. (2007). Crystal Structure of the *Bacillus subtilis* Penicillin-binding Protein 4a, and its Complex with a Peptidoglycan Mimetic Peptide. J. Mol. Biol. *371*, 528–539.

Sauvage, E., Kerff, F., Terrak, M., Ayala, J. a., and Charlier, P. (2008). The penicillin-binding

proteins: Structure and role in peptidoglycan biosynthesis. FEMS Microbiol. Rev. *32*, 234–258.

Sawers, R.G. (2005). Formate and its role in hydrogen production in Escherichia coli. Biochem Soc Trans *33*, 42–46.

Scheffers, D.J. (2005). Dynamic localization of penicillin-binding proteins during spore development in *Bacillus subtilis*. Microbiology *151*, 999–1012.

Scheffers, D., and Errington, J. (2004). PBP1 Is a Component of the *Bacillus subtilis* Cell Division Machinery. J. Bacteriol. *186*, 5153–5156.

Scheffers, D., and Pinho, M.G. (2005). Bacterial Cell Wall Synthesis : New Insights from Localization Studies. Microbiol. Mol. Biol. Rev. *69*, 585–607.

Schiffer, G., and Höltje, J.V. (1999). Cloning and characterization of PBP 1C, a third member of the multimodular class A penicillin-binding proteins of *Escherichia coli*. J. Biol. Chem. *274*, 32031–32039.

Schlag, S., Fuchs, S., Nerz, C., Gaupp, R., Engelmann, S., Liebeke, M., Lalk, M., Hecker, M., and Götz, F. (2008). Characterization of the oxygen-responsive NreABC regulon of *Staphylococcus aureus*. J. Bacteriol. *190*, 7847–7858.

Schnellmann, C., Gerber, V., Rossano, A., Jaquier, V., Panchaud, Y., Doherr, M.G., Thomann, A., Straub, R., and Perreten, V. (2006). Presence of new *mecA* and *mph*(C) variants conferring antibiotic resistance in Staphylococcus spp. isolated from the skin of horses before and after clinic admission. J. Clin. Microbiol. *44*, 4444–4454.

Schuster, C.F., Bellows, L.E., Tosi, T., Campeotto, I., Corrigan, R.M., Freemont, P., and Gründling, A. (2016). The second messenger c-di-AMP inhibits the osmolyte uptake system OpuC in *Staphylococcus aureus*. Sci. Signal. *9*, 1–14.

Seemann, T. (2014). Prokka: Rapid prokaryotic genome annotation. Bioinformatics *30*, 2068–2069.

Serruto, D., Rappuoli, R., Scarselli, M., Gros, P., and Van Strijp, J.A.G. (2010). Molecular mechanisms of complement evasion: Learning from staphylococci and meningococci. Nat. Rev. Microbiol. *8*, 393–399.

Shafer, W.M., and Iandolo, J.J. (1979). Genetics of staphylococcal enterotoxin B in methicillin-resistant isolates of *Staphylococcus aureus*. Infect.Immun. *25*, 902–911.

Sharff, K.A., Richards, E.P., and Townes, J.M. (2013). Clinical management of septic arthritis. Curr. Rheumatol. Rep. *15*.

Shinefield, H., Black, S., Fattom, A., Horwith, G., and Al, E. (2002). Use of a *Staphylococcus aureus* conjugate vaccine in patients receiving hemodialysis H. N. Engl. J. Med. *346*, 491–496.

Sickmier, E.A., Brekasis, D., Paranawithana, S., Bonanno, J.B., Paget, M.S.B., Burley, S.K., and Kielkopf, C.L. (2005). X-ray structure of a Rex-family repressor/NADH complex insights into the mechanism of redox sensing. Structure *13*, 43–54.

Sieradzki, K., Chung, M., and Tomasz, A. (2008). Role of a Sodium-Dependent Symporter Homologue in the Thermosensitivity of β-Lactam Antibiotic Resistance and Cell Wall Composition in *Staphylococcus aureus*. Antimicrob. Agents Chemother. *52*, 505–512.

Singh, V.K., Jayaswal, R.K., and Wilkinson, B.J. (2001). Cell wall-active antibiobitic induced proteins of *Staphylococcus aureus* identified using a proteomic approach. FEMS

Microbiol.Lett. *199*, 79–84.

Sjöström, J.E., Löfdahl, S., and Philipson, L. (1975). Transformation reveals a chromosomal locus of the gene (s) for methicillin resistance in *Staphylococcus aureus*. J. Bacteriol. *123*, 905–915.

Somerville, G.A., and Proctor, R.A. (2009). At the Crossroads of Bacterial Metabolism and Virulence Factor Synthesis in Staphylococci. Microbiol. Mol. Biol. Rev. *73*, 233–248.

Stacklies, W., Redestig, H., Scholz, M., Walther, D., and Selbig, J. (2007). pcaMethods - A bioconductor package providing PCA methods for incomplete data. Bioinformatics *23*, 1164–1167.

Stapleton, P.D., and Taylor, P.W. (2007). Methicillin resistance in *Staphylococcus aureus* : mechanisms and modulation. Sci Prog *85*, 1–14.

Steele, V.R., Bottomley, A.L., Garcia-Lara, J., Kasturiarachchi, J., and Foster, S.J. (2011). Multiple essential roles for EzrA in cell division of *Staphylococcus aureus*. Mol. Microbiol. *80*, 542–555.

Stewart, G.C., and Rosenblum, E.D. (1980). Genetic behavior of the methicillin resistance determinant in *Staphylococcus aureus*. J. Bacteriol. *144*, 1200–1202.

Stojanov, M., Moreillon, P., and Sakwinska, O. (2015). Excision of staphylococcal cassette chromosome mec in methicillin-resistant *Staphylococcus aureus* assessed by quantitative PCR. BMC Res. Notes *8*, 828.

Strandén, A.M., Ehlert, K., Labischinski, H., and Berger-Bächi, B. (1997). Cell wall monoglycine cross-bridges and methicillin hypersusceptibility in a *femAB* null mutant of methicillin-resistant *Staphylococcus aureus*. J. Bacteriol. *179*, 9–16.

Stranger-Jones, Y.K., Bae, T., and Schneewind, O. (2006). Vaccine assembly from surface proteins of *Staphylococcus aureus*. Proc Natl Acad Sci USA *103*, 16942–16947.

Strasters, K.C., and Winkler, K.C. (1963). Carbohydrate Metabolism of *Staphylococcus aureus*. J. Gen. Microbiol. *33*, 213–229.

Stryjewski, M.E., and Corey, G.R. (2014). Methicillin-resistant *Staphylococcus aureus*: An evolving pathogen. Clin. Infect. Dis. *58*.

Suzuki, E., Kuwahara-Arai, K., Richardson, J.F., and Hiramatsu, K. (1993). Distribution of *mec* regulator genes in methicillin-resistant Staphylococcus clinical strains. Antimicrob. Agents Chemother. *37*, 1219–1226.

Szybalski, W., and Bryson, V. (1952). Genetic Studies on Microbial Cross Resistance To Toxic Agents. J. Bacteriol. *64*, 489–499.

Tan, C.M., Therien, A.G., Lu, J., Lee, S.H., Caron, A., Gill, C.J., Lebeau-jacob, C., Benton-perdomo, L., Monteiro, J.M., Pereira, P.M., et al. (2012a). Restoring Methicillin-Resistant *Staphylococcus aureus* Susceptibility to b -Lactam Antibiotics. Sci. Transl. Med. *4*.

Tatusov, R., Galperin, M.Y., Natale, D.A., and Koonin, E. V. (2000). The COG database: a tool for genome-scale analysis of protein functions and evolution. Nucleic Acids Res. *28*, 33–36.

Tenover, F.C., Lancaster, M. V., Hill, B.C., Steward, C.D., Stocker, S.A., Hancock, G.A., O'Hara, C.M., Clark, N.C., and Hiramatsu, K. (1998). Characterization of Staphylococci with reduced susceptibilities to vancomycin and other glycopeptides. J. Clin. Microbiol. *36*, 1020–1027.

Throup, J.P., Zappacosta, F., Lunsford, R.D., Annan, R.S., Carr, S.A., Lonsdale, J.T., Bryant, A.P., McDevitt, D., Rosenberg, M., and Burnham, M.K.R. (2001). The *srhSR* gene pair from *Staphylococcus aureus*: Genomic and proteomic approaches to the identification and characterization of gene function. Biochemistry *40*, 10392–10401.

Tipper, D.J., and Strominger, J.L. (1965). Mechanism of action of penicillins: a proposal based on their structural similarity to acyl-D-alanyl-D-alanine. Proc. Natl. Acad. Sci. U. S. A. *54*, 1133–1141.

Tomasz, a., Nachman, S., and Leaf, H. (1991). Stable classes of phenotypic expression in methicillin-resistant clinical isolates of staphylococci. Antimicrob. Agents Chemother. *35*, 124–129.

Trevors, J.T. (1986). Plasmid curing in bacteria. FEMS Microbiol. Lett. *32*, 149–157.

Tsubakishita, S., Kuwahara-Arai, K., Sasaki, T., and Hiramatsu, K. (2010). Origin and molecular evolution of the determinant of methicillin resistance in staphylococci. Antimicrob. Agents Chemother. *54*, 4352–4359.

Turlej, A., Hryniewicz, W., and Empel, J. (2011). Staphylococcal Cassette Chromosome mec (SCCmec) classification and typing methods: An overview. Polish J. Microbiol. *60*, 95–103.

Turner, R.D., Vollmer, W., and Foster, S.J. (2014). Different walls for rods and balls: The diversity of peptidoglycan. Mol. Microbiol. *91*, 862–874.

Typas, A., Banzhaf, M., Gross, C. a., and Vollmer, W. (2012). From the regulation of peptidoglycan synthesis to bacterial growth and morphology. Nat. Rev. Microbiol. *10*, 123–136.

Tzagoloff, H., and Novick, R. (1977). Geometry of cell division in *Staphylococcus aureus*. J. Bacteriol. *129*, 343–350.

Utsui, Y., and Yokota, T. (1985). Role of an Altered Penicillin-Binding Protein in Methicillin- and Cephem-Resistant *Staphylococcus aureus*. Antimicrob. Agents Chemother. *28*, 397–403.

Vagner, V., Dervyn, E., and Ehrlich, S.D. (1998). A vector for systematic gene inactivation in *Bacillus subtilis*. Microbiology *144*, 3097–3104.

Varaldo, P.E., Montanari, M.P., Biavasco, F., Manso, E., Ripa, S., and Santacroce, F. (1993). Survey of clinical isolates of *Staphylococcus aureus* for borderline susceptibility to antistaphylococcal penicillins. Eur.J.Clin.Microbiol.Infect.Dis. *12*, 677–682.

Vega, D., and Ayala, J.A. (2006). The DD-carboxypeptidase activity encoded by *pbp4B* is not essential for the cell growth of Escherichia coli. Arch. Microbiol. *185*, 23–27.

Villanueva, M., Jousselin, A., Baek, K.T., Prados, J., Andrey, D.O., Renzoni, A., Ingmer, H., Frees, D., and Kelley, W.L. (2016). Rifampin Resistance *rpoB* Alleles or Multicopy Thioredoxin/Thioredoxin Reductase Suppresses the Lethality of Disruption of the Global Stress Regulator spx in *Staphylococcus aureus*. J. Bacteriol. *198*, JB.00261-16.

Villegas-estrada, A., Lee, M., Hesek, D., Vakulenko, S.B., and Mobashery, S. (2008). Co-opting the Cell Wall in Fighting Methicillin-Resistant *Staphylococcus aureus* : Potent Inhibition of PBP2a by Two Anti-MRSA β-Lactam Antibiotics. JACS *130*, 9212–9213.

Vollmer, W. (2008). Structural variation in the glycan strands of bacterial peptidoglycan. FEMS Microbiol. Rev. *32*, 287–306.

Vollmer, W., Höltje, J., and Ho, J. (2004). The Architecture of the Murein (Peptidoglycan) in

Gram-Negative Bacteria : Vertical Scaffold or Horizontal Layer. J. Bacteriol. *186*, 5978–5987.

Vollmer, W., Blanot, D., and De Pedro, M.A. (2008a). Peptidoglycan structure and architecture. FEMS Microbiol. Rev. *32*, 149–167.

Vollmer, W., Joris, B., Charlier, P., and Foster, S. (2008b). Bacterial peptidoglycan (murein) hydrolases. FEMS Microbiol. Rev. *32*, 259–286.

Walsh, C. (2000). Molecular mechanisms that confer antibacterial drug resistance. Nature *406*, 775–781.

Walter, W., Sánchez-Cabo, F., and Ricote, M. (2015). GOplot: An R package for visually combining expression data with functional analysis. Bioinformatics *31*, 2912–2914.

Wang, E.T., Sandberg, R., Luo, S., Khrebtukova, I., Zhang, L., Mayr, C., Kingsmore, S.F., Schroth, G.P., and Burge, C.B. (2008). Alternative isoform regulation in human tissue transcriptomes. Nature *456*, 470–476.

Wang, H., Gill, C.J., Lee, S.H., Mann, P., Zuck, P., Meredith, T.C., Murgolo, N., She, X., Kales, S., Liang, L., et al. (2013). Discovery of wall teichoic acid inhibitors as potential anti-MRSA β-lactam combination agents. Chem. Biol. *20*, 272–284.

Wang, Z., Gerstein, M., and Snyder, M. (2009). RNA-seq: A revolutionary tool for transcriptomics. Nat. Rev. Genet. *10*, 57–63.

Watanabe, Y., Cui, L., Katayama, Y., Kozue, K., and Hiramatsu, K. (2011). Impact of *rpoB* mutations on reduced vancomycin susceptibility in *Staphylococcus aureus*. J. Clin. Microbiol. *49*, 2680–2684.

Wecke, J., Madela, K., and Fischer, W. (1997). The absence of D-alanine from lipoteichoic acid and wall teichoic acid alters surface charge, enhances autolysis and increases susceptibility to methicillin in *Bacillus subtilis*. Microbiology *143*, 2953–2960.

Wehrli, W. (1983). Rifampin: mechanisms of action and resistance. Rev. Infect. Dis. *5 Suppl 3*, S407-11.

Wei, Y., Havasy, T., Mcpherson, D.C., and Popham, D.L. (2003). Rod Shape Determination by the *Bacillus subtilis* Class B Penicillin-Binding Proteins Encoded by *pbpA* and *pbpH* R. J. Bacteriol. *185*, 4717–4726.

Wheeler, R., Turner, R.D., Bailey, R.G., Salamaga, B., Mesnage, S., Mohamad, S.A.S., Hayhurst, E.J., Horsburgh, M., Hobbs, J.K., and Foster, S.J. (2015). Bacterial cell enlargement requires control of cell wall stiffness mediated by peptidoglycan hydrolases. MBio *6*, 1–10.

Wichelhaus, T.A., Schäfer, V., and Brade, V. (1999). Molecular Characterization of *rpoB* Mutations Conferring Cross-Resistance to Rifamycins on Methicillin-Resistant *Staphylococcus aureus*. Antimicrob. Agents Chemother. *43*, 2813–2816.

Witte, G., Hartung, S., Büttner, K., and Hopfner, K.P. (2008). Structural Biochemistry of a Bacterial Checkpoint Protein Reveals Diadenylate Cyclase Activity Regulated by DNA Recombination Intermediates. Mol. Cell *30*, 167–178.

Woodward, J.J., Iavarone, A.T., and Portnoy, D.A. (2010). c-di-AMP secreted by intracellular *Listeria monocytogenes* activates a host type I interferon response. Science (80). *328*, 1703–1705.

Wu, S., and de Lencastre, H. (1999). Mrp—A New Auxiliary Gene Essential for Optimal

Expression of Methicillin Resistance in *Staphylococcus aureus*. Microb. Drug Resist. *5*.

Wu, M.T., Burnham, C.A.D., Westblade, L.F., Bard, J.D., Lawhon, S.D., Wallace, M.A., Stanley, T., Burd, E., Hindler, J., and Humphries, R.M. (2016). Evaluation of Oxacillin and Cefoxitin Disk and MIC Breakpoints for Prediction of Methicillin Resistance in Human and Veterinary Isolates of *Staphylococcus intermedius* Group. J. Clin. Microbiol. *54*, 535–542.

Wu, S., Piscitelli, C., de Lencastre, H., and Tomasz, A. (1996a). Tracking the evolutionary origin of the methicillin resistance gene: cloning and sequencing of a homologue of *mecA* from a methicillin susceptible strain of *Staphylococcus sciuri*. Microb. Drug Resist. *2*, 435–441.

Wu, S., De Lencastre, H., and Tomasz, A. (1996b). Sigma-B, a putative operon encoding alternate sigma factor of *Staphylococcus aureus* RNA polymerase: Molecular cloning and DNA sequencing. J. Bacteriol. *178*, 6036–6042.

Wyke, a W., Ward, J.B., Hayes, M. V, and Curtis, N. a (1981). A role in vivo for penicillin-binding protein-4 of *Staphylococcus aureus*. Eur. J. Biochem. *119*, 389–393.

Zapun, A., Contreras-Martel, C., and Vernet, T. (2008). Penicillin-binding proteins and β-lactam resistance. FEMS Microbiol. Rev. *32*, 361–385.

Zeden, M.S., Schuster, C.F., Bowman, L., Zhong, Q., Williams, H.D., and Gründling, A. (2018). Cyclic-di-adenosine monophosphate (c-di-AMP) is required for osmotic regulation in *Staphylococcus aureus* but dispensable for viability in anaerobic conditions. J. Biol. Chem. jbc.M117.818716.

Zhang, B., Daniel, R. a., Errington, J., and Kroos, L. (1997). *Bacillus subtilis* spoIIID protein binds to two sites in the *spoVD* promoter and represses transcription by σ(E) RNA polymerase. J. Bacteriol. *179*, 972–975.

Zhang, H.Z., Hackbarth, C.J., Chansky, K.M., and Chambers, H.F. (2001). A proteolytic transmembrane signaling pathway and resistance to beta-lactams in staphylococci. Science (80-.). *291*, 1962–1965.

Zhang, K., McClure, J.A., Elsayed, S., and Conly, J.M. (2009). Novel staphylococcal cassette chromosome mec type, tentatively designated type VIII, harboring class A *mec* and type 4 *ccr* gene complexes in a Canadian epidemic strain of methicillin-resistant *Staphylococcus aureus*. Antimicrob. Agents Chemother. *53*, 531–540.

Zhou, W., Shan, W., Ma, X., Chang, W., Zhou, X., Lu, H., and Dai, Y. (2012). Molecular characterization of rifampicin-resistant *Staphylococcus aureus* isolates in a Chinese teaching hospital from Anhui, China. BMC Microbiol. *12*, 1–5.

Zhu, Y., Pham, T.H., Nhiep, T.H.N., Vu, N.M.T., Marcellin, E., Chakrabortti, A., Wang, Y., Waanders, J., Lo, R., Huston, W.M., et al. (2016). Cyclic-di-AMP synthesis by the diadenylate cyclase CdaA is modulated by the peptidoglycan biosynthesis enzyme GlmM in *Lactococcus lactis*. Mol. Microbiol. *99*, 1015–1027.

Zuber, P. (2004). Spx-RNA Polymerase Interaction and Global Transcriptional Control during Oxidative Stress. J. Bacteriol. *186*, 1911–1918.

Appendix 1

No.	Strain	Gradient plate	Oxacillin MIC
Parental strain SH1000			
1	**SH1000 p*mecA* (SJF4981)**		0.25 µg/ml
Parental strain SH1000 p*mecA* (SJF4981)			
2	**SH1000 p*mecA* -TI1 (SJF4984)**	0.5 µg/ml methicillin	2 µg/ml
3	**SH1000 p*mecA* -TI2 (SJF4989)**	0.5 µg/ml methicillin	2 µg/ml
4	**SH1000 p*mecA* -TI3 (SJF4992)**	0.5 µg/ml methicillin	4 µg/ml
5	SH1000 p*mecA* -TI4	0.5 µg/ml methicillin	1 µg/ml
6	SH1000 p*mecA* -TI5	0-20 µg/ml methicillin	2 µg/ml
7	SH1000 p*mecA* -TI6	0.5 µg/ml methicillin	2 µg/ml
8	SH1000 p*mecA* -TI7	0.5 µg/ml methicillin	2 µg/ml
9	SH1000 p*mecA* -TI8	0.5 µg/ml methicillin	2 µg/ml
10	SH1000 p*mecA* -TI9	0-20 µg/ml methicillin	1 µg/ml
11	SH1000 p*mecA* -TI10	0.5 µg/ml methicillin	1 µg/ml
12	SH1000 p*mecA* -TI11	0.5 µg/ml methicillin	4 µg/ml
13	SH1000 p*mecA* -TI12	0.5 µg/ml methicillin	2 µg/ml
14	SH1000 p*mecA* -TI13	0-20 µg/ml methicillin	4 µg/ml
Parental strain SH1000 p*mecA* -TI1 (SJF4984)			
15	**SH1000 p*mecA* -TIR1 (SJF4986)**	0-20 µg/ml methicillin	≥256 µg/ml
16	**SH1000 p*mecA* -TIR2 (SJF4987)**	0-20 µg/ml methicillin	≥256 µg/ml
17	**SH1000 p*mecA* -TIR3 (SJF4988)**	0-20 µg/ml methicillin	≥256 µg/ml
Parental strain SH1000 p*mecA* (SJF4981)			
18	**SH1000 p*mecA* -TR1 (SJF4985)**	0.5 µg/ml methicillin	≥256 µg/ml
19	**SH1000 p*mecA* -TR2 (SJF4990)**	0.5 µg/ml methicillin	≥256 µg/ml
20	**SH1000 p*mecA* -TR3 (SJF4991)**	0.5 µg/ml methicillin	≥256 µg/ml
21	SH1000 p*mecA* -TR4	0-20 µg/ml methicillin	≥256 µg/ml
22	SH1000 p*mecA* -TR5	0.5 µg/ml methicillin	≥256 µg/ml
23	SH1000 p*mecA* -TR6	0.5 µg/ml methicillin	≥256 µg/ml
24	SH1000 p*mecA* -TR7	0.5 µg/ml methicillin	≥256 µg/ml
25	SH1000 p*mecA* -TR8	0.5 µg/ml methicillin	≥256 µg/ml
26	SH1000 p*mecA* -TR9	0.5 µg/ml methicillin	≥256 µg/ml
27	SH1000 p*mecA* -TR10	0.5 µg/ml methicillin	≥256 µg/ml
28	SH1000 p*mecA* -TR11	0.5 µg/ml methicillin	≥256 µg/ml
29	SH1000 p*mecA* -TR12	0.5 µg/ml methicillin	≥256 µg/ml
30	SH1000 p*mecA* -TR13	0.5 µg/ml methicillin	≥256 µg/ml
31	SH1000 p*mecA* -TR14	0.5 µg/ml methicillin	≥256 µg/ml
32	SH1000 p*mecA* -TR15	0.5 µg/ml methicillin	≥256 µg/ml

33	SH1000 p*mecA* -TR16	0.5 µg/ml methicillin	≥256 µg/ml
34	SH1000 p*mecA* -TR17	0-20 µg/ml methicillin	≥256 µg/ml
35	SH1000 p*mecA* -TR18	0-20 µg/ml methicillin	≥256 µg/ml
36	SH1000 p*mecA* -TR19	0.5 µg/ml methicillin	≥256 µg/ml
37	SH1000 p*mecA* -TR20	0.5 µg/ml methicillin	≥256 µg/ml
38	SH1000 p*mecA* -TR21	0.5 µg/ml methicillin	64 µg/ml
39	SH1000 p*mecA* -TR22	0.5 µg/ml methicillin	≥256 µg/ml
40	SH1000 p*mecA* -TR23	0-20 µg/ml methicillin	≥256 µg/ml
41	SH1000 p*mecA* -TR24	0-20 µg/ml methicillin	128 µg/ml
42	SH1000 p*mecA* -TR25	0-20 µg/ml methicillin	≥256 µg/ml

Appendix 1 Table 1 List of isolates methicillin resistant selected from two screenings.

Representative strains are listed in bold.

Nucleo-tide position	Mutation Type	Mutation Strength	Amino acid change	Gene name/Locus Tag	SJF4981 (SH1000 p*mecA*)	SJF4984 (SH1000 p*mecA* TI1)	SJF4989 (SH1000 p*mecA* TI2)	SJF4992 (SH1000 p*mecA* TI3)	SJF4986 (SH1000 p*mecA* TIR1)	SJF4987 (SH1000 p*mecA* TIR2)	SJF4988 (SH1000 p*mecA* TIR3)	SJF4985 (SH1000 p*mecA* TR1)	SJF4990 (SH1000 p*mecA* TR2)	SJF4991 (SH1000 p*mecA* TR3)
					Parent SH1000	**Parent – SJF4981 (SH1000 p*mecA*)**			**Parent - SJF4984 (SH1000 p*mecA* TI1)**			**Parent – SJF4981 (SH1000 p*mecA*)**		
9045	Frame_Shift	Moderate	R681C	gyrA SAOUHSC_00006		T	T	T	T	T	T			
18904	Non-synonymous	Moderate	S196W	gdpP SAOUHSC_00015						G				
19188	Non-synonymous	Moderate	G291R	gdpP SAOUHSC_00015									C	
19270	Non-synonymous	Moderate	R318L	gdpP SAOUHSC_00015										T
19852	Non-synonymous	Moderate	A512E	gdpP SAOUHSC_00015								A		
19903	Non-synonymous	Moderate	F529S	gdpP SAOUHSC_00015							C			
22181					A	A	A	A	A	A	A	A	A	A
47648					T	T	T	T	T	T	T	T	T	T
110019	Non-synonymous	Moderate	V16F	SAOUHSC_00105	A	A	A	A	A	A	A	A	A	A
176626	Non-synonymous	Moderate	D784N	SAOUHSC_00162		A	A	A	A	A	A			
376633	Stop_Gained	High	E212*	SAOUHSC_00370										A
392716					A	A	A	A	A	A	A	A	A	A
405366					G	G	G	G	G	G	G	G	G	G
412759					AT	AT	AT	AT	AT	AT	AT	AT	AT	AT

412765					G	G	G	G	G	G	G	G	G	G
590401	Frame_Shift	High	R189	SAOUHSC_00591	G	G	G	G	G	G	G	G	G	.
649126	Synonymous	Low	G202	SAOUHSC_00661	T	T	T	T	T	T	T	T	T	T
653552	Synonymous	Low	G266	graS SAOUHSC_00666	G	G	G	G	G	G	G	G	G	G
653801					T	T	T	T	T	T	T	T	T	T
751285	Non-synonymous	Moderate	E449V	secA	T	T	T	T	T	T	T	T	T	T
827849	Non-synonymous	Moderate	T164S	SAOUHSC_00859	T	T	T	T	T	T	T	T	T	T
841103	Synonymous	Low	G39	SAOUHSC_00877	T	T	T	T	T	T	T	T	T	T
841139	Synonymous	Low	G51	SAOUHSC_00877	T	T	T	T	T	T	T	T	T	T
857574					A	A	A	A	A	A	A	A	A	A
939304	Non-synonymous	Moderate	E53K	SAOUHSC_00961	T	T	T	T	T	T	T	T	T	T
947897					C	C	C	C	C	C	C	C	C	C
954590	Synonymous	Low	D107	menD SAOUHSC_00983	T	T	T	T	T	T	T	T	T	T
1009713	Non-synonymous	Moderate	G64A	SAOUHSC_01041	C	C	C	C	C	C	C	C	C	C
1016979	Non-synonymous	Moderate	E220K	SAOUHSC_01048	A	A	A	A	A	A	A	A	A	A
1020577	Stop_Gained	High	S286*	mntH SAOUHSC_01053	T	T	T	T	T	T	T	T	T	T
1041999					T	T	T	T	T	T	T	T	T	T
1089537	Non-synonymous	Moderate	P216A	SAOUHSC_01137										G

1123048	Non-synonymous	Moderate	G42S	pyrE SAOUHSC_01172	A	A	A	A	A	A	A	A	A	A
1126724														T
1160513	Non-synonymous	Moderate	A106T	rimM SAOUHSC_01209	A	A	A	A	A	A	A	A	A	A
1160531	Non-synonymous	Moderate	K112E	rimM SAOUHSC_01209	G	G	G	G	G	G	G	G	G	G
1283783					C	C	C	C	C	C	C	C	C	C
1358230	Non-synonymous	Moderate	D590N	sucA	T	T	T	T	T	T	T	T	T	T
1562913					T	T	T	T	T	T	T	T	T	T
1632624							TA	TA		TA	TA	TA		
1636250					T	T	T	T	T	T	T	T	T	.
1653482	Synonymous	Low	I91	tgt SAOUHSC_01748	A	A	A	A	A	A	A	A	A	A
1683491	Non-synonymous	Moderate	K40E	infC SAOUHSC_01786	C	C	C	C	C	C	C	C	C	C
1718656	Non-synonymous	Moderate	G54D	SAOUHSC_01812					T					
1733515	Non-synonymous	Moderate	T73N	ezrA SAOUHSC_01827	T	T	T	T	T	T	T	T	T	T
1733572	Non-synonymous	Moderate	F54S	SAOUHSC_01827	G	G	G	G	G	G	G	G	G	G
1967012	Synonymous	Low	D13	SAOUHSC_02090	.	.	.	.	.	.	.	.	.	.
1981053	Non-synonymous	Moderate	F92S	SAOUHSC_02107	G	G	G	G	G	G	G	G	G	G
2087725	Non-synonymous	Moderate	F218I	groL groEL SAOUHSC_02254	T	T	T	T	T	T	T	T	T	T

2106539	Non-synonymous	Moderate	L602F	SAOUHSC_02274	T	T	T	T	T	T	T	T	T	T
2134372						AAGCCTTTAACG			AAGCCTTTAACG					.
2134726					TA	TA	TA	TA	TA	.	.	TA	TA	TA
2134749	Synonymous	Low	Y3	SAOUHSC_A02189	T	T	T	T	T	T	T	T	T	T
2166163	Non-synonymous	Moderate	T124R	murA SAOUHSC_02337	C	C	C	C	C	C	C	C	C	C
2166183	Synonymous	Low	G117	murA SAOUHSC_02337	A	A	A	A	A	A	A	A	A	A
2221850	Non-synonymous	Moderate	S244Y	SAOUHSC_02401	A	A	A	A	A	A	A	A	A	A
2244467					G	G	G	G	G	G	G	G	G	G
2244495					A	A	A	A	A	A	A	A	A	A
2244931						CT	CT	CT	CT	CT	CT	CT	CT	CT
2272936					T	T	T	T	T	T	T	T	T	T
2296653	Frame_Shift	High	A10	SAOUHSC_02473	G	G		G	G	G	G	G	G	G
2318272					A	A	A	A	A	A	A	A	A	A
2318274					T	T	T	T	T	T	T	T	T	T
2318290					A	A	A	A	A	A	A	A	A	A
2349916					T	T	T	T	T	T	T	T	T	T
2349971					A	A		A	A	A		A	A	A
2349979					T	T	T	T	T	T	T	T	T	T
2349985					A	A	A	A	A	A	A	A	A	A
2349989					A	A	A	A	A	A	A	A	A	A
2349994					T	T	T	T	T	T	T	T	T	T
2350000					AT	AT	AT	AT	AT	AT	AT	AT	AT	AT

2350007					A	A	A	A	A	A	A	A	A	A
2350015					A	A	A	A	A	A	A	A	A	A
2350100					C	C	C	C	C	C	C	C	C	C
2383630	Synonymous	Low	G68	SAOUHSC_02591	T	T	T	T	T	T	T	T	T	T
2383660	Synonymous	Low	G78	SAOUHSC_02591	T	T	T	T	T	T	T	T	T	T
2420618					AT	AT	AT	AT	AT	AT	AT	AT	AT	AT
2446160	Frame_Shift	High	N7	SAOUHSC_02661	C			C			C			
2446246	Synonymous	Low	E42	SAOUHSC_02662	T	T	T	T	T	T	T	T	T	T
2446393					A	A	A	A	A	A	A	A	A	A
2446399					C	C	C	C	C	C	C	C	C	C
2446423					A	A	A	A	A	A	A	A	A	A
2446630	Non-synonymous	Moderate	H26Y	SAOUHSC_02663	T	T	T	T	T	T	T	T	T	T
2446641	Synonymous	Low	I29	SAOUHSC_02663	A	A	A	A	A	A	A	A	A	A
2471861	Non-synonymous	Moderate	H173Y	SAOUHSC_02685				A						
2592011					A	A	A	A	A	A	A	A	A	A
2678563	Synonymous	Low	P107	queH SAOUHSC_02911	C	C	C	C	C	C	C	C	C	C
2689048	Non-synonymous	Moderate	V353L	SAOUHSC_02923	T	T	T	T	T	T	T	T	T	T
2690768	Non-synonymous	Moderate	G31R	SAOUHSC_02924	G							G	G	G
2698103	Non-synonymous	Moderate	S511L	betA SAOUHSC_02932		A								
2733480	Non-synonymous	Moderate	Q231K	SAOUHSC_02971	T	T	T	T	T	T	T	T	T	T

2762204	Non-synonymous	Moderate	N1514S	sraP sasA SAOUHSC_02990	C	C	C	C	C	C	C	C	C	C
2782815	Frame_Shift	High	Y249	hisF hisI hisIE SAOUHSC_03008	C		C		C	C	C	C		C

Appendix 1 Table 2 Identification of mutations in SH1000 p*mecA* (SJF4981) derived resistant strains

TI, Trained-intermediate resistance; TR, Trained-high-level resistance; TIR, Trained-intermediate to trained-high-level resistance.

Nucleotide position	Mutation type	Mutation strength	Amino acid change	Gene name/Locus tag	SJF4996 (SH1000 *lysA*:: p*mecA*)	SJF4998 (SH1000 *lysA*:: p*mecA* TI1)	SJF4999 (SH1000 *lysA*:: p*mecA* TI2)	SJF5001 (SH1000 *lysA*:: p*mecA* TI3)	SJF5002 (SH1000 *lysA*:: p*mecA* TI4)	SJF5000 (SH1000 *lysA*:: p*mecA* TR1)	SJF5003 (SH1000 *lysA*:: p*mecA* TR2)	SJF5004 (SH1000 *lysA*:: p*mecA* TR3)	SJF5005 (SH1000 *lysA*:: p*mecA* TR4)	SJF5006 (SH1000 *lysA*:: p*mecA* TIR1)	SJF5007 (SH1000 *lysA*:: p*mecA* TIR2)	SJF5008 (SH1000 *lysA*:: p*mecA* TIR3)
					Parent SH1000	Parent - SJF4996 (SH1000 *lysA*::p*mecA*)				Parent - SJF4996 (SH1000 *lysA*::p*mecA*)				Parent - SJF4998 (SH1000 *lysA*::p*mecA* TI1)		
22181					A	A	A	A	A	A	A	A	A	A	A	A
47648					.	.	.	.	.	.	.	G	.	.	.	G
75261							A			.	.	.				.
110019	Non synonymous	Moderate	V16F	SAOUHSC_00105	A	A	A	A	A	A	A	A	A	A	A	A
289906	Non synonymous	Moderate	L161Q	SAOUHSC_00269										A		
290618	Synonymous	LOW	T165	SAOUHSC_00270					C							
290628	Non synonymous	Moderate	S169A	SAOUHSC_00270					G							
392716					A	A	A	A	A	A	A	A	A	A	A	A
405366					G	G	G	G	G	G	G	G	.	G	G	G
412759					AT	AT	AT	AT	AT	AT	AT	AT	AT	AT	AT	
412765					G	G	G	.	G	G	G	G	G	G	G	G
524946	Non synonymous	Moderate	H929Q	rpoB SAOUHSC_00524							A	A				
525575	Non synonymous	Moderate	G1139D	rpoB SAOUHSC_00524			A									
528059	Non synonymous	Moderate	A729T	rpoC SAOUHSC_00525										A		

528062	Non synonymous	Moderate	R730S	rpoC SAOUHSC_00525						A						
528402	Non synonymous	Moderate	S843Y	rpoC SAOUHSC_00525					A							
528644	Non synonymous	Moderate	E924Q	rpoC SAOUHSC_00525									C			
528695	Non synonymous	Moderate	G941R	rpoC SAOUHSC_00525											C	
529097	Non synonymous	Moderate	I1075F	rpoC SAOUHSC_00525				T								
590401	Frameshift	High	R189	SAOUHSC_00591	.	.	.	.	.	C	C	C	.	.	.	C
649126	Synonymous	Low	G202	SAOUHSC_00661	T	T	T	T	T	T	T	T	T	T	T	T
653552	Synonymous	Low	G266	graS SAOUHSC_00666	G	G	G	G	G	G	G	G	G	G	G	G
653801					T	T	T	T	T	T	T	T	T	T	T	T
751285	Non synonymous	Moderate	E449V	secA	T	T	T	T	T	T	T	T	T	T	T	T
827849	Non synonymous	Moderate	T164S	SAOUHSC_00859	T	T	T	T	T	T	T	T	T	T	T	T
841103	Synonymous	Low	G39	SAOUHSC_00877	T	T	T	T	T	T	T	T	T	T	T	T
841139	Synonymous	Low	G51	SAOUHSC_00877	T	T	T	T	T	T	T	T	T	T	T	T
857574					A	A	A	A	A	A	A	A	A	A	A	A
939304	Non synonymous	Moderate	E53K	SAOUHSC_00961	T	T	T	T	T	T	T	T	T	T	T	T
947897	Intragenic	Modifier		SAOUHSC_00973	T	.	T	T	T	.	T	.	T	T	T	T

954590	Synonymous	Low	D107		T	T	T	T	T	T	T	T	T	T	T	T
1009713	Non synonymous	Moderate	G64A	SAOUHSC_01041	C	C	C	C	C	C	C	C	C	C	C	C
1016979	Non synonymous	Moderate	E220K	SAOUHSC_01048	A	A	A	A	A	A	A	A	A	A	A	A
1020577	Stop_Gained	High	S286*	mntH SAOUHSC_01053	T	T	T	T	T	T	T	T	T	T	T	T
1041999	Intragenic	Modifier		rpmF SAOUHSC_01078	G	G	G	G	G	G	G	G	G	G	G	G
1083427	Frameshift	High	N262K?	arcC1 SAOUHSC_01129					GA							
1123048	Non synonymous	Moderate	G42S	pyrE SAOUHSC_01172	A	A	A	A	A	A	A	A	A	A	A	A
1160513	Non synonymous	Moderate	A106T	rimM SAOUHSC_01209	A	A	A	A	A	A	A	A	A	A	A	A
1160531	Non synonymous	Moderate	K112E	rimM SAOUHSC_01209	G	G	G	G	G	G	G	G	G	G	G	G
1283783	Intragenic	Modifier		SAOUHSC_01343	A	A	A	A	A	A	A	A	A	A	A	A
1358230	Non synonymous	Moderate	D590N	sucA	T	T	T	T	T	T	T	T	T	T	T	T
1562913	Intragenic	Modifier		SAOUHSC_01649	T	T	T	T	T	T	T	T	T	T	T	T
1632624	Intragenic	Modifier		SAOUHSC_01726	TA	TA		TA		TA	TA	TA	TA		TA	TA
1636250	Intragenic	Modifier		SAOUHSC_01732	G	G	G	G	G	G	G	G	G	G	G	G
1653482	Synonymous	Low	I91	tgt SAOUHSC_01748	A	A	A	A	A	A	A	A	A	A	A	A
1683491	Non synonymous	Moderate	K40E	infC SAOUHSC_01786	C	C	C	C	C	C	C	C	C	C	C	C

1733515	Non synonymous	Moderate	T73N	ezrA SAOUHSC_01827	T	T	T	T	T	T	T	T	T	T	T	T
1733572	Non synonymous	Moderate	F54S	ezrA SAOUHSC_01827	G	G	G	G	G	G	G	G	G	G	G	G
1757732													.		A	
1967012	Synonymous	Low	D13	SAOUHSC_02090	T	.	.	.	.	.	.	.	.	.	.	.
1981053	Non synonymous	Moderate	F92S	SAOUHSC_02107	G	G	G	G	G	G	G	G	G	G	G	G
2087725	Non synonymous	Moderate	F218I	groL groEL SAOUHSC_02254	T	T	T	T	T	T	T	T	T	T	T	T
2106539	Non synonymous	Moderate	L602F	SAOUHSC_02274	T	T	T	T	T	T	T	T	T	T	T	T
2134372	Intragenic	Modifier		SAOUHSC_02301							AAGCCTTTAACG		AAGCCTTTAACG			
2134726					TA	.	TA	TA	TA	TA	.	TA	TA	TA	TA	TA
2134749	Synonymous	Low	Y3	SAOUHSC_A02189	T	T	T	T	T	T	T	T	T	T	T	T
2166163	Non synonymous	Moderate	T124R	murA SAOUHSC_02337	C	C	C	C	C	C	C	C	C	C	C	C
2166183	Synonymous	Low	G117	murA SAOUHSC_02337	A	A	A	A	A	A	A	A	A	A	A	A
2221850	Non synonymous	Moderate	S244Y	SAOUHSC_02401	A	A	A	A	A	A	A	A	A	A	A	A
2244467					G	G	G	G	G	G	G	G	G	G	G	G
2244495					A	A	A	A	A	A	A	A	A	A	A	A
2244931	Intragenic	Modifier		SAOUHSC_02417	A	A	A	A	A	A	A	A	A	A	A	A
2272936					T	T	T	T	T	T	T	T	T	T	T	T

2296653	Frameshift	High	A10	SAOUHSC_02473	T	T	T	T	T	T	T	T	T	T	T	T
2318272					A	A	A	A	A	A	A	A	A	A	A	A
2318274					T	T	T	T	T	T	T	T	T	T	T	T
2318290					A	A	A	A	A	A	A	A	A	A	A	A
2349916	Intragenic	Modifier		SAOUHSC_02555	T	T	T	T	T	T	T	T	T	T	T	T
2349971	Intragenic	Modifier		SAOUHSC_02555	C	C	C	C	C	C	C	C	C	C	C	C
2349979	Intragenic	Modifier		SAOUHSC_02555	A	A	A	A	A	A	A	A	A	A	A	A
2349985	Intragenic	Modifier		SAOUHSC_02555	T	T	T	T	T	T	T	T	T	T	T	T
2349989	Intragenic	Modifier		SAOUHSC_02555	C	C	C	C	C	C	C	C	C	C	C	C
2349994	Intragenic	Modifier		SAOUHSC_02555	C	C	C	C	C	C	C	C	C	C	C	C
2350000	Intragenic	Modifier		SAOUHSC_02555	C	C	C	C	C	C	C	C	C	C	C	C
2350007	Intragenic	Modifier		SAOUHSC_02555	G	G	G	G	G	G	G	G	G	G	G	G
2350015	Intragenic	Modifier		SAOUHSC_02555	C	C	C	C	C	C	C	C	C	C	C	C
2350100	Intragenic	Modifier		SAOUHSC_02555	C	C	C	C	C	C	C	C	C	C	C	C
2383630	Synonymous	Low	G68	SAOUHSC_02591	T	T	T	T	T	T	T	T	T	T	T	T
2383660	Synonymous	Low	G78	SAOUHSC_02591	T	T	T	T	T	T	T	T	T	T	T	T
2420618	Intragenic	Modifier		SAOUHSC_02632	AT	AT	AT	AT	AT	AT	AT	AT	AT	AT	AT	AT
2446160	Frameshift	High	G6	SAOUHSC_02661	T		T	T				T			T	
2446246	Synonymous	Low	E42	SAOUHSC_02662	T	T	T	T	T	T	T	T	T	T	T	T
2446393					A	A	A	A	A	A	A	A	A	A	A	A
2446399					T	T	T	T	T	T	T	T	T	T	T	T
2446423					A	A	A	A	A	A	A	A	A	A	A	A
2446630	Non synonymous	Moderate	H26Y	SAOUHSC_02663	T	T	T	T	T	T	T	T	T	T	T	T

2446641	Synonymous	Low	I29	SAOUHSC_02663	A	A	A	A	A	A	A	A	A	A	A	A
2592011	Intragenic	Modifier		SAOUHSC_02813	G	G	G	G	G	G	G	G	G	G	G	G
2678563	Synonymous	Low	P107	queH SAOUHSC_02911	C	C	C	C	C	C	C	C	C	C	C	C
2689048	Non synonymous	Moderate	V353L	SAOUHSC_02923	T	T	T	T	T	T	T	T	T	T	T	T
2733480	Non synonymous	Moderate	Q231K	SAOUHSC_02971	T	T	T	T	T	T	T	T	T	T	T	T
2762204	Non synonymous	Moderate	N1514S	sraP sasA SAOUHSC_02990	C	C	C	C	C	C	C	C	C	C	C	C
2782815	Frameshift	High	G248	hisF hisI hisIE SAOUHSC_03008	A	A	A	A	A	A	A	A	A	A	A	A

Appendix 1 Table 3 Identification of mutations in SH1000 *lysA*::p*mecA* (SJF4996) derived resistant strains

TI, Trained-intermediate resistance; TR, Trained-high-level resistance; TIR, Trained-intermediate to trained-high-level resistance.

Appendix 2

Alignment of *rpoB* and *rpoC* amino acid sequences using Clustal Omega. The amino acid sequence of *rpoB* and *rpoC* from clinical MRSA isolates, COL, Mu50, Mu3, MW2, USA300, JH9, MRSA252 was aligned with NCTC8325 (MSSA) strain. Identified amino acid substitutions from strains listed in Table 4.3 and Table 4.4 are highlighted in green and yellow, respectively. Asterisks indicate fully conserved residues, colons indicate conservative substitutions with strongly similar properties, periods indicate semi conservative substitutions with weakly similar properties and gaps indicate not conserved residues.

rpoB alignment results

```
JH9          MAGQVVQYGRHRKRRNYARISEVLELPNLIEIQTKSYEWFLREGLIEMFRDISPIEDFTG   60
COL          MAGQVVQYGRHRKRRNYARISEVLELPNLIEIQTKSYEWFLREGLIEMFRDISPIEDFTG   60
Mu50         MAGQVVQYGRHRKRRNYARISEVLELPNLIEIQTKSYEWFLREGLIEMFRDISPIEDFTG   60
8325         MAGQVVQYGRHRKRRNYARISEVLELPNLIEIQTKSYEWFLREGLIEMFRDISPIEDFTG   60
USA300       MAGQVVQYGRHRKRRNYARISEVLELPNLIEIQTKSYEWFLREGLIEMFRDISPIEDFTG   60
Mu3          MAGQVVQYGRHRKRRNYARISEVLELPNLIEIQTKSYEWFLREGLIEMFRDISPIEDFTG   60
MW2          MAGQVVQYGRHRKRRNYARISEVLELPNLIEIQTKSYEWFLREGLIEMFRDISPIEDFTG   60
MRSA252      MAGQVVQYGRHRKRRNYARISEVLELPNLIEIQTKSYEWFLREGLIEMFRDISPIEDFTG   60
             ************************************************************


JH9          NLSLEFVDYRLGEPKYDLEESKNRDATYAAPLRVKVRLIIKETGEVKEQEVFMGDFPLMT   120
COL          NLSLEFVDYRLGEPKYDLEESKNRDATYAAPLRVKVRLIIKETGEVKEQEVFMGDFPLMT   120
Mu50         NLSLEFVDYRLGEPKYDLEESKNRDATYAAPLRVKVRLIIKETGEVKEQEVFMGDFPLMT   120
8325         NLSLEFVDYRLGEPKYDLEESKNRDATYAAPLRVKVRLIIKETGEVKEQEVFMGDFPLMT   120
USA300       NLSLEFVDYRLGEPKYDLEESKNRDATYAAPLRVKVRLIIKETGEVKEQEVFMGDFPLMT   120
Mu3          NLSLEFVDYRLGEPKYDLEESKNRDATYAAPLRVKVRLIIKETGEVKEQEVFMGDFPLMT   120
MW2          NLSLEFVDYRLGEPKYDLEESKNRDATYAAPLRVKVRLIIKETGEVKEQEVFMGDFPLMT   120
MRSA252      NLSLEFVDYRLGEPKYDLEESKNRDATYAAPLRVKVRLIIKETGEVKEQEVFMGDFPLMT   120
             ************************************************************
```

```
JH9          DTGTFVINGAERVIVSQLVRSPSVYFNEKIDKNGRENYDATIIPNRGAWLEYETDAKDVV   180
COL          DTGTFVINGAERVIVSQLVRSPSVYFNEKIDKNGRENYDATIIPNRGAWLEYETDAKDVV   180
Mu50         DTGTFVINGAERVIVSQLVRSPSVYFNEKIDKNGRENYDATIIPNRGAWLEYETDAKDVV   180
8325         DTGTFVINGAERVIVSQLVRSPSVYFNEKIDKNGRENYDATIIPNRGAWLEYETDAKDVV   180
USA300       DTGTFVINGAERVIVSQLVRSPSVYFNEKIDKNGRENYDATIIPNRGAWLEYETDAKDVV   180
Mu3          DTGTFVINGAERVIVSQLVRSPSVYFNEKIDKNGRENYDATIIPNRGAWLEYETDAKDVV   180
MW2          DTGTFVINGAERVIVSQLVRSPSVYFNEKIDKNGRENYDATIIPNRGAWLEYETDAKDVV   180
MRSA252      DTGTFVINGAERVIVSQLVRSPSVYFNEKIDKNGRENYDATIIPNRGAWLEYETDAKDVV   180
             ************************************************************

JH9          YVRIDRTRKLPLTVLLRALGFSSDQEIVDLLGDNEYLRNTLEKDGTENTEQALLEIYERL   240
COL          YVRIDRTRKLPLTVLLRALGFSSDQEIVDLLGDNEYLRNTLEKDGTENTEQALLEIYERL   240
Mu50         YVRIDRTRKLPLTVLLRALGFSSDQEIVDLLGDNEYLRNTLEKDGTENTEQALLEIYERL   240
8325         YVRIDRTRKLPLTVLLRALGFSSDQEIVDLLGDNEYLRNTLEKDGTENTEQALLEIYERL   240
USA300       YVRIDRTRKLPLTVLLRALGFSSDQEIVDLLGDNEYLRNTLEKDGTENTEQALLEIYERL   240
Mu3          YVRIDRTRKLPLTVLLRALGFSSDQEIVDLLGDNEYLRNTLEKDGTENTEQALLEIYERL   240
MW2          YVRIDRTRKLPLTVLLRALGFSSDQEIVDLLGDNEYLRNTLEKDGTENTEQALLEIYERL   240
MRSA252      YVRIDRTRKLPLTVLLRALGFSSDQEIVDLLGDNEYLRNTLEKDGTENTEQALLEIYERL   240
             ************************************************************

JH9          RPGEPPTVENAKSLLYSRFFDPKRYDLASVGRYKTNKKLHLKHRLFNQKLAEPIVNTETG   300
COL          RPGEPPTVENAKSLLYSRFFDPKRYDLASVGRYKTNKKLHLKHRLFNQKLAEPIVNTETG   300
Mu50         RPGEPPTVENAKSLLYSRFFDPKRYDLASVGRYKTNKKLHLKHRLFNQKLAEPIVNTETG   300
8325         RPGEPPTVENAKSLLYSRFFDPKRYDLASVGRYKTNKKLHLKHRLFNQKLAEPIVNTETG   300
USA300       RPGEPPTVENAKSLLYSRFFDPKRYDLASVGRYKTNKKLHLKHRLFNQKLAEPIVNTETG   300
Mu3          RPGEPPTVENAKSLLYSRFFDPKRYDLASVGRYKTNKKLHLKHRLFNQKLAEPIVNTETG   300
MW2          RPGEPPTVENAKSLLYSRFFDPKRYDLASVGRYKTNKKLHLKHRLFNQKLAEPIVNTETG   300
MRSA252      RPGEPPTVENAKSLLYSRFFDPKRYDLASVGRYKTNKKLHLKHRLFNQKLAEPIVNTETG   300
             ************************************************************

JH9          EIVVEEGTVLDRRKIDEIMDVLESNANSEVFELHGSVIDEPVEIQSIKVYVPNDDEGRTT   360
COL          EIVVEEGTVLDRRKIDEIMDVLESNANSEVFELHGSVIDEPVEIQSIKVYVPNDDEGRTT   360
Mu50         EIVVEEGTVLDRRKIDEIMDVLESNANSEVFELHGSVIDEPVEIQSIKVYVPNDDEGRTT   360
8325         EIVVEEGTVLDRRKIDEIMDVLESNANSEVFELHGSVIDEPVEIQSIKVYVPNDDEGRTT   360
USA300       EIVVEEGTVLDRRKIDEIMDVLESNANSEVFELHGSVIDEPVEIQSIKVYVPNDDEGRTT   360
Mu3          EIVVEEGTVLDRRKIDEIMDVLESNANSEVFELHGSVIDEPVEIQSIKVYVPNDDEGRTT   360
MW2          EIVVEEGTVLDRRKIDEIMDVLESNANSEVFELHGSVIDEPVEIQSIKVYVPNDDEGRTT   360
MRSA252      EIVVEEGTVLDRRKIDEIMDVLESNANSEVFELHGSVIDEPVEIQSIKVYVPNDDEGRTT   360
             ************************************************************
```

```
JH9          TVIGNAFPDSEVKCITPADIIASMSYFFNLLSGIGYTDDIDHLGNRRLRSVGELLQNQFR   420
COL          TVIGNAFPDSEVKCITPADIIASMSYFFNLLSGIGYTDDIDHLGNRRLRSVGELLQNQFR   420
Mu50         TVIGNAFPDSEVKCITPADIIASMSYFFNLLSGIGYTDDIDHLGNRRLRSVGELLQNQFR   420
8325         TVIGNAFPDSEVKCITPADIIASMSYFFNLLSGIGYTDDIDHLGNRRLRSVGELLQNQFR   420
USA300       TVIGNAFPDSEVKCITPADIIASMSYFFNLLSGIGYTDDIDHLGNRRLRSVGELLQNQFR   420
Mu3          TVIGNAFPDSEVKCITPADIIASMSYFFNLLSGIGYTDDIDHLGNRRLRSVGELLQNQFR   420
MW2          TVIGNAFPDSEVKCITPADIIASMSYFFNLLSGIGYTDDIDHLGNRRLRSVGELLQNQFR   420
MRSA252      TVIGNAFPDSEVKCITPADIIASMSYFFNLLSGIGYTDDIDHLGNRRLRSVGELLQNQFR   420
             ************************************************************

JH9          IGLSRMERVVRERMSIQDTESITPQQLINIRPVIASIKEFFGSSQLSQFMYQSNPLSDLT   480
COL          IGLSRMERVVRERMSIQDTESITPQQLINIRPVIASIKEFFGSSQLSQFMDQANPLAELT   480
Mu50         IGLSRMERVVRERMSIQDTESITPQQLINIRPVIASIKEFFGSSQLSQFMDQANPLAELT   480
8325         IGLSRMERVVRERMSIQDTESITPQQLINIRPVIASIKEFFGSSQLSQFMDQANPLAELT   480
USA300       IGLSRMERVVRERMSIQDTESITPQQLINIRPVIASIKEFFGSSQLSQFMDQANPLAELT   480
Mu3          IGLSRMERVVRERMSIQDTESITPQQLINIRPVIASIKEFFGSSQLSQFMDQANPLAELT   480
MW2          IGLSRMERVVRERMSIQDTESITPQQLINIRPVIASIKEFFGSSQLSQFMDQANPLAELT   480
MRSA252      IGLSRMERVVRERMSIQDTESITPQQLINIRPVIASIKEFFGSSQLSQFMDQANPLAELT   480
             ************************************************ *:***::**

JH9          HKRRLSALGPGGLTRERAQMEVRDVHYSHYGRMCPIETPEGPNIGLINSLSSYARVNEFG   540
COL          HKRRLSALGPGGLTRERAQMEVRDVHYSHYGRMCPIETPEGPNIGLINSLSSYARVNEFG   540
Mu50         YKRRLSALGPGGLTRERAQMEVRDVHYSHYGRMCPIETPEGPNIGLINSLSSYARVNEFG   540
8325         HKRRLSALGPGGLTRERAQMEVRDVHYSHYGRMCPIETPEGPNIGLINSLSSYARVNEFG   540
USA300       HKRRLSALGPGGLTRERAQMEVRDVHYSHYGRMCPIETPEGPNIGLINSLSSYARVNEFG   540
Mu3          HKRRLSALGPGGLTRERAQMEVRDVHYSHYGRMCPIETPEGPNIGLINSLSSYARVNEFG   540
MW2          HKRRLSALGPGGLTRERAQMEVRDVHYSHYGRMCPIETPEGPNIGLINSLSSYARVNEFG   540
MRSA252      HKRRLSALGPGGLTRERAQMEVRDVHYSHYGRMCPIETPEGPNIGLINSLSSYARVNEFG   540
             :************************************************************

JH9          FIETPYRKVDLDTHAITDQIDYLTADEEDSYVVAQANSKLDENGRFMDDEVVCRFRGNNT   600
COL          FIETPYRKVDLDTHAITDQIDYLTADEEDSYVVAQANSKLDENGRFMDDEVVCRFRGNNT   600
Mu50         FIETPYRKVDLDTHAITDQIDYLTADEEDSYVVAQANSKLDENGRFMDDEVVCRFRGNNT   600
8325         FIETPYRKVDLDTHAITDQIDYLTADEEDSYVVAQANSKLDENGRFMDDEVVCRFRGNNT   600
USA300       FIETPYRKVDLDTHAITDQIDYLTADEEDSYVVAQANSKLDENGRFMDDEVVCRFRGNNT   600
Mu3          FIETPYRKVDLDTHAITDQIDYLTADEEDSYVVAQANSKLDENGRFMDDEVVCRFRGNNT   600
MW2          FIETPYRKVDLDTHAITDQIDYLTADEEDSYVVAQANSKLDENGRFMDDEVVCRFRGNNT   600
MRSA252      FIETPYRKVDLDTHAITDQIDYLTADEEDSYVVAQANSKLDENGRFMDDEVVCRFRGNNT   600
             ************************************************************
```

```
JH9          VMAKEKMDYMDVSPKQVVSAATACIPFLENDDSNRALMGANMQRQAVPLMNPEAPFVGTG   660
COL          VMAKEKMDYMDVSPKQVVSAATACIPFLENDDSNRALMGANMQRQAVPLMNPEAPFVGTG   660
Mu50         VMAKEKMDYMDVSPKQVVSAATACIPFLENDDSNRALMGANMQRQAVPLMNPEAPFVGTG   660
8325         VMAKEKMDYMDVSPKQVVSAATACIPFLENDDSNRALMGANMQRQAVPLMNPEAPFVGTG   660
USA300       VMAKEKMDYMDVSPKQVVSAATACIPFLENDDSNRALMGANMQRQAVPLMNPEAPFVGTG   660
Mu3          VMAKEKMDYMDVSPKQVVSAATACIPFLENDDSNRALMGANMQRQAVPLMNPEAPFVGTG   660
MW2          VMAKEKMDYMDVSPKQVVSAATACIPFLENDDSNRALMGANMQRQAVPLMNPEAPFVGTG   660
MRSA252      VMAKEKMDYMDVSPKQVVSAATACIPFLENDDSNRALMGANMQRQAVPLMNPEAPFVGTG   660
             ************************************************************

JH9          MEHVAARDSGAAITAKHRGRVEHVESNEILVRRLVEENGVEHEGELDRYPLAKFKRSNSG   720
COL          MEHVAARDSGAAITAKHRGRVEHVESNEILVRRLVEENGVEHEGELDRYPLAKFKRSNSG   720
Mu50         MEHVAARDSGAAITAKHRGRVEHVESNEILVRRLVEENGVEHEGELDRYPLAKFKRSNSG   720
8325         MEHVAARDSGAAITAKHRGRVEHVESNEILVRRLVEENGVEHEGELDRYPLAKFKRSNSG   720
USA300       MEHVAARDSGAAITAKHRGRVEHVESNEILVRRLVEENGVEHEGELDRYPLAKFKRSNSG   720
Mu3          MEHVAARDSGAAITAKHRGRVEHVESNEILVRRLVEENGVEHEGELDRYPLAKFKRSNSG   720
MW2          MEHVAARDSGAAITAKHRGRVEHVESNEILVRRLVEENGVEHEGELDRYPLAKFKRSNSG   720
MRSA252      MEHVAARDSGAAITAKHRGRVEHVESNEILVRRLVEENGVEHEGELDRYPLAKFKRSNSG   720
             ************************************************************

JH9          TCYNQRPIVAVGDVVEYNEILADGPSMELGEMALGRNVVVGFMTWDGYNYEDAVIMSERL   780
COL          TCYNQRPIVAVGDVVEYNEILADGPSMELGEMALGRNVVVGFMTWDGYNYEDAVIMSERL   780
Mu50         TCYNQRPIVAVGDVVEYNEILADGPSMELGEMALGRNVVVGFMTWDGYNYEDAVIMSERL   780
8325         TCYNQRPIVAVGDVVEYNEILADGPSMELGEMALGRNVVVGFMTWDGYNYEDAVIMSERL   780
USA300       TCYNQRPIVAVGDVVEYNEILADGPSMELGEMALGRNVVVGFMTWDGYNYEDAVIMSERL   780
Mu3          TCYNQRPIVAVGDVVEYNEILADGPSMELGEMALGRNVVVGFMTWDGYNYEDAVIMSERL   780
MW2          TCYNQRPIVAVGDVVEYNEILADGPSMELGEMALGRNVVVGFMTWDGYNYEDAVIMSERL   780
MRSA252      TCYNQRPIVAVGDVVEFNEILADGPSMELGEMALGRNVVVGFMTWDGYNYEDAVIMSERL   780
             ****************:*******************************************

JH9          VKDDVYTSIHIEEYESEARDTKLGPEEITRDIPNVSESALKNLDDRGIVYIGAEVKDGDI   840
COL          VKDDVYTSIHIEEYESEVRDTKLGPEEITRDIPNVSESALKNLDDRGIVYIGAEVKDGDI   840
Mu50         VKDDVYTSIHIEEYESEARDTKLGPEEITRDIPNVSESALKNLDDRGIVYIGAEVKDGDI   840
8325         VKDDVYTSIHIEEYESEARDTKLGPEEITRDIPNVSESALKNLDDRGIVYIGAEVKDGDI   840
USA300       VKDDVYTSIHIEEYESEARDTKLGPEEITRDIPNVSESALKNLDDRGIVYIGAEVKDGDI   840
Mu3          VKDDVYTSIHIEEYESEARDTKLGPEEITRDIPNVSESALKNLDDRGIVYIGAEVKDGDI   840
MW2          VKDDVYTSIHIEEYESEARDTKLGPEEITRDIPNVSESALKNLDDRGIVYIGAEVKDGDI   840
MRSA252      VKDDVYTSIHIEEYESEARDTKLGPEEITRDIPNVSESALKNLDDRGIVYIGAEVKDGDI   840
             ****************.*******************************************
```

```
JH9         LVGKVTPKGVTELTAEERLLHAIFGEKAREVRDTSLRVPHGAGGIVLDVKVFNREEGDDT   900
COL         LVGKVTPKGVTELTAEERLLHAIFGEKAREVRDTLLRVPHGAGGIVLDVKVFNREEGDDT   900
Mu50        LVGKVTPKGVTELTAEERLLHAIFGEKAREVRDTSLRVPHGAGGIVLDVKVFNREEGDDT   900
8325        LVGKVTPKGVTELTAEERLLHAIFGEKAREVRDTSLRVPHGAGGIVLDVKVFNREEGDDT   900
USA300      LVGKVTPKGVTELTAEERLLHAIFGEKAREVRDTSLRVPHGAGGIVLDVKVFNREEGDDT   900
Mu3         LVGKVTPKGVTELTAEERLLHAIFGEKAREVRDTSLRVPHGAGGIVLDVKVFNREEGDDT   900
MW2         LVGKVTPKGVTELTAEERLLHAIFGEKAREVRDTSLRVPHGAGGIVLDVKVFNREEGDDT   900
MRSA252     LVGKVTPKGVTELTAEERLLHAIFGEKAREVRDTSLRVPHGAGGIVLDVKVFNREEGDDT   900
            ******************************** ************************

JH9         LSPGVNQLVRVYIVQKRKIHVGDKMCGRHGNKGVISKIVPEEDMPYLPDGRPIDIMLNPL   960
COL         LSPGVNQLVRVYIVQKRKIHVGDKMCGRHGNKGVISKIVPEEDMPYLPDGRPIDIMLNPL   960
Mu50        LSPGVNQLVRVYIVQKRKIHVGDKMCGRHGNKGVISKIVPEEDMPYLPDGRPIDIMLNPL   960
8325        LSPGVNQLVRVYIVQKRKIHVGDKMCGRHGNKGVISKIVPEEDMPYLPDGRPIDIMLNPL   960
USA300      LSPGVNQLVRVYIVQKRKIHVGDKMCGRHGNKGVISKIVPEEDMPYLPDGRPIDIMLNPL   960
Mu3         LSPGVNQLVRVYIVQKRKIHVGDKMCGRHGNKGVISKIVPEEDMPYLPDGRPIDIMLNPL   960
MW2         LSPGVNQLVRVYIVQKRKIHVGDKMCGRHGNKGVISKIVPEEDMPYLPDGRPIDIMLNPL   960
MRSA252     LSPGVNQLVRVYIVQKRKIHVGDKMCGRHGNKGVISKIVPEEDMPYLPDGRPIDIMLNPL   960
            ************************************************************

JH9         GVPSRMNIGQVLELHLGMAAKNLGIHVASPVFDGANDDDVWSTIEEAGMARDGKTVLYDG   1020
COL         GVPSRMNIGQVLELHLGMAAKNLGIHVASPVFDGANDDDVWSTIEEAGMARDGKTVLYDG   1020
Mu50        GVPSRMNIGQVLELHLGMAAKNLGIHVASPVFDGANDDDVWSTIEEAGMARDGKTVLYDG   1020
8325        GVPSRMNIGQVLELHLGMAAKNLGIHVASPVFDGANDDDVWSTIEEAGMARDGKTVLYDG   1020
USA300      GVPSRMNIGQVLELHLGMAAKNLGIHVASPVFDGANDDDVWSTIEEAGMARDGKTVLYDG   1020
Mu3         GVPSRMNIGQVLELHLGMAAKNLGIHVASPVFDGANDDDVWSTIEEAGMARDGKTVLYDG   1020
MW2         GVPSRMNIGQVLELHLGMAAKNLGIHVASPVFDGANDDDVWSTIEEAGMARDGKTVLYDG   1020
MRSA252     GVPSRMNIGQVLELHLGMAAKNLGIHVASPVFDGANDDDVWSTIEEAGMARDGKTVLYDG   1020
            ************************************************************

JH9         RTGEPFDNRISVGVMYMLKLAHMVDDKLHARSTGPYSLVTQQPLGGKAQFGGQRFGEMEV   1080
COL         RTGEPFDNRISVGVMYMLKLAHMVDDKLHARSTGPYSLVTQQPLGGKAQFGGQRFGEMEV   1080
Mu50        RTGEPFDNRISVGVMYMLKLAHMVDDKLHARSTGPYSLVTQQPLGGKAQFGGQRFGEMEV   1080
8325        RTGEPFDNRISVGVMYMLKLAHMVDDKLHARSTGPYSLVTQQPLGGKAQFGGQRFGEMEV   1080
USA300      RTGEPFDNRISVGVMYMLKLAHMVDDKLHARSTGPYSLVTQQPLGGKAQFGGQRFGEMEV   1080
Mu3         RTGEPFDNRISVGVMYMLKLAHMVDDKLHARSTGPYSLVTQQPLGGKAQFGGQRFGEMEV   1080
MW2         RTGEPFDNRISVGVMYMLKLAHMVDDKLHARSTGPYSLVTQQPLGGKAQFGGQRFGEMEV   1080
MRSA252     RTGEPFDNRISVGVMYMLKLAHMVDDKLHARSTGPYSLVTQQPLGGKAQFGGQRFGEMEV   1080
            ************************************************************
```

```
JH9          WALEAYGAAYTLQEILTYKSDDTVGRVKTYEAIVKGENISRPSVPESFRVLMKELQSLGL   1140
COL          WALEAYGAAYTLQEILTYKSDDTVGRVKTYEAIVKGENISRPSVPESFRVLMKELQSLGL   1140
Mu50         WALEAYGAAYTLQEILTYKSDDTVGRVKTYEAIVKGENISRPSVPESFRVLMKELQSLGL   1140
8325         WALEAYGAAYTLQEILTYKSDDTVGRVKTYEAIVKGENISRPSVPESFRVLMKELQSLGL   1140
USA300       WALEAYGAAYTLQEILTYKSDDTVGRVKTYEAIVKGENISRPSVPESFRVLMKELQSLGL   1140
Mu3          WALEAYGAAYTLQEILTYKSDDTVGRVKTYEAIVKGENISRPSVPESFRVLMKELQSLGL   1140
MW2          WALEAYGAAYTLQEILTYKSDDTVGRVKTYEAIVKGENISRPSVPESFRVLMKELQSLGL   1140
MRSA252      WALEAYGAAYTLQEILTYKSDDTVGRVKTYEAIVKGENISRPSVPESFRVLMKELQSLGL   1140
             ************************************************************

JH9          DVKVMDEQDNEIEMTDVDDDDVVERKVDLQQNDAPETQKEVTD   1183
COL          DVKVMDEQDNEIEMTDVDDDDVVERKVDLQQNDAPETQKEVTD   1183
Mu50         DVKVMDEQDNEIEMTDVDDDDVVERKVDLQQNDAPETQKEVTD   1183
8325         DVKVMDEQDNEIEMTDVDDDDVVERKVDLQQNDAPETQKEVTD   1183
USA300       DVKVMDEQDNEIEMTDVDDDDVVERKVDLQQNDAPETQKEVTD   1183
Mu3          DVKVMDEQDNEIEMTDVDDDDVVERKVDLQQNDAPETQKEVTD   1183
MW2          DVKVMDEQDNEIEMTDVDDDDVVERKVDLQQNDAPETQKEVTD   1183
MRSA252      DVKVMDEQDNEIEMTDVDDDDVVERKVDLQQNDAPETQKEVTD   1183
             *******************************************
```

rpoC alignment results

```
JH9          MIDVNNFHYMKIGLASPEKIRSWSFGEVKKPETINYRTLKPEKDGLFCERIFGPTKDWEC   60
USA300       MIDVNNFHYMKIGLASPEKIRSWSFGEVKKPETINYRTLKPEKDGLFCERIFGPTKDWEC   60
8325         MIDVNNFHYMKIGLASPEKIRSWSFGEVKKPETINYRTLKPEKDGLFCERIFGPTKDWEC   60
COL          MIDVNNFHYMKIGLASPEKIRSWSFGEVKKPETINYRTLKPEKDGLFCERIFGPTKDWEC   60
Mu50         MIDVNNFHYMKIGLASPEKIRSWSFGEVKKPETINYRTLKPEKDGLFCERIFGPTKDWEC   60
Mu3          MIDVNNFHYMKIGLASPEKIRSWSFGEVKKPETINYRTLKPEKDGLFCERIFGPTKDWEC   60
MW2          MIDVNNFHYMKIGLASPEKIRSWSFGEVKKPETINYRTLKPEKDGLFCERIFGPTKDWEC   60
MRSA252      MIDVNNFHYMKIGLASPEKIRSWSFGEVKKPETINYRTLKPEKDGLFCERIFGPTKDWEC   60
             ************************************************************

JH9          SCGKYKRVRYKGMVCDRCGVEVTKSKVRRERMGHIELAAPVSHIWYFKGIPSRMGLLLDM   120
USA300       SCGKYKRVRYKGMVCDRCGVEVTKSKVRRERMGHIELAAPVSHIWYFKGIPSRMGLLLDM   120
8325         SCGKYKRVRYKGMVCDRCGVEVTKSKVRRERMGHIELAAPVSHIWYFKGIPSRMGLLLDM   120
COL          SCGKYKRVRYKGMVCDRCGVEVTKSKVRRERMGHIELAAPVSHIWYFKGIPSRMGLLLDM   120
Mu50         SCGKYKRVRYKGMVCDRCGVEVTKSKVRRERMGHIELAAPVSHIWYFKGIPSRMGLLLDM   120
Mu3          SCGKYKRVRYKGMVCDRCGVEVTKSKVRRERMGHIELAAPVSHIWYFKGIPSRMGLLLDM   120
MW2          SCGKYKRVRYKGMVCDRCGVEVTKSKVRRERMGHIELAAPVSHIWYFKGIPSRMGLLLDM   120
MRSA252      SCGKYKRVRYKGMVCDRCGVEVTKSKVRRERMGHIELAAPVSHIWYFKGIPSRMGLLLDM   120
             ************************************************************
```

```
JH9          SPRALEEVIYFASYVVVDPGPTGLEKKTLLSEAEFRDYYDKYPGQFVAKMGAEGIKDLLE   180
USA300       SPRALEEVIYFASYVVVDPGPTGLEKKTLLSEAEFRDYYDKYPGQFVAKMGAEGIKDLLE   180
8325         SPRALEEVIYFASYVVVDPGPTGLEKKTLLSEAEFRDYYDKYPGQFVAKMGAEGIKDLLE   180
COL          SPRALEEVIYFASYVVVDPGPTGLEKKTLLSEAEFRDYYDKYPGQFVAKMGAEGIKDLLE   180
Mu50         SPRALEEVIYFASYVVVDPGPTGLEKKTLLSEAEFRDYYDKYPGQFVAKMGAEGIKDLLE   180
Mu3          SPRALEEVIYFASYVVVDPGPTGLEKKTLLSEAEFRDYYDKYPGQFVAKMGAEGIKDLLE   180
MW2          SPRALEEVIYFASYVVVDPGPTGLEKKTLLSEAEFRDYYDKYPGQFVAKMGAEGIKDLLE   180
MRSA252      SPRALEEVIYFASYVVVDPGPTGLEKKTLLSEAEFRDYYDKYPGQFVAKMGAEGIKDLLE   180
             ************************************************************

JH9          EIDLDEELKLLRDELESATGQRLTRAIKRLEVVESFRNSGNKPSWMILDVLPIIPPEIRP   240
USA300       EIDLDEELKLLRDELESATGQRLTRAIKRLEVVESFRNSGNKPSWMILDVLPIIPPEIRP   240
8325         EIDLDEELKLLRDELESATGQRLTRAIKRLEVVESFRNSGNKPSWMILDVLPIIPPEIRP   240
COL          EIDLDEELKLLRDELESATGQRLTRAIKRLEVVESFRNSGNKPSWMILDVLPIIPPEIRP   240
Mu50         EIDLDEELKLLRDELESATGQRLTRAIKRLEVVESFRNSGNKPSWMILDVLPIIPPEIRP   240
Mu3          EIDLDEELKLLRDELESATGQRLTRAIKRLEVVESFRNSGNKPSWMILDVLPIIPPEIRP   240
MW2          EIDLDEELKLLRDELESATGQRLTRAIKRLEVVESFRNSGNKPSWMILDVLPIIPPEIRP   240
MRSA252      EIDLDEELKLLRDELESATGQRLTRAIKRLEVVESFRNSGNKPSWMILDVLPIIPPEIRP   240
             ************************************************************

JH9          MVQLDGGRFATSDLNDLYRRVINRNNRLKRLLDLGAPGIIVQNEKRMLQEAVDALIDNGR   300
USA300       MVQLDGGRFATSDLNDLYRRVINRNNRLKRLLDLGAPGIIVQNEKRMLQEAVDALIDNGR   300
8325         MVQLDGGRFATSDLNDLYRRVINRNNRLKRLLDLGAPGIIVQNEKRMLQEAVDALIDNGR   300
COL          MVQLDGGRFATSDLNDLYRRVINRNNRLKRLLDLGAPGIIVQNEKRMLQEAVDALIDNGR   300
Mu50         MVQLDGGRFATSDLNDLYRRVINRNNRLKRLLDLGAPGIIVQNEKRMLQEAVDALIDNGR   300
Mu3          MVQLDGGRFATSDLNDLYRRVINRNNRLKRLLDLGAPGIIVQNEKRMLQEAVDALIDNGR   300
MW2          MVQLDGGRFATSDLNDLYRRVINRNNRLKRLLDLGAPGIIVQNEKRMLQEAVDALIDNGR   300
MRSA252      MVQLDGGRFATSDLNDLYRRVINRNNRLKRLLDLGAPGIIVQNEKRMLQEAVDALIDNGR   300
             ************************************************************

JH9          RGRPVTGPGNRPLKSLSHMLKGKQGRFRQNLLGKRVDYSGRSVIAVGPSLKMYQCGLPKE   360
USA300       RGRPVTGPGNRPLKSLSHMLKGKQGRFRQNLLGKRVDYSGRSVIAVGPSLKMYQCGLPKE   360
8325         RGRPVTGPGNRPLKSLSHMLKGKQGRFRQNLLGKRVDYSGRSVIAVGPSLKMYQCGLPKE   360
COL          RGRPVTGPGNRPLKSLSHMLKGKQGRFRQNLLGKRVDYSGRSVIAVGPSLKMYQCGLPKE   360
Mu50         RGRPVTGPGNRPLKSLSHMLKGKQGRFRQNLLGKRVDYSGRSVIAVGPSLKMYQCGLPKE   360
Mu3          RGRPVTGPGNRPLKSLSHMLKGKQGRFRQNLLGKRVDYSGRSVIAVGPSLKMYQCGLPKE   360
MW2          RGRPVTGPGNRPLKSLSHMLKGKQGRFRQNLLGKRVDYSGRSVIAVGPSLKMYQCGLPKE   360
MRSA252      RGRPVTGPGNRPLKSLSHMLKGKQGRFRQNLLGKRVDYSGRSVIAVGPSLKMYQCGLPKE   360
             ************************************************************
```

```
JH9         MALELFKPFVMKELVQREIATNIKNAKSKIERMDDEVWDVLEEVIREHPVLLNRAPTLHR   420
USA300      MALELFKPFVMKELVQREIATNIKNAKSKIERMDDEVWDVLEEVIREHPVLLNRAPTLHR   420
8325        MALELFKPFVMKELVQREIATNIKNAKSKIERMDDEVWDVLEEVIREHPVLLNRAPTLHR   420
COL         MALELFKPFVMKELVQREIATNIKNAKSKIERMDDEVWDVLEEVIREHPVLLNRAPTLHR   420
Mu50        MALELFKPFVMKELVQREIATNIKNAKSKIERMDDEVWDVLEEVIREHPVLLNRAPTLHR   420
Mu3         MALELFKPFVMKELVQREIATNIKNAKSKIERMDDEVWDVLEEVIREHPVLLNRAPTLHR   420
MW2         MALELFKPFVMKELVQREIATNIKNAKSKIERMDDEVWDVLEEVIREHPVLLNRAPTLHR   420
MRSA252     MALELFKPFVMKELVQREIATNIKNAKSKIERMDDEVWDVLEEVIREHPVLLNRAPTLHR   420
            ************************************************************

JH9         LGIQAFEPTLVEGRAIRLHPLVTTAYNADFDGDQMAVHVPLSKEAQAEARMLMLAAQNIL   480
USA300      LGIQAFEPTLVEGRAIRLHPLVTTAYNADFDGDQMAVHVPLSKEAQAEARMLMLAAQNIL   480
8325        LGIQAFEPTLVEGRAIRLHPLVTTAYNADFDGDQMAVHVPLSKEAQAEARMLMLAAQNIL   480
COL         LGIQAFEPTLVEGRAIRLHPLVTTAYNADFDGDQMAVHVPLSKEAQAEARMLMLAAQNIL   480
Mu50        LGIQAFEPTLVEGRAIRLHPLVTTAYNADFDGDQMAVHVPLSKEAQAEARMLMLAAQNIL   480
Mu3         LGIQAFEPTLVEGRAIRLHPLVTTAYNADFDGDQMAVHVPLSKEAQAEARMLMLAAQNIL   480
MW2         LGIQAFEPTLVEGRAIRLHPLVTTAYNADFDGDQMAVHVPLSKEAQAEARMLMLAAQNIL   480
MRSA252     LGIQAFEPTLVEGRAIRLHPLVTTAYNADFDGDQMAVHVPLSKEAQAEARMLMLAAQNIL   480
            ************************************************************

JH9         NPKDGKPVVTPSQDMVLGNYYLTLERKDAVNTGAIFNNTNEVLKAYANGFVHLHTRIGVH   540
USA300      NPKDGKPVVTPSQDMVLGNYYLTLERKDAVNTGAIFNNTNEVLKAYANGFVHLHTRIGVH   540
8325        NPKDGKPVVTPSQDMVLGNYYLTLERKDAVNTGAIFNNTNEVLKAYANGFVHLHTRIGVH   540
COL         NPKDGKPVVTPSQDMVLGNYYLTLERKDAVNTGAIFNNTNEVLKAYANGFVHLHTRIGVH   540
Mu50        NPKDGKPVVTPSQDMVLGNYYLTLERKDAVNTGAIFNNTNEVLKAYANGFVHLHTRIGVH   540
Mu3         NPKDGKPVVTPSQDMVLGNYYLTLERKDAVNTGAIFNNTNEVLKAYANGFVHLHTRIGVH   540
MW2         NPKDGKPVVTPSQDMVLGNYYLTLERKDAVNTGAIFNNTNEVLKAYANGFVHLHTRIGVH   540
MRSA252     NPKDGKPVVTPSQDMVLGNYYLTLERKDAVNTGAIFNNTNEVLKAYANGFVHLHTRIGVH   540
            ************************************************************

JH9         ASSFNNPTFTEEQNKKILATSVGKIIFNEIIPDSFAYINEPTQENLERKTPNRYFIDPTT   600
USA300      ASSFNNPTFTEEQNKKILATSVGKIIFNEIIPDSFAYINEPTQENLERKTPNRYFIDPTT   600
8325        ASSFNNPTFTEEQNKKILATSVGKIIFNEIIPDSFAYINEPTQENLERKTPNRYFIDPTT   600
COL         ASSFNNPTFTEEQNKKILATSVGKIIFNEIIPDSFAYINEPTQENLERKTPNRYFIDPTT   600
Mu50        ASSFNNPTFTEEQNKKILATSVGKIIFNEIIPDSFAYINEPTQENLERKTPNRYFIDPTT   600
Mu3         ASSFNNPTFTEEQNKKILATSVGKIIFNEIIPDSFAYINEPTQENLERKTPNRYFIDPTT   600
MW2         ASSFNNPTFTEEQNKKILATSVGKIIFNEIIPDSFAYINEPTQENLERKTPNRYFIDPTT   600
MRSA252     ASSFNNPTFTEEQNKKILATSVGKIIFNEIIPDSFAYINEPTQENLERKTPNRYFIDPTT   600
            ************************************************************
```

```
JH9         LGEGGLKEYFENEELIEPFNKKFLGNIIAEVFNRFSITDTSMMLDRMKDLGFKFSSKAGI   660
USA300      LGEGGLKEYFENEELIEPFNKKFLGNIIAEVFNRFSITDTSMMLDRMKDLGFKFSSKAGI   660
8325        LGEGGLKEYFENEELIEPFNKKFLGNIIAEVFNRFSITDTSMMLDRMKDLGFKFSSKAGI   660
COL         LGEGGLKEYFENEELIEPFNKKFLGNIIAEVFNRFSITDTSMMLDRMKDLGFKFSSKAGI   660
Mu50        LGEGGLKEYFENEELIEPFNKKFLGNIIAEVFNRFSITDTSMMLDRMKDLGFKFSSKAGI   660
Mu3         LGEGGLKEYFENEELIEPFNKKFLGNIIAEVFNRFSITDTSMMLDRMKDLGFKFSSKAGI   660
MW2         LGEGGLKEYFENEELIEPFNKKFLGNIIAEVFNRFSITDTSMMLDRMKDLGFKFSSKAGI   660
MRSA252     LGEGGLKEYFENEELIEPFNKKFLGNIIAEVFNRFSITDTSMMLDRMKDLGFKFSSKAGI   660
            ************************************************************

JH9         TVGVADIVVLPDKQQILDEHEKLVDRITKQFNRGLITEEERYNAVVEIWTDAKDQIQGEL   720
USA300      TVGVADIVVLPDKQQILDEHEKLVDRITKQFNRGLITEEERYNAVVEIWTDAKDQIQGEL   720
8325        TVGVADIVVLPDKQQILDEHEKLVDRITKQFNRGLITEEERYNAVVEIWTDAKDQIQGEL   720
COL         TVGVADIVVLPDKQQILDEHEKLVDRITKQFNRGLITEEERYNAVVEIWTDAKDQIQGEL   720
Mu50        TVGVADIVVLPDKQQILDEHEKLVDRITKQFNRGLITEEERYNAVVEIWTDAKDQIQGEL   720
Mu3         TVGVADIVVLPDKQQILDEHEKLVDRITKQFNRGLITEEERYNAVVEIWTDAKDQIQGEL   720
MW2         TVGVADIVVLPDKQQILDEHEKLVDRITKQFNRGLITEEERYNAVVEIWTDAKDQIQGEL   720
MRSA252     TVGVADIVVLPDKQQILDEHEKLVDRITKQFNRGLITEEERYNAVVEIWTDAKDQIQGEL   720
            ************************************************************

JH9         MQSLDKTNPIFMMSDSGARGNASNFTQLAGMRGLMAAPSGKIIELPITSSFREGLTVLEY   780
USA300      MQSLDKTNPIFMMSDSGARGNASNFTQLAGMRGLMAAPSGKIIELPITSSFREGLTVLEY   780
8325        MQSLDKTNPIFMMSDSGARGNASNFTQLAGMRGLMAAPSGKIIELPITSSFREGLTVLEY   780
COL         MQSLDKTNPIFMMSDSGARGNASNFTQLAGMRGLMAAPSGKIIELPITSSFREGLTVLEY   780
Mu50        MQSLDKTNPIFMMSDSGARGNASNFTQLAGMRGLMAAPSGKIIELPITSSFREGLTVLEY   780
Mu3         MQSLDKTNPIFMMSDSGARGNASNFTQLAGMRGLMAAPSGKIIELPITSSFREGLTVLEY   780
MW2         MQSLDKTNPIFMMSDSGARGNASNFTQLAGMRGLMAAPSGKIIELPITSSFREGLTVLEY   780
MRSA252     MQSLDKTNPIFMMSDSGARGNASNFTQLAGMRGLMAAPSGKIIELPITSSFREGLTVLEY   780
            ************************************************************

JH9         FISTHGARKGLADTALKTADSGYLTRRLVDVAQDVIVREEDCGTDRGLLVSDIKEGTEMI   840
USA300      FISTHGARKGLADTALKTADSGYLTRRLVDVAQDVIVREEDCGTDRGLLVSDIKEGTEMI   840
8325        FISTHGARKGLADTALKTADSGYLTRRLVDVAQDVIVREEDCGTDRGLLVSDIKEGTEMI   840
COL         FISTHGARKGLADTALKTADSGYLTRRLVDVAQDVIVREEDCGTDRGLLVSDIKEGTEMI   840
Mu50        FISTHGARKGLADTALKTADSGYLTRRLVDVAQDVIVREEDCGTDRGLLVSDIKEGTEMI   840
Mu3         FISTHGARKGLADTALKTADSGYLTRRLVDVAQDVIVREEDCGTDRGLLVSDIKEGTEMI   840
MW2         FISTHGARKGLADTALKTADSGYLTRRLVDVAQDVIVREEDCGTDRGLLVSDIKEGTEMI   840
MRSA252     FISTHGARKGLADTALKTADSGYLTRRLVDVAQDVIVREEDCGTDRGLLVSDIKEGTEMI   840
            ************************************************************
```

```
JH9         EPFIERIEGRYSKKTIRHPETDEIIIRPDELITPEIAKKITDAGIEQMYIRSAFTCNARH   900
USA300      EPFIERIEGRYSKETIHHPETDEIIIRPDELITPEIAKKITDAGIEQMYIRSAFTCNARH   900
8325        EPFIERIEGRYSKETIRHPETDEIIIRPDELITPEIAKKITDAGIEQMYIRSAFTCNARH   900
COL         EPFIERIEGRYSKETIRHPETDEIIIRPDELITPEIAKKITDAGIEQMYIRSAFTCNARH   900
Mu50        EPFIERIEGRYSKETIRHPETDEIIIRPDELITPEIAKKITDAGIEQMYIRSAFTCNARH   900
Mu3         EPFIERIEGRYSKETIRHPETDEIIIRPDELITPEIAKKITDAGIEQMYIRSAFTCNARH   900
MW2         EPFIERIEGRYSKETIRHPETDEIIIRPDELITPEIAKKITDAGIEQMYIRSAFTCNARH   900
MRSA252     EPFIERIEGRYSKETIRHPETDEVIIRPDELITPEIAKKITDAGIEQMYIRSAFTCNARH   900
            *************:**:******:************************************

JH9         GVCEKCYGKNLATGEKVEVGEAVGTIAAQSIGEPGTQLTMRTFHTGGVAGSDITQGLPRI   960
USA300      GVCEKCYGKNLATGEKVEVGEAVGTIAAQSIGEPGTQLTMRTFHTGGVAGSDITQGLPRI   960
8325        GVCEKCYGKNLATGEKVEVGEAVGTIAAQSIGEPGTQLTMRTFHTGGVACSDITQGLPRI   960
COL         GVCEKCYGKNLATGEKVEVGEAVGTIAAQSIGEPGTQLTMRTFHTGGVAGSDITQGLPRI   960
Mu50        GVCEKCYGKNLATGEKVEVGEAVGTIAAQSIGEPGTQLTMRTFHTGGVAGSDITQGLPRI   960
Mu3         GVCEKCYGKNLATGEKVEVGEAVGTIAAQSIGEPGTQLTMRTFHTGGVAGSDITQGLPRI   960
MW2         GVCEKCYGKNLATGEKVEVGEAVGTIAAQSIGEPGTQLTMRTFHTGGVAGSDITQGLPRI   960
MRSA252     GVCEKCYGKNLATGEKVEVGEAVGTIAAQSIGEPGTQLTMRTFHTGGVAGSDITQGLPRI   960
            ************************************************************

JH9         QEIFEARNPKGQAVITEIEGVVEDIKLAKDRQQEIVVKGANETRSYLASGTSRIIVEIGQ   1020
USA300      QEIFEARNPKGQAVITEIEGVVEDIKLAKDRQQEIVVKGANETRSYLASGTSRIIVEIGQ   1020
8325        QEIFEARNPKGQAVITEIEGVVEDIKLAKDRQQEIVVKGANETRSYLASGTSRIIVEIGQ   1020
COL         QEIFEARNPKGQAVITEIEGVVEDIKLAKDRQQEIVVKGANETRSYLASGTSRIIVEIGQ   1020
Mu50        QEIFEARNPKGQAVITEIEGVVEDIKLAKDRQQEIVVKGANETRSYLASGTSRIIVEIGQ   1020
Mu3         QEIFEARNPKGQAVITEIEGVVEDIKLAKDRQQEIVVKGANETRSYLASGTSRIIVEIGQ   1020
MW2         QEIFEARNPKGQAVITEIEGVVEDIKLAKDRQQEIVVKGANETRSYLASGTSRIIVEIGQ   1020
MRSA252     QEIFEARNPKGQAVITEIEGVVEDIKLAKDRQQEIVVKGANETRSYLASGTSRIIVEIGQ   1020
            ************************************************************

JH9         PVQRGEVLTEGSIEPKNYLSVAGLNATESYLLKEVQKVYRMQGVEIDDKHVEVMVRQMLR   1080
USA300      PVQRGEVLTEGSIEPKNYLSVAGLNATESYLLKEVQKVYRMQGVEIDDKHVEVMVRQMLR   1080
8325        PVQRGEVLTEGSIEPKNYLSVAGLNATESYLLKEVQKVYRMQGVEIDDKHVEVMVRQMLR   1080
COL         PVQRGEVLTEGSIEPKNYLSVAGLNATESYLLKEVQKVYRMQGVEIDDKHVEVMVRQMLR   1080
Mu50        PVQRGEVLTEGSIEPKNYLSVAGLNATESYLLKEVQKVYRMQGVEIDDKHVEVMVRQMLR   1080
Mu3         PVQRGEVLTEGSIEPKNYLSVAGLNATESYLLKEVQKVYRMQGVEIDDKHVEVMVRQMLR   1080
MW2         PVQRGEVLTEGSIEPKNYLSVAGLNATESYLLKEVQKVYRMQGVEIDDKHVEVMVRQMLR   1080
MRSA252     PVQRGEVLTEGSIEPKNYLSVAGLNATESYLLKEVQKVYRMQGVEIDDKHVEVMVRQMLR   1080
            ************************************************************
```

```
JH9          KVRIIEAGDTKLLPGSLVDIHNFTDANREAFKHRKRPATAKPVLLGITKASLETESFLSA   1140
USA300       KVRIIEAGDTKLLPGSLVDIHNFTDANREAFKHRKRPATAKPVLLGITKASLETESFLSA   1140
8325         KVRIIEAGDTKLLPGSLVDIHNFTDANREAFKHRKRPATAKPVLLGITKASLETESFLSA   1140
COL          KVRIIEAGDTKLLPGSLVDIHNFTDANREAFKHRKRPATAKPVLLGITKASLETESFLSA   1140
Mu50         KVRIIEAGDTKLLPGSLVDIHNFTDANREAFKHRKRPATAKPVLLGITKASLETESFLSA   1140
Mu3          KVRIIEAGDTKLLPGSLVDIHNFTDANREAFKHRKRPATAKPVLLGITKASLETESFLSA   1140
MW2          KVRIIEAGDTKLLPGSLVDIHNFTDANREAFKHRKRPATAKPVLLGITKASLETESFLSA   1140
MRSA252      KVRIIEAGDTKLLPGSLVDIHNFTDANREAFKHRKRPATAKPVLLGITKASLETESFLSA   1140
             ************************************************************

JH9          ASFQETTRVLTDAAIKGKRDDLLGLKENVIIGKLIPAGTGMRRYSDVKYEKTAKPVAEVE   1200
USA300       ASFQETTRVLTDAAIKGKRDDLLGLKENVIIGKLIPAGTGMRRYSDVKYEKTAKPVAEVE   1200
8325         ASFQETTRVLTDAAIKGKRDDLLGLKENVIIGKLIPAGTGMRRYSDVKYEKTAKPVAEVE   1200
COL          ASFQETTRVLTDAAIKGKRDDLLGLKENVIIGKLIPAGTGMRRYSDVKYEKTAKPVAEVE   1200
Mu50         ASFQETTRVLTDAAIKGKRDDLLGLKENVIIGKLIPAGTGMRRYSDVKYEKTAKPVAEVE   1200
Mu3          ASFQETTRVLTDAAIKGKRDDLLGLKENVIIGKLIPAGTGMRRYSDVKYEKTAKPVAEVE   1200
MW2          ASFQETTRVLTDAAIKGKRDDLLGLKENVIIGKLIPAGTGMRRYSDVKYEKTAKPVAEVE   1200
MRSA252      ASFQETTRVLTDAAIKGKRDDLLGLKENVIIGKLIPAGTGMRRYSDVKYEKTAKPVAEVE   1200
             ************************************************************

JH9          SQTEVTE     1207
USA300       SQTEVTE     1207
8325         SQTEVTE     1207
COL          SQTEVTE     1207
Mu50         SQTEVTE     1207
Mu3          SQTEVTE     1207
MW2          SQTEVTE     1207
MRSA252      SQTEVTE     1207
             *******
```

Appendix 3

Alignment of *rpoB* and *rpoC* amino acid sequences using Clustal Omega tool. The amino acid sequence of *rpoB* and *rpoC* from *Bacillus subtilis*, *Escherichia coli*, *and Thermus aquaticus* was aligned with *S. aureus* NCTC8325 (MSSA) strain. Identified amino acid substitutions from strains listed in Table 4.3 and Table 4.4 are highlighted in green and yellow, respectively. Asterisks indicate fully conserved residues, colons indicate conservative substitutions with strongly similar properties, periods indicate semi conservative substitutions with weakly similar properties and gaps indicate not conserved residues.

***rpoB* alignment results**

```
E. coli           ---MVYSYTEKKRIRKDFGKRPQVLDVPYLLSIQLDSFQKFIEQDP----EGQYGLEAAF      53
T. aquaticus      ------------MEIKRFGRIREVIPLPPLTEIQVESYKKALQADVPPEKRENVGIQAAF      48
S. aureus         MAGQVVQY-GRHRKRRNYARISEVLELPNLIEIQTKSYEWFLRE----------GLIEMF      49
B. subtilis       MTGQLVQY-GRHRQRRSYARISEVLELPNLIEIQTSSYQWFLDE----------GLREMF      49
                               : :.:  :*: :* * .** .*::  :           *:   *

E. coli           RSVFPIQS---YSGNSELQYVSYRLGEPVFDVQECQIRGVTYSAPLRVKLRLVIYEREAP      110
T. aquaticus      KETFPIEEGDKGKGGLVLDFLEYRIGDPPFSQDECREKDLTYQAPLYARLQLIHKDT---      105
S. aureus         RDISPIED---FTGNLSLEFVDYRLGEPKYDLEESKNRDATYAAPLRVKVRLIIKET---      103
B. subtilis       QDISPIED---FTGNLSLEFIDYSLGEPKYPVEESKERDVTYSAPLRVKVRLINKET---      103
                  :.  **:.    .*.  *::::.* :*:* :  :*.: :. ** *** .:::*:  :

E. coli           EGTVKDIKEQEVYMGEIPLMTDNGTFVINGTERVIVSQLHRSPGVFFDSDKGKTHSSGKV      170
T. aquaticus      ----GLIKEDEVFLGHLPLMTEDGSFIINGADRVIVSQIHRSPGVYFTPDP---ARPGRY      158
S. aureus         ----GEVKEQEVFMGDFPLMTDTGTFVINGAERVIVSQLVRSPSVYFNEKI---DKNGRE      156
B. subtilis       ----GEVKDQDVFMGDFPIMTDTGTFIINGAERVIVSQLVRSPSVYFSGKV---DKNGKK      156
                        :*:::*::*.:*:**: *:*:***::******: ***.*:*  .       *:

E. coli           LYNARIIPYRGSWLDFEFDPKDNLFVRIDRRRKLPATIILRALNYTTEQILDLFFEKVIF      230
T. aquaticus      IASIIPLPKRGPWIDLEVEASGVVTMKVN-KRKFPLVLLLRVLGYDQETLVRELSAY---      214
S. aureus         NYDATIIPNRGAWLEYETDAKDVVYVRIDRTRKLPLTVLLRALGFSSDQEIVDLLGD---      213
B. subtilis       GFTATVIPNRGAWLEYETDAKDVVYVRIDRTRKLPVTVLLRALGFGSDQEILDLIGE---      213
                        :* ** *:: * : .. : ::::  **:* .::**.*.:  :  :  :
```

```
E. coli          EIRDNKLQMELVPERLRGETASFDIEANGKVYVEKGRRITARHIRQLEKDDVKLIEVPVE      290
T. aquaticus     ------------------------------------------------------------      214
S. aureus        ------------------------------------------------------------      213
B. subtilis      ------------------------------------------------------------      213

E. coli          YIAGKVVAKDYIDESTGELICAANMELSLDLLAKLSQSGHKRIETLFTNDLDHGPYISET      350
T. aquaticus     -----------------------------------------------------GDLVQGL      221
S. aureus        -----------------------------------------------------NEYLRNT      220
B. subtilis      -----------------------------------------------------NEYLRNT      220
                                                                       .  :

E. coli          LRVD-PTNDRLSALVEIYRMMRPGEPPTREAAESLFENLFFSEDRYDLSAVGRMKFNRSL      409
T. aquaticus     LDEAVLAMRPEEAMVRLFTLLRPGDPPKKDKALAYLFGLLADPKRYDLGEAGRYKAEEKL      281
S. aureus        LEKDG-TENTEQALLEIYERLRPGEPPTVENAKSLLYSRFFDPKRYDLASVGRYKTNKKL      279
B. subtilis      LDKDN-TENSDKALLEIYERLRPGEPPTVENAKSLLDSRFFDPKRYDLANVGRYKINKKL      279
                 *     :    .*::.::  :***:**. : * : : . : . .****. .** * :..*

E. coli          LREEIE--------------GS----------------------------------------      417
T. aquaticus     GVGLSG------RTLVRFEDGE----------------------------------------      297
S. aureus        HLKHRLFNQKLAEPIVNTETGEIVVEEGTVLDRRKIDEIMDVLESNANSEVFELHGSVID      339
B. subtilis      HIKNRLFNQRLAETLVDPETGEILAEKGQILDRRTLDKVLPYLENGIGFRKLYPNGGVVE      339
                               *.

E. coli          -----------------------------------GILSKDDIIDVMKKLIDIRNGKG--E      441
T. aquaticus     -----------------------------------FKDEVFLPTLRYLFALTAGVPGHE      321
S. aureus        EPVEIQSIKVYVPNDDEGRT-TTVIGNAFPDSEVKCITPADIIASMSYFFNLLSGIG--Y      396
B. subtilis      DEVTLQSIKIFAPTDQEGEQVINVIGNAYIEEEIKNITPADIISSISYFFNLLHGVG--D      397
                                                :.   ::  :  :: :  *

E. coli          VDDIDHLGNRRIRSVGEMAENQFRVGLVRVERAVKERLSLGDLDTLMPQDMINAKPISAA      501
T. aquaticus     VDDIDHLGNRRIRTVGELMADQFRVGLARLARGVRERMVMGSPDTLTPAKLVNSRPLEAA      381
S. aureus        TDDIDHLGNRRLRSVGELLQNQFRIGLSRMERVVRERMSIQDTESITPQQLINIRPVIAS      456
B. subtilis      TDDIDHLGNRRLRSVGELLQNQFRIGLSRMERVVRERMSIQDTNTITPQQLINIRPVIAS      457
                 .**********:*:***:  :***:** *: * *:**: : . ::: * .::* :*: *:

E. coli          VKEFFGSSQLSQFMDQNNPLSEITHKRRISALGPGGLTRERAGFEVRDVHPTHYGRVCPI      561
T. aquaticus     LREFFSRSQLSQFKDETNPLSSLRHKRRISALGPGGLTRERAGFDVRDVHRTHYGRICPV      441
S. aureus        IKEFFGSSQLSQFMDQANPLAELTHKRRLSALGPGGLTRERAQMEVRDVHYSHYGRMCPI      516
B. subtilis      IKEFFGSSQLSQFMDQTNPLAELTHKRRLSALGPGGLTRERAGMEVRDVHYSHYGRMCPI      517
                 ::***. ****** *: ***:.: ****:************** ::***** :****:**:
```

```
E. coli          ETPEGPNIGLINSLSVYAQTNEYGFLETPYRKVT--DGVVTDEIHYLSAIEEGNYVIAQA      619
T. aquaticus     ETPEGANIGLITSLAAYARVDALGFIRTPYRRVK--NGVVTEEVVYMTASEEDRYTIAQA      499
S. aureus        ETPEGPNIGLINSLSSYARVNEFGFIETPYRKVDLDTHAITDQIDYLTADEEDSYVVAQA      576
B. subtilis      ETPEGPNIGLINSLSSYAKVNRFGFIETPYRRVDPETGKVTGRIDYLTADEEDNYVVAQA      577
                 ***** *****.**: **:.:  **:.****:*      :* .: *::* **. *.:***

E. coli          NSNLDEEGHFVEDLVTCRSKGESSLFSRDQVDYMDVSTQQVVSVGASLIPFLEHDDANRA      679
T. aquaticus     NTPLEGD-RIATDRVVARRRGEPVIVAPEEVEFMDVSPKQVFSLNTNLIPFLEHDDANRA      558
S. aureus        NSKLDENGRFMDDEVVCRFRGNNTVMAKEKMDYMDVSPKQVVSAATACIPFLENDDSNRA      636
B. subtilis      NARLDDEGAFIDDSIVARFRGENTVVSRNRVDYMDVSPKQVVSAATACIPFLENDDSNRA      637
                 *: *: :  :  * :..* :*:  :.: :.:::**** :**.*  :  *****:**:***

E. coli          LMGANMQRQAVPTLRADKPLVGTGMERAVAVDSGVTAVAKRGGVVQYVDASRIVIKVNED      739
T. aquaticus     LMGSNMQTQAVPLIRAQAPVVMTGLEERVVRDSLAALYAEEDGEVVKVDGTRIAVRY---      615
S. aureus        LMGANMQRQAVPLMNPEAPFVGTGMEHVAARDSGAAITAKHRGRVEHVESNEILVRRLVE      696
B. subtilis      LMGANMQRQAVPLMQPEAPFVGTGMEYVSGKDSGAAVICKHPGIVERVEAKNVWVRRYEE      697
                 ***:*** **** :. : *.* **:*     ** .:  .:. * *  *:...: ::

E. coli          -EMYPGEAGIDIYNLTKYTRSNQNTCINQMPCVSLGEPVERGDVLADGPSTDLGELALGQ      798
T. aquaticus     -----EDGRLVEHPLRRYARSNQGTAFDQRPRVRVGQRVKKGDLLADGPASEEGFLALGQ      670
S. aureus        ENGVEHEGELDRYPLAKFKRSNSGTCYNQRPIVAVGDVVEYNEILADGPSMELGEMALGR      756
B. subtilis      VDGQKVKGNLDKYSLLKFVRSNQGTCYNQRPIVSVGDEVVKGEILADGPSMELGELALGR      757
                       .. :  : * :: ***..*. :* * * :*: *  .::*****: : * :***:
E. coli          NMRVAFMPWNGYNFEDSILVSERVVQEDRFTTIHIQELACVSRDTKLGPEEITADIPNVG      858
T. aquaticus     NVLVAIMPFDGYNFEDAIVISEELLKRDFYTSIHIERYEIEARDTKLGPERITRDIPHLS      730
S. aureus        NVVVGFMTWDGYNYEDAVIMSERLVKDDVYTSIHIEEYESEARDTKLGPEEITRDIPNVS      816
B. subtilis      NVMVGFMTWDGYNYEDAIIMSERLVKDDVYTSIHIEEYESEARDTKLGPEEITRDIPNVG      817
                 *: *.:* ::***:**::::**.::: * :*:***:.    :********.** ***::.

E. coli          EAALSKLDESGIVYIGAEVTGGDILVGKVTPKGETQLTPEEKLLRAIFGEKASDVKDSSL      918
T. aquaticus     EAALRDLDEEGIVRIGAEVKPGDILVGRTSFKGEQEPSPEERLLRSIFGEKARDVKDTSL      790
S. aureus        ESALKNLDDRGIVYIGAEVKDGDILVGKVTPKGVTELTAEERLLHAIFGEKAREVRDTSL      876
B. subtilis      EDALRNLDDRGIIRIGAEVKDGDLLVGKVTPKGVTELTAEERLLHAIFGEKAREVRDTSL      877
                 * ** .**: **: *****. **:***:.: **  : : **:**::****** :*:*:**

E. coli          RVPNGVSGTVIDVQVFTRDGVEKDKRALEIEEMQLKQAKKDLSEELQILEAGLFSRIRAV      978
T. aquaticus     RVPPGEGGIVVGRLRLRRGD----------------------------------------      810
S. aureus        RVPHGAGGIVLDVKVFNREE----------------------------------------      896
B. subtilis      RVPHGGGGIIHDVKVFNRED----------------------------------------      897
                 *** * .* : .   : *
```

```
E. coli          LVAGGVEAEKLDKLPRDRWLELGLTDEEKQNQLEQLAEQYDELKHEFEKKLEAKRRKITQ      1038
T. aquaticus     ------------------------------------------------------------P      811
S. aureus        ------------------------------------------------------------G      897
B. subtilis      ------------------------------------------------------------G      898


E. coli          GDDLAPGVLKIVKVYLAVKRRIQPGDKMAGRHGNKGVISKINPIEDMPYDENGTPVDIVL      1098
T. aquaticus     GVELKPGVREVVRVFVAQKRKLQVGDKLANRHGNKGVVAKILPVEDMPHLPDGTPVDVIL      871
S. aureus        DDTLSPGVNQLVRVYIVQKRKIHVGDKMCGRHGNKGVISKIVPEEDMPYLPDGRPIDIML      957
B. subtilis      D-ELPPGVNQLVRVYIVQKRKISEGDKMAGRHGNKGVISKILPEEDMPYLPDGTPIDIML      957
                 .  * *** ::*:*::. **::  ***:..*******::** * ****:  :* *:*::*

E. coli          NPLGVPSRMNIGQILETHLGMAAKGIGDKINAMLKQQQEVAKLREFIQRAYDLGADVRQK      1158
T. aquaticus     NPLGVPSRMNLGQILETHLGLAGYFLGQRYISPVFDGATEPEIKELLAEAFNLYFGKRQG      931
S. aureus        NPLGVPSRMNIGQVLELHLGMAAKNLGIHVASPVFDGANDDDVWSTIEEA----------      1007
B. subtilis      NPLGVPSRMNIGQVLELHMGMAARYLGIHIASPVFDGAREEDVWETLEEA----------      1007
                 **********:**:** *:*:*.  :* :  : : :     .: . : .*
E. coli          VDLSTFS-DEEVMRLAENLRKGMPIATPVFDGAKEAEIKELLKLGDLPTSGQIRLYDGRT      1217
T. aquaticus     EGFGVDKREKEVLARAEKLGLVSP------------GKSPEEQLKELFDLGKVVLYDGRT      979
S. aureus        ---------------------------------------------GMARDGKTVLYDGRT      1022
B. subtilis      ---------------------------------------------GMSRDAKTVLYDGRT      1022
                                                               :   .:  ******

E. coli          GEQFERPVTVGYMYMLKLNHLVDDKMHARSTGSYSLVTQQPLGGKAQFGGQRFGEMEVWA      1277
T. aquaticus     GEPFEGPIVVGQMFIMKLYHMVEDKMHARSTGPYSLITQQPLGGKAQFGGQRFGEMEVWA      1039
S. aureus        GEPFDNRISVGVMYMLKLAHMVDDKLHARSTGPYSLVTQQPLGGKAQFGGQRFGEMEVWA      1082
B. subtilis      GEPFDNRVSVGIMYMIKLAHMVDDKLHARSTGPYSLVTQQPLGGKAQFGGQRFGEMEVWA      1082
                 ** *:  : ** *:::** *:*:**:****** ***:**********************

E. coli          LEAYGAAYTLQEMLTVKSDDVNGRTKMYKNIVDGNHQMEPGMPESFNVLLKEIRSLGINI      1337
T. aquaticus     LEAYGAAHTLQEMLTIKSDDIEGRNAAYQAIIKGEDVPEPSVPESFRVLVKELQALALDV      1099
S. aureus        LEAYGAAYTLQEILTYKSDDTVGRVKTYEAIVKGENISRPSVPESFRVLMKELQSLGLDV      1142
B. subtilis      LEAYGAAYTLQEILTVKSDDVVGRVKTYEAIVKGDNVPEPGVPESFKVLIKELQSLGMDV      1142
                 *******:****:** ****  **   *: *:.*:.  .*.:****.**:**:::*.:::

E. coli          ELEDE-----------------------------------------------      1342
T. aquaticus     QTLDEKDNPVDIFEGLASKR--------------------------------      1119
S. aureus        KVMDEQDNEIEMTDVDDDDVVERKVDLQQ--NDAPETQKEVT------D--      1183
B. subtilis      KILSGDEEEIEMRDLEDEEDAKQADGLALSGDEEPEETASADVERDVVTKE       1193
                 :  .
```

***rpoC* alignment results**

```
T. aquaticus      ------------MKKEVRKVRIALASPEKIRSWSYGEVEKPETINYRTLKPERDGLFDER      48
E. coli           MKDLLKFLKAQTKTEEFDAIKIALASPDMIRSWSFGEVKKPETINYRTFKPERDGLFCAR      60
S. aureus         ----------LIDVNNFHYMKIGLASPEKIRSWSFGEVKKPETINYRTLKPEKDGLFCER      50
B. subtilis       ----------MLDVNNFEYMNIGLASPDKIRSWSFGEVKKPETINYRTLKPEKDGLFCER      50
                             ::.  :.*.****: *****:***:*********:***:****  *

T. aquaticus      IFGPIKDYECACGKYKRQRFEGKVCERCGVEVTRSIVRRYRMGHIELATPAAHIWFVKDV      108
E. coli           IFGPVKDYECLCGKYKRLKHRGVICEKCGVEVTQTKVRRERMGHIELASPTAHIWFLKSL      120
S. aureus         IFGPTKDWECSCGKYKRVRYKGMVCDRCGVEVTKSKVRRERMGHIELAAPVSHIWYFKGI      110
B. subtilis       IFGPTKDWECHCGKYKRVRYKGVVCDRCGVEVTRAKVRRERMGHIELAAPVSHIWYFKGI      110
                  **** **:** ****** :..* :*::******:: *** ********:*.:***:.*.:

T. aquaticus      PSKIGTLLDLSATELEQVLYFNKYIVLDPKGAVLDGVPVEKRQLLTDEEYRELRYGKQET      168
E. coli           PSRIGLLLDMPLRDIERVLYFESYVVIEGGMT-----NLERQQILTEEQYLDALEE----      171
S. aureus         PSRMGLLLDMSPRALEEVIYFASYVVVDPGPT-----GLEKKTLLSEAEFRDYYDK----      161
B. subtilis       PSRMGLVLDMSPRALEEVIYFASYVVTDPANT-----PLEKKQLLSEKEYRAYLDK----      161
                  **::* :**:    :*.*:** .*:* :   :      :*:: :*:: ::

T. aquaticus      YPLPAGVDALVKDGEEVVKGQELAPGVVSRMDGVALYRFPRRVRVDYLRKERAALRIPLS      228
E. coli           ------------------------------------------------------------      171
S. aureus         ------------------------------------------------------------      161
B. subtilis       ------------------------------------------------------------      161


T. aquaticus      AWVEKEAYRPGEVLAELSEPYLFRAEESGVVELKDLAEGHLIYLRQEEEVVARYFLPAGM      288
E. coli           ------------------------------------------------------------      171
S. aureus         ------------------------------------------------------------      161
B. subtilis       ------------------------------------------------------------      161

T. aquaticus      TPLVVEGEIVEVGQPLAEGKGLLRLPRHMTAKEVEAEEEGDSVHLTLFLEWTEPKDYKVA      348
E. coli           ------------------------------------------------------------      171
S. aureus         ------------------------------------------------------------      161
B. subtilis       ------------------------------------------------------------      161

T. aquaticus      PHMNVIVPEGAKVQAGEKIVAAIDPEEEVIAEAEGVVHLHEPASILVVKARVYPFEDDVE      408
E. coli           ------------------------------------------------------------      171
S. aureus         ------------------------------------------------------------      161
B. subtilis       ------------------------------------------------------------      161
```

```
T. aquaticus      VTTGDRVAPGDVLADGGKVKSEIYGRVEVDLVRNVVRVVESYDIDARMGAEAIQELLKEL      468
E. coli           ----------------------------------------FGDEFDAKMGAEAIQALLKSM      192
S. aureus         ----------------------------------------YPGQFVAKMGAEGIKDLLEEI      182
B. subtilis       ----------------------------------------YGNKFQASMGAEAIHKLLQDI      182
                                                          .: * ****.*: **:.:
T. aquaticus      DLEKLERELLEEMKHPS-RARRAKARKRLEVVRAFLDSGNRPEWMILEAVPVLPPDLRPM      527
E. coli           DLEQECEQLREELNETNSETKRKKLTKRIKLLEAFVQSGNKPEWMILTVLPVLPPDLRPL      252
S. aureus         DLDEELKLLRDELESATG-QRLTRAIKRLEVVESFRNSGNKPSWMILDVLPIIPPEIRPM      241
B. subtilis       DLVKEVDMLKEELKTSQG-QRRTRAIKRLEVLEAFRNSGNKPSWMILDVLPVIPPELRPM      241
                  ** :    * :*::      :  :  **:::::.:* :***:*.**** .:*::**::**:

T. aquaticus      VQVDGGRFATSDLNDLYRRLINRNNRLKKLLAQGAPEIIIRNEKRMLQEAVDAVIDNGRR      587
E. coli           VPLDGGRFATSDLNDLYRRVINRNNRLKRLLDLAAPDIIVRNEKRMLQEAVDALLDNGRR      312
S. aureus         VQLDGGRFATSDLNDLYRRVINRNNRLKRLLDLGAPGIIVQNEKRMLQEAVDALIDNGRR      301
B. subtilis       VQLDGGRFATSDLNDLYRRVINRNNRLKRLLDLGAPSIIVQNEKRMLQEAVDALIDNGRR      301
                  * :****************:********:**  .** **::************::*****

T.aquaticus      GSPVTNPGSERPLRSLTDILSGKQGRFRQNLLGKRVDYSGRSVIVVGPQLKLHQCGLPKR       647
E.coli           GRAITGSN-KRPLKSLADMIKGKQGRFRQNLLGKRVDYSGRSVITVGPYLRLHQCGLPKK       371
S.aureus         GRPVTGPG-NRPLKSLSHMLKGKQGRFRQNLLGKRVDYSGRSVIAVGPSLKMYQCGLPKE       360
B.subtilis       GRPVTGPG-NRPLKSLSHMLKGKQGRFRQNLLGKRVDYSGRSVIVVGPHLKMYQCGLPKE       360
                 *  :*. . :***:**:.::.**********************.*** *:::******.

T. aquaticus      MALELFKPFLLKKMEEKAFAPNVKAARRMLERQRDIKDEVWDALEEVIHGKVVLLNRAPT       707
E. coli           MALELFKPFIYGKLELRGLATTIKAAKKMVERE---EAVVWDILDEVIREHPVLLNRAPT       428
S. aureus         MALELFKPFVMKELVQREIATNIKNAKSKIERM---DDEVWDVLEEVIREHPVLLNRAPT       417
B. subtilis       MALELFKPFVMKELVEKGLAHNIKSAKRKIERV---QPEVWDVLESVIKEHPVLLNRAPT       417
                  *********:  ::  : :* .:* *:  :**    .  *** *:.**: : ********

T. aquaticus      LHRLGIQAFQPVLVEGQSIQLHPLVCEAFNADFDGDQMAVHVPLSSFAQAEARIQMLSAH       767
E. coli           LHRLGIQAFEPVLIEGKAIQLHPLVCAAYNADFDGDQMAVHVPLTLEAQLEARALMMSTN       488
S. aureus         LHRLGIQAFEPTLVEGRAIRLHPLVTTAYNADFDGDQMAVHVPLSKEAQAEARMLMLAAQ       477
B. subtilis       LHRLGIQAFEPTLVEGRAIRLHPLVCTAYNADFDGDQMAVHVPLSAEAQAEARILMLAAQ       477
                  *********:*.*:**::*:*****  *:***************:  ** ***  *::::

T. aquaticus      NLLSPASGEPLAKPSRDIILGLYYITQVRKEKKGAGMAFATPEEALAAYERGEVALNAPI       827
E. coli           NILSPANGEPIIVPSQDVVLGLYYMTRDCVNAKGEGMVLTGPKEAERLYRSGLASLHARV       548
S. aureus         NILNPKDGKPVVTPSQDMVLGNYYLTLERKDAVNTGAIFNNTNEVLKAYANGFVHLHTRI       537
B. subtilis       NILNPKDGKPVVTPSQDMVLGNYYLTLERAGAVGEGMVFKNTDEALLAYQNGYVHLHTRV       537
                  *:*.* .*:*:  **:*::** **:*       . *  :   .*.   *  * . *:: :
```

```
T. aquaticus      VVAGRET-----------------SVGRLKFVFANPDEALLAVAHGLLDLQDVVTVRYLG      870
E. coli           KVRITEYEKDANGELVAKTSLKDTTVGRAILWMIVPKGLPYSIVN---------------      593
S. aureus         GVHASSFNNPTFTEE-QNKKILATSVGKIIFNEIIPDSFAYINEPTQENL----------      586
B. subtilis       AVAANSLKNVTFTEE-QRSKLLITTVGKLVFNEILPESFPYMNEPTKSNI----------      586
                   *   .                  :**:  :    *.

T. aquaticus      RRLETSPGRILFARIVGEAVGDEKVAQELIQMDVPQEKNSLKDLVYQAFLRLGMEKTARL      930
E. coli           ---------------------------------QALGKKAISKMLNTCYRILGLKPTVIF      620
S. aureus         --ERKTPNRYFIDP-TTLGEGGLKEYFENEELIEPFNKKFLGNIIAEVFNRFSITDTSMM      643
B. subtilis       --EEKTPDRFFLEK-GA----DVKAVIAQQPINAPFKKGILGKIIAEIFKRFHITETSKM      639
                                                 *  : .::   :  : :  *  :

T. aquaticus      LDALKYYGFTLSTTSGITIGIDDAVIPEEKQRYLEEADRKLRQIEQAYEMGFLTDRERYD      990
E. coli           ADQIMYTGFAYAARSGASVGIDDMVIPEKKHEIISEAEAEVAEIQEQFQSGLVTAGERYN      680
S. aureus         LDRMKDLGFKFSSKAGITVGVADIVVLPDKQQILDEHEKLVDRITKQFNRGLITEEERYN      703
B. subtilis       LDRMKNLGFKYSTKAGITVGVSDIVVLDDKQEILEEAQSKVDNVMKQFRRGLITEEERYE      699
                   * :   **  :: :* ::*: * *:  .*:. :.* :  : .: : :. *::*  ***:

T. aquaticus      QVIQLWTETTEKVTQAVFKNFE------------ENYPFNPLYVMAQSGARGNPQQIRQL      1038
E. coli           KVIDIWAAANDRVSKAMMDNLQTETVINRDGQEEKQVSFNSIYMMADSGARGSAAQIRQL      740
S. aureus         AVVEIWTDAKDQIQGELMQSLD---------------KTNPIFMMSDSGARGNASNFTQL      748
B. subtilis       RVISIWSAAKDVIQGKLMKSLD---------------ELNPIYMMSDSGARGNASNFTQL      744
                   *:.:*: :.: :   ::..::                * :::*::*****.  :: **

T. aquaticus      CGMRGLMQKPSGETFEVPVRSSFREGLTVLEYFISSHGARKGGADTALRTADSGYLTRKL      1098
E. coli           AGMRGLMAKPDGSIIETPITANFREGLNVLQYFISTHGARKGLADTALKTANSGYLTRRL      800
S. aureus         AGMRGLMAAPSGKIIELPITSSFREGLTVLEYFISTHGARKGLADTALKTADSGYLTRRL      808
B. subtilis       AGMRGLMANPAGRIIELPIKSSFREGLTVLEYFISTHGARKGLADTALKTADSGYLTRRL      804
                  .******  * *  :* *: :.*****.**:****:****** *****:**:******:*

T. aquaticus      VDVAHEIVVREADCGTTNYISVP-LFQMDEVTRTLRLRKRSDIESGLYGRVLAREVEALG      1157
E. coli           VDVAQDLVVTEDDCGTHEGIMMTPVIEGGDVKEPLR--------DRVLGRVTAEDVLKPG      852
S. aureus         VDVAQDVIVREEDCGTDRGLLVSDIKEGTEMIEPFI--------ERIEGRYSKETIRHPE      860
B. subtilis       VDVAQDVIIRETDCGTDRGILAKPLKEGTETIERLE--------ERLIGRFARKQVKHPE      856
                  ****::::: * **** . :    : :  :  . :         . : **   . :

T. aquaticus      RR--LEEGRYLSLEDVHFLIKAAEAGEVREVPVRSPLTCQTRYGVCQKCYGYDLSMARPV      1215
E. coli           TADILVPRNTLLHEQW---CDLLEENSVDAVKVRSVVSCDTDFGVCAHCYGRDLARGHII      909
S. aureus         TDEIIIRPDELITPEI---AKKITDAGIEQMYIRSAFTCNARHGVCEKCYGKNLATGEKV      917
B. subtilis       TGEVLVNENELIDEDK---ALEIVEAGIEEVWIRSAFTCNTPHGVCKRCYGRNLATGSDV      913
                      :     *   :           :  : :** .:*:: .*** :*** :*: .  :
```

```
T. aquaticus      SIGEAVGVVAAESIGEPGTQLTMRTFHTGGVAVG-------------------------      1249
E. coli           NKGEAIGVIAAQSIGEPGTQLTMRTFHIGGAASRAAAESSIQVKNKGSIKLSNVKSVVNS      969
S. aureus         EVGEAVGTIAAQSIGEPGTQLTMRTFHTGGVAGS-------------------------      951
B. subtilis       EVGEAVGIIAAQSIGEPGTQLTMRTFHTGGVAGD-------------------------      947
                  . ***:* :**:*************** **.*

T. aquaticus      ------------------------------------------------------------      1249
E. coli           SGKLVITSRNTELKLIDEFGRTKESYKVPYGAVLAKGDGEQVAGGETVANWDPHTMPVIT      1029
S. aureus         ------------------------------------------------------------      951
B. subtilis       ------------------------------------------------------------      947

T. aquaticus      ------------------------------------------------------------      1249
E. coli           EVSGFVRFTDMIDGQTITRQTDELTGLSSLVVLDSAERTAGGKDLRPALKIVDAQGNDVL      1089
S. aureus         ------------------------------------------------------------      951
B. subtilis       ------------------------------------------------------------      947


T. aquaticus      -------------------------------------------TDITQGLPRVIELFEARR      1267
E. coli           IPGTDMPAQYFLPGKAIVQLEDGVQISSGDTLARIPQESGGTKDITGGLPRVADLFEARR      1149
S. aureus         ----------------------------------------------DITQGLPRIQEIFEARN      968
B. subtilis       ----------------------------------------------DITQGLPRIQELFEARN      964
                                                               *** ****: ::****.

T. aquaticus      PKAKAVISEIDGVVRIEE---GEDRLSVFVESEGFSKEYKLPKDARLLVKDGDYVEAGQP      1324
E. coli           PKEPAILAEISGIVSFGKETKGKRRLVITPVDGSDPYEEMIPKWRQLNVFEGERVERGDV      1209
S. aureus         PKGQAVITEIEGVVEDIKLAKDRQQEIVVK-GANETRSYLASGTSRIIVEIGQPVQRGEV      1027
B. subtilis       PKGQATITEIDGTVVEINEVRDKQQEIVVQ-GAVETRSYTAPYNSRLKVAEGDKITRGQV      1023
                  **  * ::**.* *   :   .. :  :   .     .       :: *  *: :  *:

T. aquaticus      LTRGAIDPHQLLEAKGPEAVERYLVDEIQKVYRAQGVKLHDKHIEIVVRQMLKYVEVTDP      1384
E. coli           ISDGPEAPHDILRLRGVHAVTRYIVNEVQDVYRLQGVKINDKHIEVIVRQMLRKATIVNA      1269
S. aureus         LTEGSIEPKNYLSVAGLNATESYLLKEVQKVYRMQGVEIDDKHVEVMVRQMLRKVRTIEA      1087
B. subtilis       LTEGSIDPKELLKVTDLTTVQEYLLHEVQKVYRMQGVEIGDKHVEVMVRQMLRKVRVIDA      1083
                  :: *   *:: *   .  :.  *::.*:*.*** ***:: ***:*::*****: . : :

T. aquaticus      GDSRLLEGQVLEKWDVEALNERLIAEGKVPVAWKPLLMGVTKSALSTKSWLSAASFQNTT      1444
E. coli           GSSDFLEGEQVEYSRVKIANRELEANGKVGATYSRDLLGITKASLATESFISAASFQETT      1329
S. aureus         GDTKLLPGSLVDIHNFTDANREAFKHRKRPATAKPVLLGITKASLETESFLSAASFQETT      1147
B. subtilis       GDTDVLPGTLLDIHQFTEANKKVLLEGNRPATGRPVLLGITKASLETDSFLSAASFQETT      1143
                  *.: .* *  ::   .   *..   . :  .:    *:*:**::* *.*::******:**
```

```
T. aquaticus      HVLTEAAIAGKKDELIGLKENVILGRLIPAGTGSDFVRFTQVVDQRTLKAIEEARKEAVE      1504
E. coli           RVLTEAAVAGKRDELRGLKENVIVGRLIPAGTGYAYHQDRMRR--RAAGEAPAA--PQVT      1385
S. aureus         RVLTDAAIKGKRDDLLGLKENVIIGKLIPAGTGMRRYSDVKYE--KTA--KPVA--EVES      1201
B. subtilis       RVLTDAAIKGKRDELLGLKENVIIGKLVPAGTGMMKYRKVKPV--SNV--QPTD--DMVP      1197
                  :***:**: **:*:* *******:*:*:*****

T. aquaticus      AKEKEAPRRPVRREQPGKGL------      1524
E. coli           AEDASAS----LAELLNAGLGGSDNE      1407
S. aureus         QTEVTE--------------------      1207
B. subtilis       VE------------------------      1199
```

Appendix 4

Appendix 4 Table 1 Identification of DEGs in untrained compared to SH1000, related to Figure 5.3 A.

UniProt Accession	Gene name/Locus tag	log2FC	pvalue	padj	WT-2	WT-3	Untrained-1	Untrained-2	Untrained-3
Q2FZZ6	SAOUHSC_00838	-3.623428912	0	0	6245.149812	6866.132959	517.7732717	486.7565208	547.4800408
Q2FYN4	lysA	-4.46262018	0	0	31469.09985	34143.42962	1436.991899	1420.954613	1418.517704
A0A0H2WXF8	*mecA*	11.3123129	0	0	0.85386243	2.530204996	44124.77507	47471.86576	51286.4511
Q2G253	SAOUHSC_00025	-2.944785809	2.97E-304	1.70E-301	4806.391617	4913.658103	636.3821268	558.8339287	655.3325817
Q2G035	SAOUHSC_00792	-2.453887271	1.89E-190	8.63E-188	5949.713411	6160.205765	1135.147569	1030.613326	1078.525409
Q2FVH5	SAOUHSC_02737	-1.35420084	2.50E-139	9.52E-137	4078.046965	4154.596604	1588.294221	1622.209713	1597.244772
Q2FUQ2	mnmE	-1.683908937	4.91E-133	1.60E-130	7946.043772	7903.517007	2361.532719	2505.860012	2464.173767
O50581	recG	-1.578539567	1.25E-129	3.57E-127	4168.556382	4505.451697	1373.125593	1416.274262	1537.669083
Q2FUQ1	rnpA	-2.095289139	1.52E-112	3.87E-110	1090.382323	1027.263229	226.5733259	243.3782604	258.8460981
Q2G239	SAOUHSC_00708	1.225161765	1.28E-110	2.93E-108	4320.543895	4620.997725	10186.67591	10480.24232	10832.50377
Q2FXV8	recD2	1.290060324	4.00E-110	8.30E-108	1952.783377	2014.043177	4612.820028	4966.788653	5057.770583
Q2G2B2	sasG	-1.536353721	5.38E-104	1.03E-101	6222.095526	6339.850319	1932.716089	2181.979712	2329.614883
Q2FXE2	SAOUHSC_01907	-1.638471128	8.04E-103	1.41E-100	1616.36158	1612.583984	528.4176561	497.9893636	509.4748598
Q2G0K4	SAOUHSC_00556	1.626727783	8.79E-96	1.44E-93	3680.147072	3468.067648	11142.38957	12168.91302	10194.63303
Q2FZD0	uvrC	-1.47372536	3.00E-94	4.58E-92	3590.491517	3472.284657	1212.699513	1296.457272	1273.687149
Q2FY54	SAOUHSC_01611	1.091921878	1.96E-91	2.79E-89	2787.006971	2890.337508	6001.912197	6025.484086	6195.871681
Q2FUQ3	mnmG	-1.266946107	4.75E-91	6.39E-89	11567.27434	11077.23747	4497.252426	4757.108921	4780.435478
Q2FXM1	SAOUHSC_01814	-1.345423901	3.77E-84	4.79E-82	4034.499981	3547.347405	1539.634178	1469.630265	1426.735041
Q2G2K5	ureC	1.724339142	1.26E-81	1.51E-79	373.1378818	430.1348494	1402.777806	1318.922957	1324.018335
Q2FUY3	SAOUHSC_02962	-1.688404134	2.99E-81	3.42E-79	1523.290575	1591.498943	432.6181961	463.354765	535.1540362
Q2G243	radA	-1.189714674	7.99E-80	8.70E-78	5317.00135	5319.334304	2132.678454	2357.960915	2471.363937
Q2G170	SAOUHSC_00284	-1.748696713	9.77E-73	1.02E-70	2678.566442	2596.833728	773.9988114	675.8427078	857.6844917
Q2FYZ0	SAOUHSC_01282	-1.559871213	1.32E-72	1.25E-70	2955.21787	2584.182703	859.1538869	916.4127575	1005.596548
Q2FW95	SAOUHSC_02404	-1.282952149	1.30E-72	1.25E-70	1876.789621	1993.801537	761.8338006	799.4039784	809.4076401
Q2G204	SAOUHSC_00942	-1.264027314	4.40E-72	4.02E-70	2635.873321	2713.223158	1075.843142	1103.626804	1138.101098
Q2FY14	SAOUHSC_01660	1.309698377	8.36E-72	7.35E-70	872.6474033	854.3658871	2061.969329	2223.166802	2197.110333
Q2G0Y8	SAOUHSC_00373	1.306298154	4.83E-70	4.09E-68	2394.230253	2741.055413	6036.12629	6543.130924	6643.716518

Q2FXQ3	SAOUHSC_01782	-1.379629519	7.15E-70	5.84E-68	4074.631515	4086.281069	1512.262904	1585.702974	1561.293925
Q2FY61	SAOUHSC_01604	-1.651828042	2.06E-68	1.63E-66	1425.950258	1432.93943	489.6416842	436.2087283	409.8396553
Q2G0Q8	SAOUHSC_00488	-1.26093476	2.93E-67	2.23E-65	13972.6048	13396.59205	5291.779693	5535.919354	6169.165338
Q9F1K0	dnaE	1.001370651	1.95E-64	1.44E-62	2456.562211	2430.6836	4682.76884	4907.816228	5154.324287
Q2FZ77	pyrR	2.029834725	6.35E-63	4.53E-61	485.8477226	462.1841127	2085.539037	1933.9211	1997.839924
Q2G0Q7	SAOUHSC_00489	-1.54649048	2.83E-59	1.90E-57	1351.664226	1389.925945	397.6437901	497.9893636	493.0401869
Q2FYF4	SAOUHSC_01497	-1.169539583	6.42E-58	4.20E-56	3107.205382	3208.299935	1294.053023	1458.397422	1431.870876
P0A084	msrA1	-1.335988811	1.81E-55	1.12E-53	1094.651635	1097.265567	409.8088009	414.6791129	465.3066763
Q2G0B2	SAOUHSC_00693	1.116438245	9.64E-55	5.65E-53	754.8143879	783.5201472	1639.235204	1737.346351	1660.929129
Q2FWX1	SAOUHSC_02150	-1.684985359	1.07E-53	6.12E-52	6010.337643	5147.280364	1624.02894	1725.177438	1725.640654
Q2FUX4	SAOUHSC_02971	-1.749715633	3.17E-53	1.77E-51	810.3154459	820.6298205	275.2333691	207.8075916	219.81375
Q2G0Y6	guaA	1.134068581	6.12E-53	3.33E-51	7126.335839	7644.592696	14582.04637	16863.30524	17561.47516
Q2G2J9	SAOUHSC_01412	1.172508124	1.24E-51	6.45E-50	784.699573	809.6655989	1735.034664	1874.948675	1836.574696
Q2FZD3	mutS2	1.172240604	1.41E-51	7.16E-50	1757.248881	1831.868417	3698.163279	4284.393454	4269.933452
Q2G0E5	SAOUHSC_00661	1.338498674	3.44E-51	1.67E-49	426.0773525	432.6650544	1119.941306	1090.521821	1088.797079
Q2G105	SAOUHSC_00356	-1.645860951	2.58E-45	1.18E-43	8865.653609	6895.652017	2881.58693	2295.24421	2160.132319
Q2FYM1	odhA	-1.056396989	5.06E-45	2.23E-43	3850.919558	4211.104516	1877.97354	1829.081234	2069.741618
Q2FVI5	SAOUHSC_02725	1.100804124	9.54E-45	4.04E-43	1096.35936	1122.567617	2394.986499	2342.047721	2462.119433
Q2FZE9	isdA	-1.534673475	8.83E-44	3.67E-42	1774.326129	1908.617969	574.7967597	614.0620724	675.8759228
Q2FZZ4	SAOUHSC_00840	-2.173204239	5.82E-43	2.38E-41	363.7453951	398.9289878	88.95664139	76.75775905	67.79302569
Q2FY74	xerD	-1.048061278	7.75E-43	3.11E-41	2514.624856	2205.495355	1062.917818	1148.558175	1191.513785
Q2FVM0	SAOUHSC_02682	3.131994355	4.27E-42	1.68E-40	140.0334385	85.18356821	1368.563714	743.2397645	1520.207243
Q2FZD7	rnhC	-1.123040723	2.42E-40	9.08E-39	1540.367823	1603.306566	660.7121484	754.4726073	732.3701109
Q2FXL6	SAOUHSC_01819	-1.496603269	1.83E-38	6.44E-37	2368.61438	2390.20032	762.5941138	780.6825738	925.4775174
Q2G0Z4	SAOUHSC_00367	-1.183738008	2.52E-38	8.74E-37	2355.806444	2507.433151	970.9199235	1028.741185	1177.133446
Q2FXN6	SAOUHSC_01800	-1.078018085	1.83E-37	5.96E-36	1301.286343	1247.391063	573.2761334	613.1260022	609.1100642
Q2G261	sodM	-1.281736931	4.53E-37	1.46E-35	1533.536924	1490.290743	532.9795351	621.5506343	686.1475934
Q2FXH7	SAOUHSC_01870	1.032378582	5.31E-36	1.69E-34	1094.651635	1196.786963	2531.84287	2230.655364	2325.506215
Q2G200	SAOUHSC_00941	-1.543379026	5.87E-36	1.84E-34	685.6515311	616.5266175	193.1195463	230.2732772	229.0582535
Q2FVV1	SAOUHSC_02590	1.024688605	1.18E-35	3.64E-34	1408.873009	1330.044426	2880.826617	2776.384309	2769.242383
Q2G0D7	SAOUHSC_00668	1.174335722	2.54E-35	7.65E-34	1320.925179	1260.88549	3320.287632	2908.370212	2621.330327
Q2FZQ1	SAOUHSC_00949	-1.266113252	4.02E-35	1.19E-33	592.5805263	607.2491991	246.3414685	232.1454176	257.818931
Q2G1S4	SAOUHSC_00018	1.123199184	4.17E-35	1.22E-33	3422.280619	3689.882286	7101.325047	8097.94358	8320.053153
Q2G252	rlmH	-1.693180269	2.27E-34	6.32E-33	526.8331192	474.8351377	130.0135528	161.9401502	155.1022254

Q2FZU7	SAOUHSC_00893	-1.030289243	1.97E-33	5.23E-32	2278.958825	2310.077162	1067.479697	1150.430316	1120.639258
Q2G155	lip2	-1.711560406	3.36E-33	8.82E-32	3990.099134	4002.784304	1091.049405	1100.818593	1311.69233
Q2G0Y9	xpt	1.087222027	4.09E-33	1.06E-31	660.0356582	641.8286674	1320.663984	1445.292439	1431.870876
Q2G0U0	SAOUHSC_00437	1.43171561	4.62E-33	1.19E-31	461.0857121	492.5465726	1310.019599	1189.745265	1454.468551
P72360	scdA	-1.496969614	1.64E-32	4.18E-31	829.9542818	705.0837923	269.9111769	223.7207855	297.8784462
Q2FVM2	SAOUHSC_02680	3.076035689	1.12E-31	2.76E-30	114.4175656	54.82110826	1107.776295	554.1535776	1119.612091
Q2FZ76	SAOUHSC_01165	1.520197927	2.55E-30	6.02E-29	292.8748134	343.2644779	859.9142001	1015.636202	958.3468632
Q2G145	SAOUHSC_00310	-1.309955138	3.93E-30	9.18E-29	574.6494153	547.3676809	211.3670624	221.8486451	232.1397546
Q2FVB4	SAOUHSC_02820	-2.64869542	1.19E-29	2.66E-28	400.4614796	457.9671044	42.57753776	66.4609865	55.46702102
Q2G0M2	SAOUHSC_00538	-1.07999562	1.44E-28	3.11E-27	998.1651804	1034.853844	414.37068	492.3729422	522.8280315
Q2FY13	SAOUHSC_01661	1.368880801	3.62E-28	7.52E-27	293.7286759	361.8193145	856.1126342	915.4766873	843.3041529
Q2G249	SAOUHSC_00026	-1.526805438	1.15E-27	2.32E-26	619.0502616	517.8486226	204.5242439	182.5336953	180.7814018
Q2G2J3	SAOUHSC_02573	1.010098907	1.43E-27	2.87E-26	1045.981477	1093.89196	1963.888929	2384.170882	2201.219001
Q2FVN5	SAOUHSC_02667	1.006979382	7.16E-27	1.38E-25	5818.218597	5826.218705	12558.0927	11424.73719	11510.43403
Q2G272	ureD	1.193245969	9.31E-27	1.77E-25	247.6201046	242.8996797	598.3664681	558.8339287	555.6973773
Q2G012	emp	-1.774172394	1.04E-25	1.89E-24	339.8372471	388.8081678	114.8072893	99.22344463	82.17336448
Q9RQP9	icaA	-2.080887154	1.88E-25	3.36E-24	890.5785143	916.7776104	142.9388768	250.8668223	173.5912325
Q2FVQ4	SAOUHSC_02648	1.853909774	2.46E-25	4.36E-24	913.6327999	718.578219	3530.894381	2070.587354	3848.794959
Q2FVL8	SAOUHSC_02684	2.884563077	2.89E-25	5.08E-24	233.1044433	150.9688981	2032.317115	1169.15172	2443.630426
Q2G2K7	ureF	1.295798145	4.13E-25	7.15E-24	197.2422213	178.8011531	491.9226237	457.7383436	469.4153446
Q2G016	SAOUHSC_00811	-1.958211422	1.88E-24	3.12E-23	1045.981477	1057.625689	242.5399026	258.3553841	235.2212558
Q2FVM7	nreC	1.30902281	3.80E-24	6.16E-23	342.3988343	298.5641896	824.1794809	703.9248147	918.287348
Q2FVM6	nreB	1.121107656	4.99E-24	7.98E-23	624.1734362	593.7547725	1377.687472	1211.274881	1447.278382
Q2G1D7	pflA	3.159311443	1.43E-23	2.24E-22	134.0564015	74.21934656	1361.720895	869.6092459	2208.40917
Q2FYZ3	SAOUHSC_01279	-1.065658677	2.73E-23	4.19E-22	543.0565054	583.6339525	278.2746218	251.8028925	263.9819334
Q2FY36	SAOUHSC_01630	-1.107241705	4.15E-23	6.25E-22	1060.497138	1037.384049	434.1388225	491.436872	512.5563609
Q2FXQ4	SAOUHSC_01781	-1.027282007	9.86E-23	1.44E-21	3578.537443	4163.030621	1925.87327	1805.679478	1892.041717
Q2FZ71	pyrF	1.183951733	7.24E-22	1.00E-20	263.8434908	261.4545163	627.2583687	571.938912	628.6262382
Q2FVA4	SAOUHSC_02829	-1.130611849	1.37E-20	1.83E-19	2329.336708	2380.0795	977.7627421	1136.389262	1043.601729
Q2FZL3	sspB	-1.191183294	1.97E-20	2.56E-19	480.724548	528.8128443	206.8051834	203.1272404	238.302757
Q2G172	SAOUHSC_00281	2.208576486	2.43E-20	3.14E-19	132.3486766	99.52139653	681.2406041	381.9166548	813.5163083
Q2G1N4	SAOUHSC_00074	-1.592408565	2.84E-20	3.65E-19	1619.777029	1950.788052	534.5001615	620.6145641	514.610695
Q2G2P5	SAOUHSC_00201	1.259550498	7.70E-20	9.67E-19	297.997988	253.0204996	697.9674939	586.9160357	753.9406191
Q2FYV0	SAOUHSC_01324	-1.184197327	3.22E-19	3.84E-18	669.428145	573.5131325	263.0683583	249.930752	286.5796086

P02976	spa	-2.206365432	3.78E-19	4.47E-18	13696.80724	17790.71473	1646.078022	2958.918004	3718.344743
Q2FVB3	SAOUHSC_02821	-2.094121925	4.93E-19	5.76E-18	260.4280411	254.707303	55.50286172	43.99530092	51.3583528
Q2FYL4	SAOUHSC_01425	-1.147380651	3.02E-18	3.36E-17	1583.060945	1395.829756	629.5393083	707.6690957	628.6262382
Q2FVM1	SAOUHSC_02681	2.869014337	4.65E-18	5.08E-17	365.45312	143.3782831	3190.274079	1802.871268	3775.866098
Q2G278	SAOUHSC_00773	-1.241914917	5.67E-18	6.17E-17	344.9604216	326.3964445	147.5007558	139.4744646	123.2600467
Q2G185	essB	-1.067337922	6.40E-18	6.94E-17	441.4468762	493.3899743	233.4161445	213.424013	206.4605782
Q2G2H9	mnhG1	1.352513752	1.17E-17	1.25E-16	257.0125914	304.4680012	886.5251612	732.0069217	623.490403
Q2G1D8	pflB	2.869828742	1.90E-17	2.02E-16	573.7955528	235.3090647	4923.027803	2706.179042	7712.997423
Q2FZL2	sspA	-1.359353928	1.37E-16	1.34E-15	393.6305801	410.7366111	139.8976241	153.5155181	155.1022254
Q2G1N5	SAOUHSC_00072	-1.376663903	2.29E-16	2.20E-15	565.2569285	651.1060858	199.9623648	228.4011367	241.3842581
Q2FVL5	SAOUHSC_02696	-1.154446686	4.61E-16	4.32E-15	488.4093098	508.5712043	231.8955181	204.9993809	214.6779147
Q2FZ75	pyrB	1.033311278	5.38E-16	5.02E-15	337.2756598	323.0228379	658.4312089	732.0069217	679.984591
Q2FV98	SAOUHSC_02836	1.018268577	5.45E-16	5.07E-15	274.9437024	240.3694747	567.193628	533.5600324	492.0130198
Q2G057	SAOUHSC_00765	-1.680115575	5.86E-16	5.40E-15	151.9875125	136.6310698	45.61879045	32.76245813	42.11384929
Q2FVN1	narT	2.394296685	9.85E-16	8.87E-15	490.9708971	251.3336963	3046.574889	1449.97279	3345.483101
Q2G273	ureG	1.166206736	1.36E-15	1.21E-14	314.2213742	269.0451313	753.4703557	668.3541459	602.9470618
Q2G0E3	SAOUHSC_00662	1.26244152	3.38E-15	2.90E-14	158.8184119	152.6557015	434.8991357	357.5788288	374.9159754
Q2FW50	SAOUHSC_02467	1.059870034	4.05E-15	3.44E-14	767.6223244	851.8356821	1589.054534	1746.707054	1851.982202
Q2FVW5	ureA	1.958186746	4.47E-15	3.78E-14	22.20042317	32.89266495	139.8976241	121.6891302	122.2328797
Q2FVM3	SAOUHSC_02679	2.629933289	5.87E-15	4.90E-14	18.78497346	15.18122998	208.3258097	99.22344463	217.7594159
Q2G1V2	SAOUHSC_02685	2.410897885	1.03E-14	8.47E-14	80.2630684	38.79647661	528.4176561	202.1911702	530.0182009
Q2FV02	SAOUHSC_02942	1.514137087	1.05E-14	8.54E-14	451.6932254	320.4926329	1227.905776	831.2303663	1489.392231
Q2FV66	SAOUHSC_02871	-1.046417235	1.34E-14	1.08E-13	352.6451835	391.3383728	174.8720301	172.2369228	179.7542348
Q2G2C4	tarI'	-1.038853068	3.51E-14	2.73E-13	413.269416	408.2064061	183.9957882	191.8943976	209.5420794
Q2G0Q6	SAOUHSC_00490	-1.042525482	4.10E-14	3.17E-13	346.6681465	384.5911595	149.0213821	196.5747488	175.6455666
Q2FYV4	SAOUHSC_01320	-1.095141998	4.69E-14	3.59E-13	590.8728014	707.6139973	277.5143086	314.5195981	291.7154439
Q2G1I7	SAOUHSC_00135	-1.018005354	1.75E-13	1.28E-12	722.3676156	590.3811658	301.084017	312.6474576	335.8836273
Q2G2K8	ureE	1.272856649	3.79E-13	2.67E-12	86.24010541	86.02696988	206.8051834	232.1454176	218.7865829
Q2G267	SAOUHSC_01181	-1.059828857	4.54E-13	3.18E-12	495.2402093	357.6023062	188.5576672	190.0222572	217.7594159
Q2FYJ3	tdcB	2.366717501	4.70E-13	3.26E-12	60.62423252	34.57946828	342.9012416	162.8762204	572.1320502
Q2FZ70	pyrE	1.04914101	8.78E-13	5.94E-12	192.9729091	184.7049647	362.6693841	452.1219222	393.4049824
Q2G1J7	SAOUHSC_00125	1.079521953	1.15E-12	7.72E-12	168.2108987	177.1143498	370.2725159	366.9395311	391.3506483
Q2FVW6	SAOUHSC_02557	1.484636128	1.48E-12	9.78E-12	78.55534354	60.72491991	229.6145786	248.9946818	162.2923948
Q2FYS2	SAOUHSC_01363	-1.213110887	1.80E-12	1.19E-11	345.8142841	344.1078795	144.4595031	152.5794479	128.395882

Q2FYV3	SAOUHSC_01321	-1.063325676	1.85E-12	1.21E-11	412.4155536	475.6785393	174.8720301	218.1043641	225.9767523
Q2G2R8	sspP	-1.067633209	2.16E-12	1.40E-11	346.6681465	322.1794362	138.3769977	157.259799	169.4825642
Q2G1H3	rocD	-1.319086594	2.40E-12	1.54E-11	251.8894168	259.767713	79.83288329	101.0955851	108.8797079
Q2G218	ldh1	2.541663509	4.46E-12	2.79E-11	1461.81248	569.2961242	10493.84243	6274.478768	15855.35068
Q2G140	mepA	1.142945237	5.80E-12	3.62E-11	85.38624298	91.93078154	217.4495678	201.2551	192.0802395
Q2G2K6	ureB	1.617649821	6.31E-12	3.93E-11	33.30063476	39.63987828	120.8897947	135.7301837	126.3415479
Q2FXD2	SAOUHSC_01931	1.300201795	2.15E-11	1.27E-10	347.5220089	339.8908712	1214.220139	818.1253831	683.0660922
Q2G1H7	SAOUHSC_00146	1.563813363	2.65E-11	1.54E-10	237.3737555	185.5483664	694.9262412	401.5741297	978.8902043
Q2FVK5	sbi	-1.633777724	4.28E-11	2.46E-10	1840.073536	1926.329404	517.7732717	505.4779255	543.3713726
Q2FZU1	argG	1.111985435	4.74E-11	2.71E-10	192.9729091	227.7184497	425.0150644	411.8709022	581.3765537
Q2G0D1	sarX	1.544818749	4.94E-11	2.81E-10	160.5261368	134.1008648	560.3508094	451.185852	411.8939894
Q2FWH6	SAOUHSC_02315	-1.250298147	1.00E-10	5.49E-10	158.8184119	137.4744715	54.74254854	39.31494976	82.17336448
Q2G0V2	metN1	-1.211419608	1.30E-10	6.97E-10	156.2568247	177.9577514	55.50286172	75.82168882	73.95602803
Q2FVC4	SAOUHSC_02789	1.025832791	1.44E-10	7.69E-10	116.1252905	113.8592248	239.4986499	226.5289962	262.9547663
Q2G173	SAOUHSC_00280	1.084494347	2.54E-10	1.32E-09	528.540844	505.1975976	1532.791359	997.8508677	897.7440069
Q2FV03	SAOUHSC_02941	1.621169787	3.56E-10	1.84E-09	42.69312149	57.35131325	202.2433043	117.008779	213.6507476
Q2G2A0	SAOUHSC_01694	1.008833581	4.48E-10	2.30E-09	598.5575633	706.7705957	1696.258692	1251.525901	1132.965263
Q2G1J9	SAOUHSC_00123	1.106075705	9.15E-10	4.60E-09	93.07100485	83.49676488	208.3258097	189.0861869	199.2704089
Q2G1H4	argC	-1.038352266	1.01E-09	5.08E-09	215.1733323	247.9600897	103.4025917	117.9448493	103.7438727
Q2G0G1	adh	1.971970217	2.04E-09	9.95E-09	232.2505809	126.5102498	798.3288329	520.4550492	1676.336635
Q2G0S6	SAOUHSC_00468	1.021460067	2.15E-09	1.04E-08	470.4781988	407.3630044	761.8338006	1130.772841	886.4451693
Q2FXE9	SAOUHSC_01900	-1.246695151	2.65E-09	1.28E-08	128.0793645	125.6668482	58.54411442	40.25101999	48.27685163
Q2FVA8	SAOUHSC_02825	-1.294477213	3.39E-09	1.61E-08	141.7411633	114.7026265	53.2219222	45.86744139	43.14101635
Q2FUQ8	SAOUHSC_03046	-2.034707586	7.72E-09	3.47E-08	765.0607371	1031.480237	123.9310474	87.99060184	128.395882
Q2G2Y3	SAOUHSC_01919	1.127033118	1.01E-08	4.47E-08	414.1232785	495.9201793	904.0123642	1127.96463	1127.829427
Q2FWP0	SAOUHSC_02241	1.196053425	1.24E-08	5.44E-08	97.340317	97.8345932	215.9289415	191.8943976	310.2044509
Q9RQP7	icaB	-1.333223395	2.49E-08	1.05E-07	224.565819	243.7430813	62.34568029	110.4562874	73.95602803
Q2FVL9	SAOUHSC_02683	2.069681362	2.71E-08	1.14E-07	6.830899438	4.217008327	64.62661981	21.52961534	66.76585864
Q2FZB8	SAOUHSC_01114	-1.604627824	3.34E-08	1.40E-07	193.8267716	207.4768097	42.57753776	55.22814371	57.52135513
Q2FYH4	SAOUHSC_01478	1.02871023	3.83E-08	1.59E-07	149.4259252	166.9935298	396.1231638	347.2820562	275.280771
Q2G1K0	SAOUHSC_00122	1.142068011	4.14E-08	1.71E-07	108.4405286	91.93078154	248.622408	239.6339795	216.7322488
Q2G0X2	SAOUHSC_00401	-1.738567882	4.97E-08	2.03E-07	134.9102639	88.55717488	25.85064792	18.72140465	23.62484229
Q2FYJ4	SAOUHSC_01450	1.499322103	6.19E-08	2.50E-07	139.1795761	83.49676488	369.5122027	190.0222572	532.072535
Q2FZC0	flr	-1.348357606	9.48E-08	3.76E-07	96.48645457	104.5818065	42.57753776	34.6345986	24.65200934

Q2G1J8	SAOUHSC_00124	1.338694556	1.57E-07	6.10E-07	43.54698392	40.48327994	164.2276456	110.4562874	87.30919976
Q2FXG0	SAOUHSC_01888	1.063121126	2.74E-07	1.03E-06	59.77037009	55.66450992	130.773866	140.4105349	117.0970444
Q2FV55	ssaA	1.320590045	3.11E-07	1.16E-06	862.4010541	931.1154387	2691.508637	2892.457018	2131.371641
Q2FYJ2	ald1	1.835121381	5.89E-07	2.16E-06	84.53238055	32.89266495	323.8934122	147.8990967	582.4037207
Q2G1N1	SAOUHSC_00077	-1.015653253	1.75E-06	6.11E-06	188.703597	193.9823831	100.361339	87.05453161	78.06469625
Q2G0Y5	SAOUHSC_00376	-1.068958766	1.84E-06	6.42E-06	82.82465569	104.5818065	50.94098267	35.57066883	35.95084696
Q2FYJ5	norB	1.123175429	2.15E-06	7.48E-06	105.0250789	94.46098653	253.9446002	146.9630265	307.1229497
Q2G2V7	SAOUHSC_02008	1.009072825	4.16E-06	1.38E-05	288.6055013	308.6850096	905.5329905	566.3224906	460.1708411
Q2G1K9	SAOUHSC_00113	1.630297853	4.45E-06	1.47E-05	448.2777756	346.6380845	1208.897947	823.7418045	3701.91007
Q2FZC2	SAOUHSC_01110	-1.156756762	4.62E-06	1.52E-05	138.3257136	167.8369314	60.06474076	68.33312696	55.46702102
Q2FWN9	SAOUHSC_02243	1.052572949	5.21E-06	1.70E-05	81.11693083	71.68914157	162.7070193	131.0498325	217.7594159
Q2G2G0	SAOUHSC_00717	-1.16330717	5.86E-06	1.90E-05	222.0042317	254.707303	86.67570186	92.670953	104.7710397
Q2FVA0	SAOUHSC_02833	1.010239316	5.91E-06	1.91E-05	58.91650766	84.34016655	193.1195463	152.5794479	120.1785455
Q2G0V1	SAOUHSC_00424	-1.198137331	7.56E-06	2.40E-05	70.87058167	81.80996155	29.6522138	32.76245813	23.62484229
Q2FZ03	SAOUHSC_01268	-1.08405247	1.58E-05	4.80E-05	55.50105794	59.03811658	25.09033475	20.59354511	26.70634345
Q2G1N2	SAOUHSC_00076	-1.159453273	1.85E-05	5.57E-05	96.48645457	95.3043882	42.57753776	32.76245813	35.95084696
Q2G0G9	SAOUHSC_00599	1.346217571	2.39E-05	7.10E-05	22.20042317	39.63987828	130.773866	101.0955851	72.92886097
Q2G1N3	sbnA	-1.184280884	3.28E-05	9.47E-05	53.79333308	66.62873157	24.33002158	21.52961534	20.54334112
Q2G192	SAOUHSC_00254	1.26636304	0.000105547	0.000286216	13.66179888	18.55483664	86.67570186	35.57066883	40.05951518
Q2FXD3	SAOUHSC_01930	1.399919361	0.000144572	0.000384741	4.269312149	4.217008327	139.1373109	14.97712372	15.40750584
Q2G2Y4	SAOUHSC_01918	1.038319091	0.000226046	0.000580608	394.4844426	428.4480461	903.252051	997.8508677	996.3520443
Q9EYW6	sspC	-1.05296954	0.000584879	0.001419355	44.40084635	52.29090326	15.96657666	25.27389627	16.4346729
Q2FX92	SAOUHSC_01985	1.144740058	0.001124866	0.002626602	5.977037009	5.903811658	26.6109611	19.65747488	19.51617406
Q2G0V9	SAOUHSC_00415	1.161513021	0.001186946	0.002760283	12.80793645	21.9284433	114.0469761	51.48386278	23.62484229
Q2FVB5	SAOUHSC_02819	1.19088968	0.001304336	0.003005757	1.70772486	5.903811658	24.33002158	14.97712372	14.38033878
Q2FVR2	SAOUHSC_02639	1.113070382	0.002896708	0.006247051	5.123174579	5.903811658	36.49503236	15.91319395	18.48900701
Q2FVA1	SAOUHSC_02832	1.09163811	0.003439615	0.007246967	6.830899438	8.434016655	56.26317489	35.57066883	17.46183995
Q2FVE3	SAOUHSC_02771	1.090224987	0.003498775	0.007351286	5.977037009	14.33782831	80.59319647	17.78533441	23.62484229
Q2G2F9	SAOUHSC_00718	1.070014507	0.00388212	0.008075093	119.5407402	177.1143498	1034.025917	413.7430427	217.7594159
Q2FUT6	hisZ	1.004580956	0.004697004	0.009621283	9.392486728	10.12081999	24.33002158	24.33782604	31.84217873

Appendix 4 Table 2 Identification of DEGs in trained-*rpoB* mutant compared to SH1000, related to Figure 5.4 A.

UniProt Accession	Gene name/Locus tag	log2FC	pvalue	padj	WT-2	WT-3	rpoB-1	rpoB-2	rpoB-3
Q2FYN4	lysA	-4.261094316	0	0	31469.09985	34143.42962	1572.360326	1499.619166	1868.739115
A0A0H2WXF8	*mecA*	12.43006172	0	0	0.85386243	2.530204996	99804.5093	100391.5559	111770.9285
Q9F0R1	sarR	1.225228975	0.000000424	0.000109775	93.07100485	122.2932415	362.2803184	268.5295675	200.1661981
Q2FWA5	SAOUHSC_02393	1.022828012	3.51E-05	3.30E-03	87.94783027	122.2932415	310.2224427	209.2951041	184.5282139
Q2FZ85	SAOUHSC_01155	1.047793407	4.47E-05	3.85E-03	134.9102639	171.2105381	521.6411623	288.2743887	254.8991429
Q2G0M0	SAOUHSC_00540	1.038887294	1.39E-04	8.46E-03	115.271428	150.1254965	456.8344191	259.644398	198.6023997
Q2FZM7	SAOUHSC_00973	1.25679853	4.18E-04	1.59E-02	34.15449719	46.3870916	219.9179645	86.87721303	95.39170378
Q2G021	SAOUHSC_00806	1.026916533	7.71E-04	2.35E-02	46.96243364	95.3043882	229.4796152	133.2775427	143.8694549
Q2G1V2	SAOUHSC_02685	-1.039598681	1.45E-03	3.24E-02	80.2630684	38.79647661	19.12330127	15.79585691	34.4035653

Appendix 4 Table 3 Identification of DEGs in Trained-*mecA*-cured-rpoB mutant compared to SH1000, related to Figure 5.5.

UniProt Accession	Gene name/Locus tag	log2FC	pvalue	padj	WT-2	WT-3	Trained-*mecA*-cured-rpoB-2	Trained-*mecA*-cured-rpoB-3
Q2FZZ6	SAOUHSC_00838	-3.453504864	0	0	6245.149812	6866.132959	620.8316527	532.6217821
Q2FYN4	lysA	-4.757998525	0	0	31469.09985	34143.42962	1219.119139	1084.667391
Q2G253	SAOUHSC_00025	-2.59074903	3.23E-198	2.41E-195	4806.391617	4913.658103	824.5962314	748.3284923
Q2G035	SAOUHSC_00792	-2.625535169	7.00E-177	3.92E-174	5949.713411	6160.205765	993.6774776	910.875255
Q2FVH5	SAOUHSC_02737	-1.487545138	1.69E-134	7.58E-132	4078.046965	4154.596604	1420.282468	1497.679291
O50581	recG	-1.600934521	3.93E-109	1.47E-106	4168.556382	4505.451697	1415.947051	1412.827837
Q2FXV8	recD2	1.37202931	1.91E-105	6.12E-103	1952.783377	2014.043177	5201.632799	5135.046471
Q2G239	SAOUHSC_00708	1.253284645	2.18E-97	6.11E-95	4320.543895	4620.997725	10656.45393	10778.17936
Q2FY54	SAOUHSC_01611	1.170542253	1.34E-88	3.34E-86	2787.006971	2890.337508	6513.529853	6328.078371
Q2G0Y8	SAOUHSC_00373	1.588386696	6.86E-87	1.54E-84	2394.230253	2741.055413	7976.299404	7664.233206
Q2FUQ2	mnmE	-1.467239779	6.17E-85	1.26E-82	7946.043772	7903.517007	2901.260768	2770.451112
Q2FUQ1	rnpA	-1.938137497	6.38E-79	1.19E-76	1090.382323	1027.263229	269.6629106	267.8443511
Q2FZ64	SAOUHSC_01187	1.016089275	4.74E-74	8.17E-72	4693.681777	4939.803555	9627.226033	9933.754043
Q2FXE2	SAOUHSC_01907	-1.496659505	6.65E-71	1.06E-68	1616.36158	1612.583984	574.0091537	554.0902224
Q2FZD0	uvrC	-1.371021843	6.03E-68	9.02E-66	3590.491517	3472.284657	1312.764137	1389.314783
Q2FY61	SAOUHSC_01604	-1.787426108	4.97E-64	6.97E-62	1425.950258	1432.93943	398.8583243	407.9003667
Q2G105	SAOUHSC_00356	-2.147268139	2.76E-63	3.64E-61	8865.653609	6895.652017	1800.932043	1594.798426

Q2FY14	SAOUHSC_01660	1.328817471	5.51E-63	6.87E-61	872.6474033	854.3658871	2244.011616	2138.665582
Q2G0Y6	guaA	1.348305018	2.11E-62	2.49E-60	7126.335839	7644.592696	19003.86499	19022.06046
Q2FZ77	pyrR	2.165753901	3.59E-61	4.03E-59	485.8477226	462.1841127	1960.475372	2501.584454
Q2G2J9	SAOUHSC_01412	1.377234961	1.41E-60	1.51E-58	784.699573	809.6655989	2056.72162	2137.643275
Q2G245	SAOUHSC_01854	-1.089395648	1.06E-58	1.08E-56	17124.21103	17155.63328	8001.44482	8008.750558
Q2FXM1	SAOUHSC_01814	-1.214383483	1.90E-57	1.85E-55	4034.499981	3547.347405	1626.648297	1612.17764
Q2G077	SAOUHSC_00743	1.00031206	6.19E-57	5.79E-55	4425.568974	4123.390743	8660.428138	8523.993127
Q2FZD3	mutS2	1.334807145	2.89E-56	2.59E-54	1757.248881	1831.868417	4786.299892	4374.450299
Q2G0E5	SAOUHSC_00661	1.487292488	2.49E-54	2.15E-52	426.0773525	432.6650544	1261.606222	1185.875753
Q2FUX4	SAOUHSC_02971	-1.986894618	2.47E-53	2.05E-51	810.3154459	820.6298205	218.5049951	171.7475228
Q2FZU6	rocD	-1.85008255	2.06E-52	1.59E-50	993.0420059	1082.927738	254.0554109	301.5804716
Q2G2B2	sasG	-1.177474092	3.33E-52	2.49E-50	6222.095526	6339.850319	2708.768272	2797.031086
Q2G170	SAOUHSC_00284	-1.604243615	1.88E-51	1.36E-49	2678.566442	2596.833728	908.7033129	785.1315329
Q2G0Y7	guaB	1.006213567	1.98E-49	1.39E-47	9050.941756	9956.356661	19270.05957	19130.42497
Q2FUY3	SAOUHSC_02962	-1.419143129	8.69E-49	5.90E-47	1523.290575	1591.498943	587.0154034	557.1571425
Q2FXQ3	SAOUHSC_01782	-1.242883022	9.29E-48	5.95E-46	4074.631515	4086.281069	1702.084545	1706.229855
Q9RQP9	icaA	-3.27273042	2.30E-47	1.43E-45	890.5785143	916.7776104	91.04374795	52.13764086
Q2G2N5	SAOUHSC_01354	1.019888282	5.04E-46	3.05E-44	2909.963161	3175.407271	6051.374447	6371.015251
Q2G0Y9	xpt	1.364992936	4.46E-44	2.56E-42	660.0356582	641.8286674	1728.097044	1679.649881
Q2G2J8	SAOUHSC_01413	1.176387549	6.48E-43	3.54E-41	496.0940717	489.172966	1156.689141	1093.868151
Q2G204	SAOUHSC_00942	-1.057079918	9.24E-43	4.93E-41	2635.873321	2713.223158	1250.334138	1301.396408
Q2FYZ0	SAOUHSC_01282	-1.271910327	2.83E-41	1.44E-39	2955.21787	2584.182703	1176.632057	1083.645084
Q2FXL6	SAOUHSC_01819	-1.709113603	3.67E-41	1.83E-39	2368.61438	2390.20032	684.1287346	719.7039052
Q2FYM1	odhA	-1.095023665	3.66E-40	1.78E-38	3850.919558	4211.104516	1927.526207	1809.48283
Q2G171	SAOUHSC_00282	1.052133641	6.11E-40	2.92E-38	819.7079326	786.8937539	1648.32538	1711.341388
Q2G0Q7	SAOUHSC_00489	-1.372602437	2.22E-39	1.04E-37	1351.664226	1389.925945	523.7183215	514.2202618
Q2G019	SAOUHSC_00808	-1.389032025	3.14E-39	1.44E-37	1659.908564	1529.930621	639.0404023	552.0456091
Q2FWX1	SAOUHSC_02150	-1.548008609	1.83E-38	8.04E-37	6010.337643	5147.280364	1967.412039	1739.965975
Q2G0B2	SAOUHSC_00693	1.008401952	3.78E-38	1.63E-36	754.8143879	783.5201472	1564.218298	1553.906159
Q2FYF4	SAOUHSC_01497	-1.025801776	1.12E-37	4.75E-36	3107.205382	3208.299935	1520.864132	1555.950772
Q2FVI5	SAOUHSC_02725	1.093217677	1.70E-37	7.06E-36	1096.35936	1122.567617	2224.0687	2560.878242
Q2G1S4	SAOUHSC_00018	1.263054337	3.44E-37	1.38E-35	3422.280619	3689.882286	8843.382717	8496.390846
P72360	scdA	-1.790347684	1.44E-36	5.55E-35	829.9542818	705.0837923	226.3087449	195.2605765
Q2G2J3	SAOUHSC_02573	1.238102216	1.23E-34	4.59E-33	1045.981477	1093.89196	2604.718275	2525.097508

Q2FZ76	SAOUHSC_01165	1.758507065	1.44E-34	5.31E-33	292.8748134	343.2644779	1004.082477	1253.347994
Q2G1W4	metK	1.160609343	6.10E-34	2.21E-32	3079.881784	3262.277642	7287.835252	7080.49609
Q2FZZ4	SAOUHSC_00840	-2.012149212	5.29E-31	1.74E-29	363.7453951	398.9289878	85.84124807	86.89606809
Q2G2K5	ureC	1.145458229	5.52E-31	1.79E-29	373.1378818	430.1348494	917.374146	885.3175879
Q2FZ72	carB	1.013754861	2.64E-30	8.01E-29	1684.670574	1803.192761	3460.529505	3653.724087
Q2FXN6	SAOUHSC_01800	-1.059108242	6.34E-30	1.87E-28	1301.286343	1247.391063	600.8887365	608.2724767
Q2FZU7	SAOUHSC_00893	-1.052385225	5.19E-29	1.45E-27	2278.958825	2310.077162	1107.265392	1079.555858
Q2FXM0	SAOUHSC_01815	-1.054783899	1.05E-28	2.88E-27	3352.263899	2929.133984	1508.724966	1478.255464
Q2G296	fhs	-1.000987061	2.48E-26	6.11E-25	6350.17489	6090.203426	3069.474931	3077.143117
Q2FUS7	SAOUHSC_03024	1.051543601	5.74E-26	1.35E-24	1676.985812	1541.738245	3192.600761	3568.872632
Q2FZ74	pyrC	1.153052471	1.81E-25	4.06E-24	625.0272986	659.5401024	1409.010385	1499.723905
Q2G200	SAOUHSC_00941	-1.410113579	2.25E-25	5.00E-24	685.6515311	616.5266175	259.2579108	212.6397902
Q2FZQ1	SAOUHSC_00949	-1.16994686	4.98E-25	1.10E-23	592.5805263	607.2491991	250.5870777	272.9558845
Q2FYZ3	SAOUHSC_01279	-1.219381871	4.53E-24	9.49E-23	543.0565054	583.6339525	235.8466614	236.1528439
Q2G252	rlmH	-1.495139155	5.55E-23	1.08E-21	526.8331192	474.8351377	186.4229125	151.3013892
Q2G145	SAOUHSC_00310	-1.237418403	1.83E-22	3.39E-21	574.6494153	547.3676809	225.4416616	238.1974572
Q2FZ71	pyrF	1.267720746	1.69E-21	2.96E-20	263.8434908	261.4545163	585.2812368	717.6592918
Q2FY13	SAOUHSC_01661	1.282096854	2.20E-21	3.82E-20	293.7286759	361.8193145	832.3999812	812.7338133
Q2FY36	SAOUHSC_01630	-1.133684763	3.57E-20	5.97E-19	1060.497138	1037.384049	473.4274893	461.0603142
Q2G249	SAOUHSC_00026	-1.411756056	3.90E-20	6.47E-19	619.0502616	517.8486226	187.2899958	221.8405503
Q2FZ75	pyrB	1.257300079	7.07E-20	1.16E-18	337.2756598	323.0228379	753.4953997	875.094521
Q2G261	sodM	-1.000307091	8.64E-20	1.39E-18	1533.536924	1490.290743	756.0966496	731.9715854
Q9RQP7	icaB	-2.414933108	4.41E-19	6.50E-18	224.565819	243.7430813	35.55041587	28.62458714
Q2FYI3	SAOUHSC_01464	-1.007963715	5.83E-19	8.54E-18	864.9626414	798.7013772	395.3899911	418.1234335
Q2FXQ4	SAOUHSC_01781	-1.012822938	9.35E-19	1.36E-17	3578.537443	4163.030621	2011.633288	1757.345189
Q2G012	emp	-1.626979587	1.40E-18	2.03E-17	339.8372471	388.8081678	108.3854142	109.3868151
Q2FVB4	SAOUHSC_02820	-2.172604357	3.18E-18	4.53E-17	400.4614796	457.9671044	71.10083173	81.78453468
Q2G1F9	SAOUHSC_00166	-1.221599648	2.28E-17	3.00E-16	433.7621143	415.7970211	185.5558292	165.6136827
Q2G0P8	ctsR	-1.063657246	1.15E-15	1.35E-14	642.1045472	700.866784	323.422076	302.6027783
Q2G176	SAOUHSC_00271	-1.090160912	1.49E-15	1.73E-14	579.7725898	627.4908391	279.200827	271.9335778
Q2G185	essB	-1.075681991	4.05E-15	4.61E-14	441.4468762	493.3899743	228.0429115	203.43903
Q2FVL5	SAOUHSC_02696	-1.218218612	8.16E-15	9.06E-14	488.4093098	508.5712043	178.6191626	233.0859238
Q2G155	lip2	-1.168736258	4.40E-14	4.67E-13	3990.099134	4002.784304	1850.355792	1573.329986
Q2G278	SAOUHSC_00773	-1.154015353	2.83E-13	2.74E-12	344.9604216	326.3964445	137.8662469	152.3236958

Q2G0E3	SAOUHSC_00662	1.240382106	7.95E-13	7.52E-12	158.8184119	152.6557015	435.2758235	337.3612055
Q2G194	SAOUHSC_00251	-1.238764791	1.09E-12	1.01E-11	1034.027402	1132.688437	466.4908228	402.7888333
Q2FZ70	pyrE	1.125289581	1.26E-12	1.16E-11	192.9729091	184.7049647	396.2570744	460.0380076
Q2FZL2	sspA	-1.270838963	1.54E-12	1.39E-11	393.6305801	410.7366111	149.13833	165.6136827
Q2FYV4	SAOUHSC_01320	-1.120417755	2.05E-12	1.81E-11	590.8728014	707.6139973	307.8145764	266.8220444
Q2G196	SAOUHSC_00249	-1.021205458	2.09E-12	1.84E-11	987.9188313	1009.551794	503.7754053	450.8372474
Q2FW50	SAOUHSC_02467	1.015420532	4.62E-12	3.95E-11	767.6223244	851.8356821	1642.255796	1727.698295
Q2G1N4	SAOUHSC_00074	-1.281170271	7.52E-12	6.27E-11	1619.777029	1950.788052	683.2616513	695.1685448
Q2G267	SAOUHSC_01181	-1.086279549	1.60E-11	1.28E-10	495.2402093	357.6023062	201.1633288	185.0375097
Q2G057	SAOUHSC_00765	-1.514086714	1.86E-11	1.48E-10	151.9875125	136.6310698	39.01874912	50.09302749
Q2G177	SAOUHSC_00270	-1.415939789	5.71E-11	4.37E-10	411.5616912	516.1618193	163.011663	149.2567758
Q2FUQ8	SAOUHSC_03046	-2.264925537	4.73E-10	3.28E-09	765.0607371	1031.480237	62.42999859	77.69530794
Q2G140	mepA	1.110660541	5.44E-10	3.70E-09	85.38624298	91.93078154	197.6949955	204.4613367
Q2G016	SAOUHSC_00811	-1.273216951	6.67E-10	4.49E-09	1045.981477	1057.625689	401.4595743	402.7888333
Q2FVB3	SAOUHSC_02821	-1.503158687	1.54E-09	9.99E-09	260.4280411	254.707303	92.77791458	63.38301437
Q2FVA8	SAOUHSC_02825	-1.450104798	2.01E-09	1.27E-08	141.7411633	114.7026265	38.15166581	43.95918739
Q2FZC0	flr	-1.625095006	4.75E-09	2.88E-08	96.48645457	104.5818065	23.41124947	26.57997377
Q2FWH6	SAOUHSC_02315	-1.198305755	1.52E-08	8.43E-08	158.8184119	137.4744715	58.96166534	58.27148096
Q2G1T5	SAOUHSC_02802	1.534662105	1.78E-08	9.78E-08	939.2486728	944.6098653	3677.300334	2883.927154
Q2FVF5	SAOUHSC_02759	-1.003310648	1.92E-08	1.05E-07	1784.572478	1561.136483	839.3366477	755.4846391
Q2G1N1	SAOUHSC_00077	-1.289360876	3.47E-08	1.85E-07	188.703597	193.9823831	73.70208167	64.40532106
Q2FY63	SAOUHSC_01602	-1.157765709	8.14E-08	4.17E-07	119.5407402	129.0404548	53.75916546	48.04841412
Q2G2Y3	SAOUHSC_01919	1.114819761	1.55E-07	7.60E-07	414.1232785	495.9201793	987.6078944	1132.715805
Q2FXE9	SAOUHSC_01900	-1.195360052	1.69E-07	8.22E-07	128.0793645	125.6668482	49.42374889	50.09302749
Q2G0F7	SAOUHSC_00612	-1.31265463	2.47E-07	1.17E-06	72.57830653	77.59295322	24.27833279	26.57997377
Q2G0V2	metN1	-1.054838397	2.61E-07	1.23E-06	156.2568247	177.9577514	80.63874818	69.51685448
Q2G0V1	SAOUHSC_00424	-1.285790568	8.78E-06	3.42E-05	70.87058167	81.80996155	26.01249941	24.5353604
Q2G1N3	sbnA	-1.362346531	9.45E-06	3.66E-05	53.79333308	66.62873157	15.60749965	18.4015203
Q2G1N2	SAOUHSC_00076	-1.256020785	1.63E-05	6.09E-05	96.48645457	95.3043882	32.08208261	31.69150719
Q2FZB9	SAOUHSC_01113	-1.264623159	3.53E-05	1.24E-04	127.225502	104.5818065	34.68333255	38.84765397
Q2FX11	SAOUHSC_02096	-1.043052887	5.88E-05	1.99E-04	140.0334385	110.4856182	43.35416569	64.40532106
Q2FZZ3	SAOUHSC_00841	-1.444762937	7.12E-05	2.38E-04	22.20042317	35.42286995	5.202499883	1.022306683
Q2G2Y4	SAOUHSC_01918	1.097670361	2.43E-04	7.55E-04	394.4844426	428.4480461	978.069978	1129.648885
Q2G056	SAOUHSC_00766	-1.120383887	5.05E-04	1.48E-03	35.00835962	37.95307495	11.27208308	13.28998688

Q2FYX7	SAOUHSC_01296	-1.085803355	7.20E-04	2.03E-03	40.1315342	48.9172966	19.0758329	13.28998688
Q2G021	SAOUHSC_00806	-1.077763888	1.10E-03	2.98E-03	46.96243364	95.3043882	22.54416616	24.5353604
Q2G0X2	SAOUHSC_00401	-1.031843312	0.001837451	0.004773541	134.9102639	88.55717488	52.02499883	31.69150719

Appendix 4 Table 4 Identification of DEGs in Trained-*rpoC* mutant compared to SH1000, related to Figure 5.6 A.

UniProt Accession	Gene name/Locus tag	log2FC	pvalue	padj	WT-2	WT-3	rpoC-1	rpoC-2	rpoC-3
Q2FYN4	lysA	-4.285372238	0	0	31469.09985	34143.42962	1587.841321	1668.537976	1584.775443
A0A0H2WXF8	*mecA*	11.90874463	0	0	0.85386243	2.530204996	71586.56075	73360.77192	71785.26207
Q2FW95	SAOUHSC_02404	1.760041899	1.38E-154	1.02E-151	1876.789621	1993.801537	6464.072182	6831.006237	6505.539375
Q2G2J8	SAOUHSC_01413	1.645142493	4.19E-97	2.31E-94	496.0940717	489.172966	1528.172962	1588.15013	1563.06619
Q2G2J9	SAOUHSC_01412	1.529558922	7.79E-87	3.43E-84	784.699573	809.6655989	2169.055332	2437.124211	2378.369234
Q2FW76	SAOUHSC_02428	1.833562438	2.95E-86	1.08E-83	636.1275102	679.7817424	2538.11518	2274.38784	2344.599285
Q2FWD4	murA	1.230935612	6.89E-78	2.17E-75	4785.898919	4642.926168	11309.36389	11145.48076	10929.40264
Q2FXT4	ruvB	1.1311004	3.12E-73	8.58E-71	3176.368239	3393.848302	7184.512364	7482.932062	7021.73716
Q2G025	SAOUHSC_00802	1.046832758	2.03E-68	4.97E-66	2218.334593	2330.318802	4752.474266	4690.92492	4712.113893
Q2G082	SAOUHSC_00738	-1.66352746	5.68E-65	1.25E-62	5787.479549	6080.082606	1814.360089	1819.510272	1889.911049
Q2FXT5	queA	1.197433409	6.42E-65	1.28E-62	2864.708452	3205.76973	6774.568641	7118.245736	7135.107702
Q2FZF0	isdB	1.94514882	1.92E-63	3.52E-61	239.0814803	243.7430813	988.9477954	902.8927589	967.2678121
Q2FXT3	ruvA	1.20540113	2.24E-63	3.80E-61	1649.662214	1743.311243	3944.741485	3921.358345	3951.083981
Q2FXU7	SAOUHSC_01735	1.013125459	4.26E-63	6.69E-61	2249.07364	2116.094779	4408.828719	4377.216252	4485.37281
Q2G2M9	SAOUHSC_02003	1.071921954	1.90E-61	2.79E-59	2061.223906	2189.470724	4384.519388	4499.758701	4589.094795
Q2G184	essC	-1.229501074	2.30E-60	3.16E-58	1676.985812	1798.132351	703.8656376	767.605896	730.8781723
Q2FVX0	SAOUHSC_02553	1.731006702	4.65E-56	5.68E-54	467.9166115	531.3430493	1687.288585	1589.130469	1800.6619
Q2G2J3	SAOUHSC_02573	1.441644853	1.49E-54	1.73E-52	1045.981477	1093.89196	2932.589328	2965.527248	2960.900846
Q2FX99	SAOUHSC_01978	1.571352137	2.21E-54	2.44E-52	935.8332231	1016.299007	2987.837809	2822.397669	3053.768205
Q2G188	esaA	-1.209520203	5.15E-49	5.15E-47	1508.774913	1659.814478	664.0867319	643.1027686	730.8781723
Q2FW77	SAOUHSC_02427	1.710986577	2.83E-48	2.71E-46	497.8017966	522.9090326	1837.564451	1581.287753	1733.122003
Q2FXW4	SAOUHSC_01717	1.124372816	6.39E-46	5.86E-44	2439.484962	2524.301185	5331.478338	5574.210887	5462.289179
Q2FXT1	obg	1.092834111	1.23E-44	1.08E-42	4987.410452	5284.754836	11397.76146	11108.22785	10588.08494
Q2FZU7	SAOUHSC_00893	-1.213917779	1.44E-44	1.22E-42	2278.958825	2310.077162	1004.41737	989.1626425	938.322142
Q2FZM6	SAOUHSC_00974	-2.211454929	2.45E-44	1.99E-42	1061.351	1059.312492	193.3696807	219.5960673	225.5350136
Q2FXW3	SAOUHSC_01718	1.384905119	9.00E-44	7.07E-42	1200.530576	1201.847373	3013.252109	3076.305622	3478.304701

Q2FUX4	SAOUHSC_02971	1.426526812	1.71E-42	1.30E-40	810.3154459	820.6298205	2310.491441	2207.724748	2133.537107
Q9RQP9	icaA	-2.725296204	2.15E-40	1.48E-38	890.5785143	916.7776104	133.7013221	107.8373545	106.134124
Q2FWH6	SAOUHSC_02315	2.296856528	1.02E-39	6.81E-38	158.8184119	137.4744715	779.0035706	720.5495959	829.7758787
Q2FXL7	ald2	1.109656038	1.11E-34	6.60E-33	531.1024313	528.8128443	1205.521838	1104.842714	1159.032877
Q2FXY9	SAOUHSC_01686	1.007363748	6.60E-33	3.72E-31	603.6807379	572.6697309	1228.726199	1129.351203	1222.954565
Q2FXW5	SAOUHSC_01716	1.063366577	2.36E-32	1.30E-30	3486.320301	3689.882286	7865.17364	7511.36191	7359.436645
Q2G0N7	SAOUHSC_00523	1.068599814	1.10E-30	5.48E-29	1361.056713	1434.626233	3027.616714	2867.49329	2995.876865
Q2G190	SAOUHSC_00256	-1.479755104	1.46E-30	7.00E-29	601.1191506	623.2738308	216.5740423	205.8713131	215.8864568
Q2FYV4	SAOUHSC_01320	-1.612057873	4.94E-27	2.02E-25	590.8728014	707.6139973	196.6845895	207.8319923	202.6196913
Q2FXR0	SAOUHSC_01775	1.100767	5.47E-27	2.19E-25	759.0837001	812.1958039	1771.266275	1585.209111	1769.30409
Q2G2L4	SAOUHSC_02814	1.035410352	6.91E-27	2.72E-25	774.4532238	745.5670723	1510.493448	1634.22609	1576.332956
Q2FUZ6	SAOUHSC_02949	-1.386340316	1.90E-26	7.07E-25	648.9354466	593.7547725	199.9994983	234.3011611	258.0988925
Q2G2C1	SAOUHSC_01064	-1.119304526	2.32E-26	8.35E-25	11936.14291	13358.63898	5937.001681	5687.930279	5573.247581
Q2FY23	SAOUHSC_01650	1.026446237	1.79E-25	5.88E-24	582.3341771	519.5354259	1099.444756	1144.056297	1156.620738
Q2G1F2	azoR	-1.960077071	2.10E-25	6.78E-24	252.7432792	213.3806214	49.72363217	52.93833766	59.09740997
Q2FYM4	SAOUHSC_01411	1.250960054	7.45E-25	2.34E-23	1369.595337	1515.592793	3498.333765	3413.542439	3637.505887
Q2FXT2	SAOUHSC_01752	1.214281715	1.34E-24	4.09E-23	490.9708971	601.3453875	1373.477217	1265.618406	1238.63347
Q2FVG2	SAOUHSC_02752	1.127703593	3.02E-24	8.99E-23	1064.76645	996.0573669	2405.518827	2174.393202	2297.562571
Q2FWN0	SAOUHSC_02258	-1.28309728	6.25E-22	1.66E-20	530.2485689	446.159481	182.3199846	197.0482568	205.0318305
Q2FWH7	SAOUHSC_02314	1.346166049	2.15E-21	5.20E-20	437.1775641	372.7835361	1075.135424	985.2412842	1114.408302
Q9RQP7	icaB	-2.375703944	5.57E-21	1.32E-19	224.565819	243.7430813	39.77890574	31.37086676	34.97601814
Q2FV66	SAOUHSC_02871	-1.324196265	6.14E-21	1.42E-19	352.6451835	391.3383728	144.7510181	141.1689004	144.7283509
Q2FYQ2	SAOUHSC_01383	-1.112660428	1.64E-20	3.58E-19	5951.421136	5988.995227	2703.86062	2716.520993	2699.183745
Q2FYV3	SAOUHSC_01321	-1.422157787	5.98E-20	1.25E-18	412.4155536	475.6785393	156.9056837	144.1099192	174.8800907
Q2FY13	SAOUHSC_01661	1.103356594	1.55E-18	2.92E-17	293.7286759	361.8193145	677.3463671	666.6309186	826.15767
P0A0M9	SAOUHSC_00995	1.340772952	1.95E-18	3.58E-17	144.3027506	205.7900064	437.5679631	448.9955305	488.4581844
Q2FZM5	SAOUHSC_00975	-1.302267211	3.61E-18	6.51E-17	2453.146761	2245.135234	946.9589504	869.561213	939.5282115
Q2G2C4	tarI'	-1.221737527	4.13E-18	7.39E-17	413.269416	408.2064061	184.5299238	158.815013	168.8497428
Q2G185	essB	-1.086558965	6.78E-18	1.20E-16	441.4468762	493.3899743	228.728708	221.5567465	194.1772042
Q2FVX1	SAOUHSC_02552	1.156023668	7.35E-18	1.29E-16	222.8580942	249.646893	544.7500147	499.973189	572.8830558
Q2G0W4	SAOUHSC_00410	-1.082157199	1.37E-17	2.33E-16	418.3925906	457.1237027	171.2702886	212.7336902	223.1228744
Q2G0L4	sdrD	-1.810148938	1.65E-17	2.76E-16	4237.719239	5524.280909	1190.052263	1185.23056	1362.858638
Q2G1C4	tarJ'	-1.096275683	1.98E-17	3.29E-16	570.3801031	619.9002241	282.8722186	285.2788196	246.0381966
Q2G1U4	SAOUHSC_00936	1.809483812	7.04E-16	1.03E-14	64.03968223	63.25512491	245.303252	266.6523675	229.1532223

Q2FZI8	purM	-1.200351962	2.44E-15	3.48E-14	255.3048665	234.465663	91.71247711	112.7390524	102.5159153
Q2G2L5	SAOUHSC_02813	1.098439203	2.72E-15	3.82E-14	291.1670886	243.7430813	553.5897715	585.262733	622.3319091
Q2FZI9	purF	-1.176574689	2.76E-15	3.84E-14	312.5136493	352.5418962	153.5907749	133.3261837	139.9040726
Q2G1M9	SAOUHSC_00079	1.301868424	4.86E-15	6.64E-14	163.0877241	198.1993914	475.1369296	422.5263617	489.664254
Q2FXF1	SAOUHSC_01898	1.466991299	8.69E-15	1.16E-13	108.4405286	108.7988148	308.2865194	312.728328	340.1116247
Q2FYV2	thrB	-1.290344738	1.42E-14	1.86E-13	351.7913211	392.1817744	143.6460485	154.8936546	135.0797942
Q2FZJ0	purL	-1.032889139	1.62E-14	2.09E-13	362.8915327	425.0744394	174.5851974	211.7533506	176.0861603
Q2FVL5	SAOUHSC_02696	1.038965238	1.83E-14	2.36E-13	488.4093098	508.5712043	1012.152157	1032.297584	1079.432284
Q9ZNI1	lytN	1.458854697	1.14E-13	1.39E-12	60.62423252	75.90614989	192.2647111	219.5960673	188.1468562
Q2G1I1	SAOUHSC_00142	1.726277886	1.17E-13	1.42E-12	73.43216896	73.3759449	270.7175529	300.964253	253.2746142
Q2FW41	SAOUHSC_02476	1.220999533	1.94E-13	2.30E-12	146.0104755	152.6557015	327.0710027	347.0402135	408.8575914
Q2FXX1	SAOUHSC_01709	1.02875406	6.53E-13	7.44E-12	174.1879357	187.2351697	358.0101516	399.9785512	373.8815733
Q2FXF2	sigS	1.66334419	2.17E-12	2.39E-11	49.52402093	78.43635489	226.5187688	204.8909735	267.7474492
Q2G1M8	SAOUHSC_00080	1.100119958	2.32E-12	2.54E-11	237.3737555	235.3090647	533.7003186	485.2680952	545.1434552
Q2G1N1	SAOUHSC_00077	1.39368788	7.33E-12	7.61E-11	188.703597	193.9823831	558.0096499	489.1894535	548.761664
Q2G0D1	sarX	-1.697967725	2.26E-11	2.30E-10	160.5261368	134.1008648	50.82860177	39.21358345	21.70925264
Q2FXW9	SAOUHSC_01711	1.340561916	6.25E-11	6.09E-10	99.04804186	84.34016655	274.0324617	234.3011611	237.5957095
P60647	cidA	-1.112566908	7.02E-11	6.78E-10	434.6159768	566.7659192	246.4082216	199.9892756	219.5046656
Q2FXQ8	engB	1.169271028	1.00E-10	9.44E-10	351.7913211	393.8685778	843.0918077	787.2126877	1001.037761
Q2FXN0	SAOUHSC_01805	1.326612794	8.82E-10	7.49E-09	51.23174579	67.47213324	160.2205925	166.6577297	164.0254644
Q2G2Q9	SAOUHSC_00274	1.129059861	1.37E-08	1.07E-07	84.53238055	102.8950032	198.8945287	239.202859	205.0318305
Q2FUQ8	SAOUHSC_03046	-1.992964838	1.58E-08	1.22E-07	765.0607371	1031.480237	121.5466564	106.8570149	126.6373071
Q2G0Y5	SAOUHSC_00376	1.165070612	1.86E-08	1.42E-07	82.82465569	104.5818065	217.6790119	200.9696152	244.832127
Q2G074	SAOUHSC_00746	1.064894988	3.14E-08	2.31E-07	440.5930138	407.3630044	1035.356519	800.9374419	943.1464203
Q2FYH9	SAOUHSC_01468	1.293179822	4.44E-08	3.19E-07	57.2087828	57.35131325	161.3255621	141.1689004	168.8497428
Q2FWJ9	ilvA	1.010520744	5.47E-08	3.91E-07	89.65555513	80.12315822	163.5355014	190.1858797	180.9104387
Q2FX92	SAOUHSC_01985	1.89139491	5.78E-08	4.10E-07	5.977037009	5.903811658	28.7292097	41.17426262	56.68527079
Q2G1N3	sbnA	1.43081482	8.48E-08	5.88E-07	53.79333308	66.62873157	193.3696807	177.4414651	168.8497428
Q2FZJ1	purQ	-1.140245969	1.13E-07	7.65E-07	110.1482534	109.6422165	36.46399692	51.95799807	49.44885324
Q2G1N2	SAOUHSC_00076	1.366042107	1.24E-07	8.26E-07	96.48645457	95.3043882	312.7063979	237.2421799	265.3353101
Q2FXN1	SAOUHSC_01804	1.584538155	1.25E-07	8.36E-07	13.66179888	22.77184497	69.61308504	67.64343145	69.95203629
Q2G225	SAOUHSC_00102	1.048121708	1.45E-07	9.45E-07	72.57830653	86.87037154	181.215015	166.6577297	172.4679515
Q2FWH9	kdpA	1.436791069	1.57E-07	1.01E-06	28.17746018	23.61524663	78.45284187	90.19124193	78.39452343
Q2FXG6	SAOUHSC_01881	1.620023839	2.55E-07	1.56E-06	18.78497346	20.24163997	83.97768989	57.84003559	88.04308016

Q2FWX7	SAOUHSC_02144	1.18729952	2.72E-07	1.66E-06	46.10857121	48.9172966	89.5025379	130.385165	138.698003
Q2G1T3	SAOUHSC_00831	-1.114486105	3.41E-07	2.07E-06	105.0250789	114.7026265	48.61866257	47.05630014	44.62457487
Q2G073	SAOUHSC_00747	1.108721409	4.32E-07	2.61E-06	173.3340732	188.0785714	435.3580239	386.253797	436.597192
Q2G072	SAOUHSC_00748	1.046006497	1.13E-06	6.44E-06	167.3570362	154.3425048	383.4244525	303.9052717	377.499782
P02976	spa	-1.194768359	1.27E-06	7.14E-06	13696.80724	17790.71473	5986.725313	6267.310975	6011.050843
Q2FV53	SAOUHSC_02886	1.688275621	1.68E-06	9.23E-06	15.36952374	20.24163997	72.92799385	90.19124193	107.3401936
Q2G1N0	SAOUHSC_00078	1.118839038	3.39E-06	1.78E-05	104.1712164	120.6064382	322.6511243	234.3011611	235.1835703
Q2FV70	SAOUHSC_02866	-1.226084732	3.74E-06	1.96E-05	1352.518089	1486.917136	553.5897715	532.3243953	517.4038546
Q2FYW3	SAOUHSC_01311	1.449857067	8.36E-06	4.18E-05	19.63883589	28.67565663	86.18762909	69.60411062	97.69163689
Q2FZ79	lspA	1.017031363	1.10E-05	5.39E-05	138.3257136	169.5237348	309.3914891	321.5513843	389.560478
Q2G218	ldh1	-1.589381221	1.53E-05	7.34E-05	1461.81248	569.2961242	140.3311397	150.9722963	136.2858638
Q2G187	SAOUHSC_00259	-1.015547573	1.55E-05	7.41E-05	78.55534354	96.14778986	34.25405772	41.17426262	43.41850528
Q2G180	SAOUHSC_00267	-1.312850941	4.23E-05	1.88E-04	42.69312149	44.70028827	19.88945287	9.803395862	9.64855673
Q2FXW8	SAOUHSC_01712	1.048049425	6.51E-05	2.79E-04	81.11693083	82.65336322	198.8945287	174.5004463	189.3529258
Q2G1V2	SAOUHSC_02685	-1.292772755	7.97E-05	3.34E-04	80.2630684	38.79647661	15.46957445	17.64611255	19.29711346
Q2FXX0	SAOUHSC_01710	1.053973151	1.25E-04	4.97E-04	48.6701585	37.10967328	118.2317476	94.11260028	86.83701057
Q2FXE5	crcB2	1.354620554	1.28E-04	5.12E-04	6.830899438	5.903811658	22.09939208	23.52815007	36.18208774
Q2G2A2	SAOUHSC_01044	1.281759833	2.22E-04	8.42E-04	15.36952374	16.86803331	68.50811543	44.11528138	43.41850528
Q2G183	SAOUHSC_00264	-1.067107739	3.03E-04	1.11E-03	60.62423252	43.85688661	17.67951366	26.46916883	18.09104387
Q2G192	SAOUHSC_00254	1.182858768	3.16E-04	1.15E-03	13.66179888	18.55483664	51.93357138	47.05630014	54.2731316
Q2FVM1	SAOUHSC_02681	-1.187784141	3.77E-04	1.35E-03	365.45312	143.3782831	78.45284187	96.07327945	74.77631465
Q2FXE4	SAOUHSC_01905	1.223754636	4.44E-04	1.57E-03	17.0772486	8.434016655	36.46399692	53.91867724	36.18208774
Q2FZS5	SAOUHSC_00915	1.141114926	4.79E-04	1.69E-03	16.22338617	16.02463164	50.82860177	55.87935641	30.15173978
Q2FXE3	SAOUHSC_01906	1.289016844	4.90E-04	1.72E-03	5.123174579	7.590614989	28.7292097	24.50848966	27.7396006
Q2FZZ3	SAOUHSC_00841	1.129907739	8.37E-04	2.79E-03	22.20042317	35.42286995	55.24848019	83.32886483	92.86735852
Q2FVV5	SAOUHSC_02586	1.160649581	8.55E-04	2.84E-03	7.684761868	8.434016655	38.67393613	20.58713131	25.32746142

Appendix 4 Table 5 Identification of DEGs in Trained-*rpoB* mutant compared to untrained, related to Figure 5.7 A.

UniProt Accession	Gene name/Locus tag	log2FC	pvalue	padj	Untrained-1	Untrained-2	Untrained-3	rpoB-1	rpoB-2	rpoB-3
Q2FZZ6	SAOUHSC_00838	3.175099346	0	0	517.7732717	486.7565208	547.4800408	4921.062859	4877.958063	4524.068837
Q2G253	SAOUHSC_00025	2.604026122	1.55E-281	1.77E-278	636.3821268	558.8339287	655.3325817	3716.294879	3916.385274	3821.923345
Q2G035	SAOUHSC_00792	2.118571535	1.15E-171	8.75E-169	1135.147569	1030.613326	1078.525409	4926.374887	5062.572141	4317.647445

O50581	recG	1.585864987	2.03E-157	1.16E-154	1373.125593	1416.274262	1537.669083	4454.666789	4428.763382	4173.77799
Q2FVH5	SAOUHSC_02737	1.21664534	3.52E-133	1.61E-130	1588.294221	1622.209713	1597.244772	3729.043747	3825.559096	3651.469317
Q2FXV8	recD2	-1.209449607	8.80E-118	3.35E-115	4612.820028	4966.788653	5057.770583	2097.188705	2122.568273	2078.288104
Q2G239	SAOUHSC_00708	-1.122298505	2.04E-114	6.65E-112	10186.67591	10480.24232	10832.50377	4879.629039	4605.479532	4943.166814
Q2FUQ2	mnmE	1.3250476	1.39E-100	3.96E-98	2361.532719	2505.860012	2464.173767	6433.92847	6416.07963	5615.600136
Q2FY54	SAOUHSC_01611	-1.025628383	2.37E-98	5.41E-96	6001.912197	6025.484086	6195.871681	3063.977825	2933.093181	2922.739252
Q2G2B2	sasG	1.341430085	1.35E-96	2.80E-94	1932.716089	2181.979712	2329.614883	5418.268692	5375.527556	5635.929515
Q2G2K5	ureC	-1.630005477	2.83E-87	5.40E-85	1402.777806	1318.922957	1324.018335	437.7111178	433.3988241	417.5341788
Q2FZD0	uvrC	1.287217894	2.62E-86	4.60E-84	1212.699513	1296.457272	1273.687149	3228.650697	3234.201703	2813.273362
Q2G0K4	SAOUHSC_00556	-1.370495531	1.23E-84	2.00E-82	11142.38957	12168.91302	10194.63303	4086.012037	4151.348645	4625.715734
Q2FZ77	pyrR	-2.118485496	2.17E-81	3.31E-79	2085.539037	1933.9211	1997.839924	489.7689935	478.8119127	364.3650325
Q2FXE2	SAOUHSC_01907	1.354986289	8.11E-81	1.16E-78	528.4176561	497.9893636	509.4748598	1384.31453	1330.800945	1244.783544
Q2FUQ1	rnpA	1.674834809	2.65E-80	3.56E-78	226.5733259	243.3782604	258.8460981	799.9914363	797.6907742	760.0060334
Q2G0Y8	SAOUHSC_00373	-1.263894043	2.85E-80	3.62E-78	6036.12629	6543.130924	6643.716518	2794.126796	2553.992615	2597.46918
Q2FY14	SAOUHSC_01660	-1.240357737	2.13E-77	2.56E-75	2061.969329	2223.166802	2197.110333	898.7951595	865.8104071	967.9912236
Q2FW95	SAOUHSC_02404	1.185330944	7.64E-73	8.73E-71	761.8338006	799.4039784	809.4076401	1881.520363	1848.115259	1681.083304
Q2G2N5	SAOUHSC_01354	-1.071778313	1.07E-72	1.16E-70	5735.802586	6274.478768	6121.915653	2932.239527	2884.718369	2760.104216
Q2FY61	SAOUHSC_01604	1.56534475	2.27E-72	2.36E-70	489.6416842	436.2087283	409.8396553	1307.821325	1433.474015	1279.18711
Q2G105	SAOUHSC_00356	1.878564448	1.37E-71	1.36E-69	2881.58693	2295.24421	2160.132319	9017.698952	9264.27008	9437.52348
Q2G0Q7	SAOUHSC_00489	1.552884222	1.40E-70	1.33E-68	397.6437901	497.9893636	493.0401869	1324.819815	1415.703676	1382.397806
Q2FXM1	SAOUHSC_01814	1.120240771	3.03E-70	2.77E-68	1539.634178	1469.630265	1426.735041	3137.283813	3257.895489	3313.688858
Q2G204	SAOUHSC_00942	1.127894283	2.08E-68	1.83E-66	1075.843142	1103.626804	1138.101098	2457.344213	2566.826749	2250.30593
Q2FYF4	SAOUHSC_01497	1.146717372	5.52E-67	4.67E-65	1294.053023	1458.397422	1431.870876	2986.422214	3005.161778	3334.018237
Q2G0Q8	SAOUHSC_00488	1.131366174	7.59E-67	6.20E-65	5291.779693	5535.919354	6169.165338	12864.66972	12589.29796	11986.51491
Q2G170	SAOUHSC_00284	1.523389658	1.71E-66	1.35E-64	773.9988114	675.8427078	857.6844917	2274.610445	2341.735788	2108.000274
Q2G2J9	SAOUHSC_01412	-1.22725667	2.00E-66	1.52E-64	1735.034664	1874.948675	1836.574696	745.8087493	764.1245782	800.6647924
Q2G0B2	SAOUHSC_00693	-1.096595583	2.15E-62	1.58E-60	1639.235204	1737.346351	1660.929129	774.4937012	770.0480246	800.6647924
A0A0H2WXF8	*mecA*	1.117748816	1.04E-61	7.43E-60	44124.77507	47471.86576	51286.4511	99804.5093	100391.5559	111770.9285
Q2G0E5	SAOUHSC_00661	-1.35838354	2.24E-61	1.55E-59	1119.941306	1090.521821	1088.797079	443.023146	417.6029672	409.7151867
Q2FYZ0	SAOUHSC_01282	1.29487031	3.21E-60	2.10E-58	859.1538869	916.4127575	1005.596548	2198.11724	2371.353019	2314.421665
Q2G0Y6	guaA	-1.076276495	7.30E-59	4.28E-57	14582.04637	16863.30524	17561.47516	7692.879137	7762.676432	7643.84669
Q2G171	SAOUHSC_00282	-1.099103424	1.62E-58	9.26E-57	1542.675431	1581.958693	1568.484094	759.6200225	712.7880433	700.5816933
Q2FWX1	SAOUHSC_02150	1.546755526	2.27E-55	1.21E-53	1624.02894	1725.177438	1725.640654	4389.860046	4820.698082	5912.721836
Q2FVM0	SAOUHSC_02682	-3.333634781	2.19E-54	1.14E-52	1368.563714	743.2397645	1520.207243	96.67891195	91.81341832	106.3382927

Q2FXQ3	SAOUHSC_01782	1.102580688	2.65E-54	1.35E-52	1512.262904	1585.702974	1561.293925	3583.494176	3532.348502	2939.941035
Q2FVI5	SAOUHSC_02725	-1.10743161	3.43E-54	1.70E-52	2394.986499	2342.047721	2462.119433	1103.839445	1085.965163	1130.62626
Q2FZD3	mutS2	-1.05968358	9.46E-52	4.42E-50	3698.163279	4284.393454	4269.933452	1982.448898	1974.482114	1874.994309
Q2G1S4	SAOUHSC_00018	-1.220741254	3.32E-50	1.49E-48	7101.325047	8097.94358	8320.053153	3046.979335	3187.801374	3764.062803
Q2FUY3	SAOUHSC_02962	1.219233024	2.19E-49	9.62E-48	432.6181961	463.354765	535.1540362	1063.468031	1151.123073	1144.700445
P0A084	msrA1	1.170810018	3.08E-49	1.30E-47	409.8088009	414.6791129	465.3066763	955.1026576	1003.036914	964.8636268
Q2FVV1	SAOUHSC_02590	-1.093987986	1.90E-48	7.90E-47	2880.826617	2776.384309	2769.242383	1393.876181	1178.765822	1351.121837
Q2FZT3	SAOUHSC_00907	1.003992852	1.77E-47	6.87E-46	778.5606904	770.3858012	821.7336448	1593.608439	1600.317754	1585.691601
Q2FUX4	SAOUHSC_02971	1.520160984	1.53E-46	5.63E-45	275.2333691	207.8075916	219.81375	698.0004962	701.9283916	673.9971201
Q2G2J8	SAOUHSC_01413	-1.056609124	8.23E-46	2.99E-44	957.2342864	992.2344463	977.8630373	462.1464472	450.1819221	487.9051079
Q2FVM2	SAOUHSC_02680	-3.493925708	5.64E-45	2.02E-43	1107.776295	554.1535776	1119.612091	62.68193192	48.3748118	73.49852586
Q2FVQ4	SAOUHSC_02648	-2.251737654	1.87E-43	6.27E-42	3530.894381	2070.587354	3848.794959	582.198283	584.4467058	670.8695233
Q2G0Y9	xpt	-1.128873756	5.75E-42	1.88E-40	1320.663984	1445.292439	1431.870876	652.3170543	650.5918567	591.1158037
Q2G200	SAOUHSC_00941	1.510975019	4.61E-40	1.46E-38	193.1195463	230.2732772	229.0582535	632.1313474	684.1580526	580.1692148
Q2FVL8	SAOUHSC_02684	-3.396471377	6.99E-39	2.13E-37	2032.317115	1169.15172	2443.630426	104.1157513	123.4051321	156.3798423
Q2FZE9	isdA	1.303893935	3.95E-38	1.19E-36	574.7967597	614.0620724	675.8759228	1628.667824	1727.67185	1308.89928
Q2FZD7	rnhC	1.001885656	4.01E-38	1.19E-36	660.7121484	754.4726073	732.3701109	1435.310001	1492.708478	1394.908193
Q2FZZ4	SAOUHSC_00840	1.92108695	6.38E-38	1.87E-36	88.95664139	76.75775905	67.79302569	321.9089046	330.7257541	293.9941035
Q2G0Z4	SAOUHSC_00367	1.062919111	2.28E-37	6.36E-36	970.9199235	1028.741185	1177.133446	2346.854027	2323.965449	2007.917175
Q2FYZ3	SAOUHSC_01279	1.256537942	3.62E-37	9.96E-36	278.2746218	251.8028925	263.9819334	699.0629018	610.1149733	619.2641754
Q2FXL6	SAOUHSC_01819	1.328559097	8.59E-37	2.28E-35	762.5941138	780.6825738	925.4775174	1887.894797	1930.056267	2505.205073
Q2G155	lip2	1.607588332	1.36E-35	3.49E-34	1091.049405	1100.818593	1311.69233	3120.285323	3227.291016	4719.543639
Q2G0U0	SAOUHSC_00437	-1.351464983	1.58E-35	4.02E-34	1310.019599	1189.745265	1454.468551	500.3930498	506.4546623	512.9258826
Q2G1D7	pflA	-3.717894792	3.70E-35	9.10E-34	1361.720895	869.6092459	2208.40917	57.3699038	72.06859717	64.11573533
Q2G0M2	SAOUHSC_00538	1.102227527	6.35E-35	1.55E-33	414.37068	492.3729422	522.8280315	1010.34775	1005.011396	1082.148508
Q2FWL3	SAOUHSC_02276	1.119578854	1.99E-34	4.78E-33	487.3607447	489.5647315	462.2251752	1122.962747	1098.799297	935.1514567
Q2G0M5	SAOUHSC_00535	-1.130641337	2.73E-34	6.49E-33	772.478185	841.5271389	798.1088025	348.4690453	381.0750481	356.5460404
Q2G019	SAOUHSC_00808	1.043586198	6.18E-34	1.43E-32	885.0045348	852.7599817	762.1579555	1867.70909	1726.684609	1609.148577
Q2FV87	glcB	-1.11251109	8.36E-34	1.91E-32	3259.462578	2711.795463	3232.494725	1291.885241	1309.081642	1618.531367
Q2G252	rlmH	1.551027499	2.81E-33	6.31E-32	130.0135528	161.9401502	155.1022254	414.3381941	429.4498599	514.489681
Q2G012	emp	1.878985586	3.91E-33	8.67E-32	114.8072893	99.22344463	82.17336448	365.4675353	337.6364415	472.2671236
Q2FZ76	SAOUHSC_01165	-1.441244348	1.17E-32	2.58E-31	859.9142001	1015.636202	958.3468632	351.6562622	360.3429859	298.6854987
Q2G172	SAOUHSC_00281	-2.663825404	2.48E-32	5.39E-31	681.2406041	381.9166548	813.5163083	70.11877131	73.05583823	104.7744943
Q2FVM1	SAOUHSC_02681	-3.728367515	3.94E-32	8.49E-31	3190.274079	1802.871268	3775.866098	106.2405626	80.95376669	157.9436407

Q2G261	sodM	1.086890499	5.62E-32	1.20E-30	532.9795351	621.5506343	686.1475934	1220.704064	1368.316105	1358.940829
Q2FZ71	pyrF	-1.338754229	2.22E-31	4.53E-30	627.2583687	571.938912	628.6262382	224.1675871	247.7975053	234.5697634
Q2G145	SAOUHSC_00310	1.23686555	6.08E-31	1.21E-29	211.3670624	221.8486451	232.1397546	553.5133311	572.5998131	459.7567362
Q2FW52	SAOUHSC_02465	1.138142588	8.77E-31	1.69E-29	288.158693	281.7571399	295.8241121	665.0659218	598.2680806	672.4333217
P72360	scdA	1.331586342	2.81E-30	5.22E-29	269.9111769	223.7207855	297.8784462	664.0035161	707.851838	664.6143296
Q2FVB4	SAOUHSC_02820	2.477130486	6.65E-30	1.20E-28	42.57753776	66.4609865	55.46702102	480.2073429	392.9219407	222.059376
Q2G1V2	SAOUHSC_02685	-3.450496566	8.04E-30	1.44E-28	528.4176561	202.1911702	530.0182009	19.12330127	15.79585691	34.4035653
Q2FVM6	nreB	-1.137894264	2.23E-29	3.93E-28	1377.687472	1211.274881	1447.278382	569.4494154	550.8805099	697.4540965
Q2FZQ1	SAOUHSC_00949	1.071964062	9.90E-29	1.68E-27	246.3414685	232.1454176	257.818931	545.0140861	519.2887961	500.4154952
Q2G0B8	SAOUHSC_00687	1.027354097	4.44E-28	7.35E-27	535.2604747	508.2861362	515.6378621	1122.962747	1067.207583	1022.724168
Q2FVM7	nreC	-1.265428831	8.27E-27	1.33E-25	824.1794809	703.9248147	918.287348	334.6577721	316.9043793	345.5994514
Q2FY36	SAOUHSC_01630	1.087436381	2.14E-26	3.36E-25	434.1388225	491.436872	512.5563609	1132.524397	1019.820012	936.7152551
Q2G1D8	pflB	-3.412373749	3.16E-26	4.91E-25	4923.027803	2706.179042	7712.997423	218.8555589	192.5120061	339.3442577
Q2G1G0	SAOUHSC_00164	1.074699135	4.26E-26	6.54E-25	306.4062092	285.5014209	300.9599474	606.6336124	618.0129018	689.6351044
Q2G249	SAOUHSC_00026	1.365903273	6.62E-26	1.00E-24	204.5242439	182.5336953	180.7814018	446.2103629	491.6460465	581.7330132
Q2FVN1	narT	-2.943586271	7.27E-26	1.08E-24	3046.574889	1449.97279	3345.483101	229.4796152	213.2440683	264.2819334
Q2G016	SAOUHSC_00811	1.797013337	1.57E-24	2.17E-23	242.5399026	258.3553841	235.2212558	1129.33718	1086.952404	545.7656495
Q2G176	SAOUHSC_00271	1.13633642	5.46E-24	7.39E-23	350.5043733	304.2228255	270.1449357	738.37191	735.4945876	597.3709974
Q2FV98	SAOUHSC_02836	-1.177414999	1.04E-23	1.38E-22	567.193628	533.5600324	492.0130198	247.5405108	232.0016484	207.9851902
Q2FY13	SAOUHSC_01661	-1.120420293	2.21E-23	2.89E-22	856.1126342	915.4766873	843.3041529	436.6487122	377.1260838	364.3650325
Q2G218	ldh1	-3.451150803	6.60E-22	8.03E-21	10493.84243	6274.478768	15855.35068	183.7961733	240.8868179	645.8487485
Q2G2P5	SAOUHSC_00201	-1.215606027	6.95E-22	8.32E-21	697.9674939	586.9160357	753.9406191	252.8525389	280.3764602	328.3976687
Q2G0P8	ctsR	1.049643434	6.95E-22	8.32E-21	390.8009716	359.4509692	328.6934579	852.0493119	726.6094181	691.1989028
Q2G2K7	ureF	-1.095792072	6.93E-22	8.32E-21	491.9226237	457.7383436	469.4153446	213.5435308	213.2440683	228.3145697
Q2FZ75	pyrB	-1.127525481	8.90E-22	1.05E-20	658.4312089	732.0069217	679.984591	339.9698003	334.6747184	245.5163524
Q2G1N4	SAOUHSC_00074	1.497489889	1.58E-21	1.84E-20	534.5001615	620.6145641	514.610695	1892.14442	1940.915918	1118.115872
Q9RQP9	icaA	1.742102391	2.42E-21	2.79E-20	142.9388768	250.8668223	173.5912325	655.5042711	611.1022144	785.0268082
Q2G1H7	SAOUHSC_00146	-2.005492563	4.43E-20	4.73E-19	694.9262412	401.5741297	978.8902043	154.0488157	154.996846	142.3056565
Q2FVL5	SAOUHSC_02696	1.188945365	9.59E-20	1.01E-18	231.8955181	204.9993809	214.6779147	588.5727167	523.2377603	409.7151867
Q2FYV4	SAOUHSC_01320	1.193637431	2.43E-19	2.50E-18	277.5143086	314.5195981	291.7154439	650.192243	598.2680806	835.0683577
Q2FVB3	SAOUHSC_02821	1.967058009	3.16E-19	3.21E-18	55.50286172	43.99530092	51.3583528	283.6623021	254.7081927	143.8694549
Q2FV02	SAOUHSC_02942	-1.583819519	9.87E-19	9.72E-18	1227.905776	831.2303663	1489.392231	327.2209328	329.7385131	453.5015426
Q2G185	essB	1.006744918	1.97E-18	1.91E-17	233.4161445	213.424013	206.4605782	438.7735235	455.1181273	444.118752
Q2FYJ3	tdcB	-2.723152309	4.51E-18	4.33E-17	342.9012416	162.8762204	572.1320502	28.6849519	27.6427496	48.4777511

Q2G0Q6	SAOUHSC_00490	1.10511917	4.61E-18	4.41E-17	149.0213821	196.5747488	175.6455666	376.0915915	381.0750481	387.8220088
Q2FYL4	SAOUHSC_01425	1.036906285	5.02E-18	4.78E-17	629.5393083	707.6690957	628.6262382	1497.991932	1545.032254	1057.127734
Q2FZL3	sspB	1.032609257	5.78E-18	5.44E-17	206.8051834	203.1272404	238.302757	478.0825316	479.7991538	384.694412
Q2FZU1	argG	-1.282363233	2.62E-16	2.17E-15	425.0150644	411.8709022	581.3765537	177.4217395	210.2823452	168.8902296
Q2G201	SAOUHSC_00940	1.105113574	5.02E-16	4.11E-15	163.4673325	189.0861869	183.862903	431.3366841	395.8836639	351.8546451
Q2FVW5	ureA	-1.884746529	1.05E-15	8.41E-15	139.8976241	121.6891302	122.2328797	28.6849519	26.65550854	35.96736372
Q2G273	ureG	-1.067796229	1.05E-15	8.41E-15	753.4703557	668.3541459	602.9470618	287.9119246	270.5040497	394.0772025
Q2FZC0	flr	1.858367368	2.26E-15	1.73E-14	42.57753776	34.6345986	24.65200934	168.9224945	103.660311	168.8902296
Q2FYS2	SAOUHSC_01363	1.256765565	2.38E-15	1.81E-14	144.4595031	152.5794479	128.395882	395.2148928	416.6157261	243.9525539
Q2FVM3	SAOUHSC_02679	-2.5336764	5.35E-15	4.01E-14	208.3258097	99.22344463	217.7594159	16.99849001	14.80861586	28.14837161
Q2G0E3	SAOUHSC_00662	-1.127294108	1.57E-14	1.14E-13	434.8991357	357.5788288	374.9159754	167.8600889	170.7927029	181.400617
Q2FYV3	SAOUHSC_01321	1.065099726	1.79E-14	1.29E-13	174.8720301	218.1043641	225.9767523	428.1494672	395.8836639	506.6706889
Q2G1N5	SAOUHSC_00072	1.165216166	4.42E-14	3.08E-13	199.9623648	228.4011367	241.3842581	572.6366323	619.0001428	358.1098388
Q2G057	SAOUHSC_00765	1.488515537	4.54E-14	3.14E-13	45.61879045	32.76245813	42.11384929	145.5495707	128.3413374	95.39170378
Q2G0D1	sarX	-1.634369425	6.35E-14	4.34E-13	560.3508094	451.185852	411.8939894	186.9833901	132.2903017	90.70030851
Q2G0Y5	SAOUHSC_00376	1.533614925	1.32E-13	8.79E-13	50.94098267	35.57066883	35.95084696	147.674382	138.213748	107.9020912
P02976	spa	1.671905569	1.72E-13	1.13E-12	1646.078022	2958.918004	3718.344743	10118.35118	9027.332227	11251.52965
Q2G177	SAOUHSC_00270	1.31517469	1.95E-13	1.27E-12	325.4140386	264.9078758	180.7814018	839.3004444	654.5408209	542.6380526
Q2FVK5	sbi	1.655001421	4.06E-13	2.59E-12	517.7732717	505.4779255	543.3713726	1518.177639	1403.856783	2736.64724
Q2FXE9	SAOUHSC_01900	1.414631271	4.55E-13	2.88E-12	58.54411442	40.25101999	48.27685163	162.5480608	147.0989175	115.7210833
Q2FZL2	sspA	1.072579556	2.39E-12	1.44E-11	139.8976241	153.5155181	155.1022254	379.2788084	346.5216111	242.3887555
Q2G140	mepA	-1.064400596	4.92E-12	2.86E-11	217.4495678	201.2551	192.0802395	96.67891195	92.80065937	93.82790536
Q2G0G1	adh	-2.152283134	5.77E-12	3.32E-11	798.3288329	520.4550492	1676.336635	161.4856551	148.0861586	154.8160438
Q2FZB8	SAOUHSC_01114	1.851170997	9.94E-12	5.62E-11	42.57753776	55.22814371	57.52135513	165.7352776	140.1882301	420.6617757
Q2FYJ4	SAOUHSC_01450	-1.764986993	1.18E-11	6.58E-11	369.5122027	190.0222572	532.072535	92.42928945	85.88997197	90.70030851
Q2G2K8	ureE	-1.08513213	1.52E-11	8.40E-11	206.8051834	232.1454176	218.7865829	106.2405626	96.7496236	95.39170378
Q2FWH6	SAOUHSC_02315	1.207758283	3.07E-11	1.67E-10	54.74254854	39.31494976	82.17336448	151.9240045	132.2903017	146.9970517
Q2FV03	SAOUHSC_02941	-1.605216526	3.52E-11	1.88E-10	202.2433043	117.008779	213.6507476	49.93306441	44.42584757	60.98813848
Q2FUQ8	SAOUHSC_03046	2.233828393	4.37E-11	2.31E-10	123.9310474	87.99060184	128.395882	475.9577204	589.3829111	1804.62338
Q2FVW6	SAOUHSC_02557	-1.256584738	6.91E-11	3.56E-10	229.6145786	248.9946818	162.2923948	73.30598818	95.76238254	82.8813164
Q2G2W8	SAOUHSC_00456	-1.030366051	1.02E-10	5.19E-10	208.3258097	210.6158023	212.6235806	97.74131758	100.6985878	100.083099
Q2G0X2	SAOUHSC_00401	1.944107646	1.23E-10	6.19E-10	25.85064792	18.72140465	23.62484229	75.43079943	87.86445409	226.7507713
Q2FYJ2	ald1	-2.305316732	1.63E-10	8.04E-10	323.8934122	147.8990967	582.4037207	30.80976315	25.66826749	46.91395268
Q2FVL9	SAOUHSC_02683	-2.379018343	1.68E-10	8.26E-10	64.62661981	21.52961534	66.76585864	4.249622503	3.948964229	1.563798423

Q2G2K6	ureB	-1.378486671	2.36E-10	1.15E-09	120.8897947	135.7301837	126.3415479	46.74584754	45.41308863	42.22255741
Q2FYJ5	norB	-1.395928155	3.63E-10	1.73E-09	253.9446002	146.9630265	307.1229497	81.80523319	89.8389362	70.37092902
Q2G2Y3	SAOUHSC_01919	-1.126042303	3.76E-10	1.79E-09	904.0123642	1127.96463	1127.829427	388.8404591	327.764031	669.3057249
Q2FWP0	SAOUHSC_02241	-1.174754559	1.62E-09	7.28E-09	215.9289415	191.8943976	310.2044509	89.24207257	93.78790043	118.8486801
Q2G1H3	rocD	1.054210079	2.16E-09	9.64E-09	79.83288329	101.0955851	108.8797079	237.9788602	234.9633716	148.5608501
Q2G0V2	metN1	1.060066376	2.45E-09	1.09E-08	55.50286172	75.82168882	73.95602803	148.7367876	160.9202923	134.4866643
Q2G2G0	SAOUHSC_00717	1.405479612	3.46E-09	1.52E-08	86.67570186	92.670953	104.7710397	199.7322577	197.4482114	464.4481315
Q2G017	SAOUHSC_00810	1.342014122	3.45E-09	1.52E-08	48.66004315	40.25101999	35.95084696	139.175137	129.3285785	81.31751798
Q2FZC2	SAOUHSC_01110	1.331828857	1.40E-08	5.78E-08	60.06474076	68.33312696	55.46702102	127.4886751	129.3285785	272.1009255
Q2G1E3	SAOUHSC_00182	1.44403546	2.07E-08	8.33E-08	74.51069107	49.61172232	45.19535046	234.7916433	155.984087	148.5608501
Q2FZ03	SAOUHSC_01268	1.321880164	2.18E-08	8.71E-08	25.09033475	20.59354511	26.70634345	66.93155443	69.106874	68.80713059
Q2FWG0	tenA	1.164968586	2.74E-08	1.08E-07	36.49503236	40.25101999	42.11384929	88.17966694	91.81341832	109.4658896
Q2G1K9	SAOUHSC_00113	-1.848441963	6.95E-08	2.66E-07	1208.897947	823.7418045	3701.91007	322.9713103	341.5854058	323.7062735
Q2FV35	SAOUHSC_02904	-1.000558027	1.07E-07	4.05E-07	124.6913606	140.4105349	118.1242114	64.80674318	65.15790977	50.04154952
Q2FV55	ssaA	-1.234311336	2.20E-07	8.12E-07	2691.508637	2892.457018	2131.371641	794.6794081	728.5839002	1427.74796
Q2FZB9	SAOUHSC_01113	1.352370554	3.08E-07	1.11E-06	98.84071265	45.86744139	32.86934579	226.2923983	167.8309797	140.741858
Q2G1N1	SAOUHSC_00077	1.003402951	3.68E-07	1.31E-06	100.361339	87.05453161	78.06469625	225.2299927	222.1292379	112.5934864
Q2FVA8	SAOUHSC_02825	1.033805107	6.65E-07	2.29E-06	53.2219222	45.86744139	43.14101635	103.0533457	103.660311	106.3382927
Q9RQP7	icaB	1.055746153	2.32E-06	7.55E-06	62.34568029	110.4562874	73.95602803	173.172117	145.1244354	236.1335618
Q2G2N7	SAOUHSC_02250	-1.463097518	3.41E-06	1.09E-05	63.86630664	34.6345986	47.24968457	19.12330127	10.85965163	6.25519369
Q2G1U4	SAOUHSC_00936	1.00853617	5.10E-06	1.58E-05	41.05691141	37.44280929	47.24968457	121.1142413	85.88997197	62.5519369
Q2FVC8	SAOUHSC_02785	-1.179719423	1.32E-05	3.88E-05	49.42035633	71.14133766	60.6028563	25.49773502	25.66826749	15.63798423
Q2G2Y4	SAOUHSC_01918	-1.077426855	3.93E-05	1.09E-04	903.252051	997.8508677	996.3520443	288.9743302	276.427496	656.7953375
Q2G1N2	SAOUHSC_00076	1.031050574	5.49E-05	1.49E-04	42.57753776	32.76245813	35.95084696	106.2405626	107.6092752	39.09496057
Q2FZZ3	SAOUHSC_00841	1.326768677	6.12E-05	1.66E-04	20.5284557	10.29677256	12.32600467	75.43079943	48.3748118	26.58457318
Q2G1H0	SAOUHSC_00153	1.025580601	6.15E-05	1.67E-04	715.454697	838.7189282	882.3365011	1272.76194	1336.724391	2930.558244
Q2FWH9	kdpA	-1.067136599	6.28E-05	1.70E-04	53.2219222	42.12316046	65.73869158	21.24811252	23.69378537	21.89317792
Q2FYW3	SAOUHSC_01311	1.25174263	1.07E-04	2.83E-04	19.76814253	5.616421394	8.217336448	41.43381941	42.45136546	28.14837161
Q2G1N3	sbnA	1.03520173	1.43E-04	3.70E-04	24.33002158	21.52961534	20.54334112	48.87065879	77.99204352	28.14837161
Q2FUT6	hisZ	-1.273753007	2.83E-04	7.09E-04	24.33002158	24.33782604	31.84217873	6.374433755	8.885169514	6.25519369
Q2FX92	SAOUHSC_01985	-1.248729001	3.08E-04	7.67E-04	26.6109611	19.65747488	19.51617406	7.436839381	5.923446343	3.127596845
Q2FV37	SAOUHSC_02902	-1.020016469	5.36E-04	1.29E-03	44.85847728	43.05923069	39.03234813	26.56014065	13.8213748	10.94658896
Q2FV53	SAOUHSC_02886	1.125445617	1.11E-03	2.55E-03	22.04908205	5.616421394	13.35317173	66.93155443	23.69378537	37.53116214

Appendix 4 Table 6 Identification of DEGs in Trained-*mecA*-cured-rpoB mutant compared to untrained, related to Figure 5.8 A.

UniProt Accession	Gene name/Locus tag	log2FC	pvalue	padj	Untrained-1	Untrained-2	Untrained-3	Trained-*mecA*-cured-rpoB-2	Trained-*mecA*-cured-rpoB-3
A0A0H2WXF8	*mecA*	-11.19053714	0	0	44124.77507	47471.86576	51286.4511	1.734166628	2.044613367
Q2FVM2	SAOUHSC_02680	-3.2674026	6.31E-35	7.07E-32	1107.776295	554.1535776	1119.612091	67.63249848	75.65069458
Q2FVL8	SAOUHSC_02684	-3.397071392	6.1E-34	4.56E-31	2032.317115	1169.15172	2443.630426	121.3916639	122.676802
Q2FVM0	SAOUHSC_02682	-2.74387631	4.29E-33	2.41E-30	1368.563714	743.2397645	1520.207243	148.2712467	159.4798426
Q2FZU6	rocD	-1.294875629	9.18E-30	4.12E-27	710.8928179	671.1623566	719.0169392	254.0554109	301.5804716
Q2FVM1	SAOUHSC_02681	-3.668054464	2.44E-28	9.13E-26	3190.274079	1802.871268	3775.866098	101.4487477	117.5652686
Q2G1V2	SAOUHSC_02685	-3.261430989	1.15E-24	3.69E-22	528.4176561	202.1911702	530.0182009	25.1454161	25.55766709
Q2FVN1	narT	-3.060561318	1.49E-24	4.18E-22	3046.574889	1449.97279	3345.483101	209.8341619	190.1490431
Q2G1D7	pflA	-3.149490191	2.19E-23	4.92E-21	1361.720895	869.6092459	2208.40917	117.9233307	92.00760151
Q2G172	SAOUHSC_00281	-2.404198772	2.19E-23	4.92E-21	681.2406041	381.9166548	813.5163083	104.0499977	93.02990819
Q2FVQ4	SAOUHSC_02648	-1.72109518	4.73E-22	8.16E-20	3530.894381	2070.587354	3848.794959	895.6970631	906.7860282
Q2FYJ3	tdcB	-3.113870405	6.43E-21	1.03E-18	342.9012416	162.8762204	572.1320502	20.80999953	20.44613367
Q2G218	ldh1	-3.395844092	2.32E-20	3.46E-18	10493.84243	6274.478768	15855.35068	334.6941591	294.4243248
Q2G1D8	pflB	-3.054025031	1.55E-19	2.17E-17	4923.027803	2706.179042	7712.997423	365.9091584	297.4912449
Q2FVM3	SAOUHSC_02679	-3.026421587	7.40E-19	9.76E-17	208.3258097	99.22344463	217.7594159	6.069583197	14.31229357
P02976	spa	1.904774705	1.16E-14	1.30E-12	1646.078022	2958.918004	3718.344743	11032.76808	13696.86494
Q2FUY2	clfB	1.058383329	1.49E-14	1.52E-12	10957.63347	14898.49382	16536.36243	25295.42151	35113.16766
Q2FV74	clpL	-1.704882045	4.67E-14	4.36E-12	2242.163551	1653.10003	3191.408043	629.5024858	634.8524504
Q2FV02	SAOUHSC_02942	-1.457552043	1.05E-13	9.09E-12	1227.905776	831.2303663	1489.392231	421.4024905	384.387313
Q2FYJ4	SAOUHSC_01450	-2.057641362	2.31E-13	1.92E-11	369.5122027	190.0222572	532.072535	61.56291528	74.62838789
Q2G0G1	adh	-2.339169751	1.28E-12	9.91E-11	798.3288329	520.4550492	1676.336635	125.7270805	119.609882
Q2G1K8	SAOUHSC_00114	-1.583903953	2.59E-12	1.90E-10	206.0448702	197.510819	191.0530724	58.96166534	56.22686759
Q2G1K5	SAOUHSC_00117	-1.419527589	2.63E-12	1.90E-10	549.706425	421.2316046	551.588709	182.0874959	165.6136827
Q2FZM6	SAOUHSC_00974	1.049197175	4.81E-12	3.37E-10	503.3273213	598.1488785	691.2834287	1188.771223	1369.890956
Q2G1K6	SAOUHSC_00116	-1.557499567	5.62E-12	3.82E-10	231.135205	162.8762204	202.35191	65.89833185	52.13764086
Q2FYJ2	ald1	-2.503171243	1.03E-11	6.61E-10	323.8934122	147.8990967	582.4037207	29.48083267	14.31229357
Q2FVL9	SAOUHSC_02683	-2.404815004	9.27E-11	5.47E-09	64.62661981	21.52961534	66.76585864	0.867083314	4.089226734
Q2G1K7	SAOUHSC_00115	-1.559349268	1.10E-10	6.34E-09	185.5164145	144.1548158	195.1617406	51.15791551	50.09302749
Q2G1K0	SAOUHSC_00122	-1.3586866	1.50E-10	8.19E-09	248.622408	239.6339795	216.7322488	77.17041493	92.00760151
Q2G1K2	SAOUHSC_00120	-1.272402782	2.38E-10	1.27E-08	250.1430343	226.5289962	236.2484229	91.04374795	92.00760151

Q2FV03	SAOUHSC_02941	-1.601493144	7.26E-10	3.62E-08	202.2433043	117.008779	213.6507476	56.3604154	44.98149407
Q2G1H7	SAOUHSC_00146	-1.424560745	1.28E-09	6.23E-08	694.9262412	401.5741297	978.8902043	219.3720784	253.5320575
Q2G0L4	sdrD	1.230590993	6.29E-09	2.88E-07	2267.253886	3223.82588	3855.985128	7021.640675	8970.741147
Q2FVK5	sbi	1.396832969	1.76E-08	7.61E-07	517.7732717	505.4779255	543.3713726	1792.26121	1318.775622
Q2G1J9	SAOUHSC_00123	-1.000331258	3.41E-08	1.39E-06	208.3258097	189.0861869	199.2704089	107.5183309	82.80684136
Q9RQP9	icaA	-1.191843266	3.67E-08	1.47E-06	142.9388768	250.8668223	173.5912325	91.04374795	52.13764086
Q2G0G9	SAOUHSC_00599	-1.68540005	1.73E-07	5.86E-06	130.773866	101.0955851	72.92886097	25.1454161	17.37921362
Q2G1K9	SAOUHSC_00113	-1.776140828	5.78E-07	1.75E-05	1208.897947	823.7418045	3701.91007	329.4916592	338.3835122
Q2G1K3	SAOUHSC_00119	-1.136489512	6.18E-07	1.85E-05	272.9524295	261.1635948	291.7154439	109.2524975	119.609882
P72358	lrgA	-1.046167479	8.83E-07	2.44E-05	116.3279157	95.4791637	143.8033878	51.15791551	54.18225422
Q2G021	SAOUHSC_00806	-1.530056936	1.05E-06	2.84E-05	157.3848271	87.05453161	69.8473598	22.54416616	24.5353604
Q2G1K4	SAOUHSC_00118	-1.056623133	1.22E-06	3.23E-05	285.8777535	268.6521567	288.6339427	126.5941638	125.7437221
Q2FZC2	SAOUHSC_01110	1.17365998	3.54E-06	8.81E-05	60.06474076	68.33312696	55.46702102	169.0812462	141.0783223
Q2FYJ5	norB	-1.068260094	7.02E-06	1.51E-04	253.9446002	146.9630265	307.1229497	103.1829143	105.2975884
Q2G1J8	SAOUHSC_00124	-1.143385926	7.15E-06	1.53E-04	164.2276456	110.4562874	87.30919976	52.89208214	46.00380076
Q2G1T5	SAOUHSC_02802	1.136508188	7.99E-06	1.67E-04	1212.699513	1368.53468	1318.8825	3677.300334	2883.927154
Q2FW05	SAOUHSC_02515	-1.055100579	1.35E-05	2.74E-04	476.7163602	246.1864711	223.9224182	126.5941638	143.1229357
Q2G1K1	SAOUHSC_00121	-1.166291642	1.38E-05	2.78E-04	78.31225695	94.54309347	77.0375292	31.2149993	33.73612055
Q2FXB9	SAOUHSC_01945	-1.080676331	2.00E-05	3.74E-04	99.60102582	76.75775905	71.90169392	38.15166581	32.71381387
Q9RQP7	icaB	-1.081709713	3.42E-05	5.90E-04	62.34568029	110.4562874	73.95602803	35.55041587	28.62458714
Q2FXD3	SAOUHSC_01930	-1.376840269	1.84E-04	2.17E-03	139.1373109	14.97712372	15.40750584	6.069583197	3.06692005
Q2FVE0	SAOUHSC_02774	-1.173772407	2.94E-04	3.21E-03	967.8786708	438.0808687	334.8564602	183.8216625	203.43903
Q2FVE3	SAOUHSC_02771	-1.321418965	3.99E-04	4.14E-03	80.59319647	17.78533441	23.62484229	6.069583197	6.133840101
Q2G1A1	SAOUHSC_00244	-1.074559324	4.88E-04	4.86E-03	249.3827211	118.8809195	82.17336448	71.96791504	37.82534729
Q2G2F9	SAOUHSC_00718	-1.248161312	7.57E-04	6.87E-03	1034.025917	413.7430427	217.7594159	97.98041446	121.6544953
Q2FVB5	SAOUHSC_02819	-1.074668025	3.72E-03	2.37E-02	24.33002158	14.97712372	14.38033878	4.335416569	5.111533417
Q2FVA1	SAOUHSC_02832	-1.024325094	6.03E-03	3.31E-02	56.26317489	35.57066883	17.46183995	17.34166628	0

Appendix 4 Table 7 Identification of DEGs in Trained-rpoC mutant compared to untrained, related to Figure 5.9 A.

UniProt Accession	Gene name/Locus tag	log2FC	pvalue	padj	Untrained-1	Untrained-2	Untrained-3	rpoC-1	rpoC-2	rpoC-3
Q2FZZ6	SAOUHSC_00838	4.144415201	0	0	517.7732717	486.7565208	547.4800408	9565.72186	9228.916865	9400.106394
O50581	recG	2.304819608	0	0	1373.125593	1416.274262	1537.669083	7238.655874	7071.189435	7255.714661

Q2FW95	SAOUHSC_02404	3.042994048	0	0	761.8338006	799.4039784	809.4076401	6464.072182	6831.006237	6505.539375
Q2FZD0	uvrC	2.400842498	5.86E-306	3.35E-303	1212.699513	1296.457272	1273.687149	6623.187805	6842.770312	6743.135084
Q2G035	SAOUHSC_00792	2.62364448	6.69E-265	3.06E-262	1135.147569	1030.613326	1078.525409	6449.707577	7243.729203	6691.274092
Q2G253	SAOUHSC_00025	2.413462144	1.00E-241	3.82E-239	636.3821268	558.8339287	655.3325817	3413.251106	3478.244852	3132.162728
Q2FUQ2	mnmE	1.957401928	3.63E-220	1.18E-217	2361.532719	2505.860012	2464.173767	9959.091039	9466.159045	9304.826896
Q2FUX4	SAOUHSC_02971	3.176242445	1.55E-211	4.44E-209	275.2333691	207.8075916	219.81375	2310.491441	2207.724748	2133.537107
Q2FXQ3	SAOUHSC_01782	2.104177415	9.17E-198	2.33E-195	1512.262904	1585.702974	1561.293925	6819.872394	6824.14386	6640.619169
Q2FUQ1	rnpA	2.529954496	9.86E-193	2.25E-190	226.5733259	243.3782604	258.8460981	1487.289087	1422.47274	1383.361821
Q2G245	SAOUHSC_01854	1.536158358	3.66E-171	7.60E-169	8751.204635	8536.024449	9052.423264	25521.48294	26839.73719	24461.50345
Q2FUY3	SAOUHSC_02962	2.233873528	6.65E-171	1.27E-168	432.6181961	463.354765	535.1540362	2224.303812	2307.719386	2297.562571
Q2G082	SAOUHSC_00738	-2.361671483	4.63E-159	8.14E-157	9509.23687	9677.094062	9875.184076	1814.360089	1819.510272	1889.911049
Q2FXE2	SAOUHSC_01907	1.814448795	3.46E-149	5.65E-147	528.4176561	497.9893636	509.4748598	1836.459481	1860.684535	1769.30409
Q2FUQ3	mnmG	1.437298126	8.80E-144	1.34E-141	4497.252426	4757.108921	4780.435478	13117.09417	12497.36905	12599.80902
Q2FY21	SAOUHSC_01652	1.470849646	6.31E-141	9.01E-139	5467.412036	6190.232447	6218.469357	16859.62621	16548.13222	16427.8739
Q2FY54	SAOUHSC_01611	-1.233407309	2.13E-140	2.86E-138	6001.912197	6025.484086	6195.871681	2582.313964	2479.278814	2664.207727
Q2G239	SAOUHSC_00708	-1.219542034	6.16E-135	7.82E-133	10186.67591	10480.24232	10832.50377	4402.198901	4537.991945	4534.821663
Q2G2B2	sasG	1.57968092	2.89E-134	3.48E-132	1932.716089	2181.979712	2329.614883	6375.674614	6581.999982	6436.793408
Q2FVX0	SAOUHSC_02553	2.50061713	1.08E-131	1.24E-129	311.7284014	278.9489292	276.3079381	1687.288585	1589.130469	1800.6619
Q2FVH5	SAOUHSC_02737	1.20120766	1.06E-130	1.15E-128	1588.294221	1622.209713	1597.244772	3699.438233	3761.562992	3630.26947
Q2FZF0	isdB	2.599397877	3.29E-124	3.42E-122	164.2276456	149.7712372	138.6675526	988.9477954	902.8927589	967.2678121
Q2FZ77	pyrR	-2.496693123	1.75E-109	1.74E-107	2085.539037	1933.9211	1997.839924	339.2256684	340.1778364	344.9359031
Q2FYK5	thyA	-1.564568908	1.88E-109	1.79E-107	1977.574566	2018.167421	2077.958954	660.771823	643.1027686	732.0842419
Q2FWD4	murA	1.305198263	3.52E-108	3.22E-106	4262.315655	4467.863219	4709.560952	11309.36389	11145.48076	10929.40264
Q2FXQ4	SAOUHSC_01781	1.973205903	6.67E-98	5.86E-96	1925.87327	1805.679478	1892.041717	7325.948473	7342.743501	7904.580101
Q2G0Q7	SAOUHSC_00489	1.810273935	6.61E-97	5.60E-95	397.6437901	497.9893636	493.0401869	1692.813433	1680.302051	1563.06619
Q2FWH6	SAOUHSC_02315	3.547154675	1.97E-95	1.61E-93	54.74254854	39.31494976	82.17336448	779.0035706	720.5495959	829.7758787
Q2FW76	SAOUHSC_02428	1.712215997	8.18E-95	6.45E-93	670.5962197	784.4268547	700.5279322	2538.11518	2274.38784	2344.599285
Q2FYM1	odhA	1.369142938	2.49E-91	1.89E-89	1877.97354	1829.081234	2069.741618	5038.661393	4964.439665	5028.104126
Q2FVE1	SAOUHSC_02773	-1.314055504	6.97E-90	5.14E-88	2761.457449	3031.931483	2939.752114	1135.908753	1142.095618	1209.6878
Q2G1B7	SAOUHSC_00228	-1.07940121	1.00E-86	7.18E-85	16593.83503	17078.60139	17589.20867	7870.698488	8018.197476	8272.431326
Q2FY61	SAOUHSC_01604	1.691161243	3.42E-85	2.37E-83	489.6416842	436.2087283	409.8396553	1367.952369	1482.273454	1547.387286
Q2FY74	xerD	1.328907985	1.25E-82	8.41E-81	1062.917818	1148.558175	1191.513785	2843.08679	2869.453969	2893.360949
Q2FZZ4	SAOUHSC_00840	2.74793878	1.46E-79	9.56E-78	88.95664139	76.75775905	67.79302569	520.4406834	531.3440557	659.7200664
Q2G0B2	SAOUHSC_00693	-1.225472925	2.89E-77	1.79E-75	1639.235204	1737.346351	1660.929129	699.4457592	704.8641625	736.9085202

Q2FXT1	obg	1.301584331	4.15E-77	2.49E-75	4190.846216	4574.575226	4558.567394	11397.76146	11108.22785	10588.08494
Q2G0Y8	SAOUHSC_00373	-1.198510482	5.62E-73	3.21E-71	6036.12629	6543.130924	6643.716518	2861.871274	2709.658616	2748.632598
Q2FXU3	lytH	-1.24446739	1.08E-71	6.01E-70	2611.675753	2699.62655	2555.591635	1121.544148	1099.941016	1073.401936
Q2G0Y6	guaA	-1.184869448	5.62E-71	2.99E-69	14582.04637	16863.30524	17561.47516	7395.561558	7088.835548	6927.663732
Q2FZT3	SAOUHSC_00907	1.221375358	6.56E-71	3.41E-69	778.5606904	770.3858012	821.7336448	1733.697308	1927.347627	1901.971745
Q2FUW9	SAOUHSC_02982	-1.087670449	2.56E-70	1.30E-68	7315.733362	7096.348432	7283.641594	3367.947352	3390.994629	3397.498038
Q2FXT3	ruvA	1.131861124	8.88E-70	4.41E-68	1729.712471	1783.213793	1851.982202	3944.741485	3921.358345	3951.083981
Q2G033	SAOUHSC_00794	-1.047075444	7.81E-69	3.72E-67	26269.58048	27695.50996	30195.62994	13238.64082	13772.79085	13524.8644
Q2G0K4	SAOUHSC_00556	-1.218675051	9.26E-68	4.32E-66	11142.38957	12168.91302	10194.63303	4795.56808	4684.062543	4813.423738
Q2G268	SAOUHSC_01178	1.160214378	7.95E-67	3.56E-65	1047.711554	1133.581051	1175.079112	2566.84439	2429.281495	2544.806837
Q2FZQ1	SAOUHSC_00949	1.607515415	3.57E-66	1.54E-64	246.3414685	232.1454176	257.818931	763.5339962	734.2743501	786.3573735
Q2FVL5	SAOUHSC_02696	2.193411924	3.96E-66	1.68E-64	231.8955181	204.9993809	214.6779147	1012.152157	1032.297584	1079.432284
Q2FYT4	sbcD	1.50383248	4.49E-66	1.87E-64	334.5377967	366.9395311	338.9651285	976.7931297	1045.041999	967.2678121
Q2FYH5	dinG	-1.068844566	2.93E-65	1.20E-63	4450.873322	4122.453303	4020.331857	1889.498022	1979.305625	2108.209645
Q53726	pcrB	1.138801468	9.19E-65	3.69E-63	970.1596103	967.8966203	947.0480256	2117.121761	2141.061656	2137.155316
Q2G2K5	ureC	-1.315741569	1.50E-61	5.91E-60	1402.777806	1318.922957	1324.018335	533.7003186	548.0098287	528.2584809
Q2FYZ3	SAOUHSC_01279	1.60180612	2.49E-61	9.64E-60	278.2746218	251.8028925	263.9819334	829.8321724	780.3503106	851.4851314
Q2FVM0	SAOUHSC_02682	-3.493150125	2.32E-59	8.82E-58	1368.563714	743.2397645	1520.207243	79.55781147	94.11260028	85.63094098
Q2FW75	SAOUHSC_02430	1.418612434	5.35E-59	2.01E-57	3714.129856	3499.966599	2862.714585	9512.683319	8364.25735	9449.555247
Q2FVQ4	SAOUHSC_02648	-2.642496617	1.03E-58	3.72E-57	3530.894381	2070.587354	3848.794959	475.1369296	475.4646993	426.9486353
Q2FZ10	cinA	1.194915402	1.87E-58	6.70E-57	797.5685198	938.8784431	851.5214894	1979.00056	1890.094722	2100.973228
Q2G0Q9	hslO	1.217657732	3.93E-56	1.36E-54	1614.144869	1761.684177	1710.233148	3982.310452	4054.684529	3893.19264
Q2FZI6	purH	-1.5100095	4.80E-56	1.64E-54	780.0813168	777.8743631	787.8371319	251.9330697	286.2591592	268.9535188
Q2FZD7	rnhC	1.178772033	5.56E-53	1.76E-51	660.7121484	754.4726073	732.3701109	1588.94629	1587.16979	1723.473446
Q2FX99	SAOUHSC_01978	1.371239081	4.72E-52	1.44E-50	1234.748595	1098.010383	1042.574562	2987.837809	2822.397669	3053.768205
Q2G252	rlmH	1.923645816	1.09E-51	3.27E-50	130.0135528	161.9401502	155.1022254	595.5786164	574.4789975	590.9740997
Q2FYF4	SAOUHSC_01497	1.00150329	1.73E-51	5.12E-50	1294.053023	1458.397422	1431.870876	2775.683645	2878.277025	2759.487225
Q2FVS3	SAOUHSC_02619	1.216991968	1.81E-51	5.30E-50	789.965388	723.5822896	759.0764543	1829.829664	1701.869522	1807.898317
Q2FVM2	SAOUHSC_02680	-3.736373715	1.05E-50	3.03E-49	1107.776295	554.1535776	1119.612091	43.09381455	49.9973189	56.68527079
Q2FVG4	SAOUHSC_02750	-1.026025499	5.27E-50	1.51E-48	1904.584501	1856.227271	1885.878715	923.7545887	889.1680047	945.5585595
Q2G188	esaA	-1.109867818	1.47E-49	4.12E-48	1427.868141	1498.648442	1504.799737	664.0867319	643.1027686	730.8781723
Q2G145	SAOUHSC_00310	1.552578932	2.51E-49	6.83E-48	211.3670624	221.8486451	232.1397546	664.0867319	660.7488811	666.9564839
Q2FWH7	SAOUHSC_02314	1.921943271	3.04E-49	8.17E-48	237.9780235	234.0175581	334.8564602	1075.135424	985.2412842	1114.408302
Q2FV86	SAOUHSC_02849	-1.129227344	7.69E-49	2.04E-47	11351.47569	13062.86009	12786.17551	5513.798323	5820.276123	5526.210867

Q2G0W4	SAOUHSC_00410	-1.677381741	8.51E-49	2.24E-47	603.6886603	717.029798	683.0660922	171.2702886	212.7336902	223.1228744
Q2FY23	SAOUHSC_01650	1.300571982	9.41E-48	2.39E-46	471.394168	447.4415711	442.7090011	1099.444756	1144.056297	1156.620738
Q2FZ72	carB	-1.065518879	2.15E-47	5.34E-46	3172.786876	3365.172485	3410.194626	1582.316473	1592.071488	1542.563007
Q2FVL8	SAOUHSC_02684	-3.781072212	2.31E-47	5.69E-46	2032.317115	1169.15172	2443.630426	92.81744672	106.8570149	77.18845384
Q2G1N5	SAOUHSC_00072	2.181769081	9.57E-47	2.33E-45	199.9623648	228.4011367	241.3842581	1109.389482	1025.435207	1109.584024
Q2FX96	SAOUHSC_01981	1.0041871	5.56E-46	1.32E-44	681.2406041	696.4362529	738.5331132	1349.167886	1453.843606	1462.962414
Q2FZ88	SAOUHSC_01152	1.391983391	5.74E-46	1.35E-44	559.5904962	610.3177915	672.7944216	1612.150652	1559.720282	1737.946281
Q2FWY4	sdcS	-1.510691188	1.62E-45	3.78E-44	603.6886603	676.778778	692.3105957	222.0988904	244.104557	207.4439697
Q2G057	SAOUHSC_00765	2.654715157	1.32E-44	3.02E-43	45.61879045	32.76245813	42.11384929	301.6567018	282.3378008	287.0445627
Q2FWL3	SAOUHSC_02276	1.271195066	1.51E-44	3.43E-43	487.3607447	489.5647315	462.2251752	1170.16281	1122.488826	1231.397053
Q2G0D1	sarX	-3.242786474	3.58E-44	8.03E-43	560.3508094	451.185852	411.8939894	50.82860177	39.21358345	21.70925264
Q2G278	SAOUHSC_00773	1.819186091	3.74E-44	8.30E-43	147.5007558	139.4744646	123.2600467	468.507112	537.2260933	505.3431587
Q2FVX2	SAOUHSC_02551	1.179268756	1.05E-42	2.29E-41	435.6594488	466.1629757	437.5731658	1038.671428	992.1036613	1034.807709
Q2G2U2	SAOUHSC_00023	-1.131330289	1.71E-42	3.70E-41	2293.104533	2380.426601	2386.109071	1014.362096	1074.452187	1102.347606
Q2G1D7	pflA	-4.102535871	4.32E-42	9.15E-41	1361.720895	869.6092459	2208.40917	34.25405772	46.07596055	54.2731316
Q2G0E5	SAOUHSC_00661	-1.080866405	4.50E-42	9.44E-41	1119.941306	1090.521821	1088.797079	478.4518384	532.3243953	536.7009681
Q2FUW8	gtf2	-1.010906258	5.78E-42	1.20E-40	1415.70313	1433.123526	1431.870876	738.1196953	679.3753333	692.2839453
Q2FUX3	isaB	1.093064647	1.17E-41	2.41E-40	1047.711554	985.6819547	978.8902043	2054.138493	2061.65415	2374.751025
Q2FZ71	pyrF	-1.566322586	1.49E-41	2.99E-40	627.2583687	571.938912	628.6262382	208.8392551	200.9696152	190.5589954
Q2FWC5	SAOUHSC_02373	-1.168758268	7.28E-41	1.42E-39	752.7100425	743.2397645	760.1036214	342.5405772	328.4137614	320.8145113
Q2FYS2	SAOUHSC_01363	2.080888588	9.43E-41	1.83E-39	144.4595031	152.5794479	128.395882	640.8823702	633.2993727	653.6897184
Q2FW77	SAOUHSC_02427	1.362693647	3.31E-39	6.16E-38	665.2740275	706.7330254	593.7025583	1837.564451	1581.287753	1733.122003
Q2FZL3	sspB	1.52867498	6.03E-39	1.10E-37	206.8051834	203.1272404	238.302757	626.5177653	602.9088455	689.8718062
Q2FV87	glcB	-1.191121788	1.40E-38	2.52E-37	3259.462578	2711.795463	3232.494725	1295.024376	1335.222516	1350.797942
Q2FVW0	SAOUHSC_02581	-1.579474059	1.94E-38	3.44E-37	1110.057234	1066.183995	1064.14507	337.0157291	360.7649677	353.3783902
Q2FZ76	SAOUHSC_01165	-1.570746999	1.97E-38	3.46E-37	859.9142001	1015.636202	958.3468632	339.2256684	291.1608571	295.4870498
Q2FVM1	SAOUHSC_02681	-4.056798477	1.25E-37	2.18E-36	3190.274079	1802.871268	3775.866098	78.45284187	96.07327945	74.77631465
Q2FVM6	nreB	-1.291658908	2.88E-37	4.94E-36	1377.687472	1211.274881	1447.278382	522.6506226	561.7345829	536.7009681
Q2G0M2	SAOUHSC_00538	1.131217508	4.96E-37	8.34E-36	414.37068	492.3729422	522.8280315	1083.975181	1047.983018	1023.953083
Q2FYH7	SAOUHSC_01470	1.016434663	6.96E-37	1.16E-35	816.5763491	828.4221556	803.2446378	1665.189193	1616.579978	1712.61882
Q2G1N4	SAOUHSC_00074	1.985950258	8.03E-37	1.33E-35	534.5001615	620.6145641	514.610695	2689.496016	2117.533506	2258.968344
Q2G016	SAOUHSC_00811	2.215149211	1.14E-36	1.87E-35	242.5399026	258.3553841	235.2212558	1285.079649	1261.697047	1215.718148
Q2G0M6	araB	1.215660263	1.49E-36	2.36E-35	415.8913063	431.5283771	420.1113259	961.3235553	1030.336905	992.5952736
Q2G1N1	SAOUHSC_00077	2.409341133	3.39E-36	5.27E-35	100.361339	87.05453161	78.06469625	558.0096499	489.1894535	548.761664

Q2FUS7	SAOUHSC_03024	-1.039881684	1.61E-35	2.47E-34	2524.239738	2736.133289	2545.319965	1287.289588	1235.227879	1238.63347
Q2G0F2	SAOUHSC_00617	-1.009898872	1.99E-35	3.01E-34	3105.879317	2461.864711	2642.900835	1384.526914	1301.890971	1360.446499
Q2FZI5	purD	-1.429068982	3.50E-35	5.22E-34	798.3288329	787.2350654	873.0919976	329.2809419	294.1018759	265.3353101
Q2G1M9	SAOUHSC_00079	1.915731792	5.38E-35	7.99E-34	107.2041576	121.6891302	118.1242114	475.1369296	422.5263617	489.664254
Q2FWC4	SAOUHSC_02374	-1.165108106	1.53E-34	2.19E-33	797.5685198	757.280818	732.3701109	320.4411851	369.588024	314.7841633
Q2G0Y9	xpt	-1.001668132	2.62E-34	3.74E-33	1320.663984	1445.292439	1431.870876	760.2190874	684.2770312	631.9804658
Q2G0D9	graS	-1.091170627	2.84E-34	4.04E-33	991.4483792	992.2344463	953.2110279	440.8828719	482.3270764	439.0093312
Q2FW63	SAOUHSC_02444	-1.344622537	4.10E-34	5.78E-33	5580.698699	5465.714087	4967.379883	1949.166381	2145.963354	2079.263975
Q2G1V2	SAOUHSC_02685	-3.70367064	9.03E-34	1.25E-32	528.4176561	202.1911702	530.0182009	15.46957445	17.64611255	19.29711346
Q2G249	SAOUHSC_00026	1.556219749	1.12E-33	1.54E-32	204.5242439	182.5336953	180.7814018	542.5400754	613.692581	575.295195
Q2FUQ4	rsmG	1.013517892	2.89E-33	3.96E-32	1541.915117	1743.898843	1798.569515	3650.819571	3370.407497	3328.752072
Q2G200	SAOUHSC_00941	1.366175539	5.08E-33	6.87E-32	193.1195463	230.2732772	229.0582535	561.3245587	570.5576392	584.9437517
Q2G261	sodM	1.095868059	1.13E-32	1.52E-31	532.9795351	621.5506343	686.1475934	1289.499528	1400.905269	1278.433767
Q2FVP4	SAOUHSC_02658	-1.236991186	3.62E-32	4.76E-31	583.1602046	549.4732264	554.6702102	230.9386472	242.1438778	230.3592919
Q2FXL6	SAOUHSC_01819	1.228269298	1.03E-31	1.33E-30	762.5941138	780.6825738	925.4775174	1956.901168	2027.342264	1893.529258
Q2G2M2	mprF	1.105571428	1.21E-31	1.57E-30	4210.614359	4066.289089	3812.844112	9123.734018	8121.133132	9103.413274
Q2G105	SAOUHSC_00356	1.219603137	4.31E-31	5.47E-30	2881.58693	2295.24421	2160.132319	5659.65431	6095.751547	5640.787478
Q2FVB8	SAOUHSC_02816	-1.062852764	5.26E-31	6.61E-30	1043.909988	994.1065868	952.1838609	423.2033582	503.8945473	488.4581844
Q2FW50	SAOUHSC_02467	-1.423602171	6.31E-31	7.88E-30	1589.054534	1746.707054	1851.982202	646.4072182	608.790883	624.7440482
Q2G218	ldh1	-4.13104473	1.17E-30	1.42E-29	10493.84243	6274.478768	15855.35068	140.3311397	150.9722963	136.2858638
Q2G0A0	SAOUHSC_00705	1.354740135	1.57E-30	1.90E-29	206.0448702	172.2369228	200.2975759	507.1810481	487.2287744	523.4342026
P0A0M9	SAOUHSC_00995	1.607367216	1.98E-30	2.39E-29	152.0626348	140.4105349	140.7218867	437.5679631	448.9955305	488.4581844
Q2G1H7	SAOUHSC_00146	-2.53308798	2.11E-30	2.52E-29	694.9262412	401.5741297	978.8902043	104.9721124	100.9749774	92.86735852
Q2G176	SAOUHSC_00271	1.272116729	4.68E-30	5.52E-29	350.5043733	304.2228255	270.1449357	753.5892698	767.605896	767.06026
Q2FXP2	SAOUHSC_01794	1.372068255	4.91E-30	5.75E-29	237.2177104	217.1682939	222.8952511	605.5233429	568.59696	627.1561874
Q2FW66	asp23	-1.128776491	7.74E-30	8.89E-29	18417.82633	19386.01451	18704.71209	8540.310067	8773.058957	8161.472924
Q2G0Q6	SAOUHSC_00490	1.414351309	2.04E-29	2.32E-28	149.0213821	196.5747488	175.6455666	524.8605618	434.2904367	466.7489318
Q2FZL2	sspA	1.684200371	3.40E-29	3.81E-28	139.8976241	153.5155181	155.1022254	563.5344979	457.8185868	493.2824628
Q2G1U4	SAOUHSC_00936	2.356837513	8.75E-29	9.61E-28	41.05691141	37.44280929	47.24968457	245.303252	266.6523675	229.1532223
Q2FXE9	SAOUHSC_01900	2.118521553	9.22E-29	1.01E-27	58.54411442	40.25101999	48.27685163	208.8392551	235.2815007	272.5717276
Q2FVN3	sarZ	-1.176938395	1.27E-28	1.39E-27	4290.447242	3084.351416	3393.759953	1539.222658	1477.371756	1670.406384
Q2G1D8	pflB	-3.56618182	1.73E-28	1.87E-27	4923.027803	2706.179042	7712.997423	202.2094375	235.2815007	207.4439697
Q2G0Y5	SAOUHSC_00376	2.234029378	2.14E-28	2.28E-27	50.94098267	35.57066883	35.95084696	217.6790119	200.9696152	244.832127
Q2G2W1	SAOUHSC_02629	-1.145141226	3.24E-28	3.40E-27	7911.058578	7609.314919	7181.952055	3370.157291	3308.646104	3426.443709

Q2FXT2	SAOUHSC_01752	1.159731299	1.20E-27	1.24E-26	586.2014573	546.6650157	574.1863843	1373.477217	1265.618406	1238.63347
Q2G0U0	SAOUHSC_00437	-1.151729446	6.82E-27	6.87E-26	1310.019599	1189.745265	1454.468551	620.9929173	586.2430726	542.731316
Q2FVV9	SAOUHSC_02582	-1.154171983	1.35E-26	1.33E-25	14772.88498	14353.70094	15328.41398	6522.635571	6668.269865	6440.411617
Q2G1M8	SAOUHSC_00080	1.52938539	3.32E-26	3.21E-25	197.6814253	172.2369228	147.9120561	533.7003186	485.2680952	545.1434552
Q2FW41	SAOUHSC_02476	1.628399796	3.40E-26	3.28E-25	118.6088552	117.9448493	95.5265362	327.0710027	347.0402135	408.8575914
Q2FVN1	narT	-2.960666059	3.50E-26	3.35E-25	3046.574889	1449.97279	3345.483101	238.6734344	244.104557	213.4743176
Q2G1Y2	SAOUHSC_02923	-1.159007938	1.02E-25	9.51E-25	485.8401183	458.6744139	518.7193633	204.4193767	235.2815007	201.4136217
Q2G194	SAOUHSC_00251	1.493135955	1.63E-25	1.51E-24	716.2150101	602.8292296	608.0828971	1880.658266	1705.79088	2064.79114
Q2G155	lip2	1.335750542	4.63E-25	4.23E-24	1091.049405	1100.818593	1311.69233	2970.158295	3252.766747	2880.094184
Q2FVX1	SAOUHSC_02552	1.249308533	8.57E-25	7.81E-24	222.7717601	238.6979093	202.35191	544.7500147	499.973189	572.8830558
Q2G2J2	ssaA2	1.01127079	1.11E-24	9.99E-24	23260.26094	27564.46013	28424.79394	53708.15256	56551.86937	51483.49264
Q2FVM7	nreC	-1.195614895	1.49E-24	1.32E-23	824.1794809	703.9248147	918.287348	371.2697869	356.8436094	317.1963025
Q2G1N2	SAOUHSC_00076	2.52549538	2.38E-24	2.09E-23	42.57753776	32.76245813	35.95084696	312.7063979	237.2421799	265.3353101
Q2FXJ2	isdH	1.176710214	2.73E-24	2.38E-23	190.8386067	198.4468893	188.9987383	459.6673552	452.9168888	419.7122177
Q2G0V4	SAOUHSC_00421	1.018595993	4.00E-24	3.46E-23	809.7335306	824.6778747	885.4180022	1665.189193	1833.235026	1669.200314
Q2G172	SAOUHSC_00281	-2.228088513	5.79E-24	4.98E-23	681.2406041	381.9166548	813.5163083	122.651626	106.8570149	116.9887503
Q2FZI8	purM	-1.402301019	6.35E-24	5.44E-23	294.2411984	262.0996651	290.6882768	91.71247711	112.7390524	102.5159153
P72360	scdA	1.174231925	7.21E-24	6.13E-23	269.9111769	223.7207855	297.8784462	616.5730389	569.5772996	638.0108137
Q2FZ75	pyrB	-1.177187147	9.12E-24	7.72E-23	658.4312089	732.0069217	679.984591	301.6567018	290.1805175	305.1356066
Q2G196	SAOUHSC_00249	1.187402738	1.25E-23	1.05E-22	624.9774292	663.6737947	645.0609111	1510.493448	1445.02055	1542.563007
Q2G1N3	sbnA	2.615095704	1.34E-23	1.12E-22	24.33002158	21.52961534	20.54334112	193.3696807	177.4414651	168.8497428
Q2FV98	SAOUHSC_02836	-1.15704308	2.15E-23	1.79E-22	567.193628	533.5600324	492.0130198	248.6181608	211.7533506	242.4199878
Q2FVB4	SAOUHSC_02820	2.176917904	2.26E-23	1.86E-22	42.57753776	66.4609865	55.46702102	303.866641	306.8462905	267.7474492
Q2G1J4	SAOUHSC_00128	-1.187234036	1.12E-22	9.01E-22	517.0129585	568.194631	572.1320502	239.778404	260.7703299	208.6500393
Q2FZM6	SAOUHSC_00974	-1.419655702	2.41E-22	1.90E-21	503.3273213	598.1488785	691.2834287	193.3696807	219.5960673	225.5350136
Q2G1F2	azoR	-1.708226208	3.75E-22	2.90E-21	193.8798594	173.172993	212.6235806	49.72363217	52.93833766	59.09740997
Q2G190	SAOUHSC_00256	-1.14337347	7.84E-22	6.03E-21	428.8166303	471.7793971	545.4257067	216.5740423	205.8713131	215.8864568
Q2FUZ6	SAOUHSC_02949	-1.141332817	1.76E-21	1.33E-20	511.6907663	530.7518217	518.7193633	199.9994983	234.3011611	258.0988925
Q2FW43	SAOUHSC_02474	1.046763457	2.88E-21	2.16E-20	279.7952481	303.2867553	321.5032885	611.0481909	639.1814102	645.2472313
Q2FZI9	purF	-1.2883097	3.38E-21	2.53E-20	340.6203021	332.3049325	407.7853212	153.5907749	133.3261837	139.9040726
Q2G074	SAOUHSC_00746	1.653511638	7.51E-21	5.54E-20	288.9190062	286.4374911	247.5472605	1035.356519	800.9374419	943.1464203
Q2FV02	SAOUHSC_02942	-1.668074479	1.23E-20	9.04E-20	1227.905776	831.2303663	1489.392231	337.0157291	366.6470052	335.2873464
Q2FYJ3	tdcB	-2.919159849	1.81E-20	1.32E-19	342.9012416	162.8762204	572.1320502	33.14908811	36.27256469	15.67890469
Q2G013	SAOUHSC_00814	1.652298458	2.20E-20	1.59E-19	85.91538869	72.07740789	78.06469625	240.8833736	268.6130466	289.4567019

Q2G2P8	nnrD	1.057416533	2.82E-20	2.02E-19	506.368574	541.0485943	635.8164076	1247.510683	1154.840033	1157.826808
Q2FXK4	SAOUHSC_01830	1.409669076	3.85E-20	2.75E-19	120.1294815	120.75306	125.3143808	313.8113675	300.964253	402.8272435
Q2G226	SAOUHSC_00099	-1.01319202	6.3E-20	4.4E-19	463.7910363	443.6972901	414.9754906	239.778404	201.9499548	203.8257609
Q2FVM3	SAOUHSC_02679	-2.974165868	1.11E-19	7.67E-19	208.3258097	99.22344463	217.7594159	8.83975683	6.862377104	21.70925264
Q2FUZ9	SAOUHSC_02945	-1.066179298	1.49E-19	1.02E-18	492.6829369	441.8251497	535.1540362	212.1541639	256.8489716	217.0925264
Q2FZJ0	purL	-1.100204085	3.69E-19	2.47E-18	407.5278614	393.1494976	438.6003329	174.5851974	211.7533506	176.0861603
Q2G012	emp	1.413751894	4.07E-19	2.72E-18	114.8072893	99.22344463	82.17336448	286.1871274	272.534405	277.396006
Q2FWG1	SAOUHSC_02330	1.585902832	6E-19	3.95E-18	51.70129585	62.71670557	51.3583528	172.3752582	192.1465589	167.6436732
A0A0H2WXF8	*mecA*	0.596431727	9.36E-19	6.04E-18	44124.77507	47471.86576	51286.4511	71586.56075	73360.77192	71785.26207
Q2G2R8	sspP	1.232152087	9.43E-19	6.07E-18	138.3769977	157.259799	169.4825642	369.0598477	402.9195699	350.966251
Q2FW49	SAOUHSC_02468	-1.152369488	9.8E-19	6.29E-18	4431.865493	4645.716563	5373.11087	2134.801274	2089.103658	2111.827854
Q2FZI4	SAOUHSC_01019	-1.061625141	1.61E-18	1.03E-17	408.2881746	462.4186948	430.3829964	202.2094375	212.7336902	194.1772042
Q2FZU1	argG	-1.356779638	3.82E-18	2.41E-17	425.0150644	411.8709022	581.3765537	174.5851974	183.3235026	171.261882
Q2G1U9	SAOUHSC_02689	1.186691423	6.48E-18	4.05E-17	101.8819653	112.3284279	116.0698773	248.6181608	255.868632	267.7474492
Q2FV28	SAOUHSC_02911	1.040204823	9.56E-18	5.9E-17	347.4631206	319.1999492	356.4269684	714.9153336	725.4512938	705.5507109
Q2G195	SAOUHSC_00250	1.29252876	1.39E-17	8.53E-17	520.8145243	469.9072566	444.7633352	1219.886443	1104.842714	1336.325107
Q2G0E3	SAOUHSC_00662	-1.247945611	1.88E-17	1.14E-16	434.8991357	357.5788288	374.9159754	146.9609573	144.1099192	185.734717
Q2G2Y3	SAOUHSC_01919	-1.532376593	2.14E-17	1.3E-16	904.0123642	1127.96463	1127.829427	325.9660331	345.0795344	347.3480423
Q2FWG0	tenA	1.729122117	2.21E-17	1.33E-16	36.49503236	40.25101999	42.11384929	128.176474	162.7363713	143.5222814
Q2G2H9	mnhG1	-1.207128635	3.55E-17	2.1E-16	886.5251612	732.0069217	623.490403	309.3914891	297.0428946	336.4934159
Q2FYJ4	SAOUHSC_01450	-2.169129965	1.27E-16	7.31E-16	369.5122027	190.0222572	532.072535	68.50811543	58.82037517	65.12775792
Q2FZC0	flr	1.93105345	1.3E-16	7.43E-16	42.57753776	34.6345986	24.65200934	135.9112613	147.0509379	180.9104387
Q9ZNI1	lytN	1.470436246	1.68E-16	9.59E-16	70.7091252	61.78063534	71.90169392	192.2647111	219.5960673	188.1468562
Q2G0G1	adh	-2.574256427	2.04E-16	1.16E-15	798.3288329	520.4550492	1676.336635	106.077082	108.8176941	98.89770648
Q2G1J7	SAOUHSC_00125	-1.145503873	2.51E-16	1.42E-15	370.2725159	366.9395311	391.3506483	166.8504102	180.3824839	147.1404901
Q2FZI7	purN	-1.477466763	4.37E-16	2.45E-15	189.3179804	187.2140465	161.2652278	56.35344979	72.54512938	49.44885324
Q2FUS6	pcp	1.075815013	8.32E-16	4.6E-15	199.9623648	182.5336953	177.6999007	432.0431151	397.0375324	383.53013
Q2FZ70	pyrE	-1.082756616	9.33E-16	5.14E-15	362.6693841	452.1219222	393.4049824	173.4802278	198.0285964	183.3225779
Q2G0B0	SAOUHSC_00695	-1.061949947	1.07E-15	5.83E-15	399.1644165	424.9758855	442.7090011	196.6845895	210.773011	183.3225779
Q2G0V2	metN1	1.390896785	1.49E-15	8.1E-15	55.50286172	75.82168882	73.95602803	204.4193767	191.1662193	171.261882
Q2FXQ8	engB	1.29846674	2.77E-15	1.49E-14	421.9738117	322.9442302	273.2264369	843.0918077	787.2126877	1001.037761
Q2FZU3	SAOUHSC_00897	1.061565696	3.47E-15	1.85E-14	206.0448702	148.8351669	181.8085689	383.4244525	389.1948157	378.7058516
Q2FZ03	SAOUHSC_01268	1.801379644	5.2E-15	2.75E-14	25.09033475	20.59354511	26.70634345	93.92241632	101.955317	96.4855673
Q2G0B9	SAOUHSC_00686	-1.206045795	6.26E-15	3.29E-14	264.5889846	236.8257688	240.3570911	93.92241632	115.6800712	98.89770648

Q2G2Q9	SAOUHSC_00274	1.424145474	9.93E-15	5.14E-14	85.91538869	60.8445651	78.06469625	198.8945287	239.202859	205.0318305
Q2G292	SAOUHSC_01849	1.352589601	1.62E-14	8.21E-14	58.54411442	72.07740789	62.65719041	167.9553798	168.6184088	184.5286475
Q2G177	SAOUHSC_00270	1.368686029	1.78E-14	9.01E-14	325.4140386	264.9078758	180.7814018	689.5010327	659.7685415	773.090608
Q2G0W6	SAOUHSC_00408	-1.22187689	3.26E-14	1.62E-13	315.5299673	285.5014209	318.4217873	125.9665348	129.4048254	121.8130287
Q2G0D2	SAOUHSC_00673	-1.318349223	5.21E-14	2.57E-13	884.2442216	621.5506343	557.7517114	239.778404	256.8489716	287.0445627
Q2G0S6	SAOUHSC_00468	-1.171479533	5.38E-14	2.65E-13	761.8338006	1130.772841	886.4451693	436.4629935	386.253797	364.2330165
Q8KQR1	isdC	1.395665123	7.67E-14	3.76E-13	49.42035633	50.54779255	52.38551985	152.4858053	132.3458441	144.7283509
Q2FVB3	SAOUHSC_02821	1.603469703	3.55E-13	1.68E-12	55.50286172	43.99530092	51.3583528	154.6957445	181.3628235	186.9407866
Q2G0F7	SAOUHSC_00612	1.455370232	4.51E-13	2.12E-12	50.94098267	38.37887953	43.14101635	127.0715044	124.5031275	144.7283509
Q2FV03	SAOUHSC_02941	-1.754792798	4.93E-13	2.3E-12	202.2433043	117.008779	213.6507476	47.51369296	43.13494179	45.83064447
Q2FXG6	SAOUHSC_01881	2.20048848	5.09E-13	2.37E-12	15.20626348	12.16891302	6.163002336	83.97768989	57.84003559	88.04308016
Q2G140	mepA	-1.103687933	5.55E-13	2.58E-12	217.4495678	201.2551	192.0802395	91.71247711	93.13226069	90.45521934
Q2FXW9	SAOUHSC_01711	1.331373301	9.4E-13	4.33E-12	98.08039948	87.05453161	93.47220209	274.0324617	234.3011611	237.5957095
Q2FYW3	SAOUHSC_01311	2.217282575	2.55E-12	1.14E-11	19.76814253	5.616421394	8.217336448	86.18762909	69.60411062	97.69163689
Q2G1H3	rocD	1.220931869	2.62E-12	1.17E-11	79.83288329	101.0955851	108.8797079	229.8336776	234.3011611	244.832127
Q2FYJ2	ald1	-2.51798807	2.97E-12	1.32E-11	323.8934122	147.8990967	582.4037207	22.09939208	31.37086676	25.32746142
Q2FWP0	SAOUHSC_02241	-1.36446931	2.98E-12	1.32E-11	215.9289415	191.8943976	310.2044509	86.18762909	86.26988359	86.83701057
Q2FZB8	SAOUHSC_01114	1.893138429	3.13E-12	1.38E-11	42.57753776	55.22814371	57.52135513	232.0436168	261.7506695	250.862475
Q2G1N0	SAOUHSC_00078	1.54855651	4.66E-12	2.05E-11	106.4438444	68.33312696	65.73869158	322.6511243	234.3011611	235.1835703
Q2FVW5	ureA	-1.537973551	1.07E-11	4.62E-11	139.8976241	121.6891302	122.2328797	47.51369296	38.23324386	33.76994855
Q2G1M6	SAOUHSC_00082	1.018212921	2.34E-11	9.95E-11	156.6245139	160.0680097	164.346729	355.8002124	299.0035738	349.7601814
Q2G1L6	SAOUHSC_00106	1.11353886	3.12E-11	1.32E-10	85.91538869	74.88561859	76.01036214	188.9498022	158.815013	189.3529258
Q2FWJ9	ilvA	1.115706055	5.34E-11	2.22E-10	77.55194377	87.05453161	71.90169392	163.5355014	190.1858797	180.9104387
Q2FVL9	SAOUHSC_02683	-2.414612186	8.84E-11	3.64E-10	64.62661981	21.52961534	66.76585864	3.314908811	4.901697931	1.206069591
Q2FWG2	thiM	1.393580263	8.94E-11	3.67E-10	40.29659823	58.03635441	59.57568925	125.9665348	152.9329755	174.8800907
Q2G1J5	SAOUHSC_00127	-1.017181648	1.25E-10	5.06E-10	320.8521595	264.9078758	296.8512792	145.8559877	134.3065233	142.3162118
Q2FXF1	SAOUHSC_01898	1.072946282	1.84E-10	7.36E-10	179.4339091	139.4744646	118.1242114	308.2865194	312.728328	340.1116247
Q2G0X2	SAOUHSC_00401	1.901486427	2.98E-10	1.18E-09	25.85064792	18.72140465	23.62484229	121.5466564	135.2868629	114.5766112
Q2G0L4	sdrD	-1.222131365	3.08E-10	1.22E-09	2267.253886	3223.82588	3855.985128	1190.052263	1185.23056	1362.858638
Q2FV70	SAOUHSC_02866	-1.521816008	5.24E-10	2.04E-09	1724.390279	1957.322856	1679.418136	553.5897715	532.3243953	517.4038546
Q2G1K0	SAOUHSC_00122	-1.189207722	6.53E-10	2.51E-09	248.622408	239.6339795	216.7322488	93.92241632	84.30920442	114.5766112
Q2G2G0	SAOUHSC_00717	1.463007366	7.17E-10	2.73E-09	86.67570186	92.670953	104.7710397	314.9163371	307.8266301	270.1595884
Q2G225	SAOUHSC_00102	1.102254396	1.39E-09	5.2E-09	67.66787251	71.14133766	93.47220209	181.215015	166.6577297	172.4679515
Q2G2Y4	SAOUHSC_01918	-1.584166813	1.62E-09	6.03E-09	903.252051	997.8508677	996.3520443	230.9386472	273.5147446	299.1052586

Q2FVK5	sbi	1.3758671	1.66E-09	6.16E-09	517.7732717	505.4779255	543.3713726	1450.82509	1688.144767	1420.749978
Q2FWN9	SAOUHSC_02243	-1.304402679	1.84E-09	6.81E-09	162.7070193	131.0498325	217.7594159	59.6683586	72.54512938	56.68527079
Q2FY63	SAOUHSC_01602	1.068484318	2.22E-09	8.12E-09	66.14724616	58.97242464	63.68435747	135.9112613	133.3261837	147.1404901
Q2G2K6	ureB	-1.272000114	2.75E-09	9.97E-09	120.8897947	135.7301837	126.3415479	51.93357138	58.82037517	34.97601814
Q2G056	SAOUHSC_00766	1.602824259	4.69E-09	1.67E-08	22.80939523	22.46568558	13.35317173	69.61308504	59.80071476	89.24914975
Q2G1M7	SAOUHSC_00081	1.011859852	8.33E-09	2.91E-08	91.99789408	74.88561859	81.14619742	187.8448326	170.579088	164.0254644
Q2FV53	SAOUHSC_02886	1.967934213	8.48E-09	2.96E-08	22.04908205	5.616421394	13.35317173	72.92799385	90.19124193	107.3401936
Q2G2A2	SAOUHSC_01044	1.933160819	1.28E-08	4.41E-08	3.801565871	5.616421394	15.40750584	68.50811543	44.11528138	43.41850528
Q2FV35	SAOUHSC_02904	-1.054159669	1.84E-08	6.26E-08	124.6913606	140.4105349	118.1242114	60.77332821	59.80071476	54.2731316
Q2FV74	clpL	-1.149556589	2.52E-08	8.48E-08	2242.163551	1653.10003	3191.408043	935.9092544	1035.238603	1007.068109
Q2FZZ3	SAOUHSC_00841	1.819282916	2.97E-08	9.95E-08	20.5284557	10.29677256	12.32600467	55.24848019	83.32886483	92.86735852
Q2FZC2	SAOUHSC_01110	1.294367224	3.34E-08	1.11E-07	60.06474076	68.33312696	55.46702102	170.165319	162.7363713	174.8800907
Q2FZK9	SAOUHSC_00992	1.221395472	3.41E-08	1.14E-07	34.21409284	42.12316046	33.89651285	91.71247711	102.9356566	85.63094098
Q2FXN1	SAOUHSC_01804	1.485670025	0.0000001	3.23E-07	25.85064792	16.84926418	18.48900701	69.61308504	67.64343145	69.95203629
Q9EYW6	sspC	1.528459093	1.04E-07	3.35E-07	15.96657666	25.27389627	16.4346729	75.13793306	57.84003559	77.18845384
Q2G0V1	SAOUHSC_00424	1.332247004	0.00000011	3.53E-07	29.6522138	32.76245813	23.62484229	77.34787226	78.4271669	94.07342811
Q2G1K9	SAOUHSC_00113	-1.80264562	1.44E-07	4.56E-07	1208.897947	823.7418045	3701.91007	352.4853036	325.4727426	358.2026686
Q2FUX7	arcA	-1.51362298	1.57E-07	4.94E-07	83.63444917	68.33312696	174.6183995	24.30933128	27.44950841	38.59422692
Q2G1I1	SAOUHSC_00142	1.091035845	1.59E-07	5.03E-07	93.51852043	101.0955851	171.5368983	270.7175529	300.964253	253.2746142
Q2FVI8	SAOUHSC_02722	-1.226358369	1.61E-07	5.08E-07	136.0960582	90.79881254	94.49936915	37.56896653	49.01697931	37.38815733
Q2FZB9	SAOUHSC_01113	1.338971927	3.87E-07	0.00000118	98.84071265	45.86744139	32.86934579	160.2205925	183.3235026	186.9407866
Q2G1K4	SAOUHSC_00118	-1.003301246	4.73E-07	0.00000143	285.8777535	268.6521567	288.6339427	106.077082	152.9329755	138.698003
Q2FUX9	SAOUHSC_02967	-1.071408738	5.39E-07	0.00000162	145.9801295	136.6662539	205.4334112	50.82860177	88.23056276	75.98238425
Q2G1J6	SAOUHSC_00126	-1.012910008	0.00000057	0.0000017	141.4182504	149.7712372	164.346729	66.29817623	87.25022317	57.89134038
Q2G1J8	SAOUHSC_00124	-1.163273174	0.00000085	0.00000249	164.2276456	110.4562874	87.30919976	50.82860177	49.01697931	48.24278365
Q2G1W1	SAOUHSC_02576	1.294622068	0.00000126	0.0000036	1402.017493	1680.246067	1501.718236	4322.64109	4323.297575	4476.930323
Q2FWG3	thiE	1.086937438	0.00000139	0.00000395	31.17284014	47.73958185	43.14101635	101.6572035	87.25022317	90.45521934
Q2G187	SAOUHSC_00259	-1.053689154	0.0000014	0.00000399	79.83288329	96.41523393	91.41786798	34.25405772	41.17426262	43.41850528
Q2G132	SAOUHSC_00324	-1.083791675	0.00000246	0.0000068	107.2041576	88.92667207	89.36353387	40.88387534	49.01697931	32.56387896
Q2FXB9	SAOUHSC_01945	-1.086262496	0.00000392	0.0000106	99.60102582	76.75775905	71.90169392	33.14908811	38.23324386	36.18208774
Q2FXW8	SAOUHSC_01712	1.114256841	0.00000448	0.000012	81.35350964	75.82168882	78.06469625	198.8945287	174.5004463	189.3529258
Q2FYW2	SAOUHSC_01312	1.086783598	0.00000703	0.0000185	36.49503236	31.8263879	34.9236799	76.24290266	81.36818566	84.42487138
Q2FZS6	SAOUHSC_00914	1.320304785	0.00000715	0.0000188	19.76814253	31.8263879	16.4346729	57.4584194	85.289544	63.92168833
Q2FXX0	SAOUHSC_01710	1.141760941	0.00000804	0.0000211	38.01565871	43.05923069	40.05951518	118.2317476	94.11260028	86.83701057

P02976	spa	1.011597074	0.00000829	0.0000217	1646.078022	2958.918004	3718.344743	5986.725313	6267.310975	6011.050843
Q9RQP7	icaB	-1.04248055	0.0000167	0.0000423	62.34568029	110.4562874	73.95602803	39.77890574	31.37086676	34.97601814
Q2FW51	SAOUHSC_02466	-1.237651627	0.000032	0.0000783	60.06474076	55.22814371	78.06469625	19.88945287	24.50848966	21.70925264
P31337	SAOUHSC_01763	1.127595232	0.0000993	0.00023103	25.09033475	19.65747488	18.48900701	58.563389	54.89901683	48.24278365
Q2FXE3	SAOUHSC_01906	1.409912334	0.00011289	0.00026146	7.603131742	4.680351162	5.13583528	28.7292097	24.50848966	27.7396006
Q2FUX8	argF	-1.130361298	0.00012627	0.0002904	79.07257012	64.58884603	168.4553972	27.62424009	43.13494179	48.24278365
Q2G1L9	SAOUHSC_00103	1.00467535	0.00016994	0.00038502	27.37127427	31.8263879	35.95084696	71.82302424	86.26988359	54.2731316
Q2G0G9	SAOUHSC_00599	-1.115090231	0.00021142	0.00047422	130.773866	101.0955851	72.92886097	41.98884494	32.35120635	44.62457487
Q2FUR2	SAOUHSC_03041	-1.101836683	0.00027051	0.00059747	88.95664139	47.73958185	53.41268691	26.51927049	20.58713131	26.53353101
Q2FZM7	SAOUHSC_00973	-1.271171244	0.00027602	0.00060847	101.1216522	49.61172232	27.73351051	17.67951366	4.901697931	22.91532223
Q2FVY9	sarV	-1.225773809	0.00029616	0.00065036	145.2198163	38.37887953	50.33118574	25.41430089	14.70509379	31.35780937
Q2FYX0	SAOUHSC_01303	1.020857984	0.00036454	0.0007914	15.96657666	23.40175581	14.38033878	44.19878415	41.17426262	41.0063661
Q2FVR2	SAOUHSC_02639	-1.261913855	0.00075842	0.00158623	36.49503236	15.91319395	18.48900701	3.314908811	4.901697931	6.030347956
Q2FZB7	SAOUHSC_01115	1.020789873	0.00177697	0.00354264	19.76814253	14.04105349	8.217336448	47.51369296	37.25290428	26.53353101
Q2FV43	SAOUHSC_02896	-1.025855223	0.00207244	0.00409827	28.89190062	37.44280929	15.40750584	6.629817623	9.803395862	13.2667655
Q2FUT6	hisZ	-1.064286594	0.00218713	0.00429903	24.33002158	24.33782604	31.84217873	15.46957445	6.862377104	6.030347956
Q2FVE3	SAOUHSC_02771	-1.016410671	0.00613419	0.01124519	80.59319647	17.78533441	23.62484229	11.04969604	6.862377104	20.50318305

Appendix 4 Table 8 Identification of DEGs in Trained-*mecA*-cured-rpoB mutant compared to trained-rpoB mutant, related to Figure 5.10 A.

UniProt Accession	Gene name/Locus tag	log2FC	pvalue	padj	rpoB-1	rpoB-2	rpoB-3	Trained-*mecA*-cured-rpoB-2	Trained-*mecA*-cured-rpoB-3
A0A0H2WXF8	*mecA*	-12.30828595	0	0	99804.5093	100391.5559	111770.9285	1.734166628	2.044613367
Q2FZZ6	SAOUHSC_00838	-3.005175298	1.25E-294	1.43E-291	4921.062859	4877.958063	4524.068837	620.8316527	532.6217821
Q2G253	SAOUHSC_00025	-2.249989343	6.18E-172	4.71E-169	3716.294879	3916.385274	3821.923345	824.5962314	748.3284923
Q2G035	SAOUHSC_00792	-2.290219433	1.62E-156	9.24E-154	4926.374887	5062.572141	4317.647445	993.6774776	910.875255
O50581	recG	-1.608259941	1.28E-127	5.86E-125	4454.666789	4428.763382	4173.77799	1415.947051	1412.827837
Q2FVH5	SAOUHSC_02737	-1.349989637	1.58E-126	6.02E-124	3729.043747	3825.559096	3651.469317	1420.282468	1497.679291
Q2FXV8	recD2	1.291418593	5.51E-110	1.80E-107	2097.188705	2122.568273	2078.288104	5201.632799	5135.046471
Q2FZ64	SAOUHSC_01187	1.139194721	1.82E-108	5.19E-106	4340.989387	4557.10472	4366.125196	9627.226033	9933.754043
Q2G239	SAOUHSC_00708	1.150421385	1.63E-97	4.13E-95	4879.629039	4605.479532	4943.166814	10656.45393	10778.17936
Q2G0Y8	SAOUHSC_00373	1.545982585	2.43E-97	5.55E-95	2794.126796	2553.992615	2597.46918	7976.299404	7664.233206
Q2FY54	SAOUHSC_01611	1.104248758	6.45E-93	1.34E-90	3063.977825	2933.093181	2922.739252	6513.529853	6328.078371
Q2G105	SAOUHSC_00356	-2.379971635	4.16E-91	7.92E-89	9017.698952	9264.27008	9437.52348	1800.932043	1594.798426

Q2FZ77	pyrR	2.254404673	1.83E-76	3.23E-74	489.7689935	478.8119127	364.3650325	1960.475372	2501.584454
Q2G2J9	SAOUHSC_01412	1.431983508	5.04E-75	8.22E-73	745.8087493	764.1245782	800.6647924	2056.72162	2137.643275
Q2G0Y7	guaB	1.087521659	5.36E-68	7.94E-66	8795.656176	9132.96702	9027.808294	19270.05957	19130.42497
Q2G0Y6	guaA	1.290512932	5.56E-68	7.94E-66	7692.879137	7762.676432	7643.84669	19003.86499	19022.06046
Q2FY14	SAOUHSC_01660	1.259476832	5.65E-66	7.60E-64	898.7951595	865.8104071	967.9912236	2244.011616	2138.665582
Q2FY61	SAOUHSC_01604	-1.700942815	6.85E-66	8.70E-64	1307.821325	1433.474015	1279.18711	398.8583243	407.9003667
Q2G0E5	SAOUHSC_00661	1.507177354	1.76E-63	2.02E-61	443.023146	417.6029672	409.7151867	1261.606222	1185.875753
Q2G2N5	SAOUHSC_01354	1.109413257	2.24E-63	2.43E-61	2932.239527	2884.718369	2760.104216	6051.374447	6371.015251
Q2FZU6	rocD	-1.846596032	4.24E-59	4.10E-57	989.0996377	950.713138	1169.72122	254.0554109	301.5804716
Q2G245	SAOUHSC_01854	-1.002780358	4.30E-59	4.10E-57	15840.46788	17199.7137	15326.78834	8001.44482	8008.750558
Q2FZD0	uvrC	-1.184514378	5.81E-59	5.31E-57	3228.650697	3234.201703	2813.273362	1312.764137	1389.314783
Q2G171	SAOUHSC_00282	1.198691271	8.10E-58	7.12E-56	759.6200225	712.7880433	700.5816933	1648.32538	1711.341388
Q2FVE1	SAOUHSC_02773	1.136675118	1.34E-57	1.14E-55	1582.984382	1670.411869	1490.299897	3450.124506	3570.917245
Q2FUQ2	mnmE	-1.108378442	1.88E-57	1.54E-55	6433.92847	6416.07963	5615.600136	2901.260768	2770.451112
Q2FZD3	mutS2	1.222250122	6.44E-56	4.90E-54	1982.448898	1974.482114	1874.994309	4786.299892	4374.450299
Q2G2J8	SAOUHSC_01413	1.260455685	8.03E-55	5.92E-53	462.1464472	450.1819221	487.9051079	1156.689141	1093.868151
Q2G0Y9	xpt	1.406644665	9.64E-54	6.89E-52	652.3170543	650.5918567	591.1158037	1728.097044	1679.649881
Q2G019	SAOUHSC_00808	-1.512842833	2.43E-53	1.68E-51	1867.70909	1726.684609	1609.148577	639.0404023	552.0456091
Q2FUQ1	rnpA	-1.517683167	3.48E-53	2.34E-51	799.9914363	797.6907742	760.0060334	269.6629106	267.8443511
Q2FXE2	SAOUHSC_01907	-1.213174666	2.17E-52	1.38E-50	1384.31453	1330.800945	1244.783544	574.0091537	554.0902224
Q2FXW6	udk	1.10144833	2.47E-52	1.52E-50	2083.377432	2075.180702	1884.377099	4411.719901	4308.000364
Q2G1S4	SAOUHSC_00018	1.360596407	1.73E-50	1.04E-48	3046.979335	3187.801374	3764.062803	8843.382717	8496.390846
Q2FUX4	SAOUHSC_02971	-1.757339969	1.12E-46	6.22E-45	698.0004962	701.9283916	673.9971201	218.5049951	171.7475228
Q2G0Q7	SAOUHSC_00489	-1.378996178	2.07E-45	1.10E-43	1324.819815	1415.703676	1382.397806	523.7183215	514.2202618
Q2G170	SAOUHSC_00284	-1.378936559	2.17E-44	1.08E-42	2274.610445	2341.735788	2108.000274	908.7033129	785.1315329
Q2FVI5	SAOUHSC_02725	1.099845164	5.65E-44	2.75E-42	1103.839445	1085.965163	1130.62626	2224.0687	2560.878242
Q9RQP9	icaA	-2.933945657	4.06E-43	1.89E-41	655.5042711	611.1022144	785.0268082	91.04374795	52.13764086
Q2G1W4	metK	1.203743499	8.56E-43	3.84E-41	3228.650697	3324.040639	2677.2229	7287.835252	7080.49609
Q2FYF4	SAOUHSC_01497	-1.002979565	8.02E-42	3.40E-40	2986.422214	3005.161778	3334.018237	1520.864132	1555.950772
Q2FZ65	SAOUHSC_01186	1.006379128	1.65E-41	6.84E-40	1026.283835	1098.799297	991.4481999	2120.885786	2091.639474
Q2FYM1	odhA	-1.019571751	9.00E-41	3.67E-39	3625.990401	3759.413946	4086.205278	1927.526207	1809.48283
Q2FXL6	SAOUHSC_01819	-1.541069431	4.16E-39	1.64E-37	1887.894797	1930.056267	2505.205073	684.1287346	719.7039052
Q2FYI3	SAOUHSC_01464	-1.349506098	9.38E-38	3.58E-36	1110.213879	1002.049673	1057.127734	395.3899911	418.1234335
Q2FWX1	SAOUHSC_02150	-1.409778776	1.09E-37	4.10E-36	4389.860046	4820.698082	5912.721836	1967.412039	1739.965975

Q2FZ76	SAOUHSC_01165	1.679553487	1.03E-36	3.58E-35	351.6562622	360.3429859	298.6854987	1004.082477	1253.347994
Q2G023	smpB	1.054869081	7.22E-36	2.43E-34	576.8862548	624.9235892	680.2523138	1343.112053	1275.838741
Q2FYZ3	SAOUHSC_01279	-1.410261136	1.01E-35	3.35E-34	699.0629018	610.1149733	619.2641754	235.8466614	236.1528439
Q2FXM0	SAOUHSC_01815	-1.07865466	7.13E-35	2.20E-33	3031.043251	2997.26385	3549.822419	1508.724966	1478.255464
P72360	scdA	-1.624964411	3.78E-34	1.14E-32	664.0035161	707.851838	664.6143296	226.3087449	195.2605765
Q2G2J3	SAOUHSC_02573	1.111391757	4.56E-33	1.32E-31	1277.011562	1188.638233	1044.617346	2604.718275	2525.097508
Q2FYZ0	SAOUHSC_01282	-1.006909424	1.86E-30	4.83E-29	2198.11724	2371.353019	2314.421665	1176.632057	1083.645084
Q2FZ74	pyrC	1.175800792	1.91E-30	4.90E-29	683.1268174	679.2218473	525.43627	1409.010385	1499.723905
Q2G2K5	ureC	1.051124564	2.93E-30	7.37E-29	437.7111178	433.3988241	417.5341788	917.374146	885.3175879
Q2FZ71	pyrF	1.422523242	9.18E-30	2.26E-28	224.1675871	247.7975053	234.5697634	585.2812368	717.6592918
Q2FWL3	SAOUHSC_02276	-1.165580207	1.21E-29	2.87E-28	1122.962747	1098.799297	935.1514567	491.6362389	432.4357271
Q2G0M5	SAOUHSC_00535	1.106624567	1.63E-27	3.54E-26	348.4690453	381.0750481	356.5460404	795.9824821	788.1984529
Q2G200	SAOUHSC_00941	-1.377709571	2.47E-27	5.23E-26	632.1313474	684.1580526	580.1692148	259.2579108	212.6397902
Q2FZZ4	SAOUHSC_00840	-1.760031922	2.59E-26	5.30E-25	321.9089046	330.7257541	293.9941035	85.84124807	86.89606809
Q2FZ75	pyrB	1.351514282	8.48E-26	1.67E-24	339.9698003	334.6747184	245.5163524	753.4953997	875.094521
Q2G1G0	SAOUHSC_00164	-1.181281302	1.32E-24	2.48E-23	606.6336124	618.0129018	689.6351044	295.67541	252.5097508
Q2G176	SAOUHSC_00271	-1.287957371	4.53E-24	8.22E-23	738.37191	735.4945876	597.3709974	279.200827	271.9335778
Q2G0P8	ctsR	-1.238832836	1.23E-23	2.16E-22	852.0493119	726.6094181	691.1989028	323.422076	302.6027783
Q2FVN8	SAOUHSC_02664	-1.033136625	1.58E-23	2.76E-22	1226.016092	1061.284136	1171.285019	535.8574879	575.5586628
Q2G012	emp	-1.73179278	2.11E-23	3.63E-22	365.4675353	337.6364415	472.2671236	108.3854142	109.3868151
Q2FV87	glcB	1.01617885	2.10E-23	3.63E-22	1291.885241	1309.081642	1618.531367	2837.963686	2913.574048
Q2FWB1	SAOUHSC_02387	-1.035012929	1.98E-22	3.19E-21	1408.74986	1470.989175	1488.736098	684.1287346	714.5923717
Q2G145	SAOUHSC_00310	-1.164328815	2.60E-22	4.12E-21	553.5133311	572.5998131	459.7567362	225.4416616	238.1974572
Q2FY36	SAOUHSC_01630	-1.113879439	2.70E-22	4.25E-21	1132.524397	1019.820012	936.7152551	473.4274893	461.0603142
Q2G177	SAOUHSC_00270	-1.942700618	4.02E-22	6.25E-21	839.3004444	654.5408209	542.6380526	163.011663	149.2567758
Q2G252	rlmH	-1.352986385	3.01E-21	4.46E-20	414.3381941	429.4498599	514.489681	186.4229125	151.3013892
Q2FW52	SAOUHSC_02465	-1.034980263	6.16E-21	8.86E-20	665.0659218	598.2680806	672.4333217	306.0804098	312.8258451
Q2G1F9	SAOUHSC_00166	-1.25650025	2.04E-20	2.87E-19	424.9622503	392.9219407	491.0327047	185.5558292	165.6136827
Q2G2E9	SAOUHSC_00030	-1.075221862	1.06E-19	1.44E-18	1945.264701	1556.879147	1566.926019	844.5391476	726.8600519
Q2FVG2	SAOUHSC_02752	1.006249499	1.73E-19	2.27E-18	1145.273265	1083.990681	827.2493656	2017.702871	2157.067102
Q2G0W4	SAOUHSC_00410	1.051446014	3.45E-19	4.42E-18	420.7126278	391.9346997	426.9169694	887.02623	856.6930007
Q2FUZ9	SAOUHSC_02945	1.110100873	2.09E-18	2.56E-17	303.848009	264.5806033	279.9199176	616.4962361	633.8301437
Q2G249	SAOUHSC_00026	-1.250853891	4.63E-18	5.58E-17	446.2103629	491.6460465	581.7330132	187.2899958	221.8405503
Q2FVL5	SAOUHSC_02696	-1.252717292	1.41E-17	1.64E-16	588.5727167	523.2377603	409.7151867	178.6191626	233.0859238

Q2FVB4	SAOUHSC_02820	-2.001039423	1.66E-17	1.92E-16	480.2073429	392.9219407	222.059376	71.10083173	81.78453468
Q2FY13	SAOUHSC_01661	1.033636346	8.72E-17	9.72E-16	436.6487122	377.1260838	364.3650325	832.3999812	812.7338133
Q9RQP7	icaB	-2.137455866	1.14E-16	1.25E-15	173.172117	145.1244354	236.1335618	35.55041587	28.62458714
Q2FYV4	SAOUHSC_01320	-1.218913188	1.97E-16	2.10E-15	650.192243	598.2680806	835.0683577	307.8145764	266.8220444
Q2FZC0	flr	-2.135104769	3.78E-16	3.96E-15	168.9224945	103.660311	168.8902296	23.41124947	26.57997377
Q2FWF6	SAOUHSC_02335	-1.142805294	7.99E-16	8.05E-15	507.8298891	455.1181273	423.7893725	203.7645787	202.4167233
Q2G194	SAOUHSC_00251	-1.288794636	1.31E-15	1.30E-14	1326.944627	1221.217188	802.2285908	466.4908228	402.7888333
Q2G185	essB	-1.015088988	3.86E-15	3.65E-14	438.7735235	455.1181273	444.118752	228.0429115	203.43903
Q2G196	SAOUHSC_00249	-1.055176264	4.77E-15	4.46E-14	1096.402606	1181.727545	774.0802192	503.7754053	450.8372474
Q2G0L5	sdrC	1.007749484	7.42E-15	6.87E-14	1012.472561	997.1134677	1124.371066	2004.696621	2290.989278
Q2G201	SAOUHSC_00940	-1.165511529	2.53E-14	2.23E-13	431.3366841	395.8836639	351.8546451	187.2899958	150.2790825
Q2G1T3	SAOUHSC_00831	-1.643953877	3.31E-14	2.89E-13	161.4856551	152.0351228	217.3679807	48.55666557	52.13764086
Q2FY81	SAOUHSC_01584	-1.002177115	5.82E-14	4.96E-13	738.37191	738.4563108	794.4095987	414.465824	318.9596852
Q2G155	lip2	-1.064764183	8.43E-14	7.09E-13	3120.285323	3227.291016	4719.543639	1850.355792	1573.329986
Q2FUQ8	SAOUHSC_03046	-2.464046344	2.78E-12	2.00E-11	475.9577204	589.3829111	1804.62338	62.42999859	77.69530794
Q2FYT5	SAOUHSC_01340	-1.171882968	6.02E-12	4.23E-11	1094.277795	913.1979779	764.6974287	377.1812415	404.8334466
Q2G0E3	SAOUHSC_00662	1.105234695	6.52E-12	4.57E-11	167.8600889	170.7927029	181.400617	435.2758235	337.3612055
Q2G1N4	SAOUHSC_00074	-1.186251596	7.41E-12	5.18E-11	1892.14442	1940.915918	1118.115872	683.2616513	695.1685448
Q2FWH7	SAOUHSC_02314	-1.027890366	1.03E-11	7.12E-11	436.6487122	436.3605473	511.3620842	215.9037451	218.7736303
Q2G021	SAOUHSC_00806	-2.104680421	1.76E-11	1.18E-10	229.4796152	133.2775427	143.8694549	22.54416616	24.5353604
Q2FW05	SAOUHSC_02515	-1.584296953	6.09E-11	3.88E-10	619.3824799	393.9091818	406.5875899	126.5941638	143.1229357
Q2G0F7	SAOUHSC_00612	-1.559343159	1.20E-10	7.39E-10	98.8037232	81.94100774	89.13651009	24.27833279	26.57997377
Q2G0Y5	SAOUHSC_00376	-1.451727906	1.93E-10	1.17E-09	147.674382	138.213748	107.9020912	38.15166581	47.02610744
Q2FXE9	SAOUHSC_01900	-1.363296171	2.87E-10	1.68E-09	162.5480608	147.0989175	115.7210833	49.42374889	50.09302749
Q2FZB9	SAOUHSC_01113	-1.820829621	2.94E-10	1.72E-09	226.2923983	167.8309797	140.741858	34.68333255	38.84765397
Q2G195	SAOUHSC_00250	-1.052965044	5.79E-10	3.29E-09	941.2913845	914.1852189	586.4244085	425.7379071	324.0712187
Q2G140	mepA	1.0321159	8.33E-10	4.64E-09	96.67891195	92.80065937	93.82790536	197.6949955	204.4613367
Q2G057	SAOUHSC_00765	-1.322486676	9.63E-10	5.30E-09	145.5495707	128.3413374	95.39170378	39.01874912	50.09302749
Q2G1K6	SAOUHSC_00116	-1.39569134	1.00E-09	5.50E-09	144.4871651	154.996846	236.1335618	65.89833185	52.13764086
Q2FXK4	SAOUHSC_01830	-1.072376994	1.19E-09	6.51E-09	248.6029164	246.8102643	214.2403839	121.3916639	92.00760151
Q2G1T5	SAOUHSC_02802	1.549663114	1.21E-09	6.60E-09	742.6215325	697.9794274	1390.216798	3677.300334	2883.927154
Q2FY39	SAOUHSC_01627	-1.070586639	1.66E-09	8.86E-09	1286.573213	1075.105511	1038.362153	540.1929045	489.6849014
Q2FV35	SAOUHSC_02904	1.210756578	2.27E-09	1.20E-08	64.80674318	65.15790977	50.04154952	152.6066632	149.2567758
Q2FY63	SAOUHSC_01602	-1.223281053	2.58E-09	1.36E-08	143.4247595	133.2775427	109.4658896	53.75916546	48.04841412

Q2FZZ3	SAOUHSC_00841	-2.082156438	3.27E-09	1.71E-08	75.43079943	48.3748118	26.58457318	5.202499883	1.022306683
Q9F0R1	sarR	-1.437144776	4.34E-09	2.25E-08	362.2803184	268.5295675	200.1661981	114.4549974	65.42762774
Q2FVB3	SAOUHSC_02821	-1.37609477	4.56E-09	2.35E-08	283.6623021	254.7081927	143.8694549	92.77791458	63.38301437
Q2G016	SAOUHSC_00811	-1.112018866	6.56E-09	3.29E-08	1129.33718	1086.952404	545.7656495	401.4595743	402.7888333
Q2FXQ8	engB	-1.076456908	6.88E-09	3.44E-08	650.192243	483.748118	415.9703804	235.8466614	226.9520837
Q2G1N1	SAOUHSC_00077	-1.277110574	7.1E-09	3.54E-08	225.2299927	222.1292379	112.5934864	73.70208167	64.40532106
Q2FWH6	SAOUHSC_02315	-1.15576589	9.8E-09	4.83E-08	151.9240045	132.2903017	146.9970517	58.96166534	58.27148096
Q2G2Y3	SAOUHSC_01919	1.113828946	1.65E-08	7.94E-08	388.8404591	327.764031	669.3057249	987.6078944	1132.715805
Q2G1K8	SAOUHSC_00114	-1.286637599	2.04E-08	9.7E-08	122.176647	139.2009891	222.059376	58.96166534	56.22686759
Q2FX11	SAOUHSC_02096	-1.361016472	2.5E-08	1.17E-07	195.4826352	125.3796143	153.2522454	43.35416569	64.40532106
Q2G017	SAOUHSC_00810	-1.324035112	1.06E-07	4.69E-07	139.175137	129.3285785	81.31751798	41.61999906	40.89226734
Q2G1K7	SAOUHSC_00115	-1.292382362	1.27E-07	5.59E-07	109.4277795	125.3796143	200.1661981	51.15791551	50.09302749
Q2G1A1	SAOUHSC_00244	-1.622928728	1.35E-07	5.92E-07	307.0352259	227.0654431	176.7092218	71.96791504	37.82534729
Q2FXB3	SAOUHSC_01952	-1.10977957	2.04E-07	8.65E-07	162.5480608	142.1627122	143.8694549	68.49958179	59.29378764
Q9RQP6	icaC	-1.443641274	0.00000024	0.00000101	241.1660771	138.213748	145.4332533	59.82874865	44.98149407
Q2FV74	clpL	-1.164706866	2.71E-07	0.00000112	1393.876181	1408.792989	1920.344463	629.5024858	634.8524504
Q2FVA8	SAOUHSC_02825	-1.189432691	3.05E-07	0.00000125	103.0533457	103.660311	106.3382927	38.15166581	43.95918739
Q2G0W9	SAOUHSC_00405	-1.066591565	4.15E-07	0.00000167	483.3945598	309.0064509	353.4184435	199.4291622	139.033709
Q2G1K5	SAOUHSC_00117	-1.034575811	4.27E-07	0.00000171	288.9743302	323.8150667	542.6380526	182.0874959	165.6136827
Q2G0M0	SAOUHSC_00540	-1.346586355	9.42E-07	0.0000036	456.8344191	259.644398	198.6023997	105.7841643	97.11913493
Q2FYI5	gpsB	-1.22788072	9.51E-07	0.00000362	183.7961733	132.2903017	129.7952691	63.29708191	48.04841412
Q2FWG0	tenA	-1.108407358	0.00000155	0.00000578	88.17966694	91.81341832	109.4658896	45.95541563	33.73612055
Q2FZ03	SAOUHSC_01268	-1.19875322	0.00000303	0.000011	66.93155443	69.106874	68.80713059	30.34791598	20.44613367
Q2G1U4	SAOUHSC_00936	-1.134214364	0.00000372	0.0000134	121.1142413	85.88997197	62.5519369	33.81624924	38.84765397
Q2G2N7	SAOUHSC_02250	1.517097175	0.0000046	0.0000163	19.12330127	10.85965163	6.25519369	57.22749871	49.07072081
Q2G1I2	SAOUHSC_00141	-1.081521362	0.00000666	0.000023	164.672872	118.4689269	175.1454233	69.3666651	59.29378764
Q2FWX0	SAOUHSC_02151	-1.049838491	0.00000707	0.0000244	531.2028129	387.9857355	364.3650325	199.4291622	175.8367496
Q2FV70	SAOUHSC_02866	1.175501365	0.00000865	0.0000294	818.0523319	869.7593714	1834.33555	3192.600761	2947.310168
Q2FYV5	SAOUHSC_01319	-1.081336017	0.0000103	0.0000346	103.0533457	88.85169514	89.13651009	45.08833232	33.73612055
Q2G132	SAOUHSC_00324	1.070196842	0.000012	0.0000398	58.43230942	57.25998131	32.83976687	109.2524975	125.7437221
Q2FXN1	SAOUHSC_01804	-1.372038606	0.0000145	0.0000475	43.55863066	46.40032969	29.71217003	10.40499977	11.24537352
Q2FV53	SAOUHSC_02886	-1.546038223	0.0000169	0.0000546	66.93155443	23.69378537	37.53116214	9.537916452	2.044613367
Q2FZ85	SAOUHSC_01155	-1.084084226	0.0000254	0.0000802	521.6411623	288.2743887	254.8991429	147.4041633	149.2567758
Q2FZM7	SAOUHSC_00973	-1.494104072	0.0000286	0.0000894	219.9179645	86.87721303	95.39170378	28.61374936	31.69150719

Q2FWA5	SAOUHSC_02393	-1.029207923	0.0000337	0.00010461	310.2224427	209.2951041	184.5282139	99.71458109	109.3868151
Q2G1E3	SAOUHSC_00182	-1.145574991	0.0000343	0.00010634	234.7916433	155.984087	148.5608501	98.84749777	42.93688071
Q2G1N3	sbnA	-1.213267377	0.0000429	0.00013075	48.87065879	77.99204352	28.14837161	15.60749965	18.4015203
Q2G1N2	SAOUHSC_00076	-1.127618086	0.0000509	0.00015351	106.2405626	107.6092752	39.09496057	32.08208261	31.69150719
Q2G2Y4	SAOUHSC_01918	1.136778125	0.0000553	0.00016574	288.9743302	276.427496	656.7953375	978.069978	1129.648885
Q2FV37	SAOUHSC_02902	1.241405944	0.0000642	0.00019007	26.56014065	13.8213748	10.94658896	52.02499883	53.15994754
Q2FVC8	SAOUHSC_02785	1.148310173	0.0000721	0.00021186	25.49773502	25.66826749	15.63798423	65.03124853	55.20456091
Q2G0X2	SAOUHSC_00401	-1.237383075	0.0000911	0.00026355	75.43079943	87.86445409	226.7507713	52.02499883	31.69150719
Q2FXE0	SAOUHSC_01923	-1.055802167	0.00010362	0.00029537	110.4901851	76.0175614	65.67953375	28.61374936	41.91457402
Q2FVE0	SAOUHSC_02774	-1.252200217	0.00011297	0.00031962	640.6305924	472.8884664	752.1870413	183.8216625	203.43903
Q2G0V1	SAOUHSC_00424	-1.074539716	0.0001138	0.00032155	48.87065879	85.88997197	54.73294479	26.01249941	24.5353604
Q2FZL0	SAOUHSC_00991	-1.240841072	0.00029866	0.00078206	1461.870141	917.1469421	548.8932463	266.1945773	302.6027783
Q2G0G9	SAOUHSC_00599	-1.139753374	0.00047116	0.00118455	103.0533457	49.36205286	40.65875899	25.1454161	17.37921362
Q2FZS7	SAOUHSC_00913	-1.006207333	0.00079698	0.0019444	54.18268692	51.33653497	37.53116214	22.54416616	17.37921362
Q2FVE3	SAOUHSC_02771	-1.246993595	0.00084624	0.00205799	61.6195263	21.71930326	31.27596845	6.069583197	6.133840101
Q2G2F9	SAOUHSC_00718	-1.208685793	0.00111015	0.00266297	875.4222357	435.3733062	289.3027082	97.98041446	121.6544953
Q2FYG3	SAOUHSC_01489	-1.205738433	0.00119155	0.00284033	11.68646188	11.84689269	15.63798423	2.601249941	0
Q2FY44	SAOUHSC_01622	-1.049966658	0.00155146	0.00362271	744.7463437	432.411583	461.3205347	194.2266623	206.5059501
Q2FYW8	SAOUHSC_01305	-1.093828521	0.00186941	0.0043036	77.55561069	16.78309797	9.382790536	0.867083314	2.044613367
Q2FW59	SAOUHSC_02458	-1.096491801	0.00239056	0.00541072	14.87367876	6.9106874	7.818992113	0.867083314	0
Q2FZN9	SAOUHSC_00961	-1.011684026	0.00477113	0.01021902	22.31051814	19.74482114	17.20178265	7.803749824	4.089226734
Q2G2B1	sarT	-1.039547532	0.00516104	0.010975	29.74735752	21.71930326	17.20178265	7.803749824	4.089226734

Appendix 4 Table 9 Identification of DEGs in Trained-rpoC mutant compared to trained-rpoB mutant, related to Figure 5.11 A.

UniProt Accession	Gene name/Locus tag	log2FC	pvalue	padj	rpoB-1	rpoB-2	rpoB-3	rpoC-1	rpoC-2	rpoC-3
Q2FW95	SAOUHSC_02404	1.857663103	3.73E-207	8.05E-204	1881.520363	1848.115259	1681.083304	6464.072182	6831.006237	6505.539375
Q2G2J8	SAOUHSC_01413	1.72921063	7.55E-123	8.14E-120	462.1464472	450.1819221	487.9051079	1528.172962	1588.15013	1563.06619
Q2FWD4	murA	1.390780982	1.08E-120	7.79E-118	4253.872126	4491.94681	3893.858072	11309.36389	11145.48076	10929.40264
Q2FW76	SAOUHSC_02428	1.944538281	2.15E-114	1.16E-111	635.3185642	630.8470355	555.14844	2538.11518	2274.38784	2344.599285
Q2G025	SAOUHSC_00802	1.226602946	8.64E-111	3.73E-108	2037.69399	2078.142425	1893.75989	4752.474266	4690.92492	4712.113893
Q2G2J9	SAOUHSC_01412	1.584307468	7.88E-110	2.83E-107	745.8087493	764.1245782	800.6647924	2169.055332	2437.124211	2378.369234
Q2FXT4	ruvB	1.172828624	1.56E-95	4.79E-93	3239.274753	3334.900291	2989.982584	7184.512364	7482.932062	7021.73716

Q2FXU7	SAOUHSC_01735	1.137243931	3.28E-94	8.85E-92	1942.077484	2098.874488	1961.003222	4408.828719	4377.216252	4485.37281
Q2G024	rnr	1.095793805	9.59E-88	2.30E-85	6992.753829	7078.51838	7037.092902	15813.22	14952.13937	14535.55071
Q2G082	SAOUHSC_00738	-1.72370508	6.08E-85	1.31E-82	5846.418159	5431.800296	7304.502432	1814.360089	1819.510272	1889.911049
Q2FVX0	SAOUHSC_02553	1.960318613	3.89E-83	7.62E-81	448.3351741	451.1691631	367.4926293	1687.288585	1589.130469	1800.6619
Q2FZD0	uvrC	1.113624604	4.52E-71	7.50E-69	3228.650697	3234.201703	2813.273362	6623.187805	6842.770312	6743.135084
Q2FXT5	queA	1.125988391	1.89E-70	2.92E-68	3369.950645	3268.75514	2928.994446	6774.568641	7118.245736	7135.107702
Q2G2M9	SAOUHSC_02003	1.033992741	2.38E-69	3.43E-67	2110.999979	2092.951041	2362.899417	4384.519388	4499.758701	4589.094795
Q2FUX4	SAOUHSC_02971	1.65608146	5.37E-67	6.81E-65	698.0004962	701.9283916	673.9971201	2310.491441	2207.724748	2133.537107
Q2FXT3	ruvA	1.109864246	1.37E-65	1.65E-63	1882.582769	1902.413517	1645.115941	3944.741485	3921.358345	3951.083981
Q2FZF0	isdB	1.802811256	1.68E-65	1.91E-63	278.350274	269.5168086	251.771546	988.9477954	902.8927589	967.2678121
Q2FXW4	SAOUHSC_01717	1.210870698	2.94E-64	3.17E-62	2317.10667	2489.821946	2201.828179	5331.478338	5574.210887	5462.289179
Q2FXT1	obg	1.170979213	2.07E-62	2.12E-60	5102.734221	5136.61522	4339.540623	11397.76146	11108.22785	10588.08494
Q2FW77	SAOUHSC_02427	1.693778895	1.09E-56	1.02E-54	571.5742267	545.9443046	428.4807678	1837.564451	1581.287753	1733.122003
Q2G2J3	SAOUHSC_02573	1.314934394	1.59E-55	1.43E-53	1277.011562	1188.638233	1044.617346	2932.589328	2965.527248	2960.900846
Q2G184	essC	-1.043990035	8.40E-51	6.97E-49	1521.364856	1526.274674	1526.26726	703.8656376	767.605896	730.8781723
Q2FZM6	SAOUHSC_00974	-2.129975092	1.42E-48	1.05E-46	876.4846413	876.6700588	1236.964552	193.3696807	219.5960673	225.5350136
Q2FWH6	SAOUHSC_02315	2.339396392	6.91E-48	4.81E-46	151.9240045	132.2903017	146.9970517	779.0035706	720.5495959	829.7758787
Q2FXQ3	SAOUHSC_01782	1.001596727	1.17E-47	7.89E-46	3583.494176	3532.348502	2939.941035	6819.872394	6824.14386	6640.619169
Q2G188	esaA	-1.097507495	2.09E-47	1.33E-45	1460.807736	1441.371943	1491.863695	664.0867319	643.1027686	730.8781723
Q2FZ43	trmD	1.074059068	2.10E-47	1.33E-45	1603.170089	1667.450146	1538.777648	3481.759221	3409.621081	3320.309585
Q2FXW3	SAOUHSC_01718	1.301060171	3.91E-47	2.35E-45	1445.934057	1287.362339	1086.839904	3013.252109	3076.305622	3478.304701
Q2FXW5	SAOUHSC_01716	1.158437351	2.12E-46	1.24E-44	3467.691963	3442.509566	3172.946999	7865.17364	7511.36191	7359.436645
Q2FX99	SAOUHSC_01978	1.291044686	1.21E-45	6.86E-44	1328.007032	1135.327216	1107.169283	2987.837809	2822.397669	3053.768205
Q2FXL7	ald2	1.14790158	3.58E-43	1.98E-41	492.9562104	523.2377603	536.382859	1205.521838	1104.842714	1159.032877
Q2FY23	SAOUHSC_01650	1.249027553	1.94E-42	1.05E-40	427.0870616	475.8501895	516.0534795	1099.444756	1144.056297	1156.620738
Q2FXY9	SAOUHSC_01686	1.062287502	2.87E-42	1.51E-40	570.5118211	573.5870542	553.5846416	1228.726199	1129.351203	1222.954565
Q2FUY3	SAOUHSC_02962	1.014640504	6.37E-40	3.27E-38	1063.468031	1151.123073	1144.700445	2224.303812	2307.719386	2297.562571
Q2FZU7	SAOUHSC_00893	-1.00906718	4.81E-37	2.16E-35	1979.261681	2182.789977	1774.91121	1004.41737	989.1626425	938.322142
Q9RQP9	icaA	-2.386511441	2.25E-36	9.70E-35	655.5042711	611.1022144	785.0268082	133.7013221	107.8373545	106.134124
Q2G2C1	SAOUHSC_01064	-1.181907697	1.17E-35	4.95E-34	14289.35567	14017.83577	11229.63647	5937.001681	5687.930279	5573.247581
Q2FYV4	SAOUHSC_01320	-1.710553305	1.96E-35	8.14E-34	650.192243	598.2680806	835.0683577	196.6845895	207.8319923	202.6196913
Q2FVX2	SAOUHSC_02551	1.085993056	4.08E-35	1.66E-33	495.0810216	474.8629485	456.6291394	1038.671428	992.1036613	1034.807709
Q2G0I4	SAOUHSC_00581	1.017720074	2.59E-31	8.87E-30	516.3291342	536.071894	500.4154952	1091.709969	1025.435207	1063.753379
Q2G0J2	SAOUHSC_00572	1.113037191	7.29E-30	2.38E-28	429.2118728	437.3477883	380.0030167	874.0309566	945.0473611	925.0553764

Q2FVG2	SAOUHSC_02752	1.142818266	7.45E-30	2.40E-28	1145.273265	1083.990681	827.2493656	2405.518827	2174.393202	2297.562571
P0A0M9	SAOUHSC_00995	1.628704809	1.65E-29	5.17E-28	138.1127314	146.1116765	142.3056565	437.5679631	448.9955305	488.4581844
Q2G2G3	mntH	1.076192827	9.87E-26	2.54E-24	402.6517322	356.3940216	293.9941035	767.9538746	746.0384251	757.4117033
Q2FYQ2	SAOUHSC_01383	-1.120125694	3.87E-25	9.49E-24	5249.346197	5267.918281	7446.808088	2703.86062	2716.520993	2699.183745
Q2FWZ8	ftnA	-1.033337659	1.47E-23	3.48E-22	2268.236011	2498.707116	2204.955776	1085.080151	1205.817691	1067.371588
Q2G1F2	azoR	-1.781985998	1.68E-23	3.93E-22	199.7322577	179.6778724	236.1335618	49.72363217	52.93833766	59.09740997
Q2FV72	SAOUHSC_02864	1.087132223	2.06E-23	4.78E-22	223.1051814	222.1292379	228.3145697	483.9766864	460.7596055	510.1674371
Q2FYV3	SAOUHSC_01321	-1.423931837	4.63E-23	1.04E-21	428.1494672	395.8836639	506.6706889	156.9056837	144.1099192	174.8800907
Q2G190	SAOUHSC_00256	-1.164522068	4.44E-22	9.13E-21	464.2712585	462.0288147	544.2018511	216.5740423	205.8713131	215.8864568
Q2FWY4	sdcS	-1.05642676	7.49E-22	1.51E-20	475.9577204	445.2457168	514.489681	222.0988904	244.104557	207.4439697
Q2FWN0	SAOUHSC_02258	-1.158045935	1.18E-20	2.19E-19	423.8998447	439.3222704	475.3947205	182.3199846	197.0482568	205.0318305
Q2G1M8	SAOUHSC_00080	1.351618108	2.21E-20	4.07E-19	220.9803702	215.2185505	148.5608501	533.7003186	485.2680952	545.1434552
Q2FWH7	SAOUHSC_02314	1.168278146	1.04E-19	1.74E-18	436.6487122	436.3605473	511.3620842	1075.135424	985.2412842	1114.408302
Q2G1M9	SAOUHSC_00079	1.39140592	1.65E-19	2.69E-18	172.1097114	200.4099346	129.7952691	475.1369296	422.5263617	489.664254
Q2FVX1	SAOUHSC_02552	1.110864853	2.32E-19	3.74E-18	267.7262177	241.874059	220.4955776	544.7500147	499.973189	572.8830558
Q9RQP7	icaB	-2.098226702	1.40E-18	2.15E-17	173.172117	145.1244354	236.1335618	39.77890574	31.37086676	34.97601814
Q2G1T3	SAOUHSC_00831	-1.75943506	2.34E-18	3.56E-17	161.4856551	152.0351228	217.3679807	48.61866257	47.05630014	44.62457487
Q2G185	essB	-1.025965962	2.44E-18	3.68E-17	438.7735235	455.1181273	444.118752	228.728708	221.5567465	194.1772042
Q2FZM5	SAOUHSC_00975	-1.178590427	4.58E-18	6.82E-17	1931.453428	1956.711775	2541.172437	946.9589504	869.561213	939.5282115
Q2FV66	SAOUHSC_02871	-1.143675946	6.70E-18	9.83E-17	348.4690453	333.6874773	290.8665066	144.7510181	141.1689004	144.7283509
Q2FYV2	thrB	-1.333794554	7.91E-18	1.15E-16	381.4036197	327.764031	439.4273568	143.6460485	154.8936546	135.0797942
Q2FZJ0	purL	-1.060855818	2.04E-17	2.91E-16	406.9013547	367.2536733	434.7359615	174.5851974	211.7533506	176.0861603
Q2G1C4	tarJ'	-1.013286112	2.07E-17	2.94E-16	552.4509254	514.3525908	616.1365785	282.8722186	285.2788196	246.0381966
Q2G2W4	SAOUHSC_02631	-1.203771031	2.19E-17	3.09E-16	627.8817249	503.4929391	444.118752	230.9386472	204.8909735	229.1532223
Q2FXX1	SAOUHSC_01709	1.132832424	2.37E-17	3.31E-16	161.4856551	148.0861586	200.1661981	358.0101516	399.9785512	373.8815733
Q2FZI8	purM	-1.191390503	6.64E-17	8.89E-16	246.4781052	222.1292379	264.2819334	91.71247711	112.7390524	102.5159153
Q9ZNI1	lytN	1.503247753	3.94E-16	5.01E-15	71.18117693	62.1961866	65.67953375	192.2647111	219.5960673	188.1468562
Q2FVL5	SAOUHSC_02696	1.004466559	4.23E-16	5.33E-15	588.5727167	523.2377603	409.7151867	1012.152157	1032.297584	1079.432284
P60647	cidA	-1.270036519	4.55E-16	5.70E-15	484.4569654	550.8805099	642.7211517	246.4082216	199.9892756	219.5046656
Q2FZI9	purF	-1.107331528	1.68E-15	2.03E-14	299.5983865	290.2488708	364.3650325	153.5907749	133.3261837	139.9040726
Q2G136	SAOUHSC_00319	-1.161348642	2.33E-15	2.78E-14	313.4096596	308.0192098	398.7685978	131.4913828	157.8346734	148.3465597
Q2G0L4	sdrD	-1.523435156	4.31E-15	5.02E-14	3689.734739	3464.22887	4550.65341	1190.052263	1185.23056	1362.858638
A0A0H2WXF8	*mecA*	-0.521317089	1.05E-14	1.18E-13	99804.5093	100391.5559	111770.9285	71586.56075	73360.77192	71785.26207
Q2G1N1	SAOUHSC_00077	1.405938182	6.13E-14	6.51E-13	225.2299927	222.1292379	112.5934864	558.0096499	489.1894535	548.761664

Q2FUS6	pcp	1.0207799	7.35E-14	7.58E-13	182.7337676	233.9761305	161.0712375	432.0431151	397.0375324	383.53013
Q2G1M6	SAOUHSC_00082	1.168060115	1.03E-13	1.06E-12	163.6104664	158.9458102	101.6468975	355.8002124	299.0035738	349.7601814
Q2G2Q9	SAOUHSC_00274	1.381516989	2.27E-13	2.24E-12	82.86763882	81.94100774	65.67953375	198.8945287	239.202859	205.0318305
Q2G074	SAOUHSC_00746	1.233652692	2.74E-12	2.54E-11	471.7080979	412.6667619	231.4421665	1035.356519	800.9374419	943.1464203
Q2G1N5	SAOUHSC_00072	1.016552915	8.55E-12	7.35E-11	572.6366323	619.0001428	358.1098388	1109.389482	1025.435207	1109.584024
Q2FXW9	SAOUHSC_01711	1.283537554	1.43E-11	1.20E-10	84.99245007	75.03032034	134.4866643	274.0324617	234.3011611	237.5957095
Q2G0D1	sarX	-1.608417048	1.63E-11	1.35E-10	186.9833901	132.2903017	90.70030851	50.82860177	39.21358345	21.70925264
Q2G1I1	SAOUHSC_00142	1.438805317	1.71E-11	1.42E-10	82.86763882	81.94100774	117.2848817	270.7175529	300.964253	253.2746142
Q2G057	SAOUHSC_00765	1.16619962	2.01E-11	1.65E-10	145.5495707	128.3413374	95.39170378	301.6567018	282.3378008	287.0445627
Q2G1U4	SAOUHSC_00936	1.348301343	3.69E-11	2.92E-10	121.1142413	85.88997197	62.5519369	245.303252	266.6523675	229.1532223
Q2FXF1	SAOUHSC_01898	1.134672186	4.20E-11	3.29E-10	169.9849001	127.3540964	120.4124785	308.2865194	312.728328	340.1116247
Q2FUQ8	SAOUHSC_03046	-2.192085645	1.03E-10	7.66E-10	475.9577204	589.3829111	1804.62338	121.5466564	106.8570149	126.6373071
Q2G1N3	sbnA	1.579893974	3.85E-10	2.71E-09	48.87065879	77.99204352	28.14837161	193.3696807	177.4414651	168.8497428
P60643	lrgB	1.042861736	4.73E-10	3.28E-09	188.0457958	193.4992472	193.9110044	426.518267	405.8605887	398.0029651
Q2G1N2	SAOUHSC_00076	1.494444806	6.46E-10	4.45E-09	106.2405626	107.6092752	39.09496057	312.7063979	237.2421799	265.3353101
Q2FWH9	kdpA	1.62530423	7.85E-10	5.36E-09	21.24811252	23.69378537	21.89317792	78.45284187	90.19124193	78.39452343
Q2FZM7	SAOUHSC_00973	-2.141307125	8.19E-10	5.57E-09	219.9179645	86.87721303	95.39170378	17.67951366	4.901697931	22.91532223
Q2G225	SAOUHSC_00102	1.151505098	8.54E-10	5.78E-09	72.24358256	66.14515083	86.00891324	181.215015	166.6577297	172.4679515
P72358	lrgA	1.15652628	1.23E-09	8.23E-09	72.24358256	77.99204352	60.98813848	161.3255621	172.5397672	168.8497428
Q2G1P1	norG	-1.064549375	2.32E-09	1.49E-08	184.8585789	144.1371943	162.635036	65.19320662	87.25022317	69.95203629
Q2FZJ1	purQ	-1.191948541	4.05E-09	2.52E-08	112.6149963	100.6985878	129.7952691	36.46399692	51.95799807	49.44885324
Q2FX92	SAOUHSC_01985	1.995383853	5.95E-09	3.65E-08	7.436839381	5.923446343	3.127596845	28.7292097	41.17426262	56.68527079
Q2G1M7	SAOUHSC_00081	1.047928325	7.16E-09	4.34E-08	94.5541007	69.106874	78.18992113	187.8448326	170.579088	164.0254644
Q2FWX7	SAOUHSC_02144	1.200508941	3.40E-08	1.91E-07	52.05787567	40.47688334	51.60534795	89.5025379	130.385165	138.698003
Q2FXX2	SAOUHSC_01708	1.13846179	6.15E-08	3.33E-07	53.12028129	60.22170449	106.3382927	182.3199846	164.6970505	160.4072556
Q2FXN0	SAOUHSC_01805	1.062550862	9.31E-08	4.85E-07	70.11877131	90.82617726	57.86054164	160.2205925	166.6577297	164.0254644
Q2G1N0	SAOUHSC_00078	1.1750574	1.58E-07	8.07E-07	122.176647	124.3923732	73.49852586	322.6511243	234.3011611	235.1835703
Q9F0R1	sarR	-1.080792704	1.30E-06	5.94E-06	362.2803184	268.5295675	200.1661981	135.9112613	119.6014295	109.7523328
Q2FXG6	SAOUHSC_01881	1.333340569	7.36E-06	3.07E-05	27.62254627	30.60447277	17.20178265	83.97768989	57.84003559	88.04308016
Q2G1L8	phnC	1.166249408	9.75E-06	3.98E-05	19.12330127	27.6427496	26.58457318	57.4584194	68.62377104	60.30347956
Q9RQP6	icaC	-1.128738536	1.21E-05	4.87E-05	241.1660771	138.213748	145.4332533	85.08265949	65.68275228	62.71561874
P31337	SAOUHSC_01763	1.256883255	2.43E-05	9.22E-05	13.81127314	23.69378537	18.76558107	58.563389	54.89901683	48.24278365
Q2G1X0	hly	-1.034609545	1.57E-04	5.20E-04	83.93004444	79.96652563	175.1454233	56.35344979	50.97765848	34.97601814
Q2G056	SAOUHSC_00766	1.022214198	1.58E-04	5.22E-04	31.87216878	33.56619594	31.27596845	69.61308504	59.80071476	89.24914975

Q2FXE4	SAOUHSC_01905	1.226912348	2.96E-04	9.30E-04	5.312028129	17.77033903	17.20178265	36.46399692	53.91867724	36.18208774
Q2G2A2	SAOUHSC_01044	1.023759581	2.21E-03	5.62E-03	26.56014065	18.75758009	17.20178265	68.50811543	44.11528138	43.41850528

Appendix 4 Table 10 Identification of DEGs in Trained-*mecA*-cured-rpoB mutant compared to trained-rpoC mutant, related to Figure 5.12 A.

UniProt Accession	Gene name/Locus tag	log2FC	pvalue	padj	rpoC-1	rpoC-2	rpoC-3	Trained-*mecA*-cured-rpoB-2	Trained-*mecA*-cured-rpoB-3
Q2FZZ6	SAOUHSC_00838	-3.974491153	0	0	9565.72186	9228.916865	9400.106394	620.8316527	532.6217821
Q2FW95	SAOUHSC_02404	-2.624581142	0	0	6464.072182	6831.006237	6505.539375	1062.177059	1048.886657
A0A0H2WXF8	*mecA*	-11.78696886	0	0	71586.56075	73360.77192	71785.26207	1.734166628	2.044613367
O50581	recG	-2.327214562	6.48E-270	3.70E-267	7238.655874	7071.189435	7255.714661	1415.947051	1412.827837
Q2G035	SAOUHSC_00792	-2.795292377	4.99E-234	2.28E-231	6449.707577	7243.729203	6691.274092	993.6774776	910.875255
Q2FZD0	uvrC	-2.298138981	8.59E-223	3.27E-220	6623.187805	6842.770312	6743.135084	1312.764137	1389.314783
Q2FUX4	SAOUHSC_02971	-3.413421429	3.55E-180	1.16E-177	2310.491441	2207.724748	2133.537107	218.5049951	171.7475228
Q2G245	SAOUHSC_01854	-1.666455598	1.02E-160	2.91E-158	25521.48294	26839.73719	24461.50345	8001.44482	8008.750558
Q2G253	SAOUHSC_00025	-2.059425365	3.56E-144	9.05E-142	3413.251106	3478.244852	3132.162728	824.5962314	748.3284923
Q2FUQ2	mnmE	-1.74073277	1.77E-140	4.05E-138	9959.091039	9466.159045	9304.826896	2901.260768	2770.451112
Q2FXQ3	SAOUHSC_01782	-1.967430917	9.04E-139	1.88E-136	6819.872394	6824.14386	6640.619169	1702.084545	1706.229855
Q2FUQ1	rnpA	-2.372802854	7.18E-134	1.37E-131	1487.289087	1422.47274	1383.361821	269.6629106	267.8443511
Q2FY54	SAOUHSC_01611	1.312027684	1.20E-129	2.10E-127	2582.313964	2479.278814	2664.207727	6513.529853	6328.078371
Q2FVH5	SAOUHSC_02737	-1.334551958	2.65E-124	4.32E-122	3699.438233	3761.562992	3630.26947	1420.282468	1497.679291
Q2G082	SAOUHSC_00738	2.262569086	5.04E-119	7.68E-117	1814.360089	1819.510272	1889.911049	8858.990217	9268.232392
Q2G239	SAOUHSC_00708	1.247664914	1.74E-114	2.49E-112	4402.198901	4537.991945	4534.821663	10656.45393	10778.17936
Q2FUY3	SAOUHSC_02962	-1.964612523	1.65E-107	2.22E-105	2224.303812	2307.719386	2297.562571	587.0154034	557.1571425
Q2FVE1	SAOUHSC_02773	1.58022337	5.82E-107	7.39E-105	1135.908753	1142.095618	1209.6878	3450.124506	3570.917245
Q2FZ77	pyrR	2.632612299	1.94E-101	2.33E-99	339.2256684	340.1778364	344.9359031	1960.475372	2501.584454
Q2FXE2	SAOUHSC_01907	-1.672637172	5.00E-101	5.71E-99	1836.459481	1860.684535	1769.30409	574.0091537	554.0902224
Q2FVX0	SAOUHSC_02553	-2.301991003	3.64E-90	3.97E-88	1687.288585	1589.130469	1800.6619	318.2195762	346.5619657
Q2G0Y8	SAOUHSC_00373	1.480599024	4.74E-90	4.92E-88	2861.871274	2709.658616	2748.632598	7976.299404	7664.233206
Q2FZ64	SAOUHSC_01187	1.018955691	4.21E-88	4.18E-86	4851.92153	4830.133141	4744.677772	9627.226033	9933.754043
Q2FY21	SAOUHSC_01652	-1.281694763	1.21E-86	1.16E-84	16859.62621	16548.13222	16427.8739	7024.241925	6552.985841
Q2FZF0	isdB	-2.386169713	1.59E-84	1.45E-82	988.9477954	902.8927589	967.2678121	185.5558292	164.591376
Q2FWD4	murA	-1.275012748	6.22E-83	5.47E-81	11309.36389	11145.48076	10929.40264	4557.389897	4585.045475
Q2FYK5	thyA	1.484301344	1.46E-81	1.24E-79	660.771823	643.1027686	732.0842419	1852.957042	1982.252659

Q2G0Y6	guaA	1.399105885	1.34E-79	1.09E-77	7395.561558	7088.835548	6927.663732	19003.86499	19022.06046
Q2FXQ4	SAOUHSC_01781	-1.958746834	8.33E-78	6.56E-76	7325.948473	7342.743501	7904.580101	2011.633288	1757.345189
Q2FYM1	odhA	-1.407769613	6.43E-77	4.90E-75	5038.661393	4964.439665	5028.104126	1927.526207	1809.48283
Q2FY61	SAOUHSC_01604	-1.826759309	2.02E-76	1.49E-74	1367.952369	1482.273454	1547.387286	398.8583243	407.9003667
Q2FWD1	pyrG	1.096471427	2.33E-76	1.67E-74	7135.893701	7224.122411	7215.914364	15244.19174	15665.82762
Q2FWH6	SAOUHSC_02315	-3.495162282	7.45E-74	5.01E-72	779.0035706	720.5495959	829.7758787	58.96166534	58.27148096
Q2G077	SAOUHSC_00743	1.044371693	4.13E-73	2.69E-71	4205.514312	4022.333322	4217.62536	8660.428138	8523.993127
Q2FUQ3	mnmG	-1.125406709	5.75E-72	3.65E-70	13117.09417	12497.36905	12599.80902	5904.837367	5709.582827
Q2FV86	SAOUHSC_02849	1.515562676	2.69E-70	1.66E-68	5513.798323	5820.276123	5526.210867	15436.68424	17141.01616
Q2FW76	SAOUHSC_02428	-1.647085377	3.41E-70	2.05E-68	2538.11518	2274.38784	2344.599285	749.1599831	752.417719
Q2G1B7	SAOUHSC_00228	1.071844842	3.28E-69	1.92E-67	7870.698488	8018.197476	8272.431326	17476.06419	16549.10059
Q2G033	SAOUHSC_00794	1.145324016	2.54E-66	1.45E-64	13238.64082	13772.79085	13524.8644	29502.50975	30647.73206
Q2G2B2	sasG	-1.220801291	6.99E-66	3.90E-64	6375.674614	6581.999982	6436.793408	2708.768272	2797.031086
Q2G0Y7	guaB	1.063611244	2.86E-65	1.56E-63	9285.05958	9239.7006	8882.702539	19270.05957	19130.42497
Q2G0Q7	SAOUHSC_00489	-1.636385891	4.37E-64	2.32E-62	1692.813433	1680.302051	1563.06619	523.7183215	514.2202618
Q2FXU3	lytH	1.291446585	2.35E-63	1.22E-61	1121.544148	1099.941016	1073.401936	2689.692439	2739.781912
Q2G0W4	SAOUHSC_00410	2.049038456	1.17E-61	5.93E-60	171.2702886	212.7336902	223.1228744	887.02623	856.6930007
Q2FZI6	purH	1.713725175	5.05E-61	2.51E-59	251.9330697	286.2591592	268.9535188	872.2858137	938.4775354
Q2FXT1	obg	-1.244885163	4.85E-57	2.36E-55	11397.76146	11108.22785	10588.08494	4505.364898	4727.146104
Q2FZZ4	SAOUHSC_00840	-2.586883753	4.97E-57	2.37E-55	520.4406834	531.3440557	659.7200664	85.84124807	86.89606809
Q2FY74	xerD	-1.222573233	2.02E-56	9.43E-55	2843.08679	2869.453969	2893.360949	1191.372473	1246.191847
Q2FYZ3	SAOUHSC_01279	-1.755529314	8.77E-56	4.01E-54	829.8321724	780.3503106	851.4851314	235.8466614	236.1528439
Q2FVL5	SAOUHSC_02696	-2.25718385	2.72E-55	1.22E-53	1012.152157	1032.297584	1079.432284	178.6191626	233.0859238
Q2FUW9	SAOUHSC_02982	1.065903236	6.21E-55	2.68E-53	3367.947352	3390.994629	3397.498038	7109.21609	7151.035251
Q2FZM6	SAOUHSC_00974	2.468852877	6.36E-55	2.69E-53	193.3696807	219.5960673	225.5350136	1188.771223	1369.890956
Q2FXT3	ruvA	-1.110754989	7.03E-54	2.92E-52	3944.741485	3921.358345	3951.083981	1764.514544	1862.642777
Q2FZT3	SAOUHSC_00907	-1.186966368	2.64E-53	1.08E-51	1733.697308	1927.347627	1901.971745	776.9066492	839.3137871
Q2G0B2	SAOUHSC_00693	1.117436632	4.00E-53	1.60E-51	699.4457592	704.8641625	736.9085202	1564.218298	1553.906159
Q2FUS7	SAOUHSC_03024	1.408733337	1.53E-52	6.04E-51	1287.289588	1235.227879	1238.63347	3192.600761	3568.872632
Q2FZU6	rocD	-1.710665855	5.93E-51	2.22E-49	934.8042848	906.8141173	975.7102993	254.0554109	301.5804716
Q2G019	SAOUHSC_00808	-1.463928694	3.50E-50	1.29E-48	1731.487369	1611.67828	1692.115636	639.0404023	552.0456091
Q2FWH7	SAOUHSC_02314	-2.196168512	8.24E-50	2.99E-48	1075.135424	985.2412842	1114.408302	215.9037451	218.7736303
Q2FX99	SAOUHSC_01978	-1.494302401	3.83E-49	1.37E-47	2987.837809	2822.397669	3053.768205	1101.195809	958.9236691
Q2FVS3	SAOUHSC_02619	-1.333729525	1.91E-48	6.61E-47	1829.829664	1701.869522	1807.898317	704.0716508	689.0347046

Q2G2L4	SAOUHSC_02814	-1.449128367	1.89E-48	6.61E-47	1510.493448	1634.22609	1576.332956	546.2624877	587.826343
Q2G105	SAOUHSC_00356	-1.721010324	2.15E-48	7.34E-47	5659.65431	6095.751547	5640.787478	1800.932043	1594.798426
Q2FUX3	isaB	-1.316460576	5.72E-47	1.89E-45	2054.138493	2061.65415	2374.751025	877.4883136	835.2245604
Q2FZQ1	SAOUHSC_00949	-1.511349023	1.14E-46	3.66E-45	763.5339962	734.2743501	786.3573735	250.5870777	272.9558845
Q2FZ72	carB	1.163029948	5.57E-46	1.77E-44	1582.316473	1592.071488	1542.563007	3460.529505	3653.724087
Q2G0Y9	xpt	1.279439041	8.88E-46	2.78E-44	760.2190874	684.2770312	631.9804658	1728.097044	1679.649881
Q2G0E5	SAOUHSC_00661	1.229660219	3.66E-45	1.13E-43	478.4518384	532.3243953	536.7009681	1261.606222	1185.875753
Q2G268	SAOUHSC_01178	-1.056693381	7.23E-45	2.20E-43	2566.84439	2429.281495	2544.806837	1186.169973	1214.50034
P60639	cidB	1.188315309	2.50E-44	7.42E-43	1602.205925	1597.953526	1481.053458	3403.302007	3786.623956
Q2FW75	SAOUHSC_02430	-1.362711034	3.06E-44	8.96E-43	9512.683319	8364.25735	9449.555247	3348.675758	3625.0995
Q2FZ76	SAOUHSC_01165	1.809056137	2.78E-42	7.67E-41	339.2256684	291.1608571	295.4870498	1004.082477	1253.347994
Q2FZ10	cinA	-1.113768891	5.12E-41	1.36E-39	1979.00056	1890.094722	2100.973228	915.6399794	904.7414149
Q53726	pcrB	-1.00239031	7.53E-41	1.96E-39	2117.121761	2141.061656	2137.155316	1081.252892	1031.507444
Q2G188	esaA	1.10452336	1.44E-40	3.65E-39	664.0867319	643.1027686	730.8781723	1532.136215	1409.760916
Q2FVH8	SAOUHSC_02733	1.051384452	3.65E-40	9.18E-39	1211.046686	1185.23056	1180.74213	2457.314111	2525.097508
Q2FZI5	purD	1.663651758	1.37E-39	3.38E-38	329.2809419	294.1018759	265.3353101	907.8362295	1037.641284
Q2FUW8	gtf2	1.078341405	2.23E-39	5.42E-38	738.1196953	679.3753333	692.2839453	1487.914966	1508.924665
Q2G0Q9	hslO	-1.1256787	5.18E-39	1.23E-37	3982.310452	4054.684529	3893.19264	1741.103294	1868.776617
Q2FZ71	pyrF	1.650091599	7.30E-39	1.70E-37	208.8392551	200.9696152	190.5589954	585.2812368	717.6592918
Q2FWL3	SAOUHSC_02276	-1.317196418	7.95E-38	1.78E-36	1170.16281	1122.488826	1231.397053	491.6362389	432.4357271
Q2G2U2	SAOUHSC_00023	1.175280839	1.43E-37	3.17E-36	1014.362096	1074.452187	1102.347606	2358.466614	2506.695988
Q2FZ88	SAOUHSC_01152	-1.397243638	3.46E-37	7.61E-36	1612.150652	1559.720282	1737.946281	636.4391523	580.6701962
Q2FYT4	sbcD	-1.234265209	4.51E-37	9.82E-36	976.7931297	1045.041999	967.2678121	395.3899911	442.6587939
Q2G194	SAOUHSC_00251	-2.011946472	4.14E-36	8.59E-35	1880.658266	1705.79088	2064.79114	466.4908228	402.7888333
Q2G145	SAOUHSC_00310	-1.480042197	6.36E-36	1.31E-34	664.0867319	660.7488811	666.9564839	225.4416616	238.1974572
Q2G1N1	SAOUHSC_00077	-2.683048756	1.81E-35	3.68E-34	558.0096499	489.1894535	548.761664	73.70208167	64.40532106
Q2G1W4	metK	1.076489714	9.49E-35	1.90E-33	3486.1791	3274.334218	3348.049185	7287.835252	7080.49609
Q2FXL6	SAOUHSC_01819	-1.440779632	2.04E-34	4.02E-33	1956.901168	2027.342264	1893.529258	684.1287346	719.7039052
Q2FUW7	gtf1	1.004613029	2.66E-34	5.20E-33	723.7550905	739.176048	697.1082237	1417.681218	1499.723905
Q2G252	rlmH	-1.725604702	2.72E-34	5.27E-33	595.5786164	574.4789975	590.9740997	186.4229125	151.3013892
Q2FY23	SAOUHSC_01650	-1.208770125	2.01E-33	3.85E-32	1099.444756	1144.056297	1156.620738	502.908322	464.1272343
Q2G196	SAOUHSC_00249	-1.595376987	8.04E-33	1.52E-31	1510.493448	1445.02055	1542.563007	503.7754053	450.8372474
Q2G057	SAOUHSC_00765	-2.488686296	1.37E-32	2.55E-31	301.6567018	282.3378008	287.0445627	39.01874912	50.09302749
Q2G278	SAOUHSC_00773	-1.731286526	2.54E-32	4.64E-31	468.507112	537.2260933	505.3431587	137.8662469	152.3236958

Q2FZI8	purM	1.741327242	1.83E-31	3.19E-30	91.71247711	112.7390524	102.5159153	349.4345755	374.1642461
Q2G1U8	SAOUHSC_02690	1.124857085	3.81E-31	6.49E-30	1071.820516	1050.924036	1111.996163	2361.067863	2401.398399
Q2G0L4	sdrD	2.452722358	7.91E-31	1.31E-29	1190.052263	1185.23056	1362.858638	7021.640675	8970.741147
Q2G1F2	azoR	2.168380175	8.18E-31	1.34E-29	49.72363217	52.93833766	59.09740997	250.5870777	293.4020182
Q2FZ74	pyrC	1.175046114	1.12E-30	1.83E-29	623.2028565	636.2403915	641.6290225	1409.010385	1499.723905
Q2G0U5	SAOUHSC_00431	1.002064538	4.91E-30	7.91E-29	532.595349	555.8525454	498.1067412	1080.385809	1061.154337
Q2FZI3	SAOUHSC_01021	1.0408508	2.04E-29	3.24E-28	1026.516762	961.7131341	1058.929101	2115.683286	2107.996381
Q2G176	SAOUHSC_00271	-1.423737679	2.35E-29	3.70E-28	753.5892698	767.605896	767.06026	279.200827	271.9335778
Q2FWY4	sdcS	1.30899576	8.63E-29	1.35E-27	222.0988904	244.104557	207.4439697	556.6674875	585.7817296
Q2FWC5	SAOUHSC_02373	1.065388706	1.89E-28	2.85E-27	342.5405772	328.4137614	320.8145113	696.267901	705.3916116
P72360	scdA	-1.467609995	3.98E-28	5.83E-27	616.5730389	569.5772996	638.0108137	226.3087449	195.2605765
Q2FWC4	SAOUHSC_02374	1.145744563	6.51E-28	9.38E-27	320.4411851	369.588024	314.7841633	726.615817	784.1092262
Q2FUZ9	SAOUHSC_02945	1.403477513	6.52E-28	9.38E-27	212.1541639	256.8489716	217.0925264	616.4962361	633.8301437
Q2FZ75	pyrB	1.401175948	8.94E-28	1.27E-26	301.6567018	290.1805175	305.1356066	753.4953997	875.094521
Q2FZI9	purF	1.611345367	9.27E-28	1.31E-26	153.5907749	133.3261837	139.9040726	447.4149899	463.1049276
Q2FV87	glcB	1.094789548	6.01E-27	8.08E-26	1295.024376	1335.222516	1350.797942	2837.963686	2913.574048
Q2FW77	SAOUHSC_02427	-1.240050182	1.03E-26	1.36E-25	1837.564451	1581.287753	1733.122003	689.3312345	741.1723455
Q2FYS2	SAOUHSC_01363	-1.818924875	2.92E-26	3.82E-25	640.8823702	633.2993727	653.6897184	168.2141629	171.7475228
Q2FW41	SAOUHSC_02476	-1.861704261	3.01E-26	3.90E-25	327.0710027	347.0402135	408.8575914	79.77166487	105.2975884
Q2G0A0	SAOUHSC_00705	-1.412234701	4.04E-26	5.18E-25	507.1810481	487.2287744	523.4342026	177.7520793	191.1713498
Q2G1U4	SAOUHSC_00936	-2.482515706	1.19E-25	1.49E-24	245.303252	266.6523675	229.1532223	33.81624924	38.84765397
Q2G1N5	SAOUHSC_00072	-1.723556979	4.56E-25	5.51E-24	1109.389482	1025.435207	1109.584024	300.0108266	316.9150719
Q2FZL3	sspB	-1.3351558	1.02E-24	1.22E-23	626.5177653	602.9088455	689.8718062	240.1820779	252.5097508
Q2G0M6	araB	-1.101637059	1.23E-24	1.46E-23	961.3235553	1030.336905	992.5952736	446.5479066	467.1941543
Q2FW50	SAOUHSC_02467	1.379152669	3.98E-24	4.64E-23	646.4072182	608.790883	624.7440482	1642.255796	1727.698295
Q2FVP4	SAOUHSC_02658	1.165684619	4.58E-24	5.29E-23	230.9386472	242.1438778	230.3592919	508.9779052	566.3579026
Q2FXP2	SAOUHSC_01794	-1.36896424	4.82E-24	5.52E-23	605.5233429	568.59696	627.1561874	233.2454114	216.7290169
Q2G249	SAOUHSC_00026	-1.441170367	9.31E-24	1.05E-22	542.5400754	613.692581	575.295195	187.2899958	221.8405503
Q2G2M2	mprF	-1.051996722	1.54E-23	1.72E-22	9123.734018	8121.133132	9103.413274	4253.043654	4094.338267
Q2G177	SAOUHSC_00270	-1.996211957	2.49E-23	2.77E-22	689.5010327	659.7685415	773.090608	163.011663	149.2567758
Q2G1Y2	SAOUHSC_02923	1.200846352	3.33E-23	3.65E-22	204.4193767	235.2815007	201.4136217	489.034989	519.3317952
Q2G1M9	SAOUHSC_00079	-1.681110169	9.33E-23	1.01E-21	475.1369296	422.5263617	489.664254	127.4612471	145.1675491
Q2FXQ8	engB	-1.799846272	1.54E-22	1.63E-21	843.0918077	787.2126877	1001.037761	235.8466614	226.9520837
Q2FXE9	SAOUHSC_01900	-2.067186453	1.67E-22	1.76E-21	208.8392551	235.2815007	272.5717276	49.42374889	50.09302749

Q2G1N3	sbnA	-2.793161351	2.41E-22	2.54E-21	193.3696807	177.4414651	168.8497428	15.60749965	18.4015203
Q2G1N4	SAOUHSC_00074	-1.674711965	3.22E-22	3.37E-21	2689.496016	2117.533506	2258.968344	683.2616513	695.1685448
Q2G200	SAOUHSC_00941	-1.232910091	3.44E-22	3.59E-21	561.3245587	570.5576392	584.9437517	259.2579108	212.6397902
Q2G1N2	SAOUHSC_00076	-2.622062892	5.08E-22	5.24E-21	312.7063979	237.2421799	265.3353101	32.08208261	31.69150719
Q2FY81	SAOUHSC_01584	-1.275634552	6.18E-22	6.33E-21	866.2961693	909.755136	979.3285081	414.465824	318.9596852
P0A0M9	SAOUHSC_00995	-1.503640124	6.33E-22	6.46E-21	437.5679631	448.9955305	488.4581844	156.0749965	154.3683092
Q2G0Y5	SAOUHSC_00376	-2.15214236	6.4E-22	6.48E-21	217.6790119	200.9696152	244.832127	38.15166581	47.02610744
Q2FZL2	sspA	-1.595685406	1.26E-21	1.25E-20	563.5344979	457.8185868	493.2824628	149.13833	165.6136827
Q2G190	SAOUHSC_00256	1.241326844	1.64E-21	1.63E-20	216.5740423	205.8713131	215.8864568	540.1929045	491.7295147
Q2G195	SAOUHSC_00250	-1.608693615	1.75E-21	1.72E-20	1219.886443	1104.842714	1336.325107	425.7379071	324.0712187
Q2FVW0	SAOUHSC_02581	1.281787836	1.98E-21	1.94E-20	337.0157291	360.7649677	353.3783902	876.6212302	878.1614411
Q2FZJ0	purL	1.256696518	7.54E-21	7.24E-20	174.5851974	211.7533506	176.0861603	447.4149899	478.4395279
Q2G0Q6	SAOUHSC_00490	-1.300444427	1.66E-20	1.57E-19	524.8605618	434.2904367	466.7489318	190.758329	181.9705897
Q2G0D1	sarX	2.334852193	1.96E-20	1.84E-19	50.82860177	39.21358345	21.70925264	265.327494	222.862857
Q2FXT2	SAOUHSC_01752	-1.088059979	4.94E-20	4.5E-19	1373.477217	1265.618406	1238.63347	595.6862366	600.0940232
Q2G2L5	SAOUHSC_02813	-1.283889203	1.21E-19	1.06E-18	553.5897715	585.262733	622.3319091	251.454161	214.6844035
Q2FXK4	SAOUHSC_01830	-1.565750729	1.8E-19	1.57E-18	313.8113675	300.964253	402.8272435	121.3916639	92.00760151
Q2FWZ8	ftnA	1.015862679	5.61E-19	4.79E-18	1085.080151	1205.817691	1067.371588	2432.168695	2168.312476
P60643	lrgB	-1.656210304	1.34E-18	1.12E-17	426.518267	405.8605887	398.0029651	109.2524975	130.8552555
Q2FY24	SAOUHSC_01649	-1.12287651	1.39E-18	1.15E-17	1039.776397	1087.196601	1209.6878	503.7754053	493.7741281
Q2FXF1	SAOUHSC_01898	-1.701572293	1.5E-18	1.24E-17	308.2865194	312.728328	340.1116247	91.04374795	89.96298814
Q2G0F7	SAOUHSC_00612	-2.081322484	1.85E-18	1.51E-17	127.0715044	124.5031275	144.7283509	24.27833279	26.57997377
Q2G2W1	SAOUHSC_02629	1.005394078	3.29E-18	2.66E-17	3370.157291	3308.646104	3426.443709	6724.231098	7030.403062
Q2FZU3	SAOUHSC_00897	-1.333567842	4.49E-18	3.6E-17	383.4244525	389.1948157	378.7058516	158.6762464	132.8998688
Q2G1I1	SAOUHSC_00142	-2.05851571	5.34E-18	4.27E-17	270.7175529	300.964253	253.2746142	52.02499883	59.29378764
Q2FW43	SAOUHSC_02474	-1.05811166	1.55E-17	1.21E-16	611.0481909	639.1814102	645.2472313	325.1562427	267.8443511
Q2FVX1	SAOUHSC_02552	-1.148675103	2.32E-17	1.78E-16	544.7500147	499.973189	572.8830558	219.3720784	256.5989775
Q2FW49	SAOUHSC_02468	1.22187115	2.62E-17	1.99E-16	2134.801274	2089.103658	2111.827854	4740.344476	5447.872316
Q2FZC0	flr	-2.207790851	2.88E-17	2.18E-16	135.9112613	147.0509379	180.9104387	23.41124947	26.57997377
Q2G2Q9	SAOUHSC_00274	-1.755118157	5.93E-17	4.43E-16	198.8945287	239.202859	205.0318305	54.62624877	60.31609432
Q2FY17	SAOUHSC_01657	-1.003125449	6.01E-17	4.48E-16	1150.273358	1036.218943	1237.427401	557.5345708	561.2463692
Q2G1T5	SAOUHSC_02802	2.097977043	2.06E-16	1.49E-15	605.5233429	696.0411062	535.4948985	3677.300334	2883.927154
Q2FV70	SAOUHSC_02866	2.161524406	3.31E-16	2.38E-15	553.5897715	532.3243953	517.4038546	3192.600761	2947.310168
Q2G101	SAOUHSC_00359	-1.07032264	4.04E-16	2.89E-15	755.799209	632.3190331	693.4900149	317.3524928	329.1827521

Q2FY64	SAOUHSC_01601	-1.041788042	4.64E-16	3.31E-15	502.7611697	472.5236806	432.9789832	226.3087449	219.7959369
Q2FZI7	purN	1.590202855	5.33E-16	3.77E-15	56.35344979	72.54512938	49.44885324	175.1508294	219.7959369
Q2FZM5	SAOUHSC_00975	1.215256954	5.52E-16	3.89E-15	946.9589504	869.561213	939.5282115	2310.777031	2098.795621
Q2FZI4	SAOUHSC_01019	1.072648563	6.41E-16	4.48E-15	202.2094375	212.7336902	194.1772042	467.3579061	407.9003667
Q2G1M8	SAOUHSC_00080	-1.286694248	6.78E-16	4.73E-15	533.7003186	485.2680952	545.1434552	198.5620789	213.6620968
Q2FWF6	SAOUHSC_02335	-1.136341498	9.49E-16	6.52E-15	455.2474767	397.0375324	534.2888289	203.7645787	202.4167233
Q2G016	SAOUHSC_00811	-1.530154739	1.17E-15	7.98E-15	1285.079649	1261.697047	1215.718148	401.4595743	402.7888333
Q2G0L5	sdrC	1.02234049	2.74E-15	1.84E-14	1019.886944	1019.55317	1058.929101	2004.696621	2290.989278
Q2FZ70	pyrE	1.158905186	4.12E-15	2.76E-14	173.4802278	198.0285964	183.3225779	396.2570744	460.0380076
Q2G2Y3	SAOUHSC_01919	1.520163235	1.63E-14	1.07E-13	325.9660331	345.0795344	347.3480423	987.6078944	1132.715805
Q2G0E3	SAOUHSC_00662	1.225886197	2.63E-14	1.7E-13	146.9609573	144.1099192	185.734717	435.2758235	337.3612055
Q2FYT5	SAOUHSC_01340	-1.293901203	2.71E-14	1.74E-13	994.4726434	905.8337777	1133.705416	377.1812415	404.8334466
Q2G1Z0	SAOUHSC_00655	-1.113648194	1.07E-13	6.64E-13	266.2976745	248.0259153	262.9231709	120.5245806	110.4091218
Q2FWG0	tenA	-1.672560889	1.24E-13	7.58E-13	128.176474	162.7363713	143.5222814	45.95541563	33.73612055
Q2FZZ3	SAOUHSC_00841	-2.574670676	1.81E-13	1.1E-12	55.24848019	83.32886483	92.86735852	5.202499883	1.022306683
Q2G012	emp	-1.266559087	4.72E-13	2.8E-12	286.1871274	272.534405	277.396006	108.3854142	109.3868151
Q2FVB4	SAOUHSC_02820	-1.70082684	5.02E-13	2.97E-12	303.866641	306.8462905	267.7474492	71.10083173	81.78453468
P72358	lrgA	-1.520998716	6.58E-13	3.84E-12	161.3255621	172.5397672	168.8497428	51.15791551	54.18225422
Q9ZNI1	lytN	-1.423753971	7.05E-13	4.1E-12	192.2647111	219.5960673	188.1468562	65.89833185	74.62838789
Q2FVF5	SAOUHSC_02759	-1.181247662	7.67E-13	4.44E-12	1916.017293	1834.215366	1933.329555	839.3366477	755.4846391
Q2G292	SAOUHSC_01849	-1.416327486	8.47E-13	4.89E-12	167.9553798	168.6184088	184.5286475	65.89833185	54.18225422
Q2G1U9	SAOUHSC_02689	-1.088599226	1.3E-12	7.45E-12	248.6181608	255.868632	267.7474492	113.5879141	120.6321886
Q2G013	SAOUHSC_00814	-1.369853453	2.31E-12	1.31E-11	240.8833736	268.6130466	289.4567019	72.83499836	121.6544953
Q2G074	SAOUHSC_00746	-1.344468448	3.98E-12	2.2E-11	1035.356519	800.9374419	943.1464203	319.0866595	367.0080994
Q2G097	SAOUHSC_00724	1.053466496	1.41E-11	7.43E-11	141.4361093	130.385165	164.0254644	311.2829097	310.7812318
Q2FXF2	sigS	-1.600596425	1.69E-11	8.85E-11	226.5187688	204.8909735	267.7474492	71.96791504	62.36070769
Q2FV53	SAOUHSC_02886	-2.38852682	2.13E-11	1.1E-10	72.92799385	90.19124193	107.3401936	9.537916452	2.044613367
Q2FZ03	SAOUHSC_01268	-1.678252699	2.56E-11	1.31E-10	93.92241632	101.955317	96.4855673	30.34791598	20.44613367
Q2FWG1	SAOUHSC_02330	-1.296960948	2.55E-11	1.31E-10	172.3752582	192.1465589	167.6436732	71.96791504	63.38301437
Q2G056	SAOUHSC_00766	-2.006340443	3.64E-11	1.85E-10	69.61308504	59.80071476	89.24914975	11.27208308	13.28998688
Q2FXN1	SAOUHSC_01804	-2.052838562	3.73E-11	1.89E-10	69.61308504	67.64343145	69.95203629	10.40499977	11.24537352
Q2FXW9	SAOUHSC_01711	-1.363027408	4.56E-11	2.3E-10	274.0324617	234.3011611	237.5957095	91.04374795	88.94068146
Q2FY63	SAOUHSC_01602	-1.315254886	1.09E-10	5.37E-10	135.9112613	133.3261837	147.1404901	53.75916546	48.04841412
Q2G2Q6	SAOUHSC_00277	-1.043523202	1.26E-10	6.19E-10	244.1982824	239.202859	291.8688411	125.7270805	115.5206552

Q2G0V2	metN1	-1.234315573	1.36E-10	6.66E-10	204.4193767	191.1662193	171.261882	80.63874818	69.51685448
Q2G140	mepA	1.071403237	1.48E-10	7.23E-10	91.71247711	93.13226069	90.45521934	197.6949955	204.4613367
Q2G0W6	SAOUHSC_00408	1.111339706	3.2E-10	1.54E-09	125.9665348	129.4048254	121.8130287	280.9349937	289.3127914
Q2FV35	SAOUHSC_02904	1.264358221	3.66E-10	1.73E-09	60.77332821	59.80071476	54.2731316	152.6066632	149.2567758
Q2FZB9	SAOUHSC_01113	-1.807430994	3.79E-10	1.79E-09	160.2205925	183.3235026	186.9407866	34.68333255	38.84765397
Q2G1F8	SAOUHSC_00167	1.186624503	6.04E-10	2.79E-09	87.2925987	119.6014295	90.45521934	266.1945773	214.6844035
Q2G1P1	norG	1.157268709	1.23E-09	5.56E-09	65.19320662	87.25022317	69.95203629	187.2899958	164.591376
Q2G2Q8	SAOUHSC_00275	-1.244771759	1.58E-09	7.1E-09	232.0436168	264.6916883	268.9535188	82.37291481	118.5875753
Q2FXG6	SAOUHSC_01881	-1.923589296	1.89E-09	8.4E-09	83.97768989	57.84003559	88.04308016	13.87333302	14.31229357
Q2G1N0	SAOUHSC_00078	-1.468095853	1.92E-09	8.49E-09	322.6511243	234.3011611	235.1835703	70.23374842	99.1637483
Q2FV45	SAOUHSC_02894	1.337885109	2.96E-09	1.29E-08	38.67393613	46.07596055	51.86099242	130.9295804	123.6991087
Q2G0X3	SAOUHSC_00400	1.344718171	3.36E-09	1.45E-08	176.7951366	246.0652361	201.4136217	673.7237348	503.9971949
Q2G1M6	SAOUHSC_00082	-1.000283654	3.64E-09	1.57E-08	355.8002124	299.0035738	349.7601814	154.3408299	169.7029095
Q2FYW3	SAOUHSC_01311	-1.950338922	4.01E-09	1.71E-08	86.18762909	69.60411062	97.69163689	9.537916452	18.4015203
Q2G2Y4	SAOUHSC_01918	1.643518083	5.93E-09	2.48E-08	230.9386472	273.5147446	299.1052586	978.069978	1129.648885
Q2FWH9	kdpA	-1.525741984	4.13E-08	1.62E-07	78.45284187	90.19124193	78.39452343	27.74666604	19.42382699
Q2FWN6	SAOUHSC_02246	-1.054564516	5.81E-08	2.23E-07	176.7951366	143.1295796	180.9104387	72.83499836	78.71761463
Q2G132	SAOUHSC_00324	1.329365422	6.89E-08	2.61E-07	40.88387534	49.01697931	32.56387896	109.2524975	125.7437221
Q2FYH9	SAOUHSC_01468	-1.265540889	1.03E-07	3.84E-07	161.3255621	141.1689004	168.8497428	61.56291528	55.20456091
Q2G1M7	SAOUHSC_00081	-1.012795543	2.15E-07	7.79E-07	187.8448326	170.579088	164.0254644	84.97416475	79.73992131
P31337	SAOUHSC_01763	-1.649708789	2.15E-07	7.79E-07	58.563389	54.89901683	48.24278365	14.74041633	9.200760151
Q2G0V1	SAOUHSC_00424	-1.419900241	0.00000024	8.65E-07	77.34787226	78.4271669	94.07342811	26.01249941	24.5353604
Q8KQR1	isdC	-1.024698671	3.72E-07	0.00000133	152.4858053	132.3458441	144.7283509	68.49958179	64.40532106
Q2FWX0	SAOUHSC_02151	-1.162673181	6.24E-07	0.00000219	443.0928111	482.3270764	473.9853493	199.4291622	175.8367496
Q2G2A2	SAOUHSC_01044	-1.703681735	0.00000122	0.0000042	68.50811543	44.11528138	43.41850528	7.803749824	11.24537352
Q2FW05	SAOUHSC_02515	-1.149565058	0.00000219	0.00000733	337.0157291	329.394101	354.5844598	126.5941638	143.1229357
Q2G1W1	SAOUHSC_02576	-1.351657273	0.00000251	0.0000083	4322.64109	4323.297575	4476.930323	1288.485804	1513.013892
Q2G073	SAOUHSC_00747	-1.010854052	0.00000417	0.0000135	435.3580239	386.253797	436.597192	182.9545792	207.5282567
Q2FZS6	SAOUHSC_00914	-1.44912054	0.00000442	0.0000143	57.4584194	85.289544	63.92168833	22.54416616	15.33460025
Q2G021	SAOUHSC_00806	-1.440450575	0.00000465	0.000015	110.4969604	67.64343145	115.7826808	22.54416616	24.5353604
Q2G1H7	SAOUHSC_00146	1.108527235	0.00000494	0.0000158	104.9721124	100.9749774	92.86735852	219.3720784	253.5320575
Q2FW42	SAOUHSC_02475	-1.152568847	0.00000992	0.0000309	67.40314583	74.50580855	80.80666261	30.34791598	27.60228045
Q2FWG2	thiM	-1.007323324	0.0000138	0.0000421	125.9665348	152.9329755	174.8800907	72.83499836	66.44993442
Q2FVB3	SAOUHSC_02821	-1.012506465	0.0000174	0.0000523	154.6957445	181.3628235	186.9407866	92.77791458	63.38301437

Q2FYW2	SAOUHSC_01312	-1.127364537	0.0000207	0.0000616	76.24290266	81.36818566	84.42487138	29.48083267	35.78073392
Q2FYX0	SAOUHSC_01303	-1.310468555	0.0000271	0.0000792	44.19878415	41.17426262	41.0063661	13.87333302	11.24537352
Q2FXX0	SAOUHSC_01710	-1.131336254	0.0000451	0.00012833	118.2317476	94.11260028	86.83701057	29.48083267	51.11533417
Q2FV56	crtO	-1.043682325	0.000055	0.00015492	67.40314583	71.56478979	71.15810588	25.1454161	35.78073392
Q2FXW8	SAOUHSC_01712	-1.058246277	0.0000595	0.00016623	198.8945287	174.5004463	189.3529258	67.63249848	95.07452156
Q9EYW6	sspC	-1.194319427	0.0000845	0.0002307	75.13793306	57.84003559	77.18845384	14.74041633	35.78073392
Q2G0X2	SAOUHSC_00401	-1.194761856	0.00015598	0.00040611	121.5466564	135.2868629	114.5766112	52.02499883	31.69150719
Q2G0X4	SAOUHSC_00399	1.116179185	0.00048046	0.0011772	36.46399692	34.31188552	34.97601814	110.9866642	82.80684136
Q2FV37	SAOUHSC_02902	1.064610034	0.00051031	0.00124633	23.20436168	19.60679172	19.29711346	52.02499883	53.15994754
Q2FV43	SAOUHSC_02896	1.202546982	0.00052478	0.00127894	6.629817623	9.803395862	13.2667655	32.08208261	34.75842724
Q2FXE3	SAOUHSC_01906	-1.26051598	0.00065551	0.00157571	28.7292097	24.50848966	27.7396006	6.069583197	7.156146784
Q2FX92	SAOUHSC_01985	-1.167346749	0.00067044	0.00160484	28.7292097	41.17426262	56.68527079	15.60749965	14.31229357
Q2FYM5	SAOUHSC_01410	-1.260608335	0.00067583	0.00161605	19.88945287	20.58713131	16.88497428	4.335416569	1.022306683
Q2G293	SAOUHSC_01847	-1.147365425	0.00099136	0.00229378	36.46399692	32.35120635	21.70925264	12.13916639	6.133840101
Q2FZS5	SAOUHSC_00915	-1.067963835	0.00111441	0.00254245	50.82860177	55.87935641	30.15173978	17.34166628	17.37921362
Q2FVY9	sarV	1.114597602	0.00157511	0.00351283	25.41430089	14.70509379	31.35780937	71.96791504	77.69530794
Q2FXF0	SAOUHSC_01899	-1.168050234	0.00164146	0.00364664	165.7454406	117.6407503	212.2682481	41.61999906	30.6692005
Q2FYR6	trpC	1.047032044	0.00280033	0.00591641	7.734787226	8.823056276	13.2667655	36.41749918	20.44613367
Q2G2T5	SAOUHSC_00012	1.062661401	0.00298009	0.00626724	6.629817623	6.862377104	9.64855673	26.01249941	21.46844035
Q2FZN9	SAOUHSC_00961	-1.000973462	0.00513837	0.01036745	15.46957445	20.58713131	22.91532223	7.803749824	4.089226734